POLYTECHNIQUE MONTRÉAL

affiliée à l'Université de Montréal

et

l'Université du Québec en Abitibi-Témiscamingue

Integrating multidisciplinary modeling tools to support upstream mine waste management

YOUSSEF TOUBRI

Département des génies civil, géologique et des mines

Thèse présentée en vue de l'obtention du diplôme de *Philosophiae Doctor*

Génie Minéral

Août 2022

© Youssef Toubri, 2022.

POLYTECHNIQUE MONTRÉAL

affiliée à l'Université de Montréal

et

l'Université du Québec en Abitibi-Témiscamingue

Cette thèse intitulée:

Integrating multidisciplinary modeling tools to support upstream mine waste management

présentée par : **Youssef TOUBRI**

en vue de l'obtention du diplôme de *Philosophiae Doctor*

a été dûment acceptée par le jury d'examen constitué de :

Bruno BUSSIÈRE, président
Isabelle DEMERS, membre et directrice de recherche
Nicholas BEIER, membre et codirecteur de recherche
Bas VRIENS, membre externe
Hooman ASKARI, membre externe

DEDICATION

To my parents Naima and Abderazzak

To my family and friends.

« Et dis : Ô mon Seigneur, accroit mes connaissances »

« Quand le fils d'Adam meurt, son œuvre s'arrête sauf dans trois choses : Une aumône continue, Une science dont les gens tirent profit, Un enfant pieux qui invoque pour lui »

ACKNOWLEDGEMENTS

Praise be to Allah for helping me throughout my life and particularly during the last four years. Without His guidance this work would not exist, I would like to thank Him for making me audacious to quit my comfort zone and patient to accomplish the most challenging journey I have ever experienced up until now.

I would like to express my sincere gratitude and my cordial acknowledgements to my supervisor Professor Isabelle Demers who believed in my capabilities and believed in my manners to manage this project. She trusted me and gave me the helm of the project to steer this outstanding journey. Besides, she was always available to support me during tough times when I got lost in the project maze and there was nothing but dead-ends. She was continuously providing me hope, autonomy and confidence along with resources. Although she did not know me before this project, she was willing to accept my application in her research team after a short virtual meeting. This meeting completely changed my personal life and my professional career. Professor Isabelle Demers is the key person who offered me promising horizons to tackle my scientific metamorphosis. My gratitude could not be summarized in few words but I would like to say thank you dear Professor.

I would like to thank my co-supervisor Professor Nicholas Beier for hosting me at the University of Alberta to acquire new modeling skills. My co-supervisor Professor Nicholas Beier was always available to review my papers and he always returned his reviews with no delay. Thank you for your time dedicated to improve my manuscripts.

I was honored to work with Benoît Plante and Mathieu Fillion throughout a Mitacs training. Thanks to their scientific contributions and commitment, I was able to issue a scientific article in one of the high-ranked journals in environmental sciences.

I am also grateful to the UQAT academic staff who provided me with professional information and guidance regarding the scientific research. I would also like to thank all the members of the URSTM technical team who have contributed to the accomplishment of this project.

Special thanks to the jury members Bas Vriens and Hooman Askari and the jury president Bruno Bussière.

Without them, I would not accomplish my ambitions, my parents Naima and Abderazzak made priceless sacrifices for the sake of my education. Although they are illiterate and cannot read these words, they know that I am proud of them for making me the first family member who attended college and the first doctor in my family. They forgave my selfishness when I decided to quit my comfort zone and leave their nearness even they needed my presence. I would like to apologize and to thank you for respecting my ambitions.

Friendship saved me when I was unable to bear troubles related to the adaptation issue. I was weak and afraid to confront the new environment. Did I make the right choice? This self-interrogation started to devastate my self-confidence. Fortunately, my rescuer Marouen Jouini afforded me assistance and pure friendship. He dedicated a good portion of his time to create warm ambience, much warmer than Canada's winter. He cooked for us the best-known Tunisian dishes, we laughed together, we sang together and we fell together when we tried skating. Marouen is my friend and much more than a friend, he is my model and my brother. Thank you dear Marouen.

Special thanks to my friends Rihem Jaidi, Rachid Amrou, Mouna Ettoumi, Khadija Elmahboub, Hssan Youssef Mahdoui and Safa Chlahbi who contributed to extracting me from my alienation. I would also thank my friends from Morocco who encouraged me to be a better version of myself: Jamal El Jabali, Radouan El Bamiki, Aiman Elmachi, Yassir Astati, Ibtissam Chraiki and Âouatif El hali.

I express my sincere gratitude to Hajar Nasserallah for the blessed positive energy that she was continuously providing me.

I would also like to thank my colleagues in my former job: Abdellatif Errami, Taha Ghadi, Mohamed Bazzi and Rachid El Haloui.

These acknowledgements could not be complete without thanking my childhood friends: Jamal Chafik, Charaf Elaarissa, Hamza Ait Saleh, Younes Boundir, Radouan Lahder and Kamal Ghadbane.

PREFACE

The scientific research performed throughout the present dissertation project was shared as original research articles, conference articles or communications presented in national and international conferences and symposiums. The present dissertation includes three original research articles featured in chapters 4, 5 and 7 respectively, while the chapter 6 consists of a conference article. The dissertation author is the first author of the scientific publications presented herein.

This work is a part of the Natural Sciences and Engineering Research Council of Canada (NSERC) TERRE-NET program, led by Dr. D. Blowes. The entire dissertation is written in English to enable the research availability to the University of Alberta, our main academic partner, as well as Anglophone universities members of the TERRE-NET program.

Details of our scientific contributions are provided below.

Research articles submitted, accepted and/or published in international scientific journals:

Toubri, Y., Demers, I., Poirier, A., Pépin, G., Gosselin, M. C., & Beier, N. A. (2021). Merging 3D geological modeling and stochastic simulation to foster waste rock upstream management. Journal of Geochemical Exploration, 224, 106739. (https://doi.org/10.1016/j.gexplo.2021.106739).

Toubri, Y., Vermette, D., Demers, I., Beier, N., & Benzaazoua, M. (2021). Incorporating Kinetic Modeling in the Development Stages of Hard Rock Mine Projects. Minerals, 11(12), 1306. (https://doi.org/10.3390/min11121306).

Toubri, Y., Demers, I., & Beier, N. (2022). A novel approach integrating 3D geological and kinetic modeling to inform upstream mine waste classification. (Accepted by Environmental Pollution).

Conference article with review committee:

Toubri, Y., Demers, I., & Beier, N. (2021). Integrating multidisciplinary modeling tools to foster scoping surveys and upstream mine waste management. In: Proceedings of Tailings and Mine Waste 2021 Banff, AB, Canada, 585-594.

International conference presentations with review committee:

Toubri, Y., Demers, I., & Beier, N. (2021). Integrating multidisciplinary modeling tools to foster scoping surveys and upstream mine waste management. In: Proceedings of Tailings and Mine Waste 2021 Banff, AB, Canada, 585-594.

Toubri, Y., Demers, I., & Beier, N. A novel approach integrating 3D geological and kinetic modeling to inform upstream mine waste classification (2022). GAC-MAC-IAH Halifax 2022.

Presentation at RIME UQAT-Polytechnique annual colloquium:

Toubri, Y., Demers, I., & Beier, N. (2021). Intégrer des outils de modélisation multidisciplinaires pour promouvoir la gestion en amont des rejets miniers. RIME UQAT-Polytechnique annual colloquium.

Presentation at the virtual symposium 2021 on mines and the environment:

Toubri, Y., Vermette, D., Demers, I., Beier, N., & Benzaazoua, M. (2021). Entailing multicomponent kinetic modeling for upstream geochemical assessment of metallic orebodies. The virtual symposium 2021 on mines and the environment.

TERRE-NET annual general meeting presentations:

Toubri, Y., Demers, I., & Beier, N. (2019). Integration of geo-environmental aspects in TMSim dynamic model to assess waste rock and tailings management approaches. TERRE-NET AGM.

Toubri, Y., Vermette, D., Demers, I., Beier, N., & Benzaazoua, M. (2020). Kinetic geochemical modeling to simulate low acid generating potential waste rock disposal scenarios in upstream mine waste management. TERRE-NET AGM.

Toubri, Y., Vermette, D., Demers, I., Beier, N., & Benzaazoua, M. (2021). Entailing multicomponent kinetic modeling for upstream geochemical assessment of metallic orebodies. TERRE-NET AGM.

Toubri, Y., Demers, I., & Beier, N. (2022). A novel approach integrating 3D geological and kinetic modeling to inform upstream mine waste classification. TERRE-NET AGM.

TERRE-NET annual general meeting posters:

Toubri, Y., Demers, I., & Beier, N. (2019). Integration of geo-environmental aspects in TMSim dynamic model to assess waste rock and tailings management approaches. TERRE-NET AGM.

Toubri, Y., Vermette, D., Demers, I., Beier, N., & Benzaazoua, M. (2020). Kinetic geochemical modeling to simulate low acid generating potential waste rock disposal scenarios in upstream mine waste management. TERRE-NET AGM.

Toubri, Y., Vermette, D., Demers, I., Beier, N., & Benzaazoua, M. (2021). Entailing multicomponent kinetic modeling for upstream geochemical assessment of metallic orebodies. TERRE-NET AGM.

Toubri, Y., Demers, I., & Beier, N. (2022). A novel approach integrating 3D geological and kinetic modeling to inform upstream mine waste classification. TERRE-NET AGM.

Research article related to other projects:

The author was also involved in a Mitacs project not related to his dissertation thematic. In this regard, the following research article was issued in the peer-reviewed international Journal of Cleaner Production.

Toubri, Y., Plante, B., Demers, I., & Fillion, M. (2022). Probing cleaner production opportunities of the Lac Tio pyrite-enriched tailings generated to alleviate sulfur dioxide emissions. Journal of Cleaner Production, 132027. (https://doi.org/10.1016/j.jclepro.2022.132027)

RÉSUMÉ

Le drainage minier acide (DMA), suivant l'oxydation des sulfures déclenchée par l'oxygène atmosphérique et l'eau libre, occasionne une détérioration de la qualité de l'eau en terme d'acidité et de concentration des métaux et oxyanions. Le DMA constitue un danger environnemental d'ampleur mondiale vu son effet néfaste sur les systèmes aquatiques et les formes de vies fauniques et floristiques. Les contributions scientifiques menées par le gouvernement, l'industrie minière, les universités et les établissements de recherche se concentrent sur l'évaluation, la prévention et le traitement du DMA pour préserver les écosystèmes avoisinant les installations minières. La plupart des contributions scientifiques abordent les aspects avals de la gestion du DMA impliquant les étapes opérationnelles et post-fermeture du cycle minier. Peu de solutions pratiques ont été suggérées pour la phase de développement en raison du manque de rejets solides in-situ et les données expérimentales nécessaires pour envisager lesdites contributions scientifiques. Par conséquent, le concept de gestion en amont a reçu très peu d'attention. De même, les approches de modélisation utilisées pour prévoir le DMA sont largement étudiées. Bien qu'elles offrent de nombreux avantages, la majorité de ces études de modélisation sont réalisées pendant les phases d'exploitation et de fermeture du cycle minier, car elles abordent les stratégies de conception et la performance des scénarios de restauration. En outre, la recherche scientifique basée sur des approches interdisciplinaires pour atténuer le risque environnemental du DMA devrait être davantage mise en évidence et développée.

La revue de la littérature souligne trois concepts principaux ; la géométallurgie, le principe de conception pour la fermeture et la réflexion en amont. La géométallurgie a été principalement développée pour dissoudre les limites interdisciplinaires entre le géologue, le métallurgiste et l'ingénieur minier afin d'optimiser les profits économiques et d'atténuer les risques techniques. Plus récemment, divers chercheurs ont inclus les enjeux environnementaux miniers dans la réflexion holistique de la géométallurgie. Le principe de conception pour la fermeture exige que les problèmes environnementaux potentiels soient pris en compte et planifiés avant et pendant les étapes de l'exploitation minière. De même, la réflexion en amont propose d'introduire des pratiques préventives dans les filières de gestion des rejets miniers. Ces pratiques doivent être entreprises dès les premières étapes possibles du cycle minier, appelées étapes en amont. Bien que de nombreuses contributions scientifiques aient abordé les concepts susmentionnés, elles se sont

principalement concentrées sur des expériences en laboratoire et/ou sur le terrain. Aucune recherche n'a abordé la réconciliation entre les approches de modélisation pour soutenir l'atténuation des risques environnementaux du DMA. Le lien entre le géologue et le géochimiste environnemental est une préoccupation croissante qui devrait être abordée pour fournir au gestionnaire des rejets miniers de nouvelles options pour aller au-delà des méthodes de gestion conventionnelles.

L'objectif principal du présent travail est de dissoudre les limites interdisciplinaires entre les approches de modélisation pertinentes pour améliorer la gestion en amont des rejets miniers solides et la prévention du DMA. Ainsi, trois objectifs principaux ont été définis : (1) lier la modélisation géologique et les attributs environnementaux du DMA pour effectuer une classification spatiale proactive des rejets miniers en fonction de leur risque environnemental inhérent; (2) réconcilier les outils de modélisation cinétique avec les contraintes des stades amonts du cycle minier (ex. le stade de développement) et (3) intégrer la composante spatiale développée selon le premier objectif et la dimension temporelle de la modélisation cinétique pour concevoir une approche de modélisation holistique permettant la classification en amont des rejets miniers et supportant l'atténuation des risques environnementaux. Pour atteindre ces objectifs, l'approche méthodologique a consisté dans un premier temps à lier les informations géologiques, collectées tout au long des campagnes du logging géologique, à la modélisation numérique. Ce lien a été établi par une approche stochastique qui relie les variables discrètes et continues du logging géologique. Le résultat de la simulation stochastique soutient la modélisation géologique 3D en accomplissant la densité spatiale adéquate des données numériques. Cette partie permettait d'établir des modèles numériques 3D décrivant la distribution spatiale d'un contaminant donné contenu dans la roche hôte. Par la suite, l'approche de modélisation cinétique a été réalisée pour simuler le pH résultant des principales réactions de génération et de neutralisation de l'acidité. Le modèle cinétique prend en compte des conditions hautement oxydantes et des réactions contrôlées par la réactivité minérale et la surface disponible. Par conséquent, la diffusion d'oxygène n'a pas été considérée comme l'étape limitant le processus d’oxydation-neutralisation. Le modèle a été calibré et étalonné par rapport à des tests cinétiques expérimentaux dont les conditions opératoires sont conformes à l'hypothèse du modèle. Enfin, les modèles spatiaux et cinétiques susmentionnés ont été intégrés pour permettre une classification dynamique de la roche abritant le minerai. Le modèle spatio-temporel intégré implique le logging

géologique, la simulation stochastique, la modélisation géologique 3D, la modélisation cinétique et la modélisation de l'écoulement non saturé. Cette approche holistique décrit la distribution spatiale des principaux minéraux générateurs et neutralisants d'acide et entreprend une modélisation du transport réactif 1D pour chaque constituant volumétrique élémentaire, nommé voxel. Par la suite, une classification en amont des rejets miniers pourrait être effectuée en fonction de la teneur inhérente d'un contaminant donné dans la roche hôte et en fonction du pH qui pourrait être libéré à l'emplacement X, Y, Z du corps minéralisé si l'assemblage minéral correspondant est soumis à des conditions oxydantes. Les résultats de chaque axe sont résumés ci-dessous.

L'utilisation de la modélisation géologique 3D pour la gestion des rejets miniers a permis de visualiser la distribution spatiale des contaminants dans un corps minéralisé et sa roche hôte. Par la suite, les responsables en matière de gestion pourraient facilement entreprendre la classification des stériles. À cet égard, le site minier Éléonore a fourni une base de données restreinte des teneurs en arsenic, l'élément le plus délétère dans son environnement minier, pour créer un modèle spatial 3D de la teneur en arsenic. Leapfrog Geo a été utilisé pour effectuer la modélisation géologique 3D et le logiciel de modélisation géostatistique de Stanford (SGeMS) a été utilisé pour entreprendre l'analyse du variogramme spatial. Le résultat de ce travail consiste en un modèle spatial 3D en multi-réalisation de la teneur en arsenic à travers le gisement et la roche encaissante. Chaque réalisation a été évaluée à l'aide des analyses chimiques mesurées pour souligner la fiabilité du modèle. Les résultats ont révélé un vaste halo géochimique d'arsenic qui s'étend jusqu'à 500 m du gisement d'or, avec jusqu'à 94 % des teneurs en arsenic dépassant 50 ppm.

Les résultats de la modélisation cinétique à l'aide de PHREEQC ont montré un bon accord avec les données des mini-cellules d'altération. L'objectif principal de simulation du pH à l'aide de la modélisation cinétique des essais en mini-cellules d'altération a été atteint. Cependant, le modèle n'inclut pas les processus de rétention géochimique tels que la coprécipitation et la sorption. Étant conscient de ces limites, le modèle cinétique PHREEQC n'est pas conforme aux objectifs de conception liés à la restauration minière. Cependant, il est conforme aux études préliminaires tout au long de la phase de développement, qui a peu bénéficié des outils de modélisation géochimique. Le principal atout du modèle cinétique proposé est la capacité d'entreprendre une analyse paramétrique pour l'identification en amont des risques en se basant sur une base de données restreinte et un raisonnement de modélisation conservateur. À cet égard, les données d'entrée sont

constituées de la caractérisation minéralogique habituelle, les tests de mini-cellule d'altération et les taux de réactivité minérale tirés de la littérature, respectant ainsi deux contraintes principales qui orientent l'étape de développement : la disponibilité des matériaux et le coût d'évaluation.

Les résultats du modèle intégrant la modélisation spatiale et la modélisation du transport réactif montrent l'évolution spatio-temporelle du pH tout au long du plan central d'exploitation minière. À cet égard, 527 simulations de transport réactif ont été effectuées tout au long du plan minier composé de voxels de 40x40x40 mètres. Le géomodèle spatio-temporel met en évidence l'effet de la réactivité des minéraux neutralisants sur le pH lors de l'oxydation des sulfures.

L'intégration de la géologie et la géochimie environnementale est la solution clé pour des opportunités de production plus propres. Le présent projet a fait progresser les connaissances sur la classification en amont des rejets miniers et a mis en place des méthodes prometteuses pour intégrer des approches de modélisation multidisciplinaires en vue d'un meilleur contrôle des rejets solides dans les mines métalliques. Les méthodes appliquées ici ne se limitent pas aux études de cas abordées et pourraient être appliquées à d'autres projets miniers atteignant les stades de développement et/ou d'exploitation.

Mots clés: Logging géologique, Modélisation géologique, Simulation Stochastique, Cinétique minérale, Classification des rejets miniers.

ABSTRACT

Acid mine drainage (AMD), following oxidation of sulphides triggered by atmospheric oxygen and through-flowing water, causes water quality exceedances in terms of water acidity and metals and oxyanions concentrations. AMD is a worldwide ecological-security threat with the ability to toxify freshwaters and impair life forms and their support systems. Scientific research contributions adopted by governments, the mining industry, universities, and research establishments focus on assessment, prevention, and treatment of AMD to safeguard ecosystems neighbouring mine facilities. Most of the scientific research contributions tackle downstream aspects of the AMD management involving operational and post-closure stages of the mine life. Few practical solutions were suggested during the development stage because of the lack of in-situ waste materials and the data-intensive nature of the solutions being used. Consequently, the concept of upstream management has received very little attention. Likewise, modeling approaches used to forecast AMD are extensively investigated. Although they provide many benefits, the majority of these modeling case studies are carried out during the operation and closure stages of the mine life cycle as they tackle design strategies and the performance of reclamation scenarios. Besides, scientific research based upon cross-disciplinary approaches to mitigate AMD environmental risk should be further highlighted and developed.

The literature review underlines three main concepts; the geometallurgy, the design for closure principle and the upstream thinking. The geometallurgy was primarily developed to dissolve the interdisciplinary barriers among the geologist, the metallurgist and the mining engineer to optimize the economic profits and mitigate technical risks. More recently, miscellaneous researchers included the mining environmental issues in the geometallurgical holistic thinking. The design for closure principle requires that potential environmental issues are considered and planned for both before and during the production stages of mining operation. Likewise, the upstream thinking proposes introducing preventive practices into mine waste management streams. These practices should be undertaken at the earliest possible stages of a mine's life cycle, known as upstream stages. Although numerous scientific contributions tackled the aforementioned concepts, they were mainly focused on lab and/or field experiments. No research has addressed the bridging among modeling approaches to support the AMD environmental risk mitigation. The nexus between the geologist and the environmental geochemist is a growing concern that should be addressed to

provide the mine waste manager with novel options to move beyond conventional management methods.

The main aim of the present work is to dissolve interdisciplinary barriers among the relevant modeling approaches to enhance mine waste upstream management and AMD prevention. Accordingly, three main objectives were defined: (1) bridging geological modeling and AMD environmental attributes to perform proactive spatial classification of mine waste based on their inherent environmental risk; (2) using the time dimension of the AMD geochemical modeling modules that should comply with the framework of the upstream stages of the mine life (e.g., the development stage); and (3) integrating the spatial component developed according to the first objective and the temporal dimension mentioned in the second objective to conceive a holistic modeling approach enabling upstream mine waste classification and supporting environmental risk mitigation. To achieve these objectives, the methodological approach consisted firstly of linking the geological information, collected throughout the geological logging surveys, to the numerical modeling. This linkage was established through a stochastic approach that relates the discrete and continuous variables of the geological logging. The outcome of the stochastic simulation supports the subsequent 3D geological modeling as it fulfills the data-density requirement. This part enables the establishment of 3D numerical models describing the spatial distribution of a given contaminant contained in the host rock. Thereafter, the kinetic modeling approach was performed to simulate the pH resulting from the main acid-generating and acid-neutralizing reactions. The kinetic model considers highly oxidizing conditions and surface-controlled reactions. Consequently, oxygen diffusion was not considered as the rate-limiting step. The model was calibrated and benchmarked against experimental kinetic tests whose operating conditions comply with the model hypothesis. Finally, the aforementioned spatial and kinetic models were integrated to enable a dynamic classification of the ore hosting rock. The spatiotemporal integrated model involves geological logging, stochastic simulation, 3D geological modeling, kinetic modeling and unsaturated environment modeling. This holistic approach portrays the spatial distribution of the main acid-generating and acid-neutralizing minerals and undertakes a 1D reactive transport modeling for each elementary volumetric constituent, named voxel. Subsequently, an upstream mine waste classification could be carried out based on the inherent content of a given contaminant in the host rock and based upon the pH that could be released at X, Y, Z location of the orebody if the

corresponding mineral assemblage undergoes highly oxidizing conditions. Results of each part are summarized in the following.

Repurposing the 3D geological modeling for mine waste management allowed for the visualization of hazardous metals spatial distribution throughout an orebody and its hosting rock. Subsequently, a mine manager could seamlessly undertake waste rock classification. In this respect, the Éléonore mine site provided restricted grades of arsenic, the most deleterious element within the mine setting, to create a 3D spatial model of arsenic content. Leapfrog Geo was used to perform the 3D geological modeling and the Stanford Geostatistical Modeling Software (SGeMS) was used to undertake the spatial variogram analysis. The outcome of this work consists of multi-realization 3D spatial model of arsenic grade across the ore deposit and the hosting rock. Each realization was assessed using available chemical analyses to underline the model's reliability. The results revealed a spacious geochemical halo of arsenic that reaches up to 500 m away from the gold deposit, with up to 94% of arsenic grades exceeding 50 ppm.

Results from the kinetic modeling using PHREEQC exhibited a good agreement with weathering cell data. The main objective of simulating the pH using kinetic modeling of weathering cell tests was fulfilled. However, the model does not include geochemical retention processes such as coprecipitation and sorption. Being cognizant of these limitations, the PHREEQC kinetic model does not conform to design purposes related to mine reclamation. However, it complies with the upstream scoping studies along the development stage, which has barely benefited from geochemical modeling tools. The main asset of the present kinetic model is the ability to undertake parametric analysis for upstream risk identification based upon restricted datasets and conservative modeling reasoning. In this regard, the input datasets consist of the usual mineralogical characterization, weathering cell tests, and literature rate laws, thereby abiding by two main constraints that steer the development stage: material availability and assessment cost.

Results from the model integrating the spatial modeling and reactive transport modeling displays the spatio-temporal evolution of the pH throughout the central plane of mining. In this regard, 527 reactive transport simulations were performed throughout the mining plane consisting of 40x40x40 meters voxels. The spatiotemporal geomodel highlights the effect of neutralizing minerals reactivity on the pH during the sulphide oxidation.

Geology and environmental geochemistry integration is the key solution for cleaner production opportunities. The present project progressed the knowledge of upstream mine waste classification and set up promising methods to integrate multidisciplinary modeling approaches for the sake of a better control over solid waste in hard rock mines. Methods applied herein are not limited to the case studies framework and could be applied to other mining projects reaching development and/or operation stages.

Keywords: Geological logging, Geological modeling, Stochastic simulation, Mineral kinetics, Mine waste classification.

TABLE OF CONTENTS

DEDICATION III

ACKNOWLEDGEMENTS IV

PREFACE VI

RÉSUMÉ IX

ABSTRACT XIII

TABLE OF CONTENTS XVII

LIST OF TABLES XXI

LIST OF FIGURES XXII

LIST OF SYMBOLS AND ABBREVIATIONS XXVII

LIST OF APPENDICES XXX

CHAPTER 1 INTRODUCTION 1

1.1 The project framework 1

1.2 The general problematic 3

1.3 The project novelty 3

1.4 The research hypotheses 4

1.5 Objectives 4

1.6 The dissertation content 4

1.7 The project sequence 8

CHAPTER 2 LITERATURE REVIEW 12

2.1 Acid mine drainage formation 12

2.2 Overview on mine waste management approaches 17

2.3 Geological modeling 22

2.3.1 Key concepts: from statistics to geostatistics 23

2.3.2 Spatial continuity 25
2.3.3 Practical steps for building spatial models 27
2.4 Monte Carlo simulation 29
2.4.1 Estimation and simulation 29
2.4.2 Probability concepts 30
2.4.3 Monte Carlo simulation and applications 32
2.5 Reactive transport modeling 35
2.6 Final remarks 37
CHAPTER 3 METHODOLOGY 39
CHAPTER 4 ARTICLE 1: MERGING 3D GEOLOGICAL MODELING AND STOCHASTIC SIMULATION TO FOSTER THE WASTE ROCK UPSTREAM MANAGEMENT 43
4.1 Abstract 43
4.2 Introduction 44
4.3 Materials and methods 46
4.3.1 Geological background 46
4.3.2 Geochemical and geological database 48
4.3.3 Modeling method 52
4.4 Results and discussion 56
4.4.1 Monte Carlo simulation results 56
4.4.2 Geological model and analysis 61
4.5 Conclusion 67
CHAPTER 5 ARTICLE 2: INCORPORATING KINETIC MODELING IN THE DEVELOPMENT STAGES OF HARD ROCK MINE PROJECTS 75

5.1 Abstract 75
5.2 Introduction 75
5.3 Materials and methods 79
5.3.1 Geological background 79
5.3.2 Samples preparation and characterization 79
5.3.3 Weathering cell test 82
5.3.4 The conceptual model 83
5.3.5 Calibration and parameter fitting 87
5.4 Results and discussion 88
5.4.1 Experimental datasets 88
5.4.2 Modeling results 92
5.4.3 Parametric analysis 101
5.5 Conclusion 104
CHAPTER 6 ARTICLE 3: INTEGRATING MULTIDISCIPLINARY MODELING TOOLS TO FOSTER SCOPING SURVEYS AND UPSTREAM MINE WASTE MANAGEMENT .. 117
6.1 Abstract 117
6.2 Introduction 117
6.3 Materials and methods 119
6.3.1 Spatial modeling for mine waste classification 119
6.3.2 Kinetic modeling approach for the pH assessment 123
6.3.3 Integration of kinetic modeling and stochastic simulation 124
6.4 Results and discussion 125
6.4.1 Spatial modeling for mine waste classification 125
6.4.2 Kinetic modeling 128

6.5 Conclusion 130

CHAPTER 7 ARTICLE 4: INTEGRATING 3D GEOLOGICAL MODELING AND KINETIC MODELING TO ALLEVIATE ACID MINE DRAINAGE THROUGH UPSTREAM MINE WASTE CLASSIFICATION 134

7.1 Abstract 134

7.2 Introduction 135

7.3 Materials and methods 137

7.3.1 Geological framework 137

7.3.2 3D implicit geomodeling 138

7.3.3 1D reactive transport modeling 143

7.4 Results and discussion 146

7.4.1 Monte Carlo simulation results 146

7.4.2 The geomodeling results 148

7.4.3 Reactive transport modeling results 150

7.5 Conclusion 153

CHAPTER 8 GENERAL DISCUSSION 161

8.1 Integrated geomodeling protocol 162

8.2 Advantages and Limitations 164

8.3 Future integration horizons 165

8.3.1 System dynamics 165

8.3.2 Mining optimization 171

CHAPTER 9 CONCLUSION AND RECOMMENDATIONS 173

REFERENCES 176

APPENDICES 193

LIST OF TABLES

Table 4.1 Error margins related to each sample size ranked based on arsenopyrite classes 51

Table 4.2 Hypotheses testing based on a 0.05 significance level 57

Table 4.3 Variogram realizations highlighting the ergodic fluctuations effect on the ranges 60

Table 5.1 List of dissolution rate parameters used in this study to kinetically simulate the neutralization potential under a wide range of pH 86

Table 5.2 Physical properties of composite samples 89

Table 5.3 Chemical analysis of the composite samples 89

Table 6.1 Number of arsenopyrite intervals per class and the sample size that was analyzed. Confidence interval: 95%. Adapted from Toubri *et al*. (2021) 121

Table 7.1 Margins of error associated to the mineral classes computed based upon the logging interval populations and the available analyzed sample size 142

LIST OF FIGURES

Figure 1.1 Visualization of the project objective 5

Figure 2.1 The staged construction methods of the tailings-made impoundments 18

Figure 2.2 Summary of integrated approaches used to overcome the issues related to conventional disposal methods 22

Figure 2.3 Three different spatial patterns presenting the same normal distribution (From Abzalov (2016)) 24

Figure 2.4 An example of experimental variogram fitted to an exponential model. 26

Figure 2.5 Practical steps to build grid and solid models (From Reed (2007)) 27

Figure 2.6 Example of a probability function of a stochastic input. 30

Figure 2.7 Example of the random sampling process used to perform Mont Carlo simulation 33

Figure 2.8 Processes included in multiscale reactive transport modeling (Vriens *et al.*, 2020) 35

Figure 3.1 The general methodology of integrating multidisciplinary modeling tools to inform upstream mine waste classification 40

Figure 3.2 The conceptual model of the reactive transport simulation carried out using PHREEQC and VS2DRTI for geochemical simulation that are not O_2 diffusion-limited. 42

Figure 4.1 Local geological setting of the Roberto deposit (Modified from Fontaine *et al.*, 2017) 47

Figure 4.2 Available geochemical arsenic data from drill core samples neighbouring the orebody (plane view) 48

Figure 4.3 Drill core logging of arsenopyrite throughout the orebody and the host rock (plane view) 49

Figure 4.4 Illustration of the geological logging concept coupled to the treemap layout of the sample size of logging intervals per class 50

Figure 4.5 The available arsenic geochemical analyses constrained to the arsenopyrite classes 51

Figure 4.6 Synthetic raw data exemplifying the iterative Monte Carlo simulation based on log-normal distributions. The simulation process is performed in steps (from a to e), A and B are two independent and continuous random variables created for illustration purposes 54

Figure 4.7 Output of the iterative stochastic simulation for each arsenopyrite class (Realization 1) 57

Figure 4.8 Data Generated through correlation-based and iterative Monte Carlo simulation. The simulation results are constrained to the available data features (Realization 1) 58

Figure 4.9 Selected values of the auxiliary variable from the generated points based on the reported interval values (Realization 1) 59

Figure 4.10 a) The spatial distribution of arsenic grades ranging from 500 ppm to 1100 ppm, b) The spatial distribution of arsenic grades ranging from 1100 ppm to 2300 ppm (Realization 1) 61

Figure 4.11 Spatial relationship between the gold deposit and the arsenic grades in Realization 1 62

Figure 4.12 a) Realization 1 of the block model delineating arsenic grades greater than 200 ppm, b) Realization 1 of the block model of the arsenic grades along the footwall of the gold deposit 63

Figure 4.13 Underground stopes assessed through realization 1 of the spatial model 64

Figure 4.14 The empirical cumulative distribution functions of the resulting realizations along with the local and the regional measured grades of arsenic 65

Figure 4.15 Spatial intersections of the mine plan overlaid with the 3D spatial model (Realization 1) and the chemical analyses performed on drill core samples 66

Figure 5.1 Blend samples prepared to assess geochemical interactions among lithological units within geo-environmental domains (the size of the boxes represent blending proportions)*. 80

Figure 5.2 The conceptual model of the weathering cell tests 85

Figure 5.3 Mineralogical composition of composite samples 90

Figure 5.4 Acid–base accounting classification based on the neutralization potential ratio 90

Figure 5.5 Weathering cell test D2 and PHREEQC modeling results using BET and geometric surface area-derived rates. (a) Experimental and simulated results of the pH. (b) sulfate. (c) sodium. (d) iron. (e) calcium. (f) magnesium. (g) aluminum. (h) potassium. (i) manganese. 94

Figure 5.6 Weathering cell test D1 and PHREEQC modeling results. (a) Experimental and simulated results of the pH. (b) sulfate. (c) sodium. (d) iron. (e) calcium. (f) magnesium. (g) aluminum. (h) potassium. (i) manganese. 97

Figure 5.7 Weathering cell test D3 and PHREEQC modeling results. (a) Experimental and simulated results of the pH. (b) sulfate. (c) sodium. (d) iron. (e) calcium. (f) magnesium. (g) aluminum. (h) potassium. (i) manganese. 99

Figure 5.8 Weathering cell test T1 and PHREEQC modeling results. (a) Experimental and simulated results of the pH. (b) sulfate. (c) sodium. (d) iron. (e) calcium. (f) magnesium. (g) aluminum. (h) potassium. (i) manganese. 100

Figure 5.9 Various scenarios underlining the effect of various mineral assemblages on leachate quality. (a) Sulfate concentrations obtained in the presence of different mineral proportions. (b) Cu concentrations obtained in the presence of different mineral proportions (c): Fe concentrations obtained in the presence of different mineral proportions. (d): Mn concentrations obtained in the presence of different mineral proportions. (e): The pH obtained from the simulated mineral proportion scenarios. 102

Figure 5.10 Various scenarios delineating the relationship between the residence time and leachate quality in weathering cell test simulation. (a) The pH obtained for various residence times. (b) Sulfate concentrations obtained for various residence times. (c): Total iron concentrations obtained for various residence times. 104

Figure 6.1 The iterative Monte Carlo simulation and the correlation based sampling. Adapted from Toubri *et al.* (2021) 122

Figure 6.2 Results of the first realization of the stochastic simulation compared to the initial sample size (G denotes the generated data by the stochastic process for each class). Adapted from Toubri *et al*. (2021) 125

Figure 6.3 Realizations of directional variograms showing the highest spatial continuity 126

Figure 6.4 Underground stopes classified in terms of their As grades 127

Figure 6.5 Experimental (empty circles) versus modeling (solid line) results from the calibration case. Adapted from Toubri *et al.* (2021b) 129

Figure 6.6 Parametric analysis using various scenarios of mineral assemblages 130

Figure 6.7 A summary of the integration reasoning suggested in this work 131

Figure 7.1 Illustration of the geological logging procedure and the associated raw data describing the occurrences of a given mineral within drill cores. The geological logging includes: the samples selected for analytical measurement of the mineral contents (double-highlighted areas), the interval of occurrence which is the length of a mineral occurrence in a drill core sample and the class which is the indicator value assigned to an interval of a mineral occurrence to describe its prevalence based upon the crystals size and their abundance. Uncoloured areas indicate the absence of the mineral 139

Figure 7.2 Workflow of the methods used to perform a dynamic classification of the host rock based upon the integration of geological logging information, Monte Carlo simulation, 3D geological modeling and the reactive transport modeling. (X denotes a reactive mineral present in the deposit setting, variable A denotes the available measurements of the X mineral weight proportions, and variable B denotes the intervals of occurrence of the mineral X reported throughout the geological logging). 145

Figure 7.3 The Monte Carlo simulation outcome depicted for each pyrite class. a. The simulated and measured datasets of the class 0.1 of pyrite. b. The simulated and measured datasets of the class 0.5 of pyrite. c. The simulated and measured datasets of the class 1 of pyrite. d. The simulated and measured datasets of the class 2 of pyrite. (N_neighbours indicates the number of points neighbouring a given point in the graph) 146

Figure 7.4 Output of the Monte Carlo simulation after cancelling the normalisation along with the measured values depicted by class. (e.g., 0.1_Cal: measured values of calcite pertaining to the class 0.1, 0.1_Cal_G: generated data via simulation for the class 0.1 of calcite). 147

Figure 7.5 The calcite numerical geo-model. a. The core casing of the calcite geo-model including values higher than 1 % along with the calcite block model in the background. b. The calcite block model along the expected plane of mining 148

Figure 7.6 The pyrite and albite numerical geo-models. a. The core casing of the pyrite geo-model including values higher than 4.5 % along with the pyrite block model in the background. b. The pyrite block model along the expected plane of mining. c. The core casing of the albite geo-model including values higher than 10 % along with the albite block model in the background. d. The albite block model along the expected plane of mining 149

Figure 7.7 The resulting pH under oxidizing conditions, after 15 days, 60 days, 180 days and 360 days, using reactive transport modeling for each voxel 152

Figure 8.1 TMSim conceptual model updated from Beier (2015) 168

Figure 8.2 A validation scenario of deposition of 30,000 m^3 of tailings of medium density using multispigot discharge along with 100,000 m^3 of water 169

Figure 8.3 Disposal validation scenario of tailings. a. deposition of 5,000 m^3 of low-density tailings. b. Deposition of 30,000 m^3 of high-density tailings using central discharge. c. deposition of 30,000 m^3 of tailings of medium density using multispigot discharge along with 100,000 m^3 of water 170

LIST OF SYMBOLS AND ABBREVIATIONS

ABA	Acid–base accounting
AMD	Acid mine drainage
AP	Acidic potential
CDF	Cumulative distribution function
CLT	Central limit theorem
CND	Contaminated neutral drainage
CPN	Carbonate neutralization potential
C_{total}	Total inorganic carbon
D_e	Effective diffusion coefficient
DMA	Drainage minier acide
ECDF	Empirical cumulative distribution function
GIS	Geographic information systems
G_s	Specific gravity
ICMM	International Council on Mining and Metals
ICP-AES	Inductively coupled plasma-atomic emission spectrometry
LLN	Law of large numbers
NLLS	The non-linear least squares method
NNP	Net neutralization potential
NP	Neutralization potential
NPV	Net present value
NSERC	Natural Sciences and Engineering Research Council of Canada
PDF	Probability density function
PMF	Probability mass function

$Q_{basal\ seepage}$	Quantity of water seepage at the impoundment base
Q_{beach}	The beach sediments quantity
$Q_{concentrate}$	The concentrate quantity
Q_{COF}	The hydrocyclone overflow quantity
Q_{CUF}	The hydrocyclone underflow quantity
$Q_{dyke\ seepage}$	Quantity of water seepage from dykes
Q_{mill_loss}	Water lost in the mill
Q_{OB_const}	Overburden dedicated to construction
Q_{ore_feed}	Ore quantity
$Q_{process\_water}$	Water used throughout ore processing
Q_{reject}	Material reject from plant intended for waste rock dumps
$Q_{release}$	Water released from tailings after sedimentation and consolidation
Q_{runoff}	The distal sediment quantity
Q_{sed_tails}	Quantity of tailings after sedimentation
Q_{sed_water}	Quantity of water released from sedimentation
Q_{tails}	Dry tailings quantity
Q_{tail_water}	Water pertaining to the tailings stream
Q_{treat_tails}	The thickened tailing quantity
Q_{treat_water}	The amount of the recovered water
RBF	Radial basis function
RMSD	Root mean square deviation
SD	System dynamics
SEM	Scanning electron microscope

S_{Geo}	Geometric surface area
SGeMS	Stanford geostatistical modeling software
Sg_{water}	Water specific gravity
SPRCSP	Soil protection and rehabilitation of contaminated sites policy
S_s	Specific surface area
S_{total}	Total sulfur
TMSim	Tailings management simulation
URSTM	Unité de Recherche et Service en Technologie Minérale
USEPA	United States environmental protection agency
VBA	Visual basic for application
W	Moisture content
WHO	World health organization
XRD	X-ray diffractometer

LIST OF APPENDICES

Appendix A Merging 3D geological modeling and stochastic simulation to foster the waste rock upstream management 193

Appendix B Incorporating Kinetic Modeling in the Development Stages of hard Rock Mine Projects 271

Appendix C Integrating 3D geological modeling and kinetic modeling to alleviate acid mine drainage through upstream mine waste classification 278

CHAPTER 1 INTRODUCTION

1.1 The project framework

Mining and quarrying activities generate overwhelming volumes of solid waste deposited in above-ground containment facilities, which receive up to 90% of the extracted ore (Mudd, 2007; Yilmaz, 2011). Mining companies are increasingly interested in low-grade, high tonnage deposits due to the expanding international demand for metals. The waste rock stream is roughly threefold higher than the ground ore in Australia and the United States, and about 1.5 times higher in Canada (Mudd, 2007). As the stripping ratio (which refers to the amount of waste that must be removed to release a given ore quantity) increases, challenges related to the geotechnical and geochemical stability of waste storage facilities exacerbate. With regard to geotechnical challenges, the International Council on Mining and Metals (ICMM) issued the global industry standard on tailings management in 2020 aiming at zero harm to people and the environment surrounding tailings facilities. One of the main axis of the standard is the integrated knowledge base that underlines the role of the interdisciplinary approach in addressing geotechnical safety issues. Regarding the geochemical aspect, the sparse sulphides in solid waste, previously sequestered in a reducing environment, are inevitably exposed to oxidizing conditions upon mine waste disposal. Atmospheric oxygen and through-flowing water trigger oxidation of sulphides such as pyrite and pyrrhotite, resulting in potentially highly contaminated effluents known as acid mine drainage (AMD). In this respect, United States Environmental Protection Agency (USEPA) ranked water contamination from mining activities as one of the top three ecological-security threats in the world (Dold, 2008). In response, mining societies started to consider environmental issues in their design plans. “Designing for closure” principle has then emerged during the last decades to deal with environmental issues even before production stages (Aubertin *et al.*, 2016). Similarly, upstream mine waste management is another promising concept that proposes introducing preventive practices into mine waste management streams. Benzaazoua *et al.* (2008) used the upstream mine waste management reasoning, suggesting that this type of management allows for better control over potential environmental issues. Upstream mine waste management involves any practice that aims to prevent or alleviate a negative environmental impact from the beginning of the mine cycle.

To face AMD environmental risks, a new research trend reconciles advanced mineralogical characterization as well as textural mineralogy of the solid waste (e.g. degree of liberation), AMD prevention and mine waste management (Brough *et al.*, 2017; Bye, 2011; Chopard, 2017; Elghali *et al.*, 2018; Erguler and Erguler, 2015; Paktunc, 1999; Parbhakar-Fox *et al.*, 2013; Weisener and Weber, 2010). Exhaustive mineralogical characterization of the solid waste bridges mineralogy, previously used exclusively by metallurgists and exploration geologists, and AMD assessment, prevention and management. Undertaking such reconciliation effort relates to the holistic thinking adopted in geometallurgy. This mineralogy-based assessment usually requires the use of time-consuming and cost-intensive techniques. Nevertheless, it can increase the efficiency of mine waste management when used as a screening tool from the very beginning stages of the mine cycle. Likewise, new studies establish geo-environmental protocols consisting of classifying the orebody in geo-environmental domains based on mineralogy and lab tests (Duvernois, 2022; Vermette, 2018). Identifying mine waste with high risk of AMD before mining helps in controlling contamination spread (Brough *et al.*, 2013; Parbhakar-Fox *et al.*, 2011; Vermette, 2018). Such protocols inherit their sequence from the geometallurgical procedures covering the exploration, the prefeasibility and the feasibility stages as they mainly depend on the available samples and their representativeness. The outcomes of such approach relate deposit typology to the geo-environmental behaviour after exposing mine wastes to atmospheric conditions. For example, volcanogenic massive sulphide base-metal deposits are deemed acid generating since the ratio of reactive neutralizing minerals to reactive sulphide minerals is low; moreover, toxic trace elements such as Cu, Zn, Pb and Cd are common to be released in such deposit type. Whereas, orogenic gold deposits mineralogy often hinder acid generation because of higher neutralizing minerals to reactive sulphide minerals ratio, nevertheless arsenic leaching from arsenopyrite is a common concern in orogenic gold deposits (Jamieson, 2011).

As pointed out earlier, integrated approaches were extensively investigated to tackle AMD-related aspects. Nonetheless, modeling disciplines frequently used in mining geology and environmental geochemistry received a very little benefit from the integration concept and the holistic thinking suggested by geometallurgy. Geologists began to establish their geological models since the exploration stages. Likewise, environmental geochemists start their modeling as soon as mine waste material is available. Nevertheless, no cross-disciplinary flow of information and skills

connects them for the sake of a better control over mine solid waste. Consequently, a new bridging approach is needed to establish a nexus between the modeling toolboxes of the geologist and the environmental geochemist to enhance mine waste classification.

1.2 The general problematic

Although numerous scientific contributions advanced the modeling of AMD geochemistry and miscellaneous geometallurgical studies carried out interdisciplinary integration to face AMD-related issues, few studies focused on integrating geological modeling, environmental geochemistry modeling and mine waste management. Besides, slight effort has been directed toward extending the capabilities of geological modeling to geochemical processes. Geostatistics is considered as an efficient tool to provide estimations because drilling could not be performed throughout the entire extent of the deposit owing to its cost and the initial investment constraints. In this regard, new insights are necessary to consolidate the high sense of teamwork and collaboration between the geologist and the environmental geochemist to implement a cross-disciplinary flow of information and skills, thereby, providing the opportunity for the formulation of proactive upstream mine waste management options that could prevent and/or alleviate future environmental liabilities.

1.3 The project novelty

Capabilities of 3D geological modeling have been extensively used to guide exploration and mining operations. The AMD-related disciplines have benefited very little from this modeling tool. Therefore, the main novelty is combining the geochemistry modeling tools and the geology modeling capabilities to create a promising way enhancing mine waste management and assisting decision makers. To the author’s knowledge, this project is the first of its type to suggest upstream management based on cross-disciplinary modeling. Other aspects of novelty may include the use of stochastic simulation in conjunction with 3D geological modeling and the use of kinetic modeling during the development stage.

1.4 The research hypotheses

This project embeds the following hypotheses:

- A 3D geological model of a given contaminant could be established based on the available data from the drilling surveys;
- Geochemical models could be envisioned since the development stage even if actually most geochemical models were performed during the operation and post-closure stages;
- Combining a geochemical model with a spatial model could result in a good risk identification and localization during the development stage.

1.5 Objectives

The general objective of this study is to develop a cross-disciplinary modeling approach that enables dynamic upstream mine waste classification (Figure 1.1).

To reach the general objective three main specific objectives were set up:

- Repurpose 3D geological modeling for mine waste classification based upon the inherent content of a given contaminant in the hosting rock;
- Develop a straightforward kinetic modeling approach that could be applied during the development stage;
- Merge the spatial and kinetic attributes of the aforementioned models into one consolidated model that enables dynamic classification of the hosting rock (upcoming waste rock).

1.6 The dissertation content

This work consists of 9 chapters; four chapters are research articles published or submitted in refereed journals or peer-reviewed conference. The present chapter discussed the general framework and the problematic of integrating multidisciplinary modeling tools. The aimed modeling aspects were succinctly evoked. Besides, linkage to upstream mine waste management was underlined. This chapter also stressed the project novelty, the research hypotheses and the objectives as well as the dissertation organization.

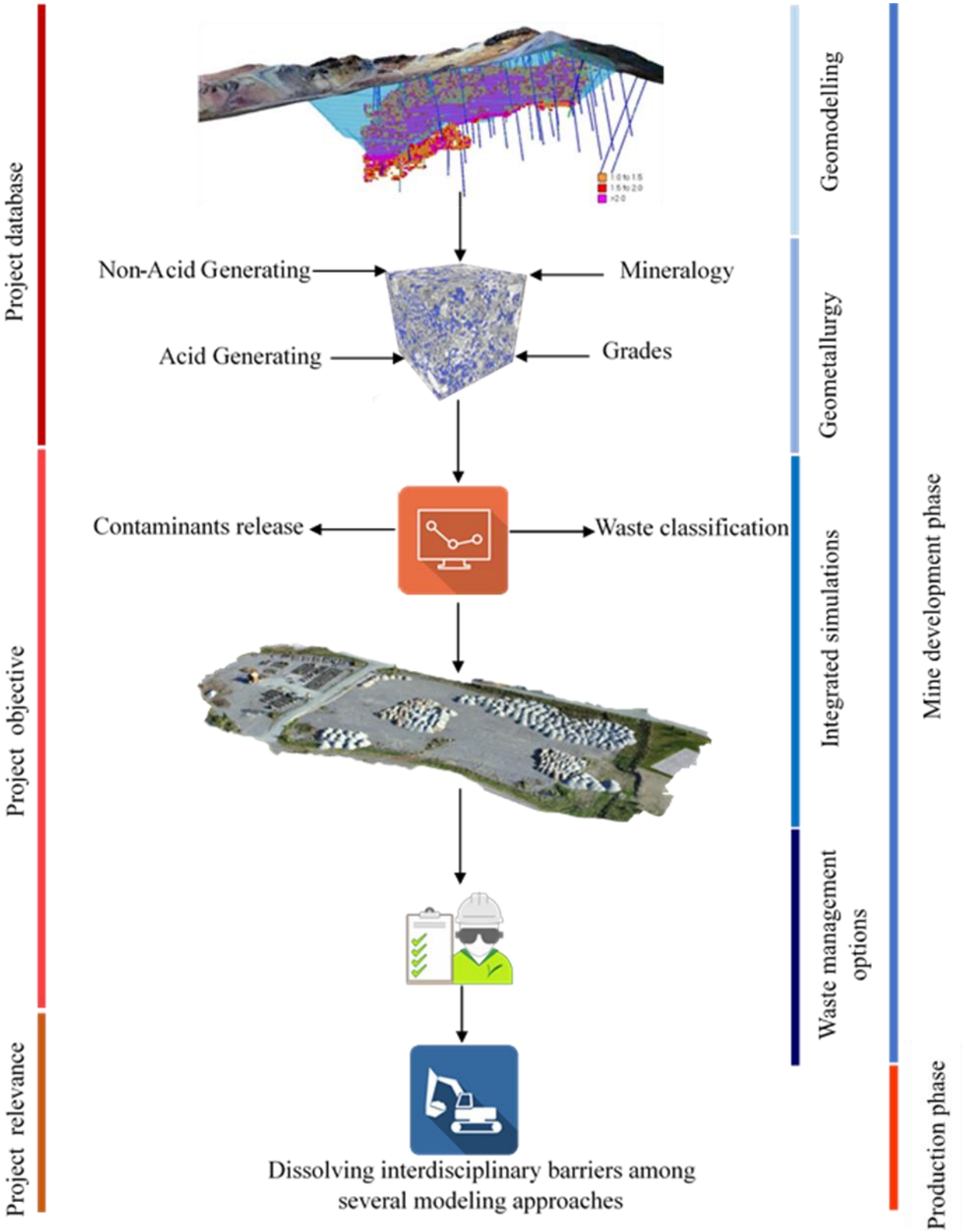


Figure 1.1 Visualization of the project objective

The chapter 2 presents a succinct critical literature review about the main axes of the project including AMD formation, conventional and integrated management approaches, stochastic simulation, geological modeling and reactive transport modeling. The field of application of each modeling approach is revisited to highlight the interdisciplinary barriers existing among the aforementioned disciplines. The main concepts of AMD formation and conventional management approaches are briefly invoked to underline the need for a research integrating management concerns and AMD mitigation before mining. Few researches tackled integrated methods to foster upstream management of mine waste. The chapter 2 ends with final remarks and considerations that guide the methodology of the project.

The chapter 3 portrays the methodology implemented throughout the project. The methodology scheme progressed as the project advanced. Therefore, the final methodological approach is slightly different from its initial version, some refinements and trade-offs were necessary in the course of this work to achieve the objectives.

The chapter 4 is a research article issued in the *Journal of Geochemical Exploration* in 2021. This chapter reconciles the upstream mine waste classification, 3D geological modeling and stochastic simulation. Therefore, it achieves the following specific objective:

- Repurposing 3D geological modeling for mine waste classification based upon the inherent content of a given contaminant in the hosting rock.

The suggested modeling method overcomes the shortcomings of the As grade database, supplied by Éléonore mine site, by coupling a correlation-based stochastic simulation with geological logging database. The 3D geological modeling coupled to the stochastic simulation via the geological logging exhibited interesting outcomes that could improve waste rock classification based upon their metal(loid) content. Through the newly developed method, mine managers could depict metal(loid) grades across the ore and its hosting rock with known margins of error based upon a restricted geochemical database. More importantly, the stochastic simulation is a powerful tool that could be applied to mine waste management to move beyond deterministic methods. Likewise, links between geology and mine waste management should be encouraged to dissolve interdisciplinary barriers and move towards integrated waste management solutions. However, the

suggested method does not include a kinetic component; it only considers the metal(loid) grade in the hosting rock as a proxy guiding the waste rock classification.

The chapter 5 is a research article issued in *Minerals* in 2021. This chapter tackles the kinetic modeling as a separate component to be used throughout the development stage despite the lack of in situ mine waste materials. Only based on the mineralogical characterization of drill core samples collected during the exploration stages, a preliminary prognosis of the pH could be performed using the previously issued kinetic rate laws and assuming highly oxidizing conditions. This article achieves the following specific objective:

- Developing a straightforward kinetic modeling approach that could be applied during the development stage.

Kinetic modeling using PHREEQC (Parkhurst and Appelo, 2013) was used to simulate weathering cell tests. This test provides highly oxidizing conditions and could be performed on 67 g of solid media. Hence, the test operating conditions foster kinetically controlled reactions mainly dependent on the minerals reactivity and their available surface for reaction. This test is a reliable tool frequently used for environmental scoping surveys during the development stage. The kinetic model was intended to simulate the pH released throughout the weathering cell test duration. The main controlling factors included in the model are the mineral rate laws, the chemical elements diffusion from the grain surfaces to the through-flowing water and chemical elements advection. After simulating the pH and benchmarking the model, a parametric analysis was undertaken to explore the effect of slow-reacting neutralizing minerals on the pH evolution. The results underlined the neutralization time lag needed for slow-reacting neutralizers to buffer the pH. Performing such parametric analysis during the development stage yields a preliminary assessment of the possible scenarios of AMD generation. However, this research article does not include a spatial component; it only considers the time-dependent evolution of the pH based on the mineral reactivity issued in the literature.

The chapter 6 is a conference article issued in *Tailings and Mine waste Proceedings* in 2021. This conference paper revisits the aforementioned approaches and initiates the concept of integrating geological modeling and kinetic modeling for a better upstream mine waste classification. The

content of the article triggers the integration thinking and its intended outcomes. The following objective was announced during the conference:

- Merging the spatial and kinetic attributes of the aforementioned models in one consolidated model that enables dynamic classification of the hosting rock.

The chapter 7 is a research article published in the journal of *Environmental Pollution* in 2022. This article addresses the general orientation of the project and fulfills the aforementioned specific objective.

The 3D geological modeling, the stochastic simulation and geological logging were used to represent the ante-mining 3D spatial distribution of pyrite, albite and calcite considered as the main acid-generating and acid-neutralizing minerals in a given case study. Along the main mining plan, a block model was produced for each mineral spatial model. The kinetic modeling approach was implemented using PHREEQC combined to VS2DRTI (Hsieh *et al.,* 2000) to consider variably saturated conditions, assuming highly oxidizing conditions. The 1D reactive modeling simulated a 1D column for each elementary component of the block model along the specified plan. Subsequently, the simulated pH for different periods was assigned to its respective voxel. The results consist of a spatiotemporal visualization of the pH circumscribing geo-environmental domains, thereby providing the opportunity for the formulation of proactive options for upstream mine waste management that could prevent future environmental liabilities.

The chapter 8 is a general discussion that begins with the advantages of the approaches developed throughout the project followed by the main limitations. An emphasis on other integration possibilities is presented to provide future research horizons that should be tackled to achieve a higher stage of integration.

Finally, the chapter 9 consists of concluding statements and recommendations.

1.7 The project sequence

To elaborate this project several steps were carried out. The following introduces these steps and yields an overview on the technical detail of each step.

The first step was to provide a critical literature review including the main axes of the project. The objective was to document the AMD-related research and explore the state of the art in hard rock

mines management methods. Subsequently, the focus was redirected to AMD modeling research to grasp the framework of the application of these models; why, when and how the geochemists establish these models? During this step, it was noticed that most AMD modeling case studies were performed during operation and post-closure stages. Accordingly, the following question emerged: why AMD modeling is not used before mining? The answer was that the programs being used to simulate water quality are data-intensive and case-specific. Furthermore, the AMD models frequently rely on laboratory and/or in situ rate laws of oxidation measured by the geochemists to take into consideration the solid waste reality in their models. Consequently, AMD geochemical models devoid of a high stage of complexity are not relevant for water quality prediction since real life AMD formation is an intricate system. Because stages before mining are data-restricted, the AMD models are not complex enough and therefore not relevant. Nonetheless, if we shift the objective from water quality prediction to preliminary scoping surveys and initial upstream risk identification there will be an opportunity to carry out geochemical modeling based upon minimal data and lower degree of complexity. Weathering cell test is the best experimental example of a geochemical tool for preliminary scoping surveys; such surveys should also include the modeling axis. However, a straightforward model of the mineral kinetics occurring in weathering cell test is insufficient as novelty.

At this stage, the concept of interdisciplinary integration emerges and it was borrowed from the geometallurgical thinking. The integration thinking was previously used by Vermette (2018) who established a staged experimental protocol merging environmental and geological information. The modeling approaches integration was not addressed by Vermette (2018), however; his work was the key knowledge to clearly define the scope of the present project. Benzaazoua *et al.* (2008) was also a key article as it discussed the relevance of upstream and integrated approaches. The following sentence stated by Benzaazoua *et al.* (2008) contributed to define the aim.

> *«For more general cases, an upstream mine waste management program that aims at reducing the downstream environmental costs corresponds well to the old saying: ‘‘prevention better than cure” (or to the principle of ‘‘designing for closure” often invoked in the mining industry).»*

Combining the straightforward geochemical model to other modeling methods that could be performed before mining was the original insight that could increase the model relevance.

Subsequently, the second step of the literature review was to explore several modeling methods including geological modeling, dynamic modeling and stochastic simulation and further learn about reactive transport modeling to find a nexus among these methods leading to a clear outcome.

Afterwards, an opportunity of a Mitacs training was offered to the author by the Éléonore mine. The training topic complied with the PhD project; the environment department in Éléonore desired to establish links with the geology department to define underground sectors containing high As grades in the orebody. Because the two departments speak different technical languages, the flow of information was lacking, thereby, halting agreement and understanding even after many meetings. Consequently, the presence of a mediator with geological background and environmental knowledge was necessary to use the available geological information for a better control of the As problematic. After realizing that the As spatial distribution is not lithology-dependent, the first original idea relied on using 3D geological modeling to depict the spatial distribution of As throughout the orebody. Geologists are frequently using this spatial modeling to depict the gold (or any other element of interest) spatial distribution based on drill cores and geostatistic methods. The geologists use these spatial geomodels for exploration purposes and the mining engineers used them to establish their mining schedule. Repurposing 3D geological modeling for contaminant visualization could become a good practice that supports proactive management of mine waste. However, such geostatistical approaches require large numerical datasets to ascertain high interpolation quality. Frequently, the available numerical data of contaminants are restricted because these elements are not of interest and do not undergo exhaustive chemical analyses. Without adequate data spatial density, 3D geological modeling could not be carried out. Consequently, the second original idea was introduced; it consists of using stochastic simulation to fulfill the requirement of data spatial density.

The stochastic process considers two continuous and independent variables A and B. Thereafter, an auxiliary variable is produced by normalizing the values of A variable by their respective values of B variable. Subsequently, the resulting power law ($y=axb$) exhibits significant correlation in the logarithmic scale and constitutes the objective function of the process. Afterwards, a Monte Carlo simulation is carried out based upon correlated random sampling of the probability density functions (PDFs) of the auxiliary variable and B variable. The PDF of the B variable is defined relying on its comprehensive sample size while the parameters of the auxiliary variable PDF are

iteratively updated until attaining a power law parameters as similar as possible to the objective function. This Monte Carlo simulation allowed the generation of a linear-shaped scatter with a large number of points. A Gaussian distribution centred on the correlation coefficient controls the scatter dispersion. The definition of the correlation as a stochastic parameter rather than a static value allows for the epistemic uncertainty approximation. Finally, the user selects the desired values of the B variable along with their respective values of the auxiliary variable and cancels the normalization to obtain the newly generated data of A variable.

Using the aforementioned stochastic process, sufficient numerical data was generated. Thereafter, variography analysis was performed using SGeMS and numerical implicit modeling was performed using Leapfrog Geo. The established 3D model of As was overlaid on the mine plan to circumscribe sectors with high to extreme As grade. These sectors could be defined and classified before mining them, thereby, fostering the upstream mine waste management.

Although the 3D geoenvironmental model supports mine waste classification before mining, it only considers the contaminant content in the host rock; it is static. Therefore, the next step was to establish a kinetic model enabling the pH simulation using a public domain software. The kinetic model is based upon minimal characterization data of drill core samples and could be used during upstream stages. The model reports the resulting pH from surface controlled reactions mainly involving oxidation and neutralization. Unsaturated flow modeling was added later to the kinetic model to enable simulations of larger-scale systems. In this respect, the 3D geoenvironmental modeling method was coupled to reactive transport modeling approach to create an integrated spatiotemporal model. This model allows the definition of geoenvironmental domains based upon the pH and supports dynamic classification of mine waste even before mining. Therefore, the third original idea was the integration of geological modeling, stochastic simulation, kinetic modeling and unsaturated flow modeling to inform dynamic mine waste classification prior and during the mining stages.

CHAPTER 2 LITERATURE REVIEW

This chapter supplements the literature review included in the introduction parts of the research articles. Furthermore, the main modeling background knowledge used in the subsequent chapters is underlined in this chapter.

2.1 Acid mine drainage formation

Mine managers tackle geotechnical issues via thorough design efforts and continuous monitoring measurements. However, in hard rock mines, besides geotechnical challenges, mine managers should meet water quality requirements. AMD is the most common dilemma in hard rock mines, as it fosters contaminants spread. This section supplies an overview on AMD and its main driving reactions.

Acid drainage is observed wherever sulfide minerals are exposed to atmospheric conditions, it occurs in naturally exhumed sulfides as well as in anthropogenic land disturbances (Blowes *et al*., 2003). Acid drainage stemming from mining activities is by far the most deleterious source of acid drainage. Nordstrom *et al*. (2000) reported one of the lowest AMD water qualities with negative pH values as low as -3.6, metal concentration amounted to 200 g/L and sulfate concentration as high as 760 g/L. Unlike the naturally exhumed ore, mining involves crushing and milling, thus the ore grain size is reduced to reach a typical range for optimal processing. Blowes *et al*. (2003) issued particle size ranging from 25 μm to 1 mm, Bussière (2007) reported a grain size as fine as silty material (2 to 80 μm). In both cases, the available grain surface of milling wastes is sharply increased, this explains to some extent the magnitude of acid drainage in mining framework.

AMD formation is a chemical process that involves miscellaneous chemical reactions; sulfides oxidation, acid neutralization and secondary minerals precipitation. The ore mineralogical assemblage is noticeably correlated to water quality, since mineralogy controls the nature of oxidation and neutralization reactions that could occur. Water and oxidant availability are also deemed as prerequisite to trigger sulfides oxidation (Akcil and Koldas, 2006; Evangelou and Zhang, 1995). Pyrite is frequently used to express oxidation reactions, note, however, that not all sulphides behave like pyrite. For the sake of clarity, this document lists chemical reactions with regard to pyrite oxidation since it is considered as the most abundant sulphide mineral in the metalliferous ore deposits as well as in coal deposits (Blowes *et al*., 2003; Bouzahzah *et al*., 2014;

Nordstrom *et al*., 2000). The oxidation of 1 mole of pyrite produces two moles of SO_4^{2-}, one mole of Fe^{2+} and two moles of H^+. The released Fe^{2+} is oxidized to Fe^{3+} consuming one mole of H^+, however, at slightly high pH, Fe^{3+} solubility drops to form iron hydroxides yielding 3 moles of H^+, the corresponding overall reaction is described as follows (Blowes *et al*., 2003; Nordstrom, 1982) :

$$FeS_2(s) + \frac{15}{4}O_2(aq) + \frac{7}{2}H_2O(aq) \longrightarrow 2SO_4^{2-}(aq) + Fe(OH)_3(s) + 4H^+(aq) \qquad 2.1$$

Equation 2.1 known as direct oxidation of pyrite shifts the pH to values as low as 4.5, high H^+ activity results in a shielding effect strengthening around Fe^{3+} atoms, and this increases the iron solubility. As Fe^{3+} becomes more available in the aqueous solution, it acts as oxidizing agent. Furthermore, it is widely accepted that Fe^{3+} oxidizes pyrite more rapidly than O_2 (Blowes *et al.*, 2003; Evangelou and Zhang, 1995). One could ask the following question regarding pyrite oxidation by Fe^{3+}: why pyrite oxidation is fostered and further accelerated when Fe^{3+} ions are available? Based on electronegativity concept, O atom is ranked second on Pauling's scale. This suggests that O atoms accept electrons much more easily than Fe atoms. However, electronegativity-based reasoning leads to erroneous insights as it speculates that O_2 should oxidize pyrite more rapidly than any other oxidizing agent should. Since electronegativity-based reasoning does not answer the previous asked question, one could adopt activation energy-based reasoning and speculate that electron transfer between pyrite and Fe^{3+} is favored through lower activation energy. Nonetheless, Wiersma and Rimstidt (1984) issued that pyrite oxidation by the aqueous ferric ion, over a temperature range of 25 to 50°C, requires an activation energy of 95 kJ/mol. McKibben and Barnes (1986) stated that pyrite oxidation by dissolved oxygen, over a temperature range of 20 to 30°C, requires an activation energy of 56.9 kJ/mol. Regardless of the crystalline structure effect on the activation energy, Blowes *et al.* (2003) related the activation energy to the pH and stated that H^+ high activity reduces the activation energy. Once again, the activation energy-based reasoning does not fully match the answer. Luther III (1987) linked the higher oxidation rate of pyrite by Fe^{3+} to orbital theory; the positively charged iron ions bond to pyrite surface more rapidly and interact with the partially-negatively charged sulfur. Thus, electrons transfer is enhanced when Fe^{3+} is involved in the pyrite oxidation. This oxidation known as indirect oxidation results in lower pH values as compared to the direct oxidation, because all oxygen atoms

of the sulfate species are released from water rather than oxygen molecules. The indirect oxidation reaction is expressed as follows (Evangelou and Zhang, 1995):

$$FeS_2 + 7Fe_2(SO_4)_3 + 8H_2O \longrightarrow 15FeSO_4 + 8H_2SO_4 \qquad 2.2$$

Although oxygen molecules initiate pyrite oxidation at circumneutral pH, Fe^{3+} ions are an effective oxidant by dint of pyrite magnetic properties (Moses *et al.*, 1987). Thus, the oxygen role consists of maintaining the process through Fe^{2+} oxidation (Evangelou, 1995; Singer and Stumm ,1970).

Biotic processes foster indirect pyrite oxidation through maintaining high rate of Fe^{2+} oxidation (Kleinmann *et al.*, 1981). Likewise, some chemical processes in abiotic framework could maintain a high rate of Fe^{2+} oxidation; Asghar and Kanehiro (1981) issued that 95% of 100 ppm of ferrous sulfate was oxidized to ferric within a day when added to a soil sample of pH 4.4 containing 3.04% of manganese oxide content. Evangelou (1995) emphasized the occurrence of sulfide oxidation under abiotic and anoxic conditions by means of transitional metal oxides; in case of manganese oxide, he suggested two possible mechanisms driven by the following reactions:

$$MnO_2 + 4H^+ + 2Fe^{2+} \longrightarrow Mn^{2+} + 2H_2O + 2Fe^{3+} \qquad 2.3$$

$$4MnO_2 + 8H^+ + 0.5FeS_2 \longrightarrow 4Mn^{2+} + SO_4 + 0.5Fe^{2+} + 4H_2O \qquad 2.4$$

As pointed out, the oxidation rate of pyrite is dependent on miscellaneous factors such the oxidant, pH, crystallography, etc. However, one could ask why under atmospheric conditions the pyrite is unstable and prefers to be disintegrated into other products. Regardless of the pyrite genesis process, once exposed to atmospheric conditions its oxidation is triggered. With regard to thermodynamic concepts, pyrite oxidation is spontaneous under isobaric conditions. Spontaneous reactions, also named exergonic reactions, imply negative change of Gibbs free energy. In terms of pyrite oxidation, the reaction is exothermic and entails a positive change in entropy since it increases the microstates of the system. These features result in a negative change of Gibbs free energy making the reaction spontaneous at all temperature ranges. Evangelou (1995) pointed out that pyrite exposed to atmospheric conditions exhibits a change of Gibbs free energy of -1200 kJ/mol. Nonetheless, the reader should notice that the magnitude of the change in Gibbs free energy does not reflect the rate at which the oxidation occurs, because spontaneity is not related to kinetics

or reaction rate. A classic example is the exergonic process of carbon in the form of a diamond turning into graphite. This reaction is very slow that it is not noticeable on the human timescale.

In terms of pyrite oxidation kinetics, Blowes *et al.* (2003) reported in his review miscellaneous rate expressions that involves either dissolved oxygen or dissolved iron in their formula. Nonetheless, dissolved oxygen and ferric ions could act simultaneously to oxidize pyrite because pyrite oxidation is a surface-controlled process. Evangelou (1995) suggested a reaction rate based on both oxidation pathways and included the surface area available for oxidation:

$$-\frac{d[FeS_2]}{dt} = [k_1(O_2)^{\nu_1} + k_2(Fe^{3+})^{\nu_2}]\,(S) \qquad 2.5$$

k_i denotes rate constants, ν_1 and ν_2 refer to reaction order with respect to O_2 and Fe^{3+} respectively, (O_2) is the partial pressure of oxygen, (Fe^{3+}) is the concentration of ferric ions and S denotes the surface area available for oxidation. As the pH controls the iron hydroxide solubility, the equation 2.5 is further developed as follows (Evangelou, 1995):

$$-\frac{d[FeS_2]}{dt} = \left[k_1(O_2)^{\nu_1} + k_2\left(K_{sp}/(OH^-)^3\right)^{\nu_2}\right](S) \qquad 2.6$$

K_{sp} denotes the solubility product constant. The equation 2.6 describes pyrite oxidation rate in abiotic conditions, it indicates that a decreasing pH results in higher oxidation rate. The iron hydroxide precipitation hinders free ferric ions adsorption on pyrite surface thereby reduces pyrite oxidation rate. Then one could expect low oxidation rate as iron hydroxide solubility drops, when the pH values shifts from 3.5 to circumneutral and neutral pH. However, Nicholson and Scharer (1994) reported that the oxidation rate at pH=6 has been found to be as much as twice the rate at pH=2 when temperature is slightly increased (at 33°C). Nicholson and Scharer (1994) findings are in line with Singer and Stumm (1970) results who found high oxidation rates at neutral pH under atmospheric conditions. Their findings supported observations related to accelerated oxidation of pyrite in the presence of limestone (Evangelou, 1995). Singer and Stumm (1970) explained this fact based on the rate-determining step of oxidation; at pH lower than 3.5 the oxidation of $Fe^{2+}$to Fe^{3+} is closely dependent on Fe^{2+} concentration and O_2 partial pressure, whereas at greater pH values, the Fe^{2+} oxidation is second order with respect to OH^-activity. Thus, OH^- ions foster Fe^{2+}oxidation, this would increase pyrite oxidation rate by Fe^{3+}as long as iron hydroxide are not precipitated and/or the formed iron hydroxide is not stable enough. No single model can describe

pyrite oxidation kinetics because of the tremendous controlling factors such as particle size, crystallinity, crystal imperfections, impurities, ionic strength, type of oxidant, mineralogical associations etc. The choice of a particular rate should be based on the scope while being cognizant of the rate limitations.

The sulfides-bearing minerals could be hosted in non-sulfide gangue minerals, reactive enough to buffer the generated acidity completely or partially. The acid-consuming minerals refer to the neutralizing minerals that trigger the neutralization mechanisms. The neutralization potential was extensively assessed by means of chemical and mineralogical approaches (Blowes *et al.*, 2003; Bouzahzah, 2013; Jambor *et al.*, 2003; Lawrence and Scheske, 1997; Paktunc, 1999; Plante *et al.*, 2012; Skousen *et al.*, 1997; Sobek, 1978). Carbonate minerals are the most effective neutralizing minerals because of their high dissolution rate. The most common carbonate minerals are calcite, dolomite, ankerite and siderite (Blowes *et al.*, 2003). One mole of pure calcite buffers two moles of acid at low pH values as follows:

$$CaCO_3 + 2H^+ \longrightarrow Ca^{2+} + H_2CO_3 \qquad 2.7$$

Dolomite is also an important acid-consuming mineral:

$$CaMg(CO_3)_2 + 2H^+ \longrightarrow Ca^{2+} + Mg^{2+} + 2HCO_3^- \qquad 2.8$$

If sufficient amount of the carbonate minerals is present and available to neutralize the produced acidity, the pore water pH is maintained at neutral values. However, depending on the chemical formula and the impurities embedded in these minerals, several cations could be released to the environment such as: Mn, Fe, Mg, Ca (Blowes *et al.*, 2003). Furthermore, the dissolution rate of carbonates varies depending on mineralogy. Bouzahzah (2013) stated that the dissolution rate of dolomite does not allow the complete release of the neutralization potential within 24-hour span. Moreover, the presence of Fe and/or Mn in the carbonate minerals induces the release of acidity following hydrolysis process and hydroxide mineral precipitation. When neutralization potential related to carbonate minerals is depleted, the Al hydroxide minerals buffer the pH at a range of 4 – 4.5 (Blowes *et al.*, 2003). The pH buffering reactions result in geochemical sequence fostered by the depletion of a given neutralizing mineral.

Strömberg (1997) compiled results that indicated the calcite dissolution rate at ambient temperature and neutral pH values is 10^6 times higher than biotite, anorthite and albite dissolution rate (Bussière

et al., 2005). Albeit silicates dissolution is slow at neutral pH values, pH-buffering capacity of silicates contribute to enhancing water quality at low pH values. Silicates dissolution is undertaken through congruent (equation 2.9) and/or incongruent mechanism (equation 2.10). Incongruent mechanism results in clay minerals formation, which fosters contaminants adsorption and a possible attenuation of the contaminants release.

$$CaAl_2Si_2O_8 + 2H^+ + 6H_2O \longrightarrow Ca^{2+} + 2Al^{3+} + 2H_4SiO_4 + 6OH^- \qquad 2.9$$

$$CaAl_2Si_2O_8 + 2H^+ + 6H_2O \longrightarrow Ca^{2+} + Al_2Si_2O_5(OH)_4 \qquad 2.10$$

AMD propagation is closely controlled by methods used to manage the mine waste facilities. Therefore, AMD and mine waste management constitute a feedback loop of causal relationships. Even though, AMD is a spontaneous geochemical process under subsurface conditions, it could be mitigated through integrated and responsible management procedures. Otherwise, it could be further exacerbated if the management approaches do not include a high sense of environmental responsibility. Therefore, the following subsection describes common mine waste management methods classified into conventional and integrated approaches.

2.2 Overview on mine waste management approaches

Tailings production is amounted to 5 billion tonnes per year worldwide (Lu and Wang, 2012). Upon closure, reclamation costs of an acid-generating tailings impoundment in Canada may raise to more than 250,000 $ per hectare (Aubertin *et al*., 2002). For instance, the reclamation cost of Lorraine mine site in Abitibi-Témiscamingue is amounted to 1.3M$ over 11 hectares in 1999 (Bussière *et al*., 2005).

Geotechnical issues and contaminants release raise serious concerns as they may result in detrimental ecological footprints. Emblematic examples include the spillage of 600 000-700 000 m^3 of caustic bauxite tailings over 40 km^2 in Hungary (Klebercz *et al*., 2012). The Bafokeng platinum tailings storage facility in South Africa crumpled because of above average rainfall, releasing more than 3 million tonnes of tailings during the resulting flowslide (Fourie, 2009), and more recently the Brumadinho dam failure affirms the hazardous risk of the conventional management approaches. Most mines around the world still adopt the conventional management approaches (Edraki *et al.*, 2014) disregarding the overall footprint and optimizing costs at the

expense of the responsible and integrated waste management plans. Aubertin *et al.* (2016) stated that the integrated management approaches and "Designing for closure" concepts are seldom being applied diligently by the industry. Nonetheless, stringent regulation has been proven reliable to streamline stakeholders' interests.

The conventional tailings management approaches consist of pouring low solid content slurry into the tailings impoundment, which is partly (side-hill dyke or closure to existing pit) or fully (complete ring-dyke) surrounded by dykes (Blight, 2009; Bussière, 2007). The slurry is hydraulically transported at solid content of 25% to 45% and discharged via a line discharge or a single-point discharge. The low solid content implies large above ground containment to store the tailings inventory. Hence, some mining frameworks impose constraints related to the available construction material. In some cases, the tailings geochemical and physical features allow dykes construction using coarse-grained tailings and/or the overburden (Beier, 2015; Blight, 2009). Beaching and/or hydrocyclone classification have proven suitable to raise the dyke height progressively. Three configurations are available for the staged dykes: upstream, downstream and centerline (Figure 2.1). The water pore pressure could be decreased using drains and filters to mitigate liquefaction. Despite the mitigation measures, Fourie (2009) reported that the presence of large quantities of stored water is the primary factor contributing to most of the recent tailings storage facility failures. For this reason, Beier (2015) carried out a simulation project to assist mine managers in water balance assessment.

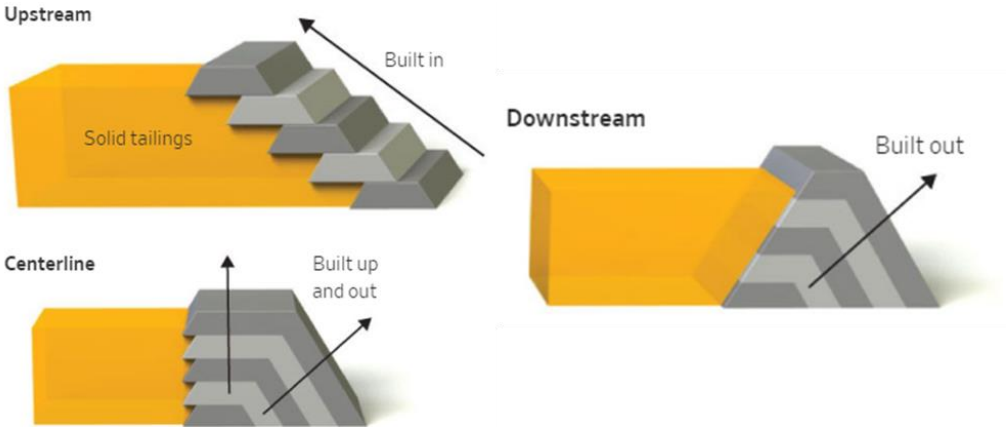


Figure 2.1 The staged construction methods of the tailings-made impoundments (Modified from The Wall Street journal www.wsj.com)

The conventional waste rock disposal methods include the end-dumping and the push-dumping practices. These methods result in a significant gravity sorting and foster physical and chemical heterogeneities (Amos *et al*., 2015). Blight (2009) stated that the end-dumping method entails a loose state that raises infiltration rates. This may cause physical issues such pore water pressure increase and fine-grained particles blowouts. Furthermore, oxygen ingress coupled to the increase of infiltration rate trigger oxidation mechanisms and could cause geochemical issues.

Emerging alternatives for mine waste management is required to enhance physical and geochemical stability. These emerging alternatives raise operational costs and may be considered at the first sight as profitability-reducing approaches. However, with regard to reclamation costs and the failure risk of the disposal areas, these alternatives should be regarded as a promising horizon for mining. For instance, the Hungarian government claimed 179M$ compensation against mine owners when the Baia Mare catastrophe in Romania resulted in the release of 100,000 m^3 of cyanide contaminated liquid into the Lapus Stream (Fourie, 2009). This section is not intended to supply detailed technical reviews. It outlines, however, the benefits of the alternative mine management methods.

Thickening, also termed gravitational sedimentation, is a dewatering technique commonly used in mineral processing and tailings classification. The thickener aims to generate a high solid content tailings, called thickened tailings, and a clear supernatant (Wills and Finch, 2015). The thickening principle relies on gravity sedimentation when the slurry exhibits a large density difference between the solid and the carrier liquid. Essentially, the slurry flows into a large cylindrical tank to settle under gravity force; thereafter the suspended solid is removed by rotating rakes as underflow while the released water is collected at the top of the vessel as overflow (Beier, 2015; Wills and Finch, 2015). There are several types of thickeners; the choice depends upon the desired final solid content. The conventional thickeners increase the solid content range to 50% or up to 70% (Bussière, 2007). With slightly improved geometry and chemical additives, the high rate thickeners yield a solid content range between 70% and 85%. High density and paste thickeners have steeper cone angles and higher sided tanks (Wills and Finch, 2015); this geometry yields higher pressure on the sediment beds and results in a solid content up to 85%.

Besides thickening, filtration is also a common technology to separate solid particles from the pulp via porous medium. The porous screen traps solid particles and supports the “cake”, via a vacuum

or pressure the filtrate passes through the medium (Beier, 2015). This type of filtration is termed "cake filtration" or "dead-end filtration" because the pulp is fed perpendicularly to the filter medium (Beier, 2015; Richardson *et al.*, 2002). Filtration normally follows thickening to achieve high quality dewatering (Wills and Finch, 2015). Filtration is essentially a mechanical process, the filtrate rate decreases as the resistance to flow increases as function of the cake build up (Richardson *et al.*, 2002). Cross flow filtration and tube press are two filtration variants that tackle the negative effects of the cake build up. The filtration process achieves a final solid content greater than 85% (Bussière, 2007). Thickening coupled to filtration technology improve the geotechnical stability and reduce pore water pressure in the tailings impoundment. Furthermore, tailings volumes are could be reduced using this technology allowing safe tailings management. These technologies reduce or eliminate the need for large retaining dykes as well.

The aforementioned technologies focus on geotechnical stability improvements. However, they do not eliminate the geochemical issues and even could foster oxidation mechanisms in some cases. The environmental desulphurization is a promising management approach that focuses on minimizing the quantities of the acid generating tailings by separating the sulphide minerals from the slurry (Leppinen *et al.*, 1997). Thereafter, the resulting fractions are managed accordingly. Bussière *et al* (1994) and Bussière *et al* (1995) performed one of the earliest studies about desulphurization as an integrated management approach. This approach was subsequently investigated and miscellaneous studies carried out desulphurization assessment (Benzaazoua *et al.*, 2008; Benzaazoua *et al.*, 2000; Benzaazoua *et al.*, 1998; Benzaazoua and Kongolo, 2003; Demers *et al.*, 2008; Leppinen *et al.*, 1997). The desulphurization efficiency has been demonstrated at the laboratory scale and at the plant scale as well (Bussière, 2007). The desulphurization increases the net neutralization potential of the treated fraction. Benzaazoua *et al.* (2008) demonstrated that the treated fraction of Doyon tailings was non-acid generating. Furthermore, Demers *et al.* (2008) demonstrated that desulphurized tailings could be used as monolayer cover at the top of the existing tailings in the Doyon impoundment. This laboratory scaled study revealed that the cover made of desulphurized tailings enhanced water quality and limited oxygen increase. With regard to the sulphide concentrate Benzaazoua *et al.* (2008) suggested that it could be used in paste backfill when thorough care is taken to choose the binder and its proportion. On the other hand, Bussière

et al (2004) demonstrated that low sulphides desulphurized tailings could be effectively used in the covers with capillary barrier effects.

In addition to the aforementioned strategies, the co-disposal of tailings and waste rocks exhibits a vigorous alternative to the conventional disposal practices. Waste rocks exhibit low compressibility and high strength but their high permeability favors oxygen ingress and water infiltration. Tailings, on the other hand, display low permeability and high saturation degree but low shear strength and slow self-consolidation process. The co-disposal of the two streams leads to a strength gain with low oxidation risk. Wickland and Wilson (2005) tested mixtures of 5:1 waste rock to tailings by dry mass, they issued that the mixtures have a hydraulic conductivity similar to tailings and total settlement similar to waste rock.

The co-disposal approaches could be carried out as layering as well. The tailings layers introduced within a waste rock dump develop the capillary barrier effect at the interface between tailings and waste rock. This naturally occurring effect could hamper AMD, nonetheless, Bussière (2007) stated that the layering co-disposal alleviates AMD and does not eliminate it completely. The co-disposal strategies include also waste rock deposition within tailings impoundment (Aubertin *et al.*, 2002). This method consists of dividing the impoundment into cells surrounded and underlaid with waste rock, this design enhance pore water drainage and strength gain. This impoundment conception opens a promising horizon to reduce geotechnical issues via favoring drainage. Nonetheless, the design geometry, the particle size and tailings and waste rock thicknesses should be considered to achieve a good agreement between tailings and waste rock hydrogeological properties (Bussière, 2007). Besides, Poirier (2015) and Vermette (2018) mentioned the waste rock segregation into geo-environmental domains to avoid downstream AMD related issues. Finally, Bussière and Guittonny (2020) provided a recent and detailed review of various mine waste management methods and hard rock mine reclamation. The subsequent chapters focus on enhancing the waste rock classification and segregation through an integrated modeling approach.

In conclusion, this axis underlines the emerging management approaches (Figure 2.2) and underscores the necessity of adopting an integrated management approaches in order to overcome failures and contaminants spread. It summarizes the main features of the emerging management approaches and outlines their benefits with regard to geotechnical and geochemical stability. However, it does not supply detailed theoretical and technical background. The aim of this part is

to highlight the existing management insights and to stress the need of practical upstream management methods. Few studies included the upstream reasoning in their mine waste management approaches and more importantly, this section underlines that most approaches are experimental. To the author's knowledge, there is no direct and practical nexus between mine waste management and geological modeling. The following section describes the geological modeling and its related techniques to seek the aforementioned nexus.

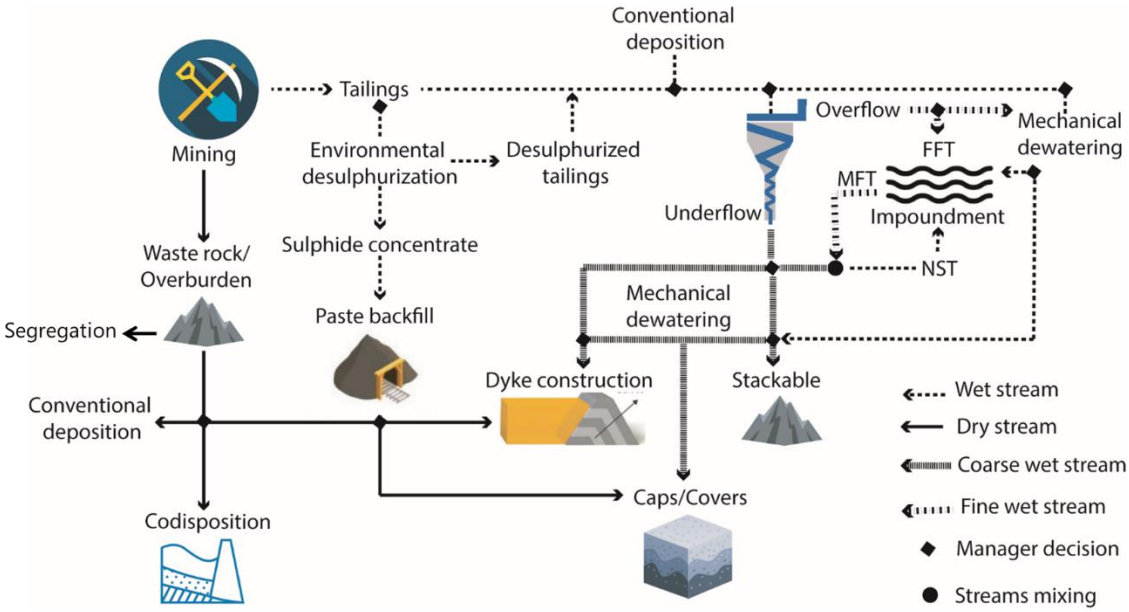


Figure 2.2 Summary of integrated approaches used to overcome the issues related to conventional disposal methods

2.3 Geological modeling

This section is intended to provide theoretical and technical background of geological modeling to determine how this modeling discipline could be repurposed for mine waste management. Generally, the term *model* is defined as a tested hypothesis regarded as the best approximation of reality, mainly based upon the observations and measurements, to solve an engineering problem (Parry *et al.*, 2014). The need of geological models emerged as geo-scientists needed to understand the Earth structure. James Hall, one of the scientists who pioneered structural geology and tectonics, performed the first roughly laboratory scale models to test the hypothesis stating that lateral compression of initially horizontal strata produces folding observed in real-scale geological structures (Ranalli, 2001). From simple physical models to more realistic physical and intricate

numerical models, geological modeling evolved to grasp various types of Earth natural resources. Modeling geology includes three main types (O'Connor, 2015):

- Geological conceptual models: these models aim at understanding the geological history based upon universal geological theories, subjective judgment and the experience of the geologist;
- Process models: the aforementioned James Hall model is an experimental process model. Examples of theoretical process models may include hydrothermal processes related to ore genesis, geological processes controlling ore traps and/or processes identifying ore primary sources. A set of connected process models are usually used to establish the conceptual model of a geological setting;
- Descriptive models: these models are spatial representations of geological surfaces and/or geological volumes known as 2D and/or 3D geological mapping. These descriptive models are extensively established to assist exploration geology and mining. Although they constitute a separate type of geological models, they implicitly incorporate geological information highlighted by the conceptual and process models. Establishing descriptive models is a staged process that evolves along with the geological information flow including subjective and quantitative types of information.

Because descriptive models are involved before and throughout mining stages, linkage to mine waste management could be feasible. Therefore, this section focuses on steps commonly used to establish descriptive models.

2.3.1 Key concepts: from statistics to geostatistics

Data processing using statistics provides quantitative parameters regarding data distribution such as the mean and the standard deviation. Although statistics is relevant for space-independent frameworks, it presents serious shortcomings regarding space-dependent processing. Abzalov (2016b) highlighted these shortcomings through three different spatial patterns presenting the same statistical parameters.

The statistical model does not consider spatial parameters such as spatial continuity and anisotropy (Figure 2.3). Therefore, geostatistics was developed (Krige, 1951; Matheron, 1963, 1965) to merge

statistical and spatial analyses. Applications of geostatistical methods in mining industry include mineral resources estimation (Bargawa and Tobing, 2020; Battalgazy and Madani, 2019; Emery and Maleki, 2019; Guo *et al.*, 2022; Taghvaeenezhad *et al.*, 2020), uncertainty assessment (Abzalov, 2016a; Mery and Marcotte, 2022; Paithankar and Chatterjee, 2018) and optimization of drilling grids (Heriawan *et al.*, 2020; Saikia and Sarkar, 2006; Silva *et al.*, 2019). In the following, the focus is on the key concepts steering spatial interpolation methods used throughout mineral resources estimation to establish descriptive models.

The key concept of geostatistics is considering the spatial distribution of a given variable, such as metal grade, as a random spatial realization Z(x) of the function z(x) which defines the spatial pattern of the considered variable at a point x (Abzalov, 2016b; Matheron, 1963). This concept is referred as regionalised variable (Abzalov, 2016b; Matheron, 1965). For instance, the tridimensional distribution of metal grades within an orebody is one realization that occurred among miscellaneous realizations of the regionalised function. Therefore, geostatistics consists of methods that aimed at defining the characteristics of the function z(x) based upon sparse values of the realizations Z(x) to estimate the values of the regionalised variable in locations lacking samples (Wackernagel, 1996).

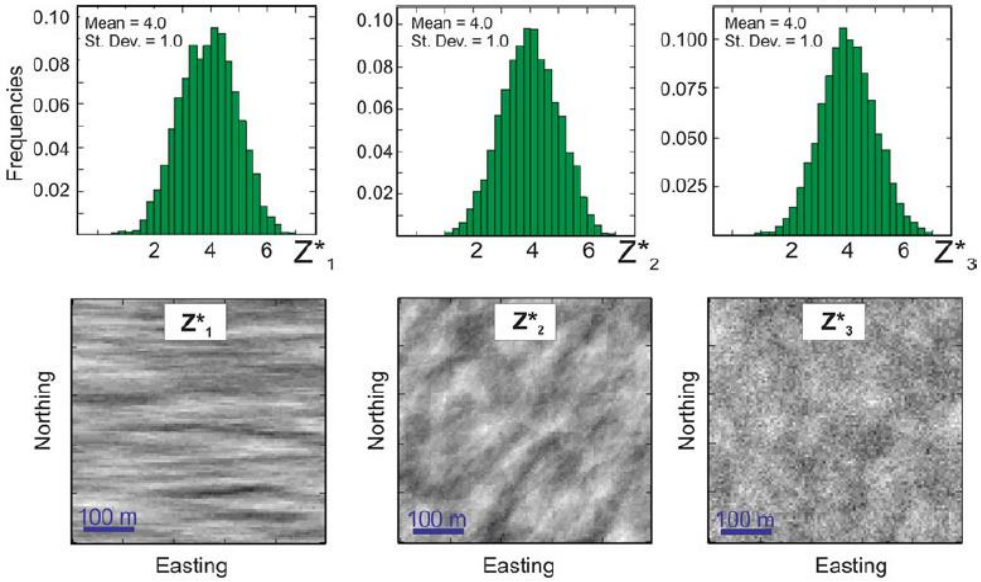


Figure 2.3 Three different spatial patterns presenting the same normal distribution (From Abzalov (2016))

To define the characteristics of the regionalised variable based upon the available experimental data considered as realizations, a second key concept is involved; two measurements z(x) and z(x+h) separated by a small distance h are belonging to realizations Z(x) and Z(x+h) whose distributions have the same first two moments (the mean and the variance) (Abzalov, 2016b; Krige, 1951; Matheron, 1963; Wackernagel, 1996). This hypothesis is known as intrinsic hypothesis or intrinsic stationarity (Haining *et al.*, 2010). Thereby, the space could be classified in multiple subdomains that validate the intrinsic stationarity. The term stationarity means that some properties of the random function are identical along spatial translations. Whereas intrinsic stationarity assumes identical parameters of the random function along small distances. Therefore, within each subdomain a spatial continuity pattern of the regionalised function could be identified and used for interpolation. The subsequent section summarizes computation methods used to define the spatial continuity within a subdomain along with an example of estimation methods.

2.3.2 Spatial continuity

Based upon the intrinsic hypothesis, z(x) and z(x+h) belong to two realizations with the same first two moments, therefore (Haining *et al.*, 2010):

$$\mathrm{E}(\mathrm{Z}(\mathrm{x}) - \mathrm{Z}(\mathrm{x}+\mathrm{h})) = 0 \qquad 2.11$$

$$\mathrm{E}([\mathrm{Z}(\mathrm{x}) - \mathrm{Z}(\mathrm{x}+\mathrm{h})]^2) = \mathrm{Var}(\mathrm{Z}(\mathrm{x}) - \mathrm{Z}(\mathrm{x}+\mathrm{h})) \qquad 2.12$$

$\mathrm{E}()$ is the first moment and $\mathrm{Var}()$ is the second moment. Using the variance addition theorem along with the intrinsic hypothesis the equation 2.12 becomes (Bachmaier and Backes, 2011):

$$\begin{aligned}\mathrm{Var}\big(\mathrm{Z}(\mathrm{x}) - \mathrm{Z}(\mathrm{x}+\mathrm{h})\big) &= \mathrm{Var}\big(\mathrm{Z}(\mathrm{x}+\mathrm{h})\big) + \mathrm{Var}\big(\mathrm{Z}(\mathrm{x})\big) - 2\mathrm{Cov}\big(\mathrm{Z}(\mathrm{x}+\mathrm{h}), \mathrm{Z}(\mathrm{x})\big) \\ &= 2\left(\mathrm{Var}\big(\mathrm{Z}(\mathrm{x})\big) - \mathrm{Cov}\big(\mathrm{Z}(\mathrm{x}+\mathrm{h}), \mathrm{Z}(\mathrm{x})\big)\right) \\ &= 2\gamma(h) \qquad 2.13\end{aligned}$$

$\gamma(\mathrm{h})$ is the variogram that only depends on the distance separating pairs of measurements. $\gamma(\mathrm{h})$ was first defined by Matheron (1963) as the half average squared differences between values

separated by a distance h. In other words, $\gamma(h)$ assesses the spatial autocorrelation exhibited by equidistant measurements. The variogram could be computed for a given distance h as follows:

$$\gamma(h) = \frac{1}{2m(h)} \sum_{i=1}^{m(h)} [z(x) - z(x+h)]^2 \qquad 2.14$$

$m(h)$ is the number of pairs separated by the distance h. If h→0, $\gamma(h)$ →0 because at infinitesimal distances the $\mathrm{Cov}(Z(x+h), Z(x)) \rightarrow \mathrm{Var}(Z(x))$. However, if $\gamma(h)$ does not tend to zero at infinitesimal distances this implies spatial discontinuities named nugget effect (Figure 2.4). Likewise, when h tends to ∞, the $\mathrm{Cov}(Z(x+h), Z(x))$ tends to 0. Accordingly, the obtained value of $\mathrm{Var}(Z(x))$ is called sill (Figure 2.4). When the sill is reached, $Z(x+h)$ and $Z(x)$ do not exhibit any spatial continuity. Values of the variograms calculated before reaching the sill, indicate the extent of the spatial continuity along a specific direction, named range (Figure 2.4) (Bachmaier and Backes, 2011; Wackernagel, 1996). Variograms calculated along a specific direction are called directional variograms and variograms computed for all directions are named omnidirectional variograms (Remy *et al.*, 2009).

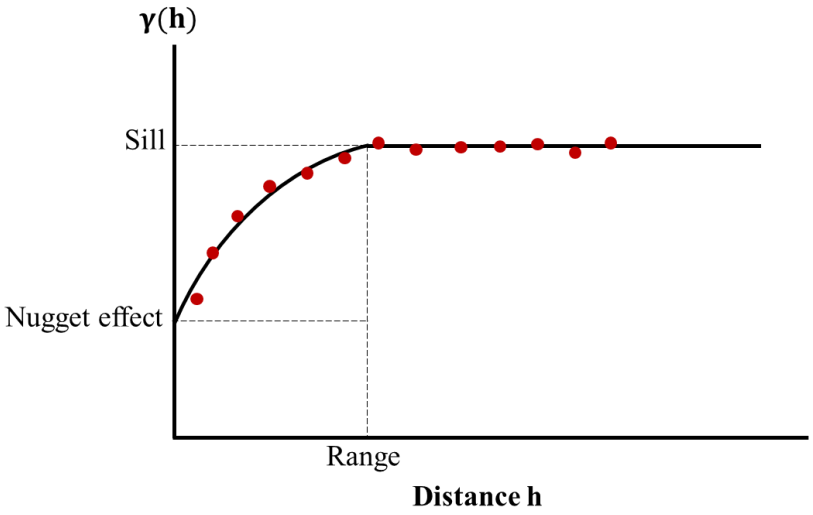


Figure 2.4 An example of experimental variogram fitted to an exponential model.

Most geostatistical methods rely on variogram parameters to perform estimation throughout locations lacking samples. Basic concepts of ordinary kriging are provided herein to exemplify geostatistical methods. Ordinary kriging performs estimation based on the neighbouring numerical

data. Each available numerical datum is associated with a weight to compute the estimation as follows (Abzalov, 2016c; Wackernagel, 1996):

$$z*(x_0) = \sum_{\alpha=1}^{n} \lambda_\alpha \, z(x_\alpha) \quad \text{where} \quad \sum_{\alpha=1}^{n} \lambda_\alpha = 1 \qquad 2.15$$

$z*(x_0)$ is the estimated value at location x_0, $z(x_\alpha)$ is the available numerical value at location x_α, λ_α is the weight of the available numerical value at location x_α, n is the number of the neighbouring numerical data. To determine the weights at locations x_α, the following matrix calculation is undertaken (Abzalov, 2016c; Wackernagel, 1996):

$$\begin{Bmatrix} \gamma(x_1 - x_1) & \cdots & \gamma(x_1 - x_n) & 1 \\ \vdots & \ddots & \vdots & \\ \gamma(x_n - x_1) & \cdots & \gamma(x_n - x_n) & 1 \\ 1 & \cdots & 1 & 0 \end{Bmatrix} \begin{Bmatrix} \boldsymbol{\lambda_1} \\ \vdots \\ \boldsymbol{\lambda_n} \\ \boldsymbol{\mu} \end{Bmatrix} = \begin{Bmatrix} \gamma(x_1 - x_0) \\ \gamma(x_n - x_0) \\ \mathbf{1} \end{Bmatrix} \qquad 2.16$$

The left-hand side of the equation 2.16 denotes values of the variogram computed for each pair of points. The right-hand side of the equation 2.16 denotes values calculated from the variogram model for pairs involving the location x_0.

2.3.3 Practical steps for building spatial models

Throughout exploration and mining stages, two types of spatial models are involved; grid models and solid models, used for surface and volume mapping respectively (Reed, 2007). In most cases,

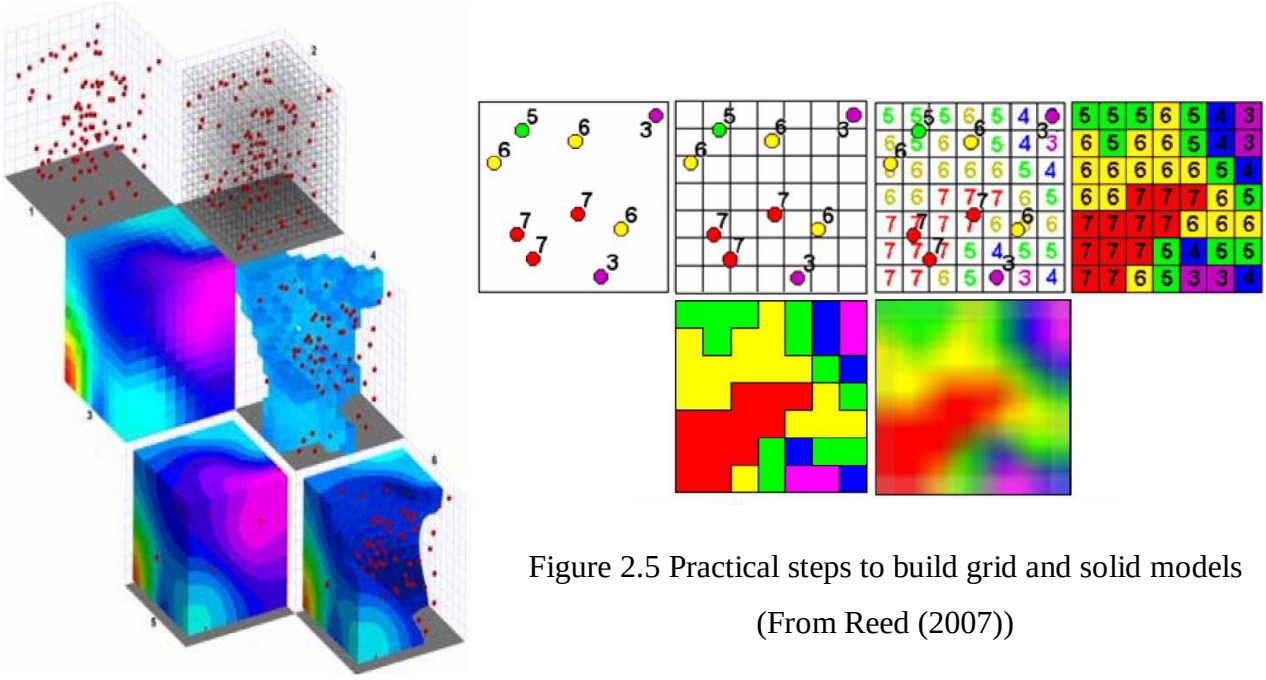


Figure 2.5 Practical steps to build grid and solid models (From Reed (2007))

numerical data are acquired through drilling surveys and subsequent quantitative assays and/or measurements. The first step for both types of spatial models is to project the available numerical data, referred as the control points, in the 2D or 3D space depending on the model objective. Thereafter, an imaginary grid defining the model resolution should be created (Figure 2.5).

The dimension of the grid, called voxel for 3D models, depends on the spatial density of the available dataset (Che and Jia, 2019; Cheng, 2021; Deng *et al.*, 2019; Gao *et al.*, 2019; Jessell, 2001; Wu and Xu, 2004; Zu *et al.*, 2012). As a guideline, Reed (2007) stated that the grid dimension could be set equal to the average minimum distance between the control points. Afterwards, the aforementioned geostatistics concepts and methods are performed to assign an estimation to each grid center node. Most software enable the creation of color-coded maps based upon the control points and the estimated points. Most geographic information systems (GIS) and spatial modeling software inherently embed algorithms that promptly undertake the aforementioned steps, however, the user is responsible for the model assessment and its compliance with geological information collected so far.

Emery and Maleki (2019) used geological modeling to unravel the relationship between the grade and the rock type for a better mineral resources estimation. Wang *et al.* (2015) established a 3D geomodel to guide exploration surveys and perform potential targeting. Carpentier *et al.* (2016) used several realizations of the geological model to schedule mining operations and take into consideration the geological uncertainty. Wang *et al.* (2012) coupled 3D geological modeling and geophysical data to establish the space-time genesis of metallogenic mineral targets. Zhang *et al.* (2018) repurposed 3D geological modeling for geotechnical engineering. Di Maio *et al.* (2020) developed a multidisciplinary approach integrating geological, geotechnical and geophysical models to identify flowslide controlling factors. Thornton *et al.* (2018) linked the bedrock geology and 3D models to grasp the main hydrological controlling factors. Høyer *et al.* (2019) developed a high-resolution 3D geological model of the geological lithology neighbouring a landfill site to grasp the leachate flow and the associated risk. Geological modeling was also applied to petroleum-related studies (e.g., Abdelwahhab *et al.* (2021), Badejo *et al.* (2021), Elatrash *et al.* (2021), Radwan *et al.* (2022)). Furthermore, Fala *et al.* (2013) used geostatistics to model 2D spatial continuity within waste rock piles. Despite the wide spectrum of geological modeling applications, few attempts were directly linked to mine waste management and/or AMD challenges.

Furthermore, geostatistics and geological modeling provide estimations of the numerical values of a variable. Nonetheless, these estimations do not capture the local spatial variability. Therefore, geological models should be coupled to a simulation method that considers uncertainty. The following section describes the most common simulation engine used to tackle uncertainties.

2.4 Monte Carlo simulation

Throughout the subsequent subsections, the Monte Carlo simulation is introduced after defining its main related concepts. Differences between estimation and simulation are underlined, afterwards an overview of basic mathematical concepts related to the theory of probability are presented. Finally, based upon the defined mathematical concepts, the Monte Carlo simulation is elucidated. Applications of Monte Carlo simulation in the mining industry are underlined.

2.4.1 Estimation and simulation

The aforementioned geostatistical concepts yield local estimation of a variable based upon the available data. Dimitrakopoulos (2011) stated that the main downside of the estimation methods is that they are unable to reproduce the regional variability that conforms to the available data initially used to perform the estimation. In other words, the geostatistical estimation methods honor the regional spatial variability, however, a smoothing effect is generated regarding the local spatial variability. Furthermore, the ultimate result of geostatistical methods is a single spatial model used for mining optimization and operation guidance (Dimitrakopoulos, 2011). Unlike the estimation, the simulation generates equiprobable realizations of the spatial model that are conditional to the available data and span a wide range of scenarios constrained to the geological uncertainty (Dimitrakopoulos, 2011; Furtado e Faria *et al.*, 2022; Kamali *et al.*, 2013). Generating equiprobable realizations to propagate uncertainty related to one or more inputs is called a stochastic approach. Unlike static inputs, stochastic inputs are mainly probability functions including all probable static values that the stochastic input could take (Figure 2.6). Dimitrakopoulos (2011) provided quantitative insights regarding the net present value (NPV) of an ore deposit computed with a deterministic estimation method that results in one model and NPV values computed based upon equiprobable realizations. It was demonstrated that the deterministic approach overestimated the NPV of the deposit. Thereby, relying on one model to preform mining optimization presents a

high-risk inherited from the accumulated geological uncertainties. Whereas simulation propagating uncertainties to the outputs generates a wide range of probable realizations. These approaches are mainly based on probability functions, the following subsection underlines basic notions of the probability theory that are used throughout the subsequent chapters; however, it is not intended to provide an advanced and detailed theoretical background.

2.4.2 Probability concepts

The main concepts of probability defined hereafter are recapitulated from the following probability textbooks; Gut (2013), Pinsky and Karlin (2010), Kolmogorov and Bharucha-Reid (2018), Gnedenko and Ushakov (2018). A probability could be intuitively defined as the relative frequency of occurrence of a given outcome when carrying out the experiment many times. Accordingly, the theory of probability relies first on the randomness of the experiment being performed and the stabilization of the relative frequencies after performing these experiments n times. A probability should be defined through the following:

- A sample space Ω that contains all the possible outcomes of the experiment;

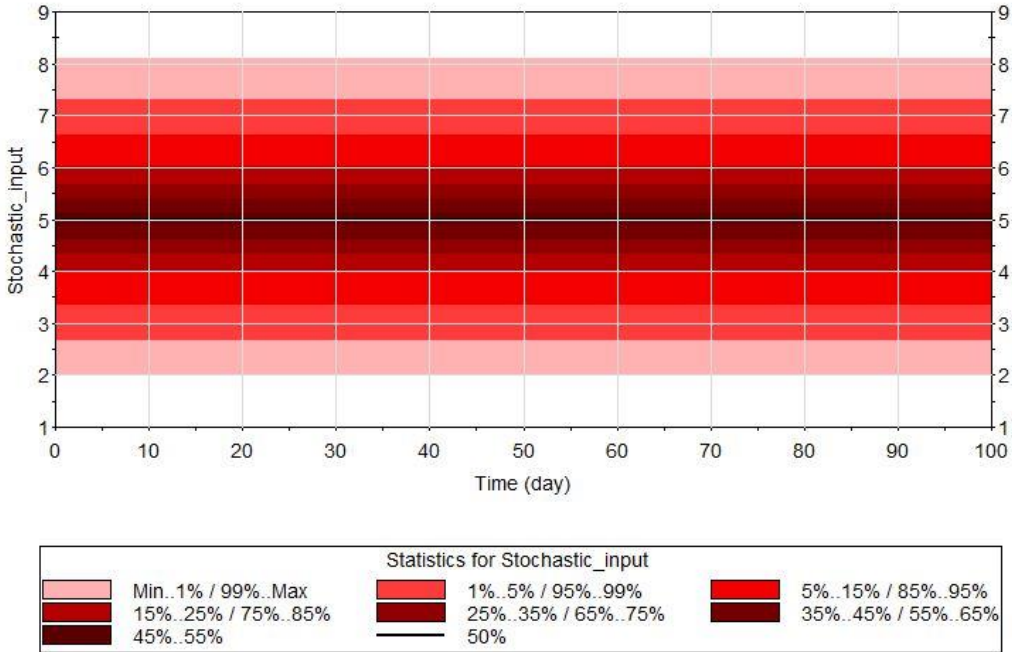


Figure 2.6 Example of a probability function of a stochastic input.

- $\mathcal{F}$ a collection of events measurable in Ω, an event is a subset of Ω including several outcomes of the random experiment;
- P is the probability measure, the relative frequency after performing the random experiment n time (n→ ∞);

Every probability triple (Ω, $\mathcal{F}$, P) should honor the Kolmogorov axioms:

- P(Ω)=1;
- A∈ $\mathcal{F}$: $0 \leq P(A) \leq 1$;
- For disjoint events : P($A_1 \cup A_2 \cup \cdots$) = $\sum_{i=1}^{+\infty} P(A_i)$, disjointed events couldn't occur at the same time;

Within a probability space, it is common to define a random variable, which is generally a function defined in Ω. The variable inherits its randomness from its random events that define the function. A random variable in a probability space should fulfill the following condition:

$$\mathrm{X}^{-1}(\mathrm{x}) = \omega \in \Omega \quad \mathrm{x} \in \mathbb{R} \qquad 2.17$$

X is the random value and x is a possible real value that X could take in the real line $\mathbb{R}$. ω is a portion of the sample space Ω that defines the random process. In other words, each possible real value x of the random variable X should stem from an event or associated events defined previously in the probability space. $\mathrm{X}^{-1}(\mathrm{x})$ is called the inverse image of x that establish the link between the probability space and the real line. For instance, X sums up the outcomes of rolling two dice once, P(X=1) = ∅ because x = 1 has no inverse images in Ω, which includes$\{1, 2, 3, 4, 5, 6\}$.

Given that the random variable X could take many values x depending on the random process to be considered, a cumulative distribution function (CDF) spanning all the possible values along with their cumulative probabilities should be defined for X such that:

$$\mathrm{F_X}(\mathrm{x}) = \mathrm{P}(\mathrm{X} \leq \mathrm{x}) \quad -\infty < \mathrm{x} < +\infty \qquad 2.18$$

$$\mathrm{P}(\mathrm{X} > \mathrm{x}) = 1 - \mathrm{F_X}(\mathrm{x}) \qquad 2.19$$

$$\mathrm{P}(\mathrm{x} < \mathrm{X} \leq \mathrm{y}) = \mathrm{F_X}(\mathrm{y}) - \mathrm{F_X}(\mathrm{x}) \qquad 2.20$$

$$\lim_{\mathrm{x}\to-\infty} \mathrm{F_X}(\mathrm{x}) = 0\,,\ \lim_{\mathrm{x}\to+\infty} \mathrm{F_X}(\mathrm{x}) = 1 \qquad 2.21$$

In this respect, two types of the random variables are defined: discrete random variables and continuous random variables. A discrete variable X implies distinct countable values x_n such that:

$$X: \{x_1, x_2, \dots, x_n\} \qquad 2.22$$

$$P(X=x_i) > 0 \text{ and } \sum_{i=1}^{i=n} P(X = x_i) = 1 \qquad 2.23$$

Unlike the CDF that cumulates the probabilities of X, a function named probability mass function (PMF) represents graphically the probability of the discrete variable X for each value x_i such that:

$$F_X(x) = P(X = x) \quad -\infty < x < +\infty \qquad 2.24$$

A random variable X is called continuous when its outcomes imply a range of the real line $\mathbb{R}$ including uncountable real values. For a continuous random variable X, a probability density function (PDF) is defined as:

$$P(a < X \leq b) = \int_a^b f_X(x)dx \quad -\infty < a < b < +\infty \qquad 2.25$$

Unlike the PMF, the PDF depicts the probability density over a continuous interval of values. Accordingly, the probability is computed through integration over a range of values. The most common PDFs are the normal and log-normal distributions that conform with a wide range of random processes because of the Central Limit Theorem (CLT). The CLT states that the combination of random variables, determined according to independent random processes, results in normally distributed random variable. In most cases, we are interested in a random variable occurring as a result of interaction amongst other parents random variables justifying the wide range of applications of the Gaussian (normal) distribution.

2.4.3 Monte Carlo simulation and applications

Monte Carlo methods belong to an experimental branch of mathematics that aims at generating random realizations using random sampling performed on distribution functions (e.g., PDFs) that define the process variables (Hammersley, 1964; Kalos and Whitlock, 1986; Niederreiter, 1992). Each realization is a simulation describing a possible outcome of the system being studied using the same initial conditions, but with different input values randomly selected from the respective random variable PDF. This random sampling process, named stochastic, results in a large number

of separate, independent and equally likely results (Bonate, 2001; Couto *et al.*, 2013; Cox *et al.*, 2003; Cox and Siebert, 2006; Papadopoulos and Yeung, 2001; Raychaudhuri, 2008).

Monte Carlo simulation is a stochastic process mainly based upon the aforementioned CLT and the Law of Large Numbers (LLN). The LLN states that the sample mean tends to the population mean when the size of the random samples is sufficiently high (Gilks *et al.*, 1995). Figure 2.7 illustrates the stochastic sampling process used to undertake a Monte Carlo simulation to propagate the epistemic uncertainty from the inputs to the degree of saturation. To carry out the process, the porosity and the volumetric water content should be defined as a stochastic input data whose PDFs were determined based upon a large dataset and the CLT. Afterwards, the PDF of the degree of saturation is portrayed using the LLN.

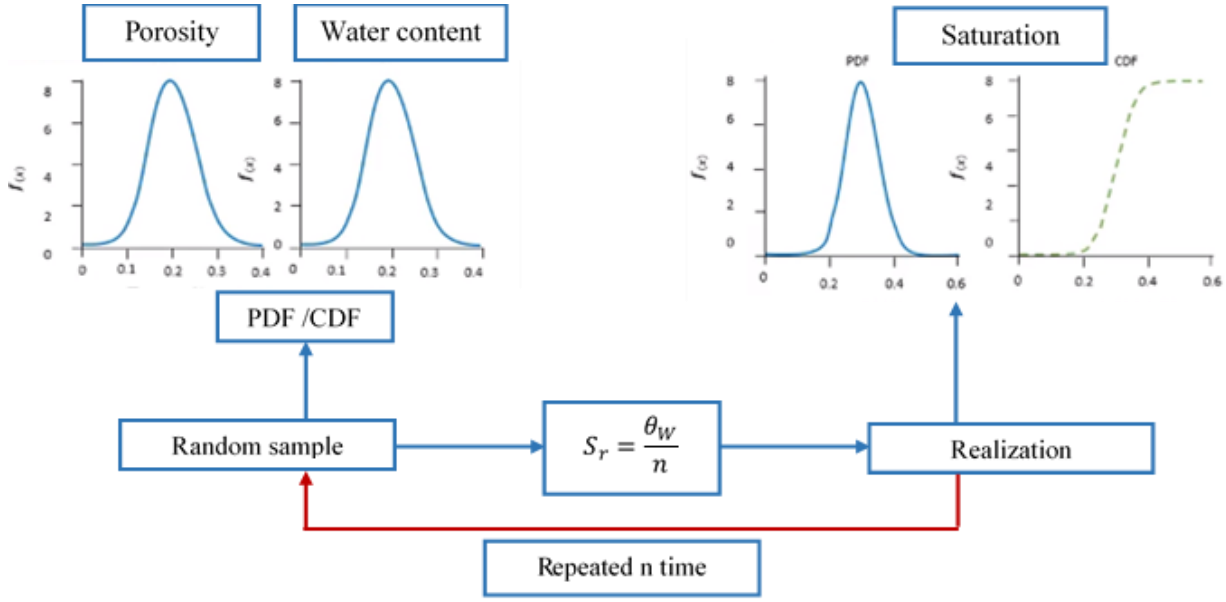


Figure 2.7 Example of the random sampling process used to perform Mont Carlo simulation

The Monte Carlo simulation methods were widely used for mining optimization. Dimitrakopoulos (1998) stated that Monte Carlo techniques provide an efficient tool to consider uncertainty regarding the ore grade variability that directly affects several aspects of open pit design and planning. In this respect, Dimitrakopoulos (1997) suggested the use of stochastic simulations to generate several deposit models that each represents a probable deposit realization. The equally probable realizations of the in situ orebody aimed at moving beyond traditional optimization method and including uncertainties from the upstream modeling stages to define the possible NPV

outcomes (Dimitrakopoulos *et al.*, 2002; Dimitrakopoulos and Sabour, 2007). Thereby, risks associated to the deposit inherent uncertainty could be alleviated and/or mitigated. Moreover, Abdel Sabour and Dimitrakopoulos (2011) suggested incorporating geological uncertainty into the mining design through Monte Carlo techniques. Kumar and Dimitrakopoulos (2021) developed a Monte Carlo simulation algorithm considering the equipment performance uncertainty to enhance the production scheduling. Ugwuegbu (2013) used Monte Carlo simulation to consider metal prices uncertainty. Given the future price fluctuations, Monte Carlo techniques are relevant to evaluate the mining projects and their respective NPV (Lima and Suslick, 2005; Lima and Suslick, 2006; Sohrabi *et al.*, 2021).

Besides, the Monte Carlo simulation is widely used to solve various problems related to a broad range of scopes (Kroese *et al.*, 2014). Specifically, Monte Carlo simulation was used to tackle geology-related problems. For instance, González-Garcia and Jessell (2016) suggested the assessment of the geological uncertainty using Monte Carlo simulation. Pakyuz-Charrier *et al.* (2018b) carried out a Monte Carlo simulation to consider uncertainty related to structural measurements and propagate it to 3D structural modeling. This enabled the establishment of a probabilistic 3D structural model consisting of a range of 3D models. Likewise, Xavier *et al.* (2022) established a probabilistic structural model through integrating uncertainty related to joints and foliation measurements. Furthermore, Pakyuz-Charrier *et al.* (2018a) simulated the uncertainty linked to drill hole locations and orientations to propagate it throughout 3D geological modeling and produce miscellaneous realizations of the geological model. Wang *et al.* (2020) used Monte Carlo simulation to approximate uncertainty related to geological, geochemical and geophysical datasets to enhance the mineral prospectivity mapping.

Up until now, sections of geological modeling and Monte Carlo simulation do not exhibit a direct link to AMD and/or mine waste management. The following section discusses the reactive transport modeling of AMD to further explore studies that may link one of the aforementioned modeling approaches to AMD modeling. Based on the findings, final remarks are provided to guide the project methodology and concretise the research originality.

2.5 Reactive transport modeling

Reactive transport modeling is regarded as a multidisciplinary and multiscale approach that integrates hydrology, geochemistry, soil physics and fluid dynamics to simulate water quality. Therefore, reactive transport models inherit all the difficulties associated with these disciplines along with complexities resulting from the coupling of the processes (Steefel *et al.*, 2005). These models integrate time-discretized mass and heat transport along with surface complexation, liquid-gas partitioning, precipitation reactions and mineral dissolution and numerous biogeochemical reactions (Seigneur *et al.*, 2019; Steefel and Lichtner, 1998). Consequently, most of the reactive transport models are highly data-intensive and require thorough characterization of the system being simulated. This characterization should include microscale and macroscale features. Vriens *et al.* (2020) summarized the main controlling factors related to solid, aqueous and gaseous phases (Figure 2.8), which are usually integrated in reactive transport models to forecast water quality stemming from geological or engineered porous media, undertake sensitivity analyses to investigate the main processes that affect water quality and to assess design or reclamation scenarios.

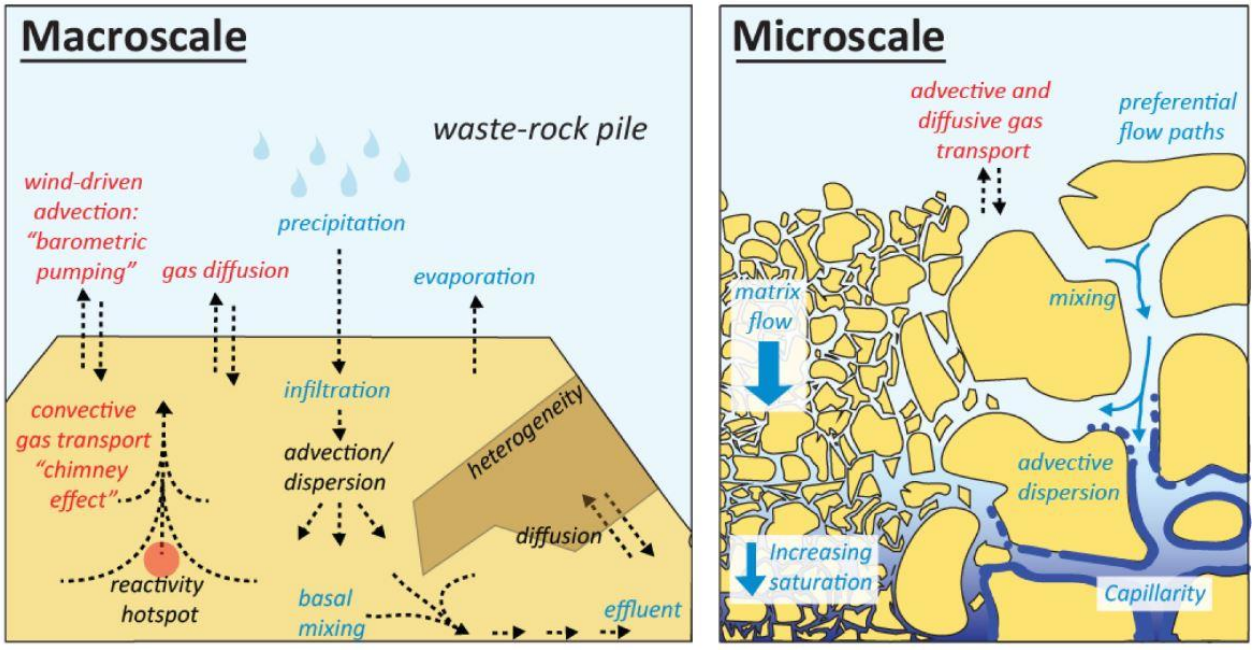


Figure 2.8 Processes included in multiscale reactive transport modeling (Vriens *et al.*, 2020)

Unlike the two aforementioned modeling approaches, geological modeling and Monte Carlo simulation, reactive transport modeling was specifically developed to solve water contamination problems including AMD. In this respect, several programs were established and used as a simulation engine incorporating simultaneously solved formulations of the physical and geochemical processes. For instance, Walter *et al.* (1994) developed the MINTRAN 2D reactive transport model that simulates advective-dispersive transport. Afterwards, Wunderly *et al.* (1996) upgraded MINTRAN through the integration of the sulphide oxidation kinetics. Then, Gerke *et al.* (1998) updated the program by adding the oxygen diffusion and unsaturated flow. Mayer *et al.* (2002) developed the MIN3P program that simulates surface and transport-controlled reaction within multiphase and unsaturated systems. Jurjovec *et al.* (2004) utilized MIN3P to simulate acid neutralization reactions occurring in column tests. Ouangrawa *et al.* (2009) used MIN3P to simulate column experiments AMD prevention through high water saturation. Likewise, Demers *et al.* (2013) performed numerical modeling of contaminated neutral drainage collected from field test cells. Wilson *et al.* (2018) used the reactive transport model MIN3P to simulate leachate quality from humidity cells performed to assess the geochemical behaviour of low-sulphide waste rock. Raymond *et al.* (2020) carried out reactive transport modeling using MIN3P to simulate leachate from laboratory-scale waste rock designed to alleviate AMD by controlling infiltration paths. Kalonji-Kabambi *et al.* (2020) used the MIN3P model to simulate the geochemical behaviour of covered and uncovered highly reactive tailings. Molson *et al.* (2005) coupled HYDRUS program and POLYMIN program to simultaneously simulate AMD flow and reactive transport occurring within 2D conceptual models of waste rock. Parkhurst and Appelo (2013) presented PHREEQC; a geochemical program also utilized to address AMD-related issues (Embile Jr *et al.*, 2019; Kirk Nordstrom, 2020; Muniruzzaman *et al.*, 2020). Lahmira *et al.* (2017) simulated waste rock pile heterogeneity and its effect on AMD. More recently, several research contributions aimed at integrating reactive transport modeling and uncertainty analysis through stochastic processes (Pedretti *et al.*, 2017, 2020). These studies underscored the importance of including such analysis in reactive transport models given the effect of heterogeneities on water quality. For instance, using Monte Carlo simulation Pedretti *et al.* (2017) demonstrated that a waste rock facility encompassing a relatively high neutralization potential could generate low-quality effluents due to spatial mineralogical heterogeneities upon disposal.

2.6 Final remarks

This chapter focuses on:

- AMD drainage formation to highlight the major problematic encountered in hard rock mines;
- Conventional mine waste management to emphasize the need for integrated management approaches that overcome the downsides of the conventional methods;
- Integrated management approaches to introduce the upstream thinking and its worthwhile outcomes regarding environmental risk mitigation and to underline that its application was only introduced in experimental approaches;
- Geological modeling to grasp how geologists model the spatial features of the orebodies;
- Monte Carlo simulation to understand how data analysts simulate and propagate uncertainty;
- Reactive transport modeling to underline modeling methods used by environmental geochemists to assess water quality;

As pointed out, several studies merged geological modeling and Monte Carlo simulation to enhance the ore descriptive models. On the other hand, recent scientific contributions incorporate Monte Carlo simulation in reactive transport models to unravel the effect of the heterogeneous configuration of waste rock piles on water quality. Other studies used geostatistics concepts to model the mineralogical spatial anisotropy within waste rock piles. However, to the author knowledge, these modeling applications are not integrated with the upstream reasoning introduced in mine waste management. Namely, modeling contributions related to AMD consider downstream configurations of the mine waste facilities. Instead of modeling complex heterogeneities within mine waste facilities, it is more convenient to apply an upstream approach to prevent them and classify hazardous mine waste beforehand. Therefore, this literature review highlights the need of upgrading the upstream thinking not only regarding experimental approaches but also in terms of modeling methods. Carrying out upstream modeling throughout the mine cycle will alleviate the modeling complexities through staged and progressive models that describe the environmental attributes of the host rock before mining. Moreover, the integration concept introduced by geometallurgical studies is barely applied when dealing with modeling. Several types of models

are built and interpreted separately. For instance, there is a firm interdisciplinary barrier between geological modeling and reactive transport modeling. Even though, information supplied by geological models, usually established before reactive transport models, could be relevant to mitigate geo-environmental risks. Therefore, this chapter underscores the need for a modeling application integrating 3D geological modeling, Monte Carlo simulation and reactive transport modeling to inform mine waste upstream management.

CHAPTER 3 METHODOLOGY

To fulfill the general objective of the project the following steps were carried out:

- Complete a critical literature review to highlight the main lack of knowledge related to the project scope;
- Learn how the geologist describes the drill cores using the geological logging;
- Learn how to project categorical and numerical geological information into the 3D space using Leapfrog Geo, a specialized spatial software;
- Acquire knowledge related to geological data analysis using geostatistical software;
- Acquire knowledge of 3D implicit modeling to establish spatial numerical models;
- Comprehend how to run a Monte Carlo simulation using specialized software (GoldSim Kossik and Miller, 2004; Rizzo *et al.,* 2006);
- Establish a methodology that merges 3D implicit modeling and Monte Carlo simulation to classify the host rock based upon their contaminants grade (more details are presented in the chapter 4);
- Acquire knowledge related to geochemical assessment of AMD during upstream stages and perform weathering cell testing;
- Grasp kinetics simulation using PHREEQC (Parkhurst and Appelo, 2013) to simulate the main controlling factors of weathering cell test to introduce kinetic modeling during the development stage of a mine cycle (more details are provided in chapter 5);
- Understand how to run unsaturated flow simulation using VS2DRTI software (Hsieh *et al.*, 2000);
- Couple PHREEQC and VS2DRTI to run reactive transport simulations embedding a degree of complexity that complies with the upstream stages;
- Integrating the use of GoldSim (Kossik and Miller, 2004; Rizzo *et al.*, 2006), Leapfrog Geo (Seequent), SGeMS (Remy *et al.*, 2009), PHREEQC and VS2DRTI to preform a dynamic classification of the host rock during the upstream stages based upon the in situ spatial distribution of the main gangue minerals and a space-discretized reactive transport simulations assuming auspicious oxidation conditions (chapter 7);

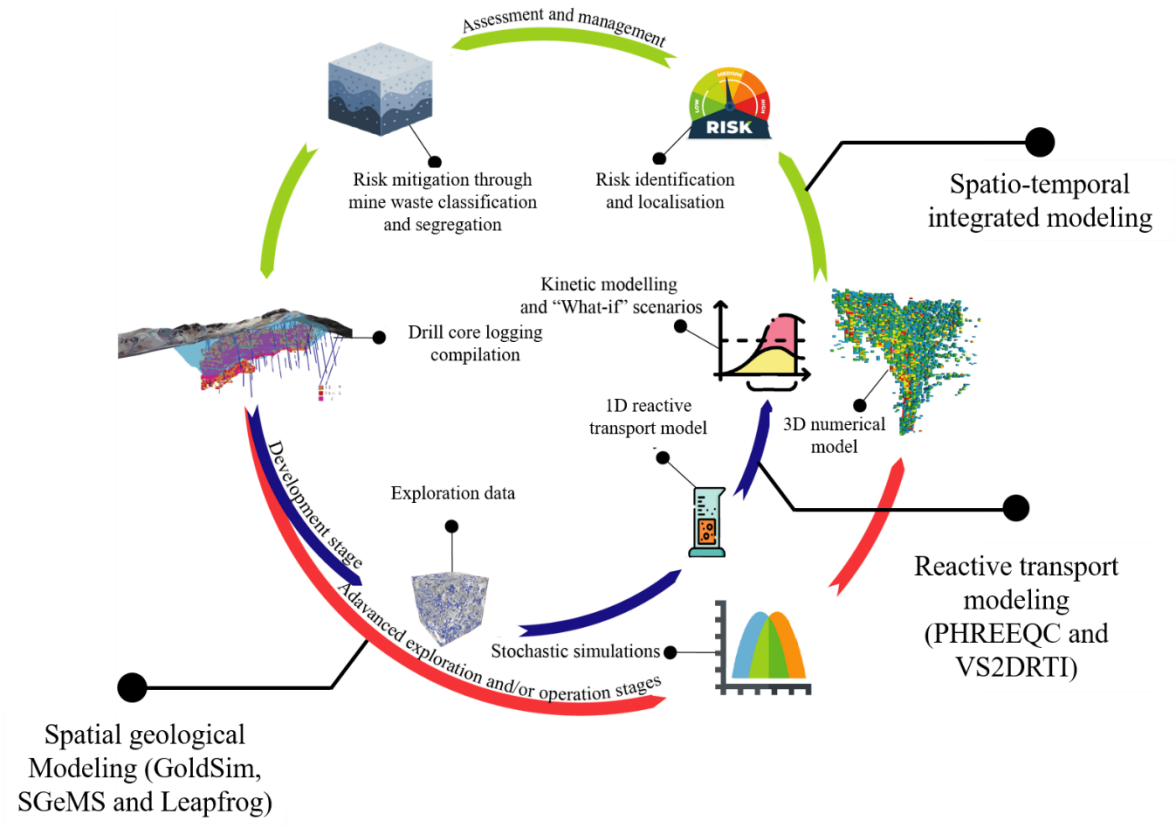


Figure 3.1 The general methodology of integrating multidisciplinary modeling tools to inform upstream mine waste classification

These steps are illustrated in the Figure 3.1. It is a staged modeling protocol that could be applied to any case study as long as it validates a main condition: the availability of drill cores and their geological logging along with the available characterization data including contaminant grades and mineral weight proportions.

In this research, Monte Carlo simulation was used to propagate uncertainty and to infer numerical data with larger sample size. This stochastic process enabled the achievement of the spatial data density requirement, which is essential for high-quality interpolation outcomes. Afterwards, the 3D implicit geological modeling was performed while maintaining the collected geological information as constraints of the model. Finally, a 3D geomodel of a contaminant is produced and benchmarked using the available numerical data. The result enabled mine waste classification beforehand based upon the contaminant grades.

Subsequently, simulation of the oxidation kinetics was suggested to be incorporated in the geochemical assessment protocol during the early stages of a mine project to perform parametric analysis based upon restricted characterization database and the weathering cell test. In this regard, four weathering cells were implemented. Each weathering cell encompasses a sample of geo-environmental domain identified previously by Vermette (2018) for a mine project in the development stage (The Akasaba West project). A geo-environmental domain consists of various proportions of the lithologies recognized through the drilling surveys. The leaching device of a weathering cell test is a Buchner funnel measuring 100 mm in diameter and containing 67 g of sample (dry mass). The sample was positioned upon two nylon membrane filters that were sealed with silica grease along their circumference. These filters inhibit the loss of fine-grained particles that could escape through Buchner holes during the flushes. The silica grease impedes undesirable seepage and allows water retention inside the Buchner funnel. A 250 mL receiving flask was placed under each funnel to recover the leachate. Each sample was flushed with 50 mL of deionized water on the first day, followed by two days of drying conditions. On the fourth day, samples were flushed again with the same volume of the leach solution and exposed to the ambient air throughout the rest of the seven-day leaching cycle. The leachates were recovered after 4 ± 0.5h of retention by applying suction on the filtering flask. The leachates were weighed and analyzed for electrical conductivity, Eh, and pH. The filtrates obtained using a 0.45 µm nylon filter were analyzed for the main dissolved elements. To ensure sample preservation, the filtrates were acidified to 2% HNO_3 prior to ICP-AES chemical analysis. Subsequently, a kinetic model was established to simulate the kinetic reactions occurring in the weathering cells. A weathering cell was used for calibration of the kinetic model while the remaining weathering cells were used for benchmarking.

Mineralogy was the main input of the kinetic model. Therefore, the mineralogical composition was identified using an X-ray diffractometer (XRD; Bruker AXS D8 ADVANCE). The XRD analyses were carried out on dried and micronized samples at room temperature. Bruker AXS equipment as well as EVA and TOPAS software were used throughout the data compilation to produce mineralogical identification and semiquantification based upon the reconciliation with chemical results. The mineralogical quantification was refined using a scanning electron microscope (SEM) equipped with energy dispersive X-ray spectroscopy probe (EDS; HITACHI S-3500N). The

mineralogical identification with SEM-EDS focused on quantifying silicate and sulphide minerals, as they are the main source of neutralization and acid generation, respectively.

Afterwards, the kinetic aspect was coupled to the unsaturated flow aspect using two synchronized public programs; PHREEQC and VS2DRTI. The conceptual model merging kinetic modeling and unsaturated flow modeling is displayed in Figure 3.2. The oxidation and neutralization kinetic reactions were implemented in PHREEQC and the drying/wetting cycles as well as the unsaturated flow were simulated using VS2DRTI.

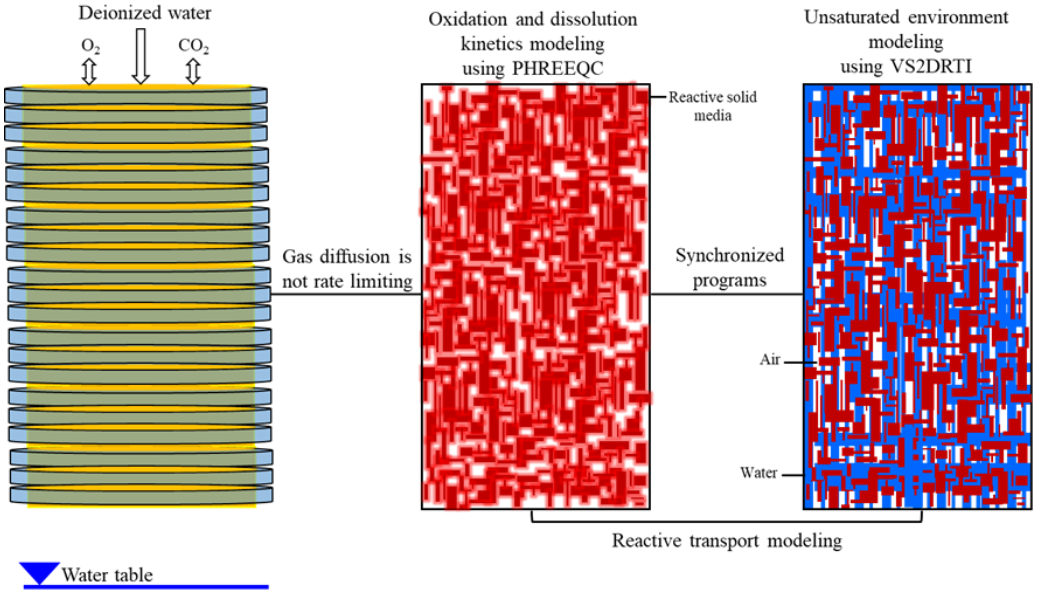


Figure 3.2 The conceptual model of the reactive transport simulation carried out using PHREEQC and VS2DRTI for geochemical simulation that are not O_2 diffusion-limited.

Finally, the realization-based simulations based upon the aforementioned 3D geomodeling approach was used to portray the spatial distribution of the main reactive minerals. A block model was produced for each reactive mineral. The generated block models of the main reactive minerals were overlapped along the plane of interest. Subsequently, the reactive transport modeling was performed for each voxel along the aforementioned plane to simulate the geochemical behaviour of a given voxel, once blasted and excavated. For each voxel a 1D column of 20 m high, containing minerals proportions designated by the block models, was simulated to assign a pH value to the given voxel. The result enabled dynamic mine waste classification based upon the pH. Specific details regarding the methods are supplied in the research articles reported in the chapters 4, 5, 6 and 7.

CHAPTER 4 ARTICLE 1: MERGING 3D GEOLOGICAL MODELING AND STOCHASTIC SIMULATION TO FOSTER THE WASTE ROCK UPSTREAM MANAGEMENT

This article was published in the *Journal of Geochemical Exploration* in 2021[1].

4.1 Abstract

Three-dimensional geological modeling is an efficient tool to visualize orebody features during both the exploration and operation phases of mines. Repurposing the 3D geological modeling for mine waste management allows for the visualization of hazardous metals distribution throughout an orebody and its host rock. With this information, a mine manager could carry out waste rock management based upon their classification. The major prerequisite to such an approach is to procure sufficiently large datasets in order to ensure high interpolation quality and suitable resolution. Apart from metals of economic interest, other elements, and more precisely the deleterious elements, usually do not undergo exhaustive geochemical analyses throughout the footwall and the hanging wall of orebodies. Based on that premise, the Éléonore mine site provided restricted grades of arsenic, the most hazardous element within the mine solid waste, to create a 3D spatial model of arsenic content. A stochastic process coupled with the geological logging of drill cores was created to fulfill the 3D modeling prerequisite with known margins of error. The outcome of this work consists of multi-realization 3D spatial model of arsenic content across the ore deposit and the hosting rock. Each realization was assessed using available chemical analyses to underline the model's reliability. The results revealed a spacious geochemical halo of arsenic that could reach up to 500 m away from the gold deposit, with up to 94% of arsenic grades exceeding 50 ppm. The process developed in this work will enable mine waste classification before

---

[1] Toubri, Y., Demers, I., Poirier, A., Pépin, G., Gosselin, M.-C. and Beier, N.A. (2021). Merging 3D geological modeling and stochastic simulation to foster the waste rock upstream management. *Journal of Geochemical Exploration*, 106739.

stripping, thereby providing the opportunity for proactive upstream mine waste management options that could prevent future environmental liabilities.

Keywords: Geological logging, Geological modeling, Monte Carlo simulation, Mine waste classification.

4.2 Introduction

Exploration geologists and mining companies are increasingly gaining interest in low-grade, high tonnage deposits due to an expanding international demand for metals. For example, porphyry copper-gold deposits supply up to 60% of copper reserves worldwide (Sun *et al*., 2010). Although these mining operations are more frequently producing favorable economic outcomes, they also usually require higher stripping ratios compared to high-grade lode swarms. Furthermore, low-grade, high-tonnage deposits exhibit thinly disseminated mineralization and/or randomly oriented thin veins (i.e., stockwork). Therefore, ore processing plants should liberate economically valuable minerals at smaller grain sizes to optimize mill recovery. For instance, in Cu mines, tailings account for up to 95% of the ground ore (Edraki *et al*., 2014). The waste rock stream is roughly threefold higher than the ground ore in Australia and the United States, and about 1.5 times higher in Canada (Mudd, 2007). These deposit-inherent features feed waste disposal sites with overwhelming amounts of the dry stream (waste rock) and require large above-ground structures to store the wet stream (tailings). Consequently, the capital investment is not only constrained by the decrease in new discoveries of metal deposits but also by the economic framework and environmental regulations. With regard to environmental considerations, the United States Environmental Protection Agency (EPA) has classified water contamination from mining activities as one of the top three ecological-security threats in the world (Dold, 2008). Acidic drainage stemming from mining activities is by far a deleterious source of water contamination in hard rock mines. The environmental surveys of acid mine drainage (AMD) may include assessment, prevention and/or treatment to safeguard the surrounding ecosystems (Akcil and Koldas, 2006; Benzaazoua *et al*., 2004; Bouzahzah *et al*., 2014; Bussière *et al*., 2001; Bussière *et al*., 2005; Evangelou, 1995; Jouini *et al*., 2020; Neculita *et al*., 2010; Plante *et al*., 2012).

Geotechnical issues and contaminant transport present serious concerns as they may result in detrimental ecological impacts (Fourie, 2009; Klebercz *et al*., 2012). Numerous improvements in

waste management practices have been proposed to enhance conventional management approaches and alleviate issues related to AMD (Benzaazoua *et al*., 2008; Benzaazoua *et al*., 2000; Benzaazoua and Kongolo, 2003; Bussière, 2007; Demers *et al*., 2015; Demers *et al*., 2008; Demers *et al*., 2017; Elghali *et al*., 2019; Lessard *et al*., 2018; Wickland and Wilson, 2005). One novel advance in mine waste management is the "design for closure" principle, which requires that potential environmental issues are considered and planned for both before and during the production stages of mining operation (Aubertin *et al*., 2016). Similarly, upstream mine waste management is another promising concept that proposes introducing preventive practices into mine waste management streams. These practices should be undertaken at the earliest possible stages of a mine's life cycle, known as upstream stages. Benzaazoua *et al*., (2008) proposed the use of the upstream mine waste management reasoning, suggesting that this type of management allows for better control over potential environmental issues. Upstream mine waste management involves any practice that aims to prevent negative environmental impacts from the beginning of a mine's life cycle. The ultimate goal of both the "design for closure" principle and upstream mine waste management is to ensure that only mine wastes with low potential of environmental contamination will be stored in above-ground waste disposal facilities, thereby avoiding the need for costly environmental remediation work.

Practically, these concepts were coupled with the geometallurgy framework resulting in more holistic geometallurgical approaches. Thus, merging advanced mineralogical surveys and mine waste management promotes the geo-environmental assessment of mine waste (Brough *et al*., 2017; Bye, 2011; Chopard, 2017; Elghali *et al*., 2018; Erguler and Erguler, 2015; Paktunc, 1999; Parbhakar-Fox *et al*., 2013; Weisener and Weber, 2010). This mineralogy-based assessment usually requires the use of time-consuming and cost-intensive techniques. Nevertheless, it can increase the efficiency of mine waste management when used as a screening tool from the very beginning stages of the mine cycle. This is because, at early stages, mine planners could, for example, segregate the waste rock stream based on the acid-generating potential of different fractions that could be firmly established by mineralogical surveys and geochemical testing (Vermette, 2018). Waste rock segregation is becoming a promising management option because it focuses on delineating the hazardous loci within the hosting lithologies in order to manage them separately. Unfortunately, this management approach is highly impacted by a lack of representative

and exhaustive sampling. Therefore, it is necessary to determine how relatively small sample sizes can be used to lead to the visualization of geo-environmental domains with known margins of error. Thus, the present study deals with the in situ classification of waste rocks based upon geochemical analyses of metal contents, with a particular focus on addressing shortcomings related to sample sizes. In this study, an integrated geo-environmental approach, based on the geological and geochemical analyses, was developed to aid in the upstream waste management of an ore deposit. The newly proposed upstream management approach relies on 3D numerical modeling to examine the spatial distribution of potential contaminants within the ore and the country rock. This approach could represent an efficient troubleshooting tool that can produce proactive assessments of country rock, even before stripping operations begin. As 3D spatial models typically require large and complete datasets, a stochastic and geology-based process was used to overcome the lack of available geochemical data in the 3D space. The aforementioned process was applied to the Éléonore gold mine to determine the spatial distribution of As within the hanging wall and the footwall of the orebody. The outcome of the stochastic, geology-based process is intended to provide a 3D visualization of As grades across the orebody and surrounding rock. This outcome will then be used to suggest effective and efficient management measures for newly produced waste rocks.

4.3 Materials and methods

4.3.1 Geological background

The Éléonore mine site is located in the Eeyou Istchee James Bay municipality in northern Quebec (Canada), 540 km northeast of Rouyn-Noranda. The main orebody, the Roberto deposit, is comprised of gold mineralization hosted in the vicinity of the tectonometamorphic contact between the La Grande and the Opinaca subprovinces that belong to the Superior Province. The Roberto deposit host rock belongs to the Low Formation, which is made of a heterogeneous metasedimentary sequence. This sequence consists of massive wacke, thinly bedded wacke, conglomerate, arenite and aluminosilicate bearing pelites (Figure 4.1) (Fontaine *et al.*, 2017). The sedimentary sequence has undergone amphibolite facies metamorphism that evolved to anataxis towards the Opinaca-La Grande contact (Ravenelle, 2013). Various dyke swarms intrude the

metasedimentary sequence, including pegmatite and dioritic dykes (Fontaine *et al.*, 2017; Ravenelle, 2013).

The Roberto deposit exhibits multiple mineralization styles along a deeply plunging orebody encompassing (Fontaine, 2019; Fontaine *et al.*, 2017): i) stockworks of quartz, dravite, microcline, phlogopite, pyrrhotite, arsenopyrite and löllingite; ii) quartz veins and breccias containing muscovite, actinolite, diopside, hedenbergite, schorl, pyrrhotite, arsenopyrite and löllingite; iii) highly deformed quartz-feldspar veins with pyrrhotite, arsenopyrite and löllingite; and iv) pervasive alteration associated with disseminated pyrrhotite, arsenopyrite and löllingite. The metallic paragenesis includes prevalent Fe-bearing sulfides and As-bearing sulfides: pyrrhotite, arsenopyrite and löllingite. The mining method is long-hole stoping (downhole drilling) longitudinal retreat with consolidated backfill (pastefill) or unconsolidated rockfill (Goldcorp, 2018).

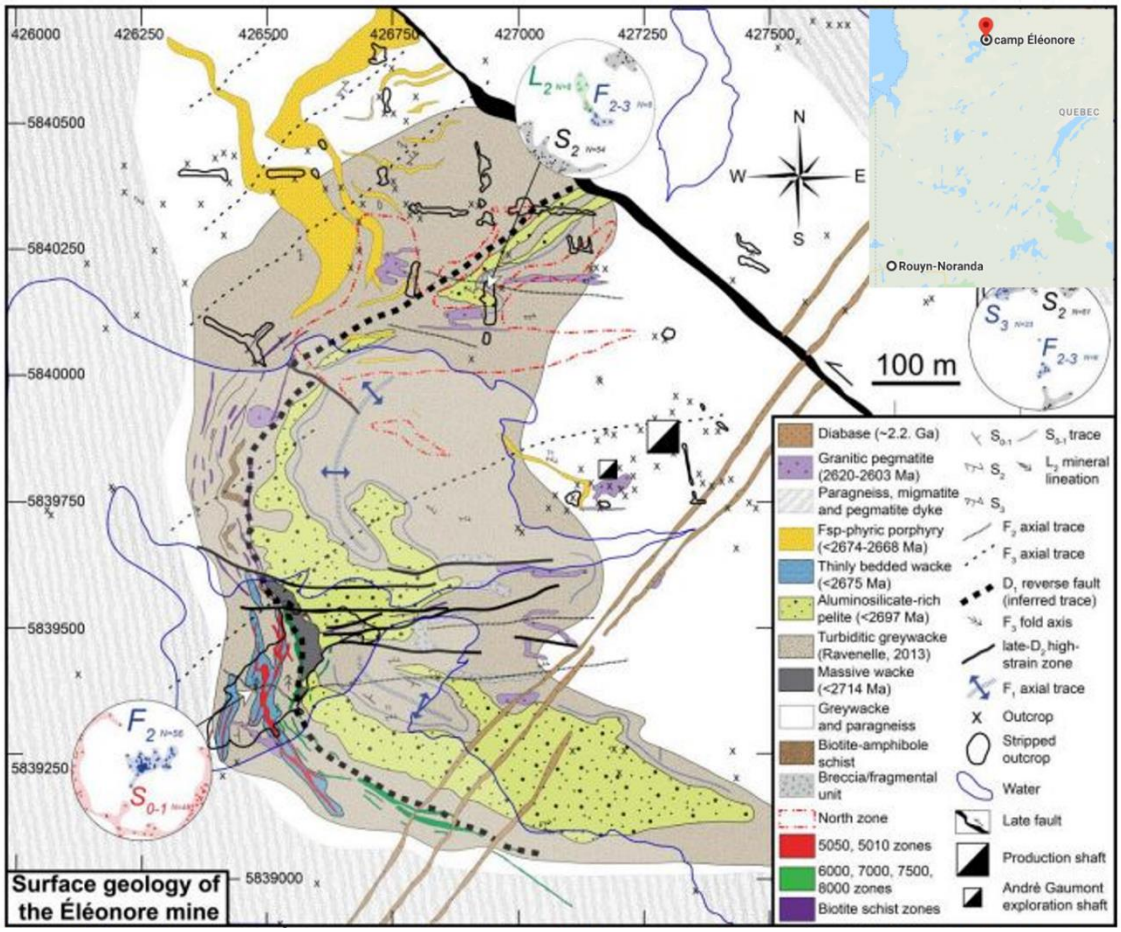


Figure 4.1 Local geological setting of the Roberto deposit (Modified from Fontaine *et al.*, 2017)

4.3.2 Geochemical and geological database

Sampling surveys are continuously conducted at the Éléonore gold mine to update the ore 3D model. In contrast, As analyses do not span the full extent of the mineralization and are insufficient to support a 3D numerical modeling approach (Figure 4.2).

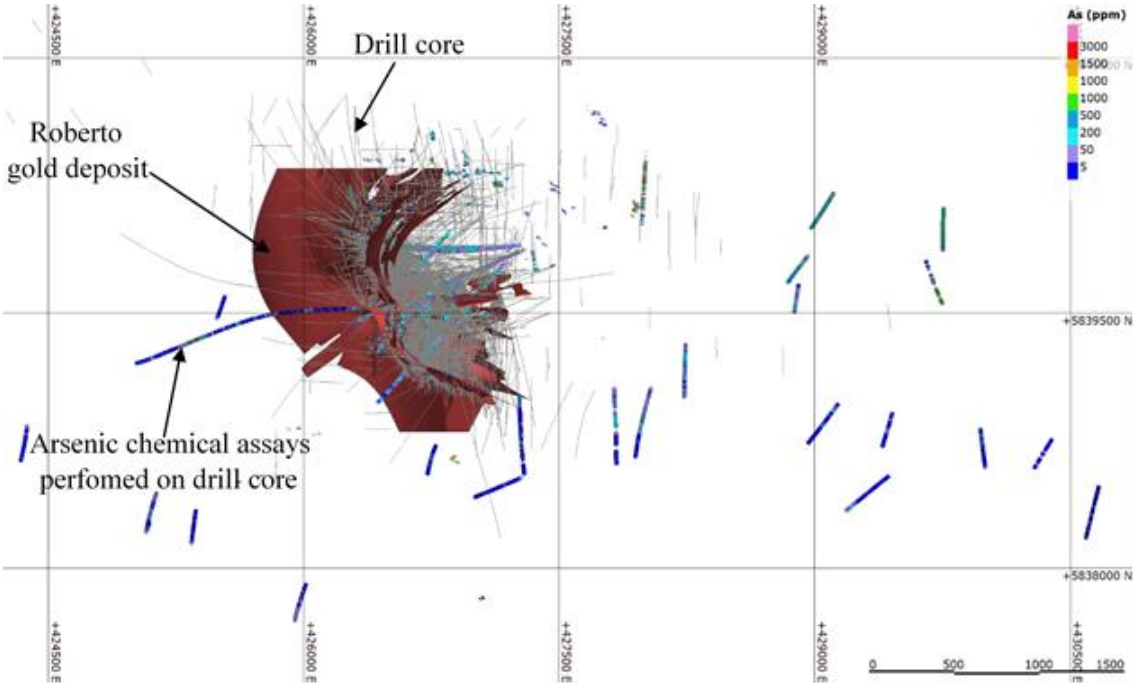


Figure 4.2 Available geochemical arsenic data from drill core samples neighbouring the orebody (plane view)

Using only the available As analyses, common geostatistical procedures yield poor interpolation results due to sparsity of these data; only about thirty drill holes with complete geochemical analysis of As versus 12,000 performed drill hole. However, up-to-date geological logging supplies qualitative insights (user-defined) about the presence of arsenopyrite within drill cores. In terms of prevalence of metal-bearing minerals, arsenopyrite is ranked second in mass percentage after pyrrhotite, with proportions ranging from 1% to 15% (Fontaine, 2019). Fontaine (2019) reported the presence of centimetric veins with up to 40% arsenopyrite content. Löllingite is also an arsenic-bearing mineral commonly found in the mineral paragenesis; however, löllingite is frequently encapsulated within arsenopyrite crystals (Fontaine, 2019). Consequently, arsenopyrite is the main As-bearing mineral and the overriding As-pathfinder. Therefore, the geological logging describing the arsenopyrite distribution can be related to the As distribution within the Roberto deposit.

In the course of geological exploration in Éléonore mine site, the geological logging included a qualitative assessment of the arsenopyrite proportions based on a standard scale (Goldcorp, 2018) ranging from 0.01 to 100 (Figure 4.3).

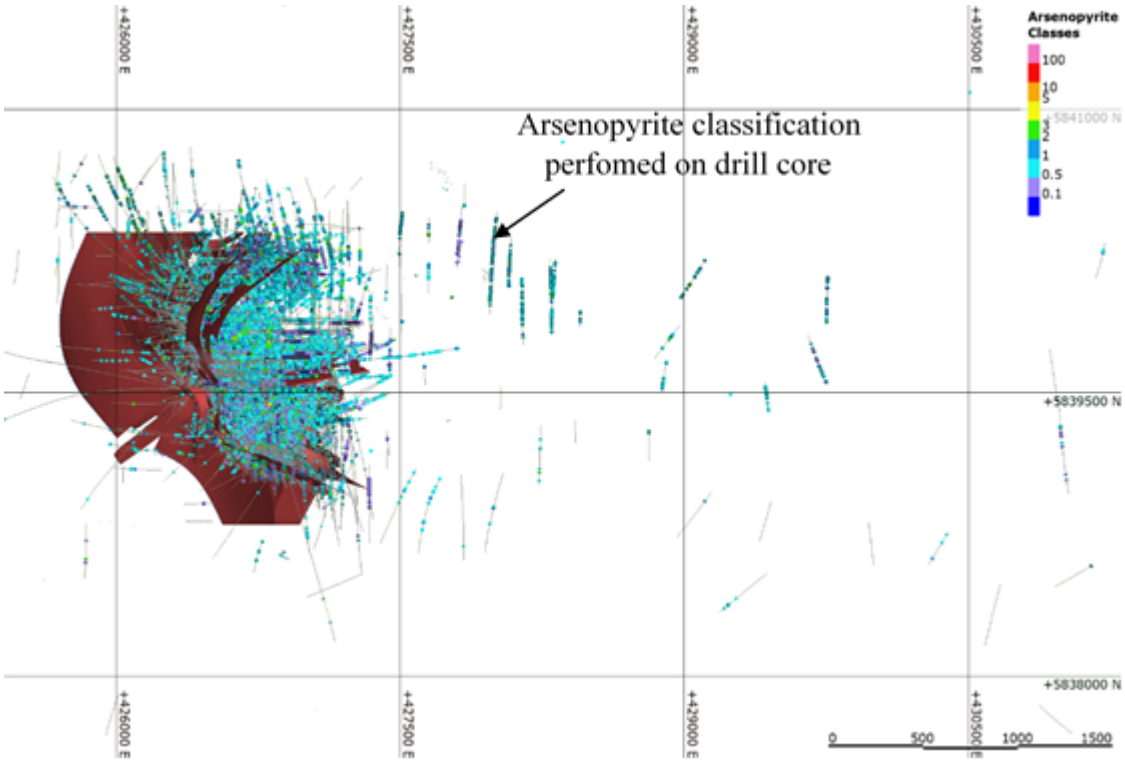


Figure 4.3 Drill core logging of arsenopyrite throughout the orebody and the host rock (plane view)

Each standard scale number refers to a class that subjectively portrays the arsenopyrite proportions. The class scale is used to describe sulfide mineral content based upon crystal size and prevalence, where a low-class number implies that a mineral is present at low proportions. However, this classification is prone to a high epistemic uncertainty that is closely related to the subjectivity of logging. Forty classes have been used from the standard scale to profile the prevalence of arsenopyrite in up to 12,000 drill cores. Furthermore, the geological logging reports class lengths within the drill cores, which are termed intervals (Figure 4.4). Up to 83,960 intervals have been measured and appraised using the standard scale classification. From the total sample size, geologists have ascribed 96% of the intervals to five classes (Figure 4.4).

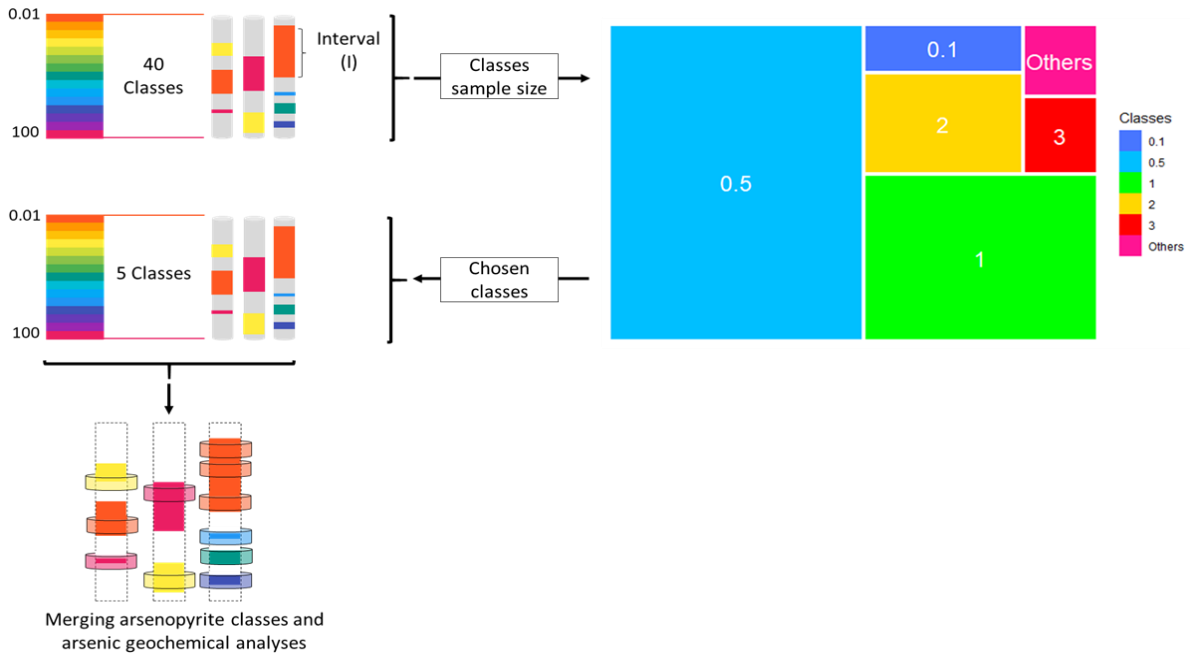


Figure 4.4 Illustration of the geological logging concept coupled to the treemap layout of the sample size of logging intervals per class

Although geological logging has been performed based on the qualitative scale, the subjectivity factor and the resulting epistemic uncertainty are unavoidable. Therefore, the main requirement identified in the process being used in the present study is that the sample size of the five qualitative classes should be constrained to the available chemical analyses of As. Firstly, this is to assess the agreement between geological logging and geochemical assays, and secondly, this allows for determination of variability in As grade within each class. As displayed in Figure 4.5, the median of As grade increases as the class number increases, thereby fulfilling agreement between geological logging and the geochemical analyses (i.e., high classes correspond to high As median and vice versa). The variability exhibited within each class (Figure 4.5) should be maintained and propagated throughout the modeling process as it reflects the extent of the epistemic uncertainty stemming from the arsenopyrite classification.

Based on limited geochemical As data and unrestricted geological logging data (Table 4.1), the present study is intended to setting up trade-offs among qualitative and quantitative datasets to overcome the lack of geochemical data. For instance, Table 4.1 shows that 71 chemical analyses of As have been performed on 37 intervals belonging to the class 0.1. Nonetheless, the sample size

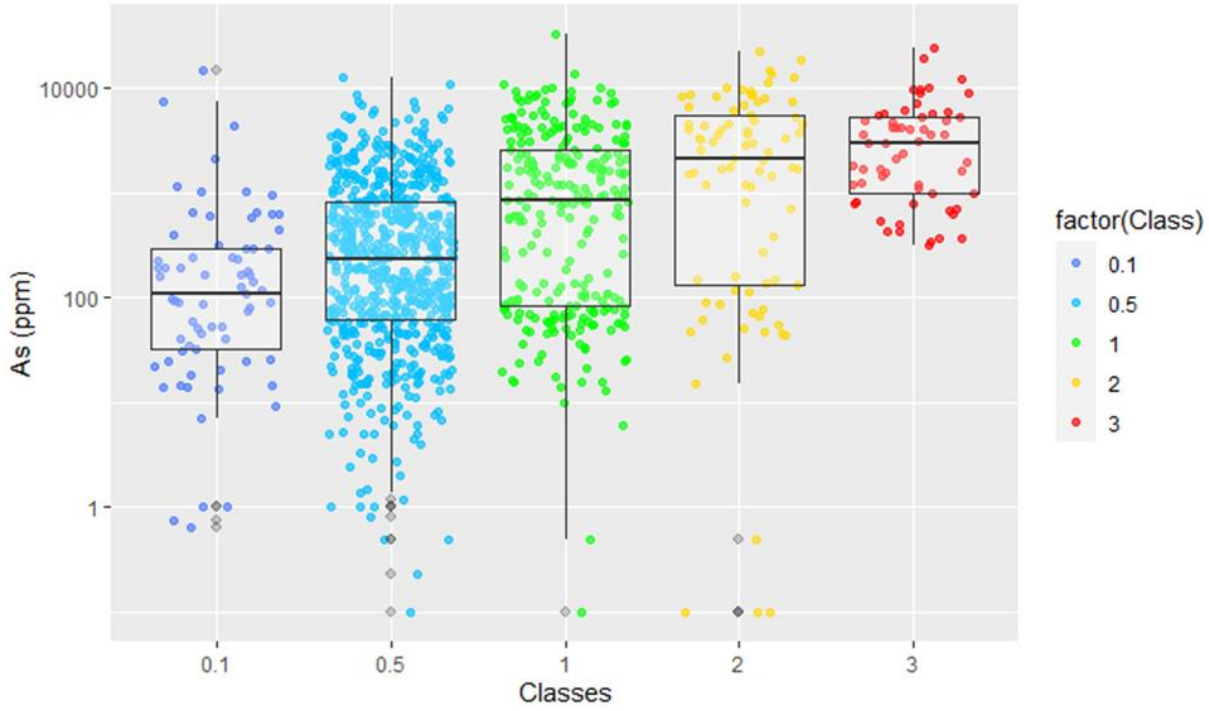


Figure 4.5 The available arsenic geochemical analyses constrained to the arsenopyrite classes

of intervals that belong to the class 0.1 is amounted to 4203 intervals. Therefore, the main concern of this study is to assign at least one simulated As grade per interval while maintaining variability (mean and standard deviation) of each class of arsenopyrite. As a primary building block of numerical models, spatial continuity should be investigated as well. The overall contribution of this work focuses on bridging geological data and mine waste management challenges via 3D numerical modeling to promote geology-based upstream management practices.

Table 4.1 Error margins related to each sample size ranked based on arsenopyrite classes

Arsenopyrite classes	0.1	0.5	1	2	3
Logging intervals	4203	43719	21193	8769	3132
Assays sample size	71	666	256	83	59
Error margin (%)	11.53	3.77	6.09	10.71	12.64
Confidence Interval (%)			95		

4.3.3 Modeling method

4.3.3.1 Stochastic simulation

Linkages among the logging data and geochemical analyses were created through a stochastic simulation intended to forecast As values that reproduce the variability (variance, mean, median) observed within each logging class (shown in Figure 4.5). A Monte Carlo simulation was performed to carry out a multi-realization process. Monte Carlo methods belong to an experimental branch of mathematics that is concerned with generating random realizations using random sampling performed on distribution functions that define the process variables (Hammersley, 1964; Kalos and Whitlock, 1986; Niederreiter, 1992). The law of large numbers proposes that the result is as accurate as desired when the size of the random samples is sufficiently high (Gilks *et al*., 1995). Monte Carlo methods usually deal with the independent variables of a system; however, several problems may involve correlated variables. In this respect, the random sampling cannot be performed independently, otherwise the generated realizations will overlook the variables' dependencies. Thus, a correlation-based Monte Carlo simulation is more effective. The modeling method used in the present study relies on a correlation-based Monte Carlo simulation to constrain the generated data against known correlation parameters, which define the results' reliability and steer the random sampling.

Before performing the Monte Carlo simulation to output equiprobable realizations, the process variables and their related distribution functions must be defined. The scope of the present study encompasses three primary variables: two continuous numerical variables (As grade and intervals), and one discrete variable (logging classes of arsenopyrite). The first step consists of classifying As grade datasets based on the discrete variable, resulting in five batches (Figure 4.5). In order to maintain the As variability of each class, computations were carried out in batches, and thus the overall process was comprised of five stages (one per class). With respect to the continuous numerical variables, they are completely independent. Monte Carlo simulation could be performed on independent variables; however, in this case, no basis is available to constrain the generated variability in As grade against the variability in the available data. Therefore, an auxiliary numerical variable was added and termed the normalized As grade. The auxiliary variable was computed by normalizing As grades to their intervals. Two main reasons warrant the use of this

auxiliary variable. First, the normalized As grade variable exhibits a power law ($y=ax^b$) when plotted against the intervals variable, thus the parameters a and b will be defined as the conformity parameters (Figure 4.6). Second, the normalization differentiates among intervals that contain the same As grade. Plotting the resulting power law on logarithmic scale displays a linear-shaped scatter stemming from a significant correlation coefficient (Figure 4.6) (A and B in Figure 4.6 could represent As grade and interval length, respectively).

Both the auxiliary variable and interval variable comply with log-normal distributions. The parameters of the probability distribution function (PDF) related to the interval variable were accurately determined because all the interval lengths are reported throughout the geological logging. In contrast, the amount of As grade data (from geochemical analyses) inherently restricts the sample size of the auxiliary variable. Therefore, PDF parameters related to the auxiliary variable were iteratively updated throughout the process until the outcome of the correlation-based Monte Carlo simulation met the initially computed parameters of the power law (a and b) of the As grade data. Regarding the dependency between the auxiliary variable and the interval variable, random sampling of the PDFs was controlled through the correlation coefficient highlighted on the logarithmic scale. Nonetheless, instead of setting the correlation as a static value, it was defined as a Gaussian PDF centred on the correlation coefficient with a standard deviation of 0.5. The correlation PDF was intended to roughly approximate the epistemic uncertainty throughout the simulation. Thereafter, the correlation-based Monte Carlo simulation was performed in order to yield numerous points displaying a linear trend on a logarithmic scale.

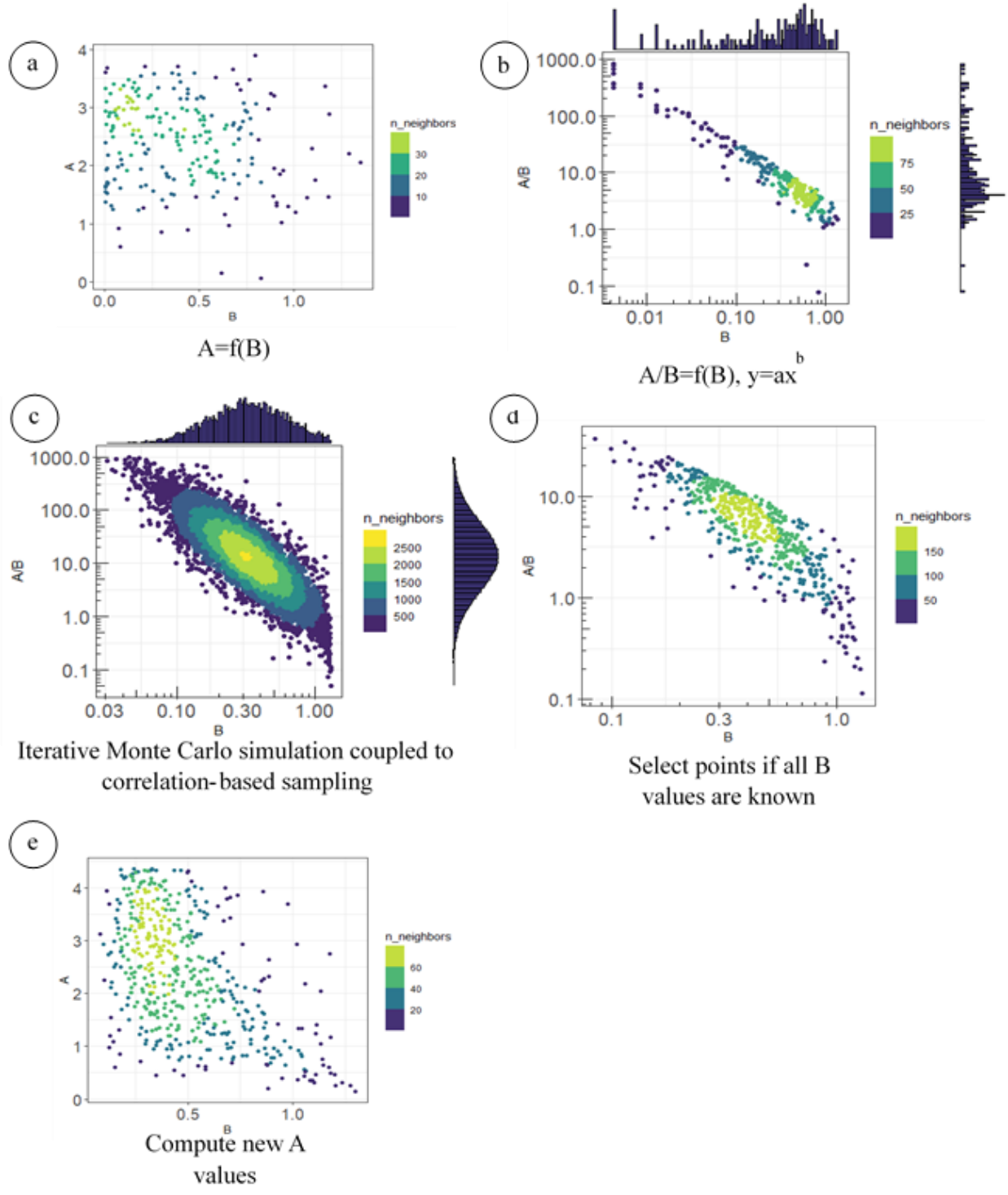


Figure 4.6 Synthetic raw data exemplifying the iterative Monte Carlo simulation based on log-normal distributions. The simulation process is performed in steps (from a to e), A and B are two independent and continuous random variables created for illustration purposes

The conformity parameters (a and b) of the simulated power law should be as close as possible to those of the available dataset, if not, the simulation should be reiterated after reconsidering the PDF parameters of the auxiliary variable. Subsequently, the values of the interval variable were selected from the simulated scatter points along with the respective values of the auxiliary variable.

Then, newly simulated As grades are calculated by cancelling the normalization through a calculation of the product of the interval variable values and their corresponding auxiliary variable values. The aforementioned steps are summarized in Figure 4.6 and applied to a synthetic raw data to highlight that this process can be performed on any data set regardless of the specific case study.

Practically, the Monte Carlo simulation was set up using the GoldSim software package to carry out calculations. GoldSim is a versatile modeling software that enables the implementation of models in a dynamic and probabilistic framework (Kossik and Miller, 2004; Rizzo *et al*., 2006). GoldSim's settings provide flexible built-in stochastic elements to run the correlation-based Monte Carlo simulation. It also embeds the importance-sampling algorithm to enhance sampling frequency of the PDF tails. Three linked stochastic elements were implemented in GoldSim: the auxiliary variable, the interval variable and the correlation.

4.3.3.2 Hypothesis testing

The hypothesis testing was required to check if the As variability (variance, mean and median) was maintained and to assess if the stochastic simulation fulfilled the homogeneity requirement between measured and simulated As grades. Levene's test is a variance homogeneity test, which is known as a statistical assessment concerned with the homoscedasticity (Gastwirth *et al*., 2009). Since the present dataset is log-normally disturbed, the Levene's test is suitable and robust in the face of non-normality (Garson, 2012). Along with the variance homogeneity test, Student's t test can be used to check if the means of two sets of data are different from each other. However, Student's t test is highly sensitive to unequal sample sizes and non-normality (Ruxton, 2006). Alternatively, Welch's t test has proven to be a robust test of equality of means as it is insensitive to both the non-normality of datasets and inequalities in sample sizes (Algina *et al*., 1994; Gamage and Weerahandi, 1998).

4.3.3.3 Spatial continuity

Geological logging marks the position of each interval within the 3D space. Accordingly, each simulated As grade inherits the coordinates of its interval. A 3D variography analysis was required to discern the spatial anisotropy of the As grades. The Stanford Geostatistical Modeling Software (SGeMS) has previously been used to investigate directional and omnidirectional variograms within the 3D space (Remy *et al.*, 2009). Several directional variograms that span the entire orebody were examined to determine the plane with the highest spatial continuity. The Leapfrog Geo software was chosen for the numerical modeling. The Leapfrog Geo software employs a rapid 3D interpolation method (the radial basis functions; RBFs) to interpolate grade and lithological data in 3D space (Cowan *et al.*, 2002). RBF interpolation techniques have increasingly gained interest as an efficient, meshless interpolation method (Aguilar *et al.*, 2005; Buhmann, 2000; Cuomo *et al.*, 2013; Floater and Iske, 1996; Hillier *et al.*, 2014; Iske, 2002; Natali *et al.*, 2013; Wright, 2003). Using the RBF interpolation method, along with the variography realizations and the structural measurements from the surface and underground mapping, ten 3D spatial models of As grades were produced.

4.4 Results and discussion

4.4.1 Monte Carlo simulation results

The simulation process was undertaken for each class of arsenopyrite, which constitutes the discrete index variable. The process thus becomes a four-sided simulation encompassing three continuous numerical variables and one discrete variable. The outcome of the iterative and correlation-based Monte Carlo simulation is shown in Figure 4.7. The trend in As grade for the five classes is maintained and the medians of the simulated grades are similar to those of the actual dataset. Figure 4.8 illustrates how the As simulated grades were generated from available analyses of As using correlation-based Monte Carlo simulation. From the generated points, values of the auxiliary variable were selected based upon the values of the interval variable reported in the geological logging dataset (Figure 4.9). Afterwards, the normalization is cancelled to obtain the newly created dataset (Figure 4.7).

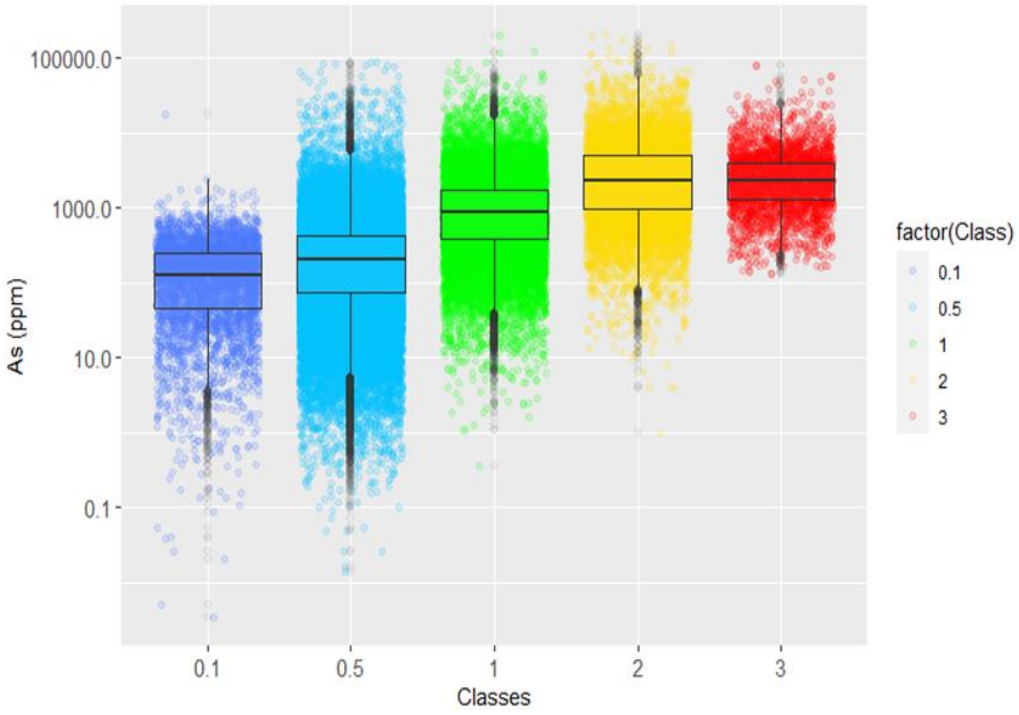


Figure 4.7 Output of the iterative stochastic simulation for each arsenopyrite class (Realization 1)

In terms of hypothesis testing, the reported p-values obtained from the Levene's test, Welch's test and even Student's t test comply with the null hypothesis (p-values > 0.05). Therefore, the difference between the actual As grade variability and the simulated As grade variability is not significant at a significance level of 0.05 (Table. 4.2). The chosen conformity parameters in the stochastic simulation appear to be reliable at propagating the logging uncertainty and producing homoscedastic datasets. Thus, the simulated As grades are adequate to undergo the spatial continuity analysis.

Table 4.2 Hypotheses testing based on a 0.05 significance level

	Sample size	Levene's test *p*-value	Student's t-test *p*-value	Welch's t-test *p*-value
As available grades	1141	0.367	0.412	0.217
As simulated grades	80977			
Significance level	0.05	Not significant	Not significant	Not significant

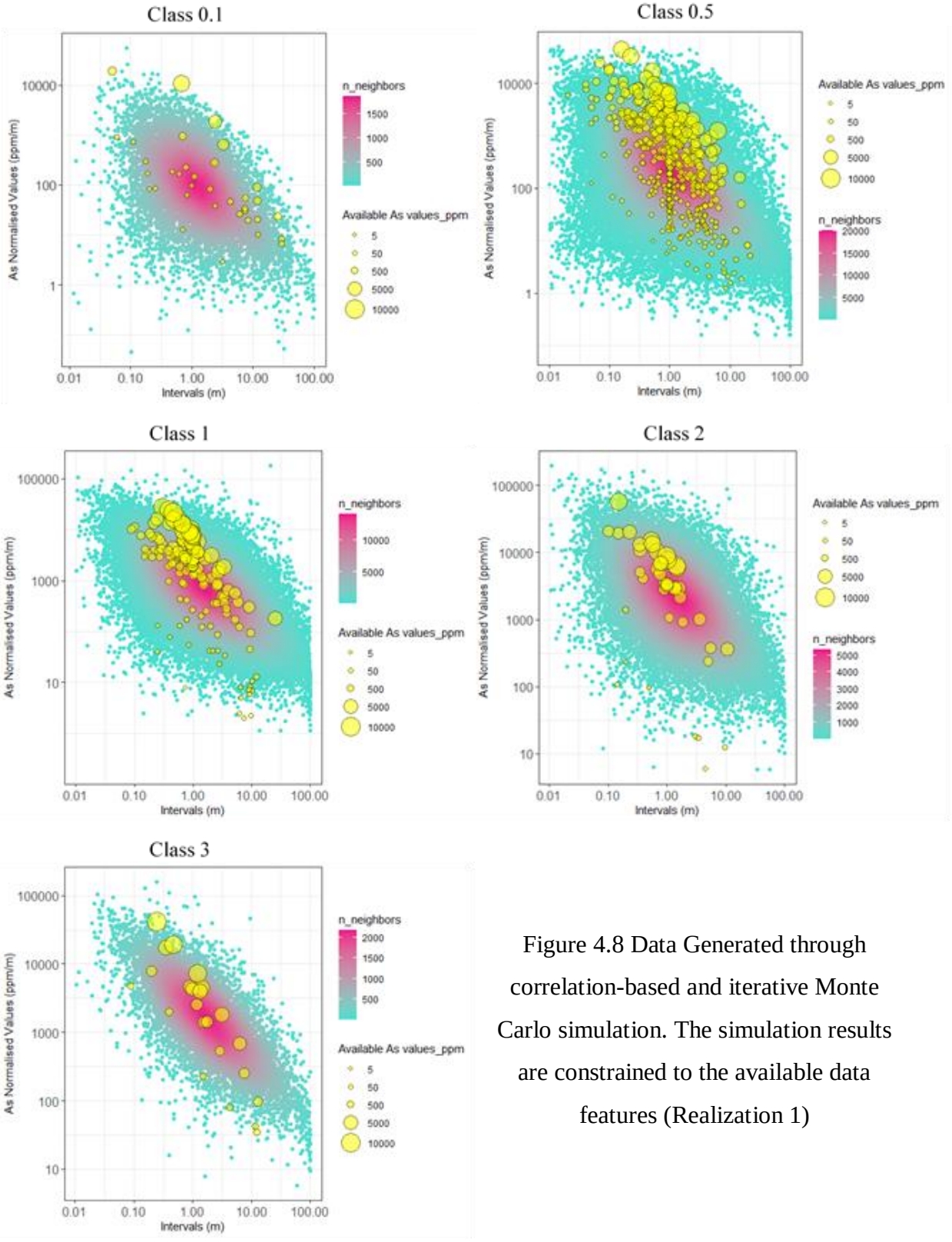


Figure 4.8 Data Generated through correlation-based and iterative Monte Carlo simulation. The simulation results are constrained to the available data features (Realization 1)

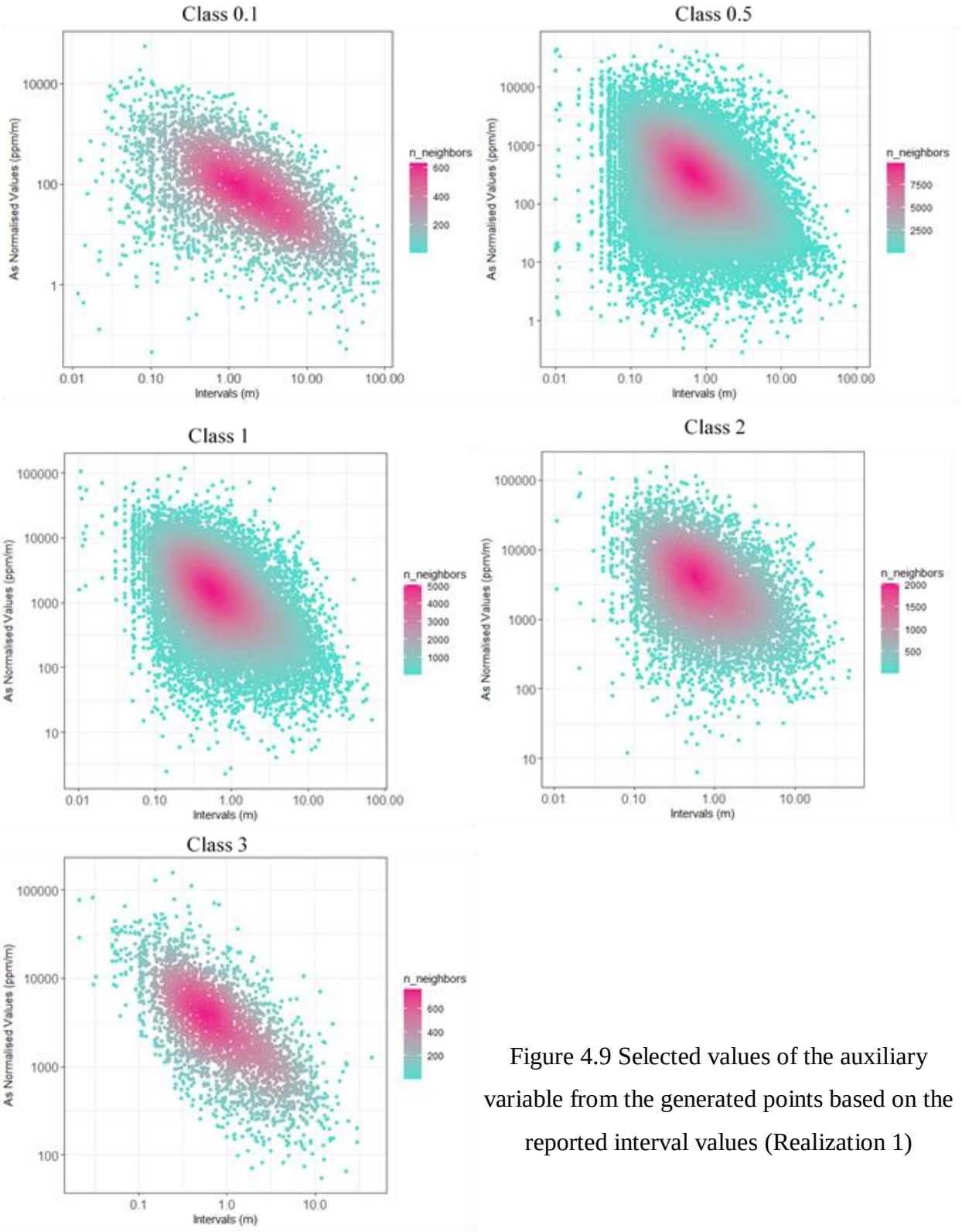


Figure 4.9 Selected values of the auxiliary variable from the generated points based on the reported interval values (Realization 1)

Results from the variography analysis showed that the plane defined at 165°N, 70°SW exhibited a variogram range of up to 28 m, whereas the other directional variograms and the omnidirectional variogram yielded lower ranges (10 to 17 m). Regardless of the anisotropy, the overall variography analysis underscores the high to extreme nugget effect, which exceeds 50% of the sill. Overall, the variography analysis highlights two features: (1) the highest spatial continuity was observed along 165°N, 70°SW. Interestingly, this plane is in agreement with the structural trend of the gold-bearing orebody; (2) the extreme nugget effect obtained in the variograms is in line with the mineralization style, which mainly consists of stockworcks and disseminations (Dominy *et al*., 2003; Dominy *et al*., 2001). Thus, the simulated As grades are in agreement with the spatial geological features of the orebody. However, the effect of ergodic fluctuations on the variography should be interrogated. Consequently, the overall modeling process was undertaken ten times to produce ten realizations of the 3D numerical models. The first four realizations, the second four realizations and the remaining two realizations were performed based on standard deviations of the correlation PDF of 0.5, 0.3, and 0.1, respectively. Table 4.3 displays the corresponding directional variograms computed along the aforementioned high-continuity plane. Variogram ranges were slightly affected by ergodic fluctuations, resulting in up to 10 m of difference. The nugget effect exceeded 50% of the sill for all realizations. The parameters of each variogram realization were used to build numerical models to visualize the effect of ergodic fluctuations in the 3D space.

Table 4.3 Variogram realizations highlighting the ergodic fluctuations effect on the ranges

Realizations	Nugget effect	Sill	Range (m)
1	1.8e+06	2.7e+06	21
2	1.7e+06	2.8e+06	22
3	2.2e+06	3.65+06	16
4	2.15e+06	3.9+06	22
5	1.8e+06	3.0+06	17
6	2.3e+06	3.4+06	24
7	2.5e+06	3.5+06	28
8	2.5e+06	3.5+06	21.5
9	2.3e+06	3.5+06	19
10	2.4e+06	3.45+06	28

4.4.2 Geological model and analysis

The results from the first realization were chosen to represent the 3D spatial models (Figure 4.10). The numerical spatial models consist of six encapsulated casings; each casing delineates the spatial distribution of a specified range of As values. Figure 4.10 displays two casings from Realization 1: the 500 ppm to 1100 ppm range, and the 1100 ppm to 2300 ppm range.

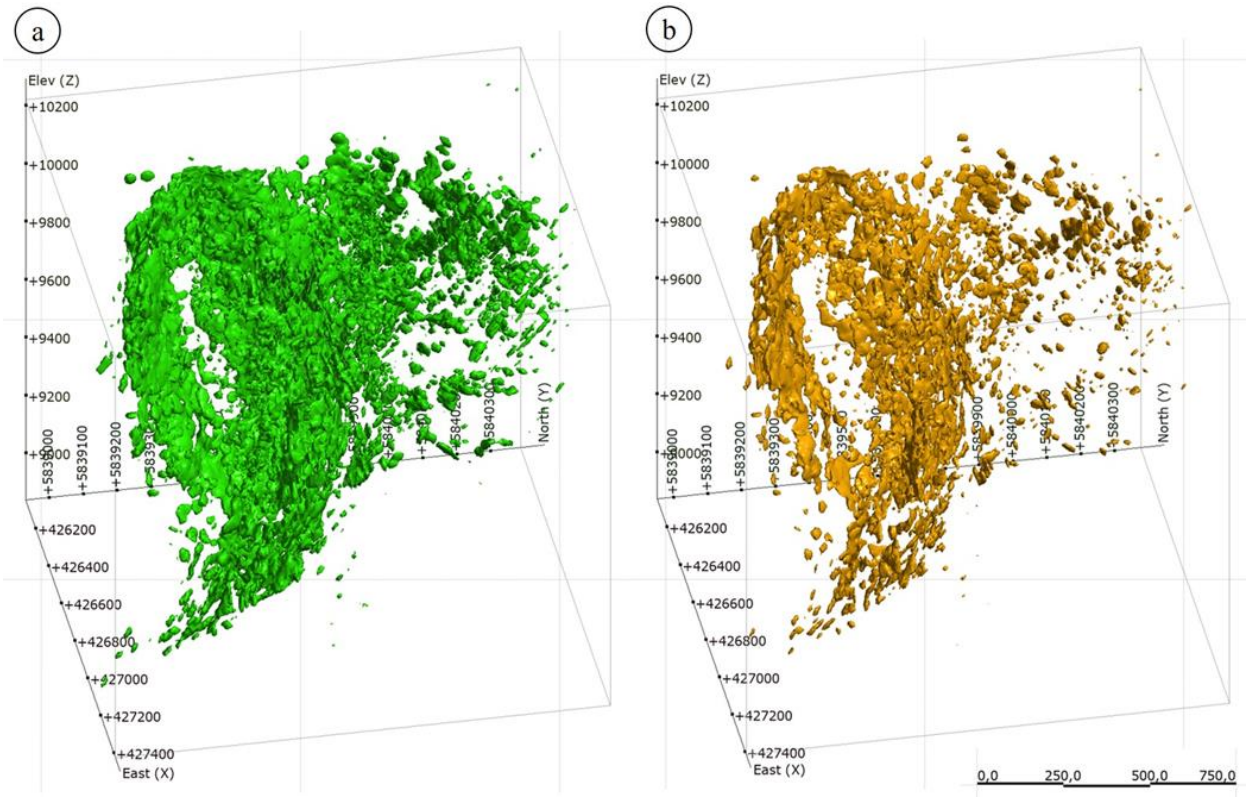


Figure 4.10 a) The spatial distribution of arsenic grades ranging from 500 ppm to 1100 ppm, b) The spatial distribution of arsenic grades ranging from 1100 ppm to 2300 ppm (Realization 1)

Since the Au mineralization is closely associated with As-bearing minerals, the first key element of the 3D spatial model is that it inherits its shape from the orebody through the directional variogram features and structural measurements. In order to visualize the spatial relationship between the As grades and the orebody, the Au mineralization was overlaid with the 3D spatial model (Figure 4.11). The orebody displays high As grades of up to 3000 ppm in some loci. The close association of the Au mineralization and the As grades is highlighted in all realizations. Nonetheless, as the geographic extent of the 3D model straddles the geological logging extent, the

3D spatial model does not span the lower part of the orebody, which is deeper than 850 metres. In spite of that, the results show that the stripped ore and perhaps the resulting subsequent tailings hold high As values. A 3D block model was created based upon an As cut-off grade of 200 ppm to spot blocks with high to extreme metal content throughout the orebody and surrounding rock; the building block dimensions are 20x20x10 m (Figure 4.12).

The 3D spatial model stresses that the geochemical halo of As is tens of meters larger than the Au mineralization extent. Consequently, it is not only the stripped ore that could contain up to 2300 ppm of As but also the country rock, which exhibits grades of up to 1100 ppm. Such a high As content in the waste rock requires proactive solution to prevent As mobilization. The upstream segregation of waste rock is a promising option to prevent, or at least mitigate the leakage of As-rich effluents. The upstream management method suggested here relies on coupling the mine plane and the 3D spatial model of As grades to distinguish between underground stopes with high to extreme As content from those with low As content (Figure 4.13)

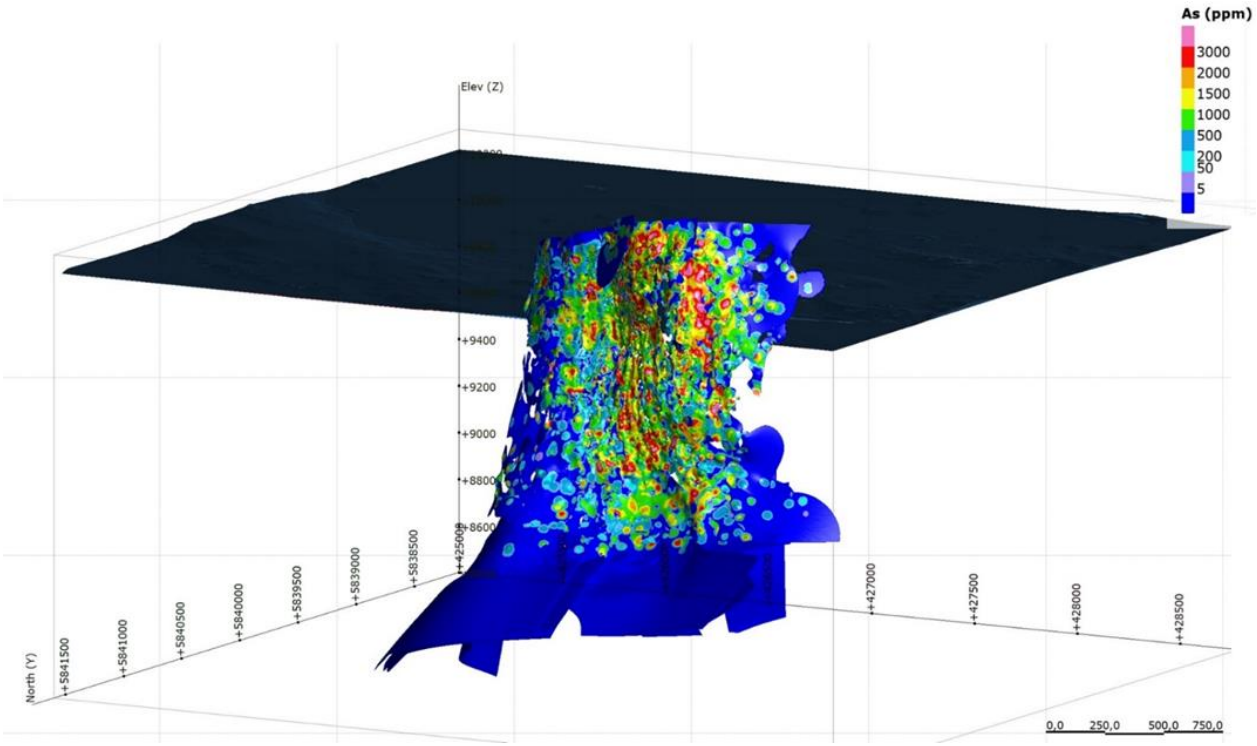


Figure 4.11 Spatial relationship between the gold deposit and the arsenic grades in Realization 1

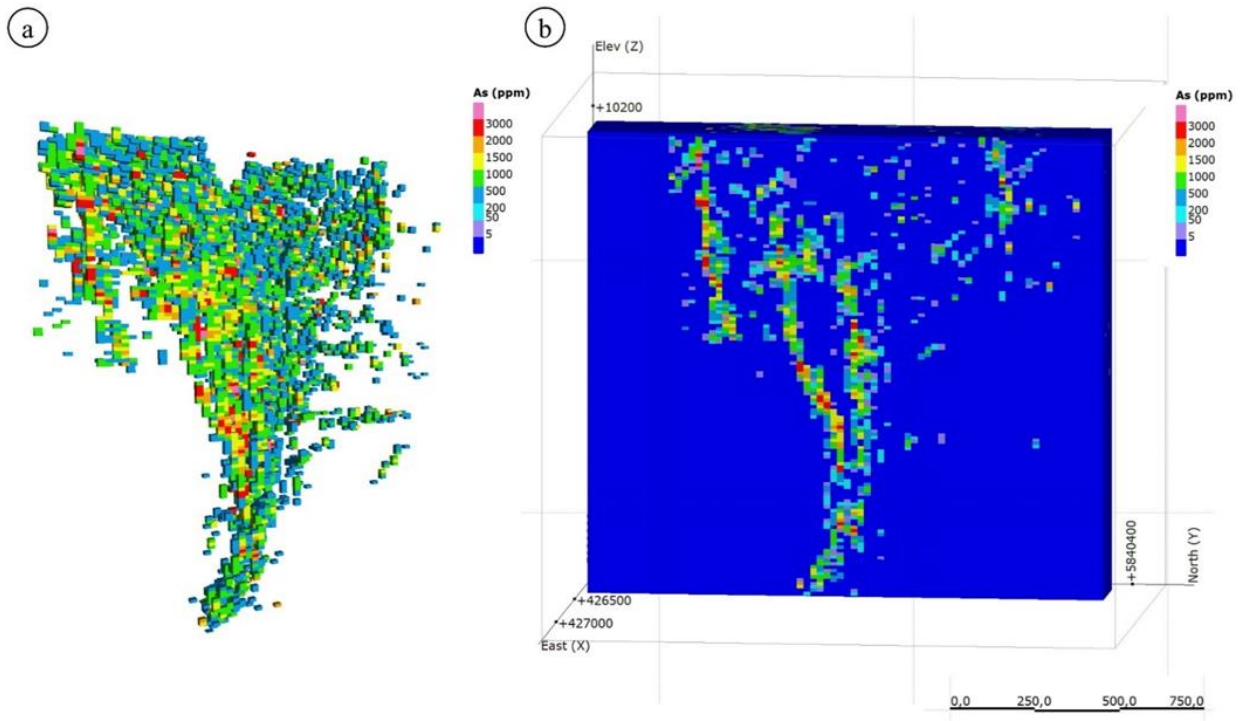


Figure 4.12 a) Realization 1 of the block model delineating arsenic grades greater than 200 ppm, b) Realization 1 of the block model of the arsenic grades along the footwall of the gold deposit

Accordingly, mine managers could seamlessly make substantive choices regarding the waste rock that should be used as backfill because of their high to extreme As grade. Therefore, only the waste rock with low to medium As content would feed the above-ground waste disposal facility. Figure 4.13 shows that few underground stopes have As grades lower than 50 ppm. Furthermore, almost all the surrounding rocks located within 100 m from the orebody exceed the "generic soil criterion A" of the Soil Protection and Rehabilitation of Contaminated Sites Policy (SPRCSP) (Beaulieu, 2020). This distance could increase to up to 500 m within the orebody's footwall. This is supported by all the spatial realizations. Thus, with respect to the Éléonore case study, the portion of the waste rock stream used in backfilling should be as high as possible. The waste rock already stored in the surface disposal facility should be managed carefully. Two preventive measures are suggested: (1) lead the progressive reclamation of the waste rock disposal areas, and (2) reuse the maximum amount of waste rock as rockfill or/and paste backfill.

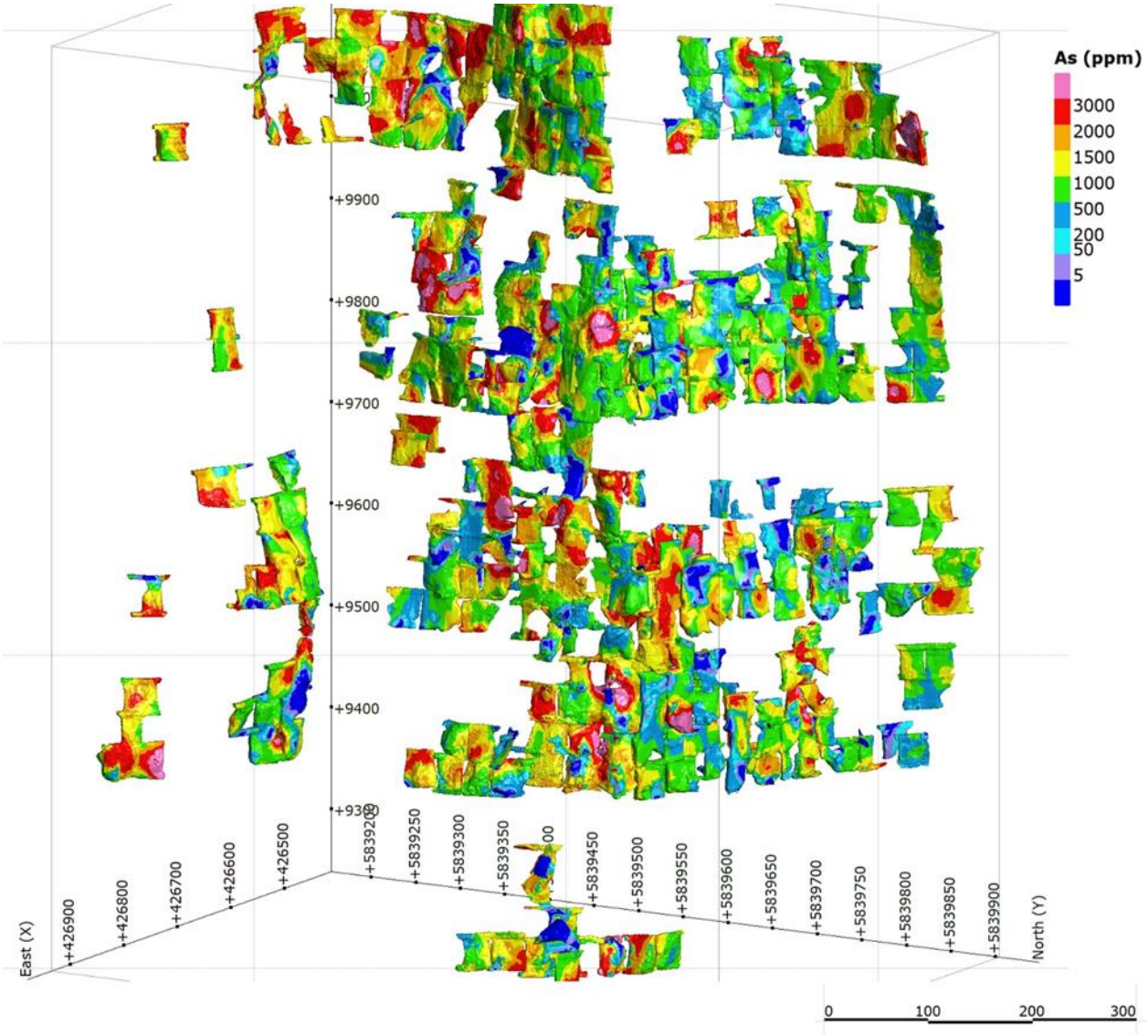


Figure 4.13 Underground stopes assessed through realization 1 of the spatial model

Analysis of the simulation results and the 3D modeling aimed at highlighting the magnitude of the ergodic fluctuations within the 3D space and their effect on the agreement between the measured and the simulated As grades. The agreement assessment was performed in two steps: the first step was to visualize the ten realizations as well as the measured As grades within the probability space using empirical cumulative density functions (ECDFs). The ECDF of each realization was computed based upon 80,977 simulated As grades. In contrast, the ECDF of the measured As grades was based on 1141 As analyses performed during the local exploration surveys (up to 1 km away from the Roberto deposit). The second step was to examine the agreement in the 3D space

by spotting the intersections of the spatial 3D model and the As geochemical analyses performed on drill cores. Figure 4.14 shows that the ECDFs of the realizations agree with the local measured ECDF values. Therefore, the stochastic simulation outcome respects the agreement requirement within the probability space, while keeping the ergodic fluctuations at an acceptable level. The process used to maintain the variability features throughout the simulation has proven to be efficient. For the sake of comparison, a supplementary ECDF pertaining to the regional exploration surveys is also plotted in Figure 4.14. It includes 23,608 As analyses located in the vicinity of the Roberto deposit (up to a distance of 9 km). The median of the As grade roughly increases by forty-fold from the regional scale to the orebody's immediate surroundings (Figure 4.14). This comparison yields insights about the extent of the geochemical halos of the Roberto deposit that could reach up to 1 km away from the main orebody.

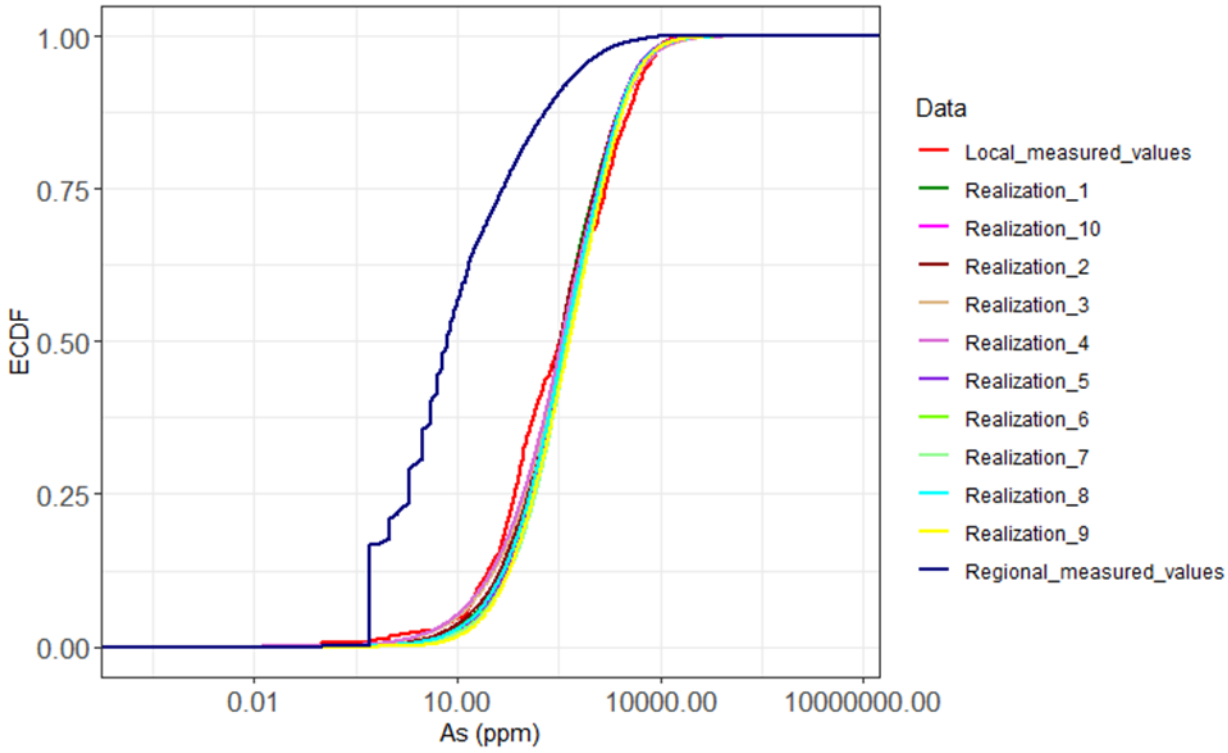


Figure 4.14 The empirical cumulative distribution functions of the resulting realizations along with the local and the regional measured grades of arsenic

In terms of the assessment of ergodic fluctuations in the 3D space, Figure 4.15 shows that the geochemical analyses of As performed on drill cores are consistent with the 3D spatial model. The

3D spatial model does not give the exact same As grade values present in the drill core intersection, but values are on the same magnitude (the same color scale is used for the analyzed drill core samples and the 3D model). Furthermore, by comparing the ten realizations of the evaluated mine plan, the effect of ergodic fluctuations is maintained at a fair level and no substantial differences were noted. The spatial visualization of the intersections of the measured and the simulated As grades underscores the effectiveness of the process being used.

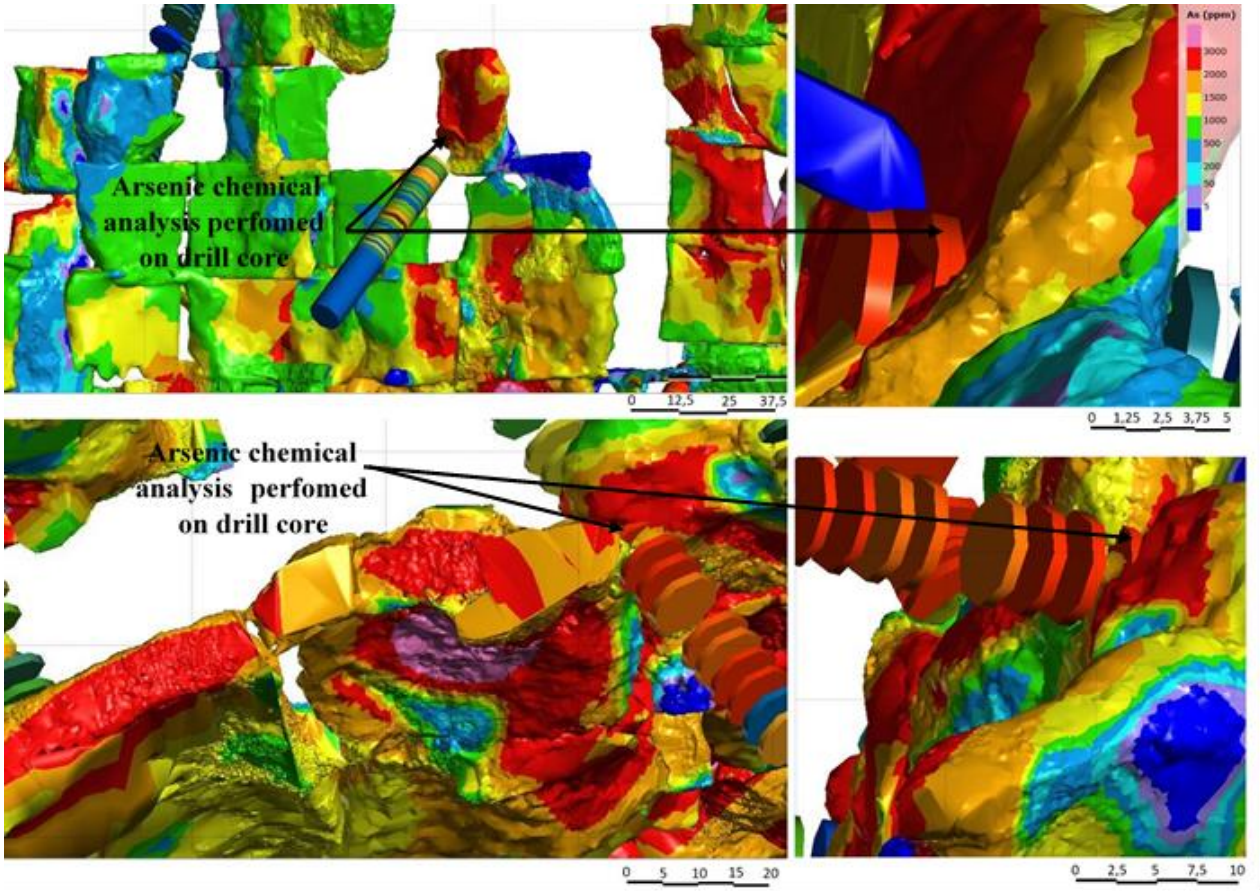


Figure 4.15 Spatial intersections of the mine plan overlaid with the 3D spatial model (Realization 1) and the chemical analyses performed on drill core samples

Although it provides many benefits, the modeling method developed in this work has some shortcomings. For example, the margins of error calculated for each class exceed 5% for the 0.1, 1, 2 and 3 classes (Table 4.1). The reported margins of error are derived from the available sample size. Therefore, to enhance the 3D model's accuracy, additional As analyses should be performed. The sample size should be increased by 281, 121, 285 and 283 samples for classes 0.1, 1, 2 and 3,

respectively in order to reach a 5% error margin. Furthermore, the suggested method does not involve kinetic considerations; it only considers the metal content in the country rock as a proxy guiding the waste rock classification for their upstream management. The As mobilization framework requires kinetic testing along with mineralogical surveys, both of which are outside the scope of the present study. Kinetic testing performed on several grain-sizes fractions is recommended. Furthermore, samples with high As content should be selected to undergo laboratory kinetic tests in order to identify links between the As content and the leaching potential. Field-scale kinetic tests are also advisable to assess the effect of climatic conditions on As mobilization.

4.5 Conclusion

The proposed modeling method overcomes the lack of available geochemical data on As content by coupling a correlation-based stochastic simulation with geological logging data. The 3D geological modeling coupled to the stochastic simulation via the geological logging revealed interesting results that could be used to enhance waste rock classification based on their metal content. Promising methods have been investigated to bridge geological modeling and upstream waste rock management. Through the newly described approach, mine managers could visualize metal content across an orebody and its host rock with known margins of error based on restricted geochemical data. Thus, the process is intended to provide an efficient troubleshooting tool for the proactive environmental assessment in hard rock mines. More importantly, the stochastic simulation represents a powerful tool that could be applied to mine waste management problems. Likewise, links between geology and mine waste management should be encouraged to overcome interdisciplinary barriers and move towards integrated waste management solutions. Promising prospects for upstream management should be further probed through integrated and multidisciplinary surveys.

Supplementary materials

The supplementary materials of this chapter are in Appendix A.

Acknowledgements

The authors thank the Éléonore mine site staff for their support and contributions and the GoldSim corporation for the reduced fees of the research license. Funding for this study was provided by a Mitacs grant to the first author, with MISA as the industrial counterpart. This work is a part of the NSERC TERRE-NET program, led by Dr. D. Blowes (University of Waterloo).

References

Aguilar, F.J., Agüera, F., Aguilar, M.A. and Carvajal, F. (2005). Effects of terrain morphology, sampling density, and interpolation methods on grid DEM accuracy. Photogrammetric Engineering & Remote Sensing, 71(7), 805-816.

Akcil, A. and Koldas, S. (2006). Acid Mine Drainage (AMD): causes, treatment and case studies. Journal of cleaner production, 14(12-13), 1139-1145.

Algina, J., Oshima, T. and Lin, W.-Y. (1994). Type I error rates for Welch's test and James's second-order test under nonnormality and inequality of variance when there are two groups. Journal of Educational Statistics, 19(3), 275-291.

Aubertin, M., Bussière, B., Pabst, T., James, M. and Mbonimpa, M. (2016). Review of the reclamation techniques for acid-generating mine wastes upon closure of disposal sites. In proceedings: Geo-Chicago 2016, pp. 343-358.

Beaulieu, M. (2020). Intervention guide - soil protection and remediation of contaminated land. quebec. Minist. Environ. Fight Clim. Chang. 280. (in French). http://www.environnement.gouv.qc.ca/sol/terrains/guide-intervention/guide-intervention-protection-rehab.pdf last access May 22, 2020.

Benzaazoua, M., Bussière, B., Dagenais, A.-M. and Archambault, M. (2004). Kinetic tests comparison and interpretation for prediction of the Joutel tailings acid generation potential. Environmental Geology, 46(8), 1086-1101.

Benzaazoua, M., Bussière, B., Demers, I., Aubertin, M., Fried, É. and Blier, A. (2008). Integrated mine tailings management by combining environmental desulphurization and cemented paste backfill: Application to mine Doyon, Quebec, Canada. Minerals engineering, 21(4), 330-340.

Benzaazoua, M., Bussière, B., Kongolo, M., McLaughlin, J. and Marion, P. (2000). Environmental desulphurization of four Canadian mine tailings using froth flotation. International journal of mineral processing, 60(1), 57-74.

Benzaazoua, M. and Kongolo, M. (2003). Physico-chemical properties of tailing slurries during environmental desulphurization by froth flotation. International Journal of Mineral Processing, 69(1-4), 221-234.

Bouzahzah, H., Benzaazoua, M., Bussiere, B. and Plante, B. (2014). Prediction of acid mine drainage: importance of mineralogy and the test protocols for static and kinetic tests. Mine Water and the Environment, 33(1), 54-65.

Brough, C., Strongman, J., Bowell, R., Warrender, R., Prestia, A., Barnes, A. and Fletcher, J. (2017). Automated environmental mineralogy; the use of liberation analysis in humidity cell testwork. Minerals Engineering, 107, 112-122.

Buhmann, M.D. (2000). Radial basis functions. Acta numerica, 9, 1-38.

Bussière, B. (2007). Colloquium 2004: Hydrogeotechnical properties of hard rock tailings from metal mines and emerging geoenvironmental disposal approaches. Canadian Geotechnical Journal, 44(9), 1019-1052.

Bussière, B., Aubertin, M. and Julien, M. (2001). Couvertures avec effets de barrière capillaire pour limiter le drainage minier acide: aspects théoriques et pratiques. Vecteur environnement, 34(3), 37-50.

Bussière, B., Aubertin, M., Zagury, G J., Potvin, R and Benzaazoua, M. (2005). Principaux défis et pistes de solution pour la restauration des aires d'entreposage de rejets miniers abandonnées. In : Paper presented at the Symposium 2005 sur l'environnement et les mines.

Bye, AR. (2011). Case studies demonstrating value from geometallurgy initiatives. GeoMet 2011-1st AusIMM International Geometallurgy Conference 2011. : AusIMM: Australasian Institute of Mining and Metallurgy.

Chopard, A. (2017). Évaluation environnementale de minerais sulfurés polymétalliques basée sur une approche minéralogique pluridisciplinaire. Ph.D. thesis, Université du Québec en Abitibi-Témiscamingue, Rouyn-Noranda.

Cowan, E., Beatson, R., Fright, W., McLennan, T. and Mitchell, T. (2002). Rapid geological modeling. In: Applied Structural Geology for Mineral Exploration and Mining, International Symposium, 23–25 September 2002, Kalgoorlie.

Cuomo, S., Galletti, A., Giunta, G and Starace, A. (2013). Surface reconstruction from scattered point via RBF interpolation on GPU Federated Conference on Computer Science and Information Systems, FedCSIS, IEEE (2013), pp. 433-440.

Demers, I., Benzaazoua, M., Mbonimpa, M., Bouda, M., Bois, D. and Gagnon, M. (2015). Valorisation of acid mine drainage treatment sludge as remediation component to control acid generation from mine wastes, part 1: Material characterization and laboratory kinetic testing. Minerals Engineering, 76, 109-116.

Demers, I., Bussière, B., Benzaazoua, M., Mbonimpa, M. and Blier, A. (2008). Column test investigation on the performance of monolayer covers made of desulphurized tailings to prevent acid mine drainage. Minerals Engineering, 21(4), 317-329.

Demers, I., Mbonimpa, M., Benzaazoua, M., Bouda, M., Awoh, S., Lortie, S. and Gagnon, M. (2017). Use of acid mine drainage treatment sludge by combination with a natural soil as an oxygen barrier cover for mine waste reclamation: Laboratory column tests and intermediate scale field tests. Minerals Engineering, 107, 43-52.

Dold, B. (2008). Sustainability in metal mining: from exploration, over processing to mine waste management. Reviews in Environmental Science and bio/technology, 7(4), 275.

Dominy, S., Platten, I. and Raine, M. (2003). Grade and geological continuity in high-nugget effect gold–quartz reefs: implications for resource estimation and reporting. Applied Earth Science, 112(3), 239-259.

Dominy, S.C., Stephenson, P.R. and Annels, A.E. (2001). Classification and reporting of mineral resources for high-nugget effect gold vein deposits. Exploration and Mining Geology, 10(3), 215-233.

Edraki, M., Baumgartl, T., Manlapig, E., Bradshaw, D., Franks, D.M. and Moran, C.J. (2014). Designing mine tailings for better environmental, social and economic outcomes: a review of alternative approaches. Journal of Cleaner Production, 84, 411-420.

Elghali, A., Benzaazoua, M., Bouzahzah, H., Bussière, B. and Villarraga-Gómez, H. (2018). Determination of the available acid-generating potential of waste rock, part I: Mineralogical approach. Applied Geochemistry, 99, 31-41.

Elghali, A., Benzaazoua, M., Bussière, B. and Bouzahzah, H. (2019). Determination of the available acid-generating potential of waste rock, part II: Waste management involvement. Applied geochemistry, 100, 316-325.

Erguler, Z.A. and Erguler, G.K. (2015). The effect of particle size on acid mine drainage generation: Kinetic column tests. Minerals Engineering, 76, 154-167.

Evangelou, V. (1995). Pyrite oxidation and its control. CRC Press, Boca Raton, FL.

Floater, M.S. and Iske, A. (1996). Multistep scattered data interpolation using compactly supported radial basis functions. Journal of Computational and Applied Mathematics, 73(1-2), 65-78.

Fontaine, A. (2019). Géologie des minéralisations aurifères de la mine Éléonore, Eeyou Istchee Baie-James, province du Supérieur, Québec, Canada. Ph.D. thesis, Université du Québec, Institut national de la recherche scientifique.

Fontaine, A., Dubé, B., Malo, M., Ravenelle, J. F., Fournier, E., McNicoll, V., Beausoleil, C., Prud'homme, N. and Goutier, J. (2017). The Éléonore Gold Mine: Exploration, Discovery and Understanding of an Emerging Gold District in Eeyou Istchee James Bay, Superior Province, Northern Québec, Canada. In: Proceedings of Exploration 17: Sixth Decenniel International Conference on Mineral Exploration. Ed. V. Tschirhart and MD Thomas, pp. 601-617.

Fourie, A. (2009). Preventing catastrophic failures and mitigating environmental impacts of tailings storage facilities. Procedia Earth and Planetary Science, 1(1), 1067-1071.

Gamage, J. and Weerahandi, S. (1998). Size performance of some tests in one-way ANOVA. Communications in Statistics-Simulation and Computation, 27(3), 625-640.

Garson, G.D. (2012). Testing statistical assumptions. Asheboro, NC: Statistical Associates Publishing.

Gastwirth, J.L., Gel, Y.R. and Miao, W. (2009). The impact of Levene's test of equality of variances on statistical theory and practice. Statistical Science, 343-360.

Gilks, W.R., Richardson, S. and Spiegelhalter, D. (1995). Markov chain Monte Carlo in practice. : Chapman and Hall/CRC.

Goldcorp. (2018). Éléonore Operations Quebec, Canada. NI 43-101 Technical Report. https://www.sec.gov/Archives/edgar/data/919239/000119312519061905/d698182dex993.htm last access May 22, 2020.

Hammersley, J. M. and Handscomb, D. C. (1964). Monte carlo methods. New York : John Wiley, pp 2.

Hillier, M.J., Schetselaar, E.M., de Kemp, E.A. and Perron, G. (2014). Three-dimensional modeling of geological surfaces using generalized interpolation with radial basis functions. Mathematical Geosciences, 46(8), 931-953.

Iske, A. (2002). Scattered data modeling using radial basis functions. In: Tutorials on Multiresolution in Geometric Modeling, Springer, Heidelberg, pp. 205–242.

Jouini, M., Neculita, C.M., Genty, T. and Benzaazoua, M. (2020). Environmental behavior of metal-rich residues from the passive treatment of acid mine drainage. Science of The Total Environment, 136541.

Kalos, M.H. and Whitlock, P.A. (1986). Monte Carlo methods, vol. 1. New York: John Wiley & Son.

Klebercz, O., Mayes, W.M., Anton, Á.D., Feigl, V., Jarvis, A.P. and Gruiz, K. (2012). Ecotoxicity of fluvial sediments downstream of the Ajka red mud spill, Hungary. Journal of Environmental Monitoring, 14(8), 2063-2071.

Kossik, R., and Miller, I. (2004). A probabilistic total system approach to the simulation of complex environmental systems. In: Proceedings of the 2004 Winter Simulation Conference.

Lessard, F., Bussière, B., Côté, J., Benzaazoua, M., Boulanger-Martel, V. and Marcoux, L. (2018). Integrated environmental management of pyrrhotite tailings at Raglan Mine: Part 2 desulphurized tailings as cover material. Journal of cleaner production, 186, 883-893.

Mudd, G.M. (2007). Global trends in gold mining: Towards quantifying environmental and resource sustainability. Resources Policy, 32(1-2), 42-56.

Natali, M., Lidal, E. M., Parulek, J., Viola, I., and Patel, D. (2013). Modeling Terrains and Subsurface Geology. In Proceedings of Eurographics State of The Art – EG STAR (Girona, Spain, 2013), Eurographics Association, pp. 155–173.

Neculita, C.M., Zagury, G.J. and Kulnieks, V. (2010). Short-term and long-term bioreactors for acid mine drainage treatment. In: Proceedings of the 22nd Conference on Soils, Sed. and Water, Amherst, University of Massachusetts, MA, October 16–18, 2006.

Niederreiter, H. (1992). Random number generation and quasi-Monte Carlo methods. Philadelphia, PA: Society for Industrial and Applied Mathematics.

Paktunc, A. (1999). Mineralogical constraints on the determination of neutralization potential and prediction of acid mine drainage. Environmental Geology, 39(2), 103-112.

Parbhakar-Fox, A., Lottermoser, B. and Bradshaw, D. (2013). Evaluating waste rock mineralogy and microtexture during kinetic testing for improved acid rock drainage prediction. Minerals Engineering, 52, 111-124.

Plante, B., Bussière, B. and Benzaazoua, M. (2012). Static tests response on 5 Canadian hard rock mine tailings with low net acid-generating potentials. Journal of Geochemical Exploration, 114, 57-69.

Ravenelle, J.F. (2013). Amphibolite facies gold mineralization: an exemple from the Roberto deposit, Eleonore property, James Bay, Quebec. Ph.D. thesis, Université du Québec, Institut national de la recherche scientifique.

Remy, N., Boucher, A. and Wu, J. (2009). Applied geostatistics with SGeMS: A user's guide. Cambridge University Press, Cambridge.

Rizzo, D.M., Mouser, P.J., Whitney, D.H., Mark, C.D., Magarey, R.D. and Voinov, A.A. (2006). The comparison of four dynamic systems-based software packages: Translation and sensitivity analysis. Environmental Modeling & Software, 21(10), 1491-1502.

Ruxton, G.D. (2006). The unequal variance t-test is an underused alternative to Student's t-test and the Mann–Whitney U test. Behavioral Ecology, 17(4), 688-690.

Sun, W., Ling, M., Yang, X., Fan, W., Ding, X. and Liang, H. (2010). Ridge subduction and porphyry copper-gold mineralization: An overview. Science China Earth Sciences, 53(4), 475-484.

Vermette, D. (2018). Approche de caractérisation géoenvironnementale axée sur l'utilisation des concepts géométallurgiques. MSc thesis, Université du Québec en Abitibi-Témiscamingue, Rouyn-Noranda.

Weisener, C. and Weber, P. (2010). Preferential oxidation of pyrite as a function of morphology and relict texture. New Zealand Journal of Geology and Geophysics, 53(2-3), 167-176.

Wickland, B.E. and Wilson, G.W. (2005). Self-weight consolidation of mixtures of mine waste rock and tailings. Canadian Geotechnical Journal, 42(2), 327-339.

Wright, G.B. (2003). Radial basis function interpolation: numerical and analytical developments. Ph.D. thesis, University of Colorado, Boulder.

CHAPTER 5 ARTICLE 2: INCORPORATING KINETIC MODELING IN THE DEVELOPMENT STAGES OF HARD ROCK MINE PROJECTS

This article was published in *Minerals* in 2021[2].

5.1 Abstract

Weathering cell test, designed specifically to overcome material-limited constraints, yields prompt and efficient experimental assessment during the development stages of mining projects. However, it has barely benefited from geochemical modeling tools despite its ease of use. Accordingly, this paper aims to strengthen the upstream geochemical assessment via parametric analysis that simulates the effect of various mineral assemblages on leachate quality recovered from weathering cells. The main objective is to simulate the pH in presence of silicate neutralizing minerals and Mn release from carbonates based upon minimal characterization data. The public domain code PHREEQC was used for geochemical kinetic modeling of four weathering cells. The kinetic model utilized a water film concept to simulate diffusion of chemical elements from mineral surfaces to the pore water. The obtained results suggest that the presence of the silicate neutralizing minerals slightly affects the Mn release from carbonates. Furthermore, plagioclase could supply a significant neutralization potential when they predominate the mineral assemblage. Finally, coupling weathering cell test and parametric analyses illuminates the pH evolution for various mineral proportion scenarios.

Keywords: Kinetic modeling; Weathering cells; Parametric analysis

5.2 Introduction

Mining and quarrying activities produce substantial volumes of solid waste deposited in above-ground containment facilities, which receive up to 90% of the extracted ore (Mudd, 2007; Yilmaz, 2011). Based on the site-specific cut-off grade, the remnant lean grades and the final solid waste

---

[2] Toubri, Y., Vermette, D., Demers, I., Beier, N. and Benzaazoua, M. (2021). Incorporating Kinetic Modeling in the Development Stages of Hard Rock Mine Projects. *Minerals*, *11*(12), 1306.

from ore processing are categorized as waste rock and tailings respectively (Park *et al.*, 2019; Tabelin *et al.*, 2021). The sparse sulphide minerals in solid waste, previously sequestered in a reducing environment, are exposed to oxidizing conditions. Atmospheric oxygen and through-flowing water trigger oxidation of sulphides such as pyrite and pyrrhotite, resulting in potentially contaminated effluents. This naturally occurring phenomenon has aroused growing interest and is termed acid mine drainage (AMD) or contaminated neutral drainage (CND), depending on the neutralizing potential and the pH (Akcil and Koldas, 2006; Barfoud *et al.*, 2019; Blowes *et al.*, 2003; Evangelou and Zhang, 1995; Heikkinen *et al.*, 2009; Kleinmann *et al.*, 1981; Moses *et al.*, 1987; Nicholson *et al.*, 1988; Nicholson and Scharer, 1994; Nordstrom *et al.*, 2000; Nordstrom, 1982; Nordstrom and Alpers, 1999; Plante *et al.*, 2010; Singer and Stumm, 1970; Weisener and Weber, 2010; Wiersma and Rimstidt, 1984). Other sources of contamination in the mine framework are also present (Ho *et al.*, 2021; Tabelin *et al.*, 2018; Tamoto *et al.*, 2015). Sulphide oxidation and the subsequent effluent result in water quality exceedances in terms of metals and oxyanions concentrations as well as low pH in the case of AMD. Contaminated mine drainage is a worldwide ecological-security threat with the ability to toxify freshwaters and impair life forms and their support systems. Research endeavors adopted by governments, the mining industry, universities, and research establishments focus on assessment, prevention, and treatment of AMD and CND to safeguard ecosystems neighboring mine facilities (Aubertin *et al.*, 1997; Benzaazoua *et al.*, 2004; Benzaazoua *et al.*, 2008; Benzaazoua *et al.*, 2000; Bouzahzah *et al.*, 2014a; Bussière, 2007; Bussière *et al.*, 2007; Demers *et al.*, 2015; Demers *et al.*, 2008; Demers *et al.*, 2009; Demers *et al.*, 2017; Elghali *et al.*, 2018; Elghali *et al.*, 2019; Jouini *et al.*, 2020; Jouini *et al.*, 2019; Michaud *et al.*, 2017; Ouangrawa *et al.*, 2010; Parbhakar-Fox *et al.*, 2011; Plante *et al.*, 2014).

Forecasting water quality through simulations of coupled physical and geochemical processes using well-vetted programs is a worthwhile endeavor to set proactive measures (Nordstrom *et al.*, 2015; Tabelin *et al.*, 2017a, 2017b). Calibrated numerical models via laboratory and/or field tests that provide long-term predictions and/or parametric analysis of water quality have been used extensively to assess the geochemical behavior of mine solid waste as well as the performance of reclamation scenarios (Demers *et al.*, 2013; Fala *et al.*, 2003; Fala *et al.*, 2013; Kalonji-Kabambi *et al.*, 2020; Molson *et al.*, 2008; Molson *et al.*, 2005; Nicholson *et al.*, 2003; Pabst *et al.*, 2018; Pabst *et al.*, 2017). For instance, Wunderly *et al.* (1996) established the PYROX model to simulate

diffusion-controlled oxidation of pyrite. Romano *et al.* (2003) utilized PYROX to perform a comparative survey of different reclamation scenarios. Graupner *et al.* (2014) also investigated PYROX capabilities to predict mining impact on groundwater. Molson *et al.* (2005) assessed design strategies intended to minimize AMD from waste rock using HYDRUS and POLYMIN. Both codes were extensively used and investigated for a wide range of problems (Abbasi *et al.*, 2004; Fala *et al.*, 2003; Fala *et al.*, 2006; Fala *et al.*, 2013; Kandelous and Šimůnek, 2010; Molson *et al.*, 2005). In this respect, the MIN3P model has proven to be an effective and versatile numerical tool to simulate kinetically controlled and transport-controlled reactions (Brookfield *et al.*, 2006; Jurjovec *et al.*, 2004; Mayer *et al.*, 2012; Mayer *et al.*, 2002; Ouangrawa *et al.*, 2009). Kalonji-Kabambi *et al.* (2020) used the MIN3P model to simulate the geochemical behavior of uncovered and covered highly reactive tailings. Pabst *et al.* (2017) used MIN3P to evaluate the hydro-geochemical behavior of covered preoxidized tailings. Although they provide many benefits, most of the geochemical modeling case studies are carried out during the operation and closure stages of the mine life cycle as they tackle design strategies and the performance of reclamation scenarios. The development stage of a mining project has received very little benefit from geochemical modeling tools because of the lack of in situ waste materials and the data-intensive nature of the programs being used. A geochemical assessment during the upstream stages of a mining project provides a proactive way to identify environmental risks and mitigate them during operation and closure stages. Advanced exploration, preliminary economic assessment, and feasibility study stages are globally referred to as the upstream stages of a mining project, during which deposit definition and preliminary environmental and operational data are gathered. As the upstream stage benefits from specific kinetic testing and suited management approaches (Amar *et al.*, 2020; Bouzahzah, 2013; Cruz *et al.*, 2001; Toubri *et al.*, 2021; Villeneuve *et al.*, 2009), it should be further expanded through geochemical modeling tools.

This research is intended to underpin the geochemical assessment of solid waste through a numerical modeling method that complies with the upstream stage constraints. In this regard, simulations of weathering cell tests, performed during material-limited stages (exploration, feasibility stages), were used to forecast scenarios that may stem from various mineral assemblages. Conservative reasoning and worse case scenarios were adopted herein to (i) address shortcomings related to material availability, and (ii) avoid underestimations of the geochemical

response of solid waste. Adding a protective margin throughout the development stage is advisable to refine risk identification. This study aims to (i) simulate weathering cells designed specifically for the upstream stage, and (ii) introduce a straightforward geochemical screening tool that expands the geochemical assessment from the interpretation of experimental results to the parametric analysis throughout the development stage. PHREEQC is the modeling engine used for this study; it is a public domain code broadly used for speciation, batch-reaction, one-dimensional transport, and inverse geochemical calculation (Parkhurst and Appelo, 1999). However, it also encompasses other advanced capabilities such as solid solutions, surface complexation, and kinetics. PHREEQC was chosen mainly because of its flexible interface that allows the implementation of time-dependent equations that could be solved using integration routines incorporated in the program. Unlike many other public codes, PHREEQC enables coupling of kinetics and 1D transport. Moreover, a wide range of geochemical databases are included in PHREEQC. Nicholson *et al*. (2003) employed PHREEQC kinetics and 1D transport keyword blocks to simulate metal leaching from acid-generating waste rock at a uranium mine. Labus and Grmela (2006) set up 1D kinetic-based model in PHREEQC to simulate pyrite oxidation within coal waste piles. Similarly, Embile Jr *et al*. (2019) introduced locally measured dissolution rates of pyrrhotite and forsterite in PHREEQC to simulate long-term kinetic tests of a milling waste. Likewise, PHREEQC was utilized in the present study to simulate kinetically controlled reactions; unlike the aforementioned examples, this study involves a multi-mineral composition in the kinetics keyword block.

The Akasaba West mining project was selected for this modeling study because it is in the early development stages. Vermette (2018) developed a staged geo-environmental protocol for the Akasaba West project based on static and weathering cell tests as well as mineralogy using materials from drill core surveys. Those findings recommended mine waste classification into geo-environmental domains in order to prevent future environmental liabilities (Vermette, 2018). A geo-environmental domain includes lithologies with nearly the same geochemical behavior. This research focuses first on the assessment of the geochemical behavior of each suggested geo-environmental domain based on the classification as well as the overall lithological units mixed. Secondly, simulation of the experimental results using PHREEQC is presented in order to perform parametric analyses. The expected outcome is to supply mine managers with a straightforward

screening method complying with data-limited and material-restricted situations to effectively simulate the pH of kinetically controlled reactions along the development stage of a mine life cycle.

5.3 Materials and methods

5.3.1 Geological background

Agnico Eagle Ltd. owns the Akasaba West Au-Cu deposit located in the Abitibi-Témiscamingue region, approximately 15 km east of Val d'Or in Quebec, Canada. The geological field of Akasaba West site belongs to Héva Formation of the Louvicourt District, consisting of volcanic and volcanoclastic rocks (Vermette, 2018). The volcanism event is mainly expressed by the presence of basalt, dacite, and quartz-feldspar bearing porphyry rocks. Dyke and sill swarms crosscut volcanic and volcanoclastic outcrops (Vermette, 2018). Low pressure-low temperature metamorphic events resulted in low-grade greenschist facies. Exploration investigations in this region resulted in the discovery of a gold-copper deposit. The mineralization style consists of thinly disseminated sulphides hosted in moderately to strongly altered basalt, andesite, volcanoclastic dacite, and trachyandesite (Vermette, 2018). Geological descriptions from diamond drill core characterization suggest that the ore is characterized by < 5% pyrite occurring as disseminations and locally as clusters, veinlets, or thin massive sulphide lenses. The Akasaba West Au-Cu deposit will yield 5.12 Mt of ore containing 0.87 ppm Au and 0.49% Cu. Up to 7.62 Mt of waste rock will be stored in above-ground facilities.

5.3.2 Samples preparation and characterization

Prior to this study, materials from drill core surveys underwent interval sampling of 3 m. Afterwards, Vermette (2018) led a staged geo-environmental protocol and identified seven lithogeochemical units spanning the extent of the future open pit. Throughout the protocol, a selection process of samples was set up according to geometallurgical directives. The final stage of the selection process provided 86 samples allocated to seven litho-geochemical units (known as geometallurgical units). The number of samples per unit was dictated by the lithology prevalence in drill cores logging. Static and kinetic tests as well as mineralogical characterization were undertaken to classify the litho-geochemical units into a set of units with nearly the same

geochemical behavior; named geo-environmental domains. Accordingly, Vermette (2018) proposed a waste disposal plan based on mine waste sorting into three geo-environmental domains (mafic domain, dacite domain, and intermediate domain). This classification was determined from the individual geochemical assessment of each litho-geochemical unit. In the present study, a composite sample from each geo-environmental domain was prepared to assess the aforementioned disposal scenario. Furthermore, a fourth composite sample encompassing all units was evaluated to compare sorted and unsorted materials and to gain insights about the geochemical behavior of the solid in the case of mixed disposal. The blending proportions originated from the number of samples that represent each lithology. Blending and homogenization were accomplished under dry conditions. Figure 5.1 displays the blending proportions for each composite sample.

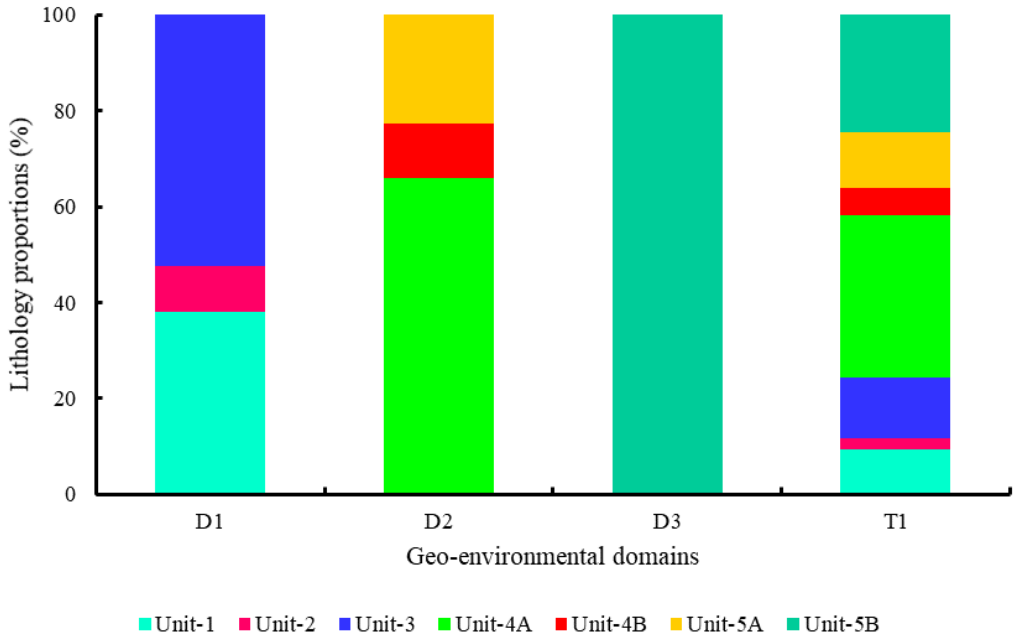


Figure 5.1 Blend samples prepared to assess geochemical interactions among lithological units within geo-environmental domains (the size of the boxes represent blending proportions)*.

*D1. the mafic domain, D2. the dacite domain, D3. the intermediate domain, T1. the all-embracing domain, Unit-1. andesitic basalt unit, Unit-2. Fe-Ti rich basalt, Unit-3. andesite, Unit-4A. dacite, dacitic tuff, dacitic intrusions, and quartz-feldspar porphyry type 1, Unit-4B. alkaline andesite and alkaline andesitic tuff, Unit-5A. dacite, dacitic tuff, dacitic intrusions, and quartz-feldspar porphyry type 2, Unit-5B. alkaline andesite and alkaline andesitic tuffs.

In previous works, kinetic assessment was undertaken on 11 ground drill core samples from Akasaba West with D_{50} ranging from 370 to 560 µm; all leachates maintained neutral to slightly alkaline pH values (Vermette, 2018). In the present study, the drill core samples were ground to less than 100 µm to deliberately expose thinly disseminated sulphides to favor optimal reaction conditions with the chosen kinetic test apparatus (Amar *et al*., 2021; Elghali *et al*., 2019).

The specific gravity (G_s) of the homogenized composite samples was measured with a Micromeritics Helium Pycnometer (Quantachrome corporation, Unité de Recherche et de Service en Technologie Minérale URSTM, Rouyn-Noranda, Canada). The specific surface area (S_s) was determined with a Micromeritics surface area analyzer (Quantachrome corporation, URSTM, Rouyn-Noranda, Canada) using the BET (Brunauer, Emmett et Teller) method (Brunauer *et al*., 1938). The geometric surface area (S_{Geo}) was calculated using the method of Chapuis and Aubertin (2003) to compute the roughness factor. The grain size distribution was gauged using a Malvern Mastersizer laser particle size analyzer (Malvern instruments Ltd, URSTM, Rouyn-Noranda, Canada). Chemical analyses were conducted using acid digestion (HNO_3-Br_2-HF-HCl) followed by ICP-AES (inductively coupled plasma-atomic emission spectrometry, PerkinElmer, URSTM, Rouyn-Noranda, Canada) analysis of the digests using a PerkinElmer OPTIMA 3100 RL. An ELTRA CS-2000 induction furnace coupled with an infrared analyzer (ELTRA Elemental Analyzers, URSTM, Rouyn-Noranda, Canada) for carbon dioxide and sulphur dioxide detection analyzed the sulphur (S_{total}) and inorganic carbon (C_{total}) contents. The C_{total} was determined after calcination of the solids for 16 h at 375 °C in a muffle furnace (Nabertherm HTCT 01/16) and then combustion in the induction furnace at 1360 °C. S_{total} is expected to correspond to sulphide sulphur given the fresh state of the solids preserved in dry conditions before handling.

The acid–base accounting (ABA) was conducted following the protocol described by Lawrence and Lawrence and Wang (1997) and modified by Bouzahzah *et al*. (2015). Lawrence and Wang (1997) modified the method of Sobek (1978) to determine the neutralization potential (NP) by adding HCl followed by back titration to an endpoint pH of 8.3 at ambient temperature. The NP was quantified after one week of acid digestion to stimulate low-reactive neutralizing minerals as suggested by Bouzahzah *et al.* (2015). The NP was also estimated based on the C_{total} content as shown in equation (5.1) assuming that C_{total} stems from carbonates (CNP) (Bouzahzah *et al*., 2014b). Similarly, the acidic potential (AP) was calculated by assuming that all the sulphide

sulphur belongs to pyrite that will oxidize and generate acidity, as expressed by equation (5.2) (Bouzahzah *et al.*, 2014b).

Thereafter, the net neutralization potential (NNP in kg $CaCO_3$/t; NNP = NP−AP) and the NP/AP ratio were computed for interpretation. CNP denotes carbonate-neutralizing potential in kg $CaCO_3$/t and AP is the acidic potential (kg $CaCO_3$/t).

$$CNP = 83.33 \times \%C_{total} \qquad 5.1$$

$$AP = 31.25 \times \%S_{total} \qquad 5.2$$

The mineralogical composition was investigated using an X-ray diffractometer (XRD; Bruker AXS D8 ADVANCE, URSTM, Rouyn-Noranda, Canada). The XRD analyses were conducted on dried and micronized samples at room temperature. Bruker AXS equipment as well as EVA and TOPAS software packages interacted throughout the data compilation to yield mineralogical identification and semiquantification based on reconciliation with chemical results, allowing a detection limit of less than 1 wt.%. The mineralogical composition and quantification were refined using a scanning electron microscope (SEM) equipped with energy dispersive X-ray spectroscopy probe (EDS; HITACHI S-3500N, detection limit around 1000 ppm, HITACHI High-Tech, URSTM, Rouyn-Noranda, Canada). The aforementioned geological setting and previous surveys from Vermette (2018) stressed that the future mine wastes from the Akasaba West open pit are expected to contain low weight proportion of calcite. Therefore, the mineralogical scrutiny with SEM-EDS had a particular focus on identifying and quantifying silicate and sulphide minerals, as they are the foremost source of neutralization and acid generation, respectively. The SEM-EDS analyses covered a range of 210–266 probed points distributed over 8 or 9 different bands on each polished section.

5.3.3 Weathering cell test

A weathering cell is a miniature version of a humidity cell. It consists of a leaching device that enables reaction rates comparable to those of humidity cells (Cruz *et al.*, 2001). However, weathering cells are slightly more aggressive than humidity cells (Bouzahzah *et al.*, 2014a; Villeneuve, 2004). Plante *et al.* (2014) reported a liquid to solid ratio for weathering cells that ranges from 5000 to 10,000 L/m^3/week versus 2000 L/m^3/week for humidity cells. The weathering cell concept was first developed by Cruz *et al.* (2001) to assess pyrite oxidation by leaching 20 g

of pyrite with 15 mL of leaching solution. Thereafter, the test was adjusted by increasing the sample mass to 67 g and maintaining the same liquid to solid ratio used by Cruz *et al*. (2001) (Bouzahzah *et al*., 2014a; Bouzahzah *et al*., 2014b; Plante *et al*., 2011). Weathering cell testing is a cost-effective method largely used during the upstream geochemical assessment for its ease of implementation and limited manipulation requirements; more importantly, weathering cells cope with material-restrained situations. Moreover, Jouini *et al*. (2019) and Park *et al*. (2020) demonstrated the effectiveness of weathering cell tests even for downstream framework. In this respect, weathering cells were selected to elucidate the differences between the mixed scenario and the geo-environmental domains partitioning.

Four weathering cells were implemented: D1, D2, D3, and T1. These samples encompass the mafic domain, the dacite domain, the intermediate domain, and the three mixed domains, respectively. The leaching device was a Buchner funnel measuring 100 mm in diameter and containing 67 g of sample (dry mass). The sample was placed upon two nylon membrane filters (Whatman 0.45 μm) that were sealed with silica grease along their circumference. The filters prevent the loss of fine-grained particles that could escape through Buchner perforations during the flushes. The silica grease hinders undesirable seepage and enables water retention inside the Buchner funnel. A 250 mL receiving flask was placed under each funnel to recover the filtrate (see supplementary materials). Each sample was flushed with 50 mL of deionized water on the first day, followed by two days of exposure to the ambient air. On the fourth day, samples were flushed again with the same volume of the leach solution and exposed to the ambient air for the rest of the seven-day leaching cycle. The leachates were recovered after 4 ± 0.5 h of retention by applying suction (with a vacuum pump) on the filtering flask. The obtained solutions were weighed and analyzed for electrical conductivity, Eh, and pH. The filtrates obtained using a 0.45 μm nylon filter (Whatman) were analyzed for the main dissolved elements. To ensure sample preservation, the filtrates were acidified to 2% HNO3 prior to ICP-AES chemical analysis.

5.3.4 The conceptual model

Weathering cell tests provide a highly oxidizing environment where atmospheric oxygen and water are not transport-limited throughout the test duration. Therefore, the effluent quality stems mainly from the inherent mineral reactivity and the available reactive surfaces. Oxidation and dissolution

reactions under such conditions are kinetically controlled (not thermodynamically controlled). The conceptual model relies on oxidation and dissolution rates of the sulphides and the gangue minerals, respectively. In accordance with the mineralogical characterization results, a kinetic reactivity rate for each mineral was selected from the literature based upon experimental conditions. The incoming leach solution as well as the pore water of the system were considered to be in equilibrium with oxygen and carbon dioxide. These equilibrium reactions allowed no restriction in oxygen supply; thus, gas transport problems were precluded, which is in line with PHREEQC limitations (Parkhurst and Appelo, 1999). This equilibrium component allowed the modeling of kinetically controlled reactions (Eary and Williamson, 2006; Salmon, 2003). Transport processes were embedded along the 1D discretized length of the system. The advective transport was intended to simulate leach solution advection as a function of the residence time and volumetric flow. The residence time would relate kinetic reactions to advective transport in order to control the time span of the water–rock interactions. The diffusive transport herein considers diffusion of dissolved species from the particle surfaces to the pore water. In this regard, the conceptual model assumed that a thin water film surrounded the particle surfaces, that kinetic reactions occurred within the water film, and that the products that were subsequently released were transferred to the bulk solution through a diffusion boundary. An oxygen reservoir was implemented within the water film to trigger and maintain sulphide oxidation (Figure 5.2). This modeling approach assumed that weathering rate laws for monomineralic samples can be utilized for mixtures of minerals (pyrite, carbonates, and silicates) evenly distributed over the uniform sample size distribution obtained after grinding (Eary and Williamson, 2006; Salmon, 2003). Opting for specific rates from literature aimed to (i) assess their reliability for a mixture of minerals and their relevance for the weathering cell test, and (ii) provide prompt scoping surveys during data-limited situations.

Plante (2010) stressed that weathering cells are less prone to precipitation of secondary phases due to the high liquid to solid ratio as well as the thickness of the solid bed sample. Furthermore, previous kinetic testing undertaken by Vermette (2018) reported low ionic strength and negative saturation indices throughout the geochemical assessment of the separate lithologies. Accordingly,

the conceptual model precluded any retention process. This assumption abides by the conservative reasoning adopted herein to avoid underestimation of the contamination potential.

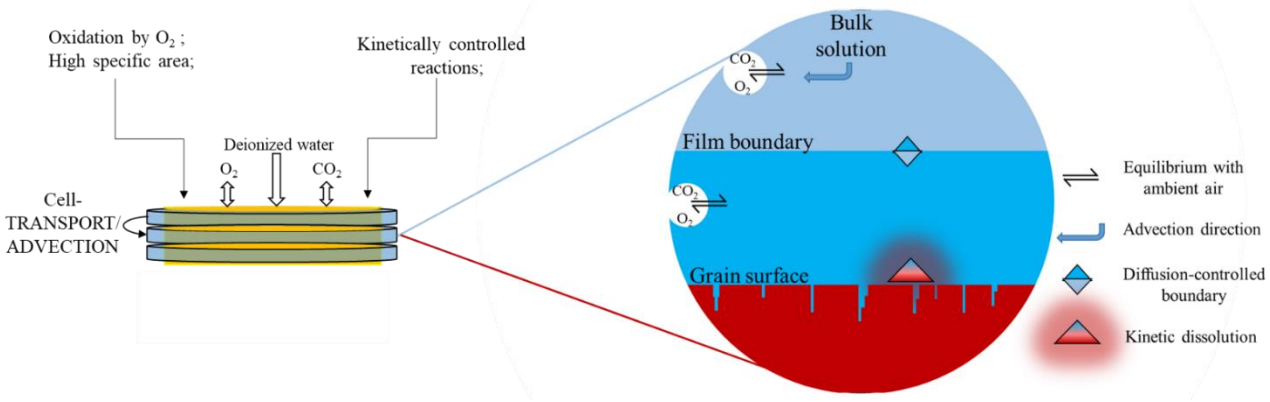


Figure 5.2 The conceptual model of the weathering cell tests

5.3.4.1 Abiotic kinetic rates

Pyrite is ubiquitous in Akasaba West ore and its host rock, representing a potential source of AMD. Pyrite was detected in all geo-environmental domains (Vermette, 2018). The specific rate of pyrite oxidation determined by Jerz and Rimstidt (2004) was chosen for the present study:

$$r_k = \frac{10^{-6.6} p^{0.5}}{t^{0.5}} \qquad 5.3$$

Where p is the partial pressure of oxygen (atm) and t is time (s). Two main reasons warranted the use of the aforementioned specific rate in this study: (i) Jerz and Rimstidt (2004) established the specific rate formula for pyrite oxidation in unsaturated medium, which is in line with the experimental approach herein. In addition to the open system approach, using a specific rate of pyrite oxidation under unsaturated conditions will aid to overcome PHREEQC limitations. (ii) The specific rate from Jerz and Rimstidt (2004) considers pyrite aging attributed to the formation of a solution film on pyrite surfaces as oxidation progresses. Including the aging effect on pyrite reactivity is relevant for the actual framework as kinetic tests are usually undertaken for a considerable time span. It is worth mentioning that the aforementioned specific rate delineates direct oxidation of pyrite that is relevant for fresh samples under kinetic testing.

The gangue minerals consisted mostly of silicates and minimal crystals of calcite (Table 5.1). To simulate gangue mineral dissolution in the KINETICS keyword block of PHREEQC the generic form of the rate expressions developed by Chou and Wollast (1985) and Casey and Ludwig (1995)

and adopted by Palandri and Kharaka (2004) was implemented for each gangue mineral (see supplementary materials). Minteq.v4 database of PHREEQC was used; it includes the speciation of all the chemical elements involved in the model.

Table 5.1 List of dissolution rate parameters used in this study to kinetically simulate the neutralization potential under a wide range of pH

Mineral	Acidic Mechanism			Neutral Mechanism		Alkaline Mechanism		
	log k	E	n	log k	E	log k	E	n
K-feldspar*	−10.06	51.7	0.5	−12.41	38	−21.2	94.1	−0.823[a]
Oligoclase*	−9.67	65	0.457	−11.84	69.8	--	--	--
Andesine*	−8.88	53.5	0.541	−11.47	57.4	--	--	--
Anorthite*	−3.5	16.6	1.411	−9.12	17.8	--	--	--
Augite*	−6.82	78	0.7	−11.97	78	--	--	--
Epidote*	−10.6	71.1	0.338	−11.99	70.7	−17.33	79.1	−0.556[a]
Calcite*	−0.3	14.4	1	−5.81	23.5	−3.48	35.4	1[b]
Tremolite*	−8.4	18.9	0.7	−10.6	94.4	--	--	--
Albite[d]**	−10.07	58	0.34	−19.29	57	−9.85	56	0.32[c]
Muscovite***	−2.5	44	0.8	−5.04	45	−0.3	61	0.6[c]
Chlorite****	−4	30	0.74	−10.32	13	−8.82	15	0.43[c]

*Palandri and Kharaka (2004), **Marty *et al.* (2015), ***Lammers *et al.* (2017), ****Smith and Carroll (2016).

[a] Reaction order with respect to H+ activity.

[b] Reaction order with respect to CO_2 partial pressure, it is a carbonate mechanism.

[c] Reaction order with respect to OH^- activity.

[d] For albite $p_1 = 0.48$ and $q_1 = 100$ (Marty *et al.*, 2015).

k: the rate constant in $mol.m^{-2}.s^{-1}$, E: the activation energy in kJ/mol, n: the reaction order, --: Not available.

5.3.4.2 Diffusive transport

Diffusion from the water film to the bulk solution along the sample height was simulated using diffusive transport in the TRANSPORT data block using a single diffusion coefficient for all chemical species (Parkhurst and Appelo, 2013). Parkhurst and Appelo (1999) included dual porosity modeling in the TRANSPORT data block to simulate diffusion between closed and interconnected porosity (named immobile and mobile cells in PHREEQC). Tiruta-Barna (2008) repurposed the Stagnant_cells modeling capability of the TRANSPORT data block for diffusion simulation in dynamic leaching tests. The same repurposing reasoning was suggested herein to bridge kinetics and transport. Regarding the drying wetting/cycles, the advection time step was at

2.5 days, which constitutes the drying period. During this period, the water retained by capillarity is reacting with minerals using immobile cell capability of PHREEQC. The Stagnant_cells capability of PHREEQC links immobile and mobile cells via diffusion. Therefore, chemical products emanating from kinetic reactions that occurred in the immobile cell were transported via diffusion to mobile cells. Based upon various discretization tests ranging from 5 to 100 cells, 30 diffusion-linked cells was determined to be an optimal 1D discretization where the first mobile cell is a transfer cell mediating kinetics and diffusive transport. The longitudinal dispersivity was estimated using equation 5.4 from Neuman (1990), then PHREEQC internally computed the hydrodynamic dispersion coefficient D_L to perform calculations of the diffusion term.

$$\alpha_L = 0.0175L^{1.46} \qquad 5.4$$

Where L is the sample height (m).

5.3.5 Calibration and parameter fitting

Model calibration was carried out by matching the model results to kinetic testing data from the D2 weathering cell. The D1, D3, and T1 weathering cells were used as benchmarking cases. The main calibration parameters used to fit the experimental results were the reactive surface area and the effective diffusion coefficient (D_e) between the film and the pore water. D_e refers to the rate of transfer of chemicals between the film and the pore water. D_e is the key fitting parameter when a conceptual model considers the water film concept. The capability of stagnant zones in PHREEQC enables D_e implementation as input. Furthermore, Mn was included in the system as a trace element in calcite according to previous work (Vermette, 2018). It is considered in this study because it could constitute an element of concern. The parameter used to calibrate Mn release was the stoichiometric coefficient of Mn within calcite. To perform the stoichiometric coefficient calibration, the fitting operation was undertaken using PHREEPLOT. The non-linear least squares (nlls) method was used in PHREEPLOT. The fineness of the fit was assessed based upon the weighted sum of the residuals (Kinniburgh and Cooper, 2011). The outcome was used to perform a parametric analysis to scope Mn leaching scenarios and highlight conditions under which CND or even AMD prevails.

5.4 Results and discussion

5.4.1 Experimental datasets

5.4.1.1 Characterization results

Characterization results are summarized in Tables 5.2 and 5.3 and Figures 5.3 and 5.4. The grain-size distribution of the composite samples is typical of the grain size of non-segregated tailings, compiled and classified by Bussière (2007) as sandy silts of low plasticity (ML). Specific gravity (G_s) values were subject to slight variations owing to high-density mineral content such as titanite, magnetite, and pyrite (Table 5.2). Likewise, the specific surface area (S_s) was affected by the presence of some phyllosilicates well known for their high specific surface (Benzaazoua *et al*., 2004). Roughness factors (the ratio between the specific surface area and the geometric area) computed based on geometric specific surface areas were 2.7, 4.24, 3.5, and 3.66 for D1, D2, D3, and T1, respectively.

The Al content confirmed that the samples were rich in aluminosilicates. The Fe content mainly originated from iron oxides such as magnetite, while iron-bearing sulphides provided a small contribution to the total iron grade as indicated by the sulfur content (S_{total}). As no graphite was associated with the Akasaba West deposit, the inorganic carbon content (C_{total}) ascertained that all composite samples were carbonate-poor materials with barely significant differences. However, SEM-EDS investigations highlighted that calcite contains traces of Mn within its crystalline lattice. Calcium exhibited high grades ascribed to epidote that pertains to the greenschist facies mineral assemblage. Figure 5.4 emphasizes the felsic composition of the Akasaba West host rock with albite contents predominating the mineral assemblage.

Regarding ABA, the NP after one week of acid digestion was twofold higher than the CNP and the NP measured after 24 h of acid digestion. Therefore, sufficient time was needed for slow-reacting silicates to neutralize acidity and shift samples from the uncertainty zone to the non-acid generating zone (Figure 5.3). Nonetheless, kinetic testing is required to investigate the reliability of the neutralization potential of the silicates and to quantify the prerequisite lag time to neutralize the sample inherent acidity produced during leaching cycles.

Table 5.2 Physical properties of composite samples

The composite samples	G_s	S_s (m^2/g)	D_{10} (μm)	D_{50} (μm)	D_{90} (μm)
D1	2.95	1.46	2	12	56
D2	2.73	2.03	2.4	12	47.1
D3	2.69	1.77	2.28	11.85	46.2
T1	2.77	1.82	2.3	11.8	48.5

G_s: the specific gravity; S_s: the specific surface area; D_x: the grain size such that x% of the particles mass is made of grains finer than the diameter D_x.

Table 5.3 Chemical analysis of the composite samples

The composite samples	Mass fraction (wt%)									
	C_{total}	Al	Ca	Cu	Fe	K	Mg	Mn	Na	S_{total}
D1	0.36	9.4	9.09	0.04	8.1	1.1	1.9	0.06	1.78	0.23
D2	0.25	8.97	2.07	0.13	4.5	1.5	1.4	0.03	2.78	0.45
D3	0.37	13.5	2.34	0.02	3	0.9	0.75	0.02	3.46	0.56
T1	0.3	9.08	3.29	0.08	3.8	1.2	1.36	0.03	2.66	0.43

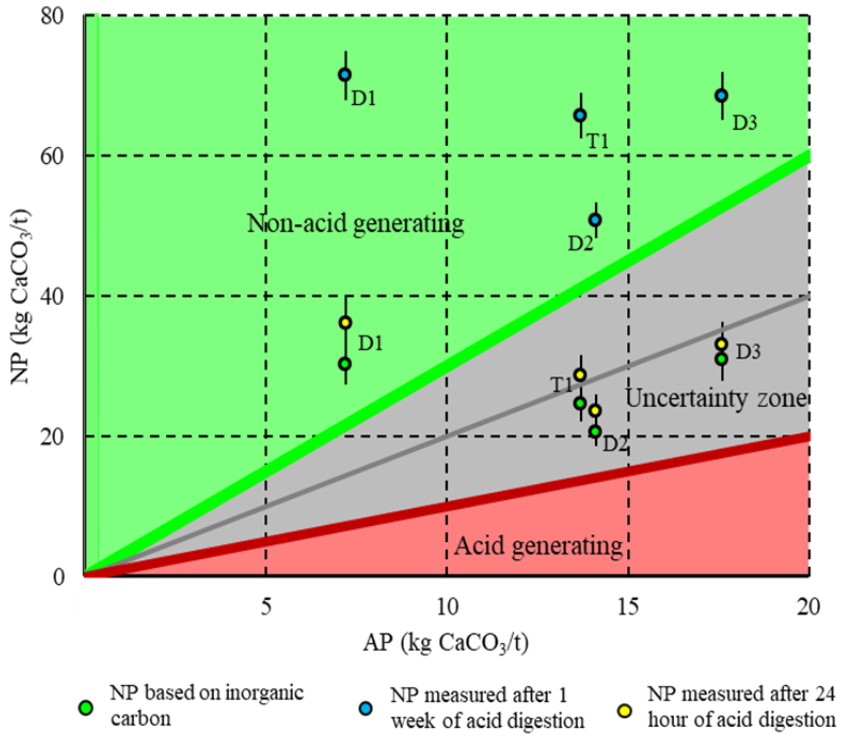


Figure 5.4 Acid–base accounting classification based on the neutralization potential ratio

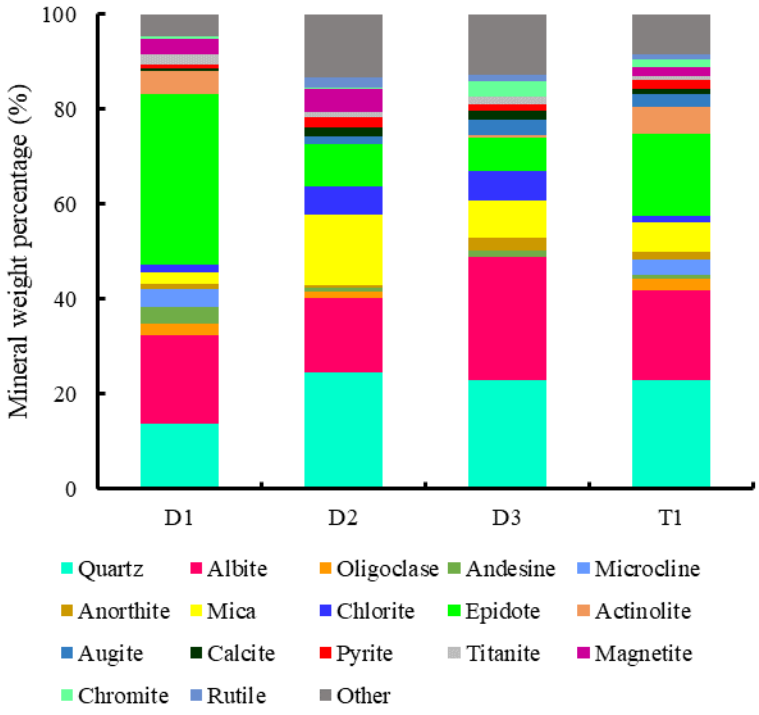


Figure 5.3 Mineralogical composition of composite samples

5.4.1.2 Weathering cells results

For modeling purposes, the accuracy of the chemical analysis was assessed to discern experimental uncertainties through the comparison of calculated and measured electrical conductivity as suggested by Appelo and Postma (2004). The calculated electrical conductivity was based upon measured molarity and molar conductivity in water at 25°C reported in the literature for each major ion (Appelo and Postma, 2004). The correlation coefficients between the calculated and the measured electrical conductivity ranged from 0.9 to 0.98 and the highest root mean square deviation (RMSD) was 10.36% (see supplementary materials). RMSD values provide some insights into experimental uncertainties related to equipment and/or manipulations. These uncertainties should be maintained as low as possible before delving into modeling. In the present study, the RMSD values were considered low enough for model calibration purposes.

The electrical conductivity was as high as 1.5 mS/cm during the first leaching cycle and progressively decreased towards the end of the kinetic tests (189 days). This could be interpreted as a decrease in metal release. Neutral to slightly alkaline pH values were maintained throughout the duration of the test for the D1, D3, and T1 weathering cells (Figures 5.6, 5.7 and 5.8). Meanwhile, the D2 weathering cell released acidic leachates during the first 14 days of the test; the pH ranged between 3.8 and 3.9 (Figure 5.5). Subsequently, the pH gradually increased to 8 by the 26th day. Sulfate concentrations SO_4^{2-} measured in the leachate from D2 started at 447 mg/L and gradually decreased to 6 mg/L after 100 days. Likewise, the Fe concentration in the D2 leachate reached 3.74 mg/L and decreased to the detection limit after 40 days (Figure 5.5). Sulfate concentrations in the D1, D3, and T1 leachates started at 100.2, 167.1, and 303 mg/L, respectively, and exhibited the same tendency as D2. Despite the content of iron-bearing sulphides in D1 and D3, Fe was below the detection limit in the leachates or sporadically released over the course of few leaching cycles. Leachates from all weathering cells displayed sporadic Cu release with low concentrations ranging from 0.003 to 0.09 mg/L. Manganese exhibited a distinctive evolution, with concentrations in the D2 leachate decreasing from 0.2 to 0.01 mg/L after 100 days; thereafter, it gradually increased to 0.045 mg/L by the end of the test (Figure 5.5). The same Mn evolution was observed in the other weathering cells, though with lower concentrations at the beginning of the test and a more abrupt increase beyond the 100th day.

At the weathering cell scale, the classification scenario showed no substantial benefits in terms of water quality. Kinetic testing results suggest that the four weathering cells contain a sufficient proportion of neutralizing minerals to prevent AMD prevalence. Nonetheless, the risk of Mn contaminated neutral drainage is conspicuous in the four weathering cells, though at variable magnitudes. The D2 weathering cell released the highest Mn concentrations; as it shifted from AMD to CND, the acidic conditions accelerated the dissolution of Mn-bearing calcite. Even though the observed concentrations did not exceed 1 mg/L, which would threaten freshwater organisms according to World Health Organization (WHO) (Le Bourre *et al.*, 2020), Mn should be carefully monitored throughout the Akasaba West lifetime. Furthermore, the assessment of the classification scenario should be undertaken at larger experimental scales during the upstream stages of the operation phase to confirm the laboratory test results.

5.4.2 Modeling results

Kinetic testing results from the D2 weathering cell were chosen to perform model calibration because the D2 sample exhibited the highest roughness factor that could underline the model sensitivity to S_{Geo} versus S_s. More importantly, the D2 weathering cell illustrates a transition from AMD to CND. The remaining weathering cells were used as benchmarking cases to highlight the model reliability and limitations.

5.4.2.1 Model calibration

Figure 5.5 compiles the D2 kinetic modeling and testing results. Generally, a good agreement between the kinetic test data and the PHREEQC model was obtained using $D_e = 8.10^{-11}$ m^2/s for chemicals diffusing from the grain surface to the bulk solution. The obtained value of D_e within the water film was roughly one order of magnitude lower than the diffusion of ions in free water. Furthermore, differences between S_s model and S_{Geo} model were scarcely significant. The calibration effort was focused on the specific surface area of albite to alleviate the Na-related discrepancy. Although the BET-based surface area of albite was reduced from 5.31 to 2 m^2/dm^3, the Na-S_s model was still prone to deviation from experimental results as time progressed (Figure 5.5). The Na-related discrepancy was substantially decreased using the albite geometric-based surface area (1.63 m^2/dm^3) (Figure 5.5).

Three main controlling factors could elucidate the Na discrepancy:

- The active surface area of albite was at least fourfold smaller than the BET-based surface area, suggesting relatively low concentrations of Na compared to the model; however, there was no noteworthy deviation of modeled Na from the experimental results at acidic to neutral pH values (before day 50).
- The albite rate used in PHREEQC under subalkaline conditions (after day 50) expedited albite dissolution, thus yielding a high Na release rate compared to the kinetic test outcomes.
- The release rate of Na was substantially slower than the dissolution rate of albite; nevertheless, plagioclase dissolution has been known to entail preferential release of Na-Ca resulting in a Na-Ca poor thin layer at the plagioclase surface (Plante, 2010). Therefore, the aforementioned factor is precluded, and the first two controlling factors may have occurred jointly to explain the geochemical behavior of Na.

Neither S_s model nor S_{Geo} model captured the increase in Mg concentration between the 10th and 50th day of the test. The calibration effort based upon specific surface areas and molar contents of the identified Mg-bearing minerals failed to improve the fit to the Mg experimental data. Presumably, a Mg-bearing mineral was not detected among the mineral phases or preferential release of Mg occurred at the surface of the Mg-bearing minerals. In contrast, the K, Al, and Ca modeling results provide a good fit to the kinetic test data (Figure 5.5).

The nlls method of PHREEPLOT yielded a good fit of the Mn experimental data when using a stoichiometric coefficient of Mn that ranged between 0.00039 and 0.0015 for 1 mole of calcite. For instance, using a stoichiometric coefficient of 0.0006, D2 PHREEPLOT fitting yielded a correlation coefficient of 0.84 between kinetic data and model results and an RMSD of 0.014. Mn lixiviation is directly related to the carbon dioxide (CO_2) partial pressure and pH that steer the calcite dissolution rate. The effect of CO_2 partial pressure during the kinetic test was assumed to be constant and proportional to the atmospheric pressure; however, we expect that a setting with biotic activity and/or organic matter degradation could increase Mn lixiviation due to an increase in CO_2 partial pressure within medium pores.

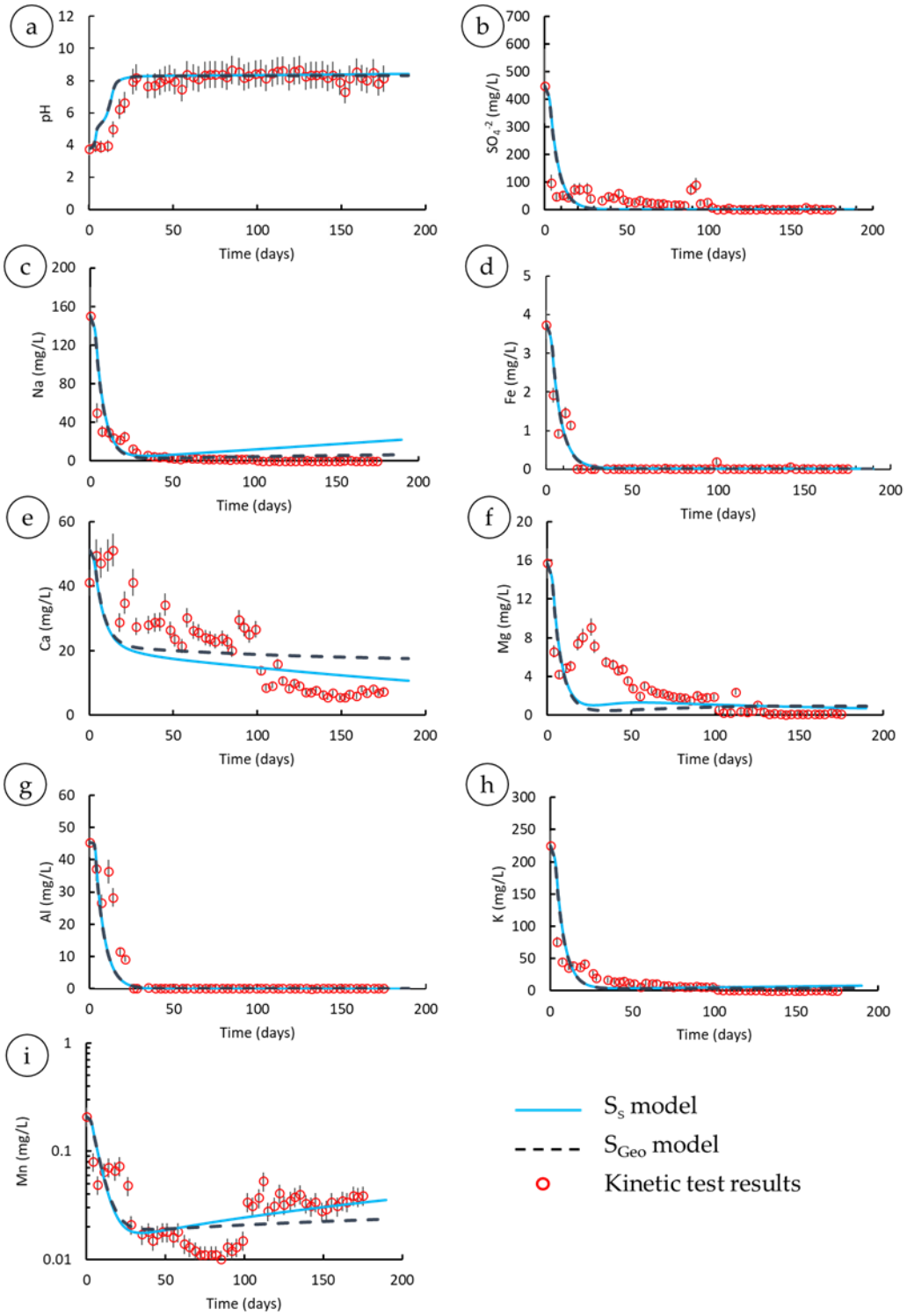


Figure 5.5 Weathering cell test D2 and PHREEQC modeling results using BET and geometric surface area-derived rates. (a) Experimental and simulated results of the pH. (b) sulfate. (c) sodium. (d) iron. (e) calcium. (f) magnesium. (g) aluminum. (h) potassium. (i) manganese.

The weathering cell setting displays the effect of sulphide oxidation on Mn lixiviation (Figure 5.5); throughout the first 50 days of the test, the Mn concentration dropped as pH values increase because calcite dissolution slowed at neutral and subalkaline conditions. This period reflects the delay needed for preponderant albite (15.6% wt) and disseminated calcite (1–1.8%) to fully neutralize acidity emanating mainly from 4.5% wt of pyrite. After the 50th day any produced acidity was promptly counteracted, thereby maintaining a relatively high pH and a low dissolution rate of calcite, thus reducing the extent of Mn lixiviation. The effect of pyrite content on Mn lixiviation will be further probed in the following sections.

5.4.2.2 Model benchmarking

(i) D1 weathering cell

Based on the calibration insights, the kinetic modeling approach was carried out to simulate the D1, D3, and T1 kinetic testing results as benchmarking proxies to delineate the reliability and limitations of the model. Figure 5.6 portrays testing and modeling results for the D1 weathering cell. With a higher plagioclase content (25.8% wt) and lower pyrite grade (0.8% wt) compared to the D2 mineral assemblage (18.2% wt plagioclase versus 4.5% wt pyrite), measured and simulated leachate pH values oscillated between 7 and 8 throughout the test duration. The mineral assemblage of D1 hindered neutralization delay and maintained neutral to subalkaline conditions throughout the full test duration. Therefore, abiding by these mineralogical proportions, silicate neutralizing minerals are deemed reliable to prevent acid generation.

On the first day, the simulated pH curve underwent a slight drop, reflecting pore water equilibrium with atmospheric CO_2, and promptly increased to 8 after seven days. This behavior is regarded as an artifact of the model as the first leachate results were used as the initial pore water composition, which was in equilibrium with atmospheric O_2 and CO_2 throughout the simulation. However, the simulated pH curve displays a good agreement with the experimental results.

The experimental sulfate concentrations indicated that the oxidation-neutralization process mainly occurred during the first 100 days of the test. The simulated SO_4^{2-} curve underestimated sulfate concentrations between the 20th and the 50th day. Nonetheless, the general trend was correlative with the experimental data. At odds with SO_4^{2-}, Fe was sporadically released or below the detection limit, thereby contradicting the oxidation implications. A geochemical retention mechanism of Fe

was suspected to occur; this mechanism will be ascertained based upon modeling results from weathering cells with a higher pyrite content (D3 and T1).

Simulated Ca and Na concentrations conformed to the testing results displaying tolerable differences. In contrast, the Mg and K modeling results exhibited only modest agreement with the testing data. The simulated Al curve roughly followed the experimental data trend (Figure 5.6). The experimental Al concentrations from the D1 weathering cell were noticeably lower than those from the D2 weathering cell indicating that the aluminosilicate dissolution rate was considerably decreased under subalkaline conditions. Nonetheless, the Na concentrations were only twofold lower than the D2 results; this probably suggests preferential release of Na over Al from plagioclase surfaces. In this respect, Hellmann 1995 demonstrated preferential release of Na with respect to Al and Si from albite leached layers over a wide range of pH values and temperatures. Accordingly, the Na-depleted leached layers are 1500 and 1200 Å thick at acid and basic pH conditions, respectively (Hellmann, 1995).

Simulated Mn concentrations completely deviated from the experimental data after the 110th day. The model was not able to capture the Mn evolution in the presence of mineral proportions as low as 0.4% wt of calcite and 0.8% wt of pyrite. The simulated Mn behavior was slightly improved when the pyrite content was increased to 3% wt (Figure 5.6). In addition to the simulated kinetic processes, perhaps other geochemical processes such as sorption and/or coprecipitation occurred and were overlooked within the PHREEQC model. Plante *et al*. (2010) demonstrated that plagioclase controlled Ni mobility through sorption in waste rock piles of the Tio mine. More recently, Reczek *et al*. (2020) and Trach *et al*. (2021) stated that volcanic tuff and basalt effectively adsorb Mn. Therefore, the next step of the geochemical assessment of Akasaba West materials should involve sorption experiments to investigate the effect of the sorption capacity of plagioclase on water quality.

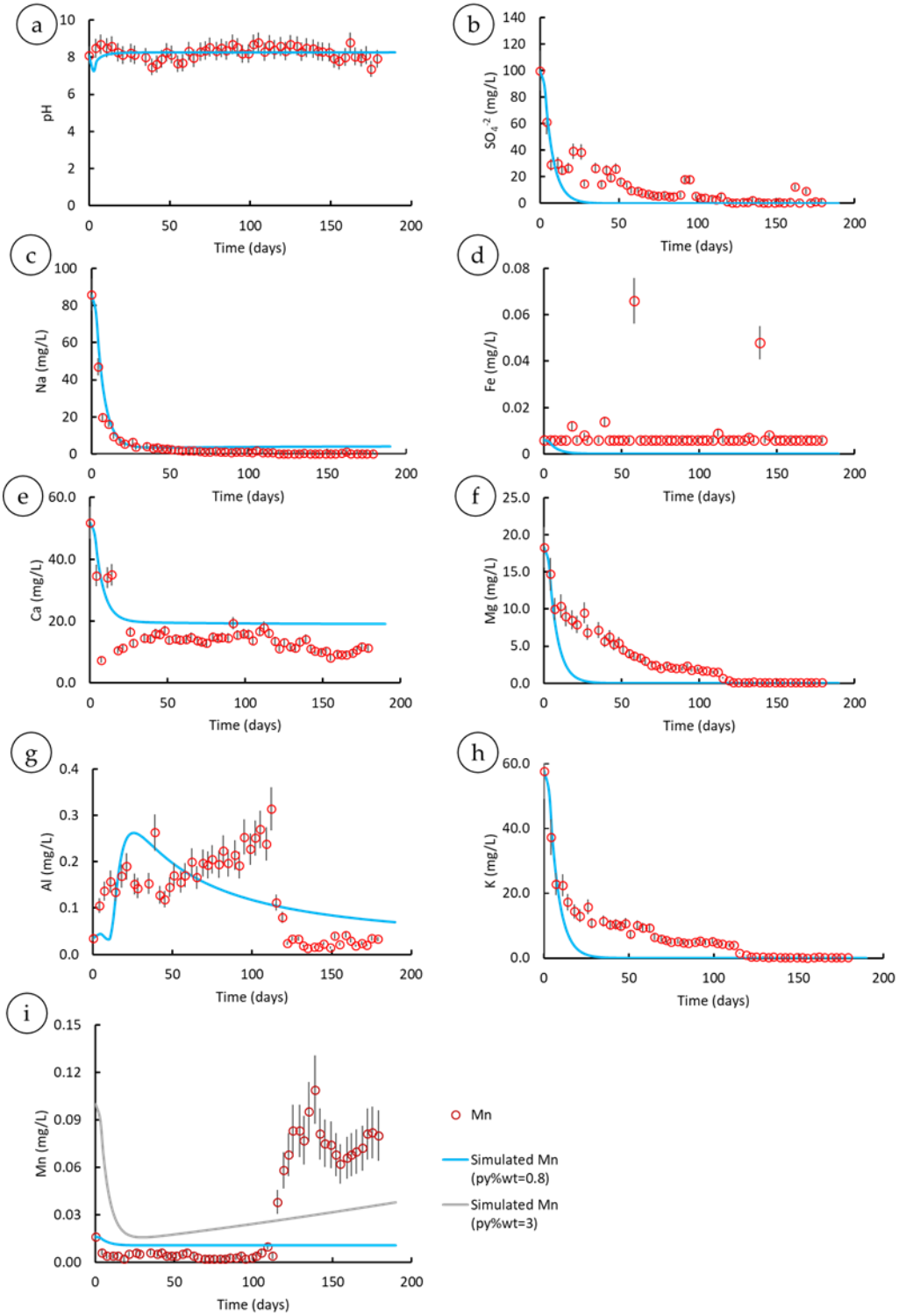


Figure 5.6 Weathering cell test D1 and PHREEQC modeling results. (a) Experimental and simulated results of the pH. (b) sulfate. (c) sodium. (d) iron. (e) calcium. (f) magnesium. (g) aluminum. (h) potassium. (i) manganese.

(ii) D3 weathering cell

Water quality from testing data and the PHREEQC model of the D3 weathering cell presented similar features as the D1 outcomes. However, the D3 mineralogical proportions were substantially different; in the presence of 26% wt of albite and 1.9% wt of calcite, the neutralization potential counteracted the overall acidity stemming from oxidation of up to 8.1% wt of pyrite. Unlike the simulated response that predicted iron and sulfate release emanating from the oxidation-neutralization process, measured Fe concentrations were generally below the detection limit throughout the test duration emphasizing the occurrence of Fe-bearing secondary minerals and/or Fe sorption on plagioclase surfaces that could affect both iron and manganese mobility (Figure 5.7).

Due to the high albite content, the PHREEQC model predicted high Na concentrations as leaching progressed and deviated from the experimental results on the 30th day. Sodium results from the D3 weathering cell support the Na controlling factor discussed earlier; the dissolution rate of albite used in PHREEQC seemed to overestimate the albite-weathering rate in subalkaline conditions.

Regarding Mn, the model roughly captured the experimental evolution. The pyrite content in D3 was higher compared to D1. The high sulphide content triggered neutralization potential of calcite and involved high Mn lixiviation; nonetheless, as long as the pH remained neutral to subalkaline the calcite dissolution rate was limited. As a result, the Mn concentrations observed in D3 were much lower than those observed in D2. Silicate neutralizing minerals, specifically albite, effectively contributed maintaining high pH values; therefore, their neutralization potential slightly attenuated Mn lixiviation.

(iii) T1 weathering cell

Modeling and testing results for the T1 weathering cell were in good agreement and supported the aforementioned insights (Figure 5.8). In summary, the modeling approach showed a good agreement with the experimental data for the four weathering cells. However, benchmarking proxies underlined two main model limitations: (i) the model did not properly capture the Mn evolution when calcite and pyrite contents were as low as 0.4% wt and 0.8% wt, respectively; and (ii) the model did not incorporate sorption kinetics of iron and manganese on plagioclase surfaces as well as coprecipitation kinetics.

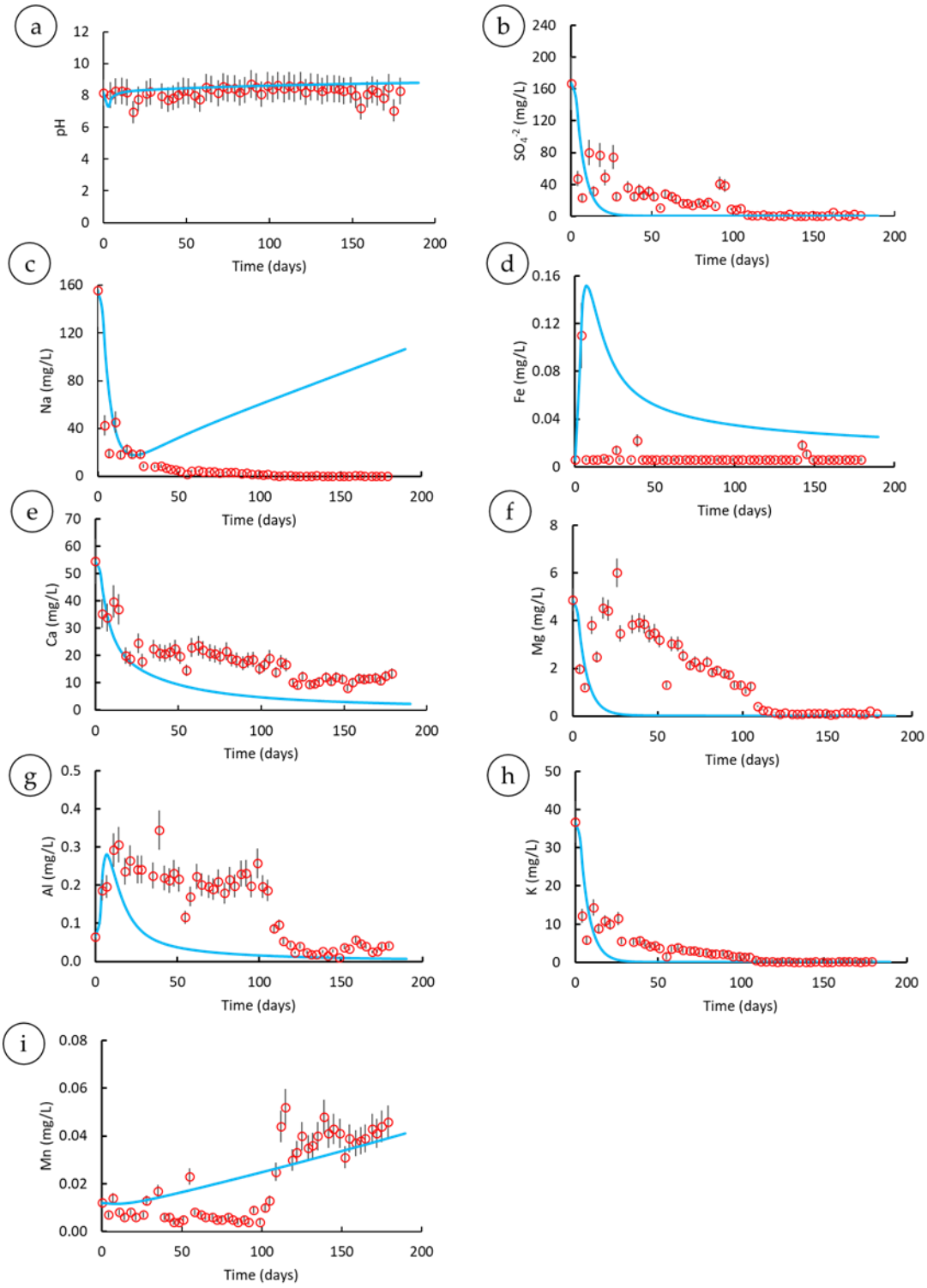


Figure 5.7 Weathering cell test D3 and PHREEQC modeling results. (a) Experimental and simulated results of the pH. (b) sulfate. (c) sodium. (d) iron. (e) calcium. (f) magnesium. (g) aluminum. (h) potassium. (i) manganese.

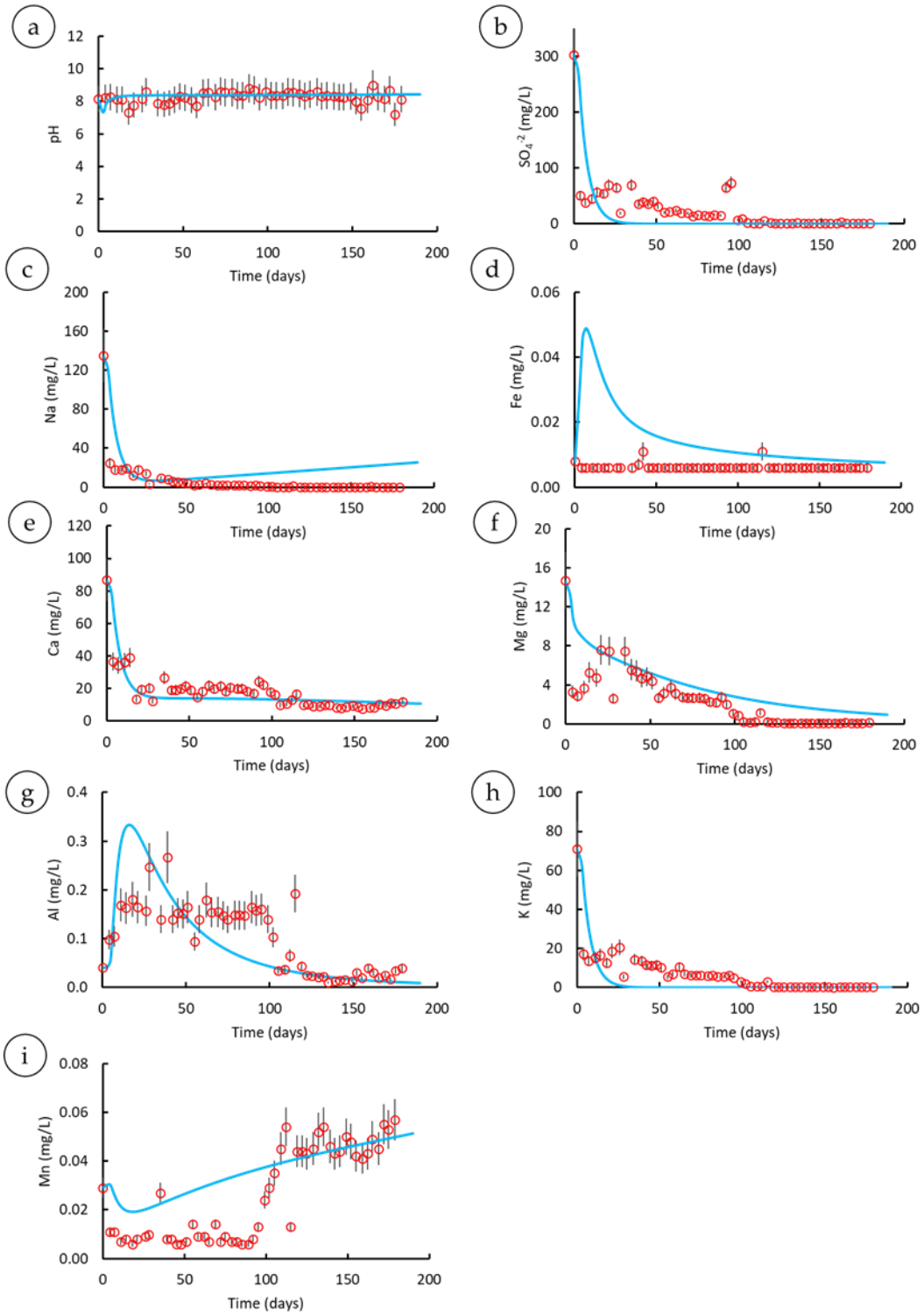


Figure 5.8 Weathering cell test T1 and PHREEQC modeling results. (a) Experimental and simulated results of the pH. (b) sulfate. (c) sodium. (d) iron. (e) calcium. (f) magnesium. (g) aluminum. (h) potassium. (i) manganese.

Nonetheless, the model capabilities complied with the conservative modeling reasoning adopted along the upstream scoping assessment studies, which overlooks geochemical retention processes in order to approach the overall leaching potential. Finally, the kinetic model captured the pH evolution in presence of silicates, which was the main objective of this modeling approach.

5.4.3 Parametric analysis

The parametric analysis performed herein was based on a what-if scenarios approach to lead an upstream scoping assessment. This scoping survey aimed at probable worse case scenarios linked to variations of mineralogical composition and water retention time. Worse case scenarios denote cases where water quality deteriorates.

5.4.3.1 Mineral assemblages

Through fixing the sulphide contents (4.2% wt of pyrite and 1.9% of chalcopyrite (Kimball *et al*., 2010)), different neutralizing mineral assemblages were assessed to stress the effectiveness of albite neutralization. The first scenario sets forth a sulphide assemblage with no neutralizing minerals. The second set of scenarios included albite as the sole neutralizing mineral present at different proportions (5, 10, 18.8 and 30% wt). The third scenario involved 18.8% wt albite and 1.1% calcite. The last scenario involved the complete mineral assemblage of T1.

The parametric analysis results are shown in Figure 5.9. From an initial pH of 8.16, the pH values dropped to 2.78 in the presence of sulphides (pyrite and chalcopyrite) with no neutralizing minerals. The pH remained acidic throughout the simulation time, whereas Fe and SO_4^{2-} reached their maximum concentrations after 139 days, with concentrations of 93.1 and 322 mg/L, respectively. In this scenario, Cu exceeded 10 mg/L after 50 days. After adding 5% wt of albite, the pH started to increase from 3 on the 80th day to 4.89 on the 189th day. The maximum concentrations reached for Fe and SO_4^{2-} were slightly lowered compared to the first scenario (253 and 73 mg/L, respectively). Water quality was further improved in the presence of 10% wt of albite; the pH attained a value of 5 after 86 days. Iron, SO_4^{2-}, and Cu concentrations were 71.3, 246, and 8.66 mg/L, respectively, after 150 days. The neutralization delay was further curtailed in the presence of 30% wt of albite, thereby achieving circumneutral pH after 65 days. In this scenario, Fe, SO_4^{2-}, and Cu concentrations after 150 days were 68.8, 238, and 2.76 mg/L, respectively.

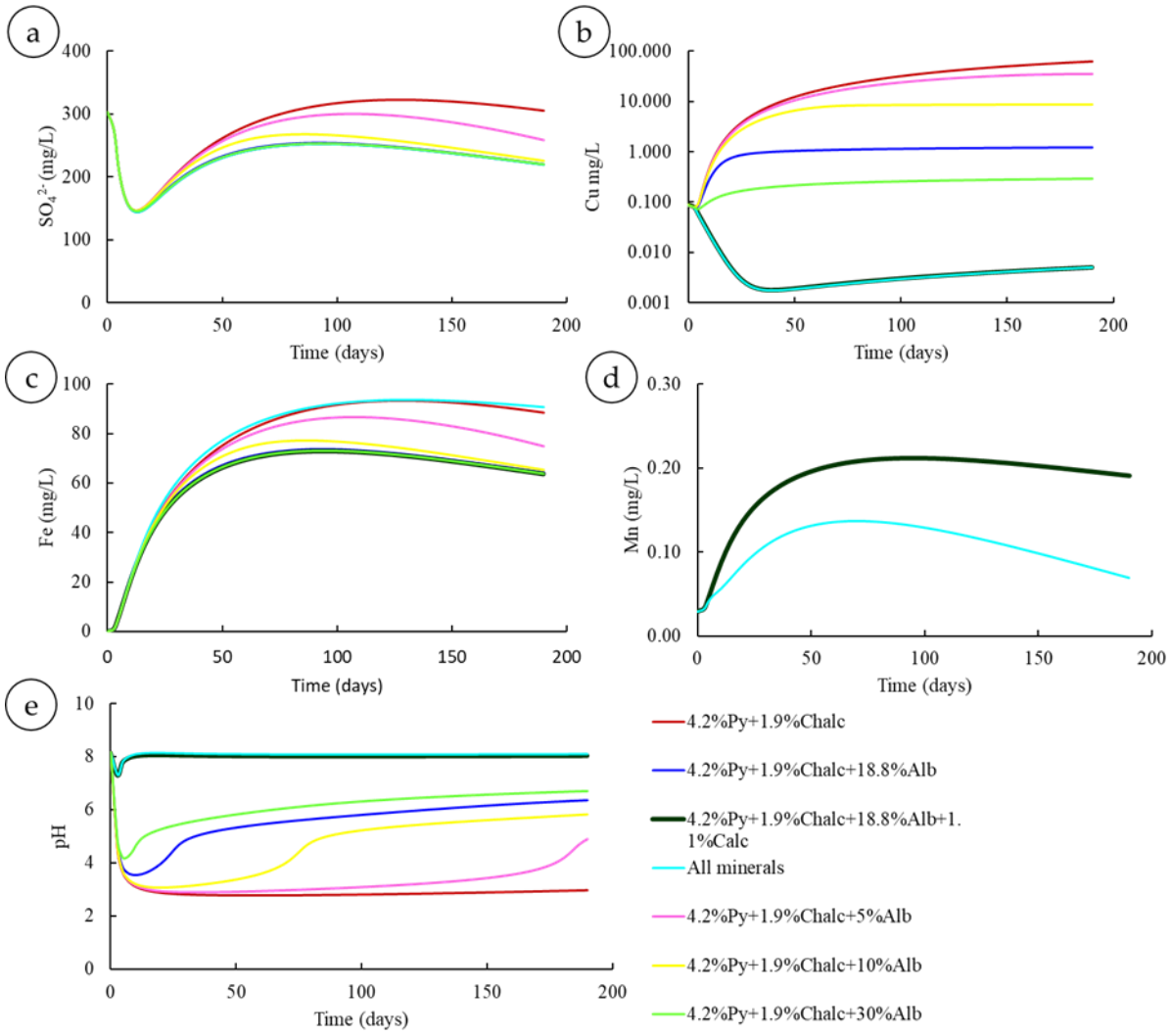


Figure 5.9 Various scenarios underlining the effect of various mineral assemblages on leachate quality. (a) Sulfate concentrations obtained in the presence of different mineral proportions. (b) Cu concentrations obtained in the presence of different mineral proportions (c): Fe concentrations obtained in the presence of different mineral proportions. (d): Mn concentrations obtained in the presence of different mineral proportions. (e): The pH obtained from the simulated mineral proportion scenarios.

According to the parametric analysis, the neutralization delay in the presence of 18.8% wt of albite was 128 days (pH reaches 6); adding 1.1% wt calcite to the mineral assemblage shifted the pH to 8 and suppressed the neutralization delay. On the other hand, including the remnant silicate neutralizing minerals (epidote, chlorite, amphibole, etc.) in the simulation did not result in a

perceptible increase in pH. Nonetheless, their contribution manifested in Mn leaching; their neutralization potential withdrew a certain amount of acidity from the system. Consequently, the pH-dependent dissolution rate of calcite was slightly decreased along with the Mn leaching rate. The concentration of Mn after 50 days decreased from 0.2 to 0.13 mg/L in the presence of the complete silicate assemblage (Figure 5.9). Iron, SO_4^{2-}, and Mn exhibited an arc-shaped evolution; this was caused by the pyrite aging effect expressed in the oxidation rate reported by Jerz and Rimstidt (2004). This behavior stresses that Mn release from calcite also relates to pyrite prevalence. The interactions between Mn-stimulating (sulphides) and Mn-hindering (silicates) components of the system determined the magnitude of Mn leaching.

5.4.3.2 Various residence times

This parametric analysis underlines the effect of residence time on water quality. Neutral flowing water leaching 4.2% wt pyrite at different volumetric flows (L/s) was simulated. Figure 5.10 features the outcomes from 10 simulated residence times (7h, 48h, 10 days, 30 days, 60 days, 100 days, 200 days, 500 days, 1000 days, and 2000 days). The range of values encompassed highly mobile and extremely slow-flowing water scenarios.

As the residence time increased, water quality worsened due to longer water–mineral interactions. Systems with a residence time less than 30 days disposed of acidity after a lag time. For instance, the system with 30 days of residence time recovered its circumneutral pH after 60 days. Residence times greater than 30 days generated acid leachates highly concentrated in Fe and sulfate throughout the simulation. A residence time of 100 days produced leachate with pH = 3.66, 20.03 mg/L sulfate, and 5.91 mg/L Fe after a simulation time of 150 days. Iron concentrations were as high as 73 mg/L in pores with extremely slow-flowing water. These outcomes indicate the impact of flow heterogeneity on water quality. The parametric analysis simulated different weathering cells with different flow conditions; however, at larger scales these heterogeneities could coexist in the same waste facility and jointly contribute to determining water quality at the effluent stream (Fala *et al.*, 2013). Conducting such parametric analyses at the upstream stage could assist in risk identification and mitigation throughout the upcoming stages.

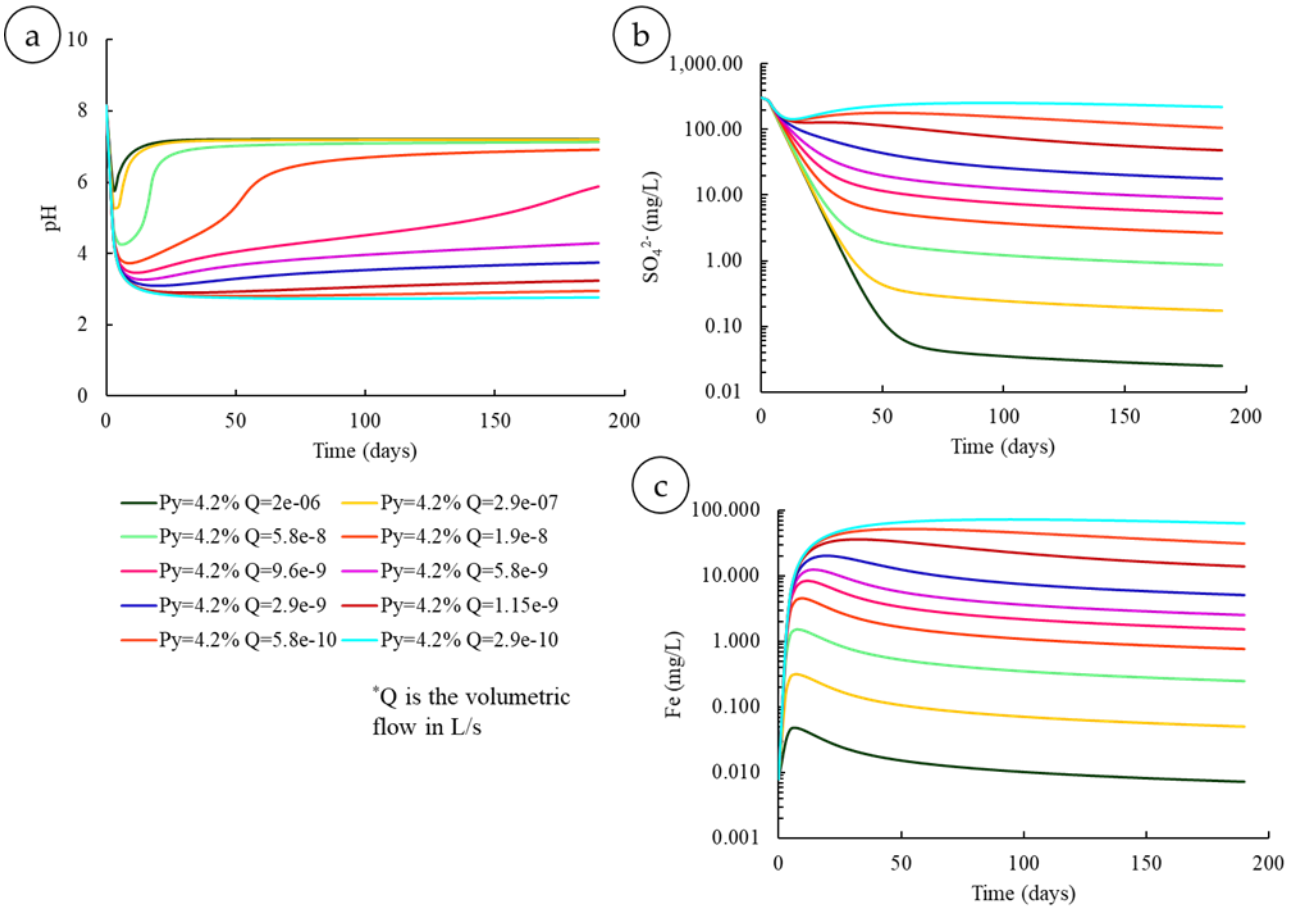


Figure 5.10 Various scenarios delineating the relationship between the residence time and leachate quality in weathering cell test simulation. (a) The pH obtained for various residence times. (b) Sulfate concentrations obtained for various residence times. (c): Total iron concentrations obtained for various residence times.

5.5 Conclusion

Preliminary kinetic testing during the development stage of hard rock mine projects is of great importance to underline the geochemical behavior of the host rock. Weathering cell tests are often used for the aforementioned purpose. The present study simulates the kinetically controlled reactions occurring in four weathering cells using a film diffusion model implemented in PHREEQC. Results from the presented kinetic modeling approach using PHREEQC exhibited a good agreement with weathering cell data. The PHREEQC capabilities coupled to the literature rate laws proved to be reliable to simulate weathering cells set up to perform inceptive assessment modeling. The main objective of simulating the pH using kinetic modeling of weathering cell tests

was fulfilled. However, the model presented herein does not include geochemical retention processes such as coprecipitation and sorption. These retention processes reduce the total dissolved concentrations and do not partake in the conservative reasoning that should be used during development stages. Being cognizant of these limitations, the PHREEQC kinetic model does not conform to design purposes related to mine reclamation. However, it complies with the upstream scoping studies along the development stage, which has barely benefited from geochemical modeling tools. The main asset of the present kinetic model is the ability to simulate various scenarios for upstream risk identification based upon restricted datasets and conservative modeling reasoning. In this regard, the input datasets consist of the usual mineralogical characterization, weathering cell tests, and literature rate laws, thereby abiding by two main constraints that steer the development stage: material availability and assessment cost. In terms of practical implications, this upstream modeling attempt was mainly performed to be combined with 3D geological modeling and stochastic simulation to undertake in situ upstream classification of the host rock and the orebody. The classification will be based on the pH that could be generated if a given mineral assemblage within the orebody is weathered under kinetically controlled conditions. This classification will be performed before mining to sort mine waste depending on their geochemical risk.

Supplementary Materials: The following are available in Appendix B and online at https://www.mdpi.com/article/10.3390/min11121306/s1.

Author contributions: Conceptualization, Y.T. and I.D.; methodology, Y.T., I.D. and D.V.; software, Y.T.; validation, D.V., N.B. and M.B.; formal analysis, Y.T., M.B. and I.D.; investigation, M.B.; resources, I.D.; data curation, Y.T and D.V.; writing—original draft preparation, Y.T.; writing review and editing, I.D., D.V., N.B and M.B.; visualization, Y.T.; supervision, I.D. and N.B.; project administration, I.D.; funding acquisition, I.D. and N.B. All authors have read and agreed to the published version of the manuscript.

Funding: Funding for this study was provided by NSERC TERRE-NET program (NSERC-TERRE-NET 479708-2015), led by Dr. D. Blowes (University of Waterloo).

Acknowledgements: The authors thank the staff of Akasaba West project for their support and contributions and the Unité de Recherche et Service en Technologie Minérale (URSTM) staff for their assistance in the laboratory. The authors are grateful for the insights and suggestions from J.

Mahoney, D. Parkhurst, and D. Kinniburgh during the formulation of the PHREEQC and PHREEPLOT models used in this work.

References

Abbasi, F., Feyen, J. and Van Genuchten, M.T. (2004). Two-dimensional simulation of water flow and solute transport below furrows: model calibration and validation. Journal of Hydrology, 290(1-2), 63-79.

Akcil, A. and Koldas, S. (2006). Acid Mine Drainage (AMD): causes, treatment and case studies. Journal of cleaner production, 14(12-13), 1139-1145.

Amar, H., Benzaazoua, M., Edahbi, M., Villeneuve, M., Joly, M.-A. and Elghali, A. (2021). Reprocessing feasibility of polymetallic waste rock for cleaner and sustainable mining. Journal of Geochemical Exploration, 220, 106683.

Amar, H., Benzaazoua, M., Elghali, A., Bussière, B. and Duclos, M. (2020). Upstream environmental desulphurisation and valorisation of waste rocks as a sustainable AMD management approach. Journal of Geochemical Exploration, 215, 106555.

Appelo, C.A.J. and Postma, D. (2004). Geochemistry, groundwater and pollution. : CRC press.

Aubertin, M., Aachib, M., Monzon, M., Joanes, A., Bussière, B. and Chapuis, R. (1997). Étude de laboratoire sur l'efficacité des barrières de recouvrement construites à partir de résidus miniers. Mine Environment Neutral Drainage (MEND) Report, 2.

Barfoud, L., Pabst, T., Zagury, G.J. and Plante, B. (2019). Effect of Dissolved Oxygen on The Oxidation of Saturated Mine Tailings. Geo-Environmental Engineering 2019, 30-31. Concordia University, Montreal, Canada

Benzaazoua, M., Bussière, B., Dagenais, A.-M. and Archambault, M. (2004). Kinetic tests comparison and interpretation for prediction of the Joutel tailings acid generation potential. Environmental Geology, 46(8), 1086-1101.

Benzaazoua, M., Bussière, B., Demers, I., Aubertin, M., Fried, É. and Blier, A. (2008). Integrated mine tailings management by combining environmental desulphurization and cemented paste backfill: Application to mine Doyon, Quebec, Canada. Minerals engineering, 21(4), 330-340.

Benzaazoua, M., Bussière, B., Kongolo, M., McLaughlin, J. and Marion, P. (2000). Environmental desulphurization of four Canadian mine tailings using froth flotation. International journal of mineral processing, 60(1), 57-74.

Blowes, D., Ptacek, C., Jambor, J. and Weisener, C. (2003). The geochemistry of acid mine drainage. Treatise on geochemistry, 9, 612.

Bouzahzah, H. (2013). Modification et amélioration des tests statiques et cinétiques pour une prédiction fiable du drainage minier acide. Université du Québec en Abitibi-Témiscamingue.

Bouzahzah, H., Benzaazoua, M., Bussiere, B. and Plante, B. (2014a). Prediction of acid mine drainage: importance of mineralogy and the test protocols for static and kinetic tests. Mine Water and the Environment, 33(1), 54-65.

Bouzahzah, H., Benzaazoua, M., Bussière, B. and Plante, B. (2014b). Revue de littérature détaillée sur les tests statiques et les essais cinétiques comme outils de prédiction du drainage minier acide. Déchets Sciences et Techniques Techniques, 66, 14-31.

Bouzahzah, H., Benzaazoua, M., Plante, B. and Bussiere, B. (2015). A quantitative approach for the estimation of the “fizz rating” parameter in the acid-base accounting tests: A new adaptations of the Sobek test. Journal of Geochemical Exploration, 153, 53-65.

Brookfield, A., Blowes, D. and Mayer, K. (2006). Integration of field measurements and reactive transport modeling to evaluate contaminant transport at a sulfide mine tailings impoundment. Journal of contaminant hydrology, 88(1-2), 1-22.

Brunauer, S., Emmett, P.H. and Teller, E. (1938). Adsorption of gases in multimolecular layers. Journal of the American chemical society, 60(2), 309-319.

Bussière, B. (2007). Colloquium 2004: Hydrogeotechnical properties of hard rock tailings from metal mines and emerging geoenvironmental disposal approaches. Canadian Geotechnical Journal, 44(9), 1019-1052.

Bussière, B., Aubertin, M., Mbonimpa, M., Molson, J.W. and Chapuis, R.P. (2007). Field experimental cells to evaluate the hydrogeological behaviour of oxygen barriers made of silty materials. Canadian Geotechnical Journal, 44(3), 245-265.

Casey, W.H. and Ludwig, C. (1995). Silicate mineral dissolution as a ligand-exchange reaction. Chemical weathering rates of silicate minerals(In: A. F. White and S. L. Brantley (eds.) Chemical Weathering Rates of Silicate Minerals, Reviews in Mineralogy Vol. 31, Mineral. Soc. Am., Washington, D.C.), 87-118.

Chapuis, R.P. and Aubertin, M. (2003). On the use of the Kozeny Carman equation to predict the hydraulic conductivity of soils. Canadian Geotechnical Journal, 40(3), 616-628.

Chou, L. and Wollast, R. (1985). Steady-state kinetics and dissolution mechanisms of albite. American Journal of Science, 285(10), 963-993.

Cruz, R., Bertrand, V., Monroy, M. and González, I. (2001). Effect of sulfide impurities on the reactivity of pyrite and pyritic concentrates: a multi-tool approach. Applied geochemistry, 16(7-8), 803-819.

Demers, I., Bouda, M., Mbonimpa, M., Benzaazoua, M., Bois, D. and Gagnon, M. (2015). Valorization of acid mine drainage treatment sludge as remediation component to control acid generation from mine wastes, part 2: field experimentation. Minerals Engineering, 76, 117-125.

Demers, I., Bussière, B., Benzaazoua, M., Mbonimpa, M. and Blier, A. (2008). Column test investigation on the performance of monolayer covers made of desulphurized tailings to prevent acid mine drainage. Minerals Engineering, 21(4), 317-329.

Demers, I., Bussiere, B., Mbonimpa, M. and Benzaazoua, M. (2009). Oxygen diffusion and consumption in low-sulphide tailings covers. Canadian Geotechnical Journal, 46(4), 454-469.

Demers, I., Mbonimpa, M., Benzaazoua, M., Bouda, M., Awoh, S., Lortie, S. and Gagnon, M. (2017). Use of acid mine drainage treatment sludge by combination with a natural soil as an oxygen barrier cover for mine waste reclamation: Laboratory column tests and intermediate scale field tests. Minerals Engineering, 107, 43-52.

Demers, I., Molson, J., Bussière, B. and Laflamme, D. (2013). Numerical modeling of contaminated neutral drainage from a waste-rock field test cell. Applied geochemistry, 33, 346-356.

Eary, L.E. and Williamson, M.A. (2006). Simulations of the neutralizing capacity of silicate rocks in acid mine drainage environments. J. Am. Soc. Min. Reclam, 2, 564-577.

Elghali, A., Benzaazoua, M., Bouzahzah, H., Bussière, B. and Villarraga-Gómez, H. (2018). Determination of the available acid-generating potential of waste rock, part I: Mineralogical approach. Applied Geochemistry, 99, 31-41.

Elghali, A., Benzaazoua, M., Bussière, B. and Bouzahzah, H. (2019). Determination of the available acid-generating potential of waste rock, part II: Waste management involvement. Applied geochemistry, 100, 316-325.

Embile Jr, R.F., Walder, I.F. and Mahoney, J.J. (2019). Multicomponent reactive transport modeling of effluent chemistry using locally obtained mineral dissolution rates of forsterite and pyrrhotite from a mine tailings deposit. Advances in Water Resources, 128, 87-96.

Evangelou, V.P. and Zhang, Y. (1995). A review: pyrite oxidation mechanisms and acid mine drainage prevention. Critical Reviews in Environmental Science and Technology, 25(2), 141-199.

Fala, O., Aubertin, M., Molson, JW., Bussière, B., Wilson, GW., Chapuis, R. and Martin, V. (2003). Numerical modeling of unsaturated flow in uniform and heterogeneous waste rock piles. Sixth International Conference on Acid Rock Drainage (ICARD), Australasian Institute of Mining and Metallurgy, Cairns, Australia, Publication Series.

Fala, O., Molson, JW., Aubertin, M., Bussière, B., and Chapuis, R. (2006). Numerical simulations of long term unsaturated flow and acid mine drainage at waste rock piles. Proceedings of the 7th International Conference on Acid Rock Drainage (ICARD).

Fala, O., Molson, J., Aubertin, M., Dawood, I., Bussière, B. and Chapuis, R. (2013). A numerical modeling approach to assess long-term unsaturated flow and geochemical transport in a waste rock pile. International Journal of Mining, Reclamation and Environment, 27(1), 38-55.

Graupner, B.J., Koch, C. and Prommer, H. (2014). Prediction of diffuse sulfate emissions from a former mining district and associated groundwater discharges to surface waters. Journal of Hydrology, 513, 169-178.

Heikkinen, P., Räisänen, M. and Johnson, R. (2009). Geochemical characterisation of seepage and drainage water quality from two sulphide mine tailings impoundments: acid mine drainage versus neutral mine drainage. Mine Water and the Environment, 28(1), 30-49.

Hellmann, R. (1995). The albite-water system: Part II. The time-evolution of the stoichiometry of dissolution as a function of pH at 100, 200, and 300 C. Geochimica et Cosmochimica Acta, 59(9), 1669-1697.

Ho, G.D., Tabelin, C.B., Tangviroon, P., Tamamura, S. and Igarashi, T. (2021). Effects of cement addition on arsenic leaching from soils excavated from projects employing shield-tunneling method. Geoderma, 385, 114896.

Jerz, J.K. and Rimstidt, J.D. (2004). Pyrite oxidation in moist air. Geochimica et Cosmochimica Acta, 68(4), 701-714.

Jouini, M., Neculita, C.M., Genty, T. and Benzaazoua, M. (2020). Environmental behavior of metal-rich residues from the passive treatment of acid mine drainage. Science of The Total Environment, 136541.

Jouini, M., Rakotonimaro, T.V., Neculita, C.M., Genty, T. and Benzaazoua, M. (2019). Prediction of the environmental behavior of residues from the passive treatment of acid mine drainage. Applied Geochemistry, 110, 104421.

Jurjovec, J., Blowes, D.W., Ptacek, C.J. and Mayer, K.U. (2004). Multicomponent reactive transport modeling of acid neutralization reactions in mine tailings. Water resources research, 40(11).

Kalonji-Kabambi, A., Demers, I. and Bussière, B. (2020). Reactive transport modeling of the geochemical behavior of highly reactive tailings in different environmental conditions. Applied Geochemistry, 122, 104761.

Kandelous, M.M. and Šimůnek, J. (2010). Numerical simulations of water movement in a subsurface drip irrigation system under field and laboratory conditions using HYDRUS-2D. Agricultural Water Management, 97(7), 1070-1076.

Kimball, B.E., Rimstidt, J.D. and Brantley, S.L. (2010). Chalcopyrite dissolution rate laws. Applied Geochemistry, 25(7), 972-983.

Kinniburgh, D. and Cooper, D. (2011). PhreePlot: Creating graphical output with PHREEQC.

Kleinmann, R.L.P., Crerar, D. and Pacelli, R. (1981). Biogeochemistry of acid mine drainage and a method to control acid formation. Min. Eng.(NY);(United States), 33(3).

Labus, K. and Grmela, A. (2006). A model of water chemistry forming in effect of pyrite oxidation in a coal mining waste pile PODZEMNÁ VODA, XII/1, 50-55. Récupéré de http://www.sah-podzemnavoda.sk/cms/e107_plugins/content/content.php?content.293

Lammers, K., Smith, M.M. and Carroll, S.A. (2017). Muscovite dissolution kinetics as a function of pH at elevated temperature. Chemical Geology, 466, 149-158.

Lawrence, R.W. and Wang, Y. (1997). Determination of neutralization potential in the prediction of acid rock drainage. Proc. 4th International Conference on Acid Rock Drainage, Vancouver, BC.

Le Bourre, B., Neculita, C.M., Coudert, L. and Rosa, E. (2020). Manganese removal processes and geochemical behavior in residues from passive treatment of mine drainage. Chemosphere, 259, 127424.

Marty, N.C., Claret, F., Lassin, A., Tremosa, J., Blanc, P., Madé, B., Giffaut, E., Cochepin, B. and Tournassat, C. (2015). A database of dissolution and precipitation rates for clay-rocks minerals. Applied Geochemistry, 55, 108-118.

Mayer, K., Amos, R., Molins, S. and Gerard, F. (2012). Reactive transport modeling in variably saturated media with MIN3P: Basic model formulation and model enhancements. (Vol. 26) : Bentham Science Publishers Sharjah, UAE.

Mayer, K.U., Frind, E.O. and Blowes, D.W. (2002). Multicomponent reactive transport modeling in variably saturated porous media using a generalized formulation for kinetically controlled reactions. Water Resources Research, 38(9), 13-11-13-21.

Michaud, M.L., Plante, B., Bussière, B., Benzaazoua, M. and Leroux, J. (2017). Development of a modified kinetic test using EDTA and citric acid for the prediction of contaminated neutral drainage. Journal of Geochemical Exploration, 181, 58-68.

Molson, J., Aubertin, M., Bussière, B. and Benzaazoua, M. (2008). Geochemical transport modeling of drainage from experimental mine tailings cells covered by capillary barriers. Applied Geochemistry, 23(1), 1-24.

Molson, J., Fala, O., Aubertin, M. and Bussière, B. (2005). Numerical simulations of pyrite oxidation and acid mine drainage in unsaturated waste rock piles. Journal of Contaminant Hydrology, 78(4), 343-371.

Moses, C.O., Nordstrom, D.K., Herman, J.S. and Mills, A.L. (1987). Aqueous pyrite oxidation by dissolved oxygen and by ferric iron. Geochimica et Cosmochimica Acta, 51(6), 1561-1571.

Mudd, G.M. (2007). Global trends in gold mining: Towards quantifying environmental and resource sustainability. Resources Policy, 32(1-2), 42-56.

Neuman, S.P. (1990). Universal scaling of hydraulic conductivities and dispersivities in geologic media. Water resources research, 26(8), 1749-1758.

Nicholson, R.V., Gillham, R.W. and Reardon, E.J. (1988). Pyrite oxidation in carbonate-buffered solution: 1. Experimental kinetics. Geochimica et Cosmochimica Acta, 52(5), 1077-1085.

Nicholson, R.V., Rinker, Michael J., Acott, Gerry. and Venhuis, M.A. (2003). Integration of field data and a geochemical transport model to assess mitigation strategies for an acid-generating mine rock pile at a uranium mine. Proceedings, Sudbury. : Citeseer.

Nicholson, R.V. and Scharer, J.M. (1994). Laboratory studies of pyrrhotite oxidation kinetics. Dans : ACS Publications.

Nordstrom, D., Alpers, C.N., Ptacek, C. and Blowes, D. (2000). Negative pH and extremely acidic mine waters from Iron Mountain, California. Environmental Science & Technology, 34(2), 254-258.

Nordstrom, D.K. (1982). Aqueous pyrite oxidation and the consequent formation of secondary iron minerals. : Soil Science Society of America.

Nordstrom, D.K. and Alpers, C.N. (1999). Negative pH, efflorescent mineralogy, and consequences for environmental restoration at the Iron Mountain Superfund site, California. Proceedings of the National Academy of Sciences, 96(7), 3455-3462.

Nordstrom, D.K., Blowes, D.W. and Ptacek, C.J. (2015). Hydrogeochemistry and microbiology of mine drainage: An update. Applied Geochemistry, 57, 3-16.

Ouangrawa, M., Aubertin, M., Molson, J., Bussière, B. and Zagury, G. (2010). Preventing acid mine drainage with an elevated water table: Long-term column experiments and parameter analysis. Water, Air, & Soil Pollution, 213(1-4), 437-458.

Ouangrawa, M., Molson, J., Aubertin, M., Bussière, B. and Zagury, G. (2009). Reactive transport modeling of mine tailings columns with capillarity-induced high water saturation for preventing sulfide oxidation. Applied Geochemistry, 24(7), 1312-1323.

Pabst, T., Bussière, B., Aubertin, M. and Molson, J. (2018). Comparative performance of cover systems to prevent acid mine drainage from pre-oxidized tailings: A numerical hydro-geochemical assessment. Journal of contaminant hydrology, 214, 39-53.

Pabst, T., Molson, J., Aubertin, M. and Bussière, B. (2017). Reactive transport modeling of the hydro-geochemical behaviour of partially oxidized acid-generating mine tailings with a monolayer cover. Applied Geochemistry, 78, 219-233.

Palandri, J.L. and Kharaka, Y.K. (2004). A compilation of rate parameters of water-mineral interaction kinetics for application to geochemical modeling. : Geological Survey Menlo Park CA.

Parbhakar-Fox, A.K., Edraki, M., Walters, S. and Bradshaw, D. (2011). Development of a textural index for the prediction of acid rock drainage. Minerals Engineering, 24(12), 1277-1287.

Park, I., Tabelin, C.B., Jeon, S., Li, X., Seno, K., Ito, M. and Hiroyoshi, N. (2019). A review of recent strategies for acid mine drainage prevention and mine tailings recycling. Chemosphere, 219, 588-606.

Park, I., Tabelin, C.B., Seno, K., Jeon, S., Inano, H., Ito, M. and Hiroyoshi, N. (2020). Carrier-microencapsulation of arsenopyrite using Al-catecholate complex: nature of oxidation products, effects on anodic and cathodic reactions, and coating stability under simulated weathering conditions. Heliyon, 6(1), e03189.

Parkhurst, D.L. and Appelo, C. (1999). User's guide to PHREEQC (Version 2): A computer program for speciation, batch-reaction, one-dimensional transport, and inverse geochemical calculations. Water-resources investigations report, 99(4259), 312.

Parkhurst, D.L. and Appelo, C. (2013). Description of input and examples for PHREEQC version 3: a computer program for speciation, batch-reaction, one-dimensional transport, and inverse geochemical calculations. (2328-7055) US Geological Survey.

Plante, B. (2010). Évaluation des principaux facteurs d'influence sur la prédiction du drainage neutre contaminé. Université du Québec à en Abitibi-Témiscamingue.

Plante, B., Benzaazoua, M. and Bussière, B. (2011). Kinetic testing and sorption studies by modified weathering cells to characterize the potential to generate contaminated neutral drainage. Mine water and the environment, 30(1), 22-37.

Plante, B., Benzaazoua, M., Bussière, B., Biesinger, M. and Pratt, A. (2010). Study of Ni sorption onto Tio mine waste rock surfaces. Applied Geochemistry, 25(12), 1830-1844.

Plante, B., Bussière, B. and Benzaazoua, M. (2014). Lab to field scale effects on contaminated neutral drainage prediction from the Tio mine waste rocks. Journal of Geochemical Exploration, 137, 37-47.

Reczek, L., Michel, M.M., Trach, Y., Siwiec, T. and Tytkowska-Owerko, M. (2020). The Kinetics of Manganese Sorption on Ukrainian Tuff and Basalt—Order and Diffusion Models Analysis. Minerals, 10(12), 1065.

Romano, C.G., Mayer, K.U., Jones, D.R., Ellerbroek, D.A. and Blowes, D.W. (2003). Effectiveness of various cover scenarios on the rate of sulfide oxidation of mine tailings. Journal of Hydrology, 271(1-4), 171-187.

Salmon, S.U. (2003). Geochemical modeling of acid mine drainage in mill tailings: Quantification of kinetic processes from laboratory to field scale. (Phd). Byggvetenskap. Phd.

Singer, P.C. and Stumm, W. (1970). Acidic mine drainage: the rate-determining step. Science, 167(3921), 1121-1123.

Smith, M.M. and Carroll, S.A. (2016). Chlorite dissolution kinetics at pH 3–10 and temperature to 275° C. Chemical Geology, 421, 55-64.

Sobek, A.A. (1978). Field and laboratory methods applicable to overburdens and minesoils. : Industrial Environmental Research Laboratory, Office of Research and Development, US Environmental Protection Agency.

Tabelin, C.B., Igarashi, T., Villacorte-Tabelin, M., Park, I., Opiso, E.M., Ito, M. and Hiroyoshi, N. (2018). Arsenic, selenium, boron, lead, cadmium, copper, and zinc in naturally contaminated rocks: A review of their sources, modes of enrichment, mechanisms of release, and mitigation strategies. Science of the Total Environment, 645, 1522-1553.

Tabelin, C.B., Park, I., Phengsaart, T., Jeon, S., Villacorte-Tabelin, M., Alonzo, D., Yoo, K., Ito, M. and Hiroyoshi, N. (2021). Copper and critical metals production from porphyry ores and E-wastes: A review of resource availability, processing/recycling challenges, socio-environmental aspects, and sustainability issues. Resources, Conservation and Recycling, 170, 105610.

Tabelin, C.B., Veerawattananun, S., Ito, M., Hiroyoshi, N. and Igarashi, T. (2017a). Pyrite oxidation in the presence of hematite and alumina: I. Batch leaching experiments and kinetic modeling calculations. Science of the Total Environment, 580, 687-698.

Tabelin, C.B., Veerawattananun, S., Ito, M., Hiroyoshi, N. and Igarashi, T. (2017b). Pyrite oxidation in the presence of hematite and alumina: II. Effects on the cathodic and anodic half-cell reactions. Science of the Total Environment, 581, 126-135.

Tamoto, S., Tabelin, C.B., Igarashi, T., Ito, M. and Hiroyoshi, N. (2015). Short and long term release mechanisms of arsenic, selenium and boron from a tunnel-excavated sedimentary rock under in situ conditions. Journal of contaminant hydrology, 175, 60-71.

Tiruta-Barna, L. (2008). Using PHREEQC for modeling and simulation of dynamic leaching tests and scenarios. Journal of hazardous materials, 157(2-3), 525-533.

Toubri, Y., Demers, I., Poirier, A., Pépin, G., Gosselin, M.-C. and Beier, N.A. (2021). Merging 3D geological modeling and stochastic simulation to foster the waste rock upstream management. Journal of Geochemical Exploration, 106739.

Trach, Y., Tytkowska-Owerko, M., Reczek, L. and Michel, M.M. (2021). Comparison the Adsorption Capacity of Ukrainian Tuff and Basalt with Zeolite–Manganese Removal from Water Solution. Journal of Ecological Engineering, 22(3).

Vermette, D. (2018). Approche de caractérisation géoenvironnementale axée sur l'utilisation des concepts géométallurgiques. Université du Québec en Abitibi-Témiscamingue. http://depositum.uqat.ca/765/1/Memoire_DVermette.pdf. Master.

Villeneuve, M. (2004). Évaluation du comportement géochimique à long terme de rejets miniers à faible potentiel de génération d'acide à l'aide d'essais cinétique. École Polytechnique de Montréal.

Villeneuve, M., Bussière, B., Benzaazoua, M. and Aubertin, M. (2009). Assessment of interpretation methods for kinetic tests performed on tailings having a low acid generating potential. Proceedings, Securing the Future and 8th ICARD, Skelleftea, Sweden.

Weisener, C. and Weber, P. (2010). Preferential oxidation of pyrite as a function of morphology and relict texture. New Zealand Journal of Geology and Geophysics, 53(2-3), 167-176.

Wiersma, C. and Rimstidt, J. (1984). Rates of reaction of pyrite and marcasite with ferric iron at pH 2. Geochimica et Cosmochimica Acta, 48(1), 85-92.

Wunderly, M., Blowes, D., Frind, E. and Ptacek, C. (1996). Sulfide mineral oxidation and subsequent reactive transport of oxidation products in mine tailings impoundments: A numerical model. Water Resources Research, 32(10), 3173-3187.

Yilmaz, E. (2011). Advances in reducing large volumes of environmentally harmful mine waste rocks and tailings. Gospodarka Surowcami Mineralnymi, 27, 89-112.

CHAPTER 6 ARTICLE 3: INTEGRATING MULTIDISCIPLINARY MODELING TOOLS TO FOSTER SCOPING SURVEYS AND UPSTREAM MINE WASTE MANAGEMENT

This article was issued in the proceedings of *Tailings and Mine waste* conference in 2021[3].

6.1 Abstract

Hard rock mines may induce water quality exceedances stemming from mine drainage. Environmental issues identification at the upstream levels of the development and/or the operation phases steer sustainable solutions design. Nonetheless, this upstream reasoning presents data-limited challenges. To overcome these challenges, the upstream reasoning was amended with a multidisciplinary modeling approach. In this regard, 3D geological modeling, core-logging datasets and stochastic simulation were combined into one modeling approach enabling mine waste classification. This modeling approach overcome issues related to small sample sizes and could be performed along the operation phase. Additionally, incorporating kinetic modeling in the upstream scoping surveys allowed a dynamic geochemical assessment that assists the aforementioned static 3D geomodel. The upstream kinetic modeling and a what-if scenario approach were used to investigate worse case scenarios along the development stage. Finally, merging kinetic and stochastic approaches will produce a holistic screening tool for both development and operation stages.

6.2 Introduction

Geochemical assessment and management of mine wastes gave rise to growing endeavor to fulfill the environmental and social commitments requested by stakeholders. Thorough weighing of trade-offs related to ore profitability, mine wastes management costs and remediation liability is

[3]Toubri, Y., Demers, I. and Beier, N. (2021). Integrating multidisciplinary modeling tools to foster scoping surveys and upstream mine waste management. In Proceedings of Tailings and mine waste conference, Banff, AB, Canada (p. 585-594).

indispensable to sustain the mining business. Surface and underground water are the main vulnerable component of the hard rock mines surroundings. Acid mine drainage (AMD) or contaminated neutral drainage (CND) are by far a potential source of water quality deterioration. The United States Environmental Protection Agency (EPA) categorized water pollution within mining facilities as one of the top three ecological-security threats in the world (Dold, 2008). Therefore, water quality exceedances increase management and remediation costs and consequently could shrink the ore profitability. In this regard, several improvements have been suggested to enhance conventional assessment and management practices (e.g. Benzaazoua *et al.*, 2004; Bussière, 2007; Demers *et al*., 2015; Jouini *et al*., 2020; Lessard *et al*., 2018; Parbhakar-Fox *et al*., 2011). Meanwhile, mining companies and academic researchers realized that proactive solutions should be designed and incorporated in the mine cycle as early as possible to mitigate geo-environmental risks and to anticipate and/or alleviate their costs. In this respect, Aubertin *et al*. (2016) proposed the "design for closure" thinking, which aims to continuously incorporate environmental issues and their respective solutions in each design effort. Likewise, Benzaazoua *et al*. (2008) suggested the upstream mine waste management as a key reasoning to mitigate environmental risks. The upstream mine waste management implies any proactive practice designed beforehand specifically to eliminate or minimize an environmental footprint.

Although an increasing attention is being given to geochemical assessment and integrated management via novel experimental approaches throughout the upstream stages of mines life, none has explored the capabilities of integrated multidisciplinary modeling approaches to support the upstream reasoning. The present paper focuses on bridging different types of modeling tools to enhance mine waste geochemical assessment and management during both the development and operation stages. Modeling approaches described herein are intended to supply efficient and cost-effective screening tools designed not to replace the experimental protocols but to support them at the upstream levels. Since upstream stages are constrained by the lack of materials and data, suitable modeling approaches are needed for environmental risk identification. The first screening tool presented, merged 3D geological modeling, core-logging data and stochastic simulation to enable mine waste classification before stripping operations. The classification is mainly based on contents of deleterious elements in the orebody and its host rock. This multidisciplinary modeling approach was designed to repurpose the advantages of 3D geological modeling for mine waste

classification. However, to fulfill the 3D geological modeling requirements, sufficient datasets are needed to yield good resolution. In this regard, core-logging data and a stochastic approach were combined to address the shortage linked to sample sizes. Although this approach assists in mine waste classification, it yields static 3D geomodels that only describe the total contents of the desired deleterious element throughout the orebody and its host rock as mining operations progress. Therefore, the second screening tool was intended to incorporate kinetic modeling in the geochemical upstream assessment to take into account the temporal dimension. A kinetic model using a water film concept was developed to simulate the likelihood of contaminant release as function of time and to perform a parametric analysis for early risk identification. Since the first modeling toolkit is applicable for mine waste classification during operation and advanced exploration stages, the second modeling approach is devoted to the geochemical assessment during the development stage. Both approaches are based on minimal characterization data and core-logging datasets. The next step will be to upgrade the kinetic model through the stochastic simulation to carry out broader scoping surveys and move beyond the deterministic thinking commonly used in geochemistry. As pointed out, the main objective is to foster the upstream modeling thinking, to overcome interdisciplinary barriers among different modeling disciplines and to move towards integrated multidisciplinary modeling reasoning during upstream geochemical assessment and mine waste management.

6.3 Materials and methods

6.3.1 Spatial modeling for mine waste classification

3D spatial modeling could be performed for economic elements that constitute the orebody as exhaustive sampling and chemical analyses are continuously undertaken for these elements of interest. However, the task is more challenging when 3D spatial modeling is repurposed for classification of mine wastes in terms of their content of deleterious elements. The chemical analyses performed for these elements do not always wrap the entire extent of the orebody and its host rock. Therefore, performing 3D geological modeling only based on the available datasets will produce poor interpolation outcome. The following describes how to overcome this challenge in

order to produce high quality 3D geomodel that could be used for mine waste classification before stripping (upstream stage of stripping operation).

6.3.1.1 Case study: Éléonore mine site

The Éléonore mine site is located in the Eeyou Istchee James Bay municipality in northern Quebec (Canada), 540 km northeast of Rouyn-Noranda. The main orebody, the Roberto deposit, consists of gold mineralization hosted in the vicinity of the tectonometamorphic contact between the La Grande and the Opinaca subprovinces. The Roberto deposit displays multiple mineralization textures along a deeply plunging orebody (Fontaine, 2019). The mineralization is closely associated with arsenopyrite. Consequently, arsenic is the main deleterious element in Éléonore setting. Visualizing the 3D spatial distribution of As throughout the orebody and its country rock will provide the opportunity for mine waste classification; only mine waste with low As content will be deposited in the above-ground facilities, the remnant mine waste should be used as paste and/or rockfill.

6.3.1.2 Stochastic simulation

The prerequisite to perform the stochastic approach described herein is to use two continuous variables and one discrete variable. In the present study, the first continuous variable is the available chemical analyses of As, the second continuous variable is the length of arsenopyrite intervals described in the core-logging reports of up to 12 000 drill cores. The discrete variable is the qualitative assessment of the arsenopyrite proportions based on a standard scale ranging from 0.01 to 100. Each number on the standard scale is referred herein as a class that qualitatively describes the prevalence of arsenopyrite in a given interval of occurrence. The class number and length were recovered from the core-logging dataset. Sufficient core-logging datasets should be available including exploration and mining drill cores. “Sufficient” refers to the required number of drill cores to portray a 3D geomodel of the orebody. This number varies depending on the geological setting and the mineralization style. This requirement justifies the use of this approach during the advanced exploration stage and/or the operation stage as they involve high number of drill cores. Table 6.1 summarizes the component of the database of core-logging as well as the number of arsenopyrite intervals that were analyzed for As.

Table 6.1 Number of arsenopyrite intervals per class and the sample size that was analyzed. Confidence interval: 95%. Adapted from Toubri *et al*. (2021)

Arsenopyrite classes	0.1	0.5	1	2	3
Arsenopyrite intervals	4203	43719	21193	8769	3132
Intervals with As grade	71	666	256	83	59
Margin of error (%)	11.53	3.77	6.09	10.71	12.64

The classes 0.1, 0.5, 1, 2, and 3 were selected from the standard scale (0.01 to 100) because more than 95% of arsenopyrite intervals fell in these classes. The margin of error in table 1 was calculated based on the known sample size (intervals with As grade) and the confidence interval.

Considering two independent continuous variables A and B (Figure. 6.1a), first we establish a power law between A and B by plotting A/B variable versus B variable. Using the logarithmic scale A/B correlates significantly with B (Figure 6.1b). The parameters of the power law (a and b) as well as the correlation coefficient should be mentioned. The second step, we perform an iterative Monte Carlo simulation coupled to correlative sampling (Figure 6.1c). Firstly, we set a normal or log-normal probability distribution functions (PDFs) for A/B and B variables based on their initial sample size shown in Figure 6.1b. The Monte Carlo simulation should sample the PDF of each variable while maintaining the correlation trend among A/B and B variables. The correlation of sampling was not set at deterministic value but it follows a Gaussian distribution centred on the aforementioned correlation coefficient value. The standard deviation of the Gaussian distribution controlled the extent of scattering. The outcome is a linear-shaped scatter that should display comparable power law parameters as the initial sample size; if not the Monte Carlo simulation should be performed again after adjusting the PDFs properties. This is an iterative process to generate a large scatter while abiding by the features of the initial dataset. Afterwards, the desired values of variable B could be selected as well as their respective values of variable A/B (Figure 6.1c). Finally, the normalization is cancelled and a larger dataset is obtained (Figure 6.1d). This method was used to enlarge the As sample size within each class. Furthermore, ten realizations were produced for each class to underline the effect of ergodic fluctuations. The available As grades were used as values of variable A, and lengths of intervals of occurrence of arsenopyrite represent the variable B.

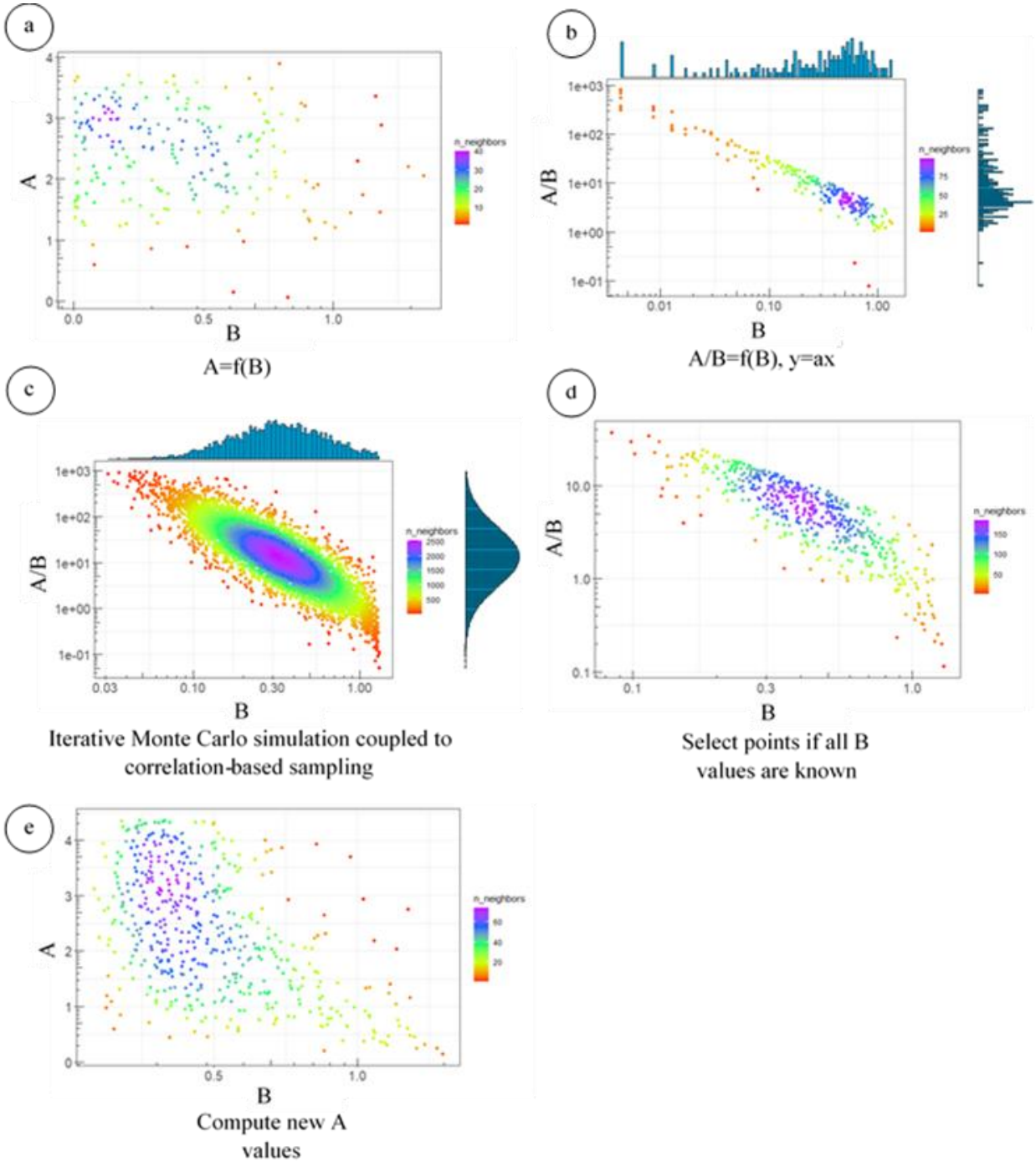


Figure 6.1 The iterative Monte Carlo simulation and the correlation based sampling. Adapted from Toubri *et al.* (2021)

6.3.1.3 Variography and spatial continuity

Geological logging dataset provides the spatial position of intervals of occurrence of arsenopyrite. Consequently, each simulated As grade obtained from the stochastic process, inherits the coordinates of its interval. A 3D variography analysis was undertaken to highlight the spatial anisotropy, the spatial continuity, and the conformity of the 3D geomodel with the geological features of the deposit. The Stanford Geostatistical Modeling Software (SGeMS) was used to establish 3D directional and omnidirectional variograms. Afterwards, the Leapfrog Geo software to perform interpolation and establish the 3D geomodel based on the variograms and the structural measurements from the surface and underground mapping.

6.3.2 Kinetic modeling approach for the pH assessment

Geochemical transport modeling is extensively utilized during operation and remediation stages (Mayer et *al.*, 2002; Wilson et *al.*, 2018). Few studies used geochemical transport modeling during the development stage because the programs being used are data-extensive. Herein, the kinetic modeling was performed based upon minimal data characterization obtained from the feasibility study of a mine project. Subsequently, a parametric analysis was carried out to enhance the upstream geochemical scoping survey and risk identification.

6.3.2.1 Case study: Akasaba West project

The Akasaba West Au-Cu deposit is located in the Abitibi-Témiscamingue region, 15 km east of Val d'Or in Quebec, Canada. The mineralization style consists of thinly disseminated sulfides hosted in moderately to strongly altered metavolcanic rocks (Vermette, 2018). Geological core-logging of diamond drill cores indicates that the ore is characterized by < 5 % pyrite and < 1% chalcopyrite occurring as disseminations and locally as clusters, veinlets, or thin massive sulfide lenses.

6.3.2.2 Laboratory testing

Four weathering cells were set up to assess the geochemical responses of different lithologies belonging to the Akasaba West orebody and its host rock. Weathering cell kinetic test is a cost-effective method for geochemical assessment when limited amount of materials is available. Prior

to testing, samples were characterized to determine their specific surface area, grain size distribution, chemical and mineralogical composition. Special attention has been paid to Mn as it was mentioned that it could be present in the effluent (Vermette, 2018).

6.3.2.3 Conceptual model

Experimental results from weathering cells were simulated by using one weathering cell for calibration and three other weathering cells for benchmarking. Weathering cell setup provides highly oxidizing conditions; atmospheric oxygen and water are not transport-limited throughout the test period. Therefore, the conceptual model considers surface controlled oxidation and dissolution reactions, see Toubri *et al*. (2021b) for details. Based upon mineralogical characterization, the rate law for each mineral was compiled from the literature and integrated in the kinetic keyword block of the model. The kinetics was coupled with equilibrium and transport processes thought relevant for the system. The leaching solution as well as the pore water of the system were considered to be in equilibrium with the partial pressures of atmospheric oxygen and carbon dioxide. These equilibrium reactions allowed no restriction in oxygen supply. The advective transport was included to simulate the advection of the leach solution as a function of the residence time and volumetric flow. The residence time would relate kinetic reactions to advective transport in order to control the time duration of the water-rock interactions. The conceptual model assumed that a thin water film is surrounding the particle surfaces. Hence, kinetic reactions are assumed to occur within the water film - the particle surface boundary. Subsequently, the products of the kinetic reactions were transferred to the bulk solution through a diffusion boundary. An oxygen reservoir was implemented within the water film to trigger and maintain sulfide oxidation. This conceptual model was solved using PHREEQC; a freely available program that can solve 1D geochemical transport problems that do not include a gas transport component.

6.3.3 Integration of kinetic modeling and stochastic simulation

Using parametric analysis to highlight risks of water contamination is an efficient approach to simulate various mineral associations that were not tested in the laboratory because of the lack of materials. However, the parametric analysis is still a deterministic approach that could overlook other leaching scenarios. Furthermore, unlike the operation stage, the development stage has not

benefited from the capabilities of Monte Carlo simulation. In this respect, stochastic 2D spatial distribution of the main sulfides and neutralizing minerals will be produced for various realizations. The 2D space will represent the cross section of waste rock piles that do not exceed the critical length in order to maintain kinetically controlled conditions (Nicholson *et al.*, 2003). Variography will be used to establish contour maps of the spatial distribution of minerals. Thereafter, kinetic modeling will be performed along mesh points to produce contour maps of water quality. This method will supply robust risk identification as it overcomes the deterministic approach and copes with a broader range of possible scenarios.

6.4 Results and discussion

6.4.1 Spatial modeling for mine waste classification

6.4.1.1 Results of Monte Carlo simulation

Results from the stochastic process suggested herein are shown in Figure 6.2. The process was able to propagate the epistemic uncertainty to the simulated sample size (Figure 6.2).

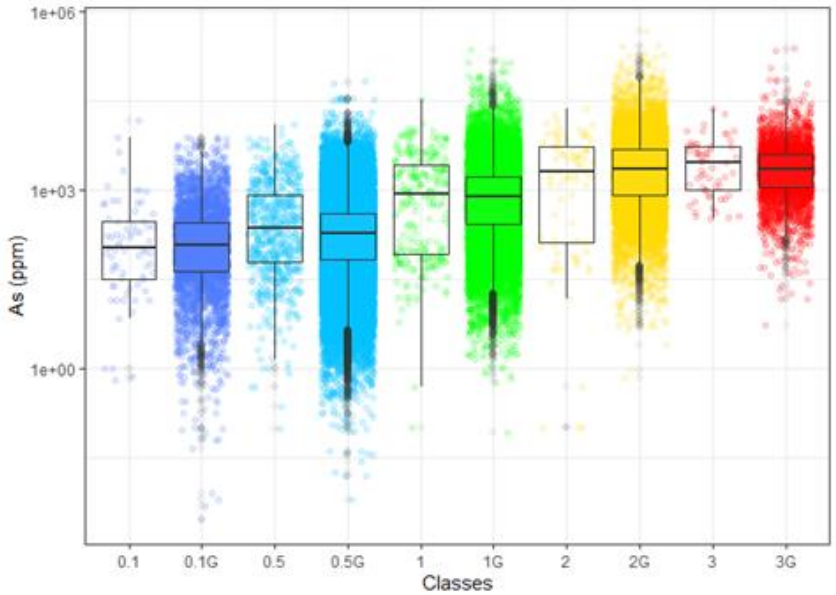


Figure 6.2 Results of the first realization of the stochastic simulation compared to the initial sample size (G denotes the generated data by the stochastic process for each class). Adapted from Toubri *et al*. (2021)

It is worth mentioning that Figure 6.2 displays the first realization, nine other realizations were produced to underline the magnitude of the ergodic fluctuations. No substantial differences were noted among the ten realizations. More details are given in Toubri *et al*. (2021).

6.4.1.2 Variography and spatial continuity

The generated sample size of As grades is now sufficient to carry out 3D geological modeling. Nonetheless, it is worth mentioning that in each realization completely different As grade is attributed to each interval. Therefore, variography analysis was performed to verify if the ten realizations produce substantial differences in terms of 3D spatial continuity. Figure 6.3 displays the differences among the ten variograms produced from the realizations. The iterative process being used has proven to be reliable in producing coherent variograms that abide by the geological features of the deposit; the highest continuity plane in these realizations complies with the structural trend of the gold-bearing ore deposit (Toubri *et al.*, 2021).

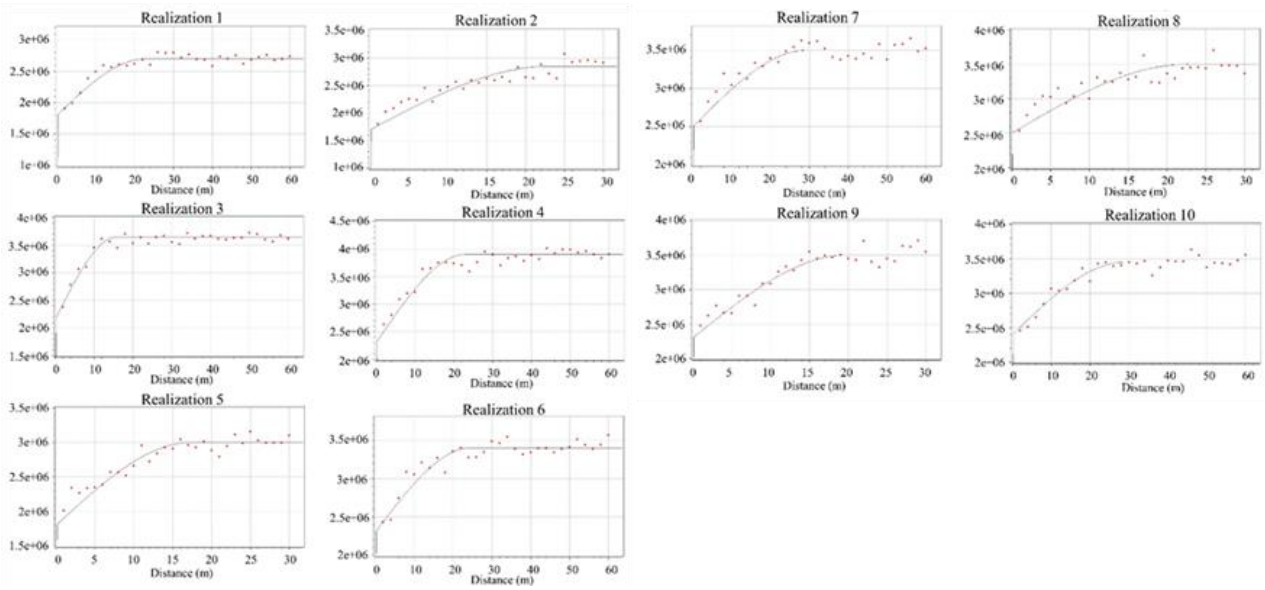


Figure 6.3 Realizations of directional variograms showing the highest spatial continuity

6.4.1.3 Mine waste classification

The 3D geomodel of As spatial distribution was produced for each variogram. Afterwards, the 3D geomodel was projected on underground stopes of Éléonore mine to visualize galleries with high to extreme content of As (Figure 6.4). Mine waste from these sectors will be mainly used in backfill

to avoid the damage that could affect water quality in case they are stored in the above-ground facilities. To validate the 3D geomodel, measured As grades were projected on it to underline the agreement. Certainly, the 3D geomodel does not display the exact measured As grade, but values are on the same magnitude. Accordingly, the agreement is good enough to perform mine waste classification based on As content in the ore and its host rock.

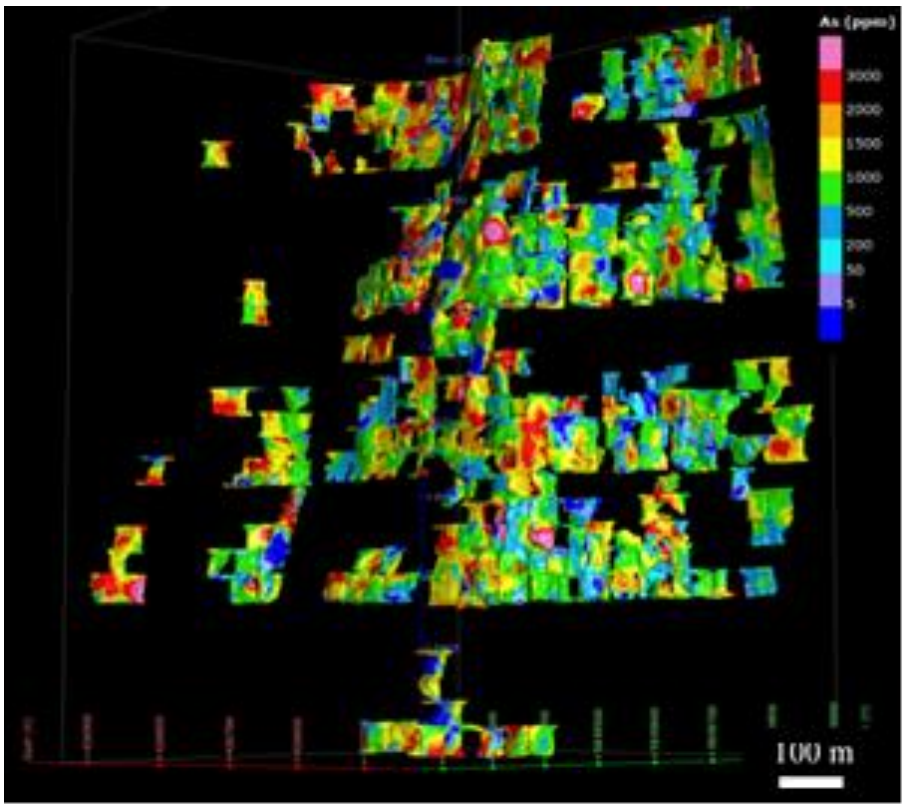


Figure 6.4 Underground stopes classified in terms of their As grades

This process was applied during the operation stage of Éléonore mine to explore its reliability using underground drill cores information. Presently, it could be applied during advanced exploration stages using the drill core information utilized to build the 3D model of the orebody. The main requirement to achieve the process is that the deleterious element should be associated to a mineral phase that could be noticed and described during drill core logging. In cases where the bearing mineral phase is imperceptible, geological logging should comprise portable X-ray fluorescence analysis. Therefore, new perspectives for mine waste management could be envisioned to decrease the environmental footprint of the mine waste disposal using drill core logging.

6.4.2 Kinetic modeling

6.4.2.1 Calibration and benchmarking

The kinetic modeling approach was designed to comply with the upstream level of the development stage of Akasaba West project. According to mineralogical characterization, Mn was mainly detected in calcite (Vermette 2018). So it was simulated as trace element in calcite. The stoichiometric coefficient of Mn in calcite was used as a calibration parameter. Other parameters were used in calibration, such as the diffusion coefficient (D_e) of a chemical element from the water film towards the pore water, available surface of reaction of albite was also used in calibration as albite is present in high weight proportions. Besides the pH, the following elements were simulated in each weathering cell: Fe, Al, K, Na, Ca, Mg and Mn. Only the pH, Ca, Mn and sulfate are presented here. A good agreement between the experimental data and the PHREEQC kinetic model was achieved using $D_e=8.10^{-11}$ m^2/s for chemicals diffusing from the water film to the pore water. The obtained value of D_e within the water film was roughly one order of magnitude lower than the diffusion of ions in free water. A stoichiometric coefficient of Mn ranging between 0.00039 and 0.0015 for 1 mole of calcite yielded a good agreement with the experimental leaching trends (Figure 6.5). The release of Mn is pH-dependent; at lower pH values the dissolution rate of calcite increases. Therefore, increasing the sulfide content would result in higher concentrations of Mn. Meanwhile, low reactive minerals such as silicates dissolve slowly and could raise the pH after a lag time. Despite their low reactivity, silicates contribute to alleviate Mn lixiviation. To underline the model reliability and limitation, three benchmarking cases were performed (not shown here). The benchmarking cases display a good agreement. However the model presented the following limitation: the model did not properly simulate the Mn leaching when calcite and pyrite contents were as low as 0.4% wt and 0.8% wt, respectively, but the simulated values are closer to laboratory results for calcite and pyrite contents above 1% wt and 4 % wt respectively.

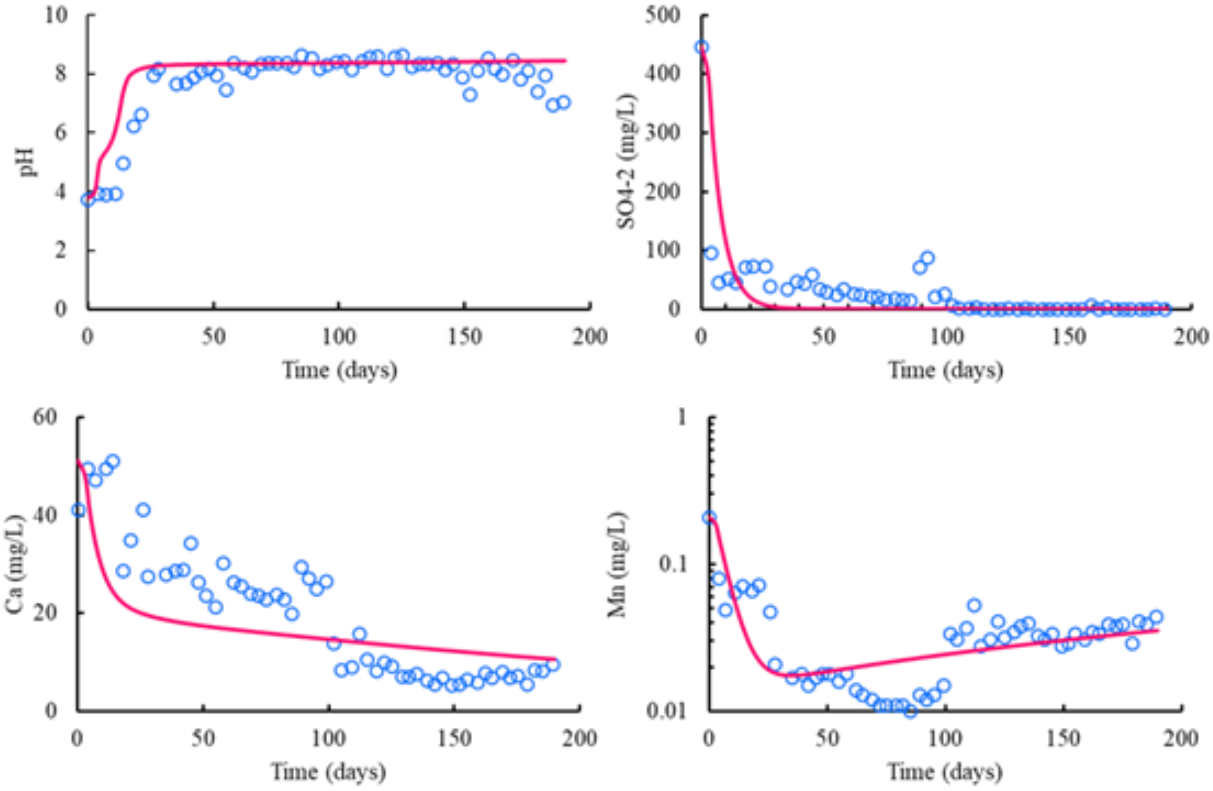


Figure 6.5 Experimental (empty circles) versus modeling (solid line) results from the calibration case. Adapted from Toubri *et al.* (2021b)

6.4.2.2 Parametric analysis

Based on results of the kinetic model, the parametric analysis was performed to underline the contamination risks under more acidic conditions (Figure 6.6). Through testing different mineral assemblages' scenarios, the parametric analysis stresses a considerable contamination potential linked to Cu and Mn lixiviation. In the absence of calcite and the presence of less than 30% wt of albite, acidic conditions would set up and foster chalcopyrite dissolution. On the other hand, in the presence of calcite, the Mn concentrations increase especially when silicates are present at low weight proportions (Figure 6.6).

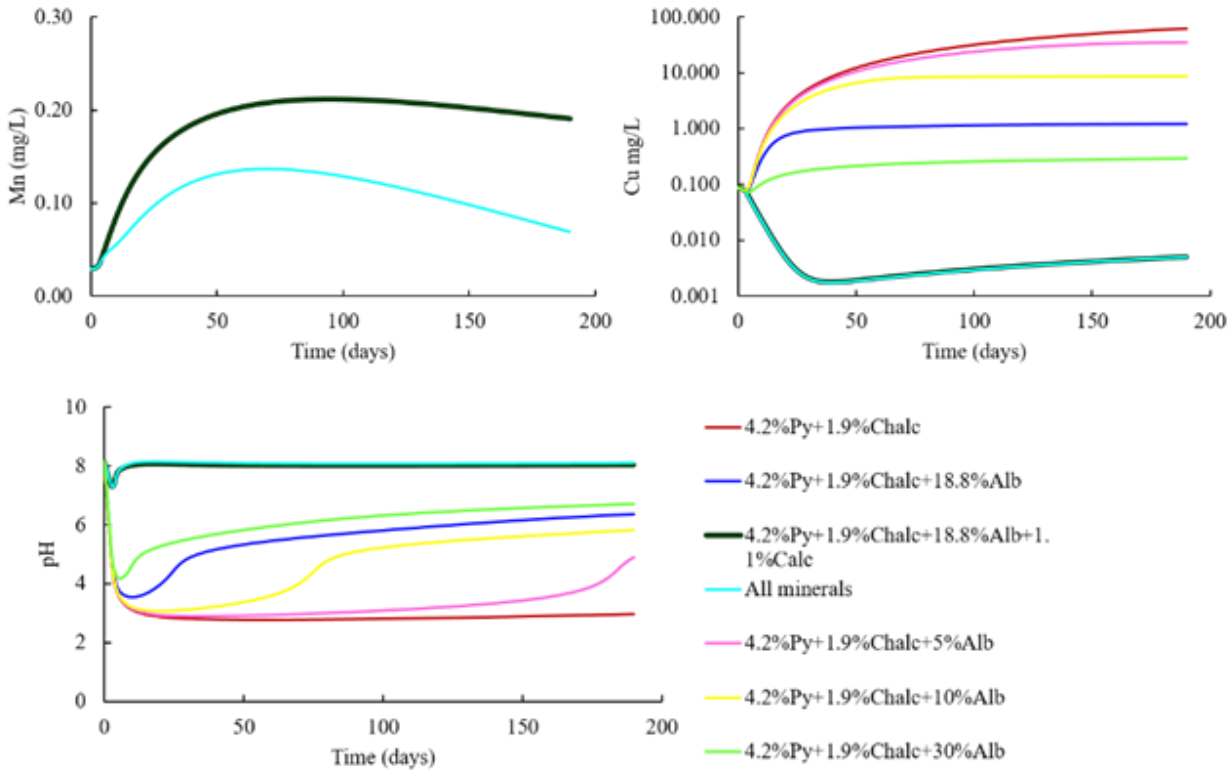


Figure 6.6 Parametric analysis using various scenarios of mineral assemblages

6.5 Conclusion

This work is a bridging effort to dissolve interdisciplinary barriers to assist mine manager's decision-making throughout different upstream stages. A 3D geomodel was built using restrained datasets to assist in mine waste classification before extraction. Figure 7.7 summarizes the approach suggested in this work. Based on core logging data, the approach aimed to cope with two types of variability; the spatial variability and the mineral assemblage variability. The first was assessed to enable mine waste spatial classification and the second was deemed necessary to perform broader scoping surveys of the geochemical behaviour of mine wastes.

This approach highlights that core-logging data are of great importance not only for geologists and mining engineers but also for mine waste managers. In this regard, core-logging data should be carefully compiled and upgraded throughout the entire life of a mine. Furthermore, using stochastic simulation to repurpose 3D geological modeling for mine waste classification revealed a promising horizon for mine waste management to be integrated with a broader spectrum of disciplines. The

present work also bridged kinetic modeling and parametric analysis to geochemical assessment during the development stage without using data-intensive programs. This approach enables a better risk identification through coupling kinetic testing, kinetic modeling and assessment of a larger spectrum of scenarios that were not evaluated in the lab owing to the lack of material. Both upstream modeling attempts, however, could be further improved through merging kinetic modeling and stochastic simulation capabilities. Future work will be focused on this subject to improve the integration thinking suggested herein.

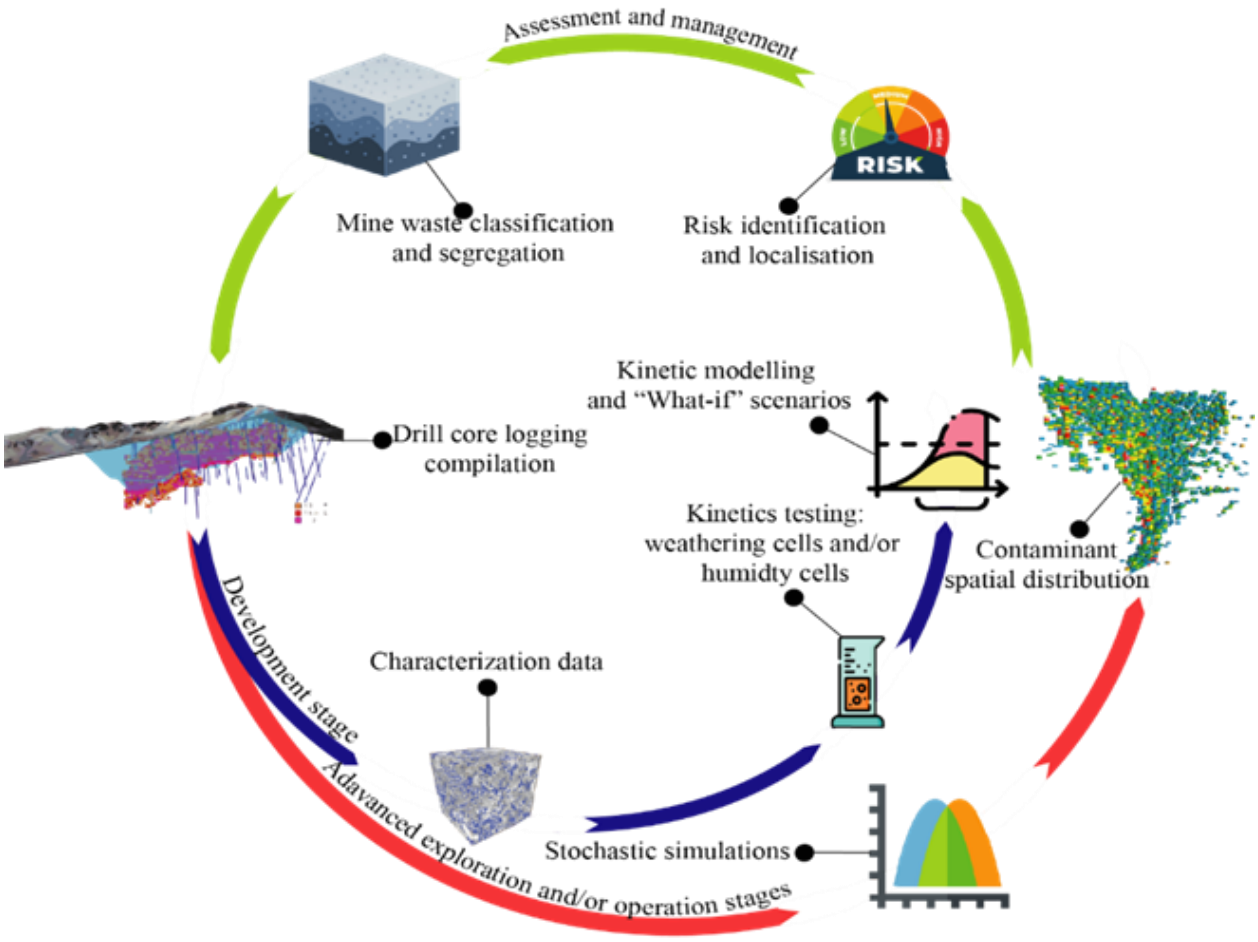


Figure 6.7 A summary of the integration reasoning suggested in this work

Acknowledgements

The authors thank the staff of Akasaba West project and Éléonore mine site for their support and the Unité de Recherche et Service en Technologie Minérale (URSTM) staff for their assistance in the laboratory. The authors are grateful for the insights and suggestions from Dr. J. Mahoney, Dr.

D. Parkhurst and Dr. D. Kinniburgh during the formulation of the PHREEQC and PHREEPLOT models used in this work. Funding for this study was provided by NSERC TERRE-NET program (NSERC-TERRE-NET 479708-2015), led by Dr. D. Blowes (University of Waterloo).

References

Aubertin, M., Bussière, B., Pabst, T., James, M. and Mbonimpa, M. (2016). Review of the reclamation techniques for acid-generating mine wastes upon closure of disposal sites. Dans Geo-Chicago 2016 (p. 343-358).

Benzaazoua, M., Bussière, B., Demers, I., Aubertin, M., Fried, É. and Blier, A. (2008). Integrated mine tailings management by combining environmental desulphurization and cemented paste backfill: Application to mine Doyon, Quebec, Canada. Minerals engineering, 21(4), 330-340.

Benzaazoua, M., Perez, P., Belem, T. and Fall, M. (2004). A laboratory study of the behaviour of surface paste disposal. Proceedings of the 8th International Symposium on Mining with Backfill, The Nonferrous Metals Society of China, Beijing.

Bussière, B. (2007). Colloquium 2004: Hydrogeotechnical properties of hard rock tailings from metal mines and emerging geoenvironmental disposal approaches. Canadian Geotechnical Journal, 44(9), 1019-1052.

Demers, I., Bouda, M., Mbonimpa, M., Benzaazoua, M., Bois, D. and Gagnon, M. (2015). Valorization of acid mine drainage treatment sludge as remediation component to control acid generation from mine wastes, part 2: field experimentation. Minerals Engineering, 76, 117-125.

Dold, B. (2008). Sustainability in metal mining: from exploration, over processing to mine waste management. Reviews in Environmental Science and bio/technology, 7(4), 275.

Fontaine, A. (2019). Géologie des minéralisations aurifères de la mine Éléonore, Eeyou Istchee Baie-James, province du Supérieur, Québec, Canada. Université du Québec, Institut national de la recherche scientifique.

Jouini, M., Benzaazoua, M., Neculita, C.M. and Genty, T. (2020). Performances of stabilization/solidification process of acid mine drainage passive treatment residues:

Assessment of the environmental and mechanical behaviors. Journal of Environmental Management, 269, 110764.

Lessard, F., Bussière, B., Côté, J., Benzaazoua, M., Boulanger-Martel, V. and Marcoux, L. (2018). Integrated environmental management of pyrrhotite tailings at Raglan Mine: Part 2 desulphurized tailings as cover material. Journal of cleaner production, 186, 883-893.

Mayer, K.U., Frind, E.O. and Blowes, D.W. (2002). Multicomponent reactive transport modeling in variably saturated porous media using a generalized formulation for kinetically controlled reactions. Water Resources Research, 38(9), 13-11-13-21

Nicholson, R.V., Rinker, Michael J., Acott, Gerry. and Venhuis, M.A. (2003). Integration of field data and a geochemical transport model to assess mitigation strategies for an acid-generating mine rock pile at a uranium mine. Proceedings, Sudbury.

Parbhakar-Fox, A.K., Edraki, M., Walters, S. and Bradshaw, D. (2011). Development of a textural index for the prediction of acid rock drainage. Minerals Engineering, 24(12), 1277-1287.

Toubri, Y., Demers, I., Poirier, A., Pépin, G., Gosselin, M.C. and Beier, N.A. (2021). Merging 3D geological modeling and stochastic simulation to foster the waste rock upstream management. Journal of Geochemical Exploration, 106739.

Toubri, Y., Vermette, D., Demers, I., Beier, N. and Benzaazoua, M. (2021). Incorporating Kinetic Modeling in the Development Stages of Hard Rock Mine Projects. Minerals, 11(12), 1306.

Vermette, D. (2018). Approche de caractérisation géoenvironnementale axée sur l'utilisation des concepts géométallurgiques. http://depositum.uqat.ca/765/1/Memoire_DVermette.pdf.

Wilson, D., Amos, R.T., Blowes, D.W., Langman, J.B., Ptacek, C.J., Smith, L. and Sego, D.C. (2018). Diavik waste rock project: A conceptual model for temperature and sulfide-content dependent geochemical evolution of waste rock–Laboratory scale. Applied geochemistry, 89, 160-172.

CHAPTER 7 ARTICLE 4: INTEGRATING 3D GEOLOGICAL MODELING AND KINETIC MODELING TO ALLEVIATE ACID MINE DRAINAGE THROUGH UPSTREAM MINE WASTE CLASSIFICATION

This article is accepted for publication[4].

7.1 Abstract

Mine waste classification preceding mining, constitutes a proactive solution to classify and segregate mine waste into geo-environmental domains based upon the magnitude of their environmental risks. However, upstream classification requires multi-disciplinary and integrated approaches. This study integrates geological modeling and kinetic modeling to inform upstream mine waste classification based on the pH generated from the main acid-generating and acid-neutralizing reactions once waste rock is stored in oxidizing conditions. Geological models were used to depict the ante-mining spatial distribution of the main reactive minerals: pyrite, albite and calcite. Subsequently, the corresponding block models were created. The dimension of the elementary voxels for each block model was set at 40x40x40 meters for this study. The kinetic modeling approach was performed using PHREEQC and VS2DRTI to consider unsaturated conditions. The kinetic modeling simulated a 1D column for each voxel. The column simulates the excavated state of the hosting rock involving kinetic reactions and unsaturated flow under highly oxidizing conditions. Subsequently, the resulting pH for different intervals of time was assigned to its respective voxel. The outcome consists of a spatio-temporal visualization of the pH defining ante-mining geo-environmental domains, thereby providing the opportunity for formulating proactive management measures regarding the hazardous geo-environmental domains.

---

[4] Toubri, Y., Demers, I. and Beier, N. (2022). Integrating 3D geological modeling and kinetic modeling to alleviate acid mine drainage through upstream mine waste classification. Accepted for publication in Environmental Pollution journal on 3 September 2022.

Keywords: Geological logging, Spatial models, Mineral kinetics, Unsaturated flow, Geo-environmental domains.

7.2 Introduction

Generally, the mining cycle begins with regional and local exploration surveys to guide the development stage. This stage involves pre-feasibility and feasibility investigations to define the deposit resources and reserves to economically remove the hosting rock and mine the orebody throughout the mining stage. Boundaries between the orebody and its hosting rock are visualized using geological modeling, which delineates the ore casings based on the cut-off grade, the geological logging data and the numerical database. Geological modeling is a staged process that evolves along with the drilling surveys to establish the ore 3D geological model to guide the mineral exploration and the subsequent mining phases (e.g. Martin-Izard *et al.* (2015), Stoch *et al*. (2018), Wu and Xu (2014)). Therefore, links between the geology and mining were established and extensively adopted as corporate governance procedures known as applied mining geology (Abzalov, 2016). The applied mining geology embeds a set of practices, currently used by mining ventures to optimise the economic outcome of a deposit.

In addition to challenges related to effective mining, tackled through efficient connection between the geologist and the mining engineer, mine stakeholders should fulfill environmental requirements and effectively manage the environmental footprint of the mine solid waste. The host rock below the cut-off grade is classified as waste rock that is frequently deposited in aboveground storage facilities in direct contact with the atmospheric conditions. Previously sequestered sulphides are exposed to oxidizing conditions upon surface disposal and become chemically unstable. Consequently, the oxidation process is triggered, manifested in most cases as acid mine drainage (Akcil and Koldas, 2006; Blowes *et al*., 2003; Evangelou, 1995; Jamieson, 2011; Nicholson and Scharer, 1994; Wunderly *et al*., 1996). Acid mine drainage (AMD), an anthropogenic process associated to mining, generates contaminated effluents known by their low pH values and high concentrations of dissolved metals and oxyanions (Nordstrom *et al*., 2000; Nordstrom and Alpers, 1999). These geochemical features entail an acute reduction of the water quality and hazardous exposure of the surroundings. Accordingly, AMD is considered by the United States Environmental Protection Agency (EPA) as one of the top three worldwide security threats (Dold,

2008). In this regard, mining companies should dedicate portfolios and corporate governance procedures for AMD prevention, prediction, treatment and rehabilitation using practices explored so far (Aachib *et al*., 1994; Aubertin *et al*., 2016; Benzaazoua *et al*., 2008; Benzaazoua *et al*., 2004; Bouzahzah *et al*., 2014; Bussière, 2007; Bussière *et al*., 2007; Demers *et al*., 2015; Demers *et al*., 2017; Demers *et al*., 2013; Jouini *et al*., 2020; Lawrence and Wang, 1997; Mbonimpa *et al*., 2008; Neculita *et al*., 2010; Parbhakar-Fox *et al*., 2011). More recently, Toubri *et al.* (2021a) used the 3D implicit geological modeling for upstream waste rock classification to support contaminant-leaching prevention. Benzaazoua *et al.* (2008) used the upstream reasoning; it refers to any proactive practice that aims at the alleviation or the elimination of a given environmental risk by acting on its upstream attributes. Toubri *et al*. (2021a) established the 3D spatial distribution of arsenic (As) contained in the hosting rock of the Roberto gold deposit in Éléonore mine site. Thereafter, an in-situ classification of the hosting rock based on its content of As was carried out before stripping operations to identify underground stopes with high to extreme As content. This classification delineated sectors that are not recommended for surface disposal owing to their high As grade, thereby preventing As leaching and its related water exceedances from the upstream level.

In this paper, the main objective is to establish the connection between geological modeling and AMD potential. In the same manners as the strong information flow between the mining engineer and the geologist to face mining-related issues, communication and concrete links between the geologist and the environmental geochemist are needed to cope with the AMD environmental challenges. Repurposing some of the geological modeling practices for AMD mitigation and dissolving interdisciplinary barriers among geological modeling tools and environmental geochemistry tools are the main intended outcomes of the present study. This cross-disciplinary study developed a new method for AMD risk mitigation. The main novelty is the integration of 3D geological modeling, kinetic modeling and unsaturated flow modeling to undertake a dynamic classification of mine waste beforehand. The modeling toolkit of the environmental geochemistry encompasses kinetic modeling and reactive transport modeling to forecast and/or simulate leachate quality. For instance, Molson *et al*. (2005) appraised design strategies intended to alleviate AMD from waste rock piles using HYDRUS and POLYMIN codes. Similarly, Pabst *et al.* (2017) used MIN3P to assess the hydro-geochemical behavior of covered pre-oxidized tailings. Most AMD-

related models are centred on operation and post-closure stages (Demers *et al*., 2013; Kalonji-Kabambi *et al*., 2020; Molson *et al*., 2008). More recently, Toubri *et al.* (2021b) used kinetic modeling during the development stage of a mine project with a focus on oxidation-neutralization kinetics and the resulting pH to foster the proactive reasoning. On the other hand, the modeling toolkit of the mining geology comprises 3D implicit numerical modeling, which is based upon spatial continuity analysis using variograms and spatial interpolation codes (Abzalov, 2016; Cowan *et al*., 2002; Hillier *et al*., 2014; Natali *et al*., 2013; Remy *et al*., 2009). Hence, the specific objectives of the present study are (i) the use of 3D implicit numerical modeling to establish the ante-mining spatial distribution of pyrite, albite and calcite; the main acid-generating and acid-neutralizing minerals of a given mine project (ii) the establishment of the block model for each numerical model, and (iii) the use of 1D reactive transport modeling for each voxel to attribute the resulting pH values to their respective voxels. The reactive transport modeling setup assumes auspicious conditions to trigger oxidation-neutralization process. Therefore, an upstream spatial classification of the hosting rock, based upon the pH under oxidizing conditions, could be undertaken beforehand to assist in AMD prevention.

7.3 Materials and methods

7.3.1 Geological framework

The study considers a gold-bearing deposit hosted in heterogeneous metasedimentary sequence. The deeply plunging and East-trending orebody exhibits three main types of mineralization types; stockworks (interconnected and randomly oriented veins), disseminations and massive occurrences. Exploration surveys delimited the deposit through meshless network of drill cores (drill core surveys without a regular mesh). Throughout the advanced exploration stages, resources and reserves were defined along with the deposit spatial features based upon the geological logging of the drill cores. The proven reserves are 500 meters deep while the indicated resources extend from 500 to 1000 meters below the surface. The definition of the mineral reserves was based upon CIM (the Canadian Institute of Mining) Definition Standards for Mineral Resources & Mineral Reserves. Comprehensive sampling of drill cores was conducted to measure the gold grades and to establish the 3D model of the mineralization accordingly. Samples were selected for mineralogical

characterization using X-ray diffraction; the most reactive gangue minerals include pyrite, calcite and albite. Pyrite described throughout the geological logging is frequently present as disseminations and seldom present as stockworks. Pyrite is present in 82% of the total number of drill core samples. The pyrite content was measured in 533 samples, the obtained mineral weight proportions found in the pyrite disseminations are ranging from 0.5 to 8 wt. %. Whereas, the stockworks could contain up to 25 wt. % of pyrite. Samples with pyrite disseminations account for 95% of the sample size, while samples containing pyrite stockworks represents 5% of the sample size. Calcite is present as disseminations with mineral weight proportions ranging from 0.4 to 2 wt.%. With regard to calcite occurrences reported throughout the geological logging, drill core samples containing calcite represent 2.65% of the total number of drill cores. Albite is present as massive occurrences with mineral weight proportions ranging from 4 to 50 wt. %. The quantitative dataset indicates that 61% of the analyzed sample size of albite ranges between 10 and 20 wt. %. Other gangue minerals include quartz, muscovite, biotite, augite and epidote. Toubri *et al.* (2021b) issued details of the mineralogical and chemical composition considered for the present study.

7.3.2 3D implicit geomodeling

The 3D implicit geo-modeling is utilized herein to build the 3D numerical models of pyrite, albite and calcite hosted within the considered orebody. Such models could be established using meshed or meshless numerical datasets depending on the used interpolation code abilities. Appropriate data density is required to ascertain suitable interpolation quality (Stoch *et al.*, 2018). Nonetheless, exhaustive quantification of mine waste related parameters is not cost-effective as most chemical and mineralogical expenses are devoted to the economically valuable ore rather than its host rock. In this regard, Toubri *et al*. (2021a) disclosed a method relying on the available numerical data, geological logging data and stochastic simulation to overcome the database shortages. This approach is used in this study to output denser mineral proportion datasets. The relevant background of the aforementioned approach is summarised herein. The novelty is to integrate the stochastic approach developed for 3D geological modeling with reactive transport modeling to perform dynamic (time-dependent) classification of mine waste.

7.3.2.1 The stochastic method components

(i) The geological logging

Along with drilling surveys, geologists carry out geological logging of the drill cores. Geological logging is a detailed description of the mineral occurrences. It mainly reports the type of the mineral occurrence (dissemination, stockwerks, massive, etc.), the occurrence length known as the interval of occurrence. The interval of occurrence is the length of a drill core sample where the described mineral occurs as disseminations, stockworks or massive lodes. In addition to a qualitative judgment on the mineral prevalence within its interval of occurrence. Accordingly, an indicator value (discrete variable, such as visual classification of a given mineral content) is attributed to each interval. This indicator variable is named "class" after Toubri *et al*. (2021a); a class refers to occurrences with same indicator value. Figure 7.1 depicts the main geological logging information as well as the aforementioned terminology; colors were used to illustrate the class variable for a particular mineral.

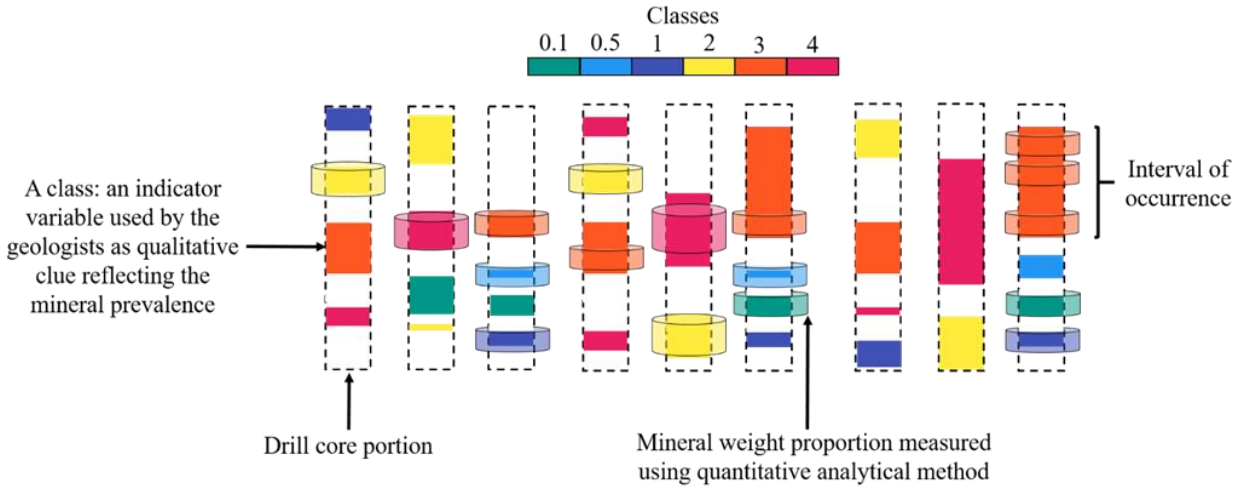


Figure 7.1 Illustration of the geological logging procedure and the associated raw data describing the occurrences of a given mineral within drill cores. The geological logging includes: the samples selected for analytical measurement of the mineral contents (double-highlighted areas), the interval of occurrence which is the length of a mineral occurrence in a drill core sample and the class which is the indicator value assigned to an interval of a mineral occurrence to describe its prevalence based upon the crystals size and their abundance. Uncoloured areas indicate the absence of the mineral

Some mineral occurrences reported in the logging reports may undergo a quantitative analytical method to measure their mineral weight proportion. Nonetheless, the analyzed sample size constitutes a slight portion of the reported intervals of occurrence. Consequently, the quantitative data do not fulfill the spatial density requirement of the 3D implicit geo-modeling.

On the other hand, the interval and the class are a continuous variable and a discrete variable respectively, with complete sample sizes. The subsequent section describes how the logging-related raw variables are coupled to the stochastic simulation to fulfill the spatial density requirement.

(ii) Monte Carlo simulation

The stochastic simulation portrayed in Figure 4.6 is a correlation-based Monte Carlo process that ensures homoscedasticity and uncertainty propagation throughout the generated data (Toubri *et al.*, 2021a). The problem to be solved using Monte Carlo simulation consists of restricted measurements of the variable A while the B variable is thoroughly sampled and measured. The purpose of the Monte Carlo simulation is to estimate the probability density function (PDF) of a restricted variable A based upon a well-defined PDF of the variable B. The first step is to consider two continuous and independent variables A and B. Figure 4.6.a depicts the sample size where both variables were measured. Thereafter, an auxiliary variable is created by normalising the values of A variable by their respective values of B variable. Using a logarithmic scale, the normalized variable (A/B) is represented in the y-axis and the B variable in x-axis. Consequently, the resulting power law ($y=ax^b$) exhibits significant correlation in the logarithmic scale and sets forth the objective function of the process being used (a and b are the power law parameters) (Figure. 4.6.b). The parameters of the power law displayed by the measured dataset are used as criterion of convergence of throughout the following steps. Afterwards, a Monte Carlo simulation is performed based on correlated random sampling of the probability density functions (PDFs) set for the auxiliary variable and B variable. The PDF of the thoroughly sampled B variable is defined relying on its comprehensive sample size while the parameters of the auxiliary variable PDF are iteratively updated until obtaining a power law parameters (a and b) as similar as possible to the objective function (Figure 4.6.c). This Monte Carlo simulation enabled the generation of a linear-shaped scatter with a large number of points (Figure 4.6.c). The scatter dispersion is controlled through a Gaussian distribution centred on the correlation coefficient defined previously (Figure 4.6.b). The

definition of the correlation as a stochastic parameter rather than a static value allows for the epistemic uncertainty approximation as discussed by Toubri *et al*. (2021a). The final steps consist of selecting the desired values of the B variable along with their respective values of the auxiliary variable (Figure 4.6.d) and cancelling the normalisation to obtain the newly generated data of A variable (Figure 4.6.e).

For a particular mineral logging information, the available quantitative data (the measured mineral proportions) were sorted by the user-defined classes. Subsequently, the aforementioned stochastic approach was performed for each class. In this case, the intervals are the continuous variable with complete sample size (B variable) and the mineral weight content assays constitute the continuous variable with incomplete sample size (A variable). The simulated values of the mineral weight proportion are then attributed to their respective intervals. Table 7.1 summarizes the number of intervals belonging to each class and the sample size that was analyzed for the mineral weight proportion. Relying on a confidence interval of 95%, margins of error were computed for each set of data. Only one class was used for describing calcite occurrences since it occurs as scarce disseminations. Given the slightly homogenous presence of albite throughout the hosting lithology, two classes were sufficient to portray its occurrences. Pyrite, though, exhibits a higher range of variability and its prevalence was described throughout logging using four classes. The margins of error computed for each mineral class are equal or lower than 15%. They could be further curtailed as more analytical data are imparted throughout the project phases. In the present study, 15% was considered low enough for the modeling purposes. Nonetheless, exhaustive logging data are the essential requirement to implement the spatial continuity analysis. Practically, the Monte Carlo simulation was performed using the GoldSim software package. GoldSim is a multipurpose modeling software that enables the implementation of models in a dynamic and probabilistic framework (Kossik and Miller, 2004; Rizzo *et al*., 2006). Three linked PDFs were implemented in GoldSim using built-in stochastic elements: the auxiliary variable, the interval variable and the correlation.

As pointed out, the power law parameters were used as conformity clues to ensure homoscedasticity between the measured and the simulated dataset in each class. Furthermore, abiding by the conformity parameters, the effect of ergodic fluctuations related to PDFs random sampling is minimal. (ergodic fluctuations are simply the differences among different realizations

generated using the same Monte Carlo simulation). Detailed insights on homoscedasticity, hypothesis testing, ergodic fluctuations as well as the method validation are issued in Toubri *et al*. (2021a).

Table 7.1 Margins of error associated to the mineral classes computed based upon the logging interval populations and the available analyzed sample size

	Pyrite classes				Albite classes		Calcite class
	0.1	0.5	1	2	3	4	0.1
Logging intervals	4187	43 446	21 002	8667	10 187	4091	2500
Analyzed sample size	62	201	99	171	76	44	47
Margins of error (%)	12	7	10	7	11	15	14
Confidence interval (%)	95						

7.3.2.2 Spatial continuity analysis

After generating denser dataset of the mineral weight proportion variable, each simulated value inherits the coordinates of its interval. Subsequently, a variogram analysis was performed using the Stanford Geostatistical Modeling Software (SGeMS) enabling the calculation of omnidirectional and directional variograms in the 3D space (Remy *et al*., 2009). The variogram analysis allows for the definition of the plane with the highest spatial continuity. The SGeMS outputs are then used in the course of the 3D implicit modeling undertaken in Leapfrog Geo. The Leapfrog Geo software employs a rapid 3D interpolation method named radial basis functions (RBFs) to interpolate grades and lithologies in 3D space based upon meshless datasets (Aguilar *et al*., 2005; Buhmann, 2000; Cowan *et al*., 2002; Cuomo *et al*., 2013; Floater and Iske, 1996; Hillier *et al*., 2014; Iske, 2002; Natali *et al*., 2013; Wright, 2003).

The variogram analysis provides the spatial continuity parameters of the dataset, including the nugget effect, the range and the sill. After, projecting the dataset in the 3D space, the variogram parameters were used for numerical modeling using Leapfrog Geo. This software undertakes spatial interpolation based upon the variogram parameters along with RBFs algorithm enabling mesh-free interpolants. Structural measurements were used to define the spatial model orientations for different depths. Finally, each numerical model was benchmarked against the available measurements of the mineral content. This process was performed for the datasets of pyrite, calcite and albite respectively. Afterwards, a block model was created for each numerical model; the dimension of the elementary volumetric constituent, known as voxel, was set at 40x40x40 meters. The dimension of the voxel could be further reduced as drill core surveys progress and computing capabilities are improved.

7.3.3 1D reactive transport modeling

Reactive transport modeling was performed for each voxel along the main plane of mining to simulate the geochemical behaviour of the given voxel, once blasted and excavated. For each voxel a 1D column of 20 m high, containing minerals proportions designated by the pyrite, albite and calcite block models, was simulated to assign a pH value to the given voxel. The simulated weathering conditions are similar to the weathering cell kinetic test. The extremely slow reacting minerals and inert minerals such as quartz and muscovite were considered as inert matrix throughout the simulation. It was demonstrated by Toubri et al. (2021b) that their effect on the pH is insignificant regarding the considered geochemical setting. The simulation sets highly oxidizing conditions assuming no oxygen restriction along the column height to assist in proactive reasoning upon disposal and conservative predictions. Accordingly, the through-flowing water and the pore water are in equilibrium with O_2 and CO_2 partial pressures during the whole duration of the simulation. Two days wetting event was simulated each month resulting in a liquid to solid ratio (L/S) of 5000 L/m^3/week, which is similar to L/S used in weathering cell kinetic test (Plante *et al.*, 2014). The drying event lasts 28 days entailing unsaturated flow towards the water table set 10 m below the column base. Thereby, free drainage boundary condition was set at the column bottom. An infiltration boundary condition is applied to the column top during recharge periods. The drying-wetting cycles were simulated throughout 1 year. PHREEQC was used to implement the

kinetic reactions of the system and VS2DRTI was used to simulate the transport environment to overcome PHREEQC limitations (a conceptual model is provided in the supplementary file). Both software are released by the United States Geological Survey and are well synchronized at solving reaction kinetics along with the unsaturated flow Richard equation (Hsieh *et al.*, 2000; Parkhurst and Appelo, 2013).

Regarding the unsaturated environment, the Van Genuchten (1980) parameters of typical fine-sand grain size were used since particles smaller than 2.4 mm contribute the most in the geochemical reactions (Elghali *et al.*, 2019). The unsaturated flow parameters are reported in the supplementary materials.

Pyrite is the main acid-generating mineral found in the orebody. The specific rate of pyrite oxidation suggested by Jerz and Rimstidt (2004) was selected for the present study:

$$r_k = \frac{10^{-6.6} P^{0.5}}{t^{0.5}} \qquad 7.1$$

P is the partial pressure of oxygen (atm) and t is time (s). Jerz and Rimstidt (2004) considered in their experiments the oxidation of pyrite under unsaturated conditions. Furthermore, they included the pyrite-aging factor in the specific rate, which passivates pyrite surface as oxidation proceeds.

The generic form of the dissolution rate of gangue minerals issued by Chou and Wollast (1985) and Casey and Ludwig (1995) and adopted by Palandri and Kharaka (2004) is defined as:

$$r_k = \begin{pmatrix} k_{H^+} e^{\frac{-E_{H^+}}{R}\left(\frac{1}{T}-\frac{1}{298.15}\right)} [H^+]^{n_1}(1-\Omega^{p_1})^{q_1} + \\ k e^{\frac{-E}{R}\left(\frac{1}{T}-\frac{1}{298.15}\right)}(1-\Omega^{p_2})^{q_2} + \\ k_{OH^-} e^{\frac{-E_{OH^-}}{R}\left(\frac{1}{T}-\frac{1}{298.15}\right)} [H^+]^{n_2}(1-\Omega^{p_3})^{q_3} \end{pmatrix} \qquad 7.2$$

Where E_{H^+}, E, and E_{OH^-} are the activation energies in acidic, alkaline, and neutral conditions, respectively; k_{H^+}, k_{OH^-}, and k are rate constants for acidic, alkaline, and neutral conditions, respectively; n_i denotes the reaction order; Ω is the mineral saturation index; and pi and qi are dimensionless empirical parameters. The rate parameters of albite and calcite, the main neutralizing minerals hosting the orebody, are listed in the supplementary file. The entire process of the integrated modeling is summarized in figure 7.2. A practical step-by-step description of the methods is available in the supplementary file.

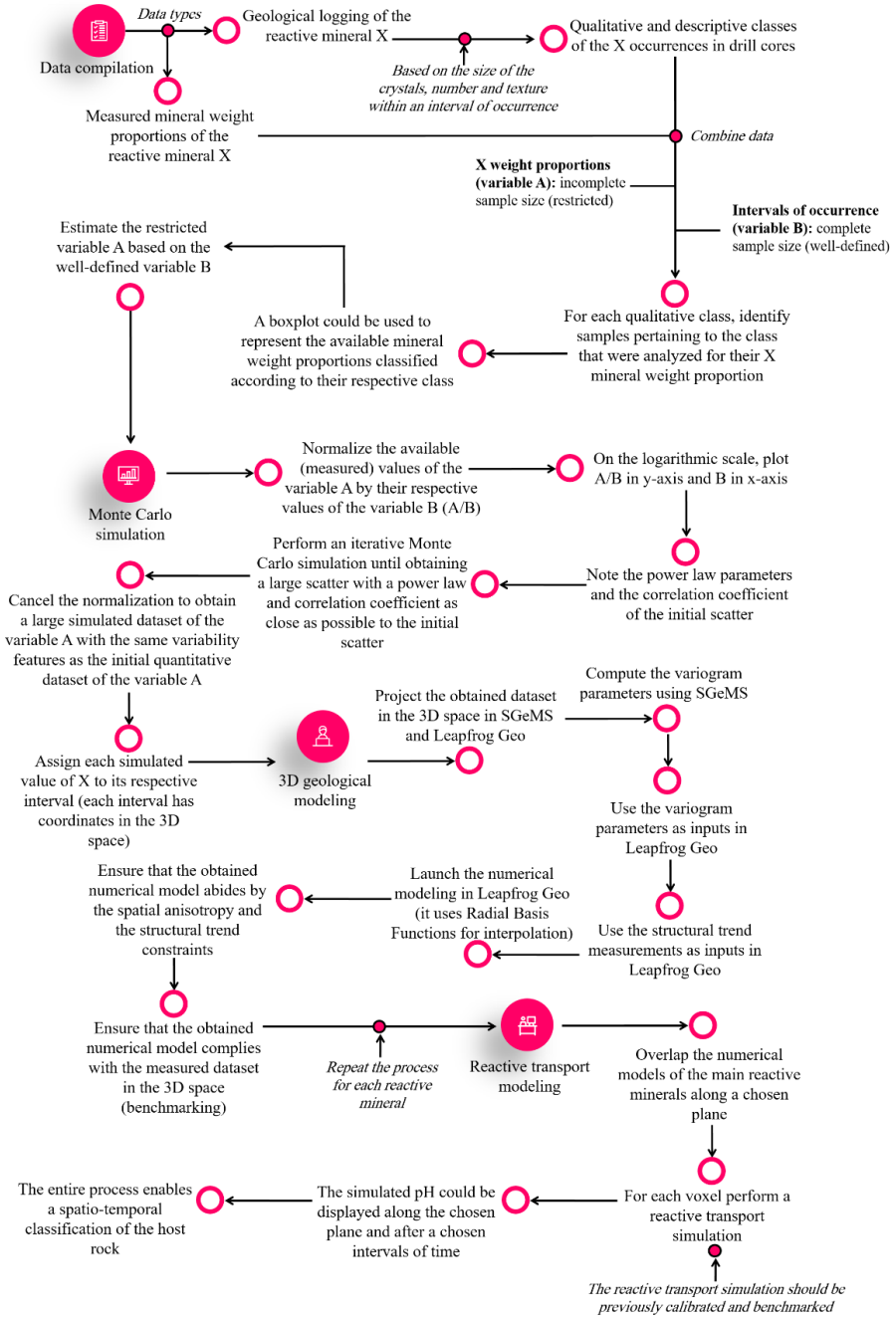


Figure 7.2 Workflow of the methods used to perform a dynamic classification of the host rock based upon the integration of geological logging information, Monte Carlo simulation, 3D geological modeling and the reactive transport modeling. (X denotes a reactive mineral present in the deposit setting, variable A denotes the available measurements of the X mineral weight proportions, and variable B denotes the intervals of occurrence of the mineral X reported throughout the geological logging).

7.4 Results and discussion

7.4.1 Monte Carlo simulation results

The iterative and correlation-based Monte Carlo simulation was carried out for each class indicator value. Figures 7.3 displays the simulation outcome constrained to the objective function (a power law; y=axb) portrayed by the available measured data. Pyrite classes, reported in Table 7.1, and their respective sample size are depicted in Figure 7.3 along with the simulated population.

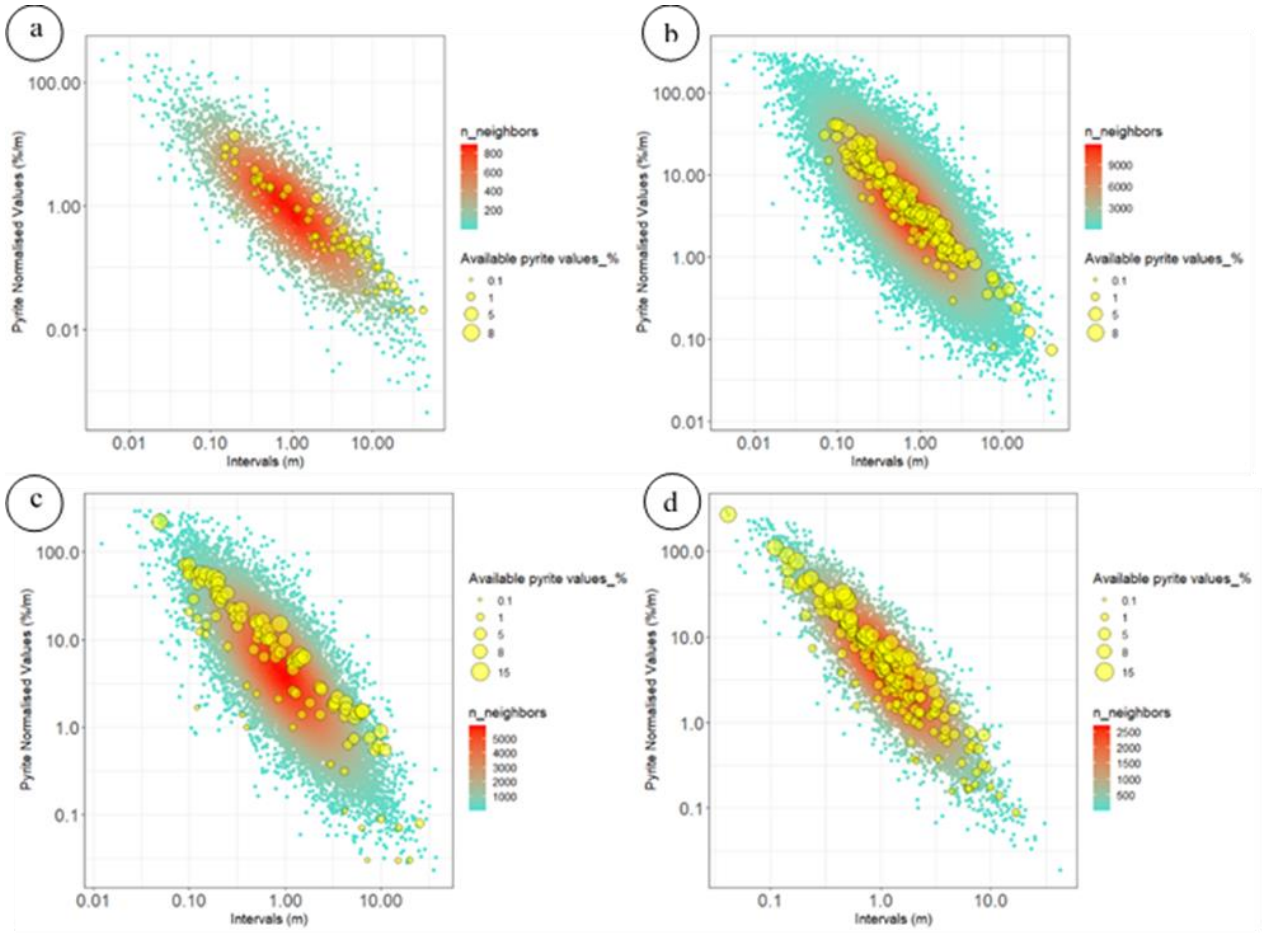


Figure 7.3 The Monte Carlo simulation outcome depicted for each pyrite class. a. The simulated and measured datasets of the class 0.1 of pyrite. b. The simulated and measured datasets of the class 0.5 of pyrite. c. The simulated and measured datasets of the class 1 of pyrite. d. The simulated and measured datasets of the class 2 of pyrite. (N_neighbours indicates the number of points neighbouring a given point in the graph)

Likewise, a figure in the supplementary material depicts the simulation results of albite and calcite classes as well as their respective related data. As stated earlier, the procedure enables the generation of linear-shaped scatter with a large number of points, mainly steered by the tendency of the normalised weight proportions obtained by analytical quantification. The number of intervals per class defines the size of the simulated dataset. For instance, 4187 simulated values were produced for the pyrite class 0.1, which classifies pyrite in 4187 intervals as feebly occurring pyrite. Thereby, each simulated normalised weight proportion was linked to its respective interval.

Figure 7.4 outlines the newly created weight proportions after cancelling the normalisation along with measured weight proportions. As issued by Toubri *et al*. (2021a), the process being used propagates the same variability features from the measured sample size to the simulated dataset. Moreover, the epistemic uncertainty related to the subjective geological logging classification is approximated through measured data boxplots and propagated throughout the generated data.

It is worth mentioning that producing other Monte Carlo realisations does not affect the variability features as long as the power law parameters are used to constrain the generated dataset (Toubri *et al*., 2021a).

This newly created database of mineral weight proportions is used to undertake spatial data analysis as the obtained population size fulfills the aforementioned data density requirement. In sum, 77 302, 14 278 and 2500 simulated weight proportions were generated for pyrite, albite and calcite respectively. Intervals of albite occurrences are much longer than pyrite and calcite intervals;

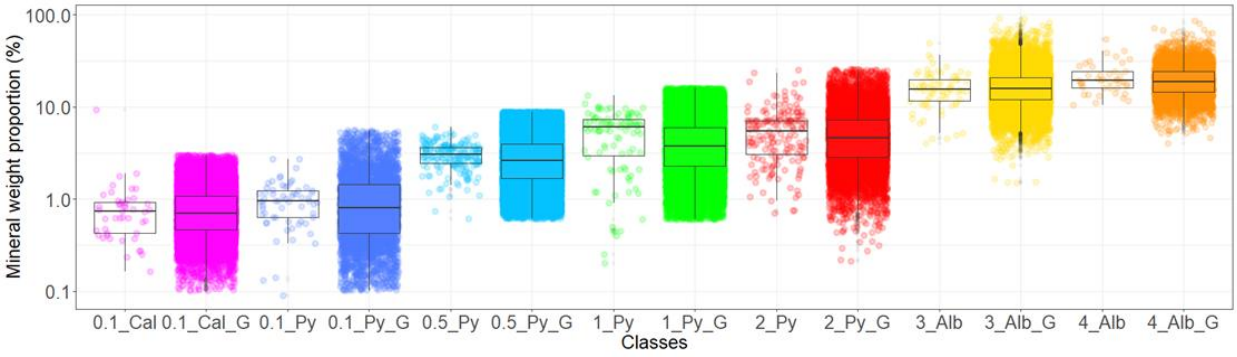


Figure 7.4 Output of the Monte Carlo simulation after cancelling the normalisation along with the measured values depicted by class. (e.g., 0.1_Cal: measured values of calcite pertaining to the class 0.1, 0.1_Cal_G: generated data via simulation for the class 0.1 of calcite).

typically, albite intervals are comprised between 2 and 10 meters consisting of massive occurrences. Pyrite and calcite intervals typically ranged between 0.05 and 4 meters frequently occurring as disseminations and veins.

7.4.2 The geomodeling results

Miscellaneous directional variograms along with the omnidirectional variogram were computed using SGeMS. The variogram parameters obtained for the omnidirectional variogram and three main directional variograms that exhibited the highest ranges are reported in the supplementary file. The range is the main geostatistical parameter that relates to the spatial continuity as it reflects the extent of the autocorrelation among neighboring points.

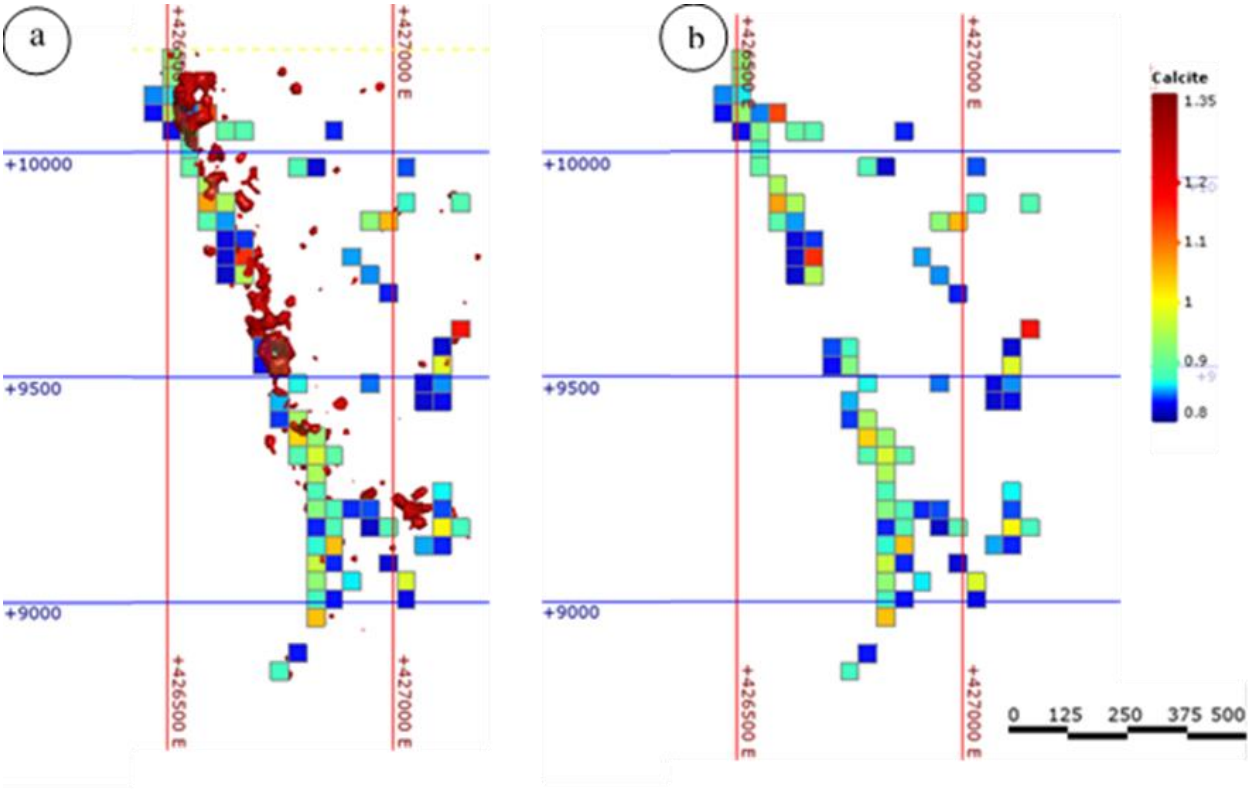


Figure 7.5 The calcite numerical geo-model. a. The core casing of the calcite geo-model including values higher than 1 % along with the calcite block model in the background. b. The calcite block model along the expected plane of mining

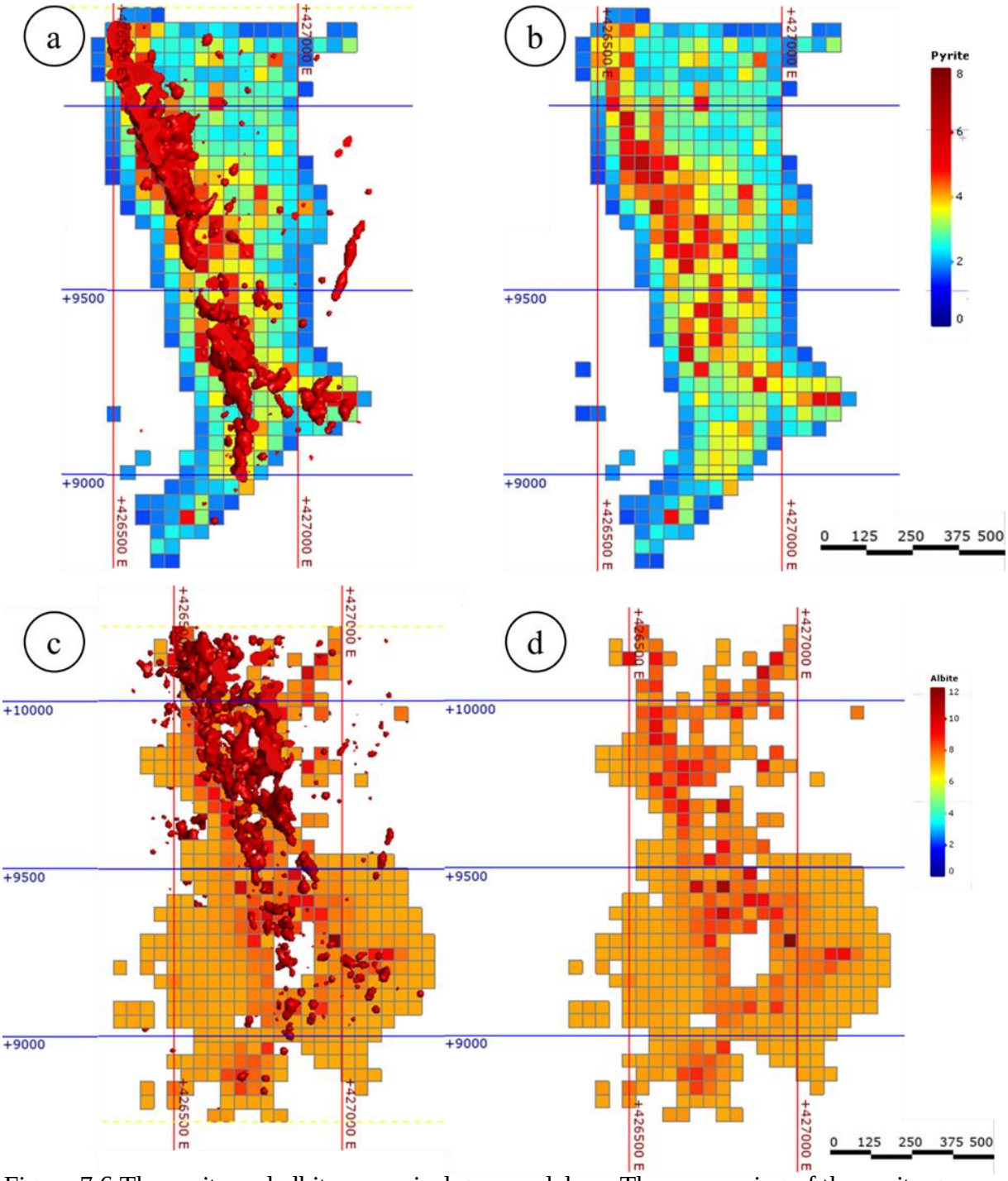


Figure 7.6 The pyrite and albite numerical geo-models. a. The core casing of the pyrite geo-model including values higher than 4.5 % along with the pyrite block model in the background. b. The pyrite block model along the expected plane of mining. c. The core casing of the albite geo-model including values higher than 10 % along with the albite block model in the background. d. The albite block model along the expected plane of mining

The direction defined as 270° N, 70° E exhibits the highest range for the three mineral datasets (see supplementary materials). This outcome complies with the major structural trend of the orebody. Consequently, the parameters of the directional variogram defined at 270° N, 70° E were used as inputs for 3D implicit modeling performed in Leapfrog Geo. The nugget effects of calcite and pyrite exceed 70% of the sill while the albite nugget effect is predominantly lower than 70% of the sill. This difference is in line with the geological characteristics of the gangue minerals; calcite and pyrite are frequently occurring as thin scattered disseminations while albite is generally described as phenocrysts throughout longer intervals of occurrences. In sum, the variography analysis underlines that the generated data conform to the geological features of the orebody.

Results of numerical geo-modeling are summarized in Figures 7.5 and 7.6 for calcite, pyrite and albite respectively. The gangue minerals are East-trending with a deeply plunging dip, this structural tendency was inherited from geological logging that straddles the ore spatial trend and the structural measurements reported throughout logging. For each numerical model, a block model was established along the mining plane to discern sectors expected to be excavated. Block models could be produced along any given horizontal or vertical view. For instance, in case of open-pit mining, equidistant horizontal sights could be produced to visualize the mining plans. For underground mining, vertical sights are more relevant. As issued by Toubri *et al*. (2021a), to underline the numerical models reliability, drill cores with measured mineral proportions were projected on the 3D model. Consistency between measured data and simulated data in the 3D space is appropriate enough for the purpose of the study (see supplementary material). However, the model reliability could be further improved through quantitative data acquisition to refine the objective function parameters and reduce the margins of error to less than 5%. In this regard, the analyzed sample size should be comprised between 310 and 350 samples for each logging class.

7.4.3 Reactive transport modeling results

The albite and the calcite block models were overlaid on the pyrite block model. Subsequently, three mineral weight proportions (albite, calcite and pyrite) were assigned to each voxel. The reactive transport modeling was performed for over 500 voxels; kinetic parameters and environment transport features were held the same, only mineral weight proportions were adjusted accordingly. The resulting pH values after 15 days, 60 days, 180 days and 360 days are displayed

in Figure 7.7, respectively. To evaluate the reactive transport modeling reliability, the experimental pH results of a kinetic test, previously issued by Toubri *et al*. (2021b) were simulated. The simulated pH values are comparable to the pH experimental measurements (see supplementary material).

After 15 days, 199 voxels display pH values lower than 3, the pH of 193 voxels is comprised between 3 and 4.5, 71 voxels exhibit pH ranging from 4.5 to 5.5 and 64 voxels indicate pH higher than 7. Voxels containing calcite; effective neutralizing mineral, promptly buffer the pH at 8 even before 15 elapsed days. Voxels encompassing albite and pyrite weight proportions ranging from 10 to 12 wt.% and 1 to 2 wt.% respectively increase the pH to 5. The effectiveness of albite neutralization mainly depends on the elapsed time and its weight proportion as it is considered as a slow-reactive neutralizing mineral (Toubri *et al*., 2021b). Likewise, voxels with pH values ranging from 3 to 4.5 generally consist of pyrite proportions comprised between 2 and 4 along with albite proportions comprised between 8 and 12 wt.%. Values of pH lower than 3 reflect voxels embodying merely pyrite with no associated neutralizing minerals. After 60 days of reactive transport, 299 voxels display pH values oscillating between 3 and 4.5; these voxels either contain 1 to 2 wt.% of pyrite with no associated neutralizing minerals or 3 to 6 wt.% of pyrite associated to albite not exceeding 12 wt.%. Besides, 111 voxels mostly consisting of 2 to 3 wt.% of pyrite and 10 to 11 wt.% of albite generated pH fluctuating between 4.6 and 5.5. Likewise, 117 voxels display pH higher than 6; the neutralization potential of 45% of these voxels stems from relatively high albite proportions associated to 1 wt.% of pyrite. These results suggest that the albite weight proportion should be at least tenfold higher than the pyrite weight proportion to achieve a circumneutral pH after 60 days of kinetic reaction. The remnant voxels rely on the calcite neutralization potential to buffer the pH at 8 as pointed out earlier.

The geochemical pseudo-steady state of the pH is approximately reached beyond 180 days. It is worth mentioning that the number of voxels with pH ranging from 4.6 to 5.5 increased to 210. On the other hand, the number of voxels with pH lower than 4.5 decreased to 200 voxels. As discussed by Toubri *et al*. (2021b), this result stresses the albite slow reactivity and the related neutralization lag time needed to increase the pH. This geochemical behaviour is further highlighted after 360 days when the number of voxels buffering the pH above 6 increased to 171; 62% of them rely on the albite neutralization potential.

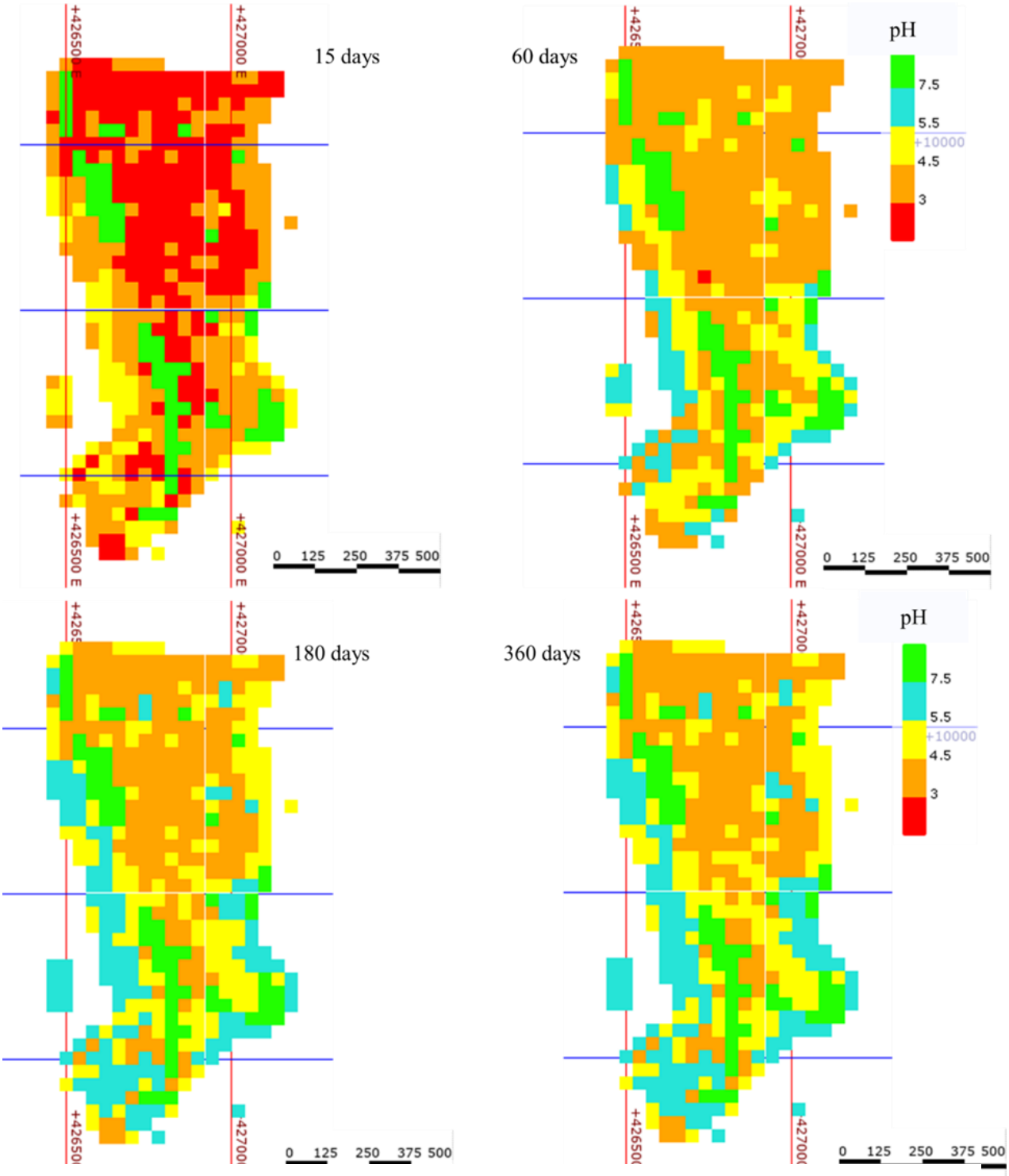


Figure 7.7 The resulting pH under oxidizing conditions, after 15 days, 60 days, 180 days and 360 days, using reactive transport modeling for each voxel

It is noteworthy that the reaction conditions assumed throughout the reactive transport-modeling step were highly oxidizing conditions and the L/S ratio was similar to the weathering cell test; considered as one of the kinetic tests involving the most aggressive weathering conditions. Therefore, the results comply with conservative scenarios and could not be directly linked to exact waste rock piles effluent quality. As discussed by Plante *et al*. (2014), lab to field scale effects are frequently limiting direct linkage between laboratory and field scale results. Therefore, the present study suggests upstream spatial classification of the hosting rock mainly based on conservative reasoning.

Hence, the aforementioned results (Figure.7.7) display a one case scenario. The mine managers could use the same approach to perform other optimistic or conservative scenarios, including alternative waste rock storage scenarios, merely by changing the reactive transport-modeling inputs

The mine managers could use the same approach to perform other optimistic scenarios, including alternative waste rock storage scenarios, merely by changing the reactive transport-modeling inputs. For instance, the user could consider the encapsulated pyrite proportion, which is not available for reaction. Therefore, different pH outputs will be generated. The user also could consider simulation duration longer than 360 days. Consequently, the pH could be slightly increased throughout time. It is always worthwhile to produce several scenarios for the sake of comparison. In sum, the present study developed a new approach to identify geo-environmental domains based on a dynamic classification of the host rock before mining. This classification enables the identification of hazardous host rock that could generate AMD upon surface disposal. Subsequently, the mine manager could avoid their surface disposal and mitigate AMD risk. Alternative management approaches could involve the use of these hazardous geo-environmental domains in underground backfill or intermingling them with other geo-environmental domains to increase their neutralization potential.

7.5 Conclusion

This study focused on bridging the spatial capabilities of geological modeling and the time-related abilities of geochemical modeling for the sake of a better control over mine solid waste environmental risk. The approach described herein could be used to perform upstream mine waste classification based on the simulated pH under oxidizing conditions. For instance, the mine

managers could seamlessly select sectors recommended for surface disposal and sectors that should be used as backfill or intermingled with other sectors to level off the pH at circumneutral values. Nonetheless, continuous refinement of the spatiotemporal model is needed throughout the mine project phases as soon as the newly acquired information is incorporated in the database. This task compels a high sense of teamwork and collaboration between the geologist and the environmental geochemist to implement a cross-disciplinary flow of information and skills. In the present paper, only one mining plane was investigated. The same procedure could be performed along numerous vertical and horizontal plans spanning the entire extent of the orebody to establish the 3D spatiotemporal distribution of the pH. However, the overriding limitation of this procedure is the reactive transport computation time, since the number of voxels dictates the number of reactive transport simulations to be performed. In this study, 527 reactive transport simulations were carried out throughout one plane consisting of 40x40x40 meters voxels. This shortcoming underlines the need of a versatile software that simultaneously integrates both the capabilities of geological modeling and reactive transport modeling to alleviate the computation time and data manipulations.

The approach presented in this research considers some environmental attributes of AMD in hard rock mines. However, in real-life mining, optimization of the mining operations is indispensable to ensure high net present value throughout the life of the mine. Consequently, to perform mine waste classification and segregation throughout mining to avoid AMD liabilities, the mining engineer should be involved in conducting the mine waste segregation based upon the best mining schedule. Therefore, the linkage between the geologist and the environmental geochemist should be completed through involving the mining engineer.

Finally, it is worth mentioning that the geochemical setting simulated throughout this study considers only controlled weathering conditions performed in the lab. Therefore, several aspects of AMD generation were not considered including the role of biotic reactions. Accordingly, the results could not be directly linked to the weathering field conditions and their interpretation should be limited to the lab scale and the development stage of the mine project. Hence, future improvements of this approach should upgrade the geochemical model conditions during the operation phase to simulate settings that are more complex such as the field experimental tests using highly specialized geochemical software.

Supplementary materials

The supplementary materials of this chapter are in Appendix C.

Acknowledgements

The authors thank the GoldSim corporation for the reduced fees of the research license and Seequent corporation for the academic license of Leapfrog Geo. Funding for this study was provided by the NSERC TERRE-NET program, led by Dr. D. Blowes (University of Waterloo).

References

Aachib, M., Aubertin, M., And Chapuis, R. (1994). Column tests investigation of milling wastes properties used to build cover systems. Proceedings of the International Land Reclamation and Mine Drainage Conference and 3rd International Conference on the Abatement of Acidic Drainage, Pittsburgh.

Abzalov, M. (2016). Introduction to Geostatistics. In Applied Mining Geology, 233-237 Springer.

Aguilar, F.J., Agüera, F., Aguilar, M.A. and Carvajal, F. (2005). Effects of terrain morphology, sampling density, and interpolation methods on grid DEM accuracy. Photogrammetric Engineering & Remote Sensing, 71(7), 805-816.

Akcil, A. and Koldas, S. (2006). Acid Mine Drainage (AMD): causes, treatment and case studies. Journal of cleaner production, 14(12-13), 1139-1145.

Aubertin, M., Bussière, B., Pabst, T., James, M. and Mbonimpa, M. (2016). Review of the reclamation techniques for acid-generating mine wastes upon closure of disposal sites. Dans Geo-Chicago 2016 (p. 343-358).

Benzaazoua, M., Bussière, B., Demers, I., Aubertin, M., Fried, É. and Blier, A. (2008). Integrated mine tailings management by combining environmental desulphurization and cemented paste backfill: Application to mine Doyon, Quebec, Canada. Minerals engineering, 21(4), 330-340.

Benzaazoua, M., Perez, P., Belem, T and Fall M. (2004). A laboratory study of the behaviour of surface paste disposal. Proceedings of the 8th International Symposium on Mining with Backfill, The Nonferrous Metals Society of China, Beijing.

Blowes, D., Ptacek, C., Jambor, J. and Weisener, C. (2003). The geochemistry of acid mine drainage. Treatise on geochemistry, 9, 612.

Bouzahzah, H., Benzaazoua, M., Bussiere, B. and Plante, B. (2014). Prediction of acid mine drainage: importance of mineralogy and the test protocols for static and kinetic tests. Mine Water and the Environment, 33(1), 54-65.

Buhmann, M.D. (2000). Radial basis functions. Acta numerica, 9, 1-38.

Bussière, B. (2007). Colloquium 2004: Hydrogeotechnical properties of hard rock tailings from metal mines and emerging geoenvironmental disposal approaches. Canadian Geotechnical Journal, 44(9), 1019-1052.

Bussière, B., Aubertin, M., Mbonimpa, M., Molson, J.W. and Chapuis, R.P. (2007). Field experimental cells to evaluate the hydrogeological behaviour of oxygen barriers made of silty materials. Canadian Geotechnical Journal, 44(3), 245-265.

Casey, W.H. and Ludwig, C. (1995). Silicate mineral dissolution as a ligand-exchange reaction. Chemical weathering rates of silicate minerals(In: A. F. White and S. L. Brantley (eds.) Chemical Weathering Rates of Silicate Minerals, Reviews in Mineralogy Vol. 31, Mineral. Soc. Am., Washington, D.C.), 87-118.

Chou, L. and Wollast, R. (1985). Steady-state kinetics and dissolution mechanisms of albite. American Journal of Science, 285(10), 963-993.

Cowan, E. J., Beatson, R. K., Fright, W. R., McLennan, T. J., and Mitchell, T. J. (2002). Rapid geological modeling. In Applied Structural Geology for Mineral Exploration and Mining, International Symposium, 23-25.

Cuomo, S., Galletti, A., Giunta, G and Starace, A. (2013). Surface reconstruction from scattered point via RBF interpolation on GPU. In federated conference on computer science and information systems, 433-440.

Demers, I., Bouda, M., Mbonimpa, M., Benzaazoua, M., Bois, D. and Gagnon, M. (2015). Valorization of acid mine drainage treatment sludge as remediation component to control acid generation from mine wastes, part 2: field experimentation. Minerals Engineering, 76, 117-125.

Demers, I., Mbonimpa, M., Benzaazoua, M., Bouda, M., Awoh, S., Lortie, S. and Gagnon, M. (2017). Use of acid mine drainage treatment sludge by combination with a natural soil as an oxygen barrier cover for mine waste reclamation: Laboratory column tests and intermediate scale field tests. Minerals Engineering, 107, 43-52.

Demers, I., Molson, J., Bussière, B. and Laflamme, D. (2013). Numerical modeling of contaminated neutral drainage from a waste-rock field test cell. Applied geochemistry, 33, 346-356.

Dold, B. (2008). Sustainability in metal mining: from exploration, over processing to mine waste management. Reviews in Environmental Science and bio/technology, 7(4), 275.

Elghali, A., Benzaazoua, M., Bussière, B. and Bouzahzah, H. (2019). Determination of the available acid-generating potential of waste rock, part II: Waste management involvement. Applied geochemistry, 100, 316-325.

Evangelou, V.P. and Zhang, Y. (1995). A review: pyrite oxidation mechanisms and acid mine drainage prevention. Critical Reviews in Environmental Science and Technology, 25(2), 141-199.

Floater, M.S. and Iske, A. (1996). Multistep scattered data interpolation using compactly supported radial basis functions. Journal of Computational and Applied Mathematics, 73(1-2), 65-78.

Hillier, M.J., Schetselaar, E.M., de Kemp, E.A. and Perron, G. (2014). Three-dimensional modeling of geological surfaces using generalized interpolation with radial basis functions. Mathematical Geosciences, 46(8), 931-953.

Hsieh, P.A., Wingle, W. and Healy, R.W. (2000). VS2DI-A graphical software package for simulating fluid flow and solute or energy transport in variably saturated porous media, 99-4130. US Geological Survey.

Iske, A. (2002). Scattered data modeling using radial basis functions. In Tutorials on Multiresolution in Geometric Modeling, 205-242. Springer, Berlin, Heidelberg.

Jamieson, H.E. (2011). Geochemistry and mineralogy of solid mine waste: essential knowledge for predicting environmental impact. Elements, 7(6), 381-386.

Jerz, J.K. and Rimstidt, J.D. (2004). Pyrite oxidation in moist air. Geochimica et Cosmochimica Acta, 68(4), 701-714.

Jouini, M., Benzaazoua, M., Neculita, C.M. and Genty, T. (2020). Performances of stabilization/solidification process of acid mine drainage passive treatment residues: Assessment of the environmental and mechanical behaviors. Journal of Environmental Management, 269, 110764.

Kalonji-Kabambi, A., Demers, I. and Bussière, B. (2020). Reactive transport modeling of the geochemical behavior of highly reactive tailings in different environmental conditions. Applied Geochemistry, 122, 104761.

Kossik. R. and Miller. I. (2004). A probabilistic total system approach to the simulation of complex environmental systems. In Proceedings of the 36th conference on Winter simulation, 1757-1761. Winter Simulation Conference.

Lawrence. R. and Wang. Y. (1997). Determination of neutralization potential in the prediction of acid rock drainage. In Proceedings 4th International Conference on Acid Rock Drainage, Vancouver, BC.

Martin-Izard, A., Arias, D., Arias, M., Gumiel, P., Sanderson, D., Castañon, C., Lavandeira, A. and Sanchez, J. (2015). A new 3D geological model and interpretation of structural evolution of the world-class Rio Tinto VMS deposit, Iberian Pyrite Belt (Spain). Ore Geology Reviews, 71, 457-476.

Mbonimpa, M., Awoh, S., Beaud, V., Bussière, B. and Leclerc, J. (2008). Spatial water quality distribution in the water cover used to limit acid mine drainage generation at the Don Rouyn site (QC, Canada). In Proceedings of the 61th Canadian Geotechnical Conference and the 9th Joint CGS/IAH-CNC Groundwater Conference, 21-24.

Molson, J., Aubertin, M., Bussière, B. and Benzaazoua, M. (2008). Geochemical transport modeling of drainage from experimental mine tailings cells covered by capillary barriers. Applied Geochemistry, 23(1), 1-24.

Molson, J., Fala, O., Aubertin, M. and Bussière, B. (2005). Numerical simulations of pyrite oxidation and acid mine drainage in unsaturated waste rock piles. Journal of Contaminant Hydrology, 78(4), 343-371.

Natali, M., Lidal, E., Parulek, J., Viola, I. and Patel, D. (2013). Modeling Terrains and Subsurface Geology. In Interactive Data Processing and 3D Visualization of the Solid Earth, pp. 1-43.

Neculita, C., Zagury, G. and Kulnieks, V. (2010). Short-term and long-term bioreactors for acid mine drainage treatment. Proceedings of the Annual International Conference on Soils, Sediments, Water and Energy, 12, 1-2.

Nicholson, R.V. and Scharer, J.M. (1994). Laboratory studies of pyrrhotite oxidation kinetics. In C.N. Alpers, D.W. Blowes (Eds.), Environmental Geochemistry of Sulfide Oxidation, ACS Symposium Series, vol. 550 (1994), pp. 14-30 Washington, DC.

Nordstrom, D., Alpers, C.N., Ptacek, C. and Blowes, D. (2000). Negative pH and extremely acidic mine waters from Iron Mountain, California. Environmental Science & Technology, 34(2), 254-258.

Nordstrom, D.K. and Alpers, C.N. (1999). Negative pH, efflorescent mineralogy, and consequences for environmental restoration at the Iron Mountain Superfund site, California. Proceedings of the National Academy of Sciences, 96(7), 3455-3462.

Pabst, T., Molson, J., Aubertin, M. and Bussière, B. (2017). Reactive transport modeling of the hydro-geochemical behaviour of partially oxidized acid-generating mine tailings with a monolayer cover. Applied Geochemistry, 78, 219-233.

Palandri, J.L. and Kharaka, Y.K. (2004). A compilation of rate parameters of water-mineral interaction kinetics for application to geochemical modeling. Geological Survey Menlo Park CA. US Geological Survey Open File Report.

Parbhakar-Fox, A.K., Edraki, M., Walters, S. and Bradshaw, D. (2011). Development of a textural index for the prediction of acid rock drainage. Minerals Engineering, 24(12), 1277-1287.

Parkhurst, D.L. and Appelo, C. (2013). Description of input and examples for PHREEQC version 3: a computer program for speciation, batch-reaction, one-dimensional transport, and inverse geochemical calculations. US geological survey techniques and methods, 6(A43), 497.

Plante, B., Bussière, B. and Benzaazoua, M. (2014). Lab to field scale effects on contaminated neutral drainage prediction from the Tio mine waste rocks. Journal of Geochemical Exploration, 137, 37-47.

Remy, N., Boucher, A. and Wu, J. (2009). Applied geostatistics with SGeMS: A user's guide. Cambridge University Press.

Rizzo, D.M., Mouser, P.J., Whitney, D.H., Mark, C.D., Magarey, R.D. and Voinov, A.A. (2006). The comparison of four dynamic systems-based software packages: Translation and sensitivity analysis. Environmental Modeling & Software, 21(10), 1491-1502.

Stoch, B., Anthonissen, C.J., McCall, M.J., Basson, I.J., Deacon, J., Cloete, E., Botha, J., Britz, J., Strydom, M., Nel, D. and Bester, M. (2018). 3D implicit modeling of the Sishen Mine: new resolution of the geometry and origin of Fe mineralization. Mineralium Deposita, 53(6), 835-853.

Toubri, Y., Demers, I., Poirier, A., Pépin, G., Gosselin, M. and Beier, N. (2021a). Merging 3D geological modeling and stochastic simulation to foster the waste rock upstream management. Journal of Geochemical Exploration, 224, 106739.

Toubri, Y., Vermette, D., Demers, I., Beier, N. and Benzaazoua, M. (2021b). Incorporating Kinetic Modeling in the Development Stages of Hard Rock Mine Projects. Minerals, 11(12), 1306.

Van Genuchten, M.T. (1980). A closed-form equation for predicting the hydraulic conductivity of unsaturated soils. Soil science society of America journal, 44(5), 892-898.

Wright, G.B. (2003). Radial basis function interpolation: numerical and analytical developments, Ph.D. thesis, University of Colorado, Boulder, 2003.

Wu, Q. and Xu, H. (2014). Three-dimensional geological modeling and its application in Digital Mine. Science China Earth Sciences, 57(3), 491-502.

Wunderly, M., Blowes, D., Frind, E. and Ptacek, C. (1996). Sulfide mineral oxidation and subsequent reactive transport of oxidation products in mine tailings impoundments: A numerical model. Water Resources Research, 32(10), 3173-3187.

CHAPTER 8 GENERAL DISCUSSION

This work started from the concept of the upstream thinking, which is inspired from designing for closure principle, and the integration concept inspired from geometallurgy to develop cost-effective modeling methods that enhance the mitigation capabilities regarding AMD and the associated environmental risks. Linkage between specialized geological modeling engines and environmental geochemistry modeling toolbox was established to bridge 3D spatial visualization to the time dimension. This linkage evolved through three main steps highlighting the research hypotheses announced in the chapter 1:

- A 3D geological model portraying the spatial distribution of a contaminant could be established based upon the available data from the drilling surveys;
- Geochemical models could be established since the development stage based upon the available mineralogical characterization;
- Combining a geochemical model with a spatial model could result in a good risk identification and localization during the development stage.

The first step involved stochastic simulation to accomplish the geological modeling requirements. Monte Carlo simulation, a straightforward stochastic process, was developed based upon the discrete and continuous variables of the geological logging. The process suggested in this study relates the independent continuous variable through the power law. The power law is subsequently used as an objective function throughout the iterative Monte Carlo simulation. The second step focused on simulating the pH generated due to surface-controlled reaction including direct oxidation and dissolution. Unlike the complex geochemical models established during the reclamation phase, the suggested geochemical model requires minimal characterization data to be applied during upstream stages. The author believes that geochemical modeling approaches should be staged approaches that evolve from the development stage until the closure stage as the information flow evolves rather than establishing complex geochemical models at one stage without progressing the geochemical model throughout the entire mine cycle. The third step resulted in a spatiotemporal model that enables upstream and dynamic classification of the host rock. This modeling approach is a holistic method requiring a multidisciplinary background and a high sense of communication among the geologist, the environmental geochemist and the mine

waste manager. In this study, the parameter displayed by the model is the pH, however, other parameters could be envisioned such as element concentrations. In this regard, the geochemical component of the model should be further enhanced through the case-specific oxidation rates, geochemical retention processes and trace-elements mineralogy. When the user reaches this stage of data acquirement, generally during downstream stages, MIN3P would be more efficient and adequate than the coupled PHREEQC and VS2DRTI.

To perform the aforementioned integrated modeling method, the practical steps are summarized in this chapter to introduce an integrated geomodeling protocol to move beyond the case-specific description. Albeit various advantages of this integrated geomodeling approach were thoroughly described throughout the preceding chapters, several limitations should be considered and/or addressed depending on the case study. This chapter provides insights on the main advantages and limitations. Finally, horizons of improvements are presented herein to suggest future studies that further improve the integration level particularly within the systems dynamics framework.

8.1 Integrated geomodeling protocol

This section is intended to provide insights on the sequence of practices that should be performed to establish a spatiotemporal model.

(1) The user should define her/his elements of concern for the static modeling and the dynamic modeling respectively;

(2) The geological logging of the drill cores should be performed based upon standard scale used by all the geologists involved in the drill core description and sampling;

(3) The user should collect and understand the geological logging information and visualize all the geological data (categorical and numerical) in the 3D space along with the ore model suggested by the geologists;

(4) An emphasis should be carried on regarding the structural measurements performed by the geologists. This enables the user to grasp and define the plane of spatial anisotropy; if the element of interest is related to the mineralization, which is the common case, the spatial model should inherit its shape from the mineralization structural trend. If not,

the user would need to infer the structural trend from geological information and structural data analysis using stereonets;

(5) Based upon the available mineralogical information, the user should focus on the elements of concern-bearing minerals and highlight their locations in each drill core;

(6) If intensive drill core surveys are already performed, the user could perform the modeling along the entire ore depth. If not, the user should proceed by progressive depth portions as the drill core surveys evolved in the vertical dimension Z;

(7) Likewise, the plane defined by X and Y coordinates could be discretized depending on the drill core availability;

(8) The user may need to perform the stochastic process described herein if insufficient numerical data of the element of concern are available. In this regard, the user should define two independents continuous variables (including the element of concern grade) and one categorical variable used to describe the elements of concern-bearing minerals;

(9) When the aforementioned steps are accomplished the static model could be built using the variogram analysis and a multi-realization analysis could be undertaken to consider uncertainties;

(10) Calibration of the stochastic parameters and benchmarking of the static model should be performed to determine its level of reliability. Margins of error should be computed as well;

(11) To establish the dynamic model, the user should choose a 2D plane or multiple 2D plans that should be discretized in voxels. The dimension of the voxel reflects the level of detail, which is closely dependent on the drill cores spatial density;

(12) Based upon the aim of the user, she/he should establish the conceptual geochemical model. The geochemical processes of interest included in the conceptual model will define the model complexity degree that will dictate the geochemical software to be used;

(13) Calibration and benchmarking of the geochemical model should be carried out;

(14) For each voxel, the user should preform a geochemical simulation and assign the output to its respective voxel center;

(15) The aforementioned step should be repeated for ascending time intervals that are specified by the user;

(16) At this stage, the dynamic model is established and could be used for mitigation purposes. A multi-realization analysis could be undertaken through stochastically changing key-controlling inputs and/or inputs with high uncertainty.

8.2 Advantages and Limitations

The advantages of the integrated modeling approach include:

- Fulfilling of the cross-disciplinary principle suggested by geometallurgy to overcome mining environmental risks using integrated modeling;
- Merging spatial visualization and the time dimension allowing for a better risk identification and localization;
- Fostering the upstream reasoning and the mine waste classification before mining;
- Relying on cost-effective modelling approaches.

Regarding the advantages of the integrated modeling approach, it could be used to enhance the "designing for closure" thinking. The host rock classification into geo-environmental domains yields the possibility to design the mine waste facilities accordingly. This design should consider the mine waste flows established based upon the aforementioned geo-environmental domains.

As most modeling methods, the present methods presents several limitations including:

- The availability of drill cores and their logging define if the modeling method could be performed or not as it is mainly contingent on the spatial density of the drill cores. Therefore, the integrated modeling could be performed as soon as the geologist is able to visualize the deposit or a portion of the deposit;
- The spatial multi-realizations are time-consuming and require intricate manipulation of data. This limitation underlines the need for a software that incorporates the capabilities of

geological modeling and geochemical modeling as well as the possibility to run Monte Carlo simulation yielding numerous spatial realizations;

- Although the high sense of integration constitutes an advantage of this method, it also presents an issue because of the versatile scientific background required to accomplish the building steps.

Regarding the limitations of the integrated modeling approach, the use of portable analytical technologies throughout the geological logging still not common in the mining industry. These technologies will enable a better classification of the sulphides occurrence and overcome the limitations of the conventional geological logging procedures mainly in terms of imperceptible sulphides occurrence. However, promising future horizons could be perceived regarding the environmental risk management thanks to the newly issued global standard on mine waste management.

8.3 Future integration horizons

This section presents other aspects of integration that should be added to the present modeling approach to render its application feasible in real life hard rock mines. The following section provides an overview on the possible modeling efforts that could be carried out for future integration research studies. Therefore, this description is intended to provide a starting point for the upcoming research.

8.3.1 System dynamics

Almost all world systems behave according to their variables change, mathematical formulation of variables interaction is a common way to foster systems understanding. Nevertheless, mathematical formulation could be complex enough to not abide by analytical solutions or simply infeasible because of the system's intricacy. To cope with these challenges, experimental investigations are pivotal to establish solutions; however, in several cases we would assess the entire system behaviour without real-life implementation. Some real-systems implementation is time-consuming, prohibitively costly or simply impractical to do when the controlling factors are not accessible and/or controllable; these controlling factors are named *disturbance inputs* (Fritzson, 2010). Likewise, some interesting outputs are not reachable for measurements, these are called

internal states (Fritzson, 2010). The model is a key concept to overcome experimental approach shortcomings, Fritzson (2010) states that

> "*A model of a system is anything an experiment can be applied to in order to answer questions about that system*"

System dynamics (SD) modeling is one of the modeling approaches that build causality among variables system to enhance understanding (Kelly *et al.*, 2013) based on nonlinear and feedback thinking (Forrester, 1996). Owing to tremendous growth in system modeling needs, SD was developed to stress that knowledge integration considering closed-loop concept is a promising way to tackle systems behaviour understanding (Peck, 1998). The growing application of SD includes economic fluctuations, dynamics of ecosystems, project management and many other domains. These extensive application case studies preclude mining fields, Zheng (2019) stated that SD integration in mining engineering is substantially curtailed, papers related to keyword "mining" amounted to less than 1% in the System Dynamics Review bibliography database (Zheng, 2019).

Several software were used to perform SD modeling such as GoldSim. GoldSim is a completely object-oriented and highly graphical program devoted to build probabilistic, dynamic simulations of complex models. Graphical objects called elements afford the basic building blocks to establish hierarchical, top-down models. These elements receive inputs and carry out calculations that solve equations embedded in the element to impart outputs. Elements could be regarded as a built-in functions represented by icons. The second building block in GoldSim is influence; automatically drawn arrows that link elements to explicitly display interdependencies. Therefore, GoldSim enables the establishment of SD models using flow diagrams.

8.3.1.1 TMSim: an example of system dynamics application

As mentioned before, the mining industry has not thoroughly used SD process as a modeling approach. Meanwhile, various fields have benefited from SD capabilities such as Li and Simonovic (2002) who selected SD modeling tools to predict floods in prairie watersheds and Cassell *et al.* (1998) integrated SD process to understand phosphorous dynamics pertaining to agriculture. Nonetheless, few examples of SD models applied to mining industry have emerged recently. These case studies are mainly related to oil sand mining industry; Jutla (2006) who simulated unsaturated soil dynamics of reconstructed watersheds, Beier (2015) developed a dynamic simulation, named

tailings management simulation (TMSim) to manage oil sand tailings and more recently Zheng (2019) set up the consolidation and unsaturated flow dynamic simulation for coarse sand tailings.

The modeling purpose behind TMSim implementation is to track tailings physical properties throughout the mine life span. Miscellaneous outputs are deemed mandatory to reach this aim, such as storage volume, construction materials quantity, water cap volume, freeboard volume, effective stress evolution, etc. Beier (2015) named these outputs as performance measures. Based on Beier (2015) findings, the conceptual model embeds mining operations from ore extraction to tailings deposition. Each operation implies a sub-model within TMSim. Therefore, TMSim envisions a versatile modeling purpose that is in line with SD capabilities. The flowchart in figure 8.1 is a communicative model of TMSim conceptual model; a communicative model is an explicit depiction of the conceptual model whereas a conceptual model pertains to the mind imaging (Robinson, 2008).

Mining extraction and ore valorization intertwine in the same sub-model within TMSim; called Mine/Extraction Sub-model. Likewise, the impoundment sub-model includes the following sub-models: containment, deposition, deposit strength, third dewatering stage and fluid storage. The first and the second dewatering stages constitute two separate sub-models respectively. Each sub-model requires some user-defined inputs and yields several outputs that may be included as inputs in other sub-models. This kind of complex interrelated sub-models enhances system dynamic understanding and complies with SD aim. The model intricacy stems from the inputs number and the complex interrelated elements, making the entire package unreadable at first sight. Nonetheless, the top-down approach is both the modeling key method and the key practice to grasp the model structure. At the highest level of detail, one can recognize three main reservoirs; mine reservoir, plant reservoir and impoundment reservoir. Likewise, the main flow originates from mining. At the lowest level, these main components are subdivided into other reservoirs and flows according to mining cycle choices. TMSim conceptual model abides by conceptualization requirements and sets up the scope and the purpose of the simulation. It also represents the model framework as simple as possible using sub-models and a top-down approach. Validating conceptual model requirements leads us over model formulation. Details on model formulation can be found in the dissertation of Beier (2015).

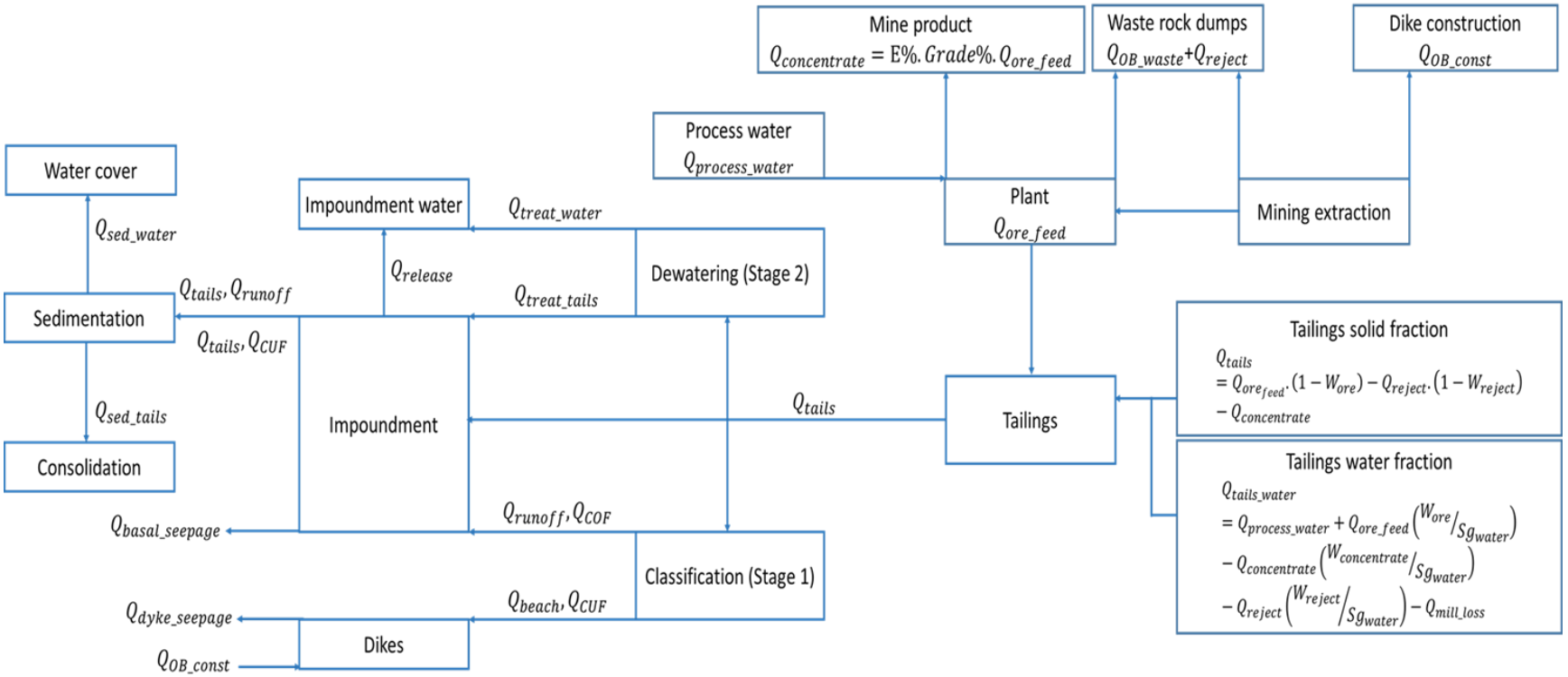


Figure 8.1 TMSim conceptual model updated from Beier (2015)

8.3.1.2 Visual Basic for application code of disposal

Beier (2015) established a code using visual basic for application (VBA) to estimate the tailings heights at any point in space and after each disposal operation. The same concept could be added to the integrated geomodeling approach when the mine manager perform mine waste segregation. Beier (2015) validated his code using several deposition scenarios. The author reproduced the validation cases and used Surfer software for spatial representation (Figures 8.2 and 8.3).

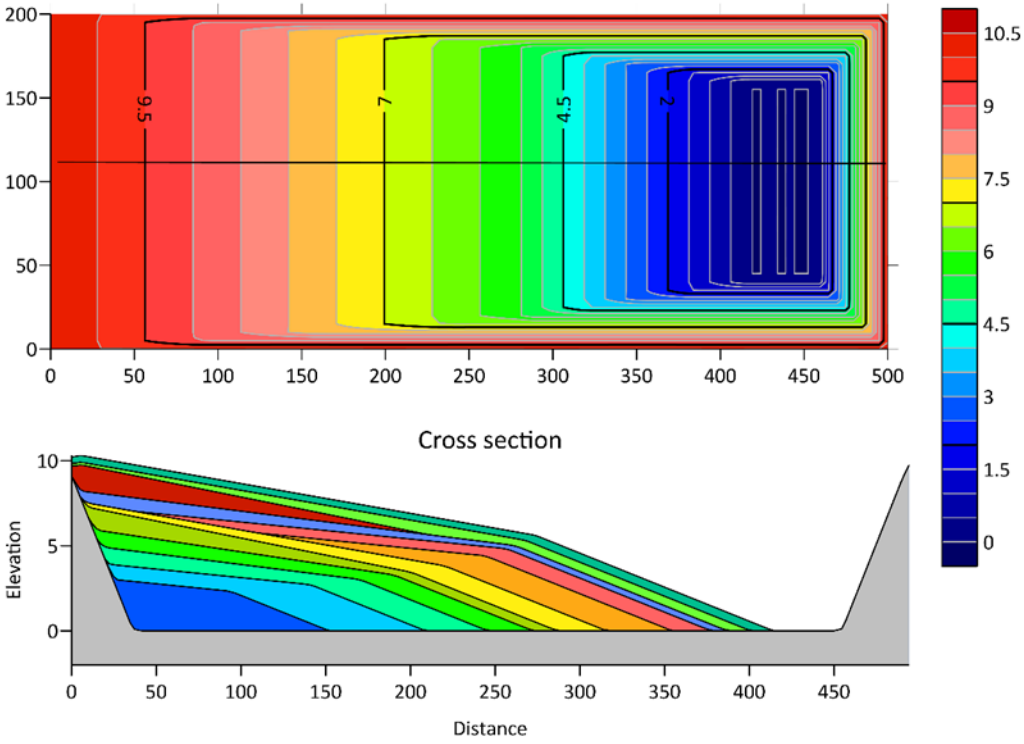


Figure 8.2 A validation scenario of deposition of 30,000 m^3 of tailings of medium density using multispigot discharge along with 100,000 m^3 of water

In conclusion, system dynamics and VBA could be used during mine waste classification and segregation to manage streams of hazardous and non-hazardous mine waste. Therefore, the approach suggested in this work could be further enhanced through relating the host rock classification to mine waste disposal dynamics based upon geo-environmental domains. The following section provides perspectives regarding SD modeling and mine waste management integration.

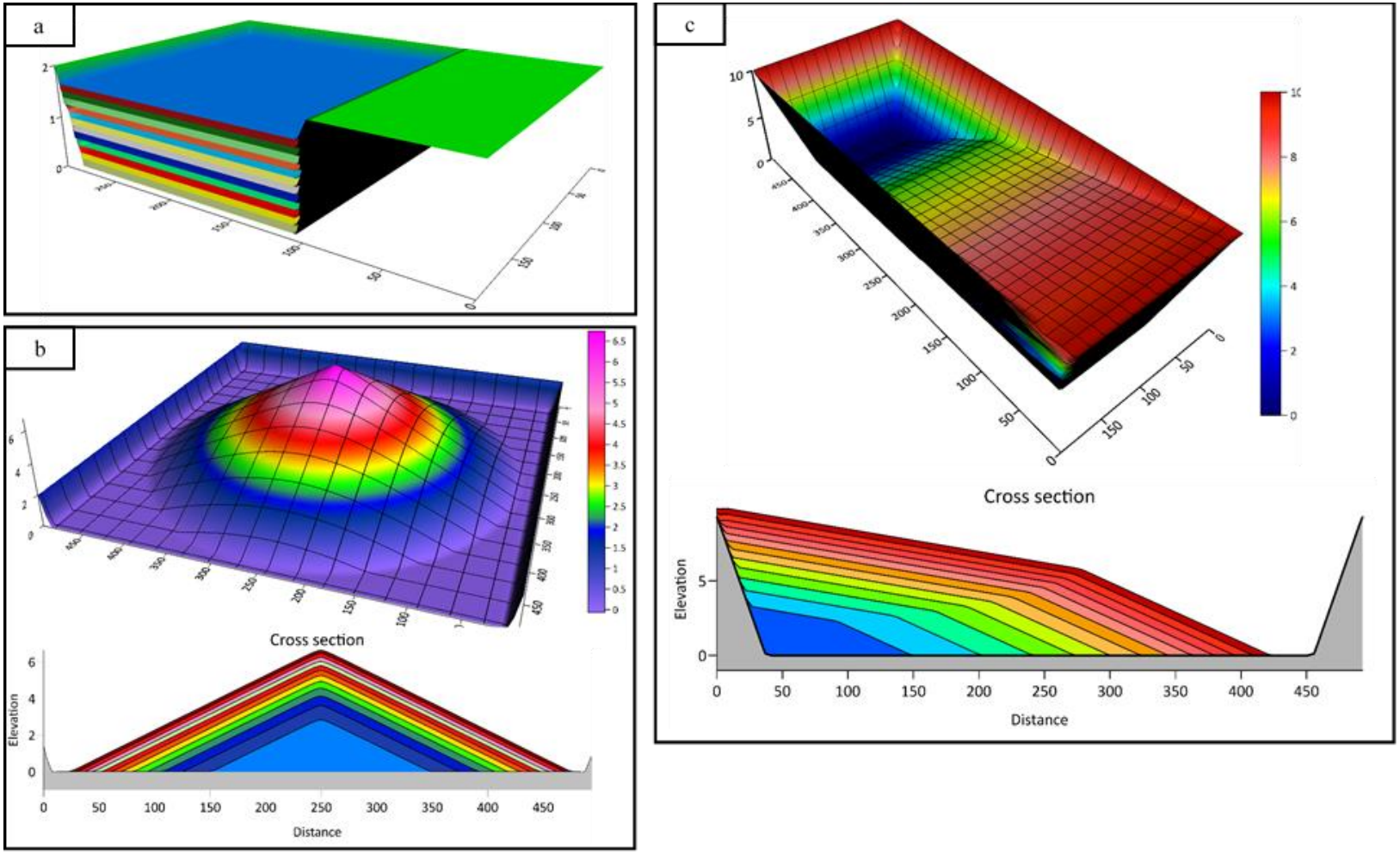


Figure 8.3 Disposal validation scenario of tailings. a. deposition of 5,000 m^3 of low-density tailings. b. Deposition of 30,000 m^3 of high-density tailings using central discharge. c. deposition of 30,000 m^3 of tailings of medium density using multispigot discharge along with 100,000 m^3 of water

8.3.1.3 System dynamics and upstream thinking

System dynamics modeling involves the holistic thinking that aims at the incorporation of the stocks and the flows of the system being considered along with the self-correcting and the self-reinforcing feedback loop relationships linking the system components. Although the SD principle is simple, it can results in highly intricate models. Therefore, SD approach could be coupled to the upstream thinking to build staged models with increasing degree of complexity throughout the mine life.

GoldSim is a software providing a specialized interface enabling SD modeling and uncertainty propagation. Furthermore, it can be linked to other external programs such as PHREEQC. Mine waste classification and segregation is a dynamic process that evolves depending on the mining operations. Practically, the mining operations schedule could be represented in GoldSim as a time series element. The geo-environmental domains could be represented by stock elements defining the tonnage, computed using geological modeling, of each geo-environmental domain. Mining operations abiding by the mining time series could be simulated using the flow elements. Environmental attributes of each geo-environmental domain, such as mineralogical associations, neutralization potential and acidic potential could be defined as stochastic elements to consider uncertainty. This uncertainty will be propagated to the outputs of PHREEQC previously linked to GoldSim. Subsequently, the generated stochastic outputs could be used to produce disposal segregation realizations. These realizations should define the time series of disposal as well as the tonnage of each segregated stream. To select the most promising disposal time series, the realizations should be assessed using mining optimization.

8.3.2 Mining optimization

The approach presented in this research considers some environmental attributes of AMD in hard rock mines. However, in real-life mining, optimization of the mining operations is indispensable to ensure high NPV. Consequently, to perform mine waste classification and segregation throughout mining to avoid AMD liabilities, the mining engineer should be involved in steering the mine waste segregation based upon the best mining schedule. Therefore, the linkage between the geologist and the environmental geochemist should be completed through involving the mining engineer. Several studies tackle the mining optimization problem using stochastic simulation and

spatial modeling (Abdel Sabour and Dimitrakopoulos, 2011; Dimitrakopoulos, 1997, 1998; Dimitrakopoulos, 2011; Dimitrakopoulos *et al.*, 2002; Dimitrakopoulos and Sabour, 2007; Kumar and Dimitrakopoulos, 2021). The results of these studies often suggest the best mining schedule based upon the ore classification. This classification is established based upon several attributes including the grade, the depth, the tonnage, the market constraints, the plant requirements… etc. Hence, the ore classification for economic purposes should be merged and reconciled with the host rock classification for environmental purposes. Without this integration, the integrated geomodeling approach suggested herein will lack realistic applications in real-life mining.

CHAPTER 9 CONCLUSION AND RECOMMENDATIONS

Nowadays, an integrated knowledge base is indispensable to overcome mining challenges mainly related to physical stability and geochemical spread of the contaminants. Regarding the geochemical aspect, the assessment and the control of AMD could prevent additional operating costs related to AMD reclamation and/or treatment. Nonetheless, to guarantee the assessment effectiveness, it should be launched as early as possible. Moreover, it should integrate all the available data related to the geological framework, which determines the nature of the upcoming mine waste. Therefore, an environmental geochemist should not merely rely on her/his knowledge; she/he should also grasp the deposit genesis and the geological model provided by the geologist to consolidate the acquired geological information in a spatial model allowing a first inference regarding the deposit typology and gitology. Accordingly, two main concepts are underlined herein to enhance AMD assessment; the integration and the earliness.

Several studies incorporated these concepts in experimental approaches suggested to support AMD assessment and/or integrated mine waste management. However, the modeling aspect is lacking such a holistic reasoning. Models established throughout the mine life, including geological models, geochemical models, mining models and mine waste management models, are used as independent compartments of knowledge. Accordingly, the general objective of this research is to introduce the integration reasoning in the modeling approaches for a better control over AMD and solid waste in hard rock mines. The aim was bridging geological modeling and geochemical modeling. Besides, upstream mine waste classification was considered as an adequate target to link geological modeling to both mine waste management and AMD control. This study combines the capabilities of 3D implicit modeling, stochastic simulation and reactive transport modeling in one consolidated modeling method that enables mine waste classification based upon the contaminant grades in the host rock and the simulated pH. A multirealization process was used to overcome the effect of uncertainties on the final decision. The method mainly relies on the geological logging information that should be collected and visualized in the 3D space. Because the suggested integrated modeling approach inherits some of its features from the geological modeling, it could be performed as soon as the geologist is able to establish his model. Furthermore, as geological models, the suggested approach is a progressive and staged procedure that could be carried out as the information flow evolves throughout drilling surveys.

The main results and conclusions of this study are summarized as follows:

- Monte Carlo simulation is efficient to repurpose the uncertainty propagation capability to infer larger and homoscedastic sample sizes;
- The conformity parameters used for the objective function are reliable to generate homoscedastic samples sizes
- The geological features underlined by the static geomodel comply with the deposit geology;
- The static geomodel established for Éléonore mine revealed a wide geochemical halo of As that could reach up to 500 m away from the gold deposit, with up to 94% of As grades exceeding 50 ppm;
- The effect of ergodic fluctuations is maintained at a fair level and no substantial differences were observed;
- The static geomodel was overlaid to the underground stopes model to enable mine waste classification based upon As grades;
- Rate laws previously issued could be used to simulate the leachate pH collected from the weathering cell tests;
- Relatively simple kinetic modeling could be performed during the development stage to carry out preliminary parametric analyses;
- Calibrated kinetic models are suggested to be used to simulate mineral assemblage that were not tested using the weathering cell test because of the lack of materials. These models should focus on the pH given their limitations;
- Kinetic models established in PHREEQC could be coupled to unsaturated flow modeling using VS2DRTI to simulate larger scale experiments that are not diffusion-limited;
- The geochemical aspects were coupled to the static geomodel to produce a dynamic geomodel that describes the temporal and the spatial evolution of the pH throughout the deposit;

- Highly oxidizing conditions were assumed to enable dynamic waste classification based upon the oxidation-neutralization process with a focus on the albite neutralization potential;
- Results circumscribe hazardous geo-environmental domains;
- The method generates several realizations that could be assessed simultaneously and other scenarios could be assessed before suggesting the final classification of the host rock;
- Data analysis and manipulation are the main limitation regarding the approach application;
- Finally, and more importantly, the present study progressed the knowledge of upstream mine waste classification and introduced promising methods to integrate multidisciplinary modeling approaches for the sake of a better control over solid waste in hard rock mines.

To improve the modeling integration and overcome the approach limitations the following recommendations are suggested:

- Models and simulations established by the mining engineer should be incorporated in the present approach to enable mine waste segregation and to determine the best mining schedule;
- System dynamics using GoldSim could be an efficient tool to simulate segregated mine waste streams and produce time series of mine waste disposal;
- A software incorporating the numerical capabilities of geological modeling and reactive transport modeling along with Monte Carlo simulation could be developed to overcome data manipulation issues;
- Other mineralogical inputs could be added if available, such as the sulphides liberation;
- Other geochemical aspects could be considered such as oxygen diffusion through the use of other unsaturated geochemical software such as MIN3P;
- The approach should be progressive, therefore, when the site specific oxidation rates are available the geomodel should be updated accordingly. Likewise, the spatial discretization should be refined as drilling surveys progress.

REFERENCES

Abdel Sabour, S. and Dimitrakopoulos, R. (2011). Incorporating geological and market uncertainties and operational flexibility into open pit mine design. Journal of Mining Science, 47(2), 191-201.

Abdelwahhab, M.A., Ali, E.H. and Abdelhafez, N.A. (2021). Petroleum system analysis-conjoined 3D-static reservoir modeling in a 3-way and 4-way dip closure setting: insights into petroleum geology of fluvio-marine deposits at BED-2 Field (Western Desert, Egypt). Petroleum.

Abzalov, M. (2016a). Grade Uncertainty. Dans Applied Mining Geology (p. 323-333) : Springer.

Abzalov, M. (2016b). Introduction to Geostatistics. Dans Applied Mining Geology (p. 233-237) : Springer.

Abzalov, M. (2016c). Methods of the Linear Geostatistics (Kriging). Dans Applied Mining Geology (p. 263-286) : Springer.

Akcil, A. and Koldas, S. (2006). Acid Mine Drainage (AMD): causes, treatment and case studies. Journal of cleaner production, 14(12-13), 1139-1145.

Amos, R.T., Blowes, D.W., Bailey, B.L., Sego, D.C., Smith, L. and Ritchie, A.I.M. (2015). Waste-rock hydrogeology and geochemistry. *Applied Geochemistry, 57*, 140-156.

Asghar, M. and Kanehiro, Y. (1981). The fate of applied iron and manganese in an oxisol and an ultisol from Hawaii. Soil Science, 131(1), 53-55.

Aubertin, M., Bussière, B., Pabst, T., James, M. and Mbonimpa, M. (2016). Review of the reclamation techniques for acid-generating mine wastes upon closure of disposal sites. Dans Geo-Chicago 2016 (p. 343-358).

Aubertin, M., Mbonimpa, M., Jolette, D., Bussière, B., Chapuis, R. P., James, M., & Riffon, O. (2002). Stabilité géotechnique des ouvrages de retenue pour les résidus miniers: problèmes persistants et méthodes de contrôle. In *Défis & Perspectives: Symposium*.

Bachmaier, M. and Backes, M. (2011). Variogram or semivariogram? Variance or semivariance? Allan variance or introducing a new term? Mathematical Geosciences, 43(6), 735-740.

Badejo, S., Fraser, A., Neumaier, M., Muxworthy, A. and Perkins, J. (2021). 3D petroleum systems modelling as an exploration tool in mature basins: A study from the Central North SeaUK. Marine and Petroleum Geology, 133, 105271.

Bargawa, W. S., and Tobing, R. F.. (2020). Iron ore resource modeling and estimation using geostatistics. AIP Conference Proceedings. : AIP Publishing LLC.

Battalgazy, N. and Madani, N. (2019). Categorization of mineral resources based on different geostatistical simulation algorithms: A case study from an iron ore deposit. Natural Resources Research, 28(4), 1329-1351.

Beier, N.A. (2015). Development of a Tailings Management Simulation and Technology Evaluation Tool. University of Alberta.

Benzaazoua, M., Bussière, B., Demers, I., Aubertin, M., Fried, É. and Blier, A. (2008). Integrated mine tailings management by combining environmental desulphurization and cemented paste backfill: Application to mine Doyon, Quebec, Canada. Minerals engineering, 21(4), 330-340.

Benzaazoua, M., Bussière, B., Kongolo, M., McLaughlin, J. and Marion, P. (2000). Environmental desulphurization of four Canadian mine tailings using froth flotation. International journal of mineral processing, 60(1), 57-74.

Benzaazoua, M., Bussière, B., Nicholson, R. V., and Bernier, L. (1998). Geochemical behavior of a multi-layered cover composed of desulfurized mine tailings. In Tailings and mine waste (pp. 389-398).

Benzaazoua, M. and Kongolo, M. (2003). Physico-chemical properties of tailing slurries during environmental desulphurization by froth flotation. International Journal of Mineral Processing, 69(1-4), 221-234.

Blight, G.E. (2009). Geotechnical engineering for mine waste storage facilities. CRC Press.

Blowes, D., Ptacek, C., Jambor, J. and Weisener, C. (2003). The geochemistry of acid mine drainage. Treatise on geochemistry, 9, 612.

Bonate, P.L. (2001). A brief introduction to Monte Carlo simulation. Clinical pharmacokinetics, 40(1), 15-22.

Bouzahzah, H. (2013). Modification et amélioration des tests statiques et cinétiques pour une prédiction fiable du drainage minier acide. Université du Québec en Abitibi-Témiscamingue.

Bouzahzah, H., Benzaazoua, M., Bussière, B. and Plante, B. (2014). Revue de littérature détaillée sur les tests statiques et les essais cinétiques comme outils de prédiction du drainage minier acide. Déchets Sciences et Techniques Techniques, 66, 14-31.

Brough, C., Strongman, J., Bowell, R., Warrender, R., Prestia, A., Barnes, A. and Fletcher, J. (2017). Automated environmental mineralogy; the use of liberation analysis in humidity cell testwork. Minerals Engineering, 107, 112-122.

Brough, C., Warrender, R., Bowell, R., Barnes, A. and Parbhakar-Fox, A. (2013). The process mineralogy of mine wastes. Minerals Engineering, 52, 125-135.

Bussière, B., Lelièvre, J., Ouellet, J., & Bois, D. (1994). Valorisation des résidus miniers: une approche intégrée. Rapports final soumis au Ministère des Ressources Naturelles dans le cadre du volet Mines Écologiques de l'Entente Auxiliaire du Développements Minéral.

Bussière, B., Lelièvre, J., Ouellet, J., & Bois, D. (1995). Utilisation de résidus miniers désulfurés comme recouvrement pour prévenir le DMA: analyse technico-économique sur deux cas réels. In Proceedings of Sudbury'95, Conference on Mining and the Environment, Ed. Hynes TP & Blanchette MC, Sudbury, Ontario (Vol. 1, pp. 59-68).

Bussière, B., Benzaazoua, M., Aubertin, M., and Mbonimpa, M. (2004). A laboratory study of covers made of low-sulphide tailings to prevent acid mine drainage. Environmental geology, 45(5), 609-622.

Bussière, B. (2007). Colloquium 2004: Hydrogeotechnical properties of hard rock tailings from metal mines and emerging geoenvironmental disposal approaches. Canadian Geotechnical Journal, 44(9), 1019-1052.

Bussière, B., Aubertin, M., Zagury, G. J., Potvin, R., and Benzaazoua, M. (2005). Principaux défis et pistes de solution pour la restauration des aires d'entreposage de rejets miniers abandonnées. In Proceedings of the Symposium 2005 sur L'environnement et les Mines (pp. 1-29).

Bussière, B., & Guittonny, M. (Eds.). (2020). Hard rock mine reclamation: from prediction to management of acid mine drainage. CRC press.

Bye, A. R. (2011,). Case studies demonstrating value from geometallurgy initiatives. In GeoMet 2011-1st AusIMM International Geometallurgy Conference 2011 (pp. 9-30). AusIMM: Australasian Institute of Mining and Metallurgy.

Carpentier, S., Gamache, M. and Dimitrakopoulos, R. (2016). Underground long-term mine production scheduling with integrated geological risk management. Mining Technology, 125(2), 93-102.

Cassell, E.A., Dorioz, J.M., Kort, R.L., Hoffmann, J.P., Meals, D.W., Kirschtel, D. and Braun, D.C. (1998). Modeling Phosphorus Dynamics in Ecosystems: Mass Balance and Dynamic Simulation Approaches. Journal of Environmental Quality, 27(2), 293-298.

Che, D. and Jia, Q. (2019). Three-dimensional geological modeling of coal seams using weighted Kriging method and multi-source data. IEEE Access, 7, 118037-118045.

Cheng, J. (2021). Construction and visualization of a three-dimensional model of an engineering geological body. Arabian Journal of Geosciences, 14(5), 1-8.

Chopard, A. (2017). Évaluation environnementale de minerais sulfurés polymétalliques basée sur une approche minéralogique pluridisciplinaire. Université du Québec en Abitibi-Témiscamingue.

Couto, P.G., Damasceno, J.C., Oliveira, S.d. and Chan, W. (2013). Monte Carlo simulations applied to uncertainty in measurement. Theory and applications of Monte Carlo simulations, 27-51.

Cox, M., Harris, P. and Siebert, B.-L. (2003). Evaluation of measurement uncertainty based on the propagation of distributions using Monte Carlo simulation. Measurement Techniques, 46(9), 824-833.

Cox, M.G. and Siebert, B.R. (2006). The use of a Monte Carlo method for evaluating uncertainty and expanded uncertainty. Metrologia, 43(4), S178.

Demers, I., Bussière, B., Benzaazoua, M., Mbonimpa, M. and Blier, A. (2008). Column test investigation on the performance of monolayer covers made of desulphurized tailings to prevent acid mine drainage. Minerals Engineering, 21(4), 317-329.

Demers, I., Molson, J., Bussière, B. and Laflamme, D. (2013). Numerical modeling of contaminated neutral drainage from a waste-rock field test cell. Applied geochemistry, 33, 346-356.

Deng, Y., Chen, D., Fan, J., Shi, Y., Hou, X., Yang, J. and Xu, W. (2019). Geological Panorama Database: Digitizing and Visualizingthe Geological Outcrops. Acta Geologica Sinica (English Edition), 1.

Di Maio, R., De Paola, C., Forte, G., Piegari, E., Pirone, M., Santo, A. and Urciuoli, G. (2020). An integrated geological, geotechnical and geophysical approach to identify predisposing factors for flowslide occurrence. Engineering Geology, 267, 105473.

Dimitrakopoulos, R. (1997). Conditional simulations: tools for modelling uncertainty in open pit optimisation. Optimizing with Whittle, Perth, Whittle Programing Pty. Ltd, 31-42.

Dimitrakopoulos, R. (1998). Conditional simulation algorithms for modelling orebody uncertainty in open pit optimisation. International journal of surface mining, reclamation and environment, 12(4), 173-179.

Dimitrakopoulos, R. (2011). Stochastic optimization for strategic mine planning: a decade of developments. Journal of Mining Science, 47(2), 138-150.

Dimitrakopoulos, R., Farrelly, C. and Godoy, M. (2002). Moving forward from traditional optimization: grade uncertainty and risk effects in open-pit design. Mining Technology, 111(1), 82-88.

Dimitrakopoulos, R.G. and Sabour, S.A.A. (2007). Evaluating mine plans under uncertainty: Can the real options make a difference? Resources Policy, 32(3), 116-125.

Dold, B. (2008). Sustainability in metal mining: from exploration, over processing to mine waste management. Reviews in Environmental Science and bio/technology, 7(4), 275.

Duvernois, A. (2022). Développement d'une méthodologie de prédiction du risque environnementale appliquée à l'exploration minière. Université du Québec en Abitibi-Témiscamingue. Master.

Edraki, M., Baumgartl, T., Manlapig, E., Bradshaw, D., Franks, D.M. and Moran, C.J. (2014). Designing mine tailings for better environmental, social and economic outcomes: a review of alternative approaches. Journal of Cleaner Production, 84, 411-420.

Elatrash, A.M., Abdelwahhab, M.A., Wanas, H.A., El-Naggar, S.I. and Elshayeb, H.M. (2021). Multi-disciplinary approach to sedimentary facies analysis of Messinian Salinity Crisis tectono-sequences (South-Mansoura Area, Nile Delta): Incised-valley fill geological model reconstruction and petroleum geology–reservoir element delineation. Journal of Petroleum Exploration and Production, 11(4), 1643-1666.

Elghali, A., Benzaazoua, M., Bouzahzah, H., Bussière, B. and Villarraga-Gómez, H. (2018). Determination of the available acid-generating potential of waste rock, part I: Mineralogical approach. Applied Geochemistry, 99, 31-41.

Embile Jr, R.F., Walder, I.F. and Mahoney, J.J. (2019). Multicomponent reactive transport modeling of effluent chemistry using locally obtained mineral dissolution rates of forsterite and pyrrhotite from a mine tailings deposit. Advances in Water Resources, 128, 87-96.

Emery, X. and Maleki, M. (2019). Geostatistics in the presence of geological boundaries: Application to mineral resources modeling. Ore Geology Reviews, 114, 103124.

Erguler, Z.A. and Erguler, G.K. (2015). The effect of particle size on acid mine drainage generation: Kinetic column tests. Minerals Engineering, 76, 154-167.

Evangelou, V. B. (1995). Pyrite oxidation and its control: solution chemistry, surface chemistry, acid mine drainage (AMD), molecular oxidation mechanisms, microbial role, kinetics, control, ameliorates and limitations, microencapsulation. CRC press.

Evangelou, V.P. and Zhang, Y. (1995). A review: pyrite oxidation mechanisms and acid mine drainage prevention. Critical Reviews in Environmental Science and Technology, 25(2), 141-199.

Fala, O., Molson, J., Aubertin, M., Dawood, I., Bussière, B. and Chapuis, R. (2013). A numerical modelling approach to assess long-term unsaturated flow and geochemical transport in a waste rock pile. International Journal of Mining, Reclamation and Environment, 27(1), 38-55.

Forrester, J.W. (1996). System dynamics and K-12 teachers. Retrieved August, 8, 2008.

Fourie, A. (2009). Preventing catastrophic failures and mitigating environmental impacts of tailings storage facilities. Procedia Earth and Planetary Science, 1(1), 1067-1071.

Fritzson, P. (2010). Principles of object-oriented modeling and simulation with Modelica 2.1. : John Wiley and Sons.

Furtado e Faria, M., Dimitrakopoulos, R. and Pinto, C. (2022). Stochastic stope design optimisation under grade uncertainty and dynamic development costs. International Journal of Mining, Reclamation and Environment, 36(2), 81-103.

Gao, M., Wang, L., Jia, J., Chen, Y., Liu, R., Shen, L., Chen, X. and Su, M. (2019). Interactive geological visualization based on quadratic-surface distance query. Journal of Electronic Imaging, 28(2), 021009.

Gerke, H.H., Molson, J.W. and Frind, E.O. (1998). Modelling the effect of chemical heterogeneity on acidification and solute leaching in overburden mine spoils. Journal of Hydrology, 209(1-4), 166-185.

Gilks, W.R., Richardson, S. and Spiegelhalter, D. (1995). Markov chain Monte Carlo in practice. : Chapman and Hall/CRC.

Gnedenko, B.V. and Ushakov, I.A. (2018). Theory of probability. : Routledge.

González-Garcia, J. and Jessell, M. (2016). A 3D geological model for the Ruiz-Tolima Volcanic Massif (Colombia): Assessment of geological uncertainty using a stochastic approach based on Bézier curve design. Tectonophysics, 687, 139-157.

Guo, J., Wang, Z., Li, C., Li, F., Jessell, M.W., Wu, L. and Wang, J. (2022). Multiple-Point Geostatistics-Based Three-Dimensional Automatic Geological Modeling and Uncertainty Analysis for Borehole Data. Natural Resources Research, 1-21.

Gut, A. (2013). Probability: a graduate course. (Vol. 75) : Springer Science and Business Media.

Haining, R.P., Kerry, R. and Oliver, M.A. (2010). Geography, Spatial Data Analysis, and Geostatistics: An Overview. . Geographical Analysis, 42(1), 7-31.

Hammersley, J. (1964). Monte carlo methods. : Springer Science and Business Media.

Heriawan, M.N., Pillayati, P., Widodo, L.E. and Widayat, A.H. (2020). Drill hole spacing optimization of non-stationary data for seam thickness and total sulfur: A case study of coal deposits at Balikpapan Formation, Kutai Basin, East Kalimantan. International Journal of Coal Geology, 223, 103466.

Høyer, A.-S., Klint, K., Fiandaca, G., Maurya, P., Christiansen, A., Balbarini, N., Bjerg, P., Hansen, T. and Møller, I. (2019). Development of a high-resolution 3D geological model for landfill leachate risk assessment. Engineering Geology, 249, 45-59.

Jambor, J., Dutrizac, J., Raudsepp, M. and Groat, L. (2003). Effect of peroxide on neutralization-potential values of siderite and other carbonate minerals. Journal of environmental quality, 32(6), 2373-2378.

Jamieson, H.E. (2011). Geochemistry and mineralogy of solid mine waste: essential knowledge for predicting environmental impact. Elements, 7(6), 381-386.

Jessell, M. (2001). Three-dimensional geological modelling of potential-field data. Computers and Geosciences, 27(4), 455-465.

Jurjovec, J., Blowes, D.W., Ptacek, C.J. and Mayer, K.U. (2004). Multicomponent reactive transport modeling of acid neutralization reactions in mine tailings. Water resources research, 40(11).

Jutla, A.S. (2006). Hydrologic modeling of reconstructed watersheds using a system dynamics approach.

Kalonji-Kabambi, A., Demers, I. and Bussière, B. (2020). Reactive transport modeling of the geochemical behavior of highly reactive tailings in different environmental conditions. Applied Geochemistry, 122, 104761.

Kalos, M.H. and Whitlock, P.A. (1986). Monte Carlo methods. : Wiley-VCH.

Kamali, M.R., Omidvar, A. and Kazemzadeh, E. (2013). 3D geostatistical modeling and uncertainty analysis in a carbonate reservoir, SW Iran. Journal of Geological Research, 2013.

Kelly, R.A., Jakeman, A.J., Barreteau, O., Borsuk, M.E., ElSawah, S., Hamilton, S.H., Henriksen, H.J., Kuikka, S., Maier, H.R. and Rizzoli, A.E. (2013). Selecting among five common modelling approaches for integrated environmental assessment and management. Environmental modelling and software, 47, 159-181.

Kirk Nordstrom, D. (2020). Geochemical modeling of iron and aluminum precipitation during mixing and neutralization of acid mine drainage. Minerals, 10(6), 547.

Klebercz, O., Mayes, W.M., Anton, Á.D., Feigl, V., Jarvis, A.P. and Gruiz, K. (2012). Ecotoxicity of fluvial sediments downstream of the Ajka red mud spill, Hungary. Journal of Environmental Monitoring, 14(8), 2063-2071.

Kleinmann, R.L.P., Crerar, D. and Pacelli, R. (1981). Biogeochemistry of acid mine drainage and a method to control acid formation. Min. Eng.(NY);(United States), 33(3).

Kolmogorov, A.N. and Bharucha-Reid, A.T. (2018). Foundations of the theory of probability: Second English Edition. Courier Dover Publications.

Krige, D.G. (1951). A statistical approach to some basic mine valuation problems on the Witwatersrand. Journal of the Southern African Institute of Mining and Metallurgy, 52(6), 119-139.

Kroese, D.P., Brereton, T., Taimre, T. and Botev, Z.I. (2014). Why the Monte Carlo method is so important today. Wiley Interdisciplinary Reviews: Computational Statistics, 6(6), 386-392.

Kumar, A. and Dimitrakopoulos, R. (2021). Production scheduling in industrial mining complexes with incoming new information using tree search and deep reinforcement learning. Applied Soft Computing, 110, 107644.

Lawrence, R.W. and Scheske, M. (1997). A method to calculate the neutralization potential of mining wastes. Environmental Geology, 32(2), 100-106.

Leppinen, J., Salonsaari, P. and Palosaari, V. (1997). Flotation in acid mine drainage control: beneficiation of concentrate. Canadian metallurgical quarterly, 36(4), 225-230.

Li, L. and Simonovic, S.P. (2002). System dynamics model for predicting floods from snowmelt in north American prairie watersheds. [Article]. Hydrological Processes, 16(13), 2645-2666. Scopus.

Lima, G. A., and Suslick, S. B. (2005, April). A quantitative method for estimation of volatility of oil production projects. In *SPE Hydrocarbon Economics and Evaluation Symposium*. OnePetro.

Lima, G.A.C. and Suslick, S.B. (2006). Estimating the volatility of mining projects considering price and operating cost uncertainties. Resources Policy, 31(2), 86-94.

Lu, X. and Wang, H. (2012). Microbial oxidation of sulfide tailings and the environmental consequences. *Elements, 8*(2), 119-124.

Luther III, G.W. (1987). Pyrite oxidation and reduction: molecular orbital theory considerations. Geochimica et Cosmochimica Acta, 51(12), 3193-3199.

Matheron, G. (1963). " Principles of geostatistics", Economic Geology, 58, pp 1246-1266.

Matheron, G. (1965). Les variables régionalisées et leur estimation: une application de la théorie des fonctions aléatoires aux sciences de la nature. : Masson et CIE.

Mayer, K.U., Frind, E.O. and Blowes, D.W. (2002). Multicomponent reactive transport modeling in variably saturated porous media using a generalized formulation for kinetically controlled reactions. Water Resources Research, 38(9), 13-11-13-21.

McKibben, M.A. and Barnes, H.L. (1986). Oxidation of pyrite in low temperature acidic solutions: Rate laws and surface textures. Geochimica et Cosmochimica Acta, 50(7), 1509-1520.

Mery, N. and Marcotte, D. (2022). Assessment of Recoverable Resource Uncertainty in Multivariate Deposits Through a Simple Machine Learning Technique Trained Using Geostatistical Simulations. Natural Resources Research, 31(2), 767-783.

Molson, J., Fala, O., Aubertin, M. and Bussière, B. (2005). Numerical simulations of pyrite oxidation and acid mine drainage in unsaturated waste rock piles. Journal of Contaminant Hydrology, 78(4), 343-371.

Moses, C.O., Nordstrom, D.K., Herman, J.S. and Mills, A.L. (1987). Aqueous pyrite oxidation by dissolved oxygen and by ferric iron. Geochimica et Cosmochimica Acta, 51(6), 1561-1571.

Mudd, G.M. (2007). Global trends in gold mining: Towards quantifying environmental and resource sustainability. Resources Policy, 32(1-2), 42-56.

Muniruzzaman, M., Karlsson, T., Ahmadi, N. and Rolle, M. (2020). Multiphase and multicomponent simulation of acid mine drainage in unsaturated mine waste: Modeling approach, benchmarks and application examples. Applied Geochemistry, 120, 104677.

Nicholson, R.V. and Scharer, J.M. (1994). Laboratory studies of pyrrhotite oxidation kinetics. Dans : ACS Publications.

Niederreiter, H. (1992). Random number generation and quasi-Monte Carlo methods. (Vol. 63) : Siam.

Nordstrom, D., Alpers, C.N., Ptacek, C. and Blowes, D. (2000). Negative pH and extremely acidic mine waters from Iron Mountain, California. Environmental Science and Technology, 34(2), 254-258.

Nordstrom, D.K. (1982). Aqueous pyrite oxidation and the consequent formation of secondary iron minerals. : Soil Science Society of America.

O'Connor, S. (2015). Geological models and their influence on geotechnical investigation. Queen's University.

Ouangrawa, M., Molson, J., Aubertin, M., Bussière, B. and Zagury, G. (2009). Reactive transport modelling of mine tailings columns with capillarity-induced high water saturation for preventing sulfide oxidation. Applied Geochemistry, 24(7), 1312-1323.

Paithankar, A. and Chatterjee, S. (2018). Grade and tonnage uncertainty analysis of an african copper deposit using multiple-point geostatistics and sequential gaussian simulation. Natural Resources Research, 27(4), 419-436.

Paktunc, A. (1999). Mineralogical constraints on the determination of neutralization potential and prediction of acid mine drainage. Environmental Geology, 39(2), 103-112.

Pakyuz-Charrier, E., Giraud, J., Ogarko, V., Lindsay, M. and Jessell, M. (2018a). Drillhole uncertainty propagation for three-dimensional geological modeling using Monte Carlo. Tectonophysics, 747-748, 16-39.

Pakyuz-Charrier, E., Lindsay, M., Ogarko, V., Giraud, J. and Jessell, M. (2018b). Monte Carlo simulation for uncertainty estimation on structural data in implicit 3-D geological modeling, a guide for disturbance distribution selection and parameterization. Solid Earth, 9(2), 385-402.

Papadopoulos, C.E. and Yeung, H. (2001). Uncertainty estimation and Monte Carlo simulation method. Flow Measurement and Instrumentation, 12(4), 291-298.

Parbhakar-Fox, A., Lottermoser, B. and Bradshaw, D. (2013). Evaluating waste rock mineralogy and microtexture during kinetic testing for improved acid rock drainage prediction. Minerals Engineering, 52, 111-124.

Parbhakar-Fox, A.K., Edraki, M., Walters, S. and Bradshaw, D. (2011). Development of a textural index for the prediction of acid rock drainage. Minerals Engineering, 24(12), 1277-1287.

Parkhurst, D.L. and Appelo, C. (2013). Description of input and examples for PHREEQC version 3: a computer program for speciation, batch-reaction, one-dimensional transport, and inverse geochemical calculations. (2328-7055). : US Geological Survey.

Parry, S., Baynes, F., Culshaw, M., Eggers, M., Keaton, J., Lentfer, K., Novotny, J. and Paul, D. (2014). Engineering geological models: an introduction: IAEG commission 25. Bulletin of engineering geology and the environment, 73(3), 689-706.

Peck, S. (1998). Group model building: facilitating team learning using system dynamics. Journal of the Operational Research Society, 49(7), 766-767.

Pedretti, D., Mayer, K.U. and Beckie, R.D. (2017). Stochastic multicomponent reactive transport analysis of low quality drainage release from waste rock piles: Controls of the spatial distribution of acid generating and neutralizing minerals. Journal of contaminant hydrology, 201, 30-38.

Pedretti, D., Mayer, K.U. and Beckie, R.D. (2020). Controls of uncertainty in acid rock drainage predictions from waste rock piles examined through Monte-Carlo multicomponent reactive transport. Stochastic Environmental Research and Risk Assessment, 34(1), 219-233.

Pinsky, M. and Karlin, S. (2010). An introduction to stochastic modeling. : Academic press.

Plante, B., Bussière, B. and Benzaazoua, M. (2012). Static tests response on 5 Canadian hard rock mine tailings with low net acid-generating potentials. Journal of Geochemical Exploration, 114, 57-69.

Poirier, A. (2019). Étude du comportement thermique d'une halde à stériles en milieu nordique. Ecole Polytechnique, Montreal (Canada).

Radwan, A.A., Abdelwahhab, M.A., Nabawy, B.S., Mahfouz, K.H. and Ahmed, M.S. (2022). Facies analysis-constrained geophysical 3D-static reservoir modeling of Cenomanian units in the Aghar Oilfield (Western Desert, Egypt): insights into paleoenvironment and petroleum geology of fluviomarine systems. Marine and Petroleum Geology, 136, 105436.

Ranalli, G. (2001). Experimental tectonics: from Sir James Hall to the present. Journal of Geodynamics, 32(1-2), 65-76.

Raychaudhuri, S. (2008, December). Introduction to monte carlo simulation. In 2008 Winter simulation conference (pp. 91-100). IEEE..

Raymond, K.E., Seigneur, N., Su, D., Poaty, B., Plante, B., Bussière, B. and Mayer, K.U. (2020). Numerical modeling of a laboratory-scale waste rock pile featuring an engineered cover system. Minerals, 10(8), 652.

Reed, J.P. (2007). Volumetric Analysis and Three-Dimensional Visualisation of Industrial Mineral Deposit. 43th Forum on Geology of Industrial Minerals.

Remy, N., Boucher, A. and Wu, J. (2009). Applied geostatistics with SGeMS: A user's guide. : Cambridge University Press.

Richardson, J.F., Harker, J.H., Backhurst, J.R. and Coulson, J.M. (2002). Coulson and Richardson's chemical engineering. Vol. 2, Particle technology and separation processes. (5th ed. / J.F. Richardson and J.H. Harker with J.R. Backhurst. éd.). Oxford : Butterworth-Heinemann.

Robinson, S. (2008). Conceptual modelling for simulation Part I: definition and requirements. Journal of the operational research society, 59(3), 278-290.

Saikia, K. and Sarkar, B. (2006). Exploration drilling optimisation using geostatistics: a case in Jharia Coalfield, India. Applied Earth Science, 115(1), 13-22.

Seigneur, N., Mayer, K.U. and Steefel, C.I. (2019). Reactive transport in evolving porous media. Reviews in Mineralogy and Geochemistry, 85(1), 197-238.

Silva, C. J. E., Bassani, M. A. A., and Costa, J. F. C. L. (2019, May). Influence of drilling spacing on the mineral resources uncertainty. In Mining goes Digital: Proceedings of the 39th International Symposium Application of Computers and Operations Research in the Mineral Industry'(APCOM 2019), June 4-6, 2019, Wroclaw, Poland (p. 184). CRC Press.

Simonovic, S.P., Fahmy, H. and El-Shorbagy, A. (1997). The use of object-oriented modeling for water resources planning in Egypt. Water Resources Management, 11(4), 243-261.

Singer, P.C. and Stumm, W. (1970). Acidic mine drainage: the rate-determining step. Science, 167(3921), 1121-1123.

Skousen, J., Renton, J., Brown, H., Evans, P., Leavitt, B., Brady, K., Cohen, L. and Ziemkiewicz, P. (1997). Neutralization potential of overburden samples containing siderite. Journal of Environmental Quality, 26(3), 673-681.

Sobek, A.A. (1978). Field and laboratory methods applicable to overburdens and minesoils. : Industrial Environmental Research Laboratory, Office of Research and Development, US Environmental Protection Agency.

Sohrabi, P., Dehghani, H. and Jodeiri Shokri, B. (2021). Determination of optimal production rate under price uncertainty—Sari Gunay gold mine, Iran. Mineral Economics, 1-15.

Steefel, C.I., DePaolo, D.J. and Lichtner, P.C. (2005). Reactive transport modeling: An essential tool and a new research approach for the Earth sciences. Earth and Planetary Science Letters, 240(3-4), 539-558.

Steefel, C.I. and Lichtner, P.C. (1998). Multicomponent reactive transport in discrete fractures: I. Controls on reaction front geometry. Journal of Hydrology, 209(1-4), 186-199.

Strömberg, B. (1997). Weathering Kinetics of Sulphidic Mining Waste : an Assessment of Geochemical Process in the Aitik Mining Waste Rock Deposits. AFR-Report 159, Department of Chemistry, Inorganic Chemistry, Royal Institue of Technology, Stockholm, Sweden.

Taghvaeenezhad, M., Shayestehfar, M., Moarefvand, P. and Rezaei, A. (2020). Quantifying the criteria for classification of mineral resources and reserves through the estimation of block model uncertainty using geostatistical methods: a case study of Khoshoumi Uranium deposit in Yazd, Iran. Geosystem Engineering, 23(4), 216-225.

Thornton, J.M., Mariethoz, G. and Brunner, P. (2018). A 3D geological model of a structurally complex Alpine region as a basis for interdisciplinary research. Scientific data, 5(1), 1-20.

Ugwuegbu, C.C. (2013). Segilola gold mine valuation using Monte Carlo simulation approach. Mineral Economics, 26(1), 39-46.

Vermette, D. (2018). Approche de caractérisation géoenvironnementale axée sur l'utilisation des concepts géométallurgiques. Université du Québec en Abitibi-Témiscamingue. http://depositum.uqat.ca/765/1/Memoire_DVermette.pdf. Master.

Vriens, B., Plante, B., Seigneur, N. and Jamieson, H. (2020). Mine waste rock: Insights for sustainable hydrogeochemical management. Minerals, 10(9), 728.

Wackernagel, H. (1996). Multivariate geostatistics: an introduction with applications. In International Journal of Rock Mechanics and Mining Sciences and Geomechanics Abstracts (Vol. 8, No. 33, p. 363A).

Walter, A., Frind, E., Blowes, D., Ptacek, C. and Molson, J. (1994). Modeling of multicomponent reactive transport in groundwater: 1. Model development and evaluation. Water resources research, 30(11), 3137-3148.

Wang, G., Li, R., Carranza, E.J.M., Zhang, S., Yan, C., Zhu, Y., Qu, J., Hong, D., Song, Y. and Han, J. (2015). 3D geological modeling for prediction of subsurface Mo targets in the Luanchuan district, China. Ore Geology Reviews, 71, 592-610.

Wang, G., Zhu, Y., Zhang, S., Yan, C., Song, Y., Ma, Z., Hong, D. and Chen, T. (2012). 3D geological modeling based on gravitational and magnetic data inversion in the Luanchuan ore region, Henan Province, China. Journal of Applied Geophysics, 80, 1-11.

Wang, Z., Yin, Z., Caers, J. and Zuo, R. (2020). A Monte Carlo-based framework for risk-return analysis in mineral prospectivity mapping. Geoscience Frontiers, 11(6), 2297-2308.

Weisener, C. and Weber, P. (2010). Preferential oxidation of pyrite as a function of morphology and relict texture. New Zealand Journal of Geology and Geophysics, 53(2-3), 167-176.

Wickland, B.E. and Wilson, G.W. (2005). Self-weight consolidation of mixtures of mine waste rock and tailings. Canadian Geotechnical Journal, 42(2), 327-339.

Wiersma, C. and Rimstidt, J. (1984). Rates of reaction of pyrite and marcasite with ferric iron at pH 2. Geochimica et Cosmochimica Acta, 48(1), 85-92.

Wills, B.A. and Finch, J. (2015). Wills' mineral processing technology: an introduction to the practical aspects of ore treatment and mineral recovery. Butterworth-Heinemann.

Wilson, D., Amos, R.T., Blowes, D.W., Langman, J.B., Ptacek, C.J., Smith, L. and Sego, D.C. (2018). Diavik waste rock project: A conceptual model for temperature and sulfide-content dependent geochemical evolution of waste rock–Laboratory scale. Applied geochemistry, 89, 160-172.

Wu, Q. and Xu, H. (2004). On three-dimensional geological modeling and visualization. Science in China Series D: Earth Sciences, 47(8), 739-748.

Wunderly, M., Blowes, D., Frind, E. and Ptacek, C. (1996). Sulfide mineral oxidation and subsequent reactive transport of oxidation products in mine tailings impoundments: A numerical model. Water Resources Research, 32(10), 3173-3187.

Xavier, B.C., Egydio-Silva, M., Sadowski, G.R., de Assis Silva, B. and Takara, V.J. (2022). Construction of Structural Geological Model Using Monte Carlo Simulation. Geotechnical and Geological Engineering, 40(3), 1345-1361.

Yilmaz, E. (2011). Advances in reducing large volumes of environmentally harmful mine waste rocks and tailings. Gospodarka Surowcami Mineralnymi, 27, 89-112.

Zhang, Y., Zhong, D., Wu, B., Guan, T., Yue, P. and Wu, H. (2018). 3D Parametric Modeling of Complex Geological Structures for Geotechnical Engineering of Dam Foundation Based on T-Splines. Computer-Aided Civil and Infrastructure Engineering, 33(7), 545-570.

Zheng, X. (2019). Development of a tailings simulation model using System Dynamics. University of Alberta, Education and Research Archive. Master's.

Zu, X.F., Hou, W.S., Zhang, B.Y., Hua, W.H. and Luo, J. (2012). Overview of three-dimensional geological modeling technology. Ieri Procedia, 2, 921-927.

APPENDIX A MERGING 3D GEOLOGICAL MODELING AND STOCHASTIC SIMULATION TO FOSTER THE WASTE ROCK UPSTREAM MANAGEMENT

Research Institute on Mines and Environment (RIME),

Université du Québec en Abitibi-Témiscamingue, Rouyn-Noranda, Québec, Canada

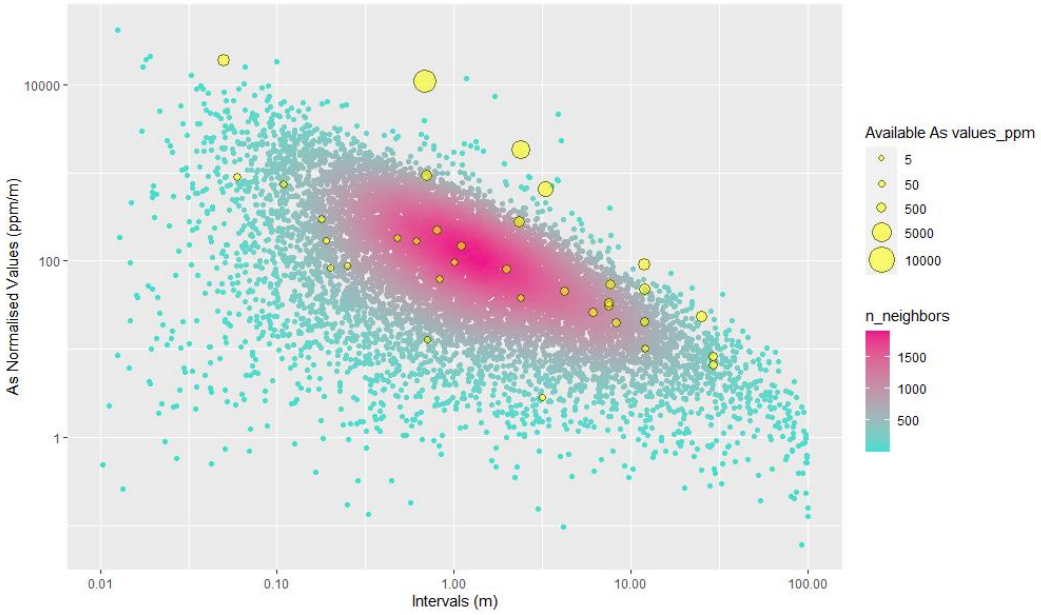


Figure. S1 Realization 2 of the arsenopyrite class 0.1.

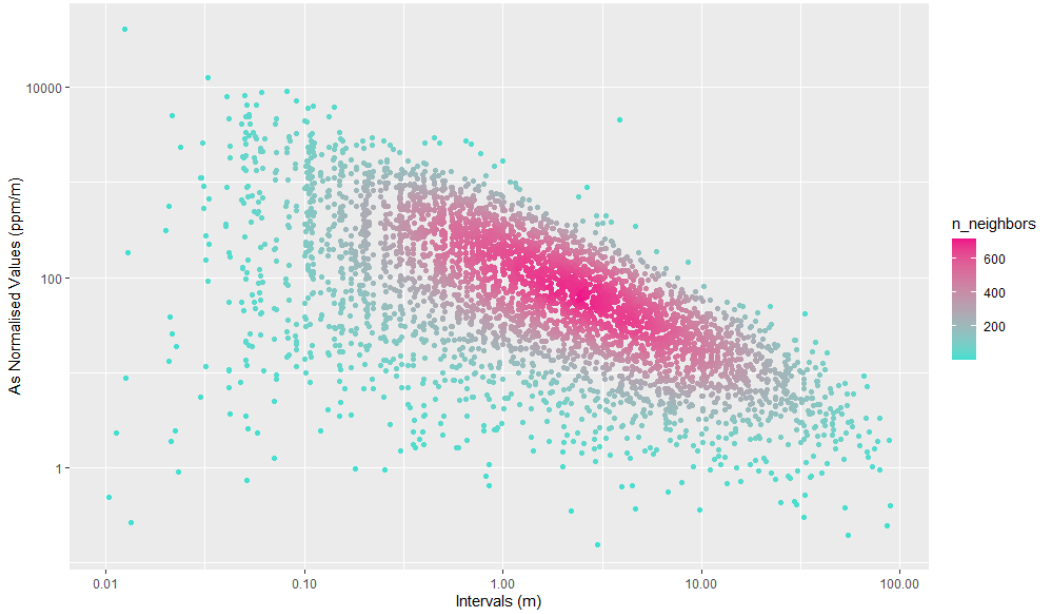


Figure. S2 The selected values of the auxiliary variable based on interval values of the class 0.1 (realization 2).

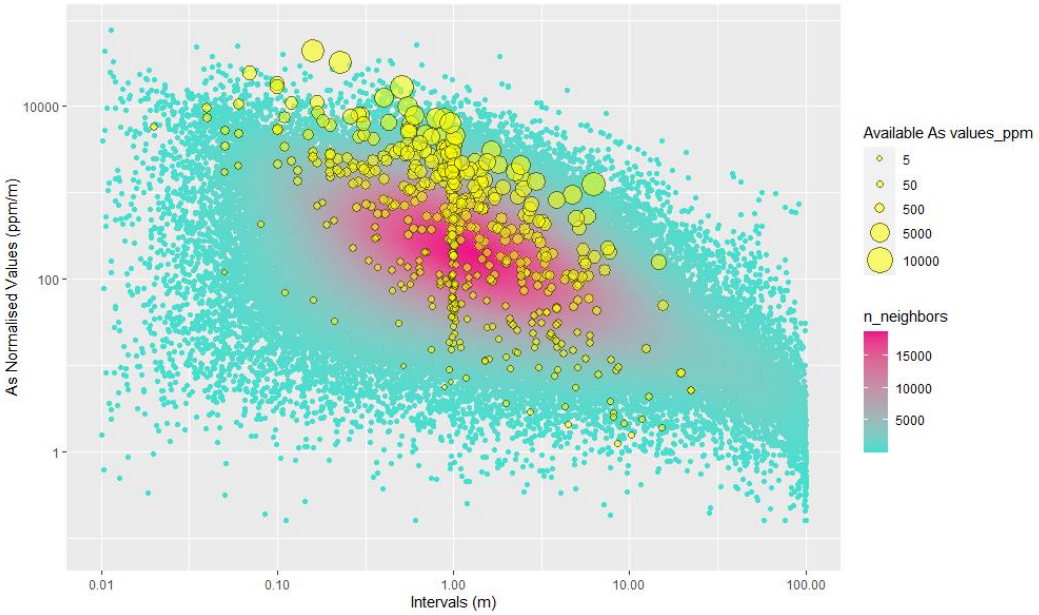


Figure. S3 Realization 2 of the arsenopyrite class 0.5.

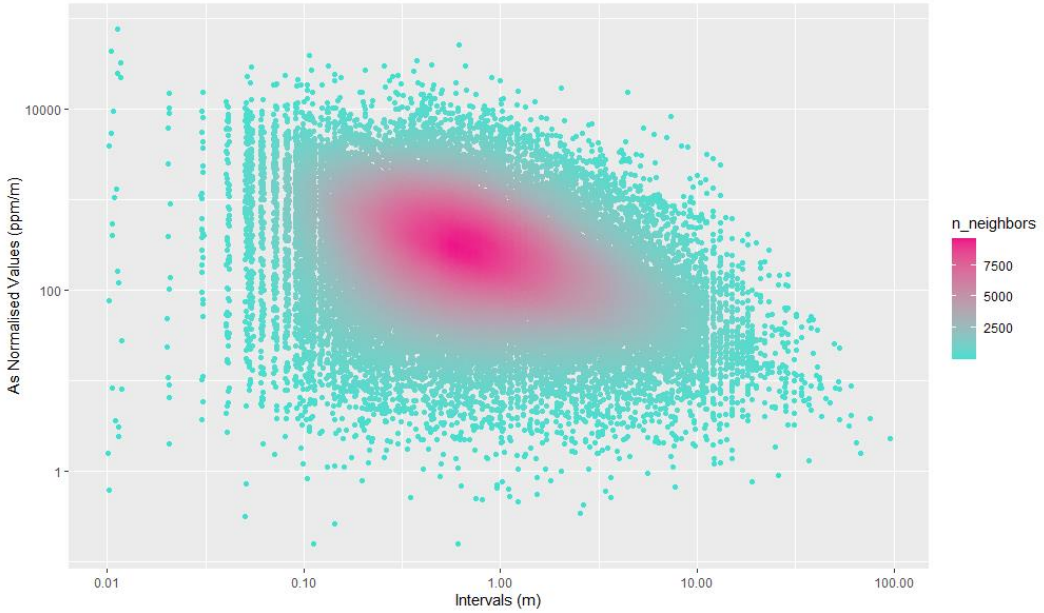


Figure. S4 The selected values of the auxiliary variable based on interval values of the class 0.5 (realization 2).

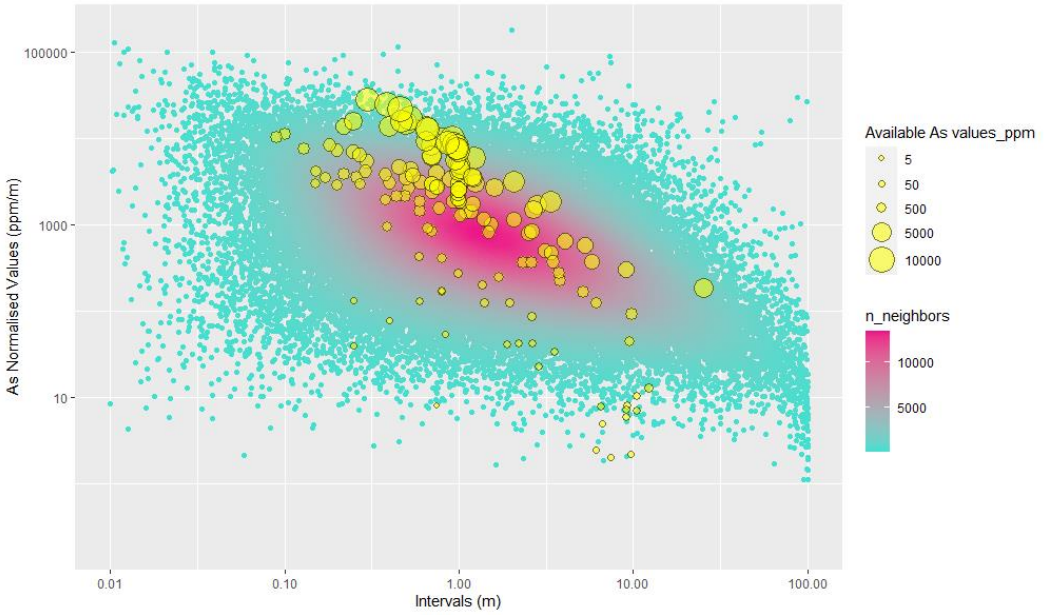


Figure. S5 Realization 2 of the arsenopyrite class 1.

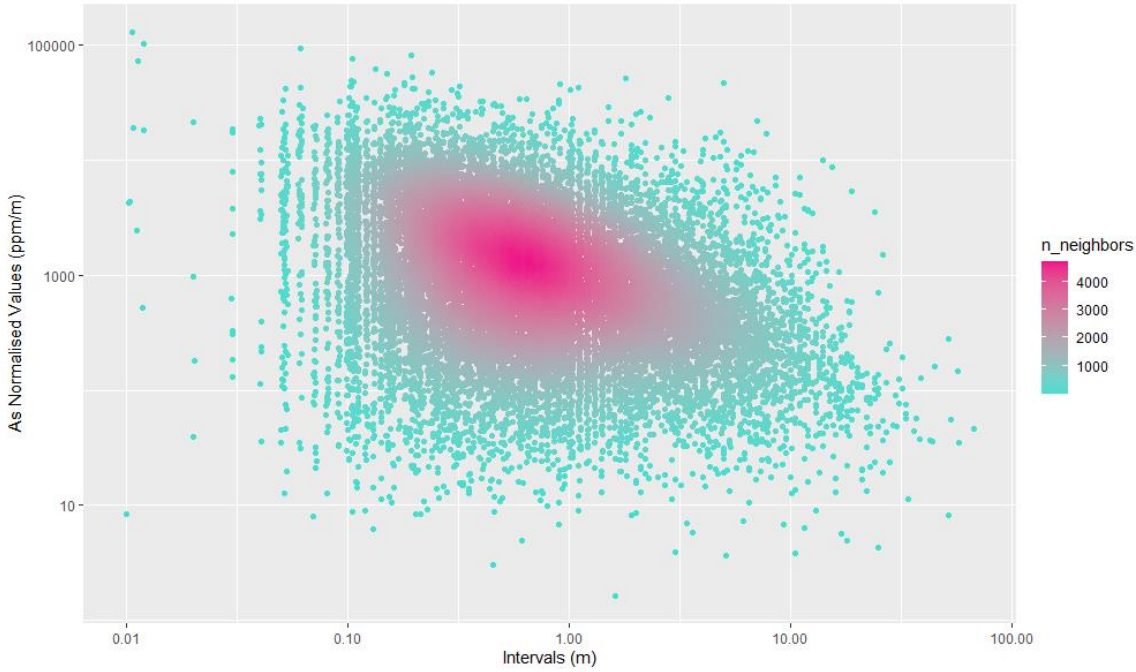


Figure. S6 The selected values of the auxiliary variable based on interval values of the class 1 (realization 2).

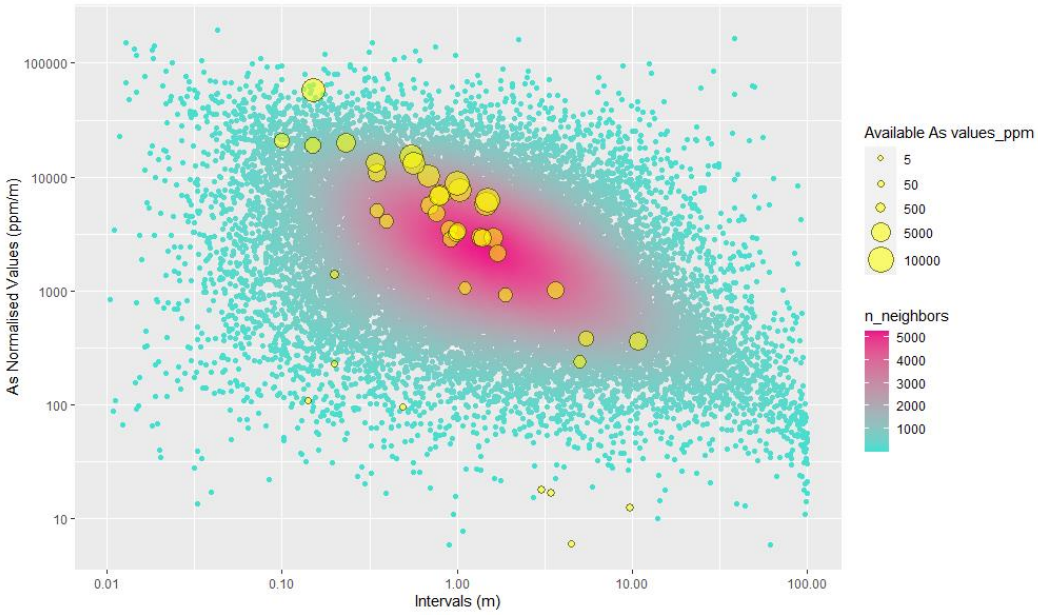


Figure. S7 Realization 2 of the arsenopyrite class 2.

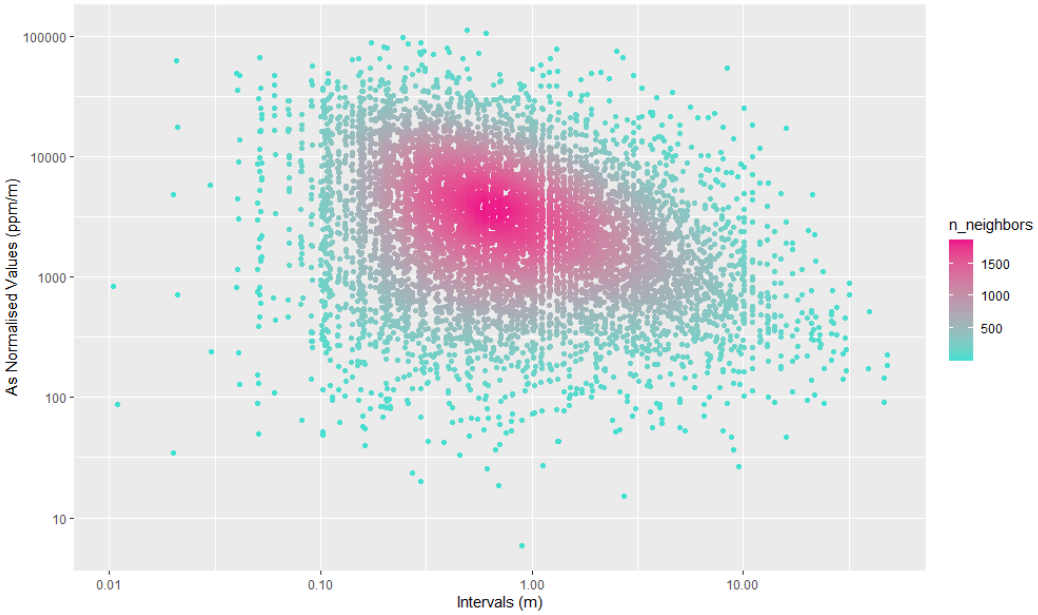


Figure. S8 The selected values of the auxiliary variable based on interval values of the class 2 (realization 2).

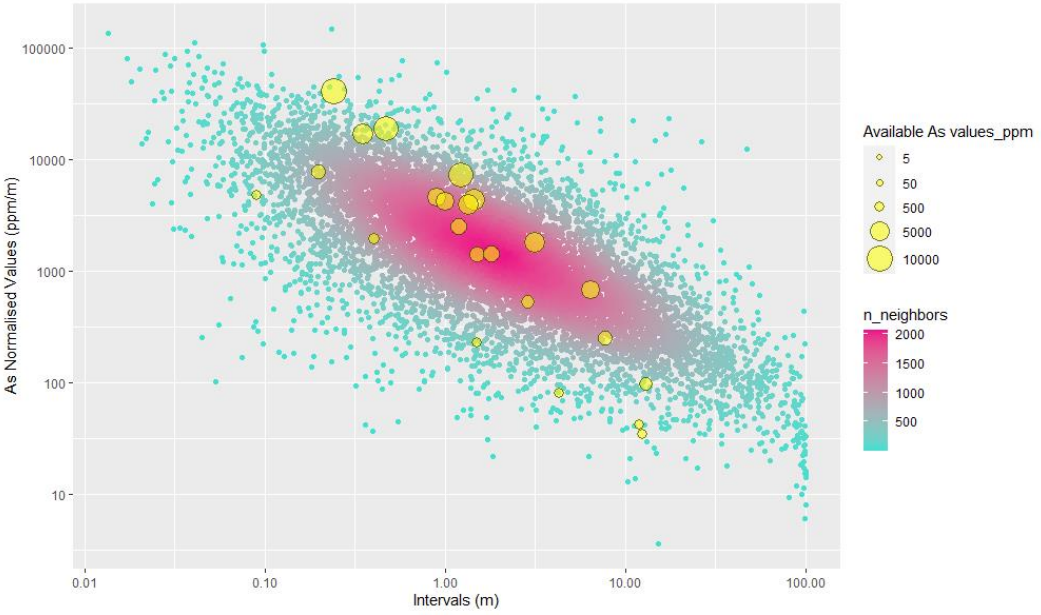


Figure. S9 Realization 2 of the arsenopyrite class 3.



Figure. S10 The selected values of the auxiliary variable based on interval values of the class 3 (realization 2).

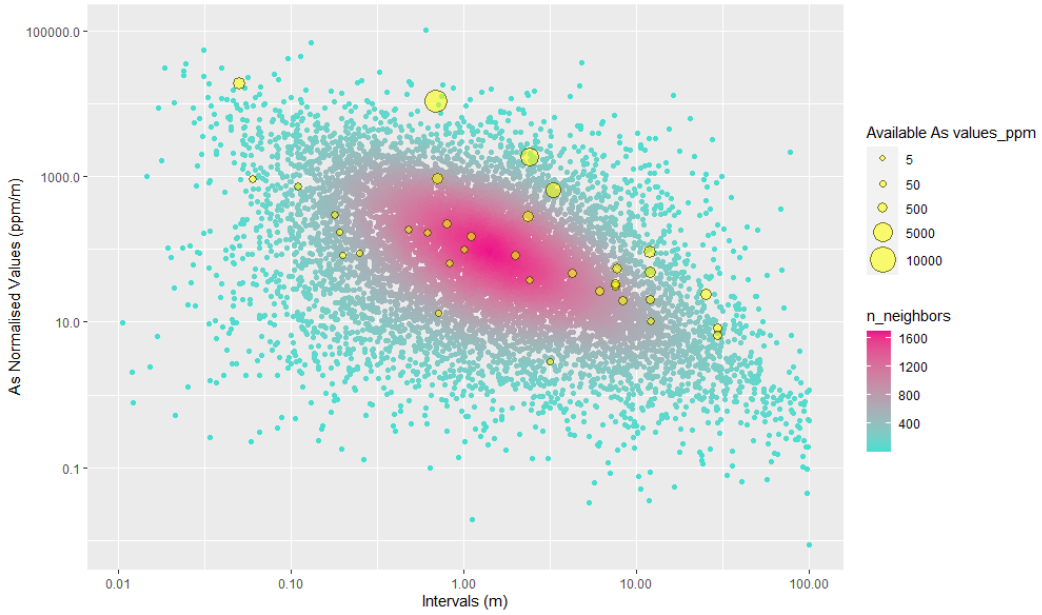


Figure. S11 Realization 3 of the arsenopyrite class 0.1.

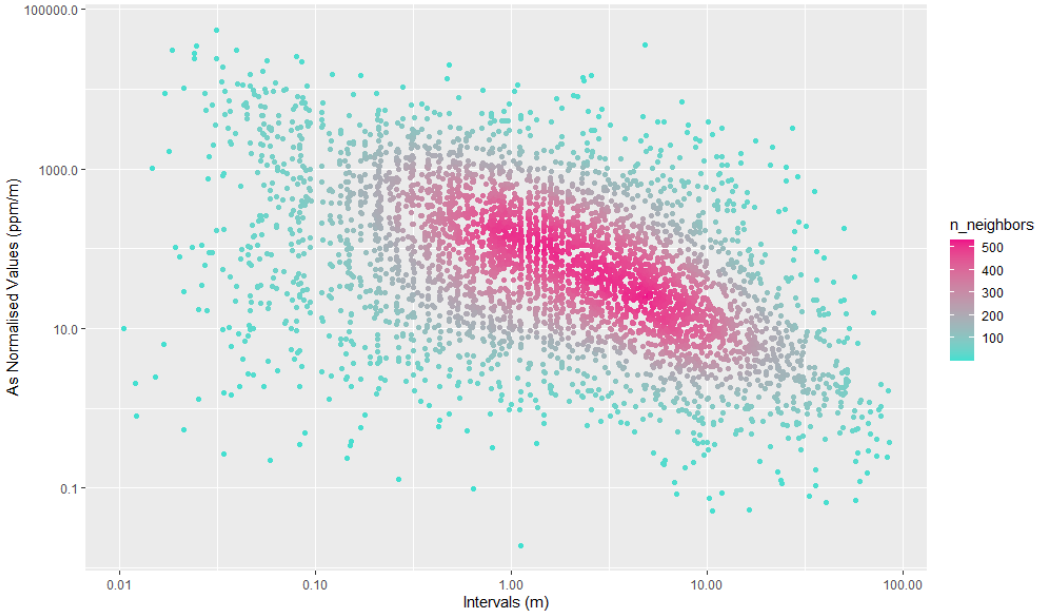


Figure. S12 The selected values of the auxiliary variable based on interval values of the class 0.1 (realization 3).

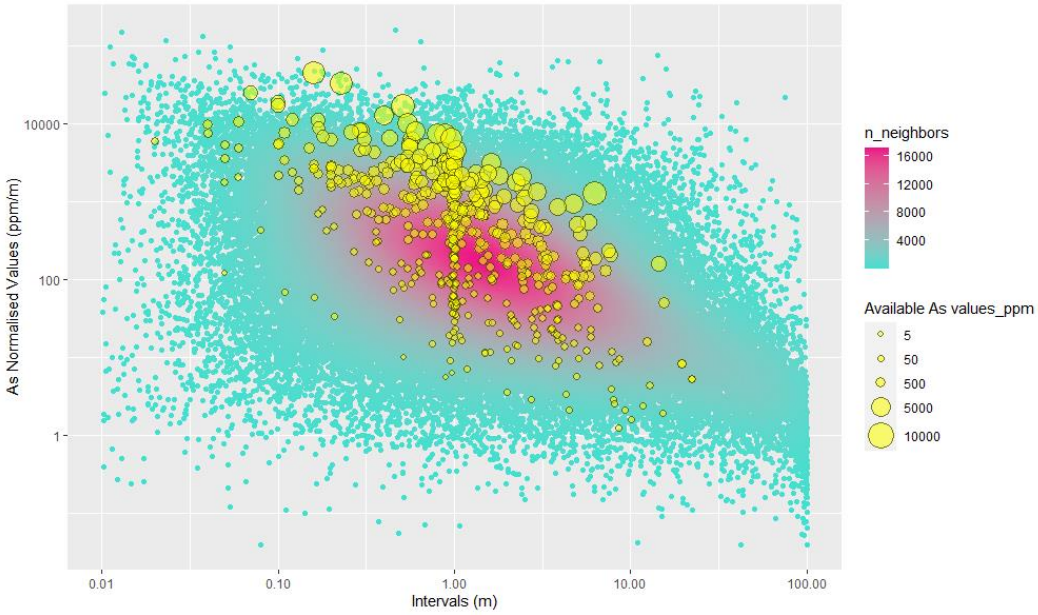


Figure. S13 Realization 3 of the arsenopyrite class 0.5 .

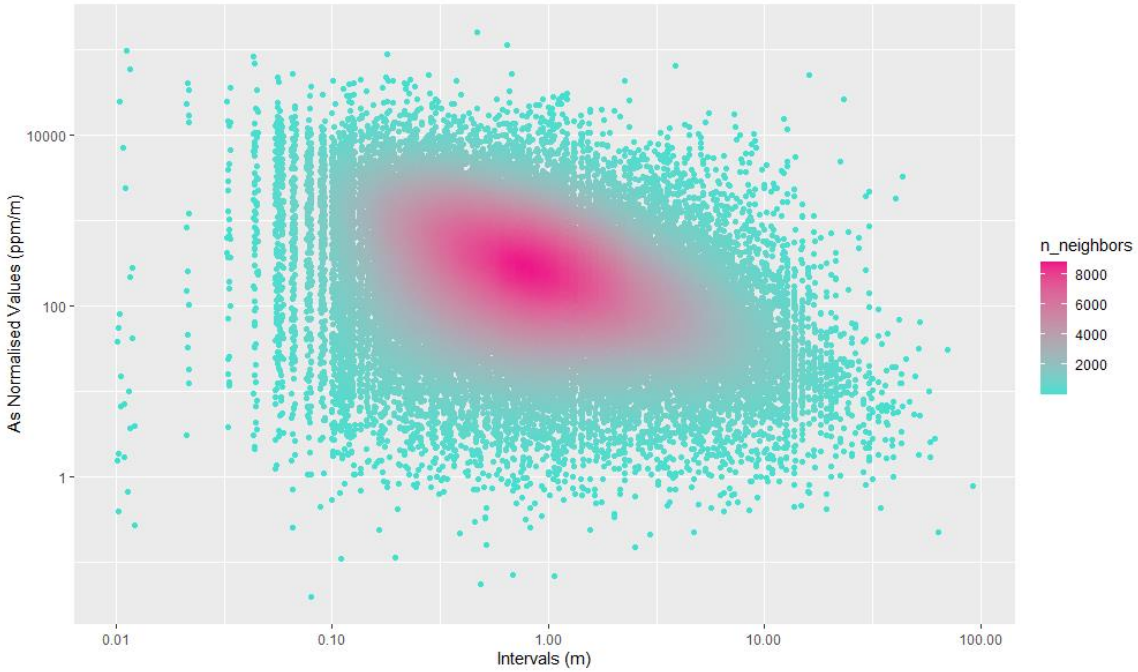


Figure. S14 The selected values of the auxiliary variable based on interval values of the class 0.5 (realization 3).

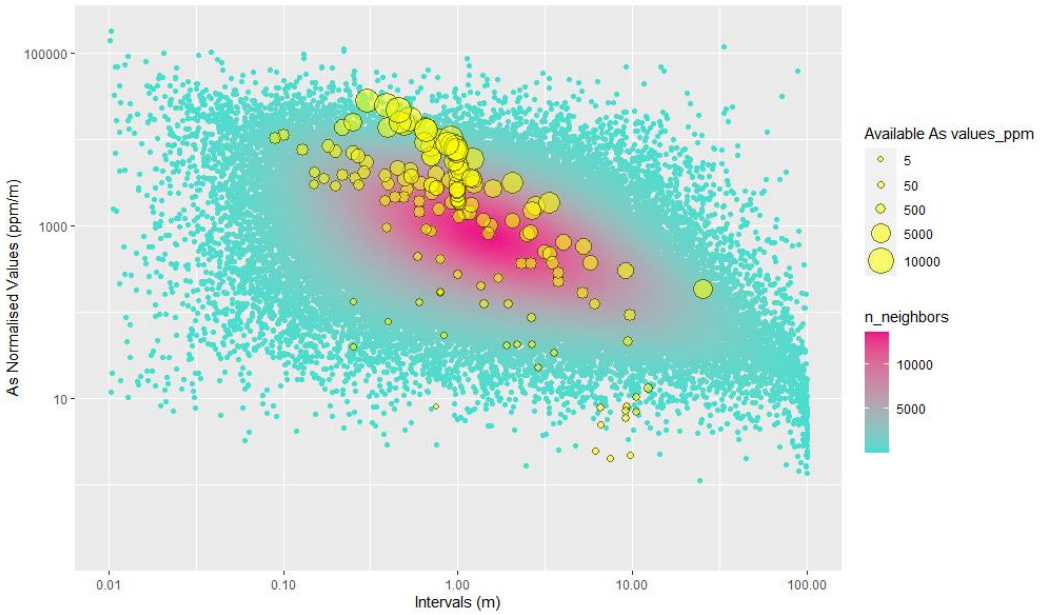


Figure. S15 Realization 3 of the arsenopyrite class 1.

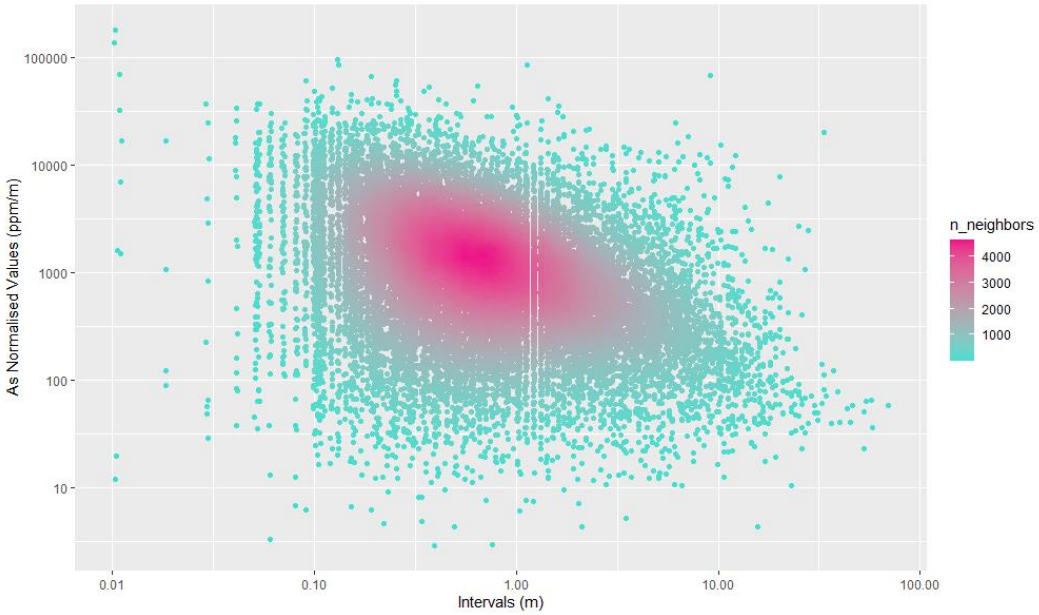


Figure. S16 The selected values of the auxiliary variable based on interval values of the class 1 (realization 3).

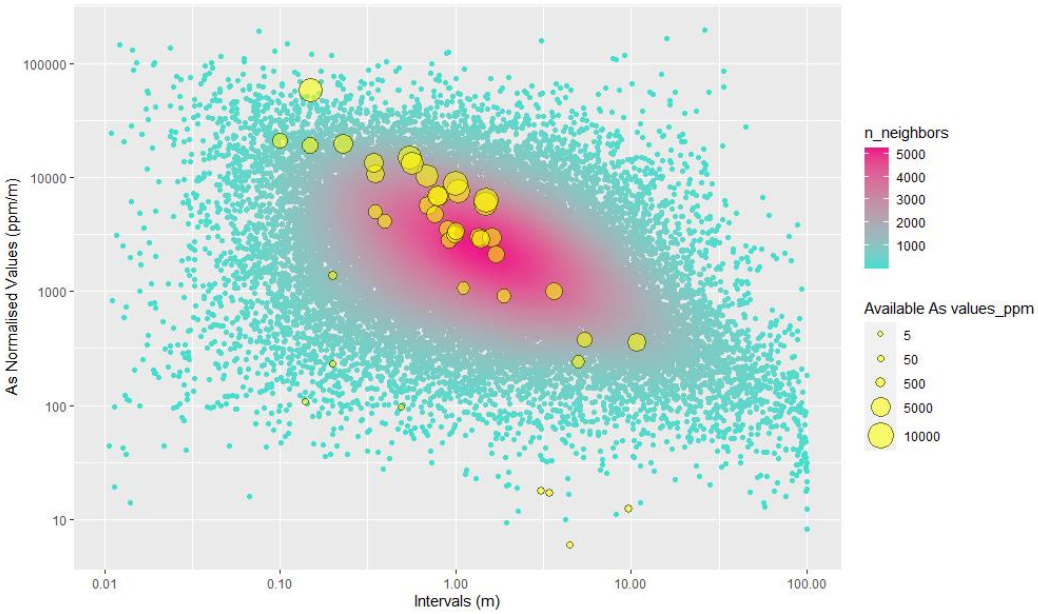


Figure. S17 Realization 3 of the arsenopyrite class 2.



Figure. S18 The selected values of the auxiliary variable based on interval values of the class 2 (realization 3).

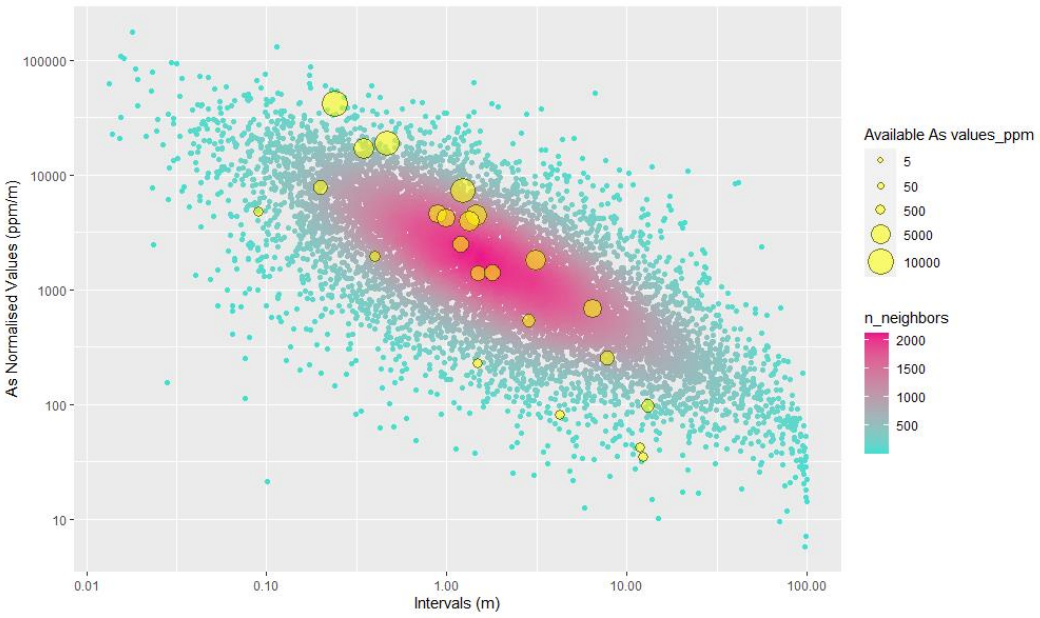


Figure. S19 Realization 3 of the arsenopyrite class 3.

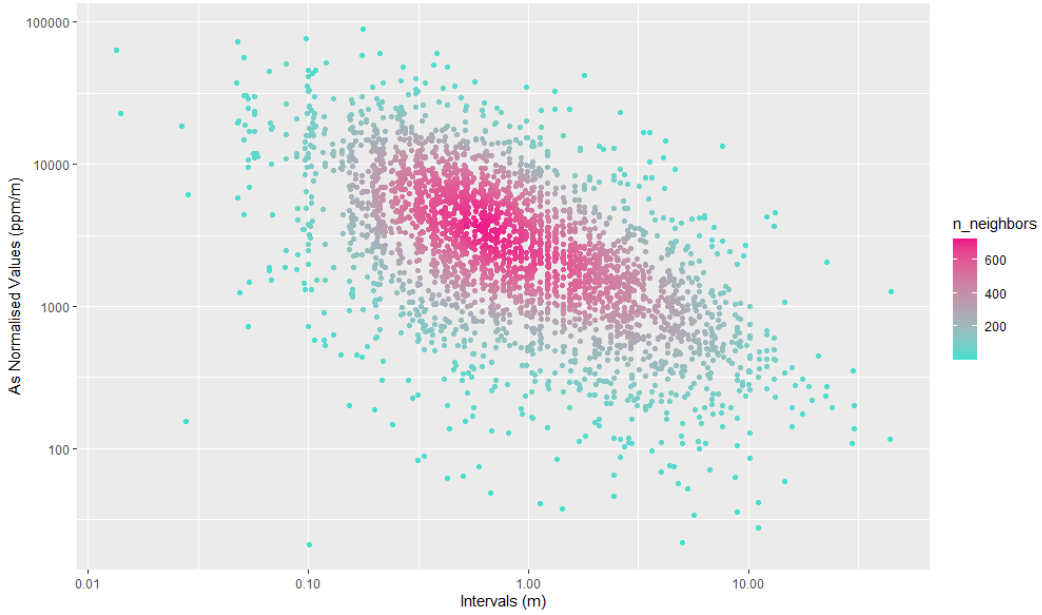


Figure. S20 The selected values of the auxiliary variable based on interval values of the class 3 (realization 3).

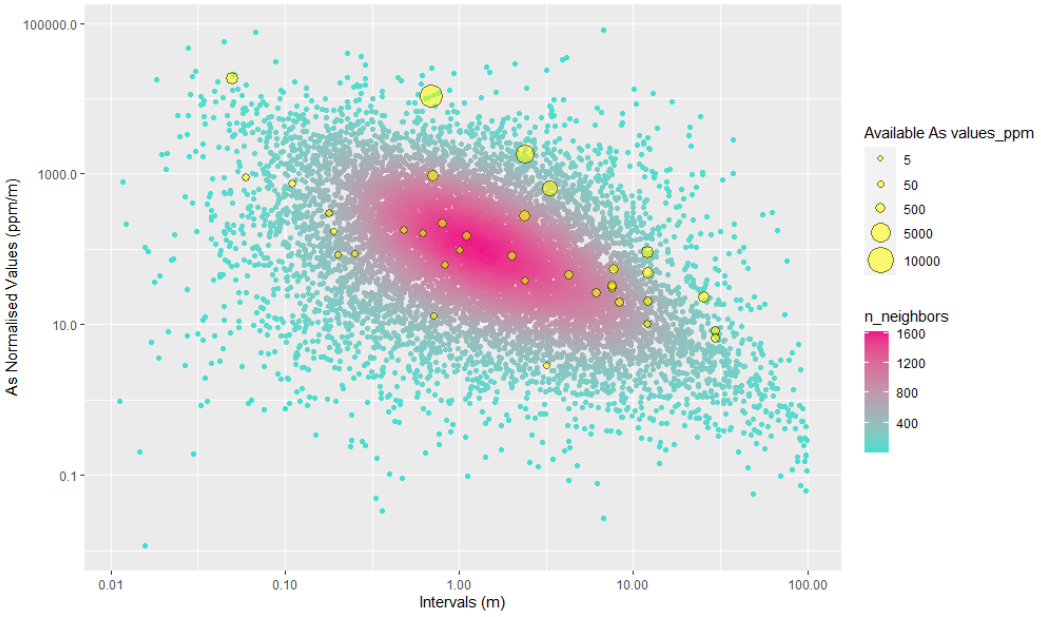


Figure. S21 Realization 4 of the arsenopyrite class 0.1.



Figure. S22 The selected values of the auxiliary variable based on interval values of the class 0.1 (realization 4).

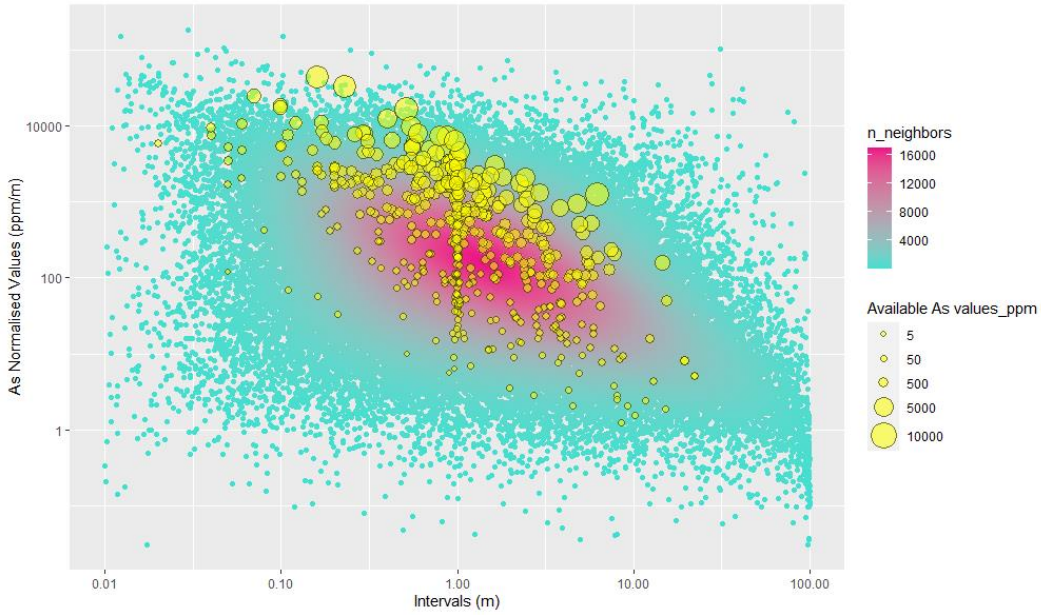


Figure. S23 Realization 4 of the arsenopyrite class 0.5.

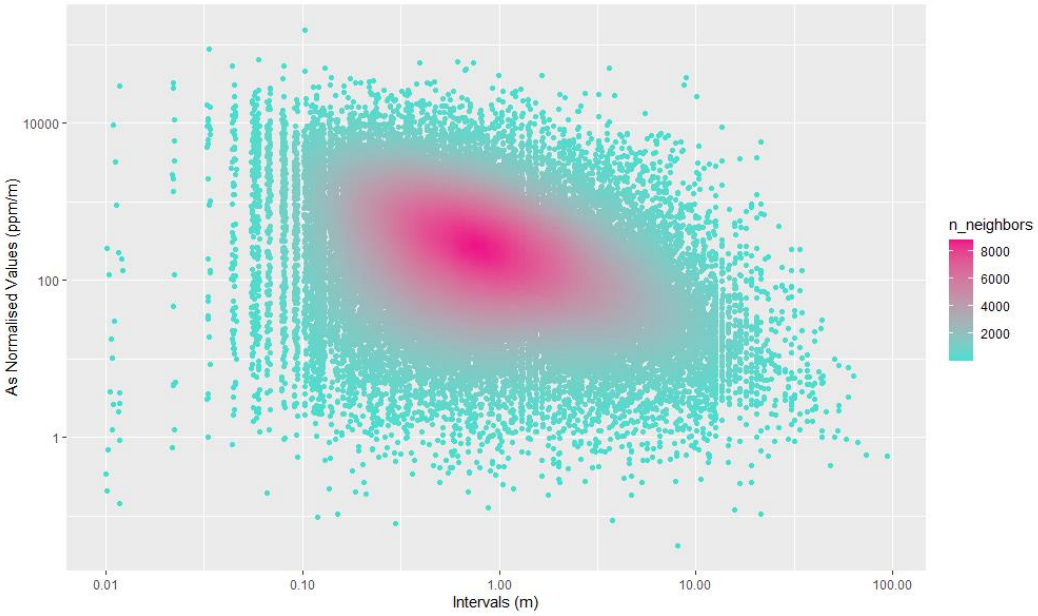


Figure. S24 The selected values of the auxiliary variable based on interval values of the class 0.5 (realization 4).

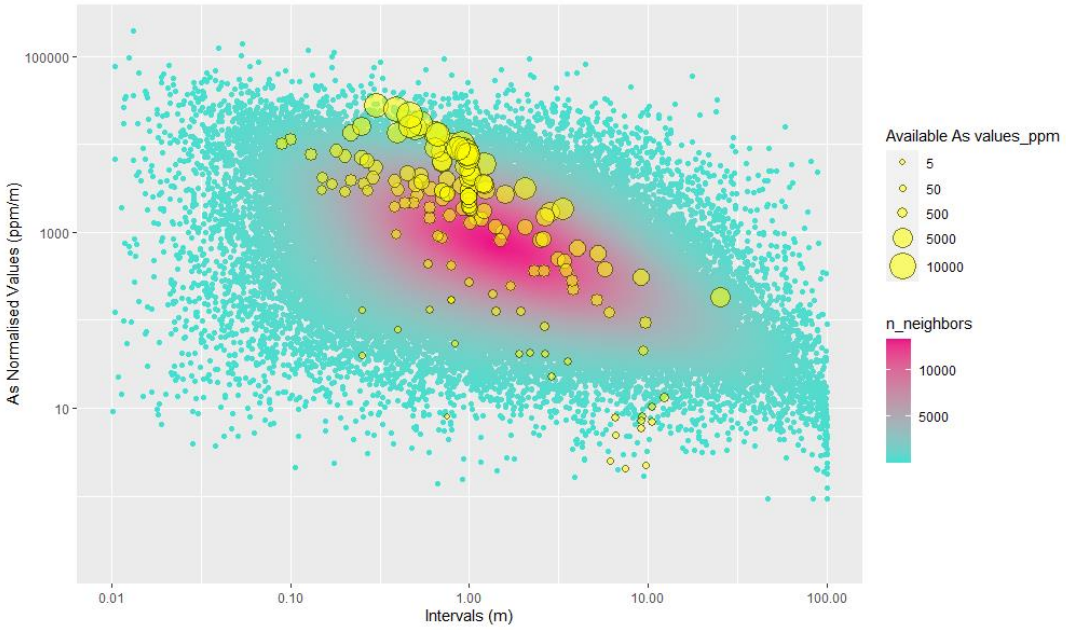


Figure. S25 Realization 4 of the arsenopyrite class 1.

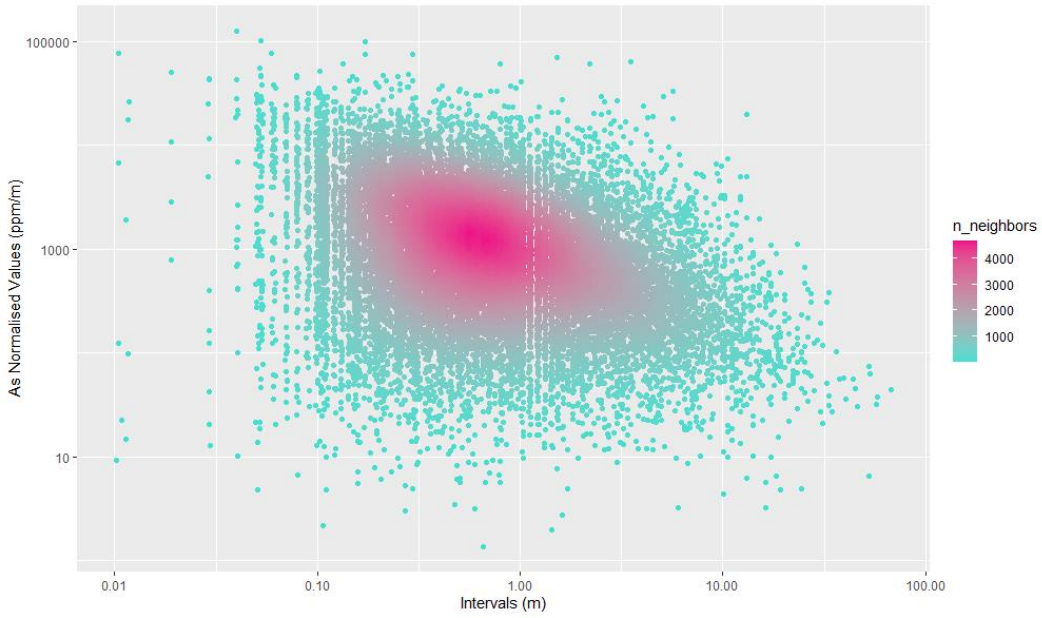


Figure. S26 The selected values of the auxiliary variable based on interval values of the class 1 (realization 4).

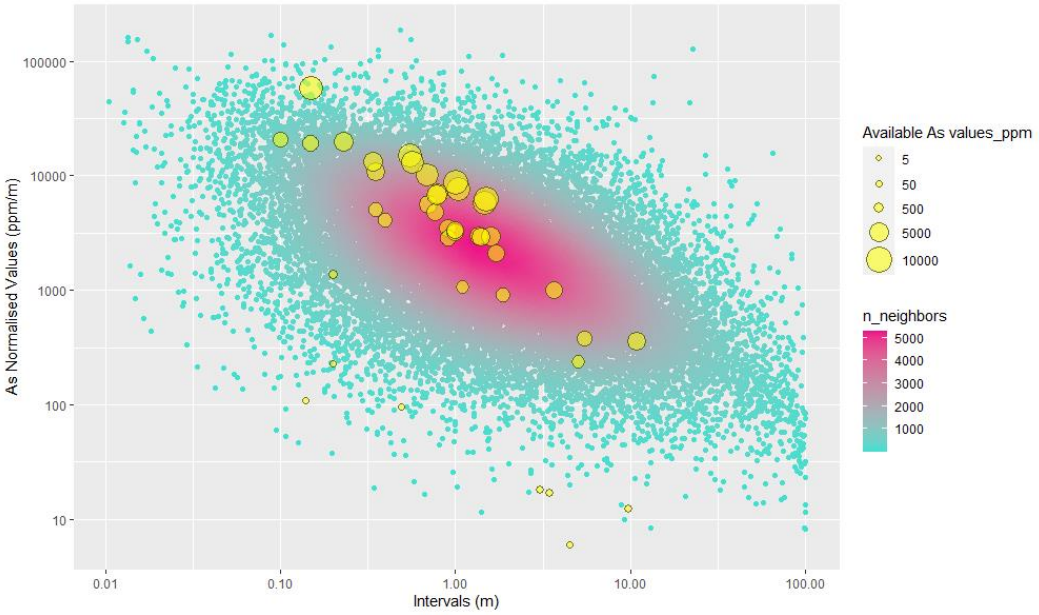


Figure. S27 Realization 4 of the arsenopyrite class 2.

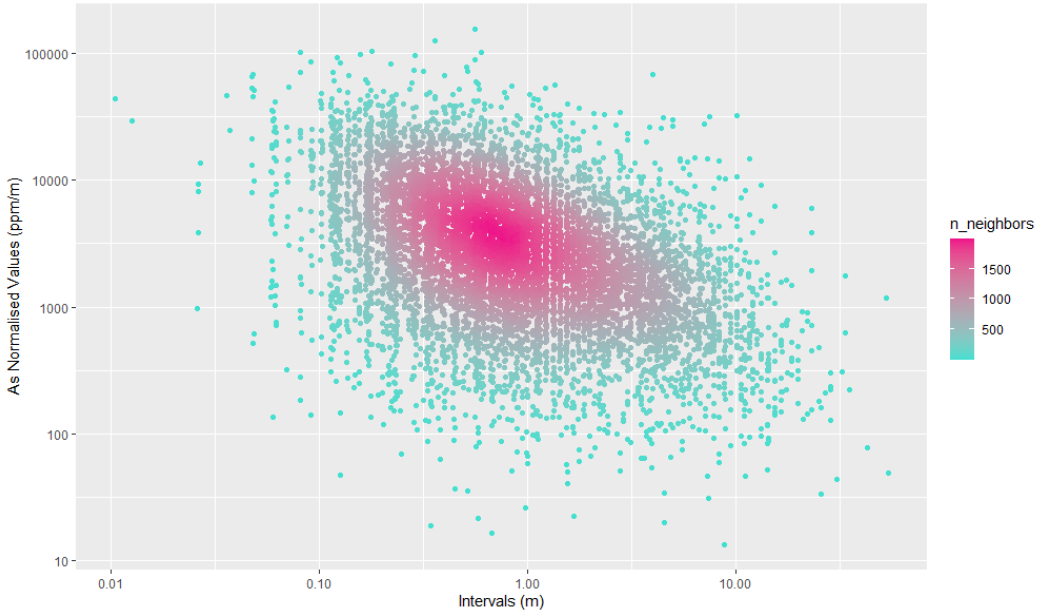


Figure. S28 The selected values of the auxiliary variable based on interval values of the class 2 (realization 4).

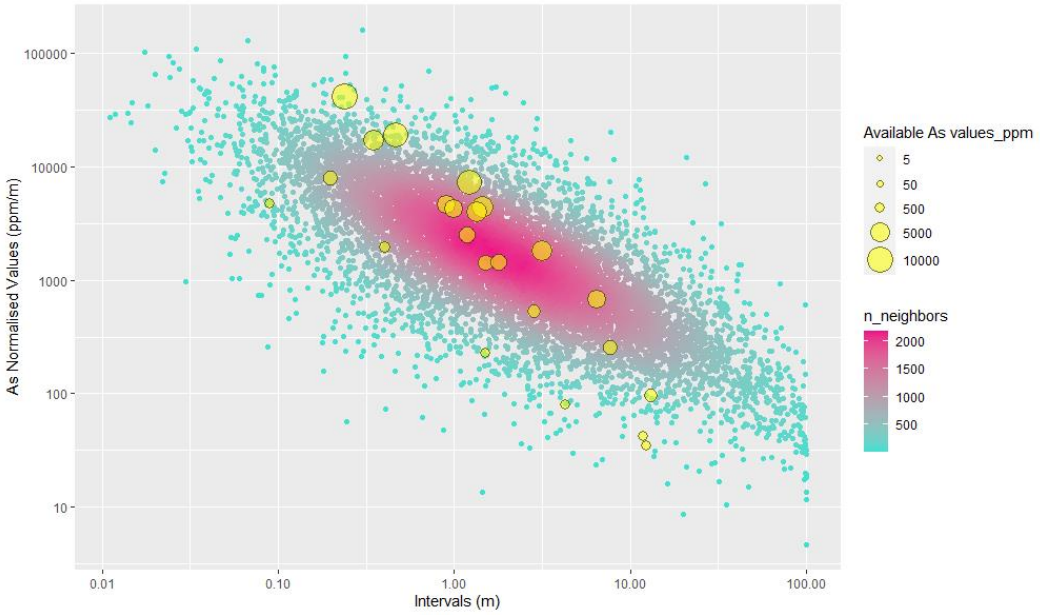


Figure. S29 Realization 4 of the arsenopyrite class 3.



Figure. S30 The selected values of the auxiliary variable based on interval values of the class 3 (realization 4).

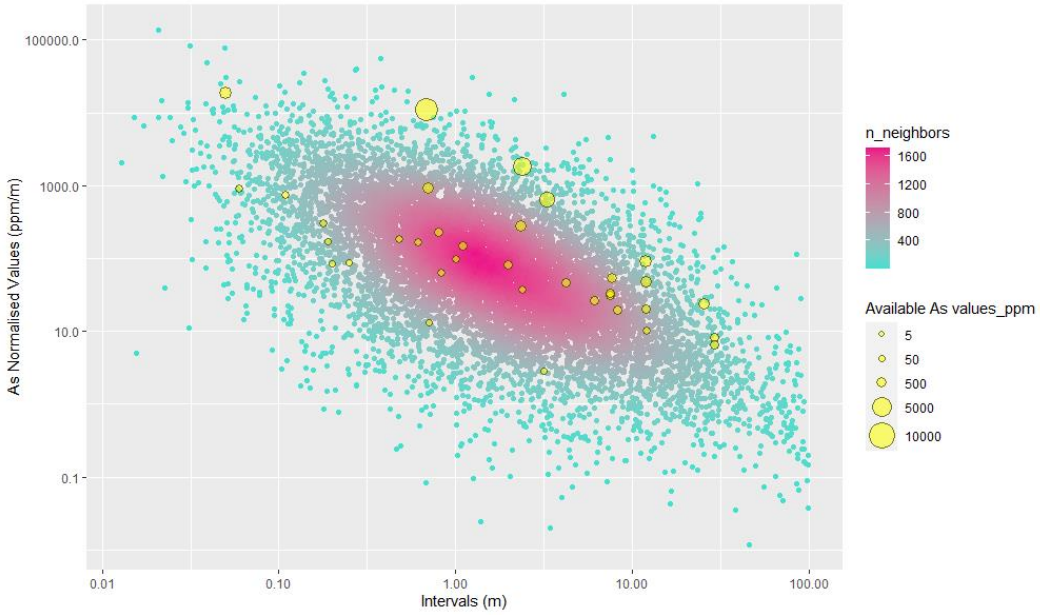


Figure. S31 Realization 5 of the arsenopyrite class 0.1.



Figure. S32 The selected values of the auxiliary variable based on interval values of the class 0.1 (realization 5).

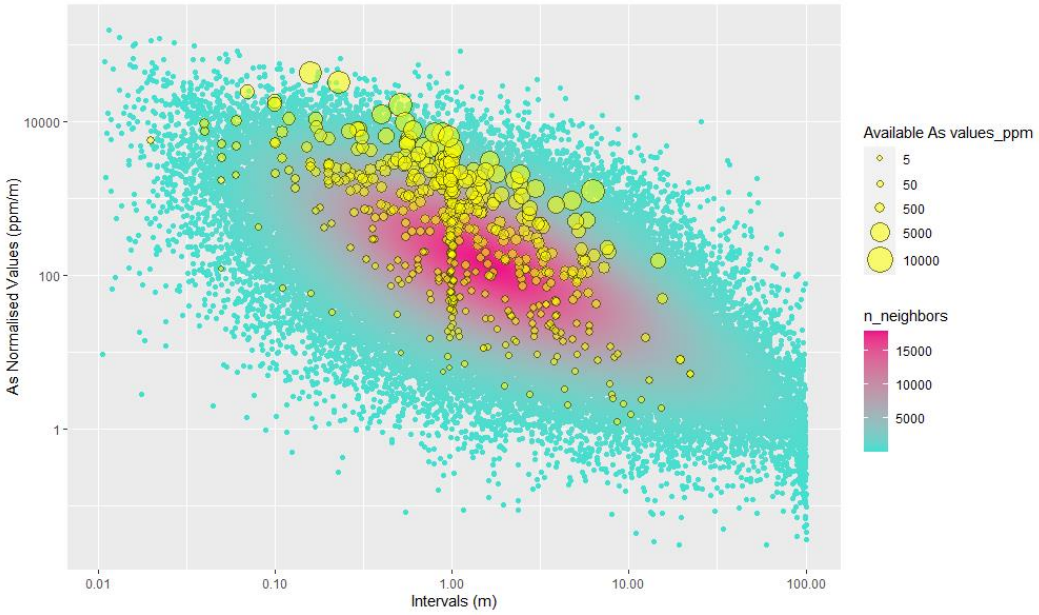


Figure. S33 Realization 5 of the arsenopyrite class 0.5.

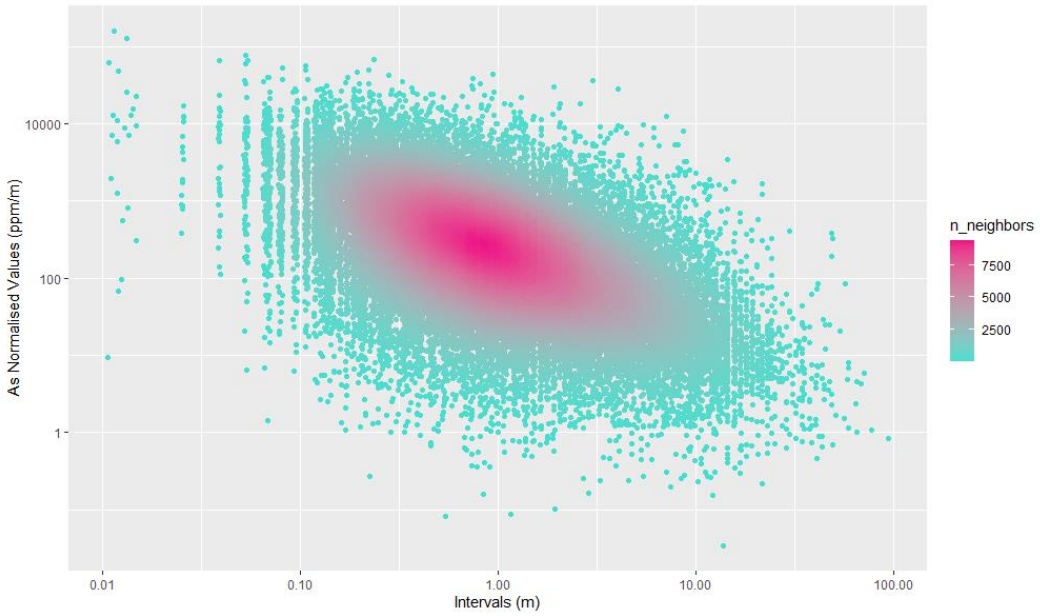


Figure. S34 The selected values of the auxiliary variable based on interval values of the class 0.5 (realization 5).

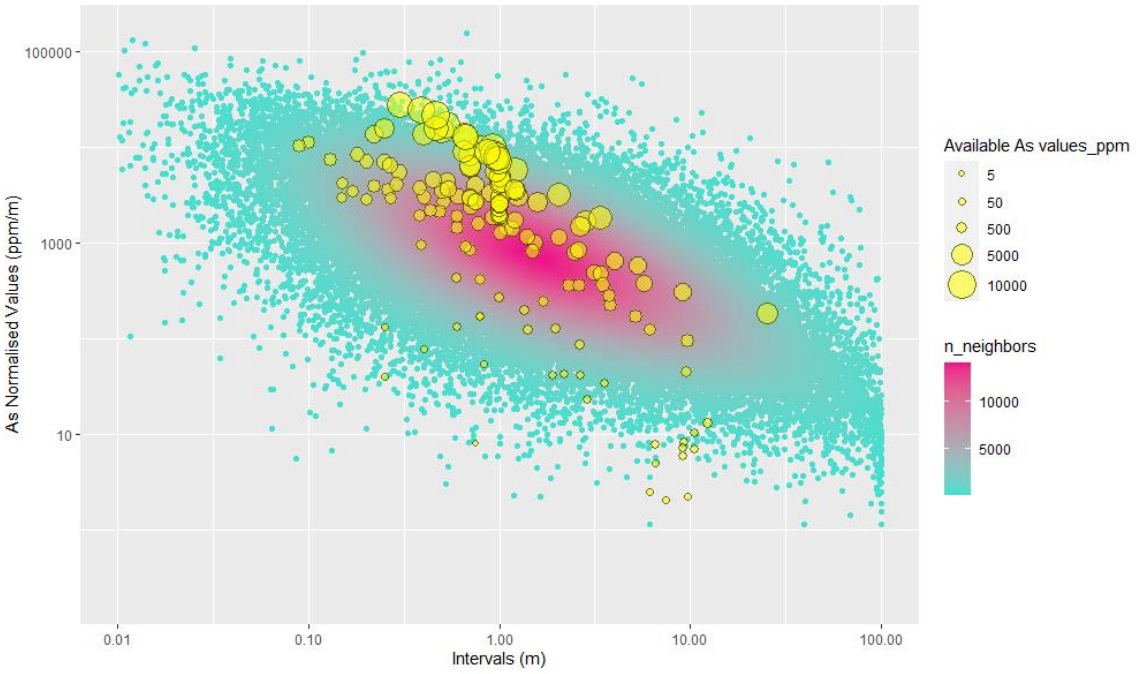


Figure. S35 Realization 5 of the arsenopyrite class 1.

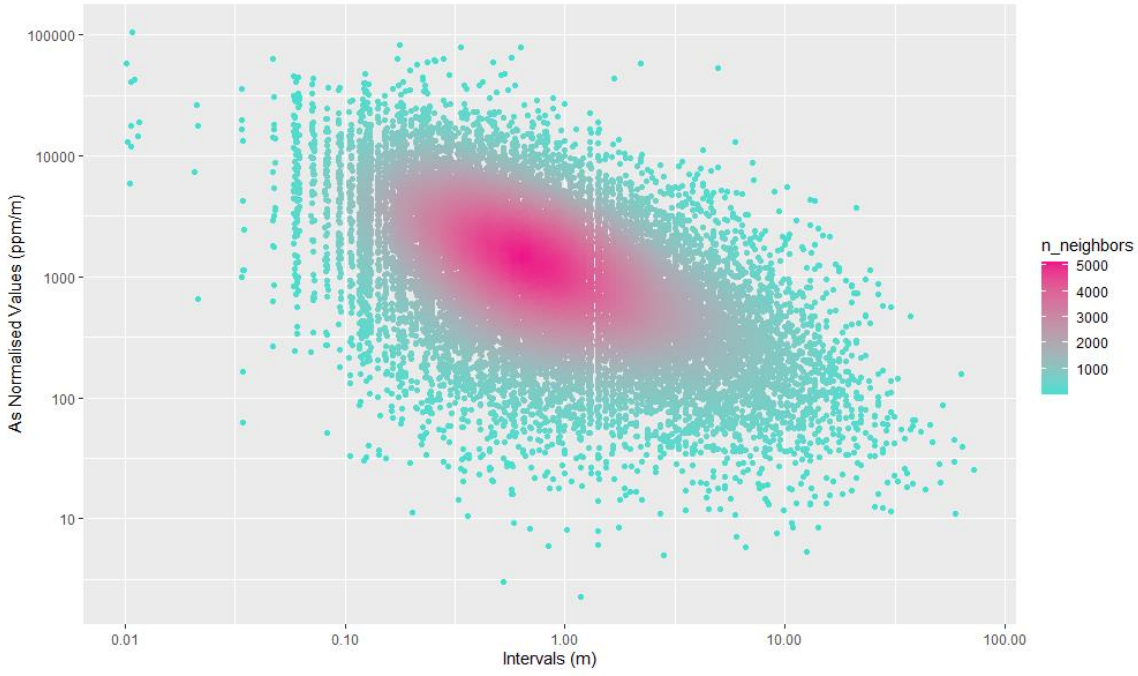


Figure. S36 The selected values of the auxiliary variable based on interval values of the class 1 (realization 5).

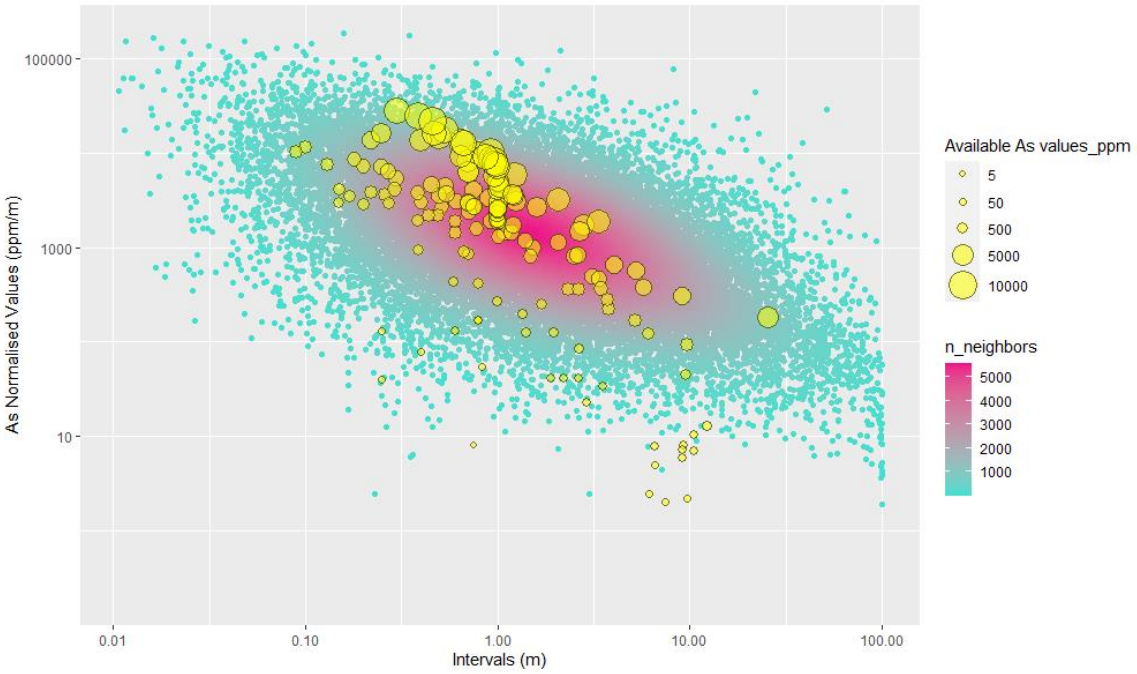


Figure. S37 Realization 5 of the arsenopyrite class 2.

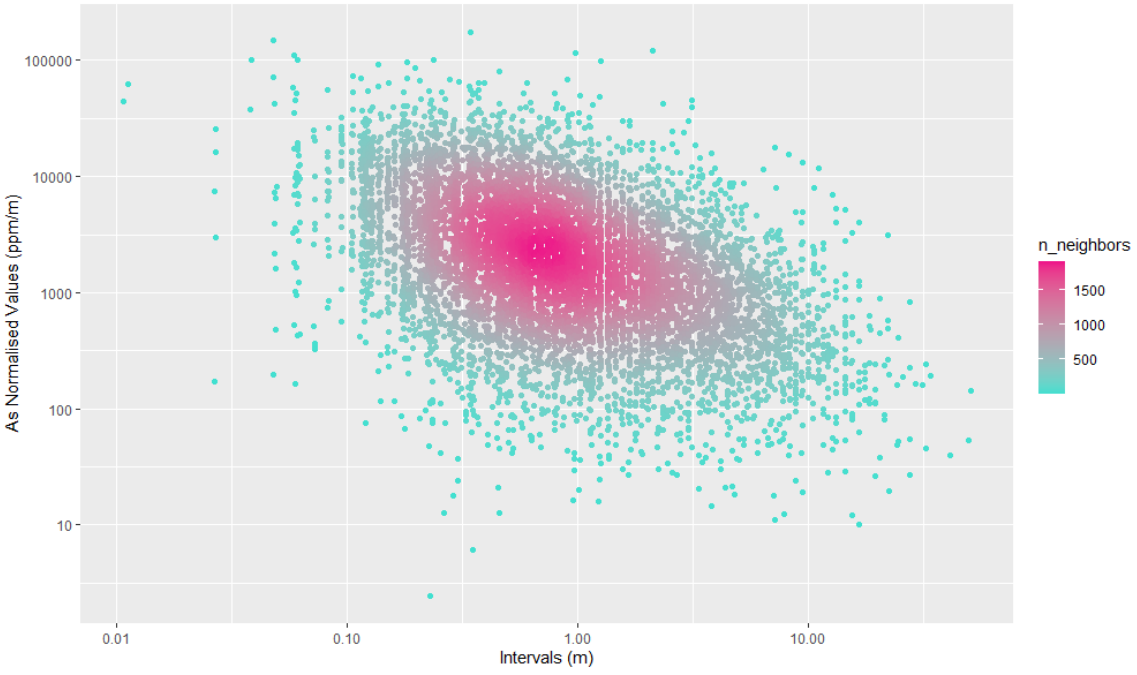


Figure. S38 The selected values of the auxiliary variable based on interval values of the class 2 (realization 5).

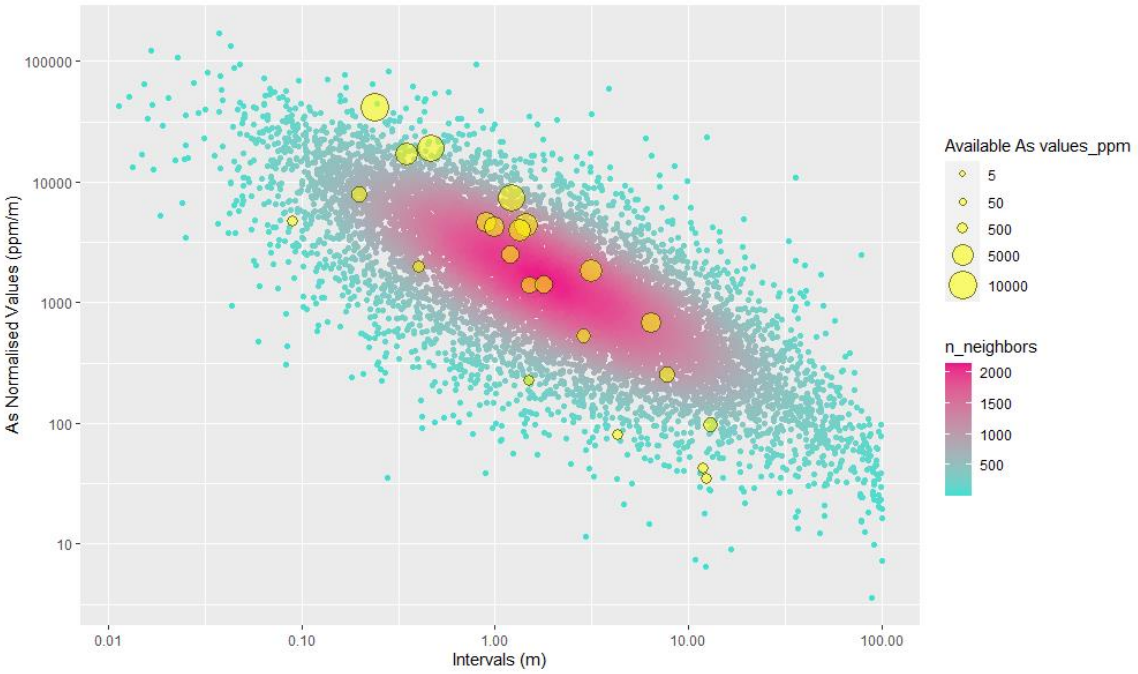


Figure. S39 Realization 5 of the arsenopyrite class 3.



Figure. S40 The selected values of the auxiliary variable based on interval values of the class 3 (realization 5).

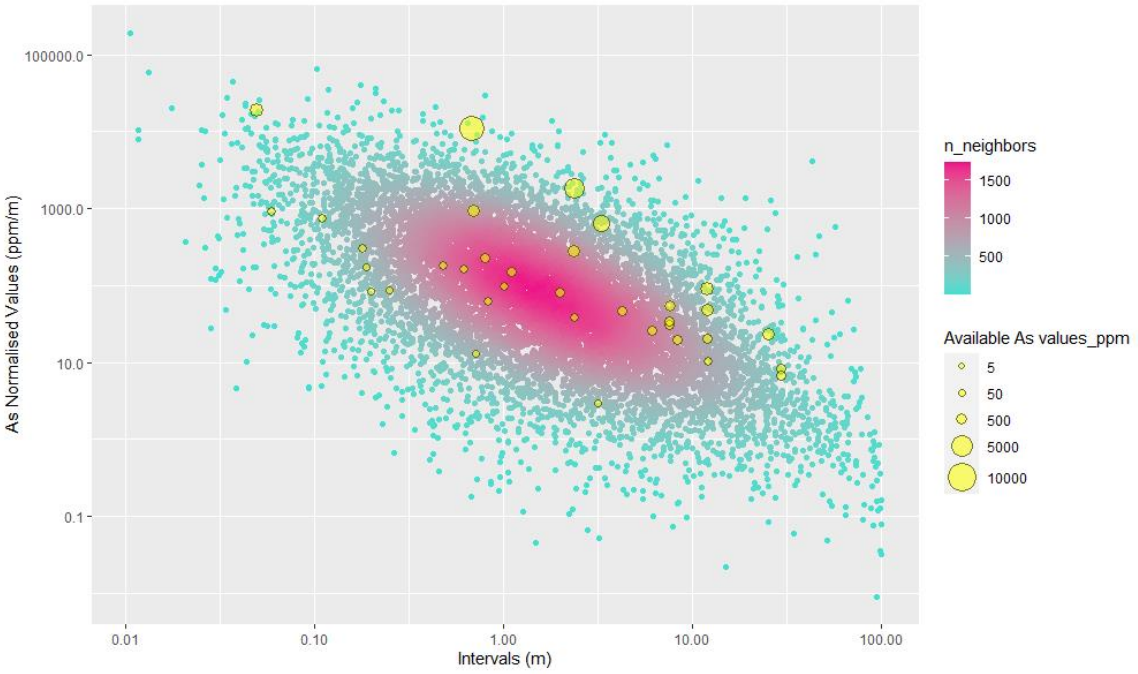


Figure. S41 Realization 6 of the arsenopyrite class 0.1.



Figure. S42 The selected values of the auxiliary variable based on interval values of the class 0.1 (realization 6).

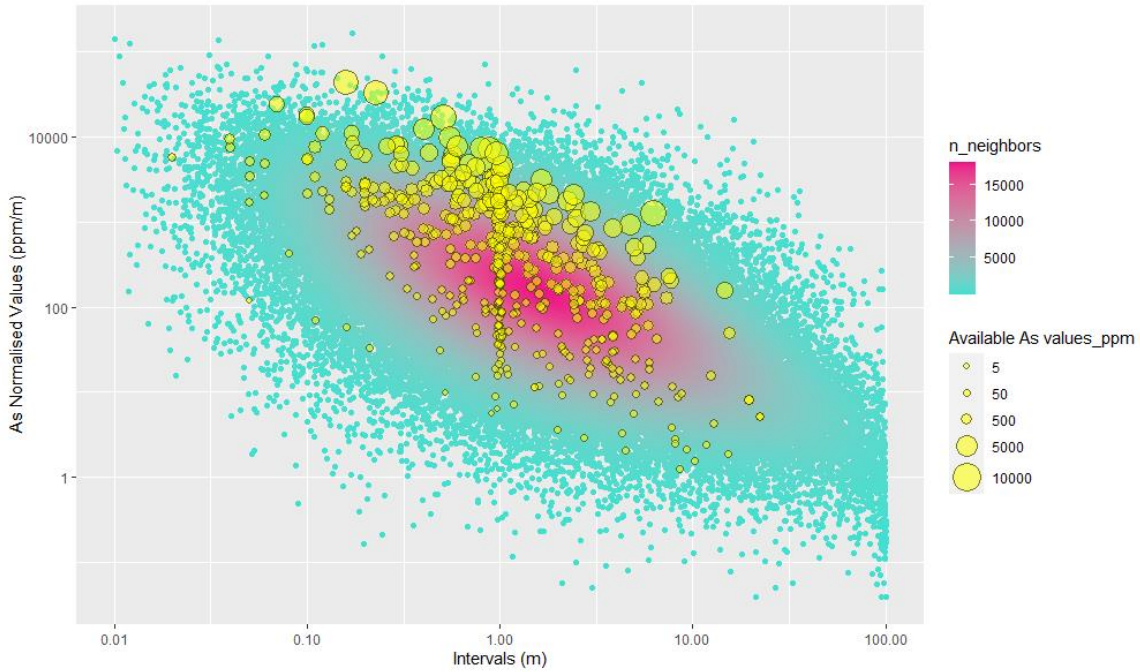


Figure. S43 Realization 6 of the arsenopyrite class 0.5.

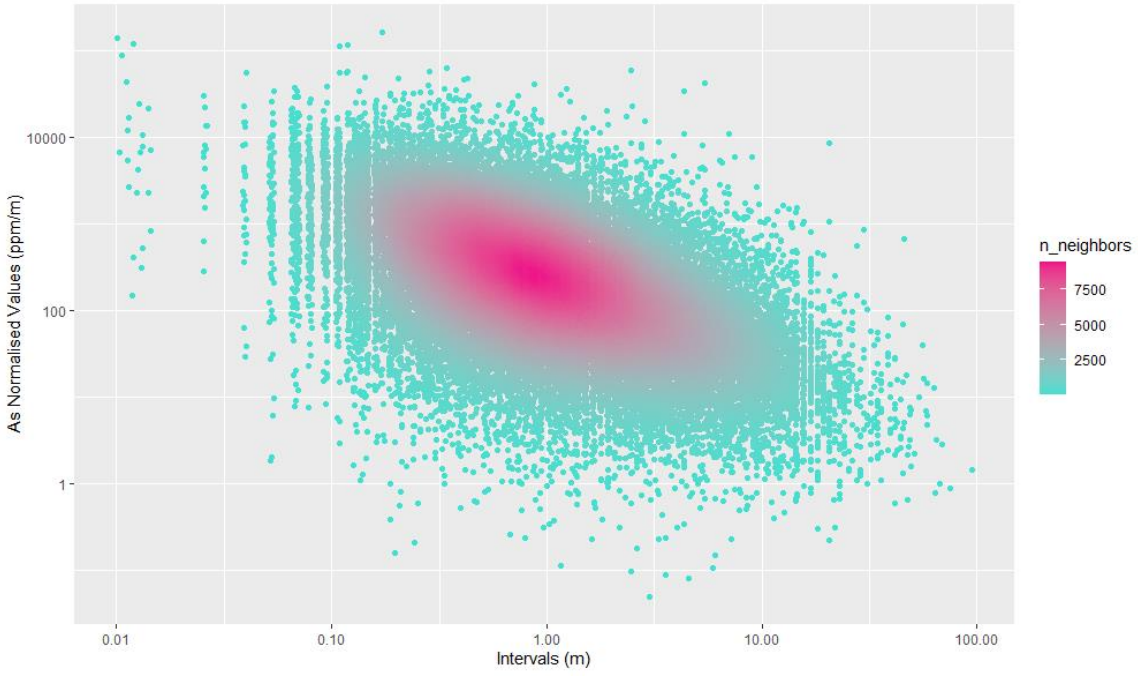


Figure. S44 The selected values of the auxiliary variable based on interval values of the class 0.5 (realization 6).

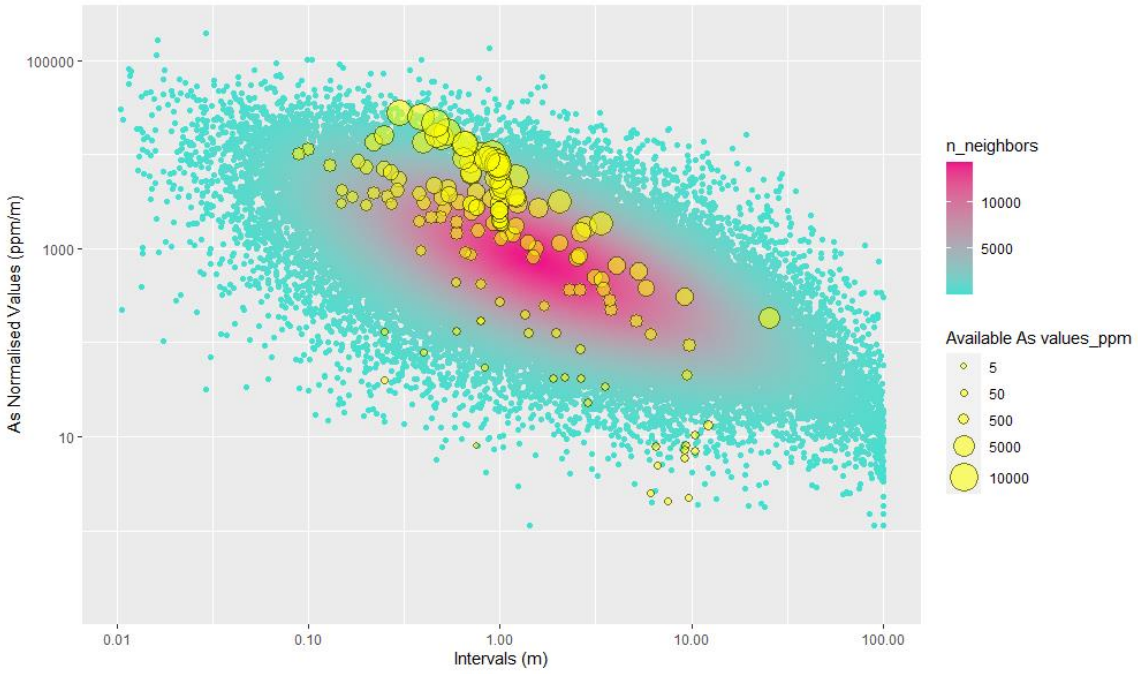


Figure. S45 Realization 6 of the arsenopyrite class 1.

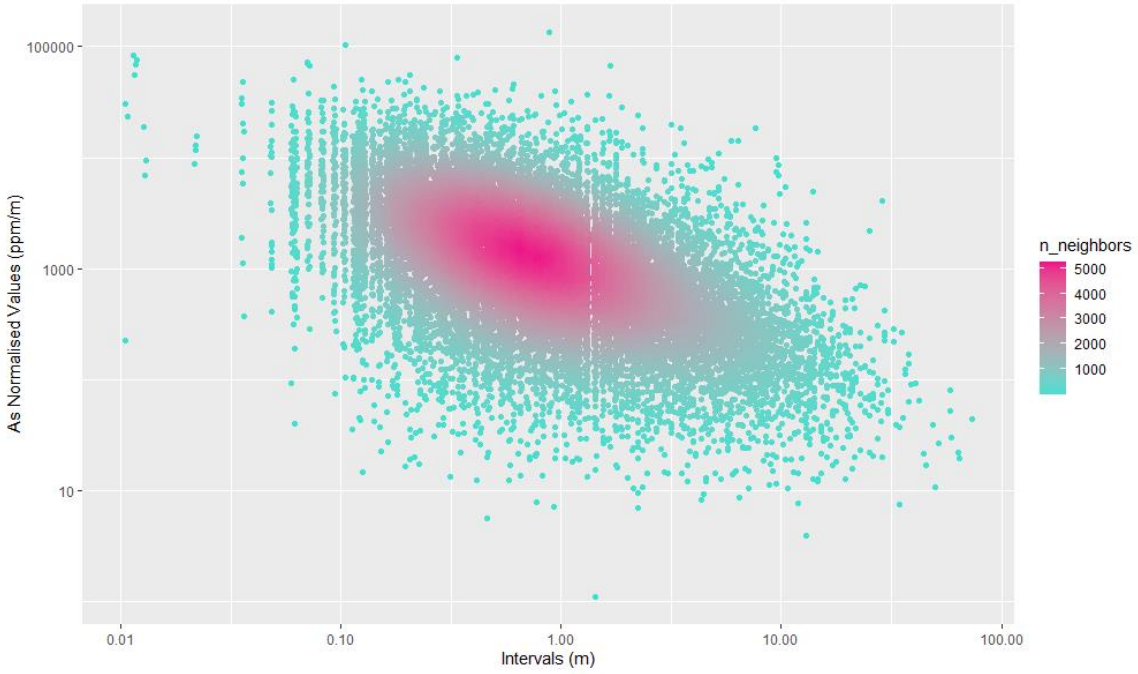


Figure. S46 The selected values of the auxiliary variable based on interval values of the class 1 (realization 6).

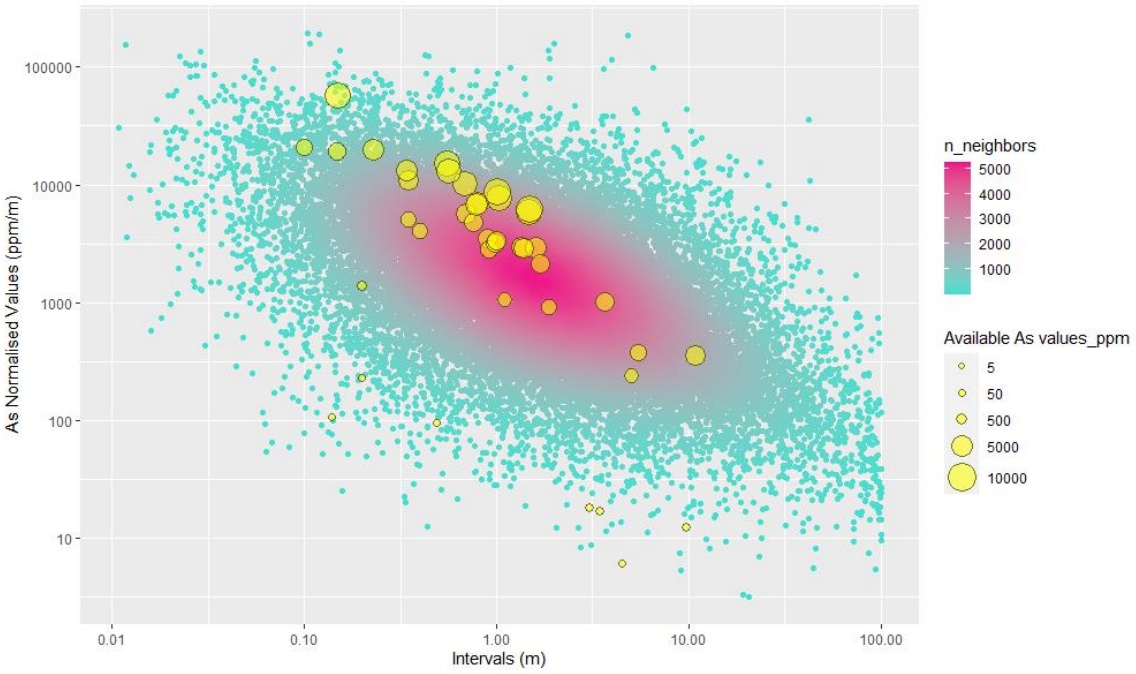


Figure. S47 Realization 6 of the arsenopyrite class 2.



Figure. S48 The selected values of the auxiliary variable based on interval values of the class 2 (realization 6).

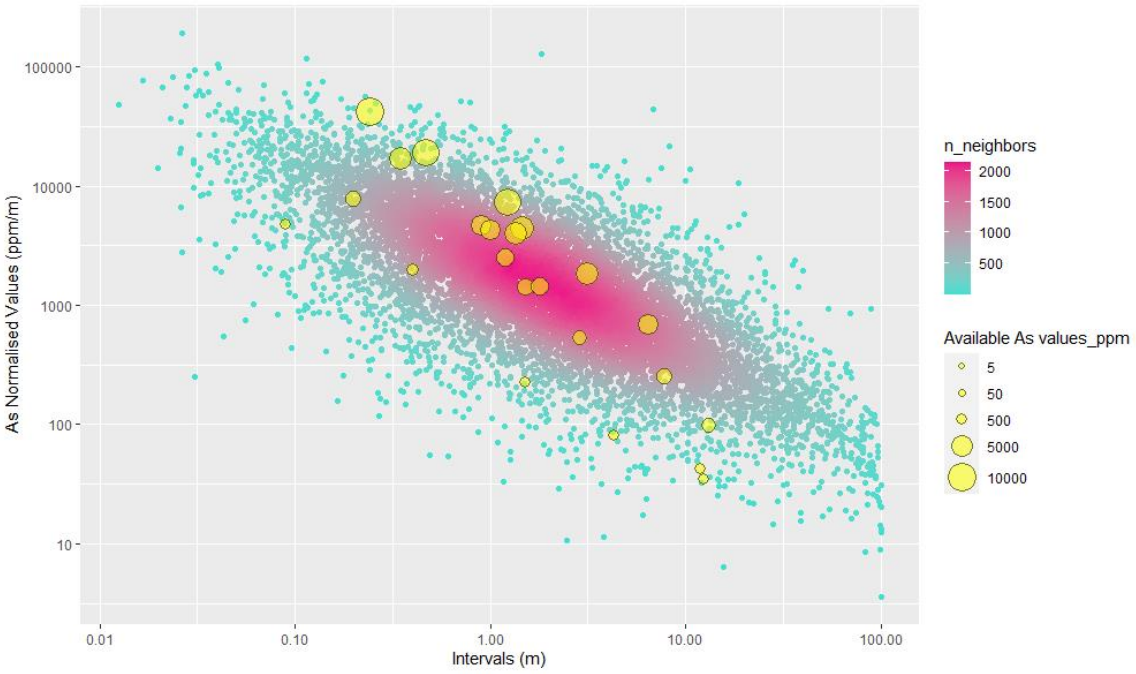


Figure. S49 Realization 6 of the arsenopyrite class 3.

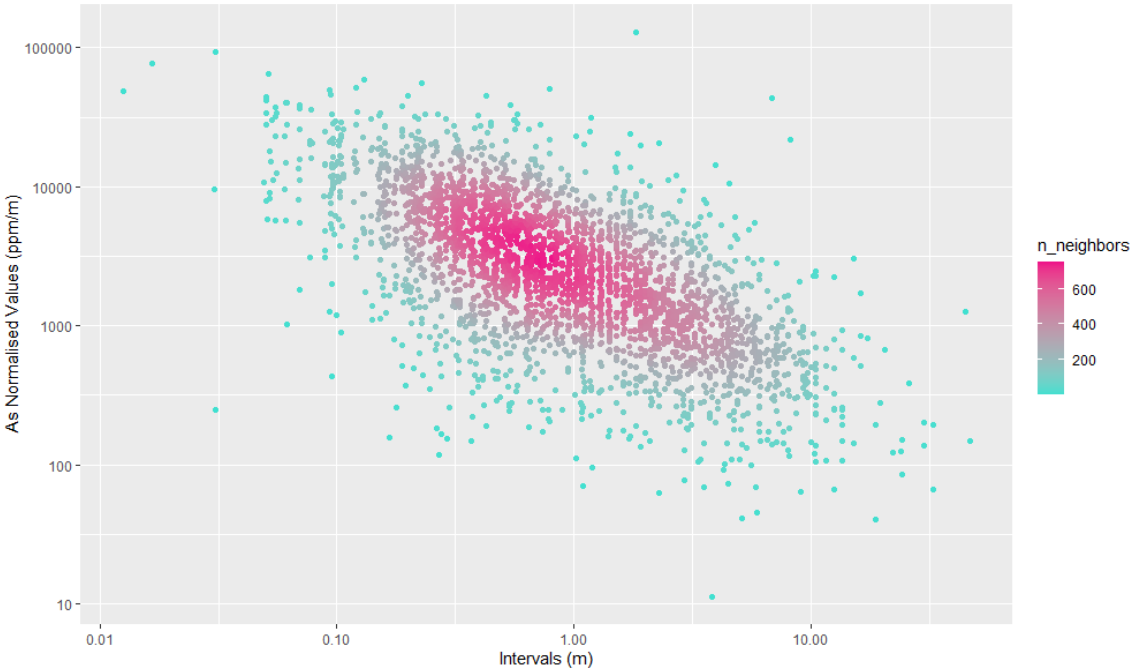


Figure. S50 The selected values of the auxiliary variable based on interval values of the class 3 (realization 6).

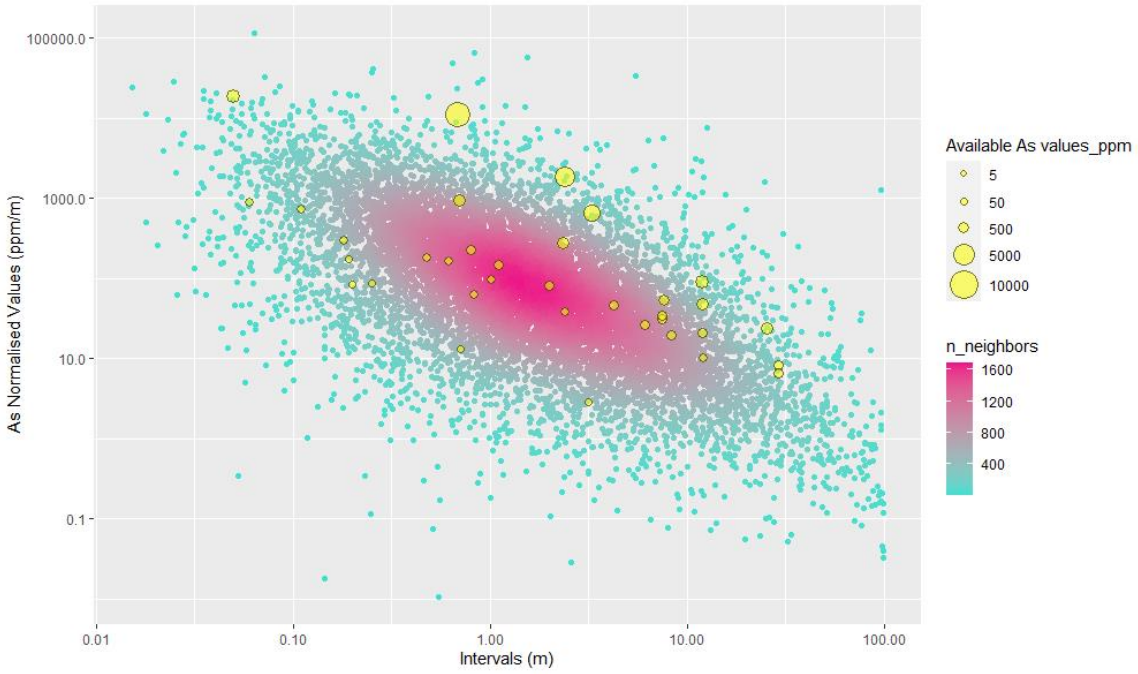


Figure. S51 Realization 7 of the arsenopyrite class 0.1.

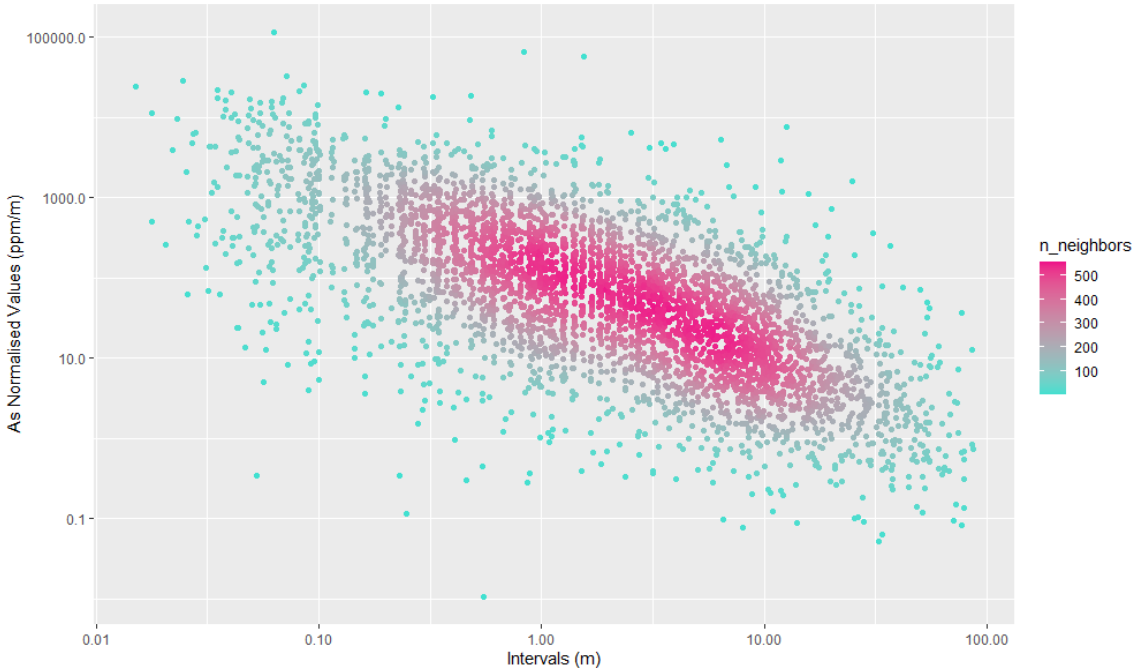


Figure. S52 The selected values of the auxiliary variable based on interval values of the class 0.1 (realization 7).

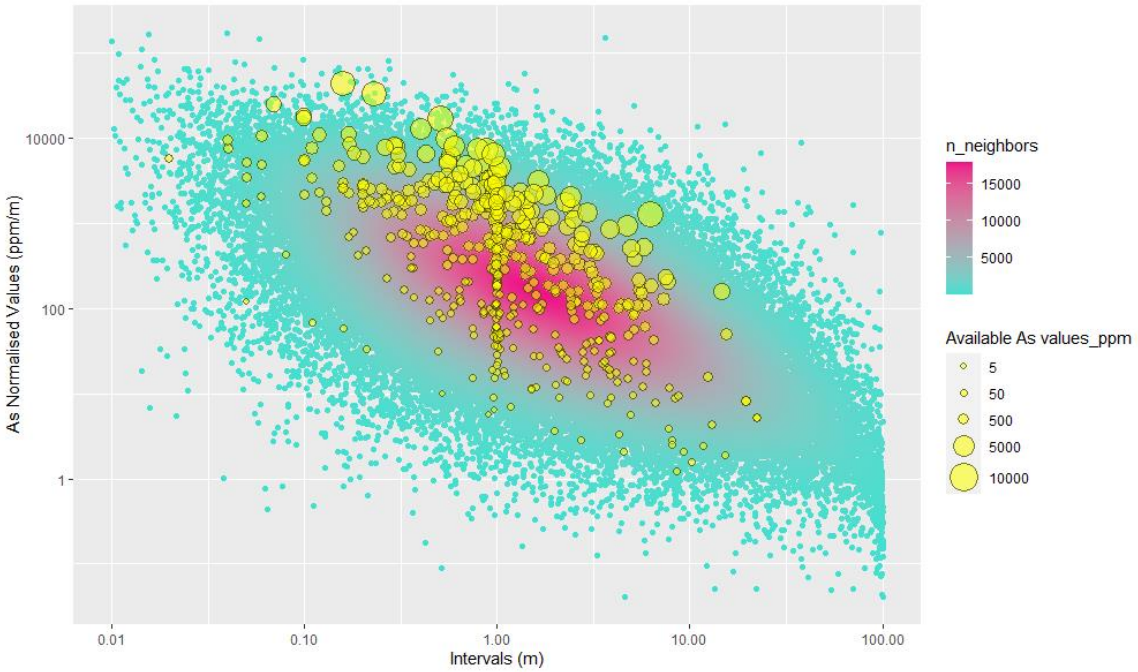


Figure. S53 Realization 7 of the arsenopyrite class 0.5.

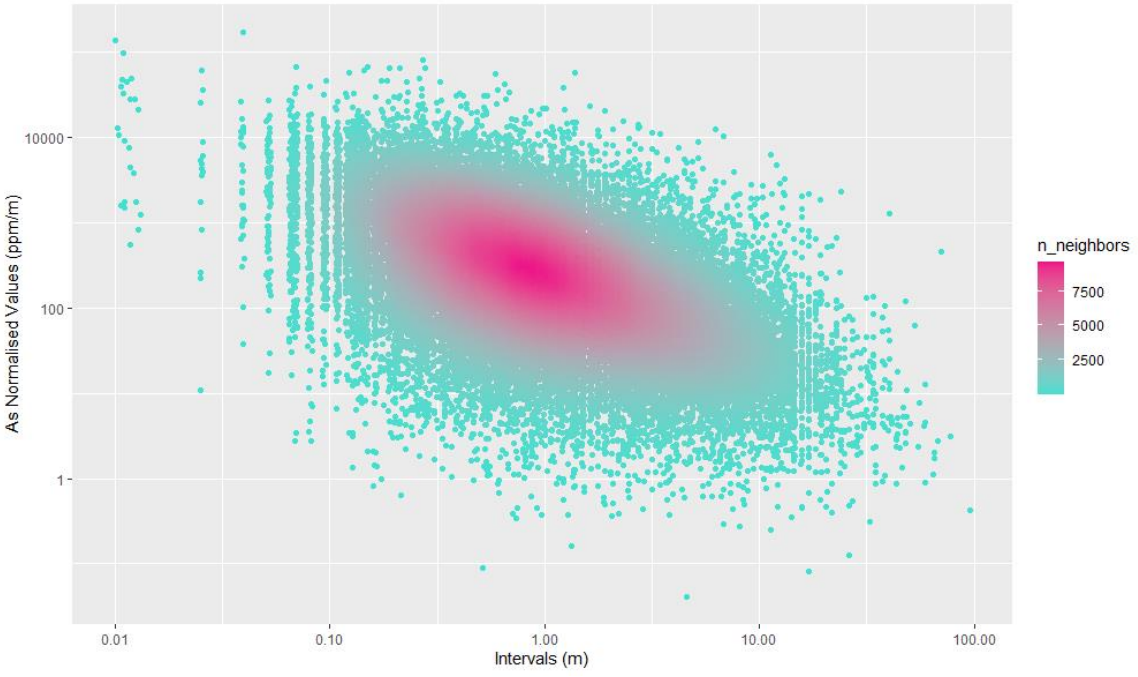


Figure. S54 The selected values of the auxiliary variable based on interval values of the class 0.5 (realization 7).

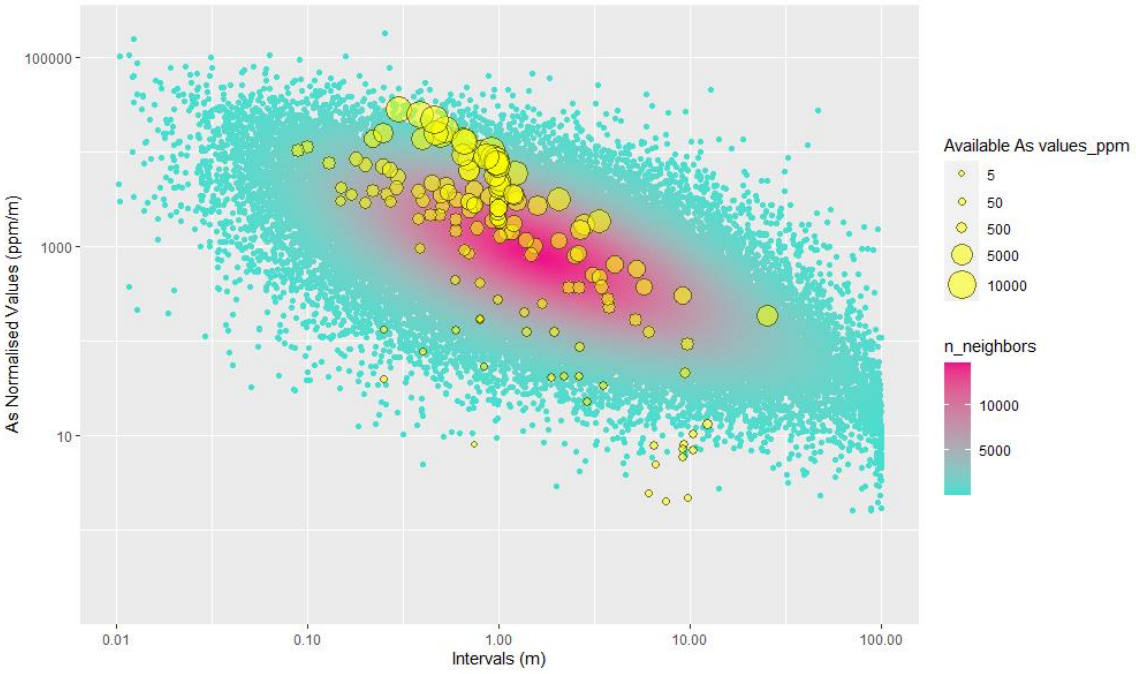


Figure. S55 Realization 7 of the arsenopyrite class 1.

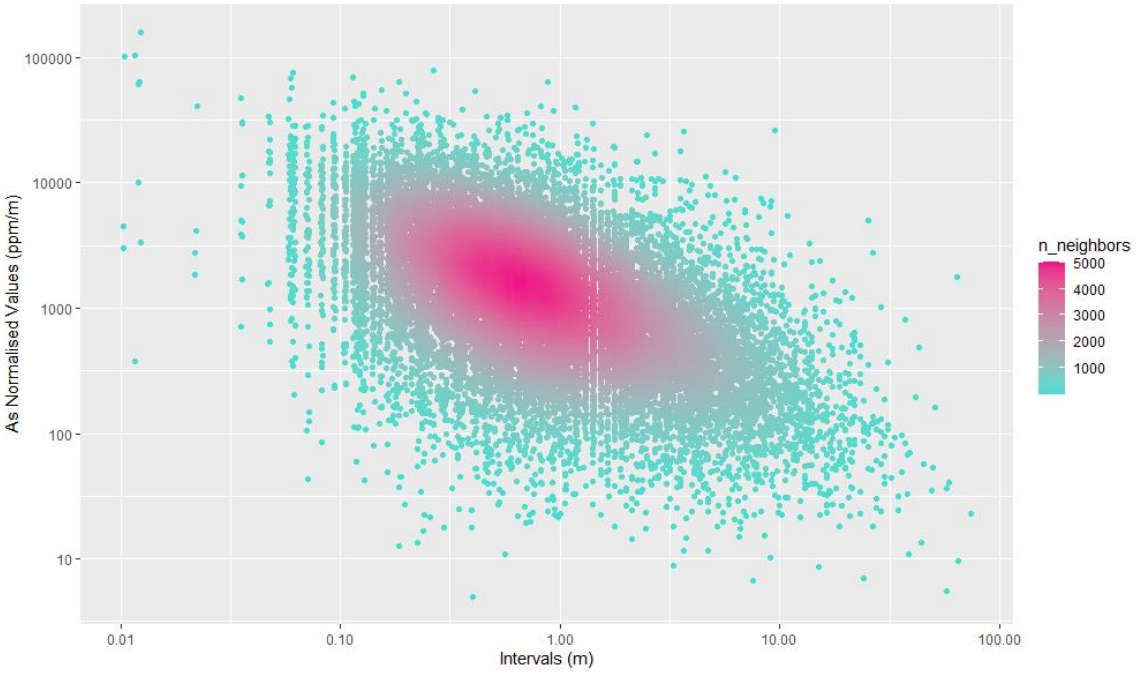


Figure. S56 The selected values of the auxiliary variable based on interval values of the class 1 (realization 7).

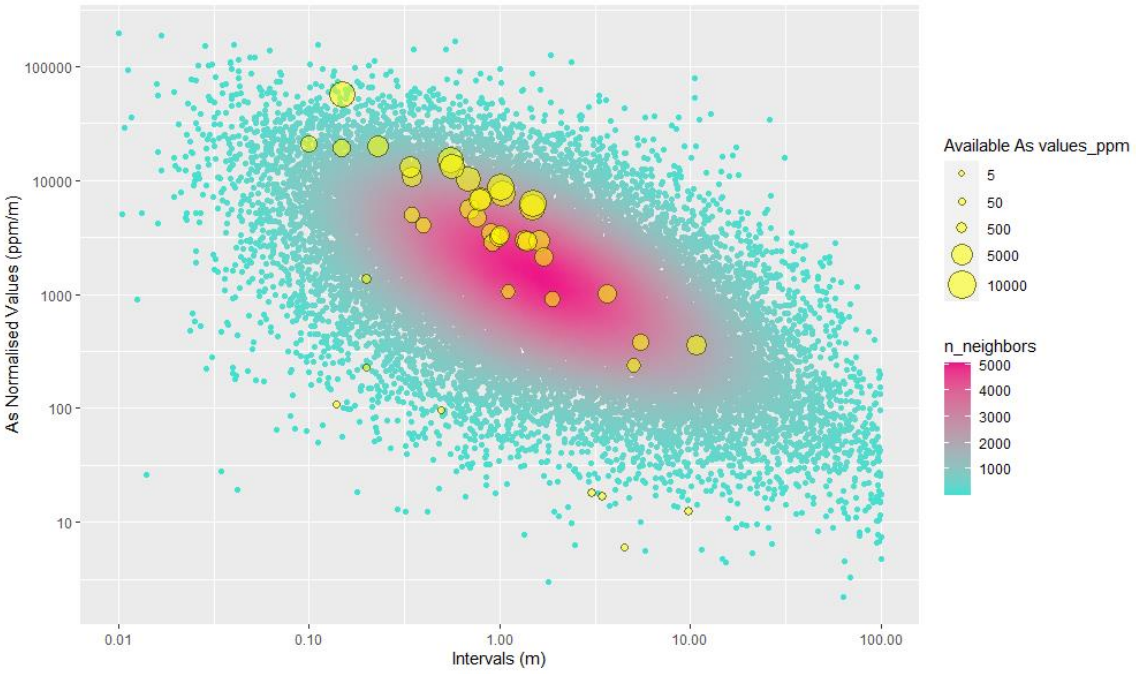


Figure. S57 Realization 7 of the arsenopyrite class 2.



Figure. S58 The selected values of the auxiliary variable based on interval values of the class 2 (realization 7).

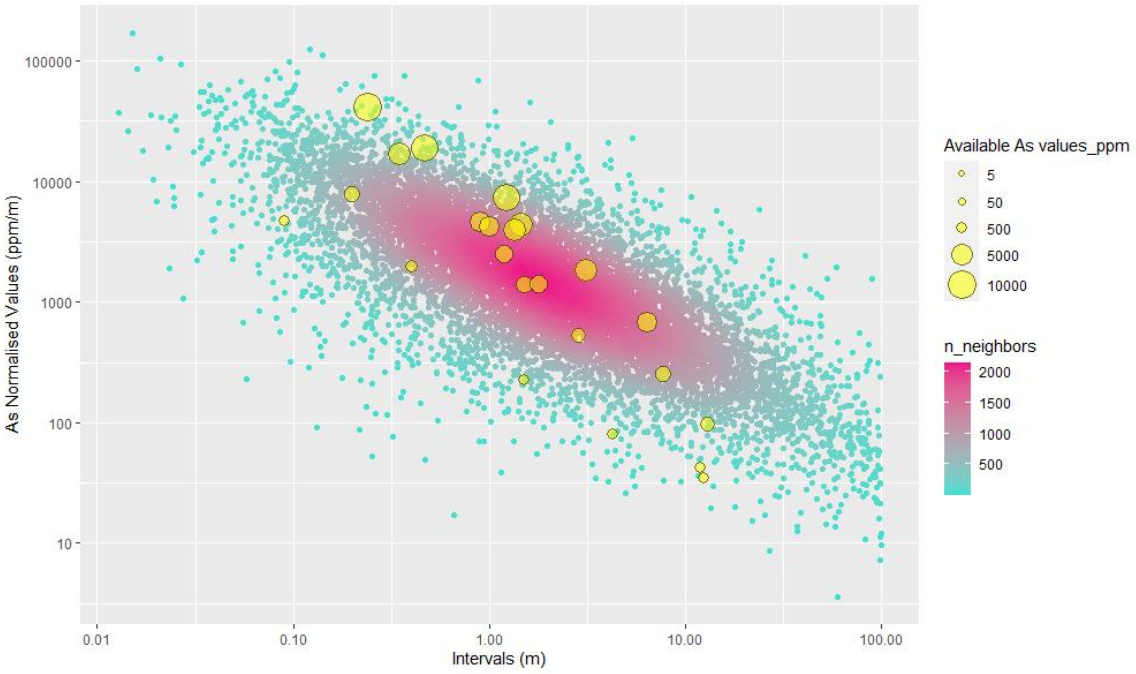


Figure. S59 Realization 7 of the arsenopyrite class 3.

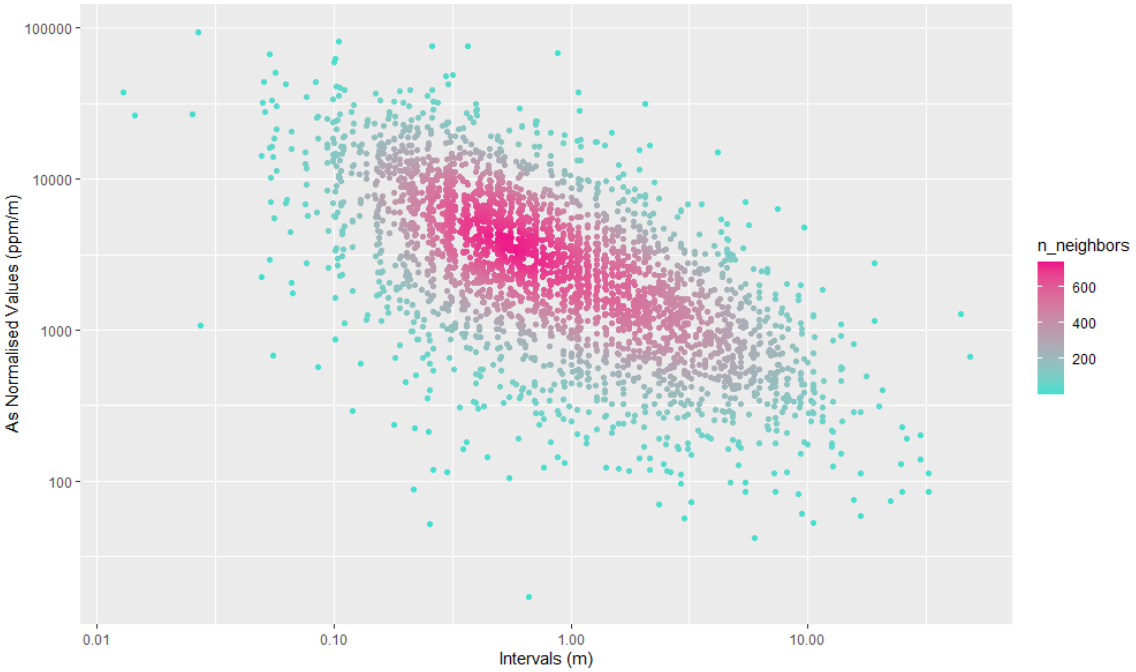


Figure. S60 The selected values of the auxiliary variable based on interval values of the class 3 (realization 7).

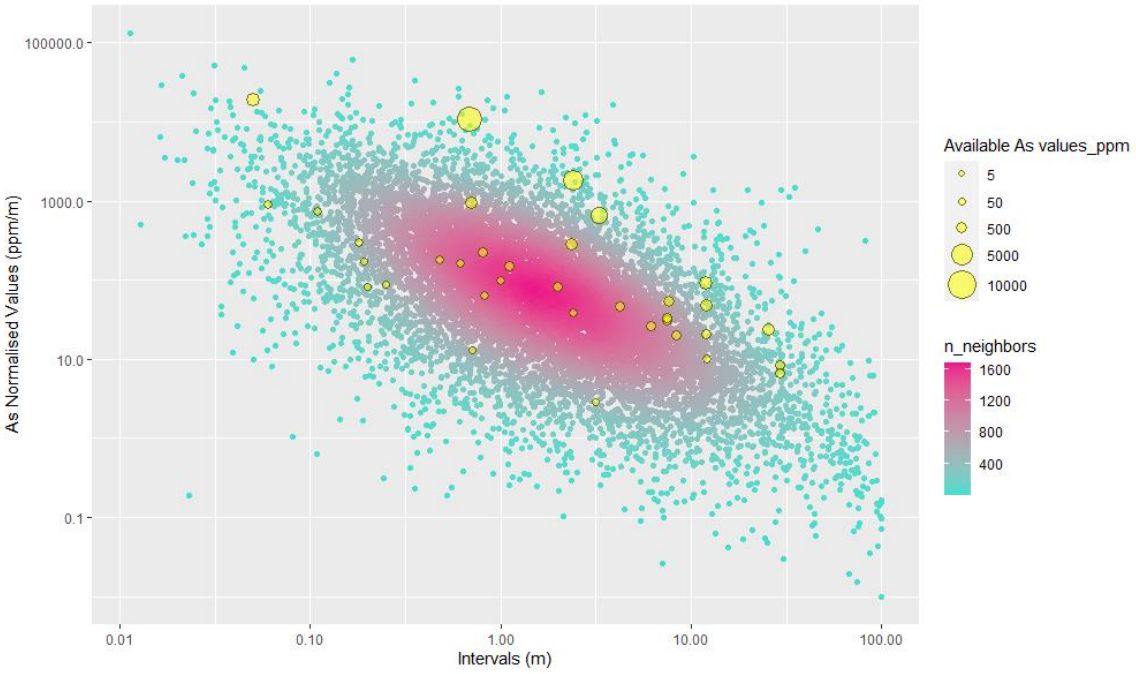


Figure. S61 Realization 8 of the arsenopyrite class 0.1.



Figure. S62 The selected values of the auxiliary variable based on interval values of the class 0.1 (realization 8).

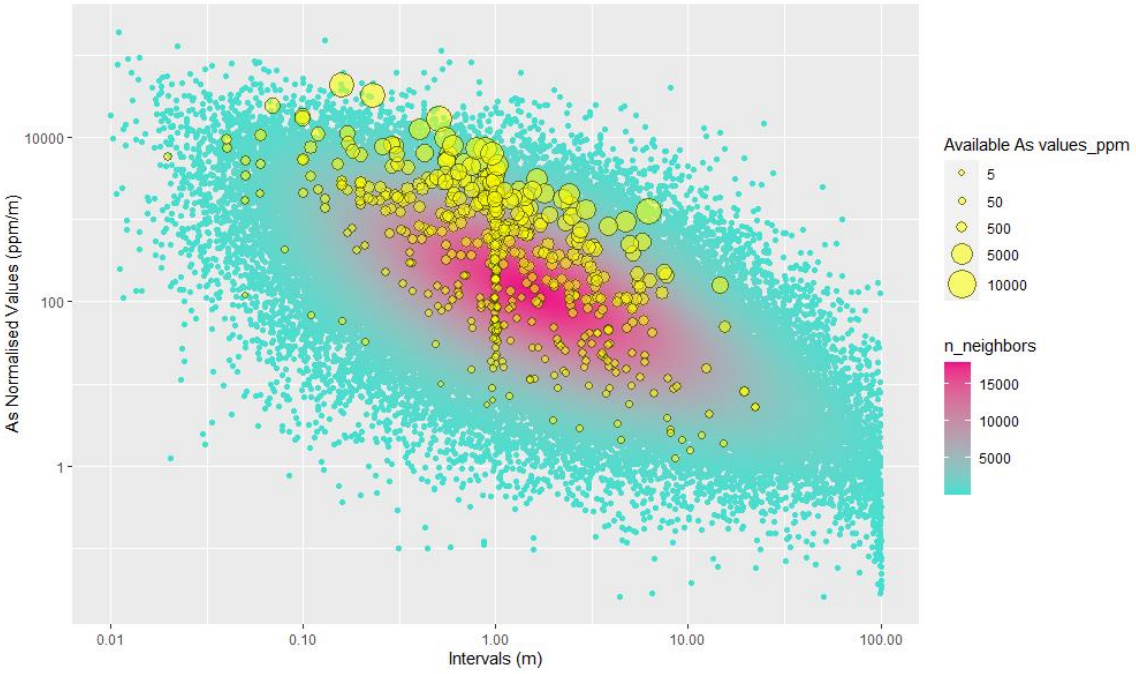


Figure. S63 Realization 8 of the arsenopyrite class 0.5.

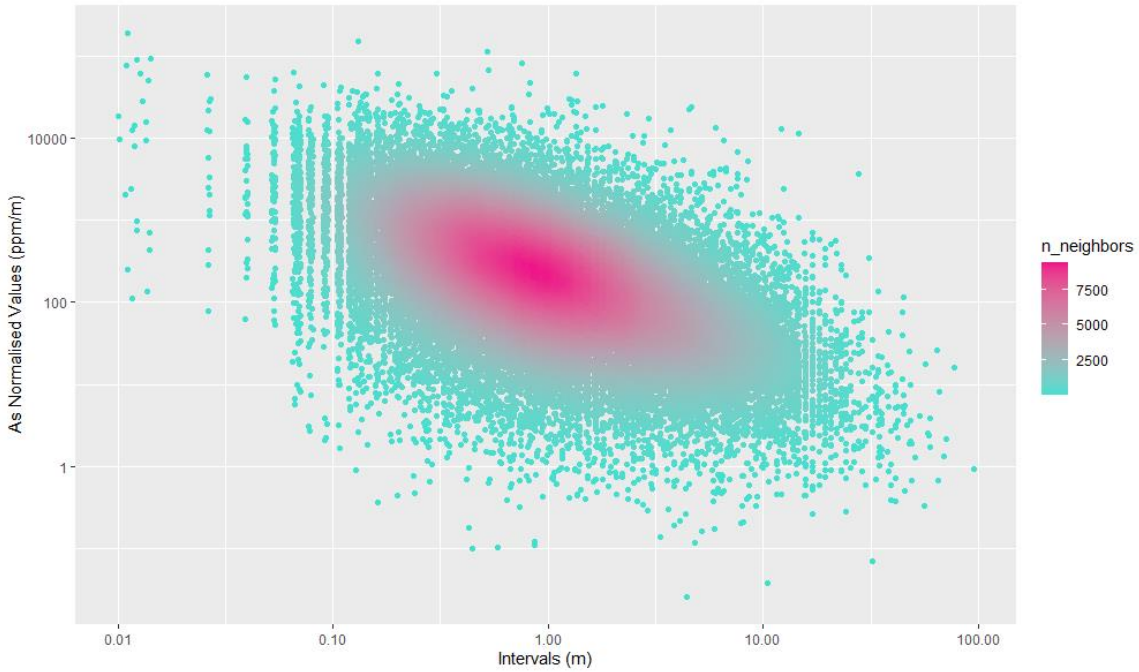


Figure. S64 The selected values of the auxiliary variable based on interval values of the class 0.5 (realization 8).

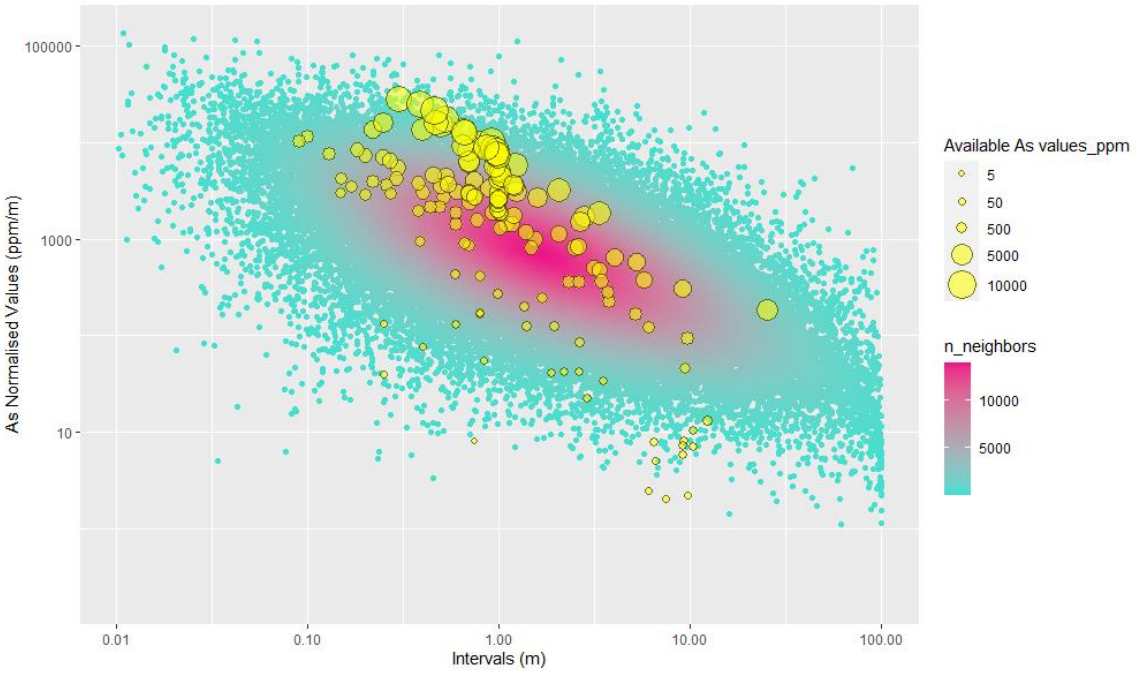


Figure. S65 Realization 8 of the arsenopyrite class 1.

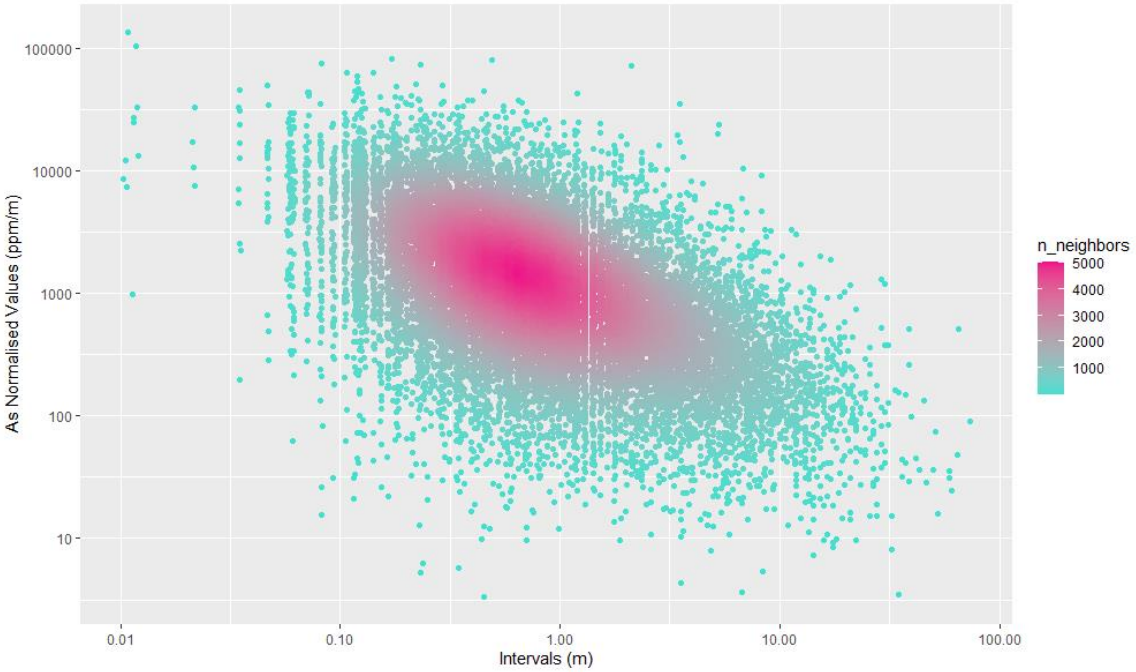


Figure. S66 The selected values of the auxiliary variable based on interval values of the class 1 (realization 8).

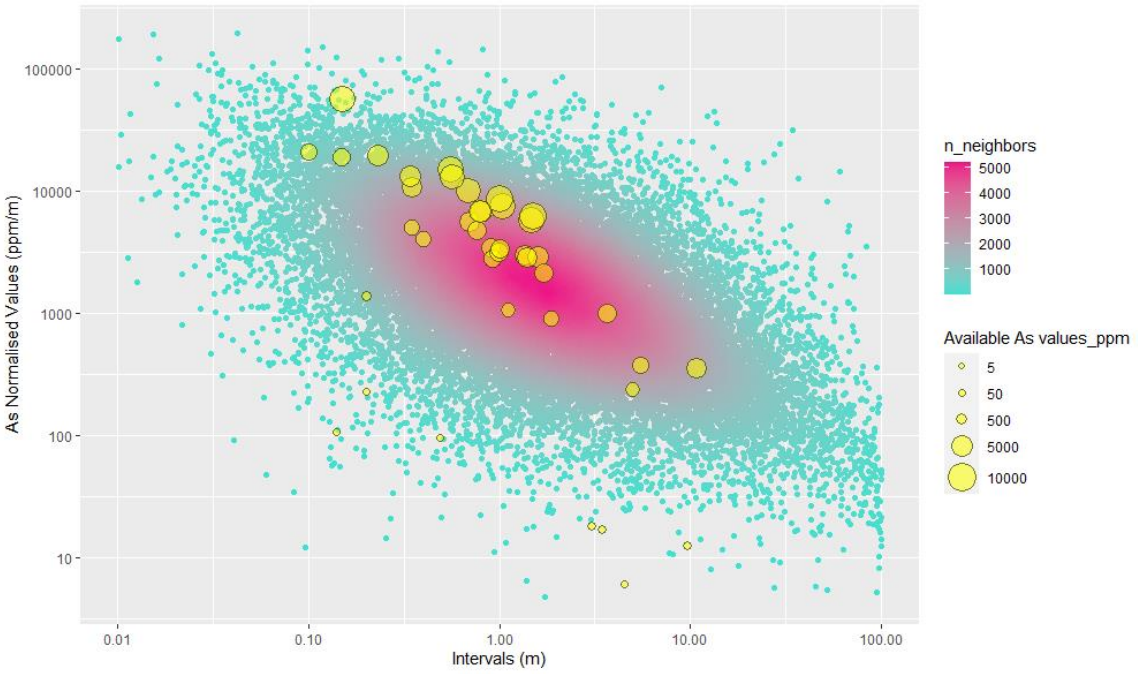


Figure. S67 Realization 8 of the arsenopyrite class 2.

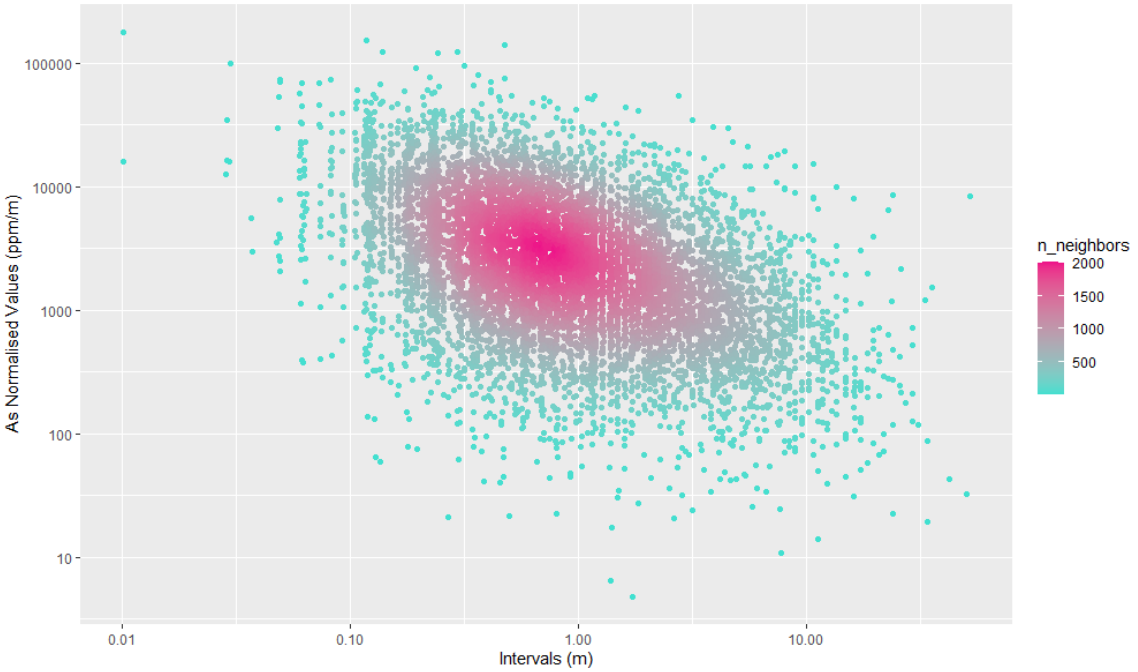


Figure. S68 The selected values of the auxiliary variable based on interval values of the class 2 (realization 8).

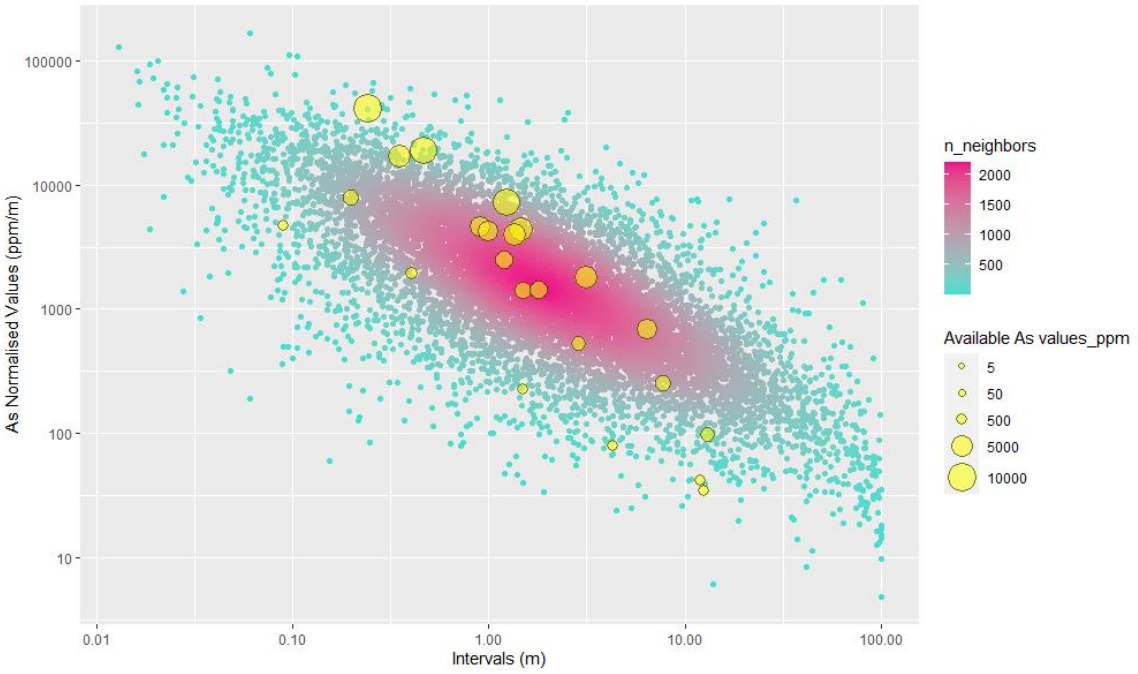


Figure. S69 Realization 8 of the arsenopyrite class 3.



Figure. S70 The selected values of the auxiliary variable based on interval values of the class 3 (realization 8).

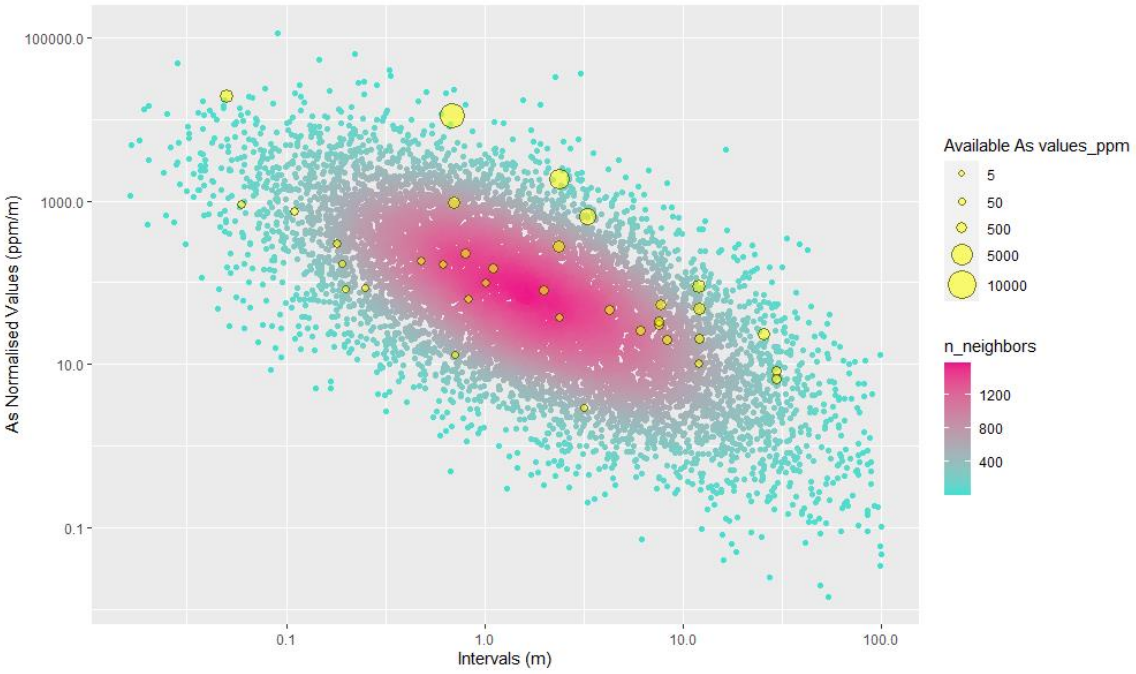


Figure. S71 Realization 9 of the arsenopyrite class 0.1.

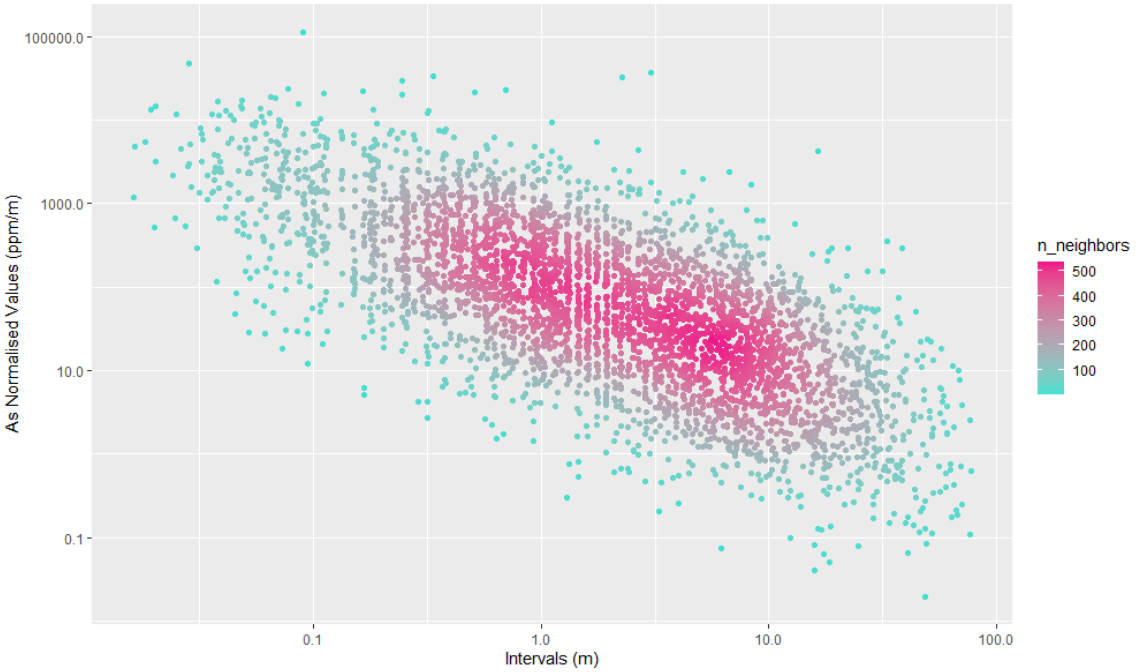


Figure. S72 The selected values of the auxiliary variable based on interval values of the class 0.1 (realization 9).

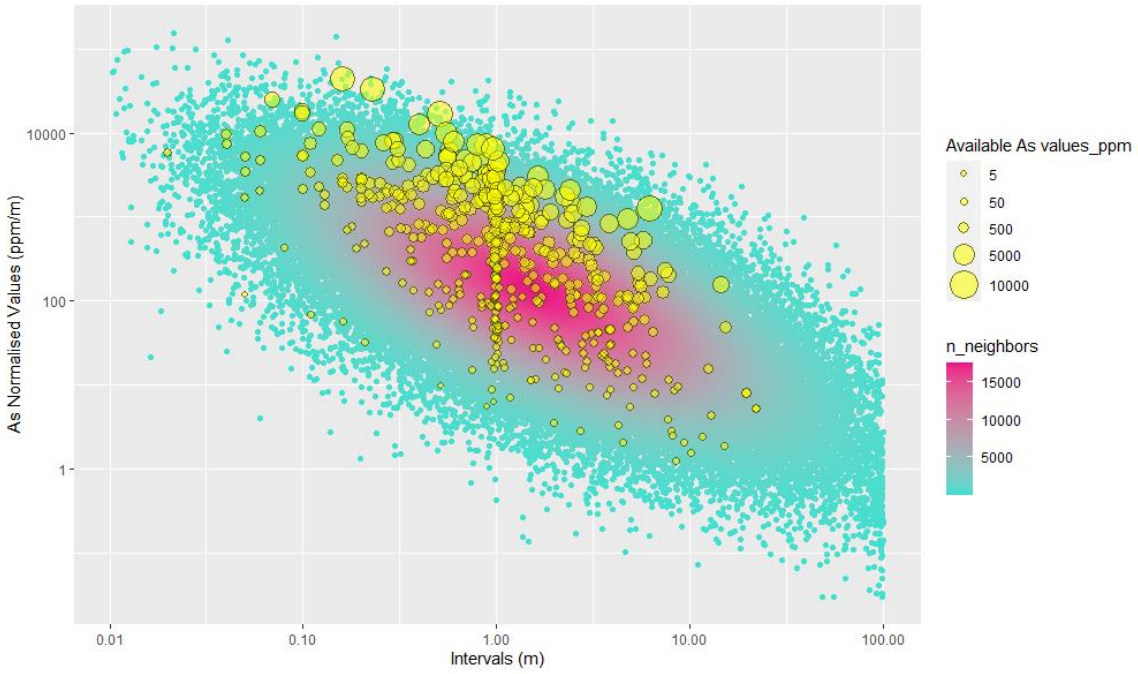


Figure. S73 Realization 9 of the arsenopyrite class 0.5.

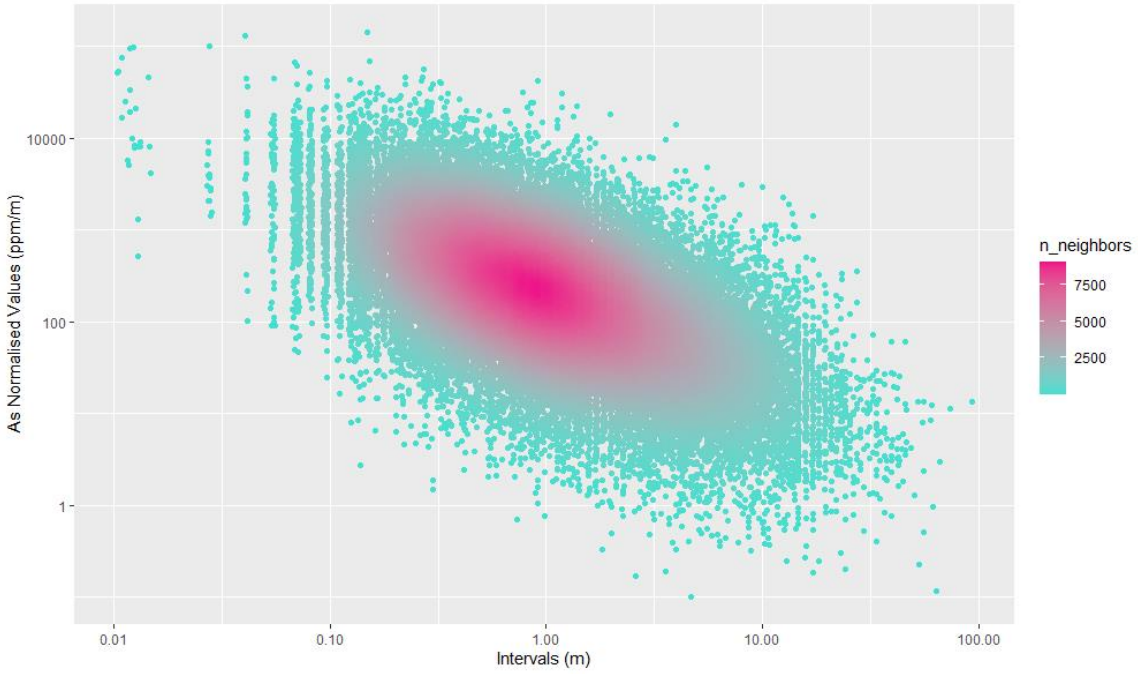


Figure. S74 The selected values of the auxiliary variable based on interval values of the class 0.5 (realization 9).

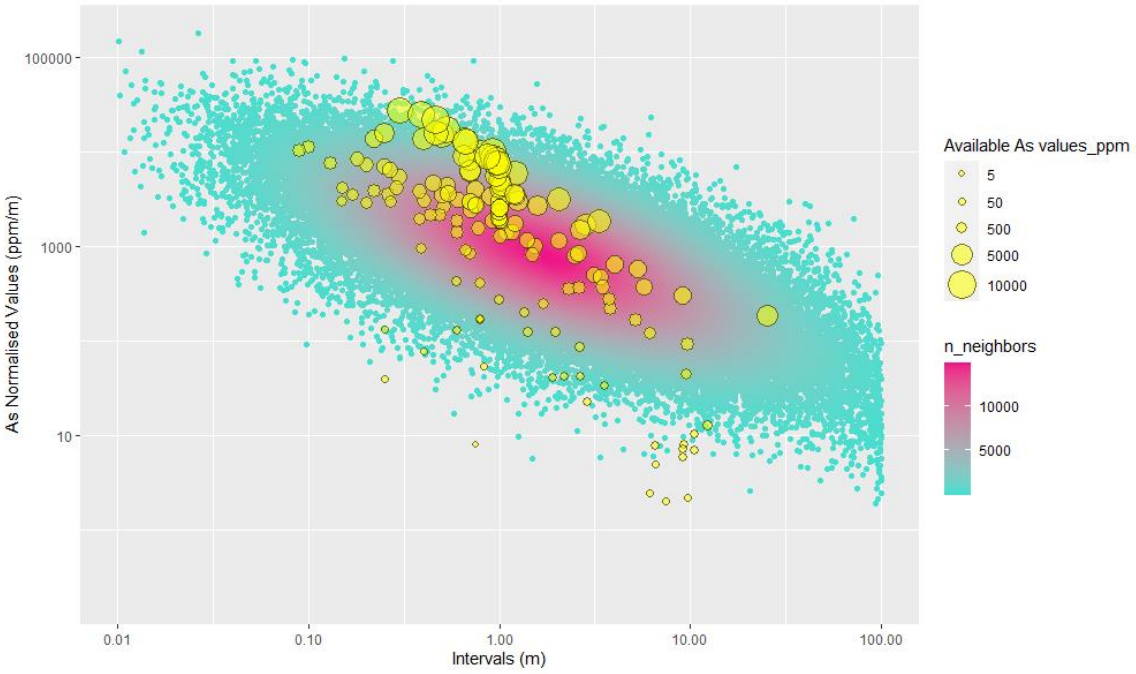


Figure. S75 Realization 9 of the arsenopyrite class 1.

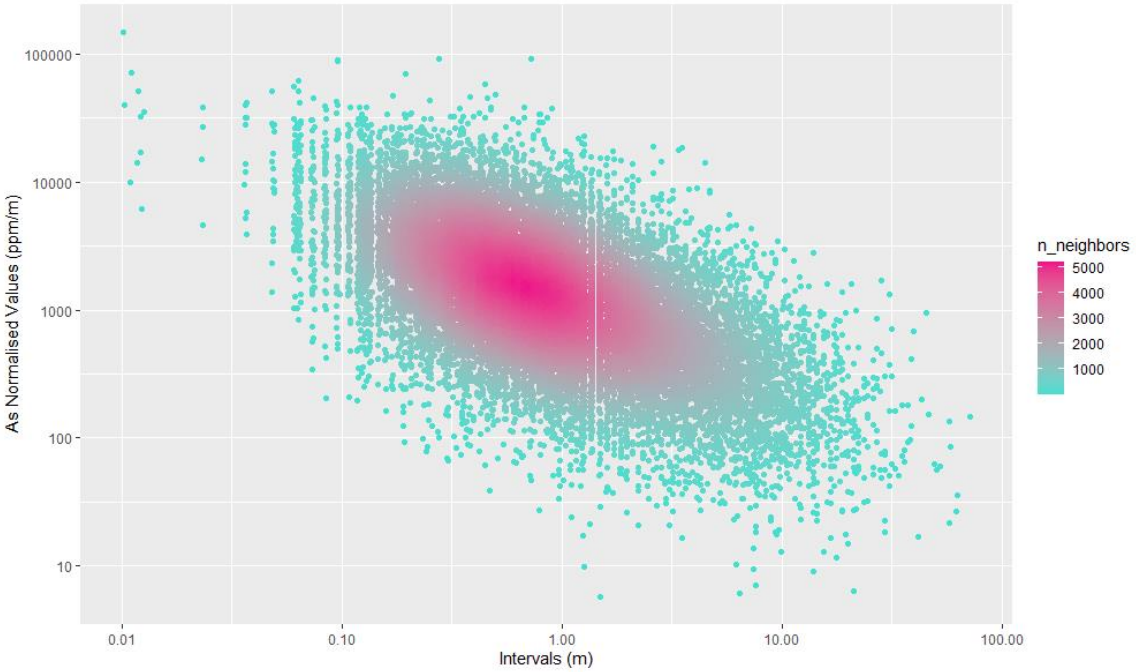


Figure. S76 The selected values of the auxiliary variable based on interval values of the class 1 (realization 9).

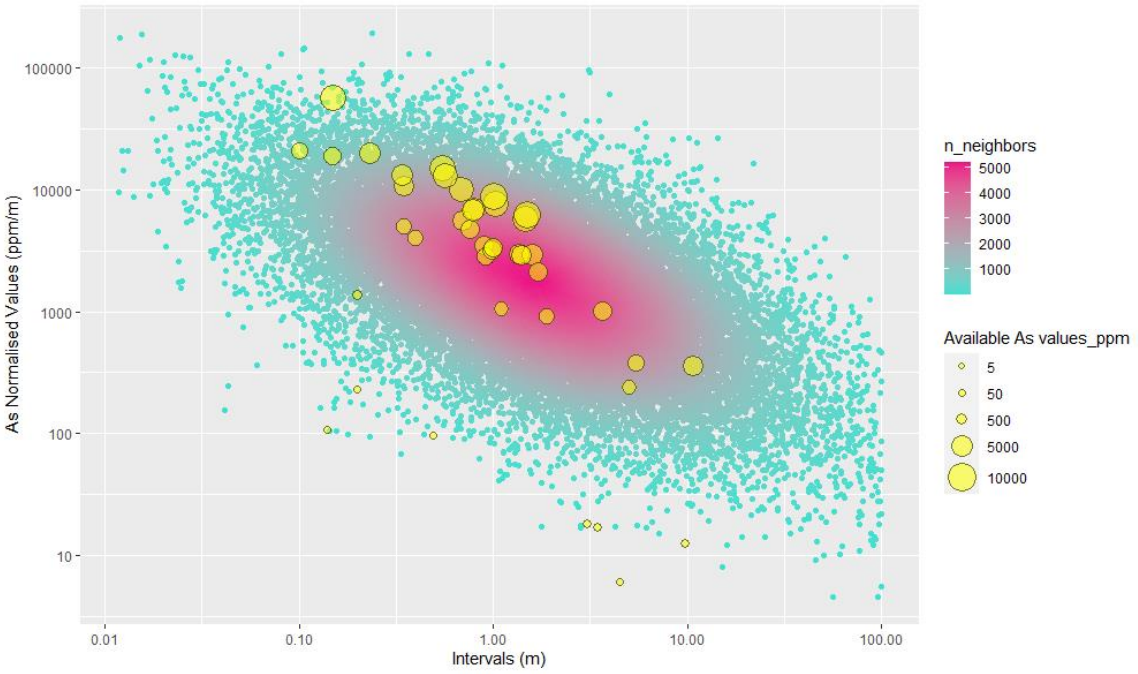


Figure. S77 Realization 9 of the arsenopyrite class 2.

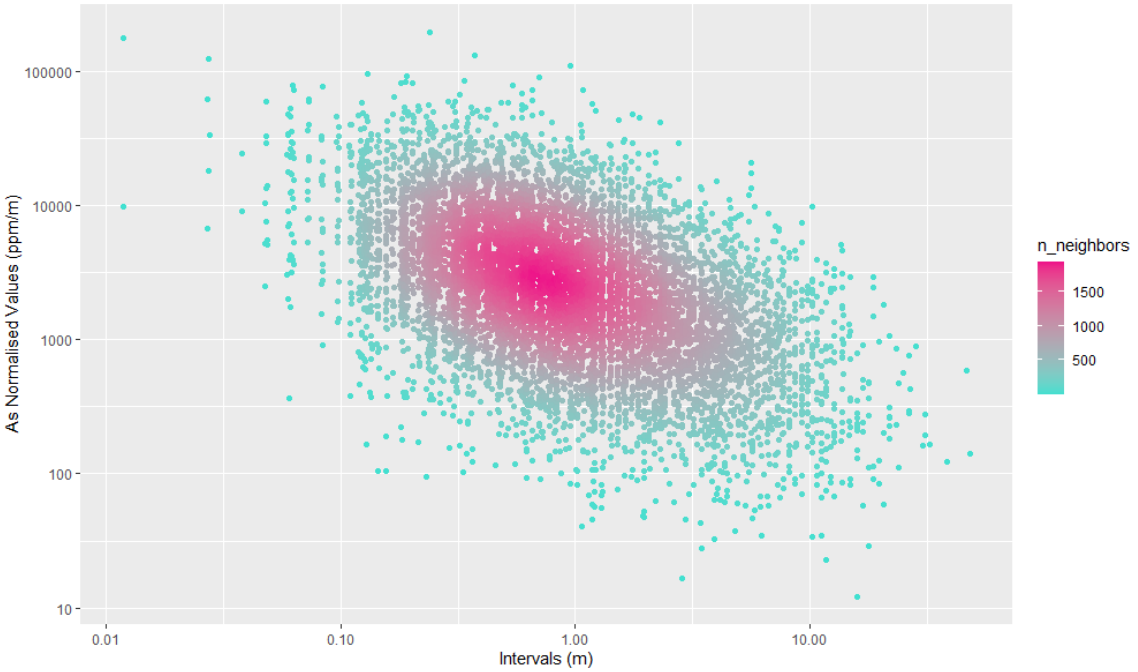


Figure. S78 The selected values of the auxiliary variable based on interval values of the class 2 (realization 9).

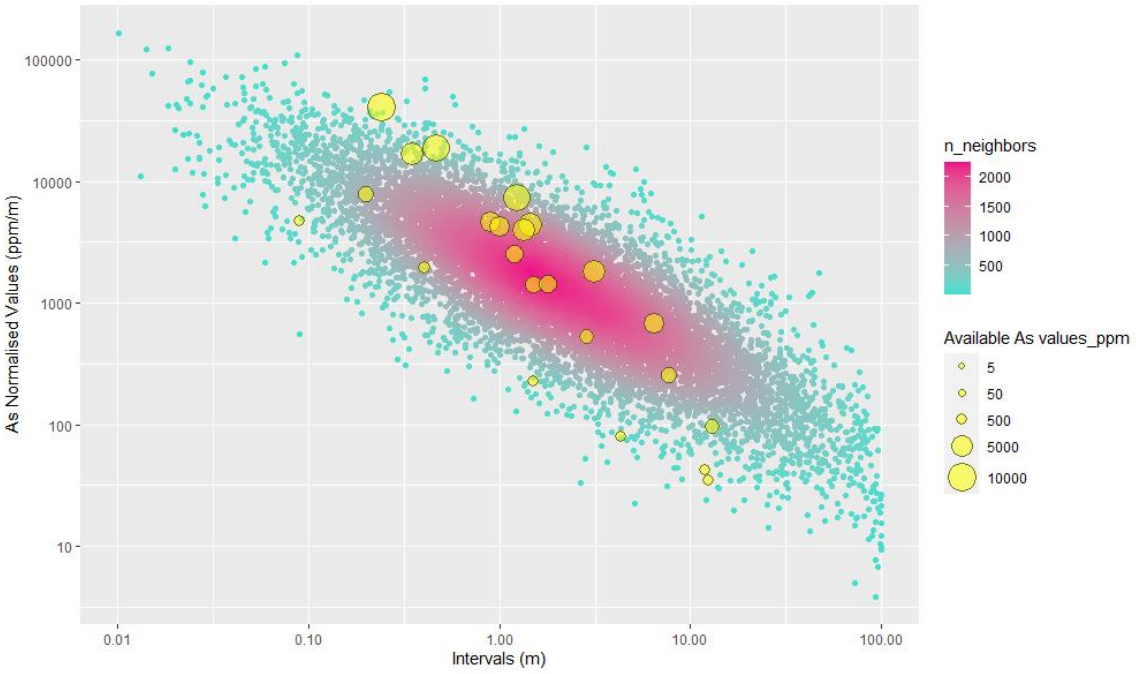


Figure. S79 Realization 9 of the arsenopyrite class 3.

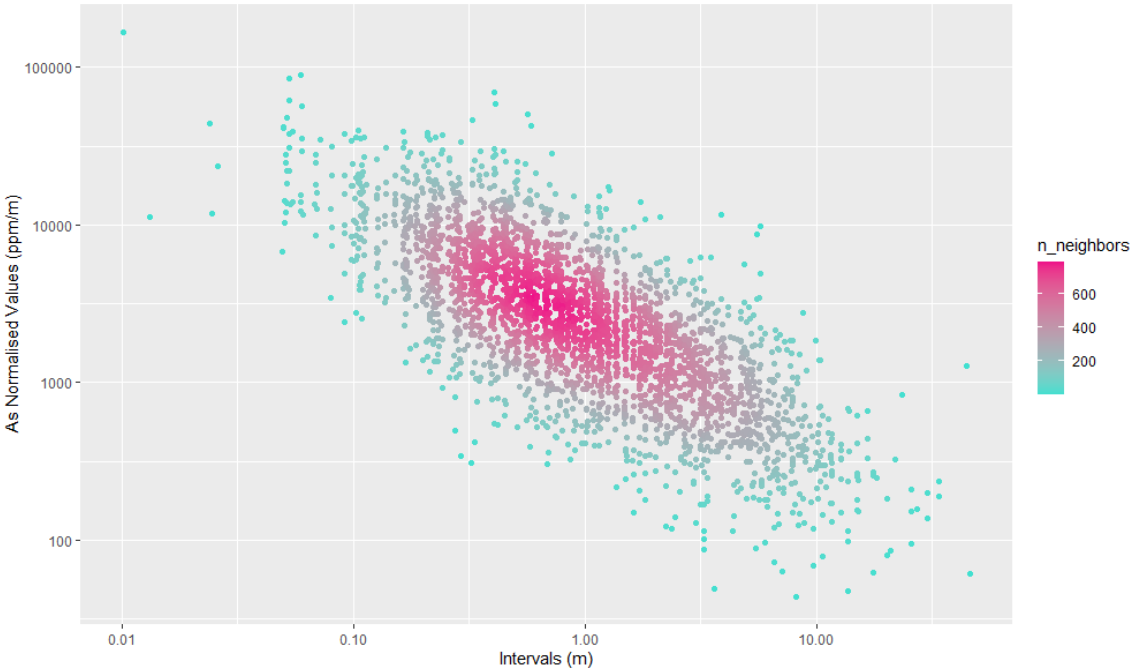


Figure. S80 The selected values of the auxiliary variable based on interval values of the class 3 (realization 9).

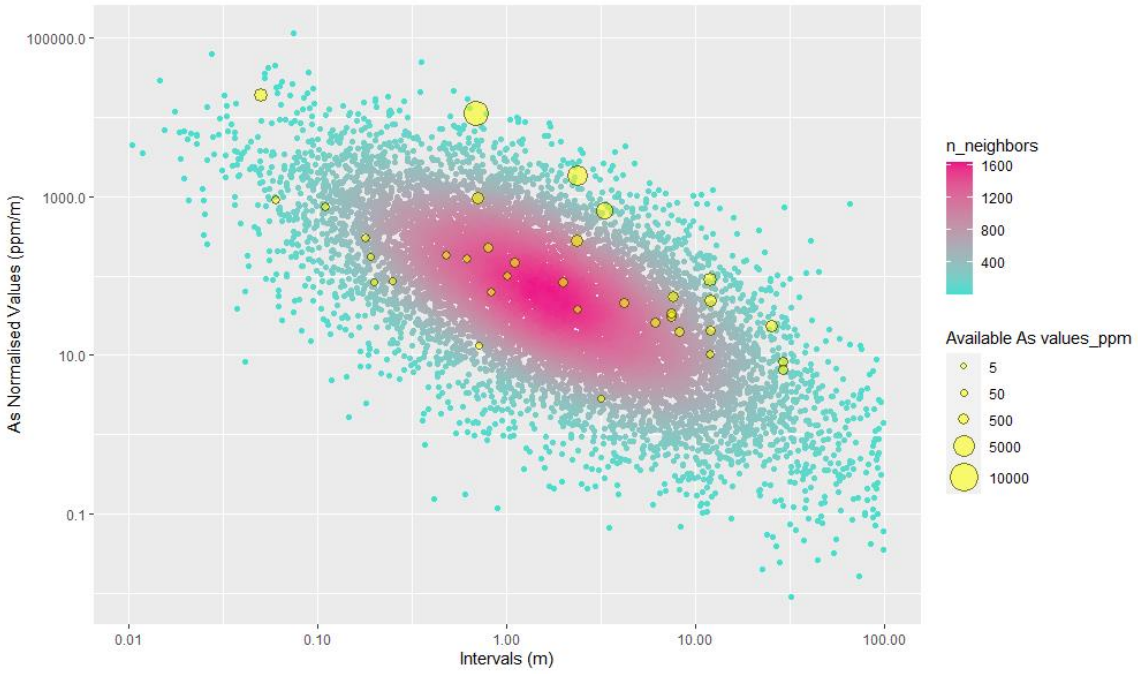


Figure. S81 Realization 10 of the arsenopyrite class 0.1.

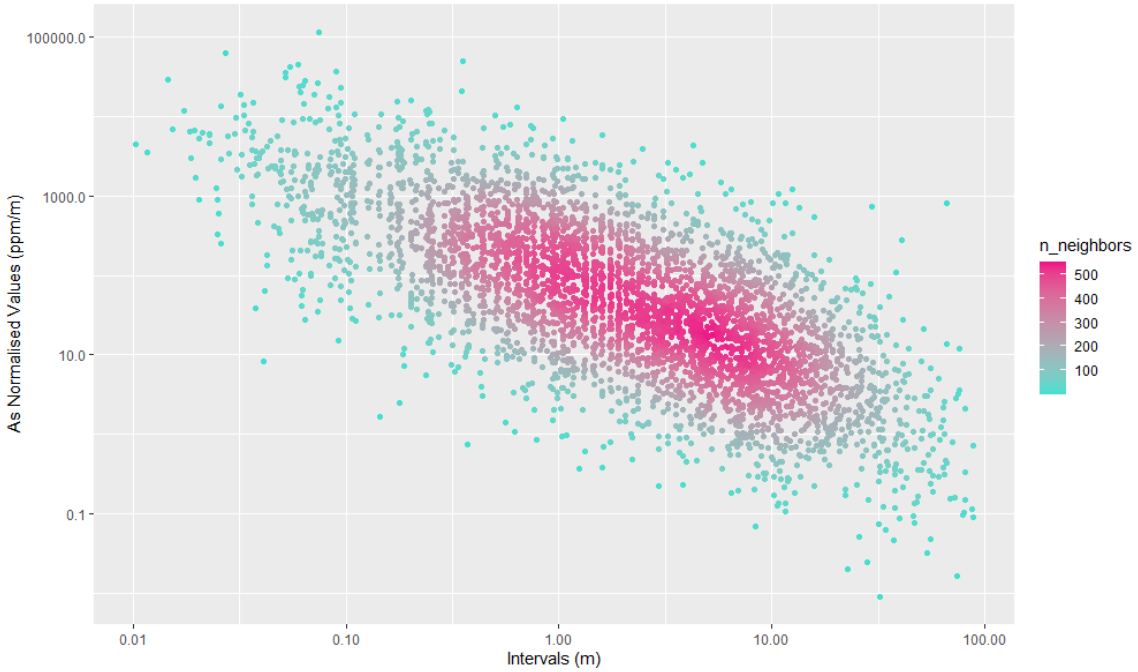


Figure. S82 The selected values of the auxiliary variable based on interval values of the class 0.1 (realization 10).

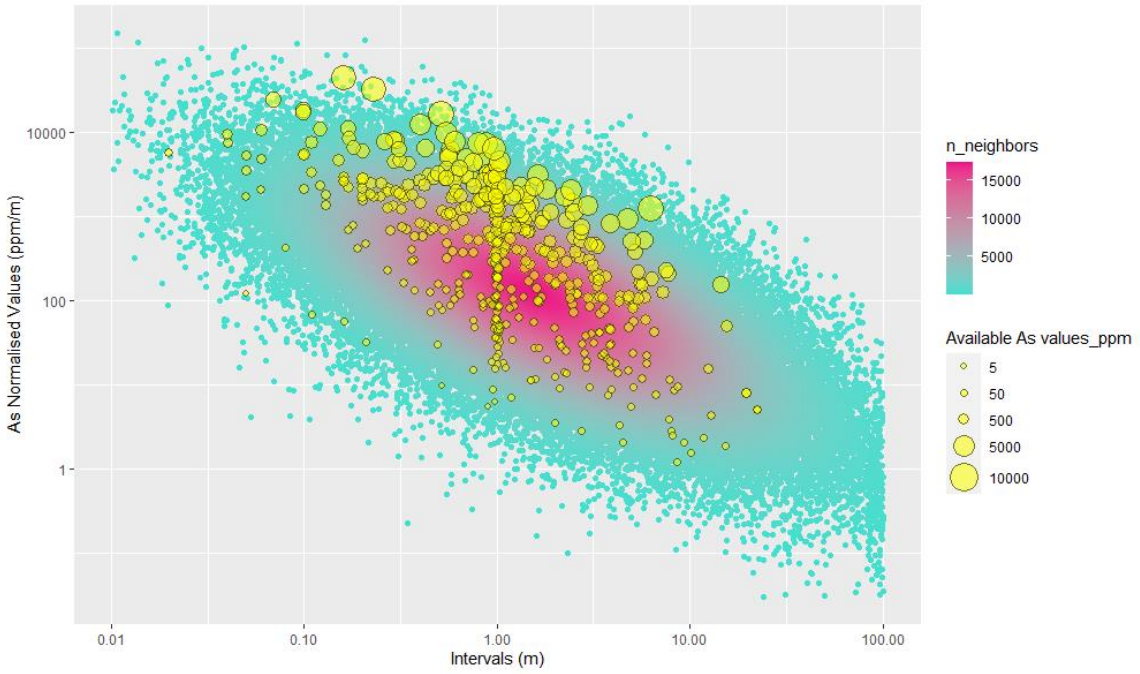


Figure. S83 Realization 10 of the arsenopyrite class 0.5.

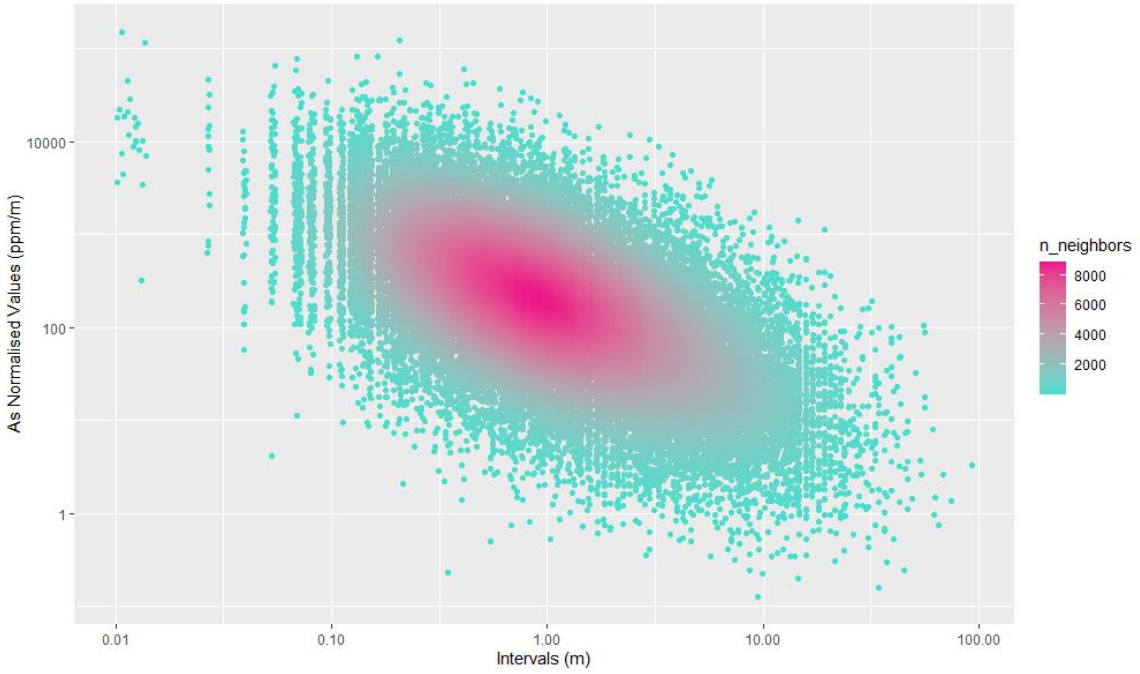


Figure. S84 The selected values of the auxiliary variable based on interval values of the class 0.5 (realization 10).

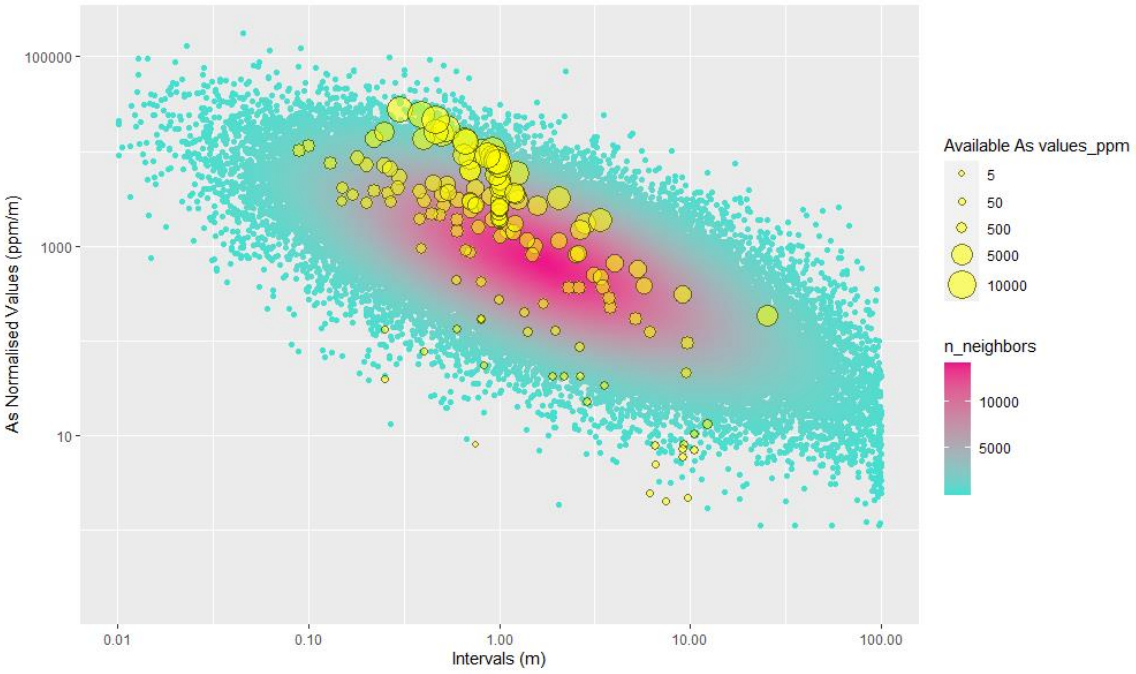


Figure. S85 Realization 10 of the arsenopyrite class 1.

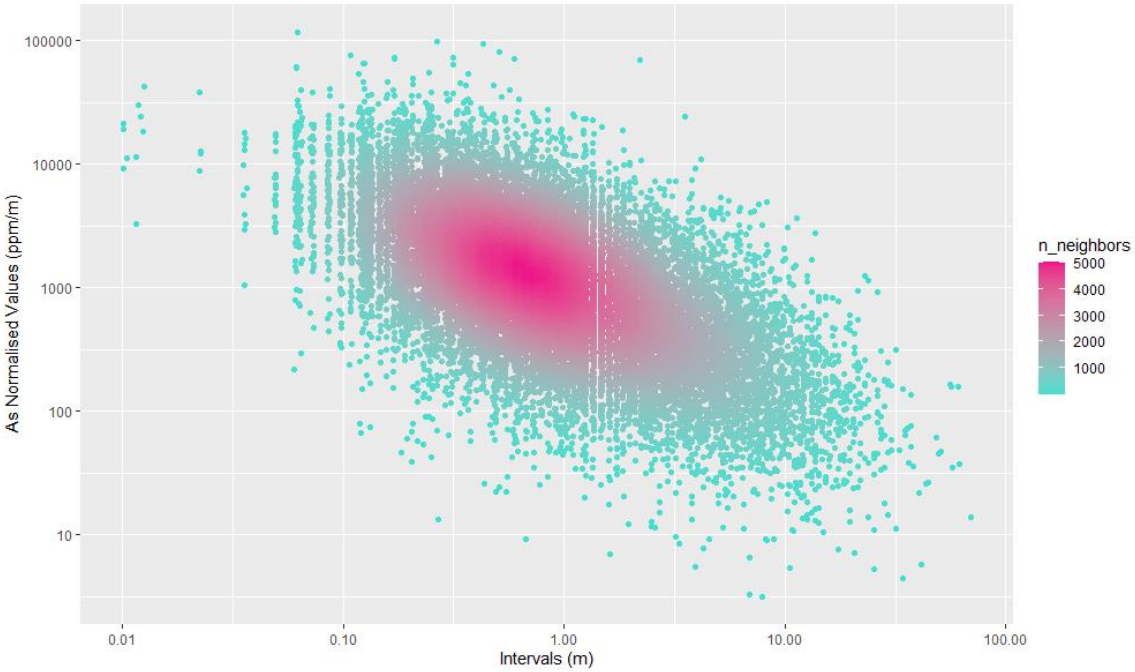


Figure. S86 The selected values of the auxiliary variable based on interval values of the class 1 (realization 10).

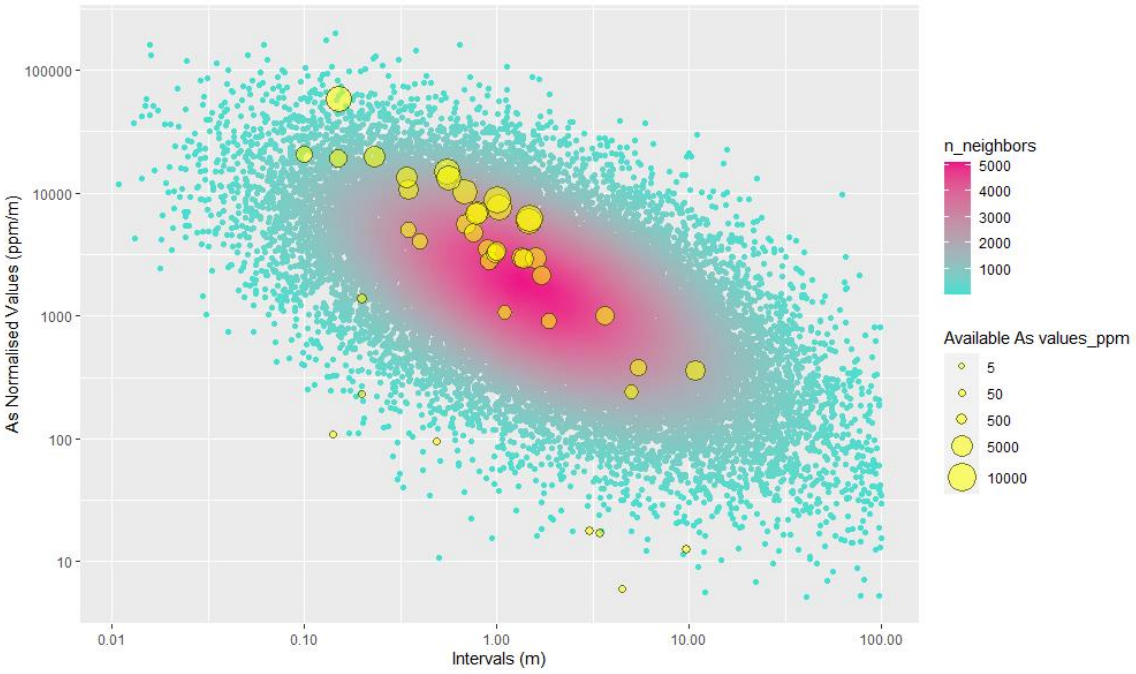


Figure. S87 Realization 10 of the arsenopyrite class 2.



Figure. S88 The selected values of the auxiliary variable based on interval values of the class 2 (realization 10).

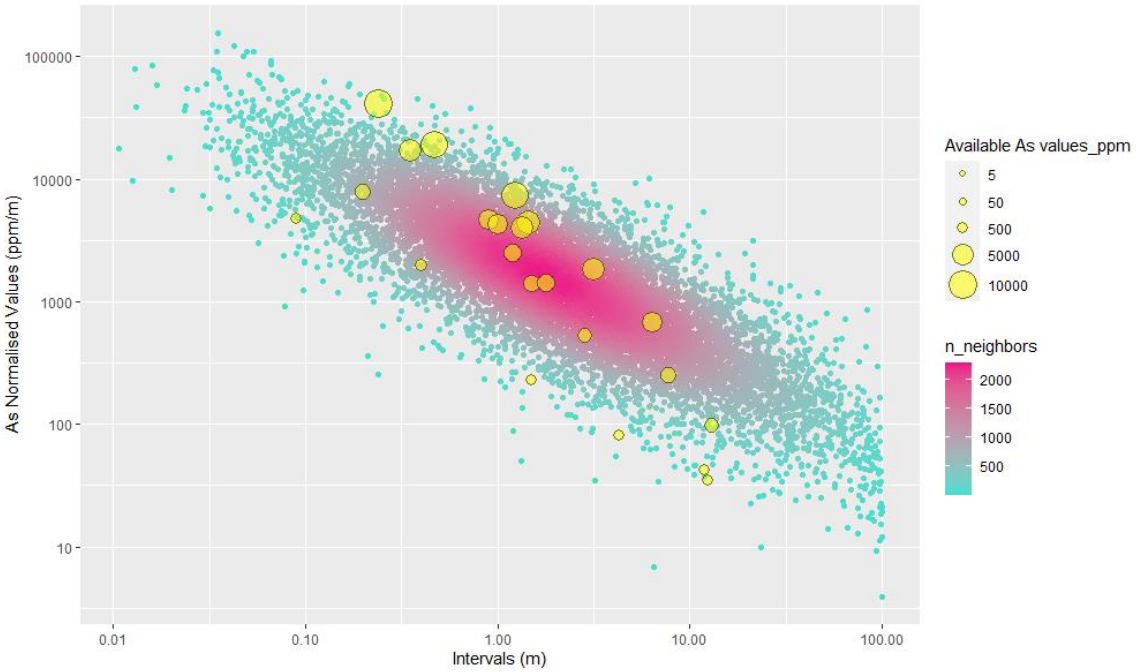


Figure. S89 Realization 10 of the arsenopyrite class 3.

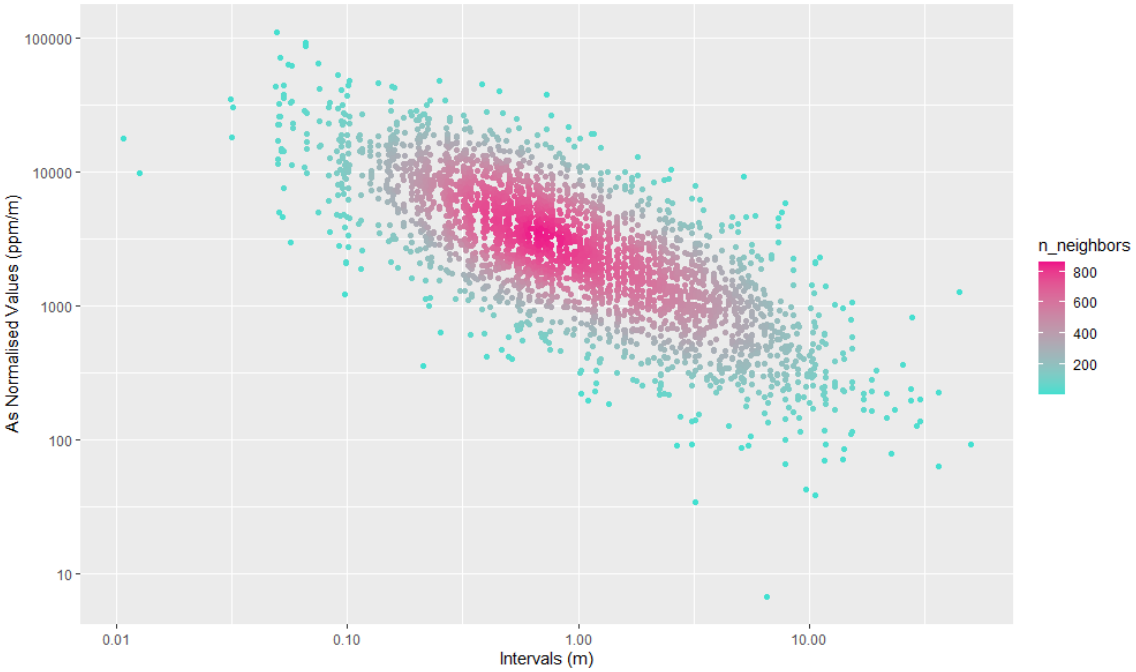


Figure. S90 The selected values of the auxiliary variable based on interval values of the class 3 (realization 10).

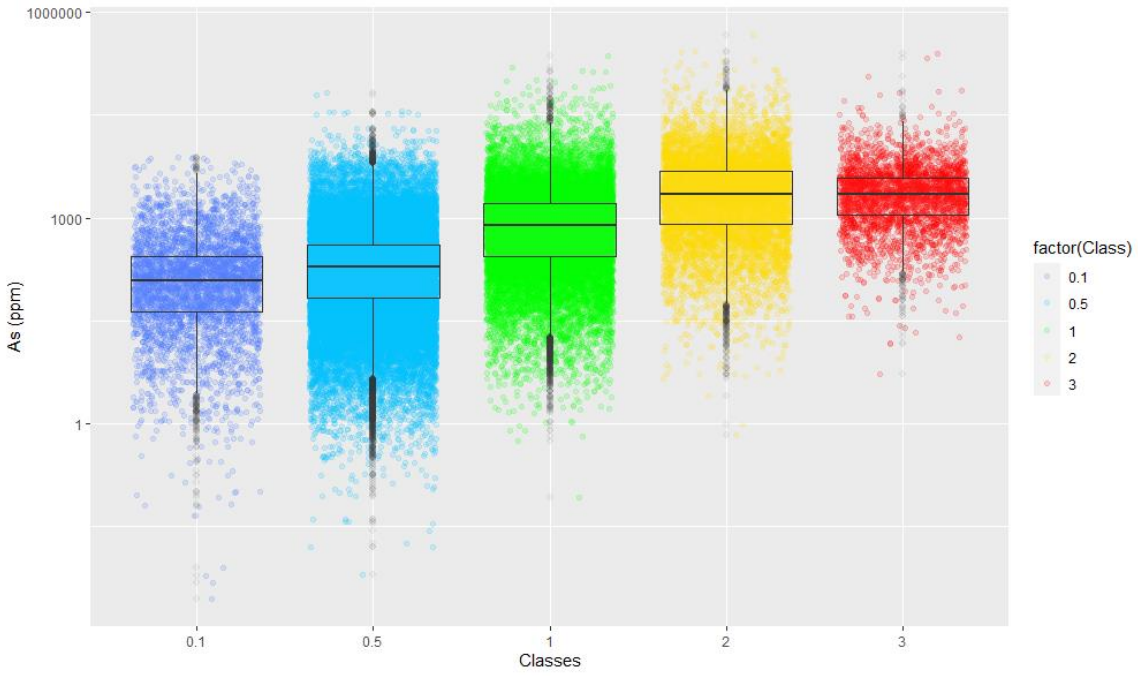


Figure. S91 The output of the iterative Monte Carlo simulation for each arsenopyrite class (realization 2).

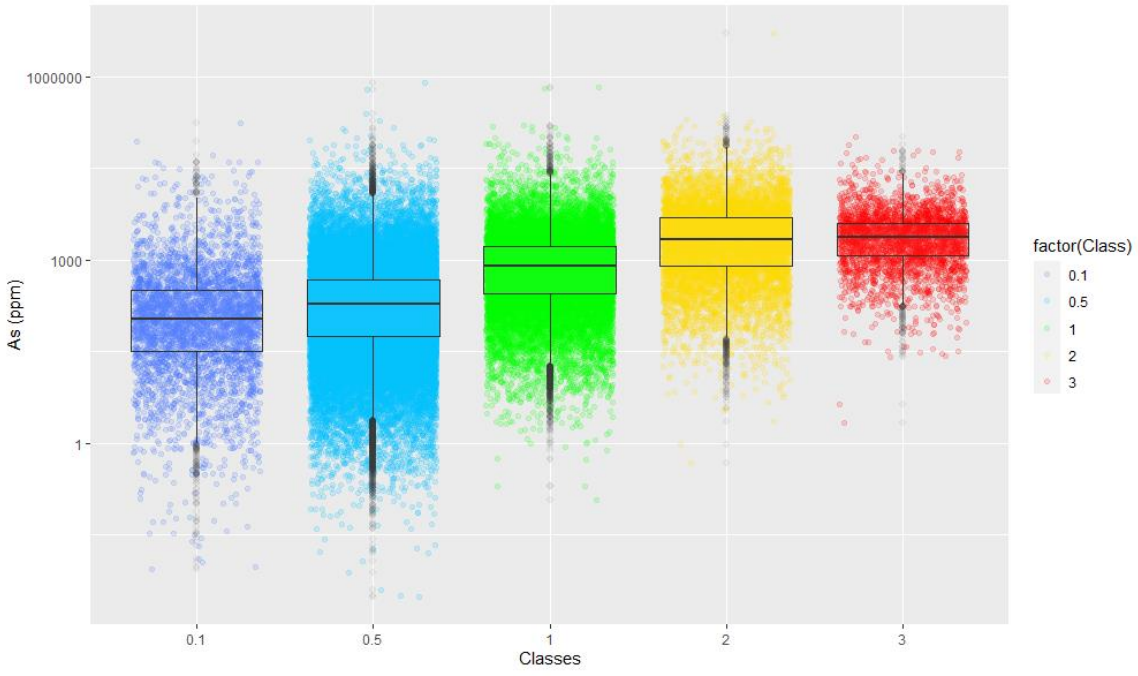


Figure. S93 The output of the iterative Monte Carlo simulation for each arsenopyrite class (realization 3).

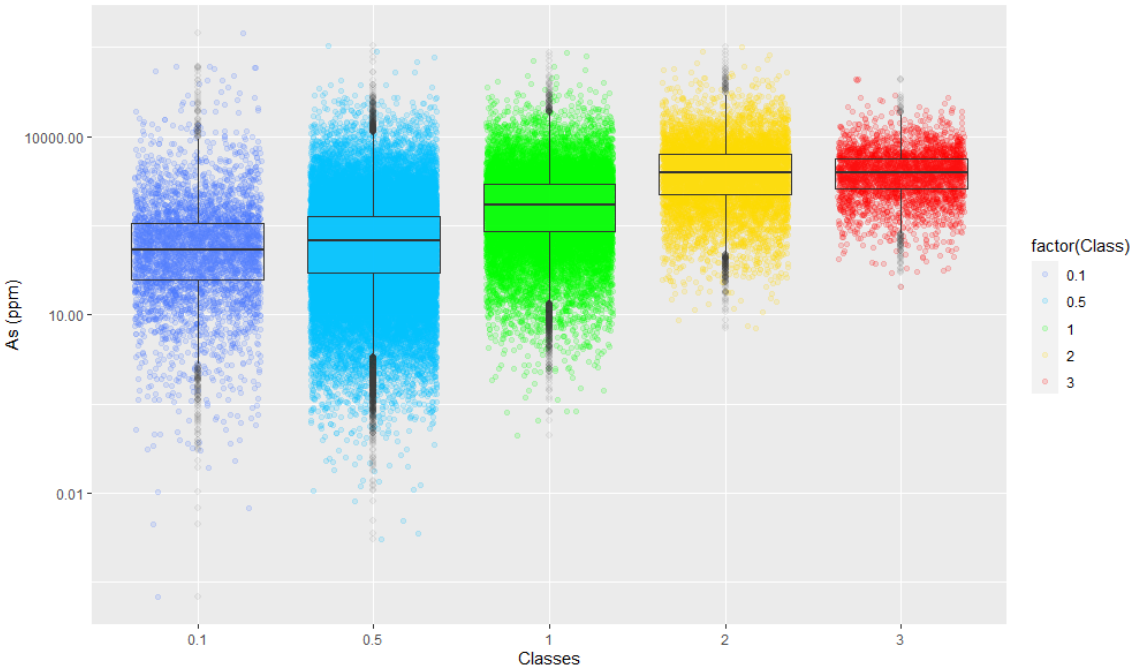


Figure. S94 The output of the iterative Monte Carlo simulation for each arsenopyrite class (realization 4).

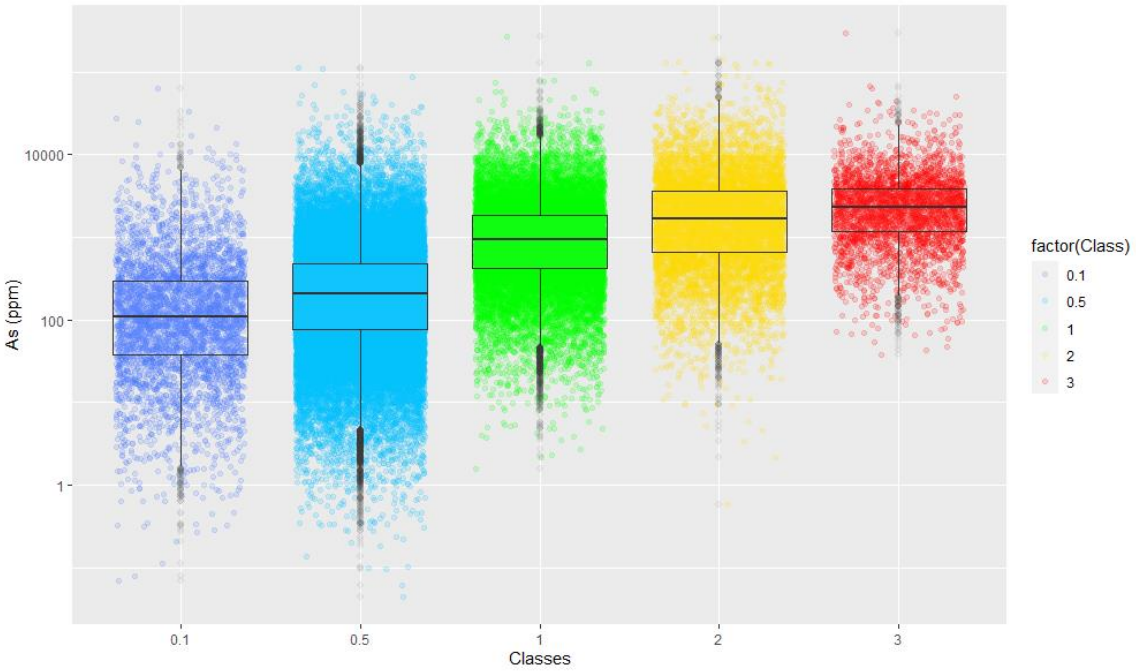


Figure. S95 The output of the iterative Monte Carlo simulation for each arsenopyrite class (realization 5).

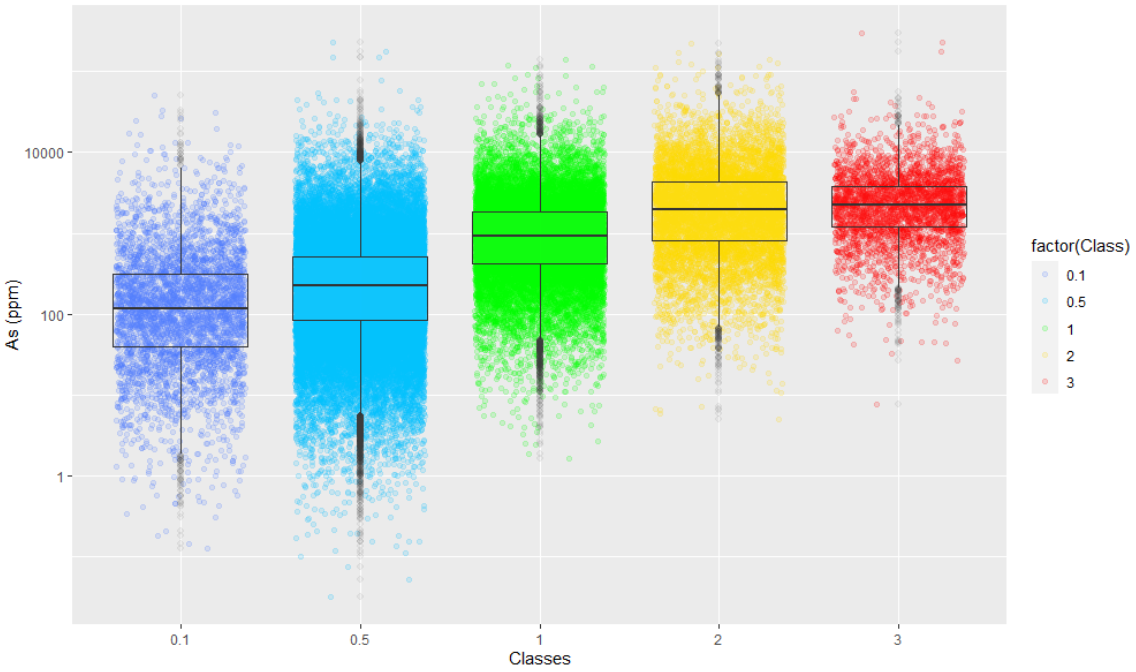


Figure. S96 The output of the iterative Monte Carlo simulation for each arsenopyrite class (realization 6).

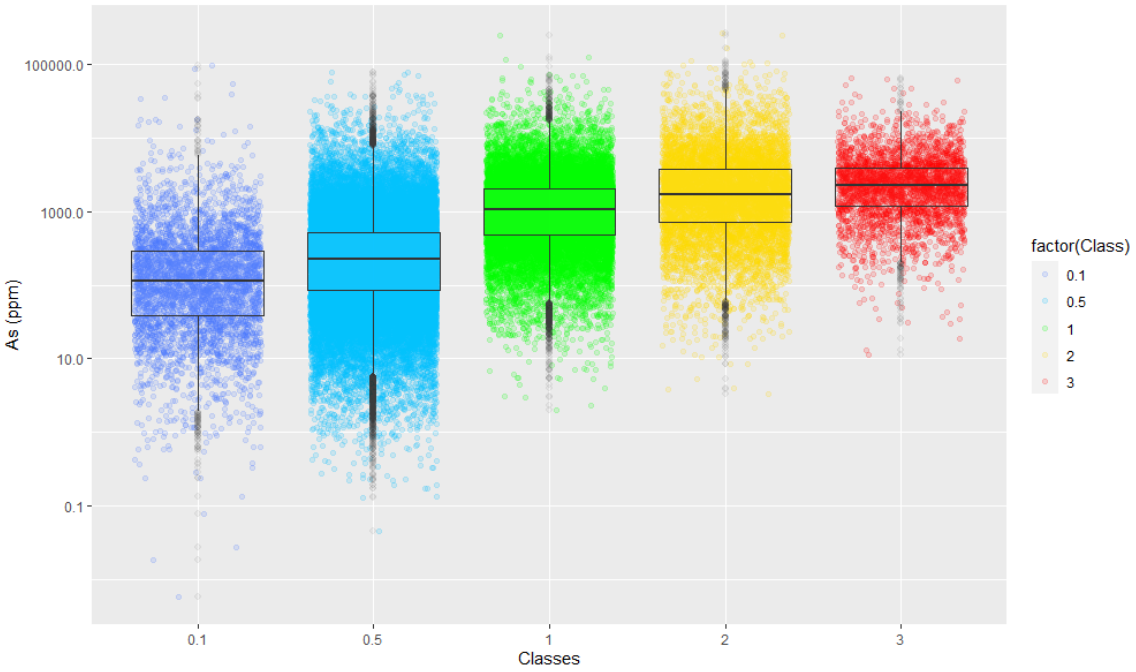


Figure. S97 The output of the iterative Monte Carlo simulation for each arsenopyrite class (realization 7).

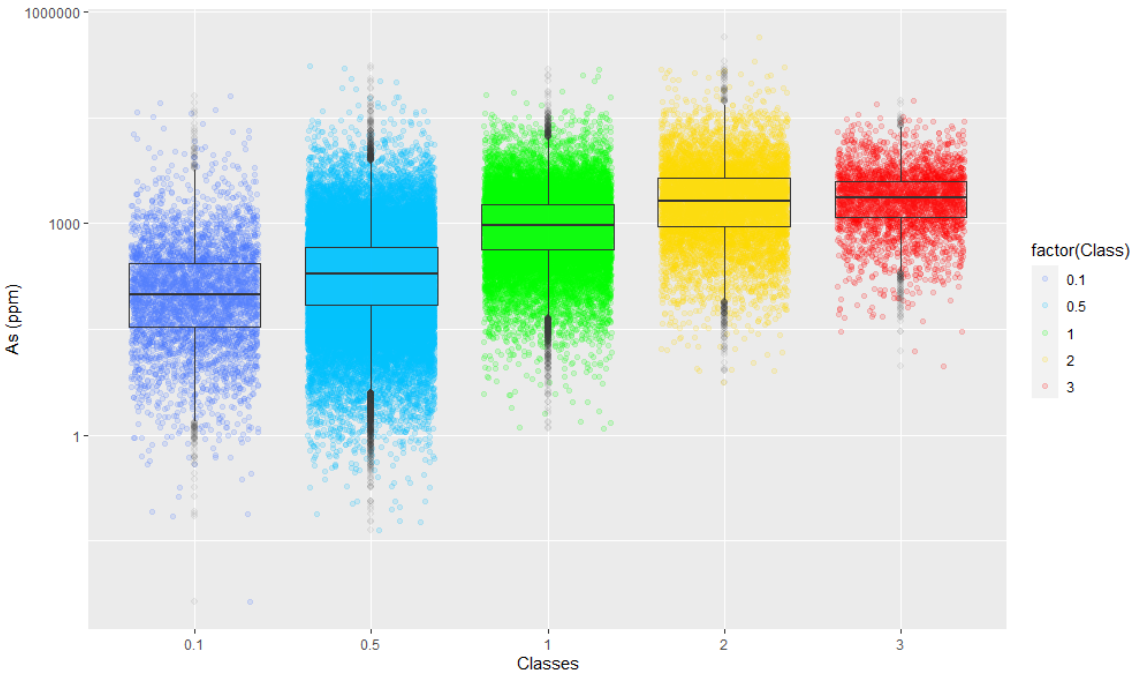


Figure. S98 The output of the iterative Monte Carlo simulation for each arsenopyrite class (realization 8).

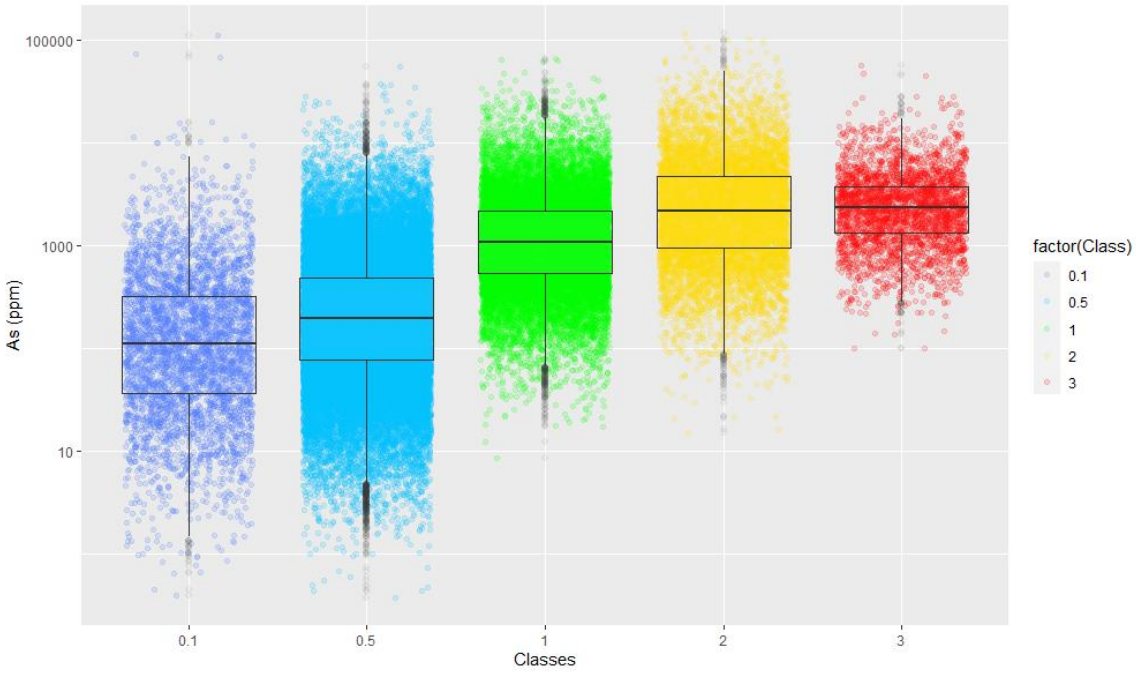


Figure. S99 The output of the iterative Monte Carlo simulation for each arsenopyrite class (realization 9).

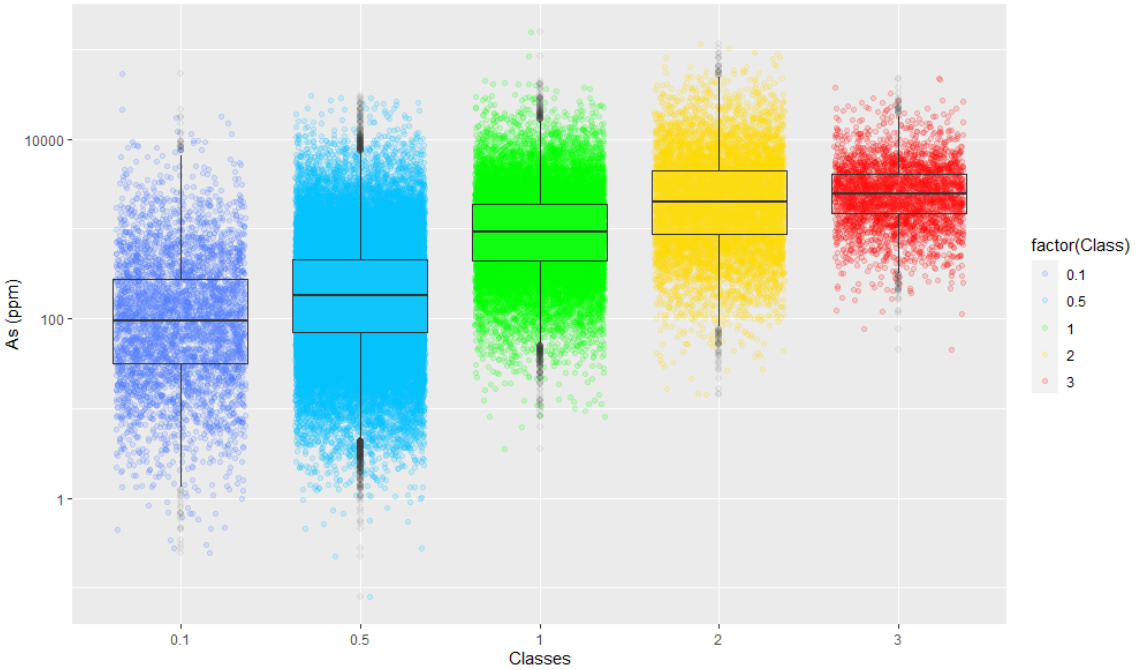


Figure. S100 The output of the iterative Monte Carlo simulation for each arsenopyrite class(realization 10).

Table S1 Hypothesis testing of the generated realizations.

	Sample size	Realizations	Levene's test	Student’s t test	Welch’s t test	Significance level 0.05
As available grades	1141	1	0.367	0.412	0.217	Not significant
		2	0.807	0.45	0.414	Not significant
		3	0.627	0.792	0.151	Not significant
		4	0.476	0.813	0.633	Not significant
		5	0.013	0.136	0.043	Significant
As simulated grades	80977	6	0.248	0.608	0.426	Not significant
		7	0.119	0.538	0.39	Not significant
		8	0.291	0.519	0.320	Not significant
		9	0.073	0.619	0.561	Not significant
		10	0.001	0.07	0.048	Significant

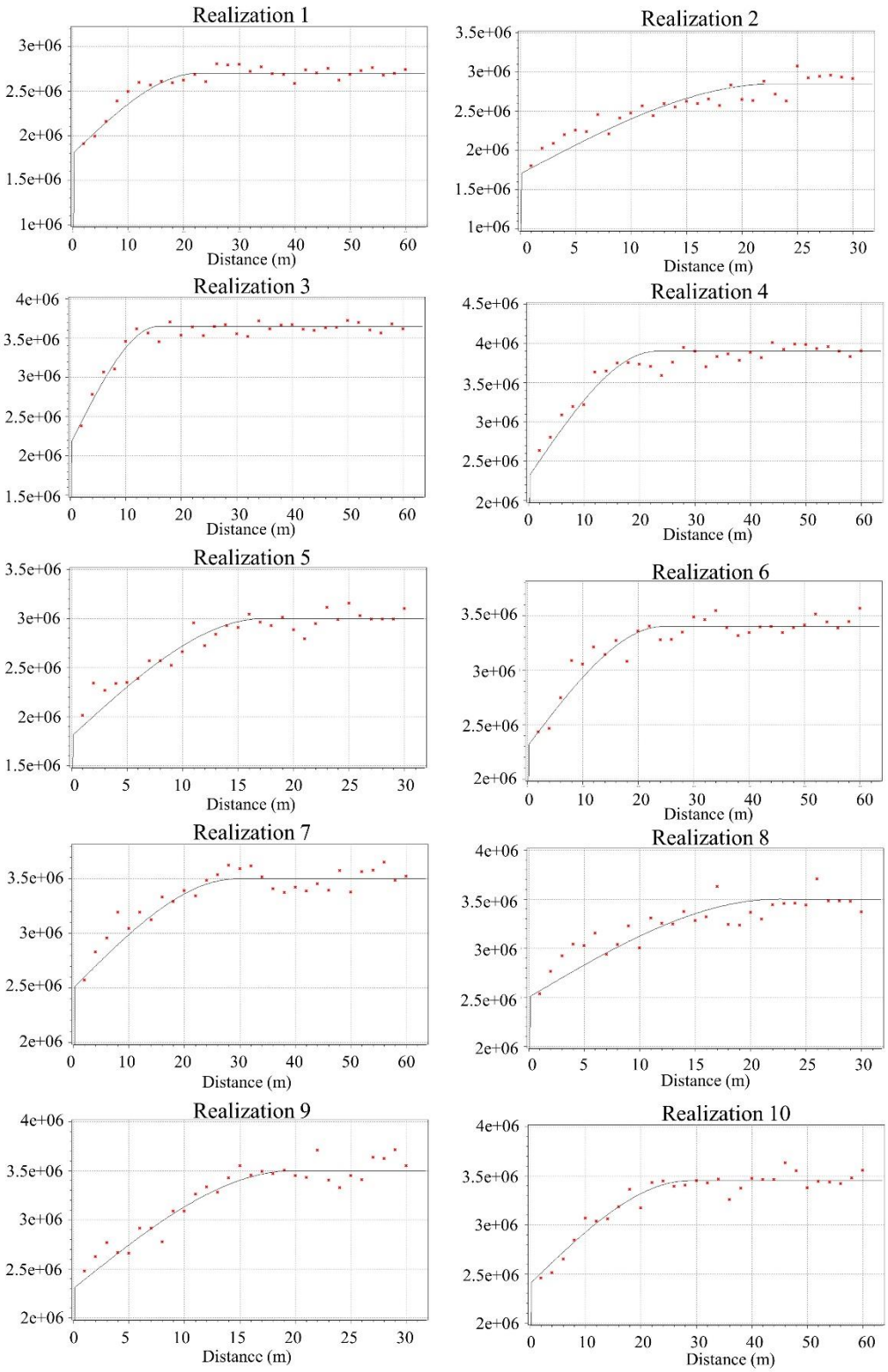


Figure. S101 The directional variograms of the generated realizations

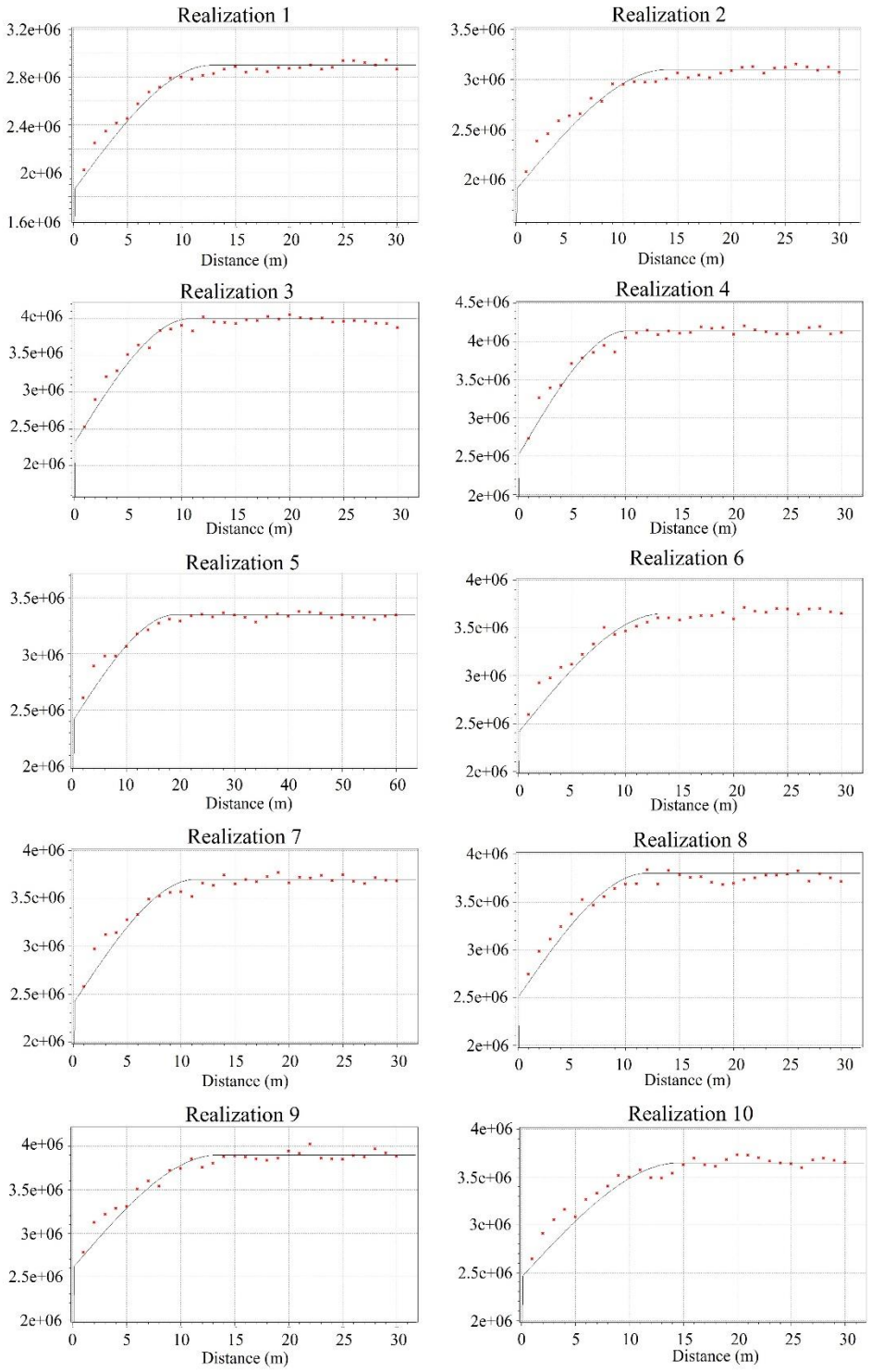


Figure. S102 The omnidirectional variograms of the generated realizations.

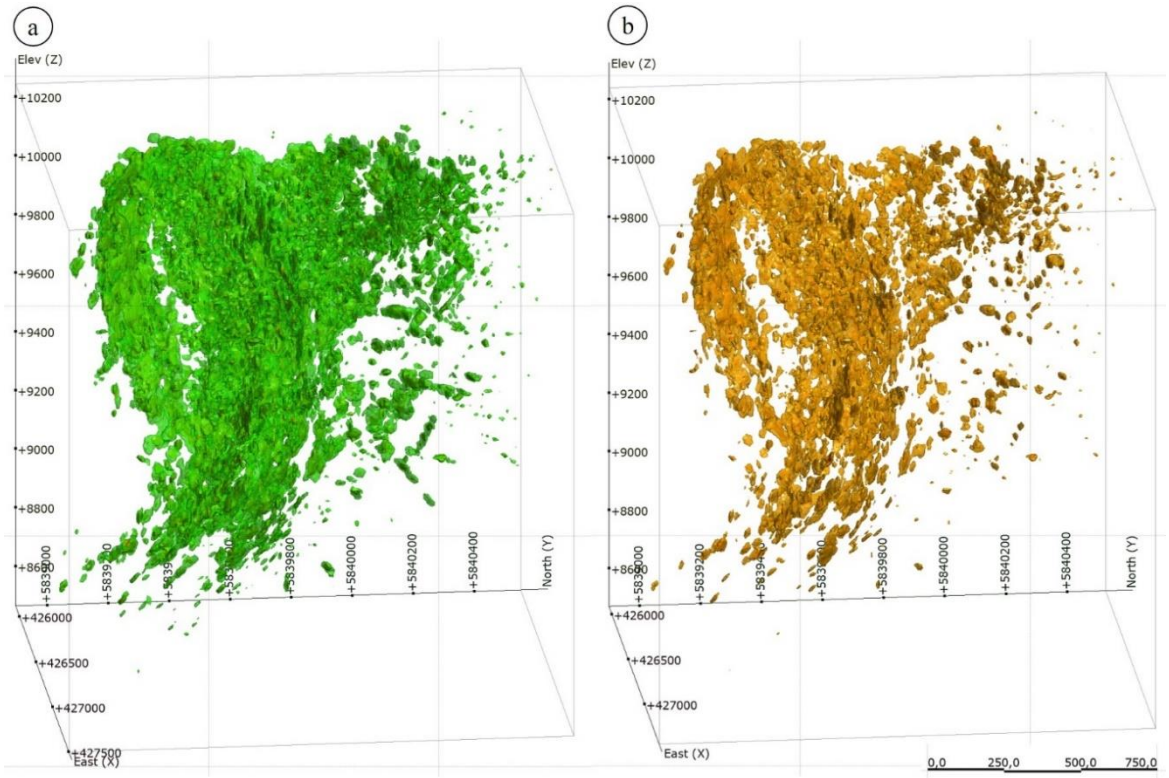


Figure. S103 a) The spatial distribution of arsenic grades ranging from 500 ppm to 1100 ppm, b) The spatial distribution of arsenic grades ranging from 1100 ppm to 2300 ppm (realization 2).

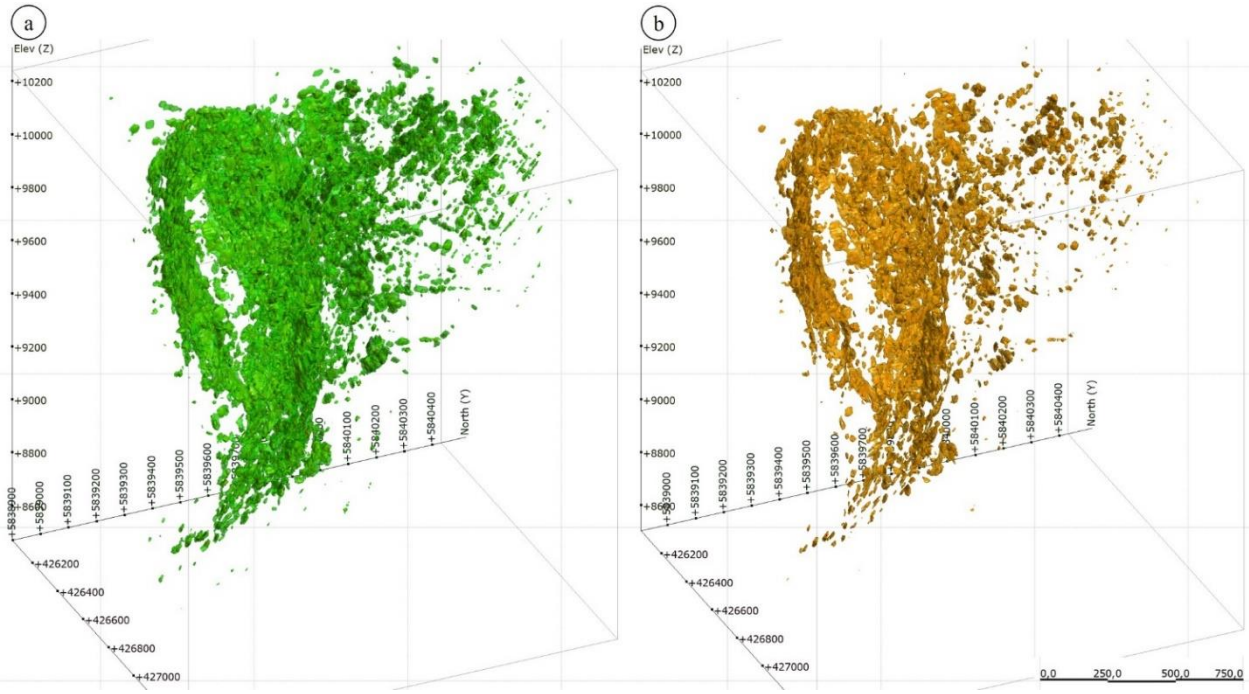


Figure. S104 a) The spatial distribution of arsenic grades ranging from 500 ppm to 1100 ppm, b) The spatial distribution of arsenic grades ranging from 1100 ppm to 2300 ppm (realization 3).

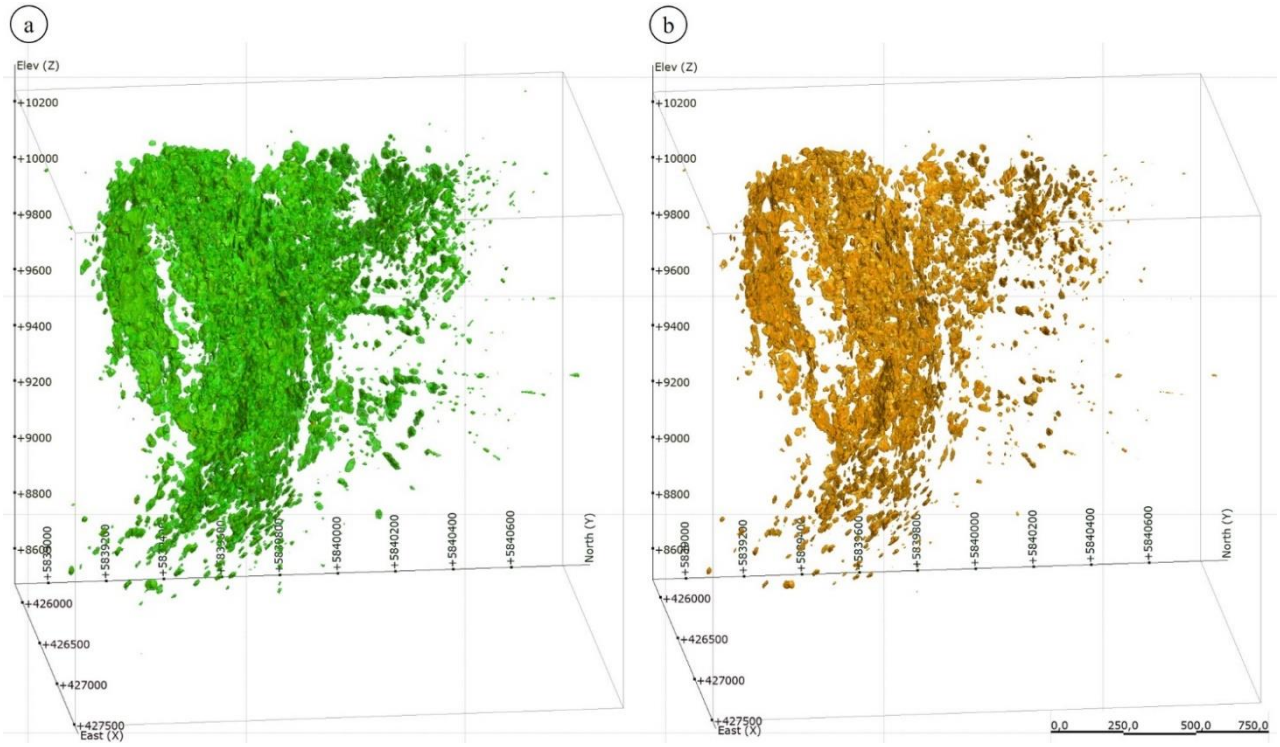


Figure. S105 a) The spatial distribution of arsenic grades ranging from 500 ppm to 1100 ppm, b) The spatial distribution of arsenic grades ranging from 1100 ppm to 2300 ppm (realization 4).

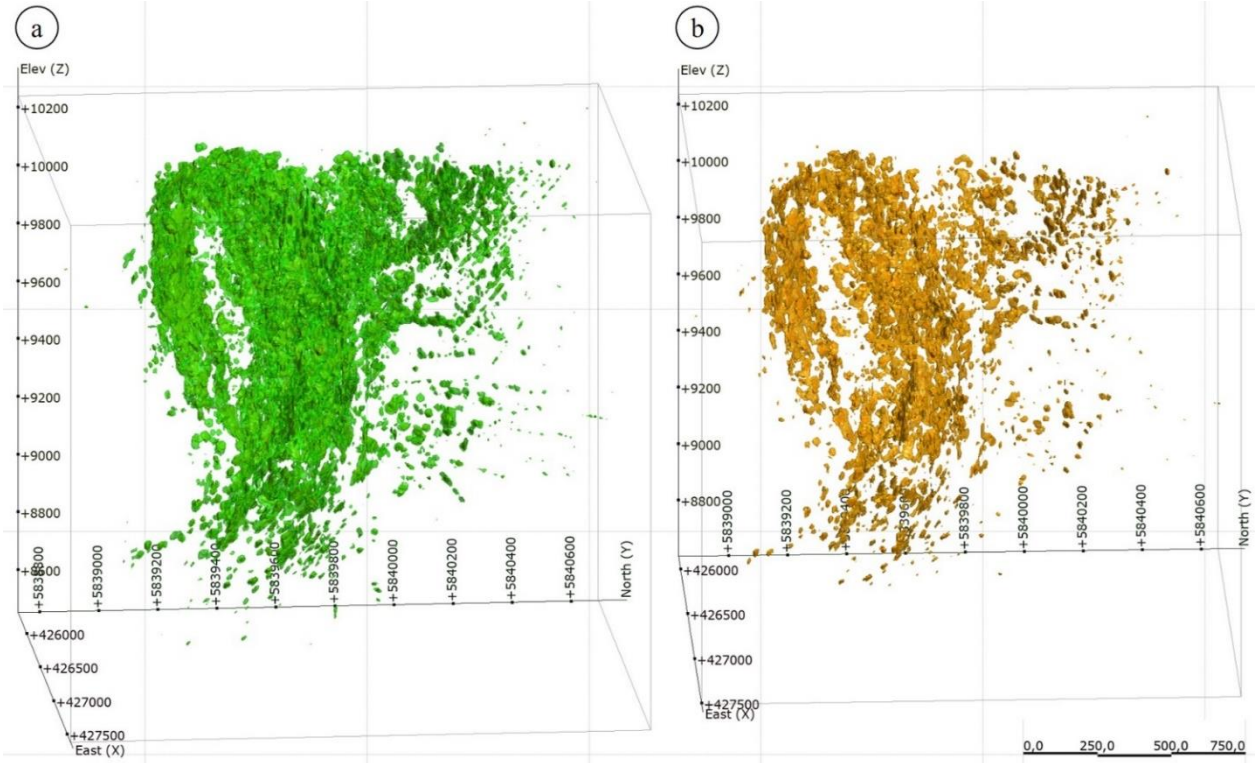


Figure. S106 a) The spatial distribution of arsenic grades ranging from 500 ppm to 1100 ppm, b) The spatial distribution of arsenic grades ranging from 1100 ppm to 2300 ppm (realization 5).

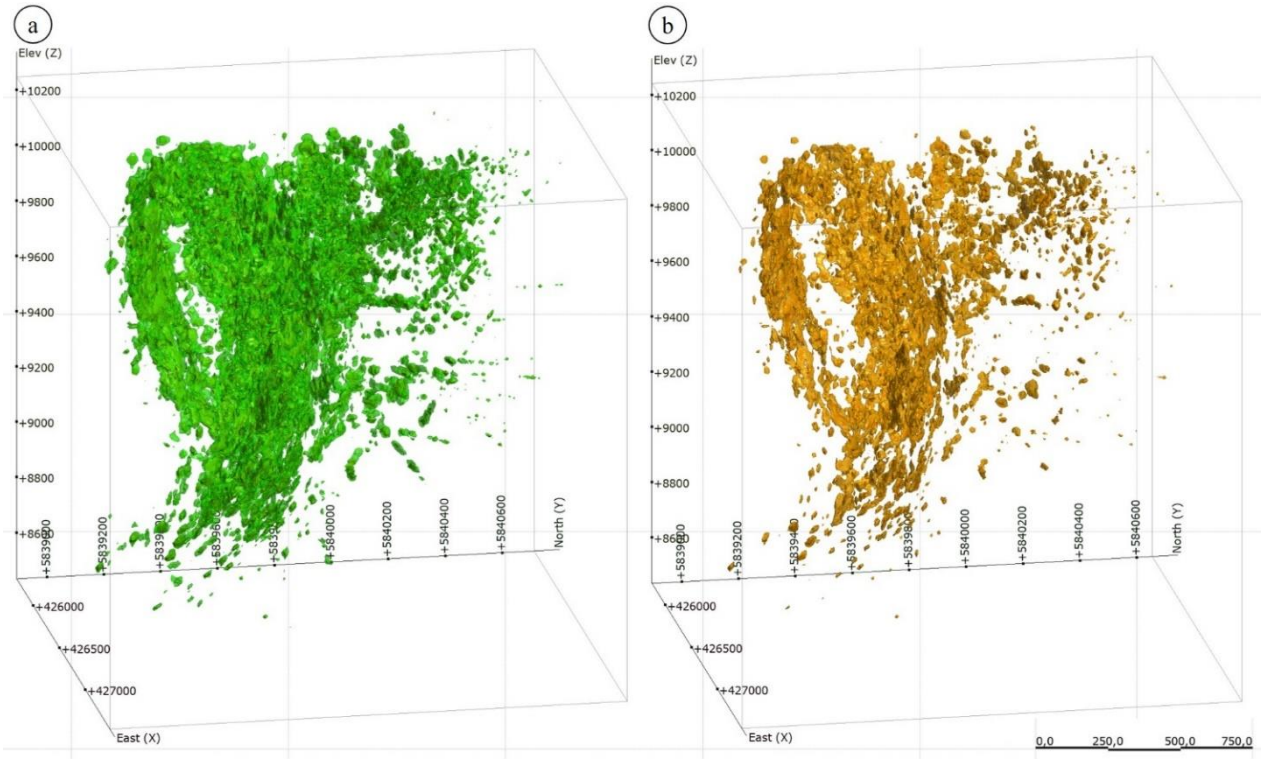


Figure. S107 a) The spatial distribution of arsenic grades ranging from 500 ppm to 1100 ppm, b) The spatial distribution of arsenic grades ranging from 1100 ppm to 2300 ppm (realization 6).

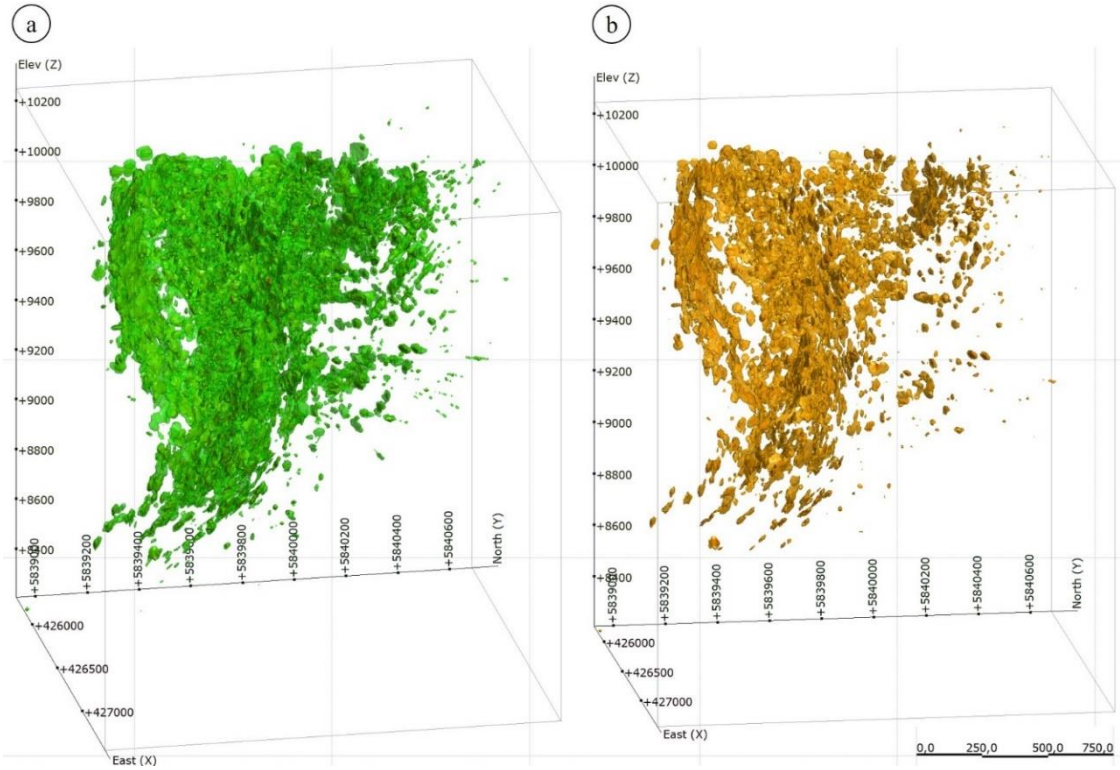


Figure. S108 a) The spatial distribution of arsenic grades ranging from 500 ppm to 1100 ppm, b) The spatial distribution of arsenic grades ranging from 1100 ppm to 2300 ppm (realization 7).

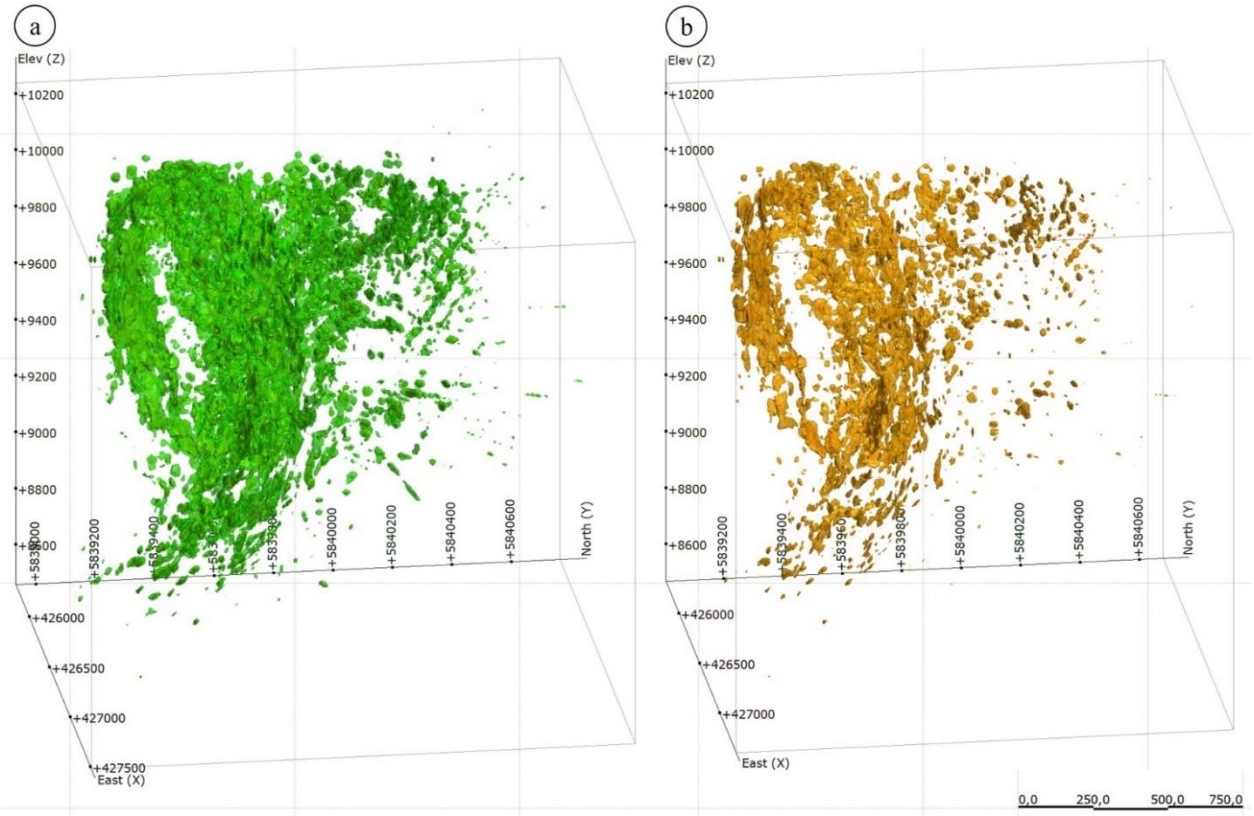


Figure. S109 a) The spatial distribution of arsenic grades ranging from 500 ppm to 1100 ppm, b) The spatial distribution of arsenic grades ranging from 1100 ppm to 2300 ppm (realization 8).

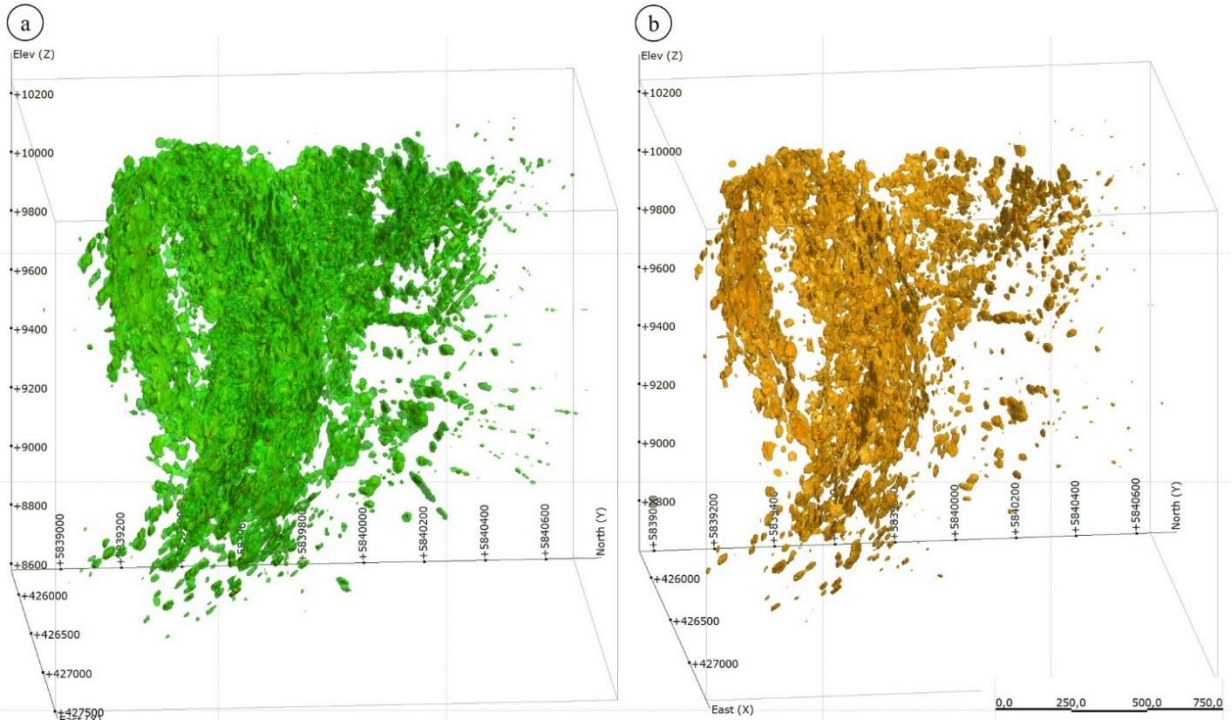


Figure. S110 a) The spatial distribution of arsenic grades ranging from 500 ppm to 1100 ppm, b) The spatial distribution of arsenic grades ranging from 1100 ppm to 2300 ppm (realization 9).

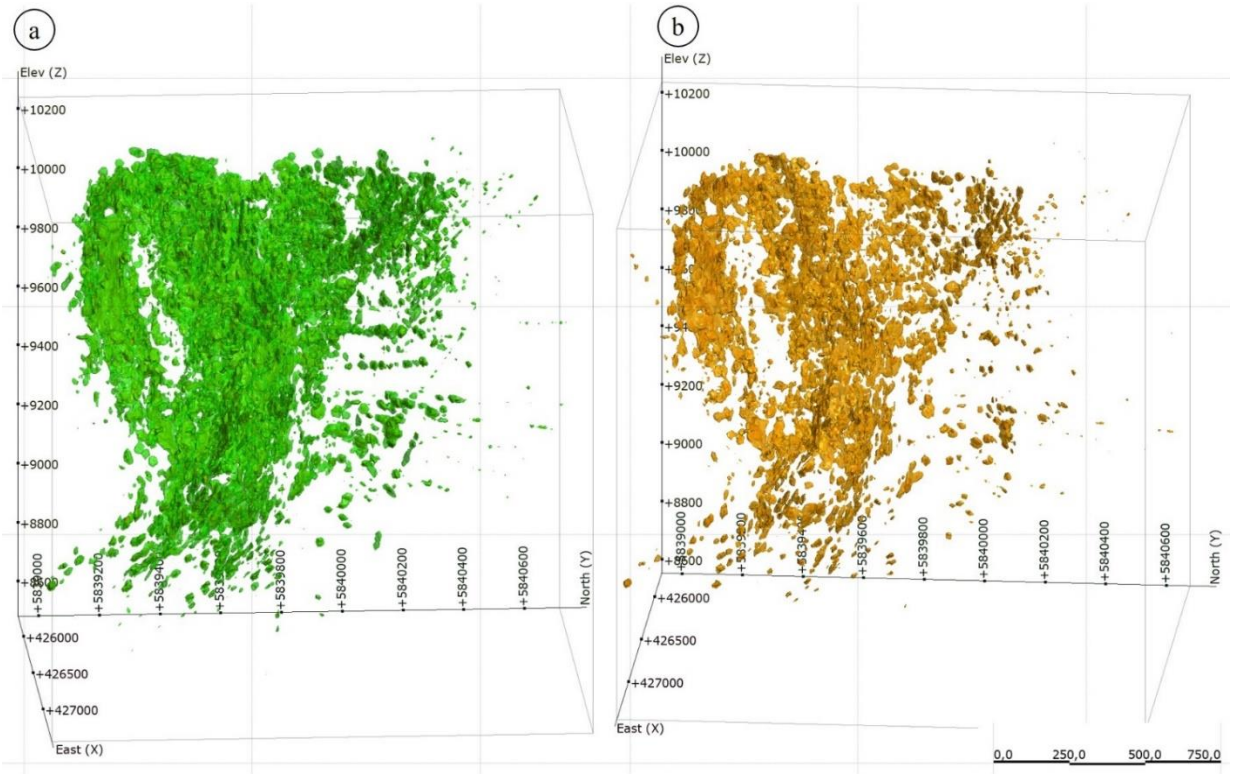


Figure. S111 a) The spatial distribution of arsenic grades ranging from 500 ppm to 1100 ppm, b) The spatial distribution of arsenic grades ranging from 1100 ppm to 2300 ppm (realization 10).

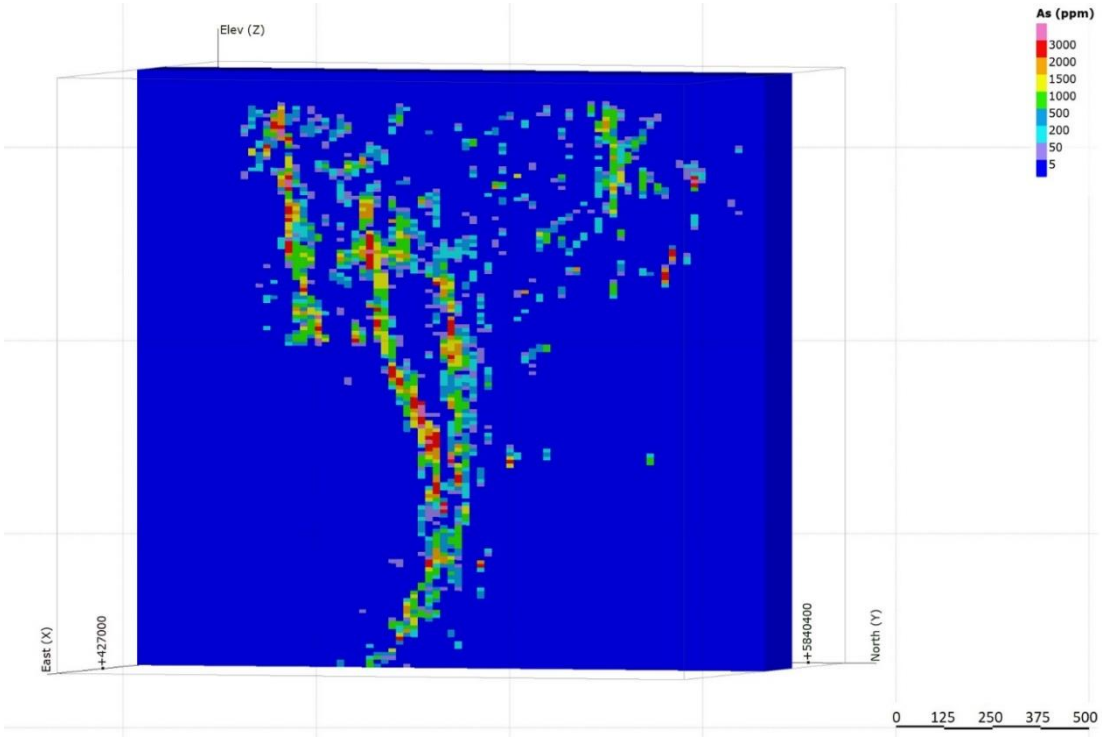


Figure. S112 Realization 2 of the block model of the arsenic grades along the footwall of the gold deposit.

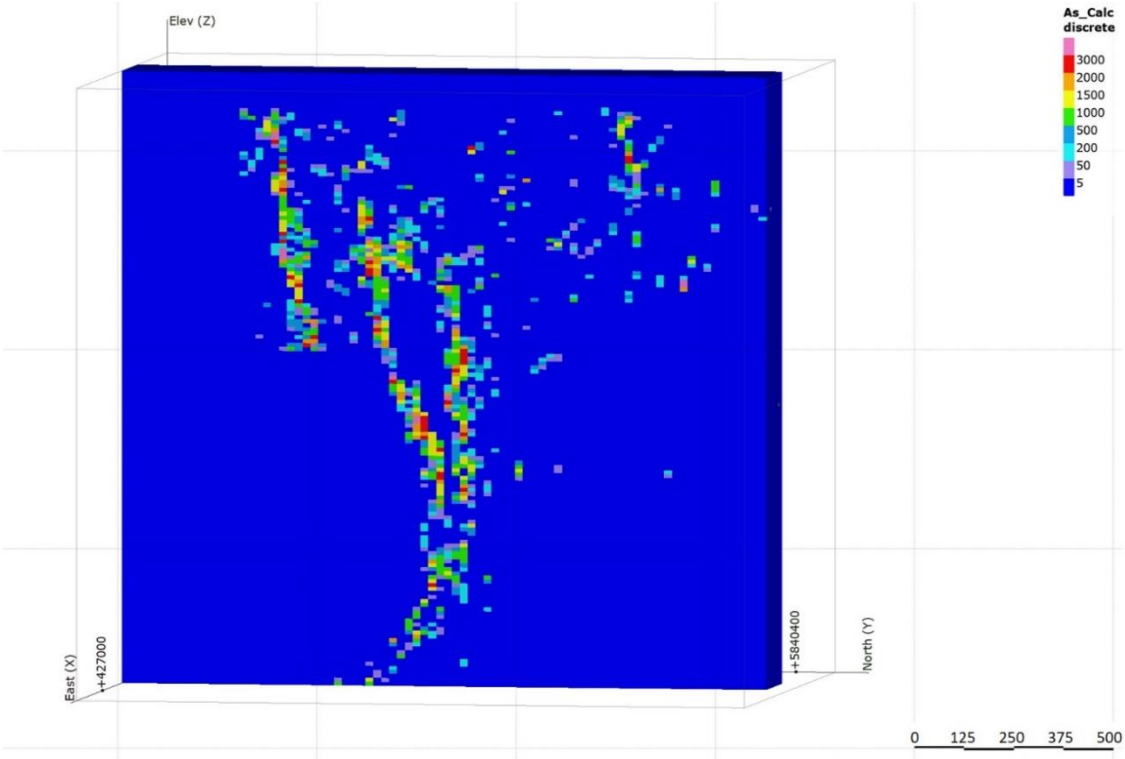


Figure. S113 Realization 3 of the block model of the arsenic grades along the footwall of the gold deposit.

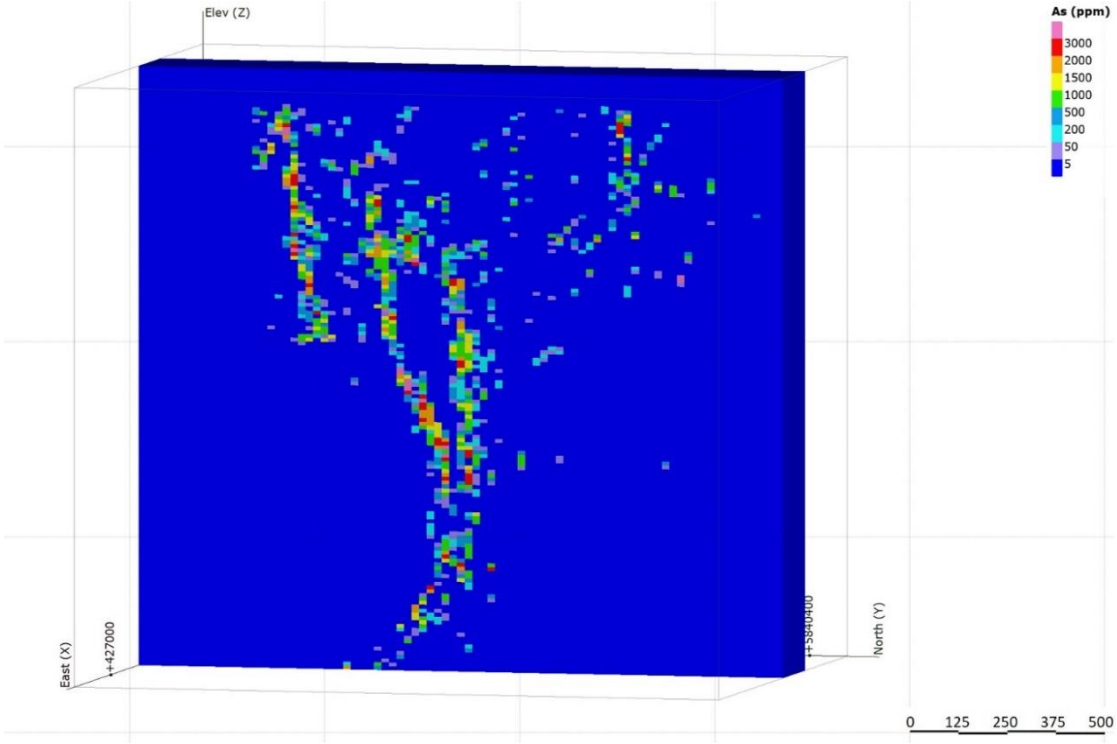


Figure. S114 Realization 4 of the block model of the arsenic grades along the footwall of the gold deposit.

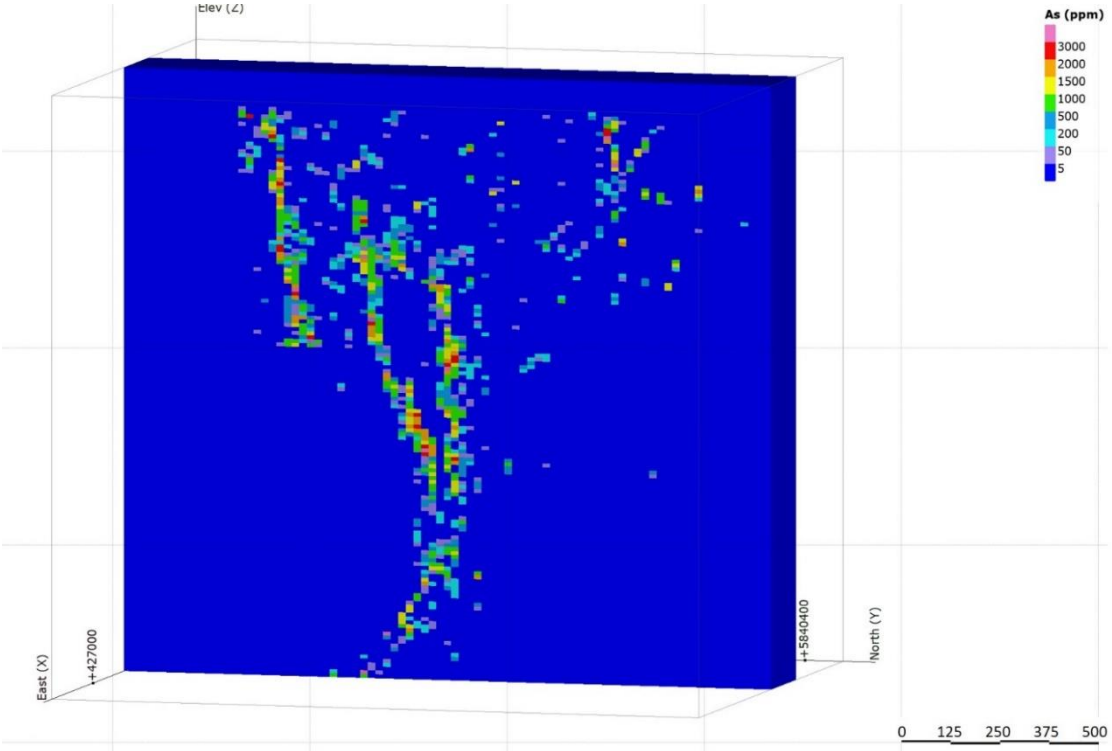


Figure. S115 Realization 5 of the block model of the arsenic grades along the footwall of the gold deposit.

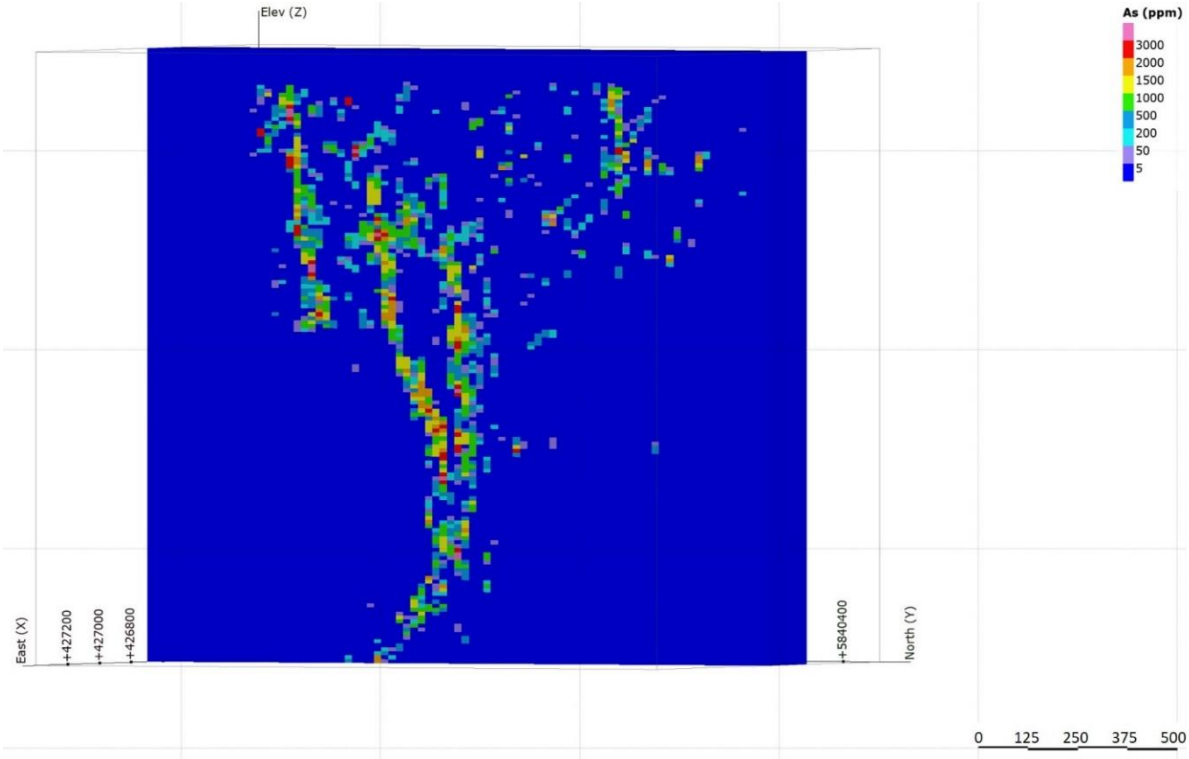


Figure. S116 Realization 6 of the block model of the arsenic grades along the footwall of the gold deposit.

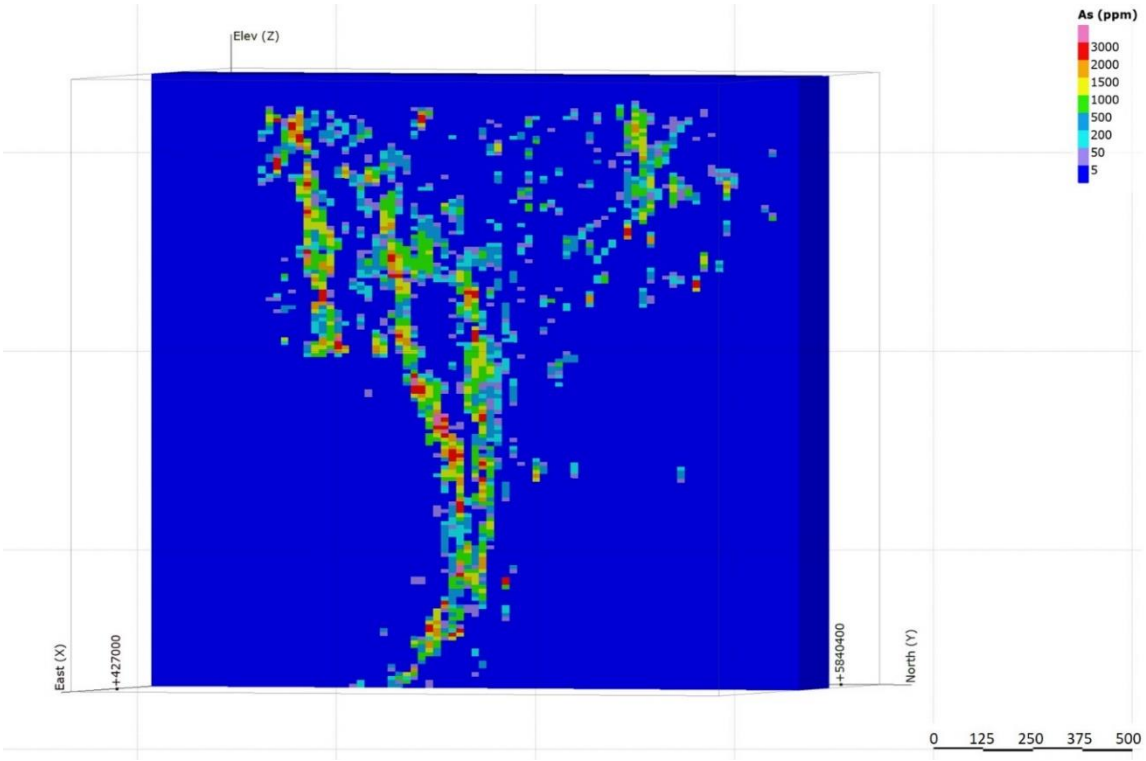


Figure. S117 Realization 7 of the block model of the arsenic grades along the footwall of the gold deposit.

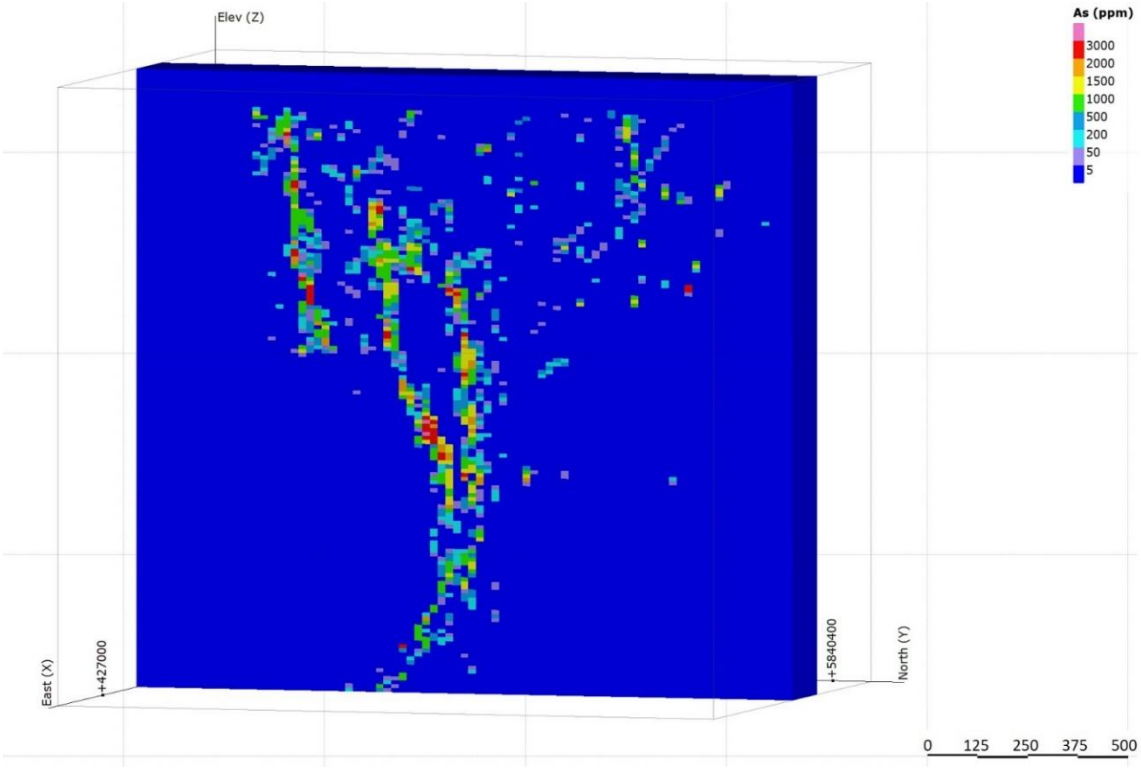


Figure. S118 Realization 8 of the block model of the arsenic grades along the footwall of the gold deposit.

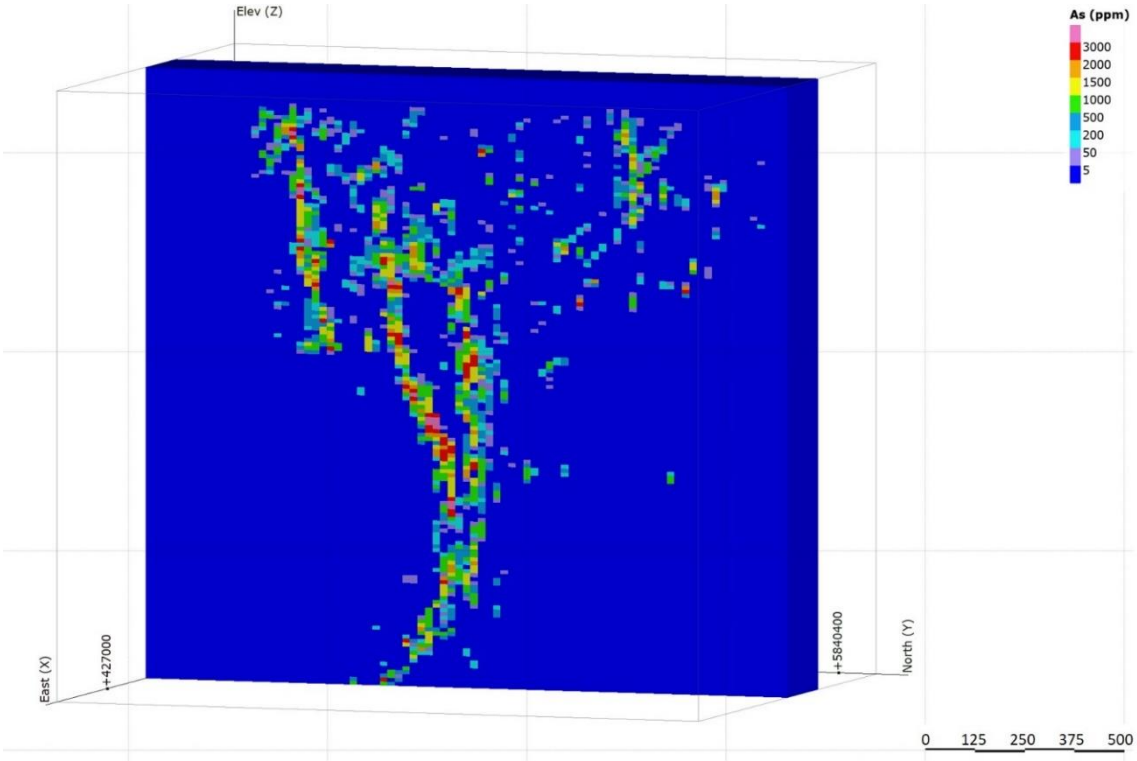


Figure. S119 Realization 9 of the block model of the arsenic grades along the footwall of the gold deposit.

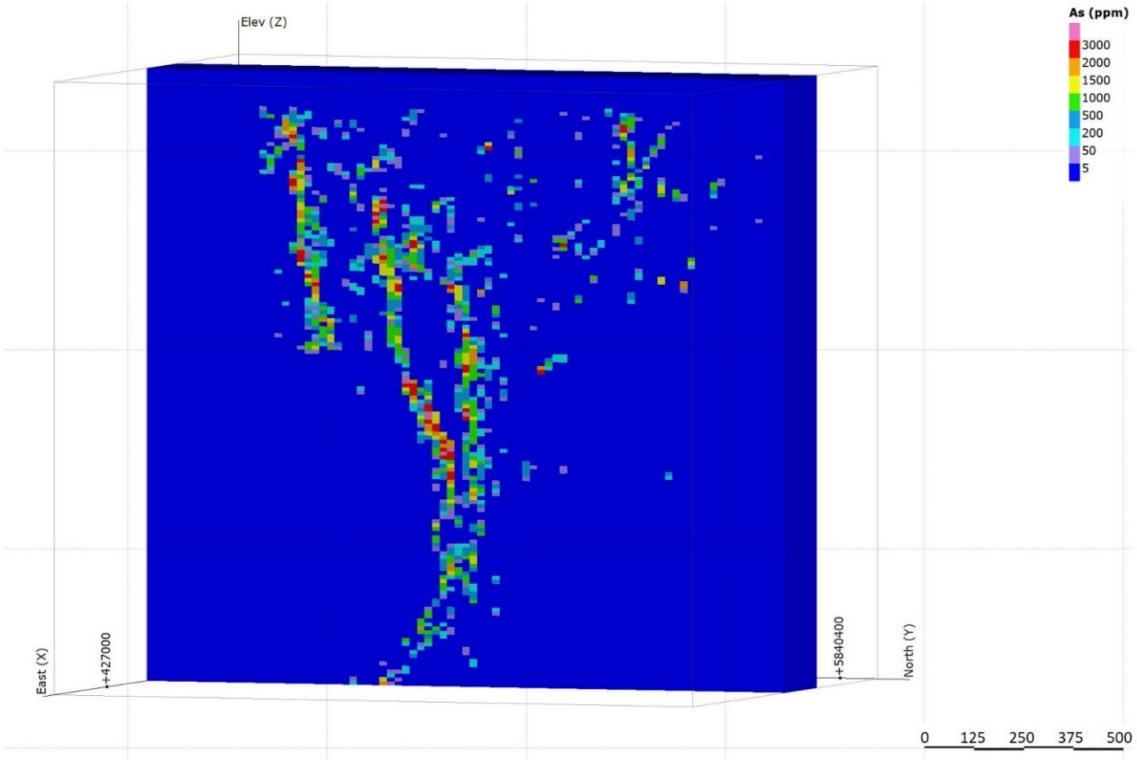


Figure. S120 Realization 10 of the block model of the arsenic grades along the footwall of the gold deposit.

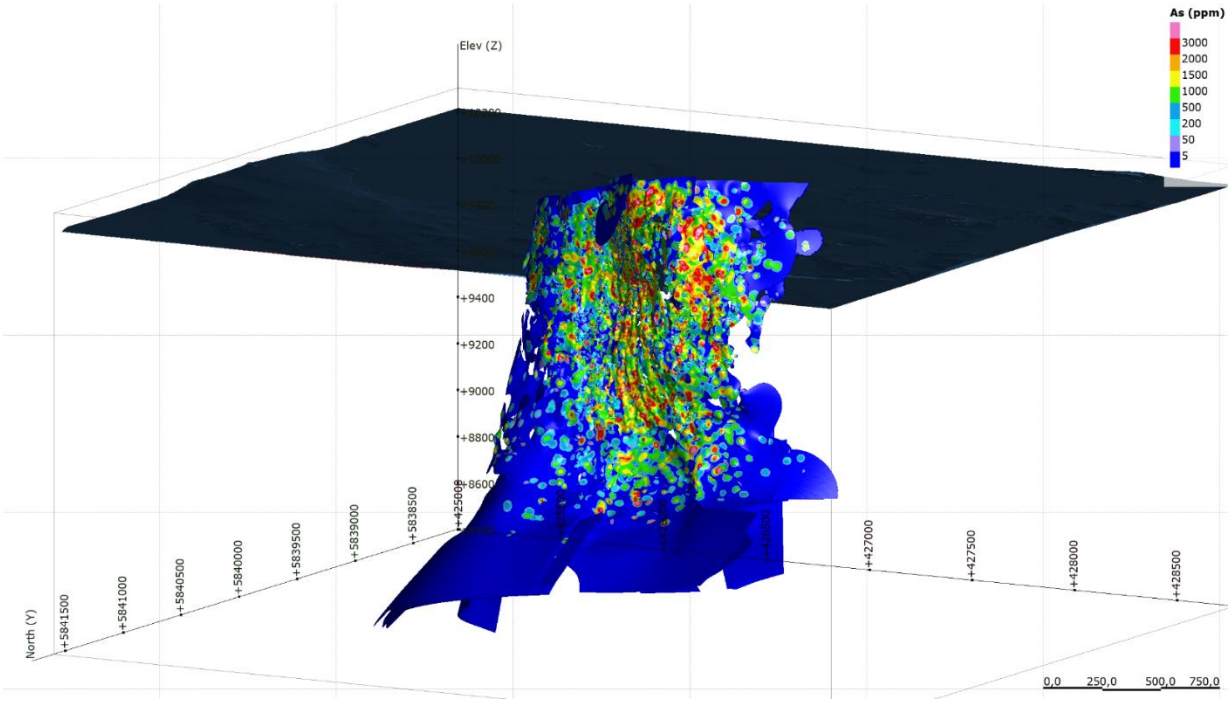


Figure. S121 Spatial relationship between the gold deposit and the arsenic grades in the realization 5.

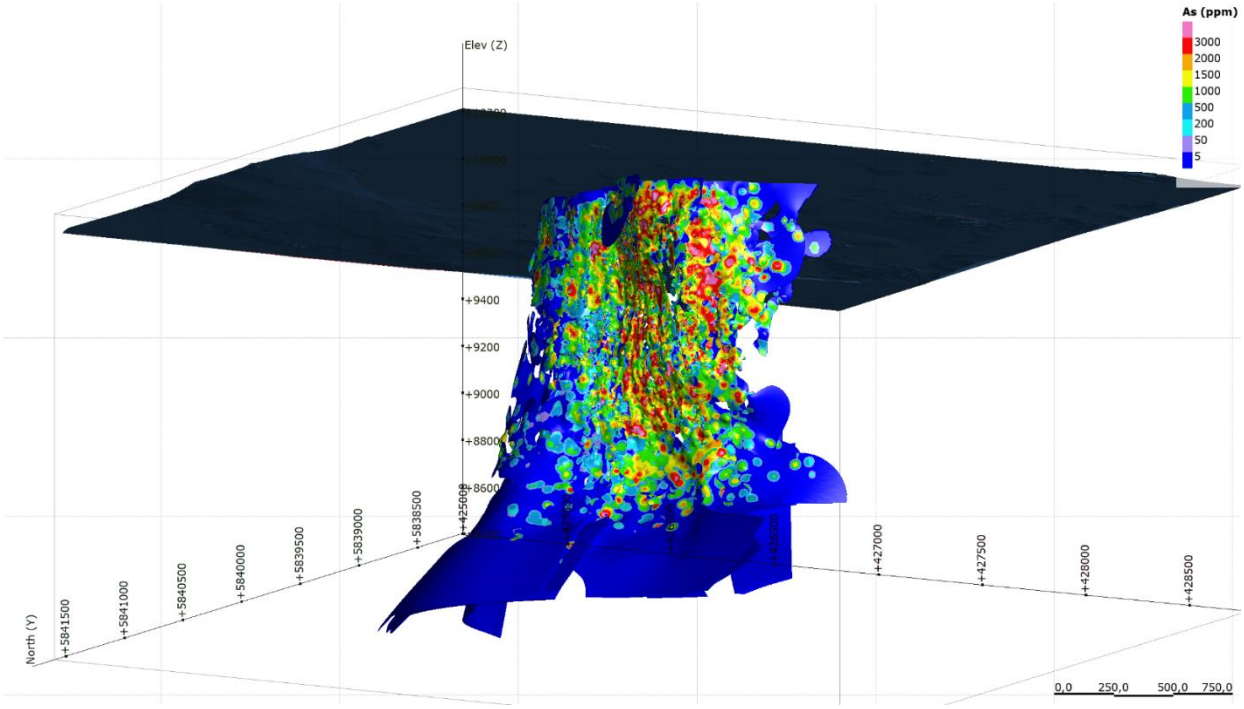


Figure. S122 Spatial relationship between the gold deposit and the arsenic grades in the realization 9.

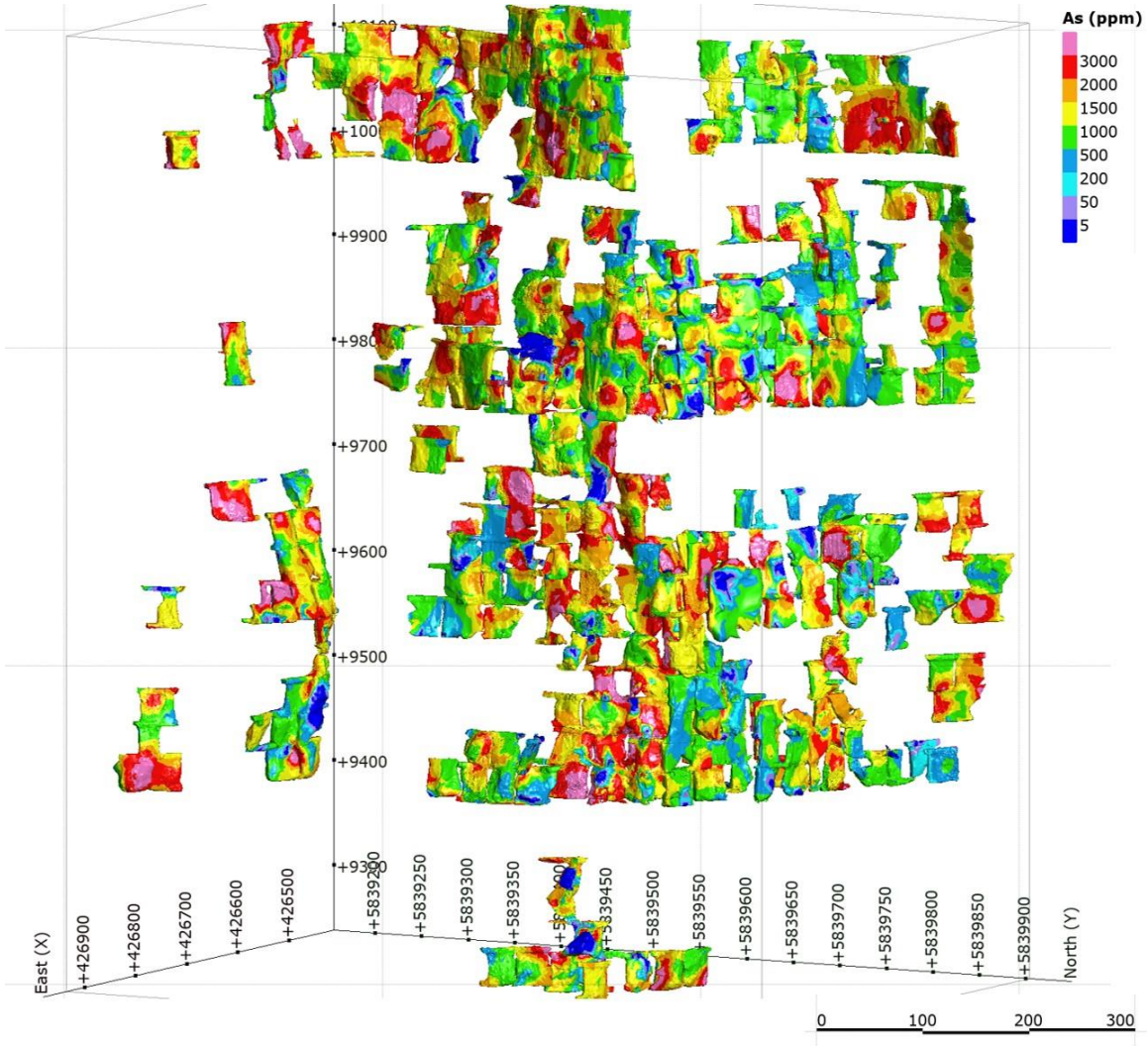


Figure. S123 The underground stopes assessed through the realization 2 of the spatial model.

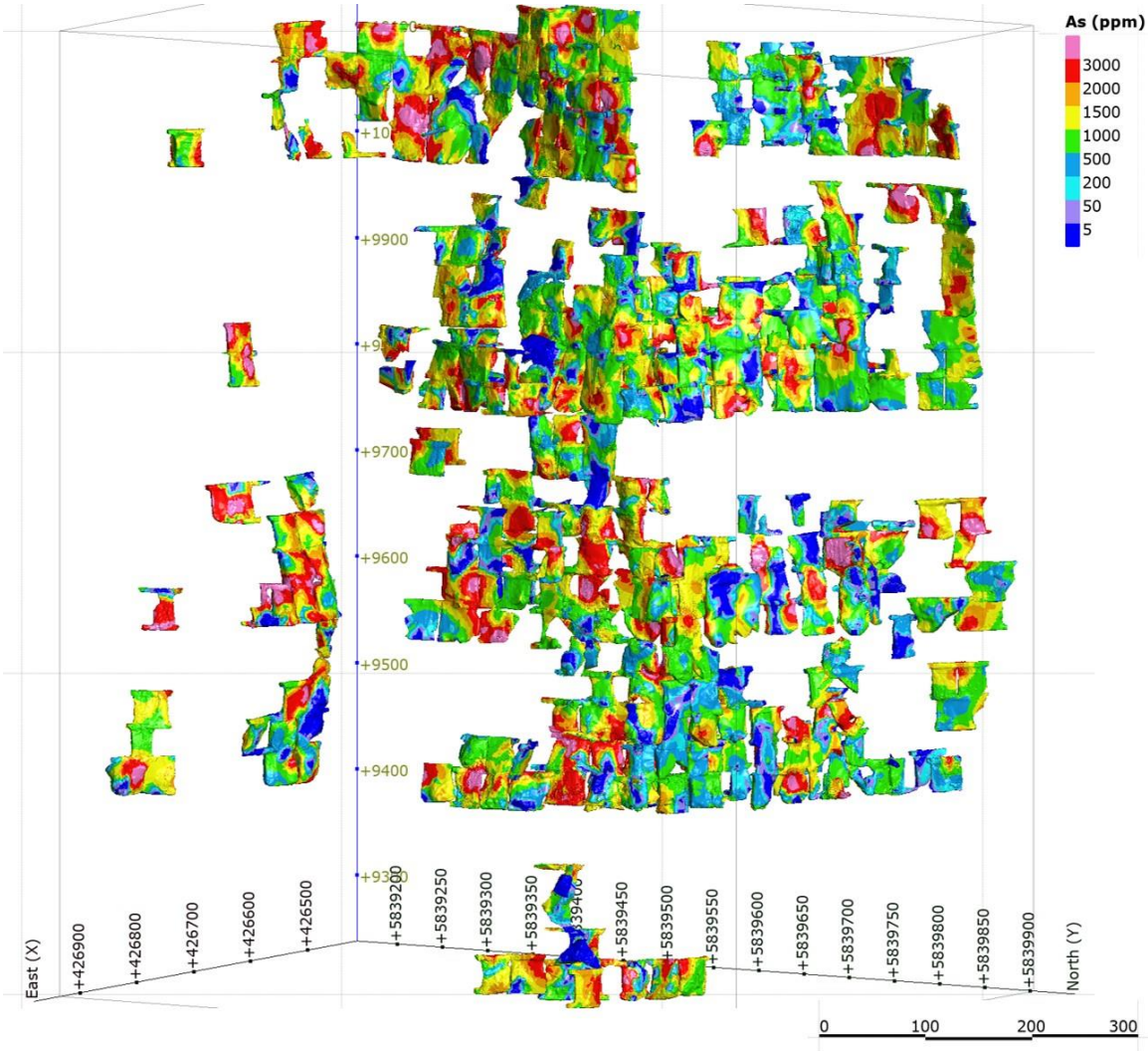


Figure. S124 The underground stopes assessed through the realization 3 of the spatial model.

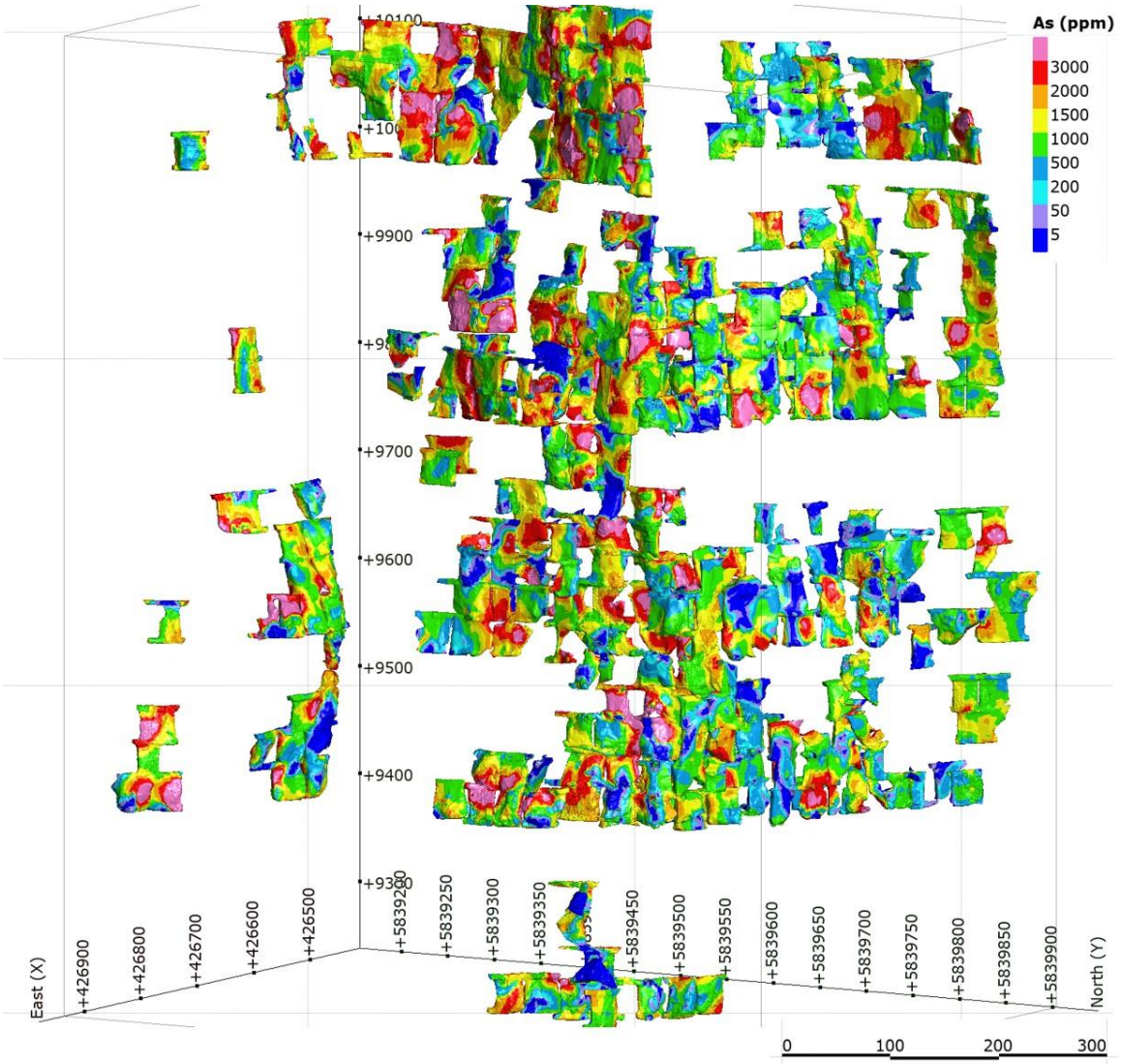


Figure. S125 The underground stopes assessed through the realization 4 of the spatial model.

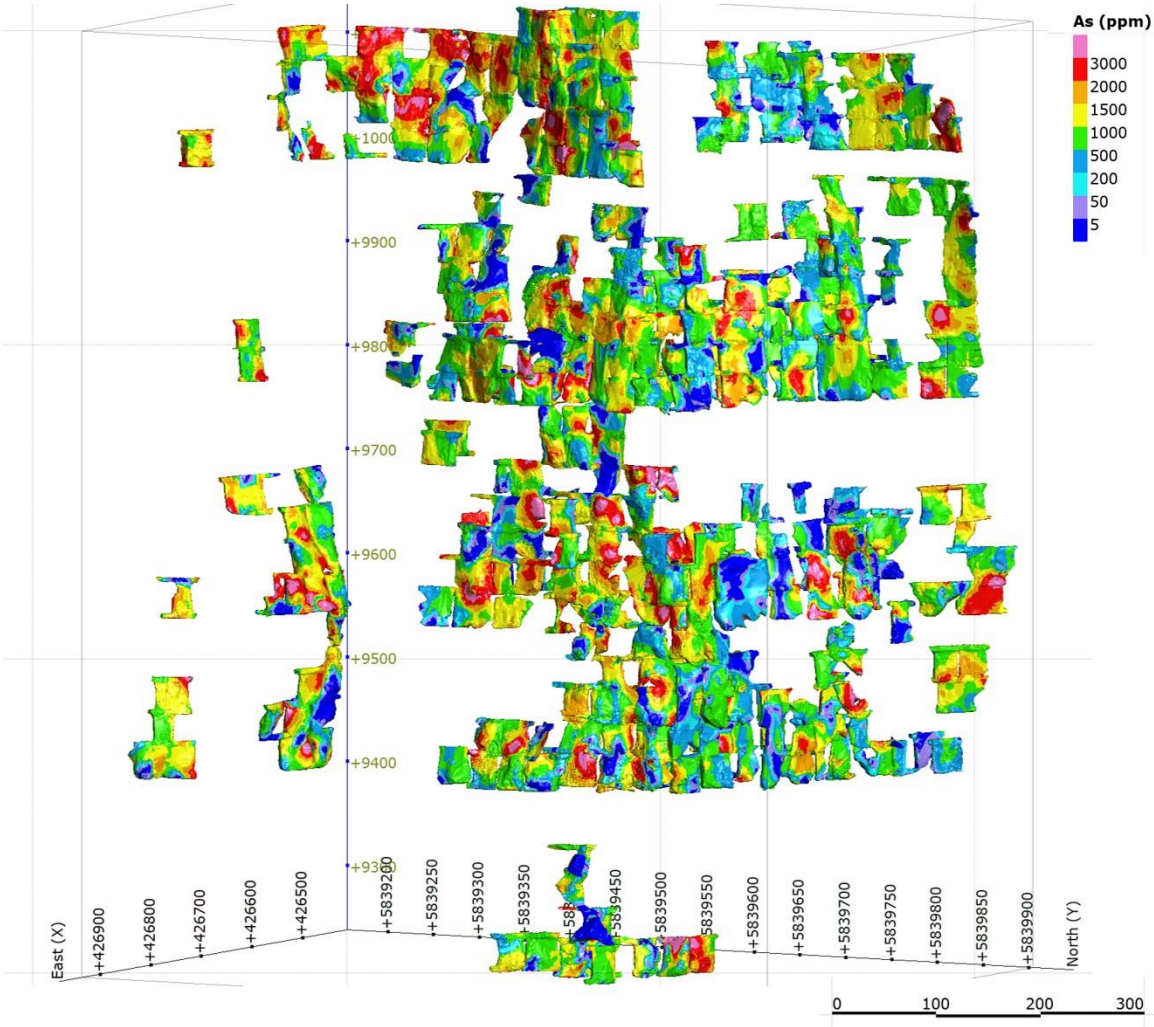


Figure. S126 The underground stopes assessed through the realization 5 of the spatial model.

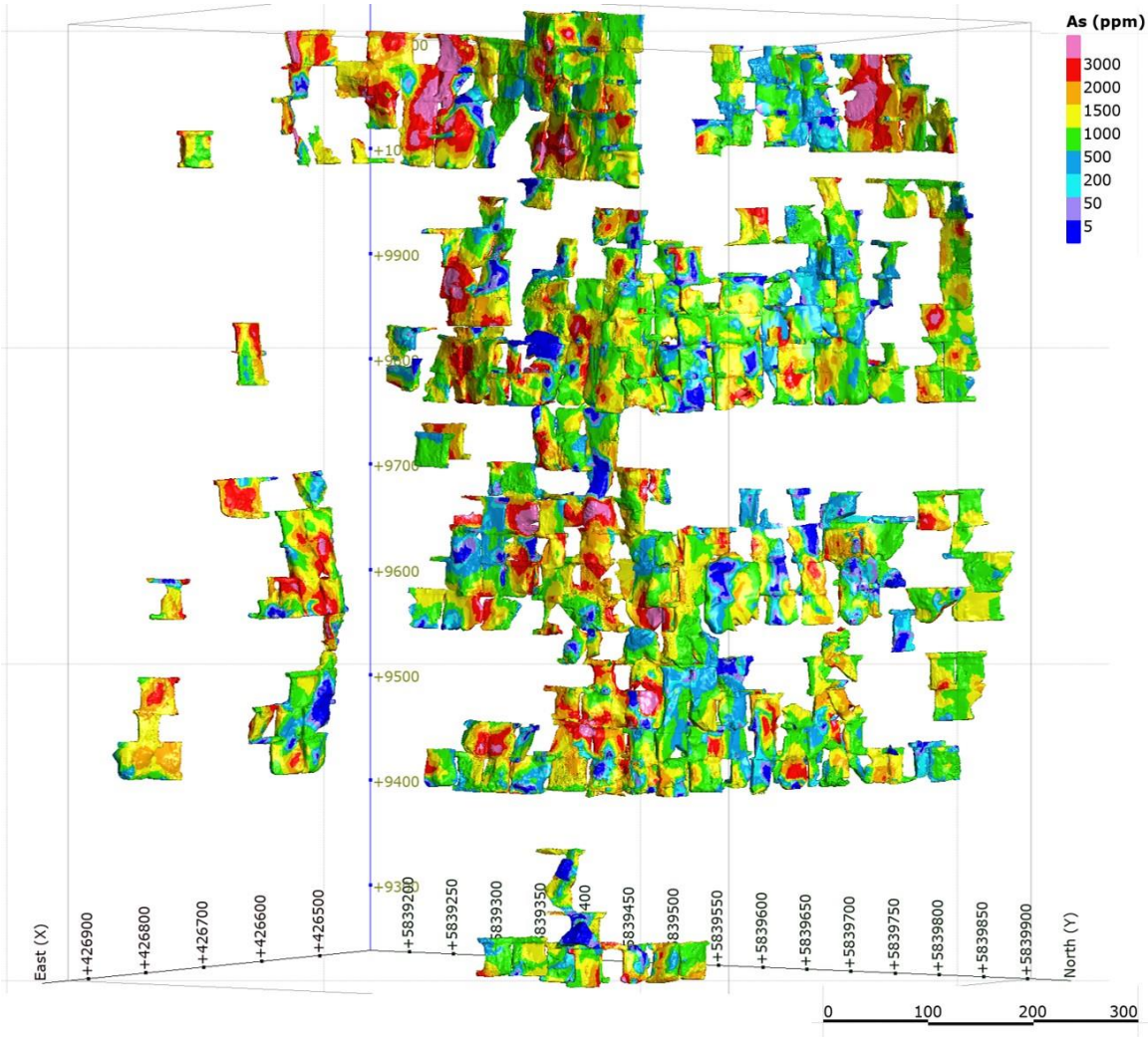


Figure. S127 The underground stopes assessed through the realization 6 of the spatial model.

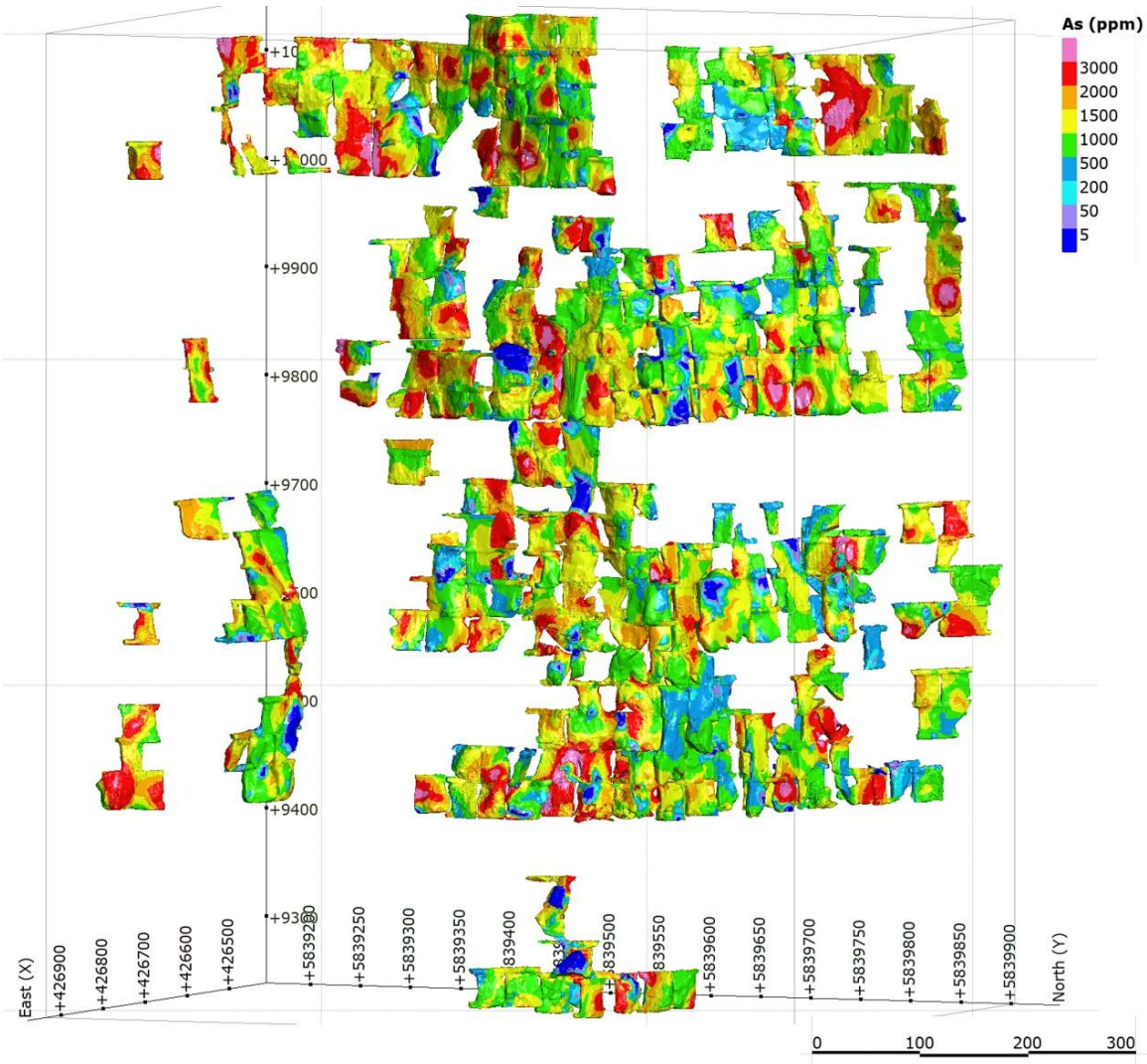


Figure. S128 The underground stopes assessed through the realization 7 of the spatial model.

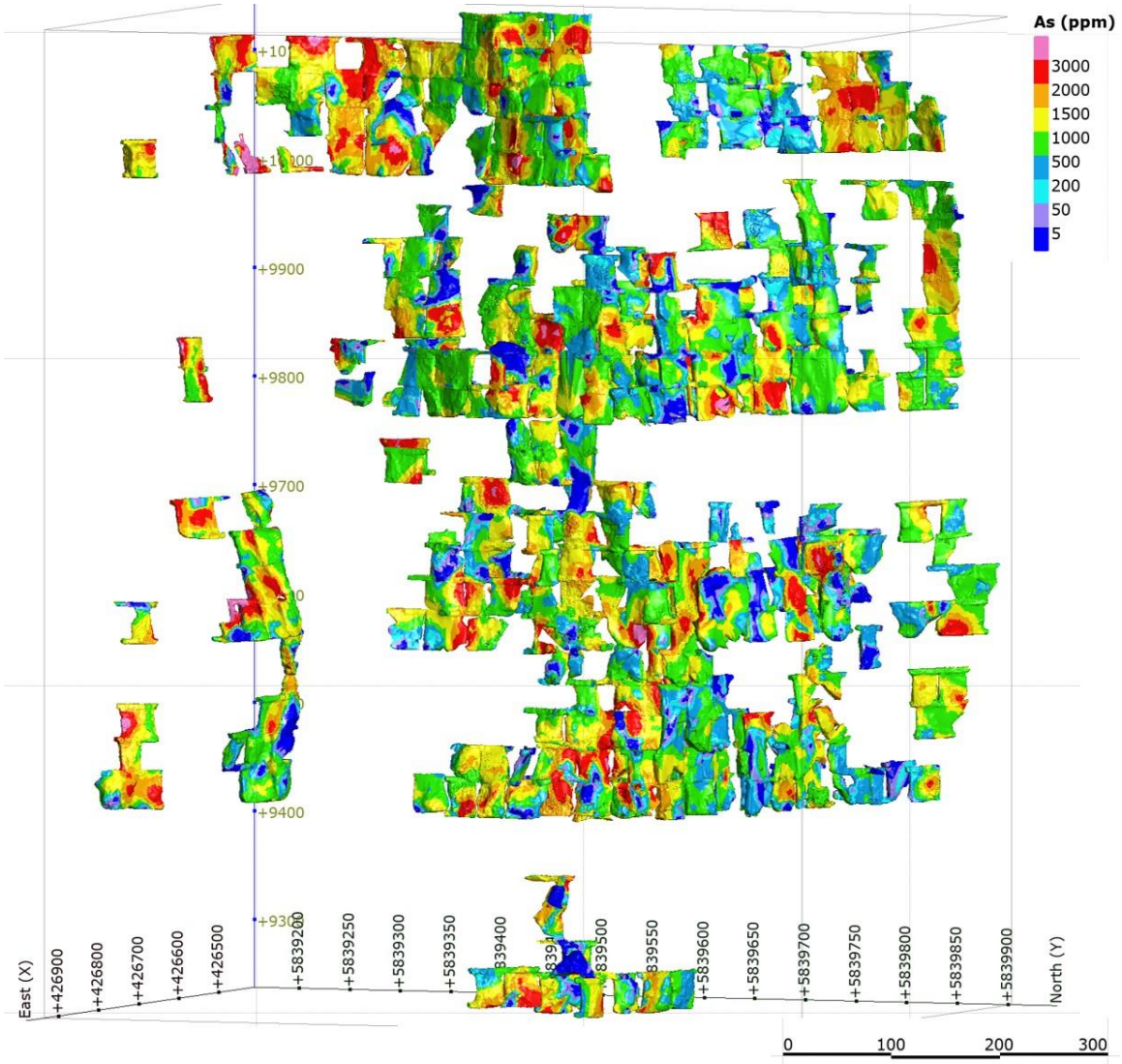


Figure. S129 The underground stopes assessed through the realization 8 of the spatial model.

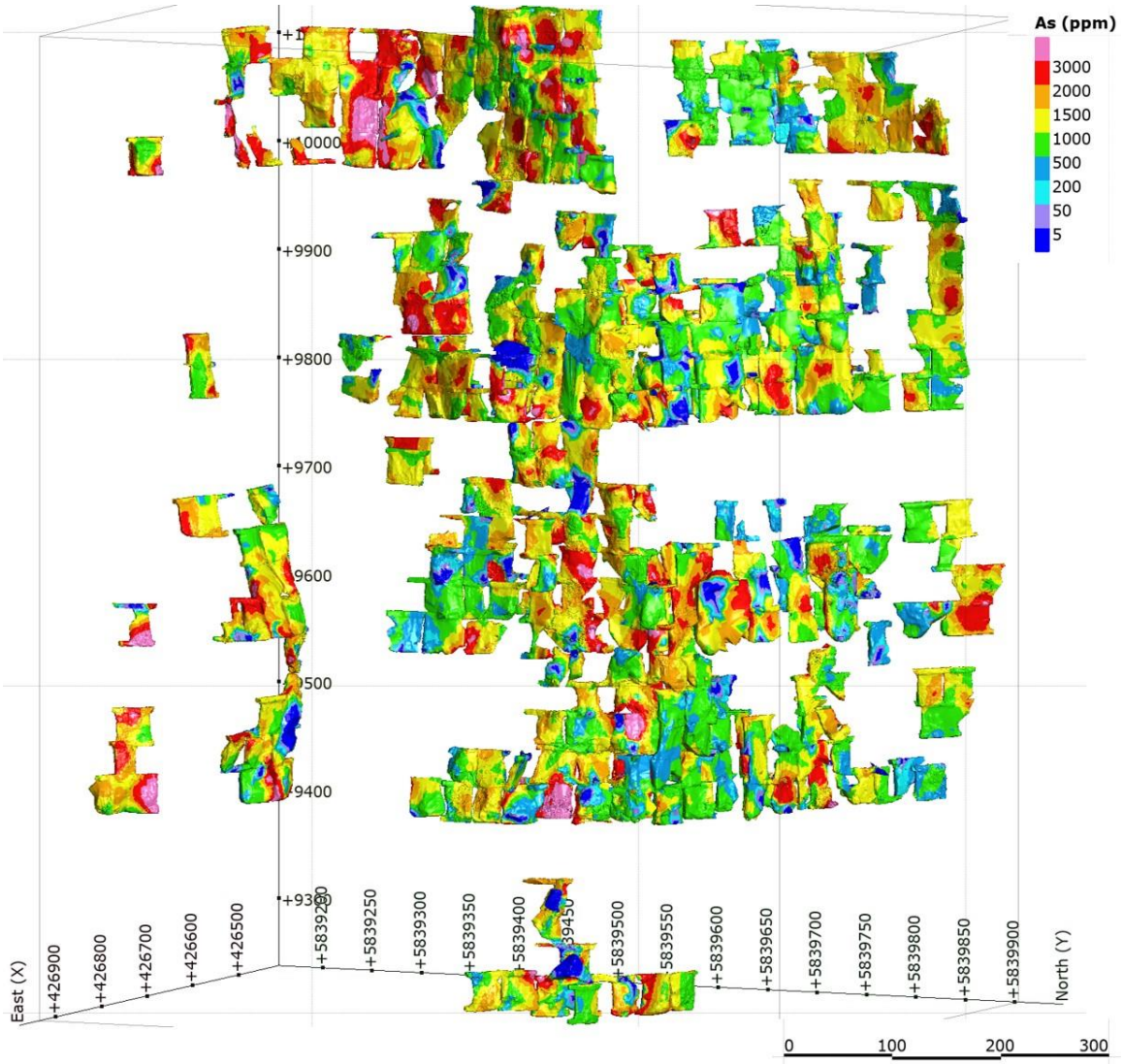


Figure. S130 The underground stopes assessed through the realization 9 of the spatial model.

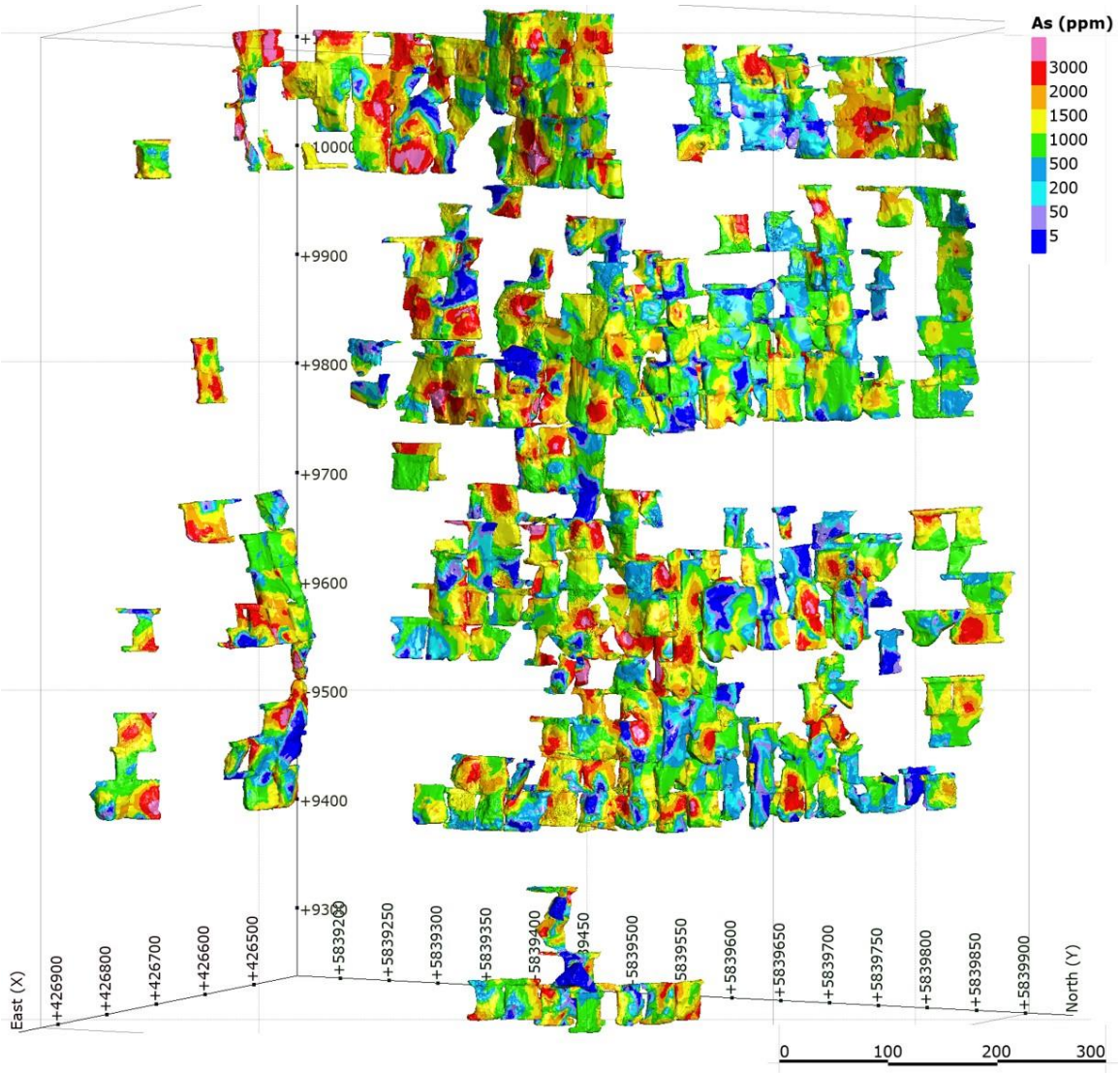


Figure. S131 The underground stopes assessed through the realization 10 of the spatial model.

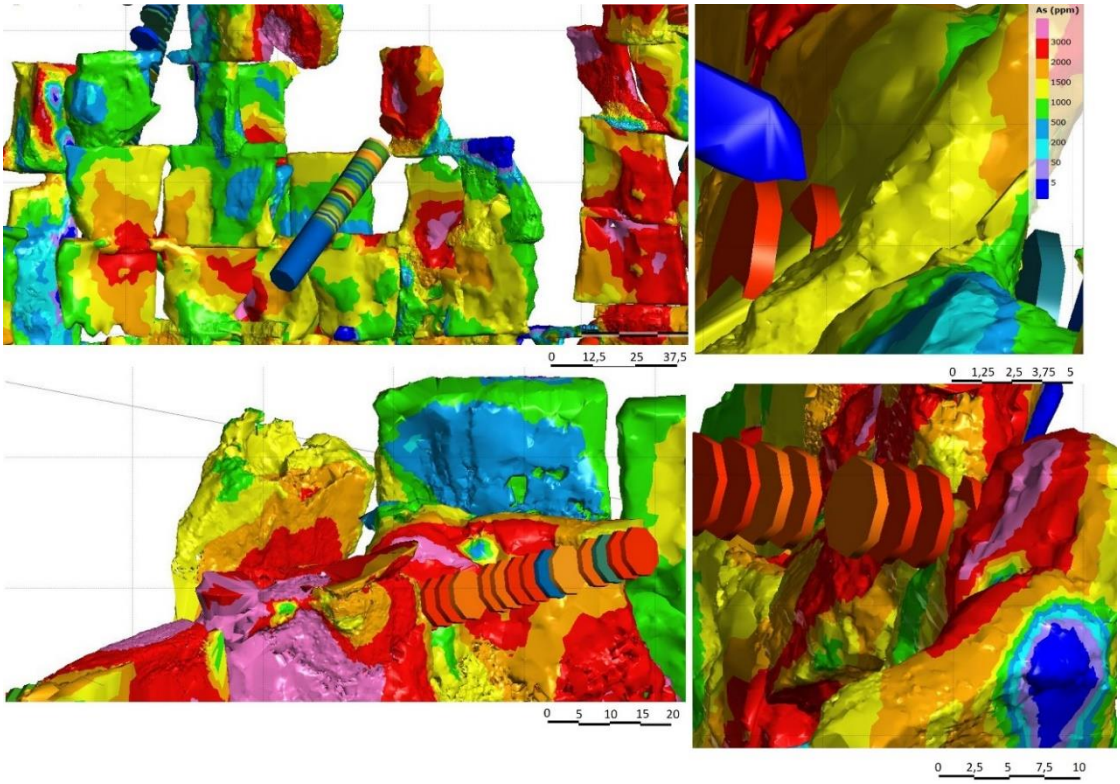


Figure. S132 The spatial intersections of the 3D spatial model (realization 2) and the chemical analyses performed on drill core samples.

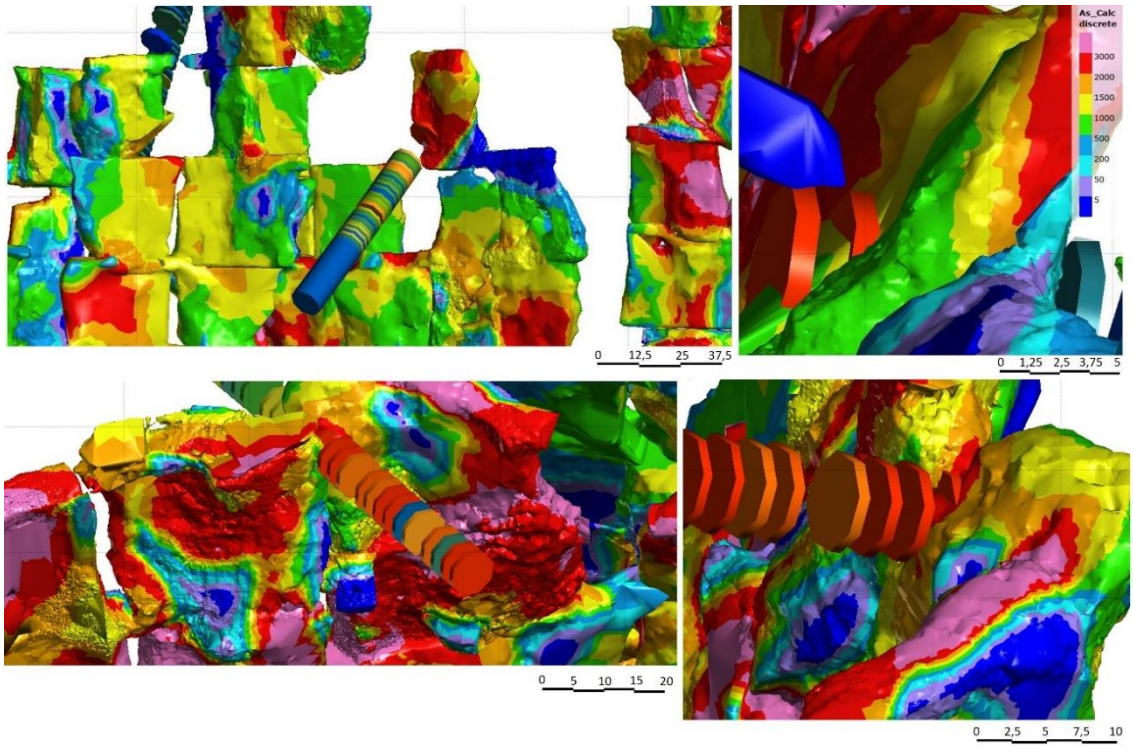


Figure. S133 The spatial intersections of the 3D spatial model (realization 3) and the chemical analyses performed on drill core samples.

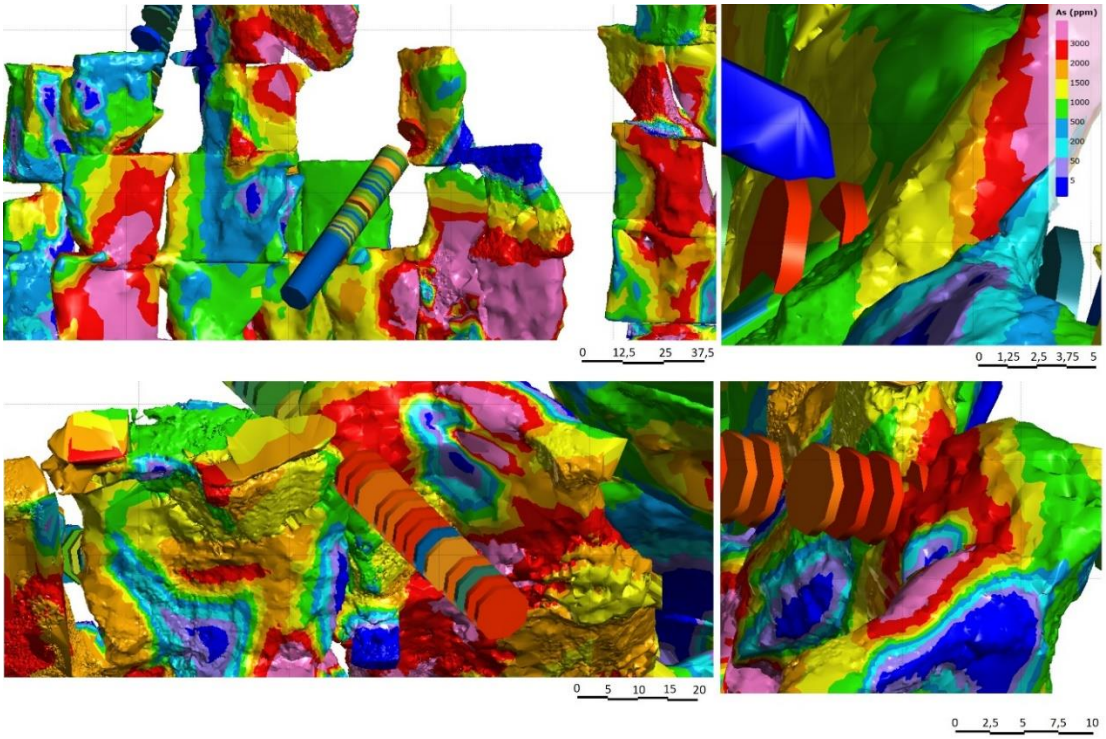


Figure. S134 The spatial intersections of the 3D spatial model (realization 4) and the chemical analyses performed on drill core samples.

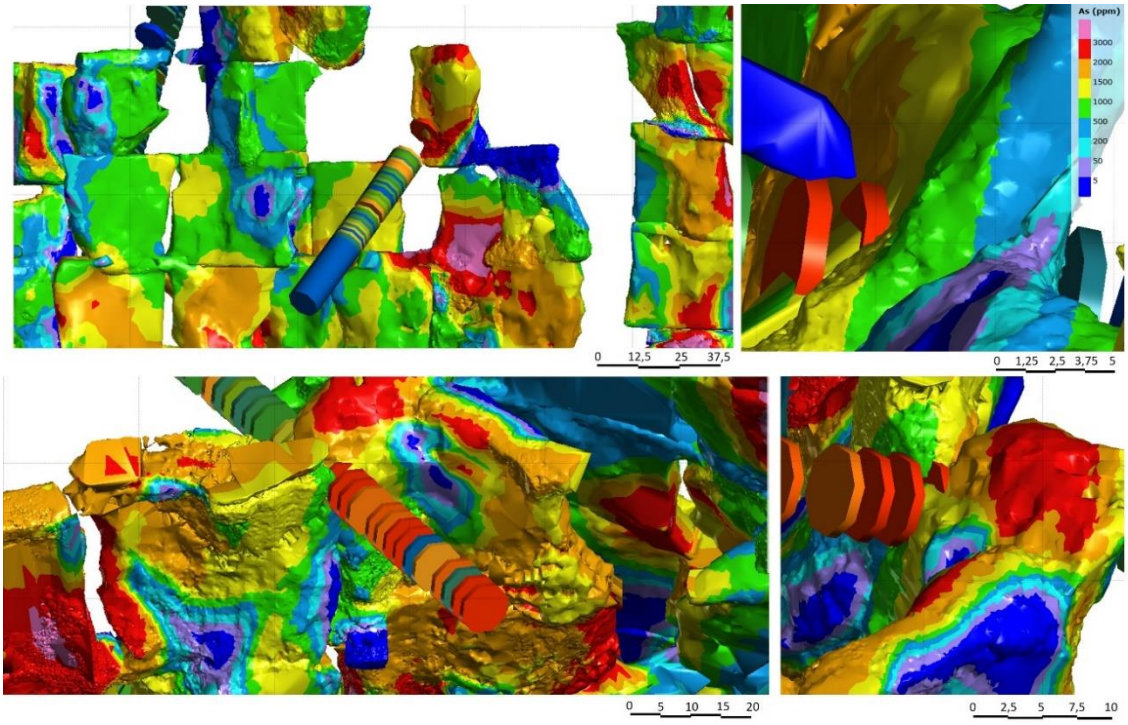


Figure. S135 The spatial intersections of the 3D spatial model (realization 5) and the chemical analyses performed on drill core samples.

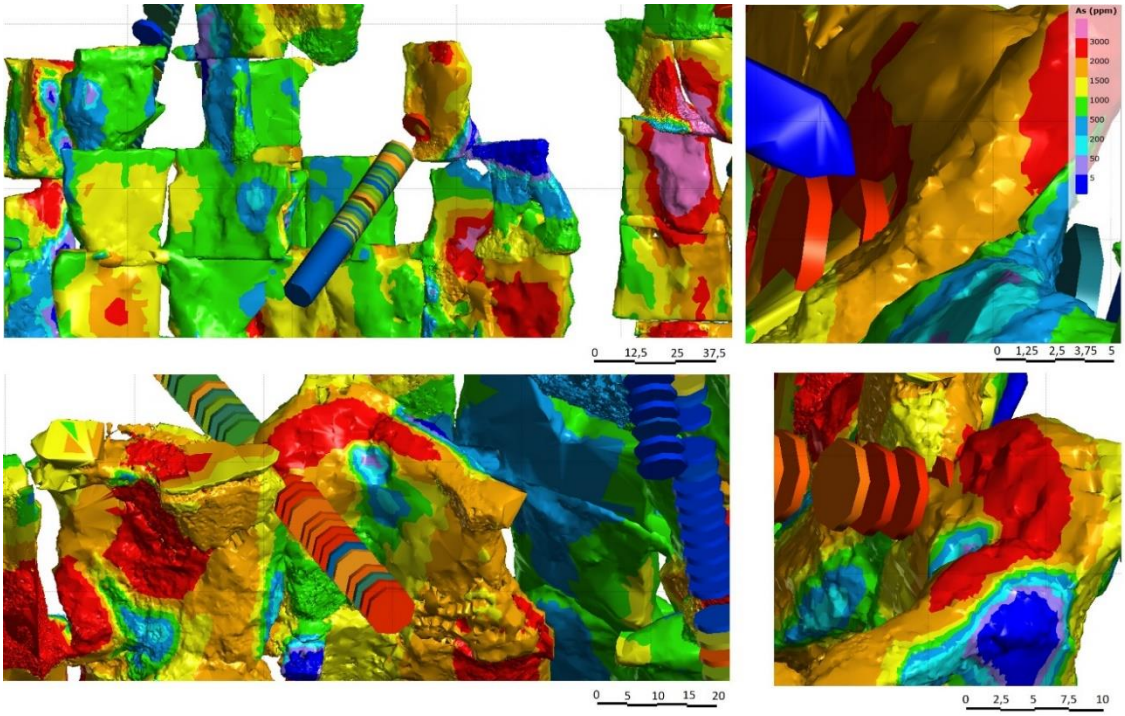


Figure. S136 The spatial intersections of the 3D spatial model (realization 6) and the chemical analyses performed on drill core samples.

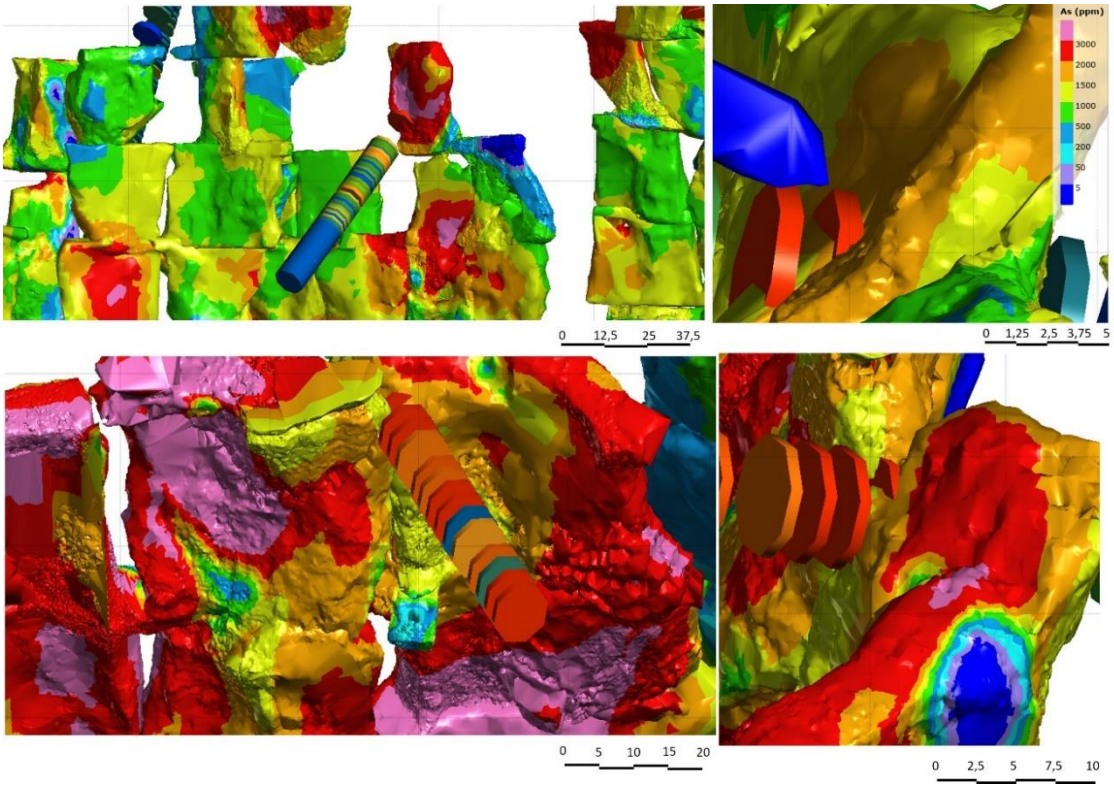


Figure. S137 The spatial intersections of the 3D spatial model (realization 7) and the chemical analyses performed on drill core samples.

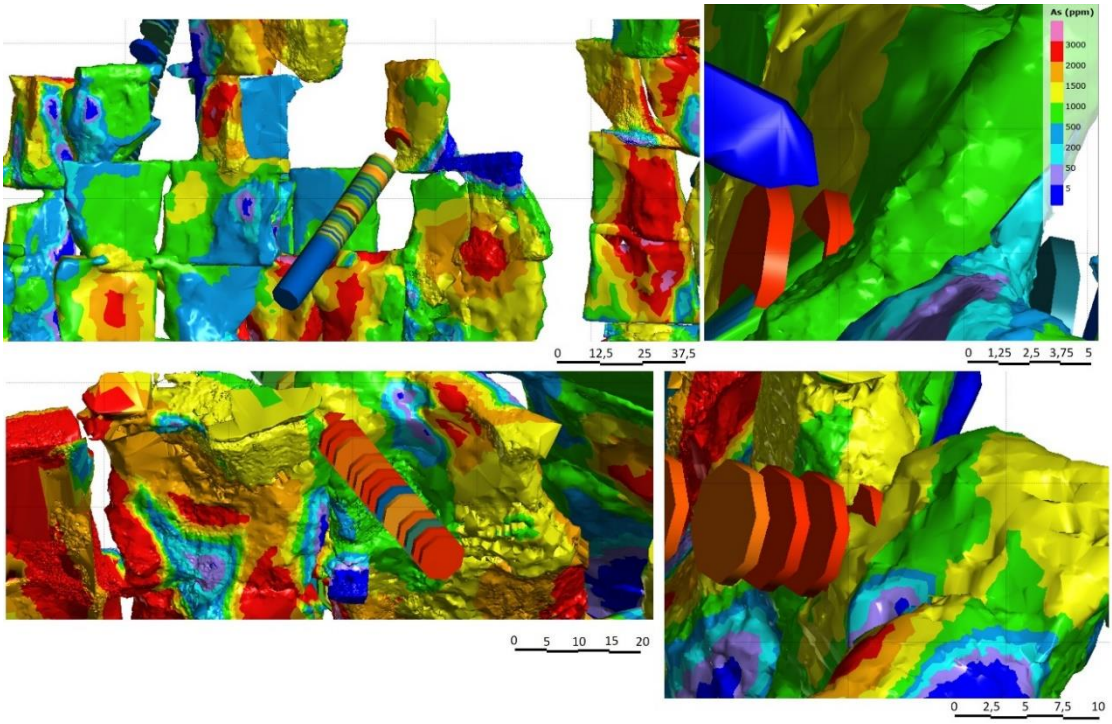


Figure. S138 The spatial intersections of the 3D spatial model (realization 8) and the chemical analyses performed on drill core samples.

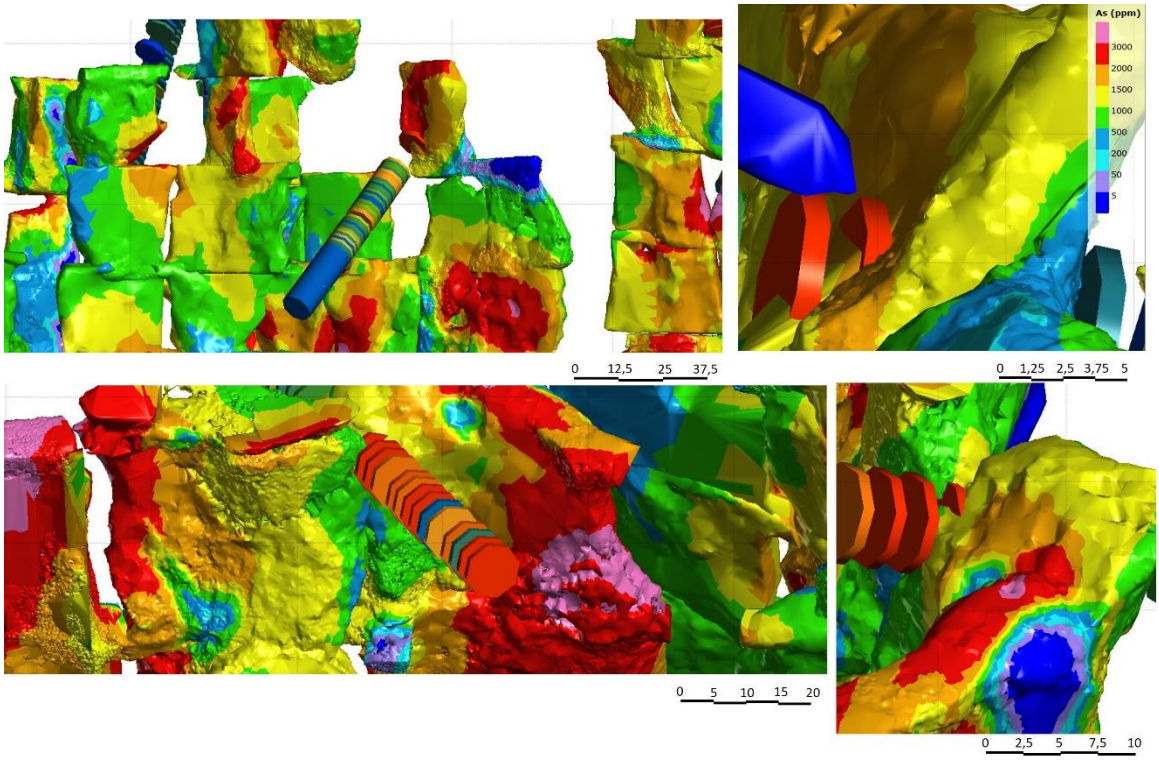


Figure. S139 The spatial intersections of the 3D spatial model (realization 9) and the chemical analyses performed on drill core samples.

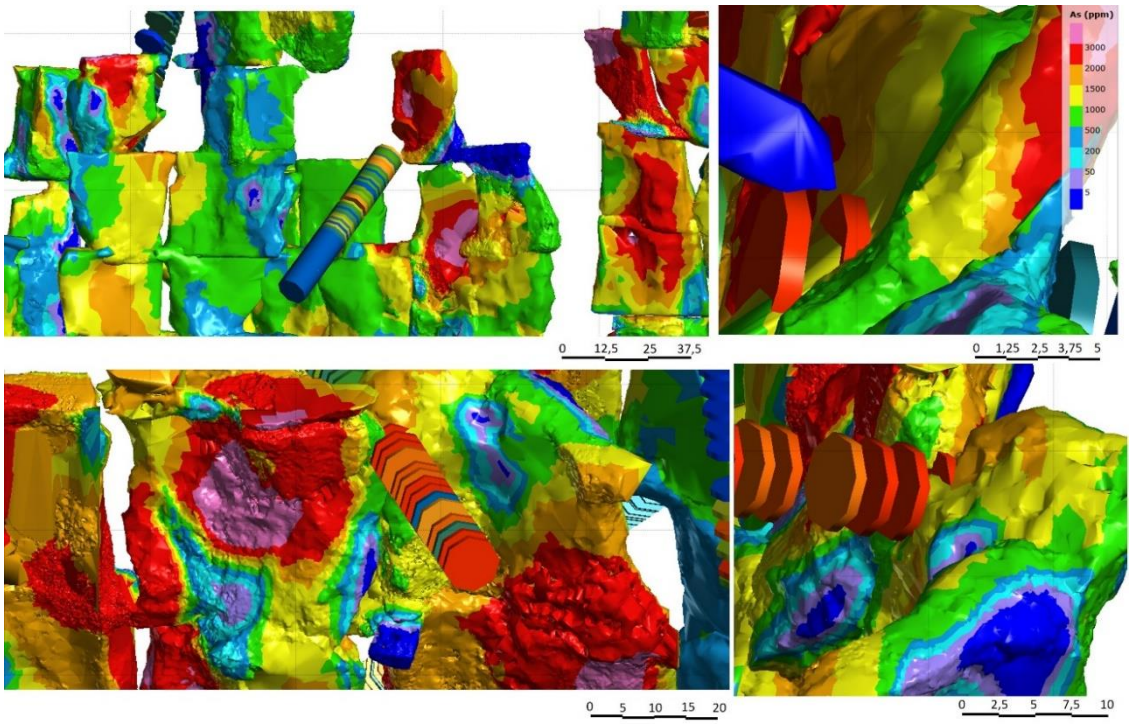


Figure. S140 The spatial intersections of the 3D spatial model (realization 10) and the chemical analyses performed on drill core samples.

APPENDIX B INCORPORATING KINETIC MODELING IN THE DEVELOPMENT STAGES OF HARD ROCK MINE PROJECTS

Research Institute on Mines and Environment (RIME),

Université du Québec en Abitibi-Témiscamingue, Rouyn-Noranda, Québec, Canada

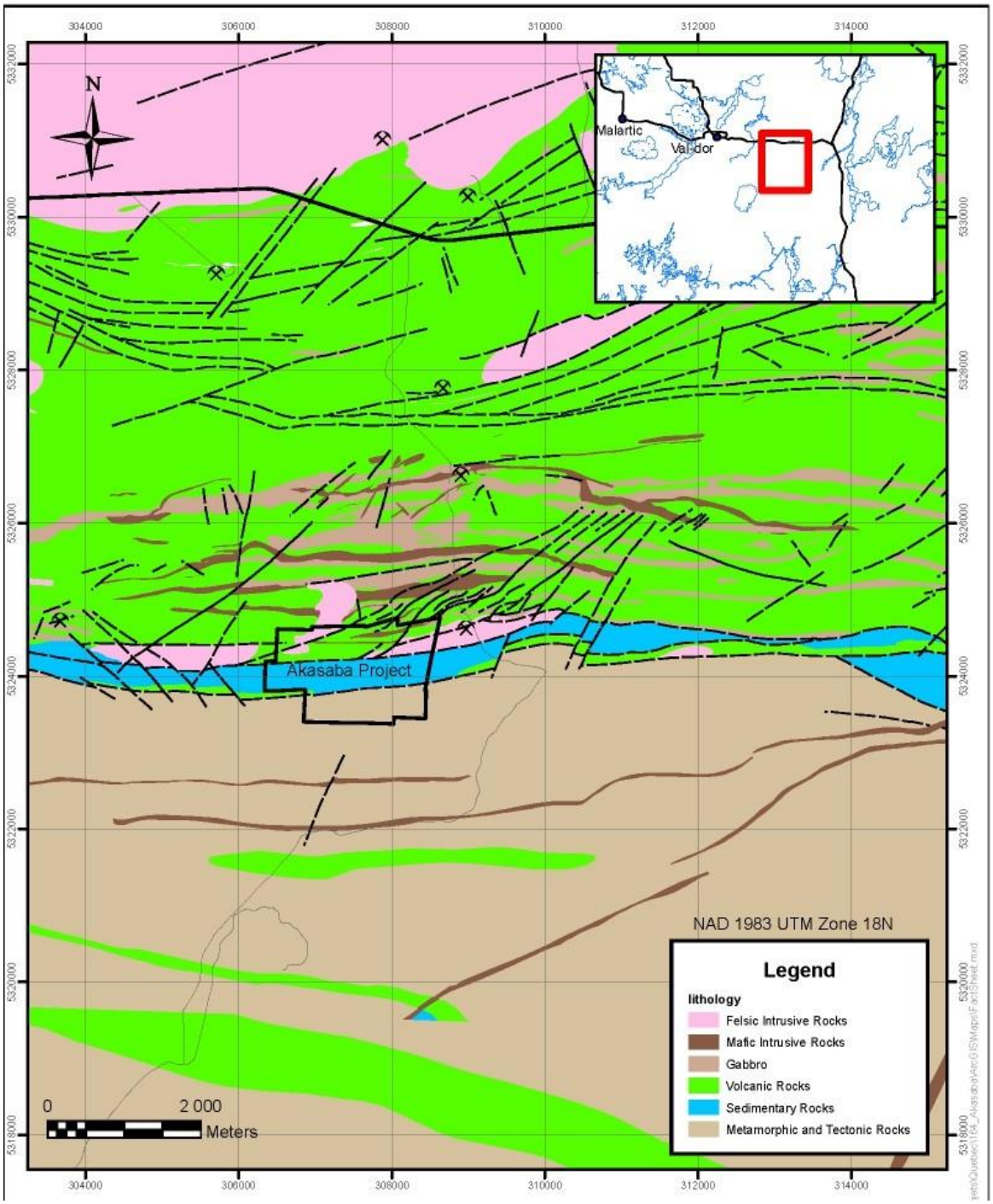


Figure S1. The geological framework of Akasaba West project (https://www.agnicoeagle.com)

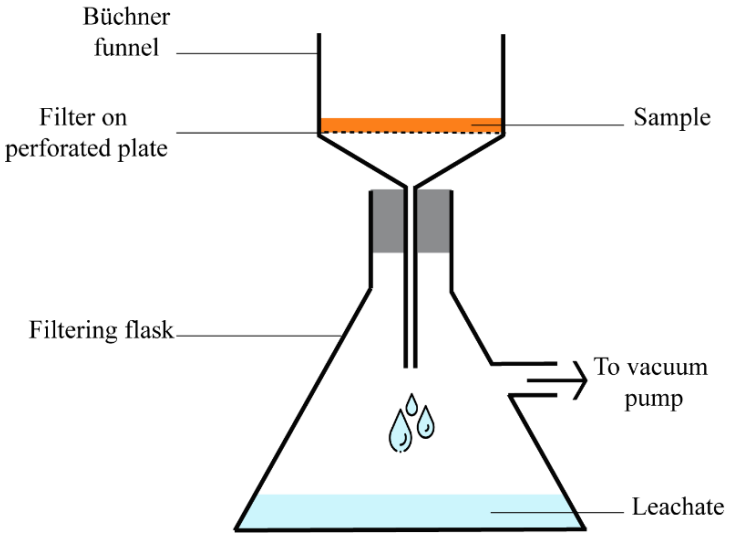


Figure S2. The experimental setup of weathering cell test.

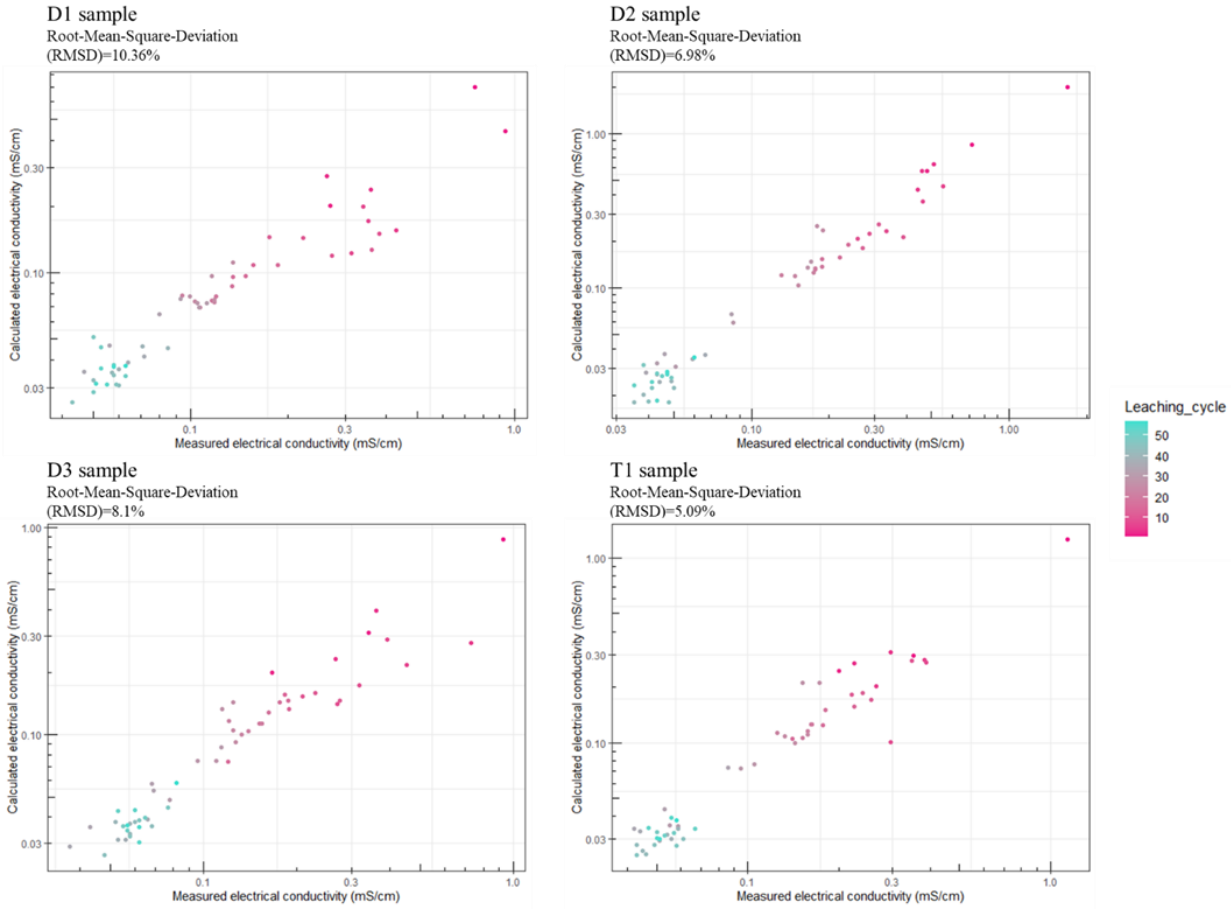


Figure S3. Comparison of calculated and measured electrical conductivity.

1. Model parameters

In order to perform 1D reactive transport in PHREEQC, the weathering cell height was discretized into 30 transport cells evenly distributed along a total height of 1 cm. A time step of 163296s with 100 shifts was chosen to achieve a total simulation time of 189 days that corresponds to the kinetic test duration. Amounts of reacting minerals in PHREEQC should be specified in moles (Parkhurst and Appelo, 2013). Eary and Williamson (2006) set forth a normalization basis for water-rock systems to compute initial molar amounts available for reaction with a specified mass of water ($m_{mineral}$):

$$m_{mineral}\left(\frac{\text{mole}}{\text{kg } H_2O}\right) = F_{\text{mineral}} \times \left(\frac{1-n}{n}\right) \times \left(\frac{\rho_{\text{solids}}}{\rho_{H_2O}}\right) \times \left(\frac{1000 \text{ g } H_2O}{1 \text{ kg } H_2O}\right) \times \left(\frac{1}{M_{\text{mineral}}}\right) \quad (1)$$

where F_{mineral} is the fractional content of the mineral in bulk sample, n is the fluid-filled porosity of the bulk sample, ρ_{solids} is the bulk solid density, ρ_{H_2O} is water density, and M_{mineral} is the molar mass of the mineral. The above-mentioned formula considers a water-rock system that contains 1 kg of water, as it is the default water mass used in PHREEQC. In the present study, the default water mass was changed to 50 g to match 50 ml of deionized water used as flushing solution throughout the kinetic test ($\rho_{H_2O} = 1\ \text{g/cm}^3$). Accordingly, the available molar amounts for reaction with $50\ \text{g}\ H_2O$ were calculated and used within the KINETIC keyword block of PHREEQC.

Water-rock interaction involves the surface area of solids available per volume of water (SA/V) as a key parameter. It is computed as a function of the initial molar amounts ($m_{mineral}$) and the estimated geometric specific surface area (S_{Geo}) or BET measurement of specific surface area (S_s) (Embile Jr *et al.*, 2019):

$$\text{Surface area}\left(\frac{m^2}{dm^3}\right) = S_{Geo} \times M_{\text{mineral}} \times m_{\text{mineral}} \times X_{\text{mineral}} \quad (2)$$

$$\text{Surface area}\left(\frac{m^2}{dm^3}\right) = S_s \times M_{\text{mineral}} \times m_{\text{mineral}} \times X_{\text{mineral}} \quad (3)$$

where X_{mineral} is the volumetric fraction of the mineral. S_{Geo} was estimated using the procedure described by Chapuis and Aubertin (2003). Samples were loosely placed in a Buchner funnel at an estimated porosity of 0.6. The average volumetric flow rate in the four weathering cells was set at $2x10^{-6}$ L/s, resulting in a residence time of 7h. The residence time was slightly increased in the

simulation from 4h±0.5 to 7h, as a portion of the recovered filtrates was retained even after applying suction. The effect of residence time on the kinetic reactions will be covered later.

2. Equilibrium reactions

PHREEQC was designed to cope with a large range of geochemical calculations in saturated medium (Parkhurst and Appelo, 2013). The conceptual model was intended to circumvent PHREEQC limitations with respect to unsaturated systems. Setting an unlimited supply of O_2 and CO_2 in mobile and immobile cells is suitable for kinetically controlled unsaturated systems. This alternative was previously employed by Embile Jr *et al.* (2019) to simulate column tests; also Nicholson *et al.* (2003)Nicholson *et al.* (2003)Nicholson *et al.* (2003)Nicholson *et al.* (2003)Nicholson *et al.* (2003)Nicholson, *et al.* [5] utilized an open system approach to assess the environmental footprint of a rock stockpile. Thus, equilibrium reactions with the atmosphere ($\log [p(O_2)] = -0.7$ and $\log [p(CO_2)] = -3.5$) were embedded at ambient temperature. The Minteq.v4 database supplied with PHREEQC package was used to carry out mass balance and mass-action calculations.

3. Abiotic kinetic rates

The general rate expression (R_k) for kinetic modeling in PHREEQC is as follows:

$$R_k = r_k \frac{A_0}{V} \left(\frac{m}{m_0}\right)^n \qquad (4)$$

where r_k is the specific rate (mol/m^2/s), A_0 is the initial surface area of the solid (m^2), V is the volume of the solution (kgw), m_0 is the initial moles of solid, m is the moles of solid after a certain time of kinetic reaction, n is the shape factor equal to 0.67 for uniformly dissolving cubes and spheres, and $\left(\frac{m}{m_0}\right)^n$ considers the surface area shrinkage throughout the mineral dissolution (Parkhurst and Appelo, 2013). As the Akasaba West project is still in the development stage, no site-specific rates were available. Therefore, monomineral specific rate expressions from literature were used to simulate the weathering cells. Opting for specific rates from literature aimed to: i) assess their reliability for a mixture of minerals and their relevance for the upstream geochemical assessment, and ii) provide prompt scoping surveys during data-limited situations.

Chalcopyrite was present as thin disseminations and could result in Cu lixiviation. However, throughout previous kinetic testing Cu concentrations remained below or slightly above the detection limit (Vermette, 2018). There are no published chalcopyrite rate laws that describe its

oxidation by O_2 alone. However, Kimball *et al.* (2010) defined a nonoxidative dissolution rate law in the presence and absence of O_2:

$$r_k = 10^{1.88} e^{\frac{-48100}{RT}} [H^+]^{0.8} [Fe^{3+}]^{0.42} \quad (5)$$

where R is the gas constant (J/mol/K) and T is temperature (K). This rate law is applicable for pH values less than 3. As Cu concentrations from kinetic tests were expected to remain below or slightly above the detection limit, the chalcopyrite rate law was not included in the simulation. Despite the shortcomings related to the nonoxidative dissolution rate law of chalcopyrite, it was used only during the parametric analysis to approach Cu lixiviation scenarios.

The generic form of the specific rate is as follows:

$$r_k = \begin{pmatrix} k_{H^+} e^{\frac{-E_{H^+}}{R}\left(\frac{1}{T}-\frac{1}{298.15}\right)} [H^+]^{n_1} (1-\Omega^{p_1})^{q_1} + \\ k e^{\frac{-E}{R}\left(\frac{1}{T}-\frac{1}{298.15}\right)} (1-\Omega^{p_2})^{q_2} + \\ k_{OH^-} e^{\frac{-E_{OH^-}}{R}\left(\frac{1}{T}-\frac{1}{298.15}\right)} [H^+]^{n_2} (1-\Omega^{p_3})^{q_3} + \end{pmatrix} \quad (6)$$

where k_{H^+}, k_{OH^-}, and k are rate constants for acidic, alkaline, and neutral conditions, respectively, E_{H^+}, E, and E_{OH^-} are the activation energies in acidic, alkaline, and neutral conditions, respectively, n_i denotes reaction order (n_2 is negative and could be positive when alkaline mechanism equation is expressed in function of OH^-), Ω is the mineral saturation index, and p_i and q_i are dimensionless empirical parameters to take into account chemical affinity that slows down the dissolution rate at near-equilibrium conditions. Palandri and Kharaka (2004) compiled a large set of rate expressions by fitting a wide range of experimental data to the generic equation. Their experimental database covers oxic and anoxic conditions, as O_2 could have a slight indirect effect on dissolution rates when iron is present in gangue minerals.

References

Chapuis, R.P. and Aubertin, M. (2003). On the use of the Kozeny Carman equation to predict the hydraulic conductivity of soils. Canadian Geotechnical Journal, 40(3), 616-628.

Eary, L.E. and Williamson, M.A. (2006). Simulations of the neutralizing capacity of silicate rocks in acid mine drainage environments. J. Am. Soc. Min. Reclam, 2, 564-577.

Embile Jr, R.F., Walder, I.F. and Mahoney, J.J. (2019). Multicomponent reactive transport modeling of effluent chemistry using locally obtained mineral dissolution rates of forsterite and pyrrhotite from a mine tailings deposit. Advances in Water Resources, 128, 87-96.

Kimball, B.E., Rimstidt, J.D. and Brantley, S.L. (2010). Chalcopyrite dissolution rate laws. Applied Geochemistry, 25(7), 972-983.

Nicholson, R. V., Rinker, M. J., Acott, G., and Venhuis, M. A. (2003). Integration of field data and a geochemical transport model to assess mitigation strategies for an acid-generating mine rock pile at a uranium mine. Proceedings, Sudbury. : Citeseer.

Palandri, J.L. and Kharaka, Y.K. (2004). A compilation of rate parameters of water-mineral interaction kinetics for application to geochemical modeling. : Geological Survey Menlo Park CA.

Parkhurst, D.L. and Appelo, C. (2013). Description of input and examples for PHREEQC version 3: a computer program for speciation, batch-reaction, one-dimensional transport, and inverse geochemical calculations. (2328-7055). : US Geological Survey.

Vermette, D. (2018). Approche de caractérisation géoenvironnementale axée sur l'utilisation des concepts géométallurgiques (Master thesis, Ecole Polytechnique, Montreal (Canada)).

APPENDIX C INTEGRATING 3D GEOLOGICAL MODELING AND KINETIC MODELING TO ALLEVIATE ACID MINE DRAINAGE THROUGH UPSTREAM MINE WASTE CLASSIFICATION

Research Institute on Mines and Environment (RIME),

Université du Québec en Abitibi-Témiscamingue, Rouyn-Noranda, Québec, Canada

Table S1. The model flow parameters based on VS2DRTI database.

D_{90} (mm)	θ_s	θ_r	α_{VG} (m^{-1})	n_{VG}	k_{sat} (m/s)
0.2	0.37	0.07	1.04	6.9	$2.4x10^{-5}$

D_{90} (mm): 90% of particles are finer than the specified diameter.

θ_s: the saturated volumetric water content.

θ_r: the residual volumetric water content.

α_{VG} and n_{VG}: Van Genuchten (1980) parameters.

k_{sat}: the saturated hydraulic conductivity.

Table S2. Reaction rate parameters of albite and calcite used in PHREEQC code (E in kJ/mol).

Mineral	Acidic mechanism			Neutral mechanism		Alkaline mechanism		
	log k	E	n	log k	E	log k	E	n
Calcite*	-0.3	14.4	1	-5.81	23.5	-3.48	35.4	1[a]
Albite**	-10.07	58	0.34	-19.29	57	-9.85	56	0.32[b]

*Palandri and Kharaka (2004), **Marty *et al.* (2015).

[a] Reaction order with respect to CO_2 partial pressure, it is a carbonate mechanism.

[b] Reaction order with respect to OH^- activity.

Table S3. Variogram parameters produced for each mineral dataset along various direction settings.

The mineral variogram	Variogram direction	Nugget effect	Sill	Range (m)
Albite	Omni-directional	13	20	30
	0° N, 90°	13	21	21
	90° N, 90°	14	20	19
	270° N, 70° E	12	19	30
Calcite	Omni-directional	0.19	0.24	29
	0° N, 90°	0.18	0.25	25
	90° N, 90°	0.17	0.24	20
	270° N, 70° E	0.17	0.23	31
Pyrite	Omni-directional	5.8	7.4	24
	0° N, 90°	5.5	7.5	20
	90° N, 90°	5.5	7.55	18
	270° N, 70° E	5.75	7.45	32

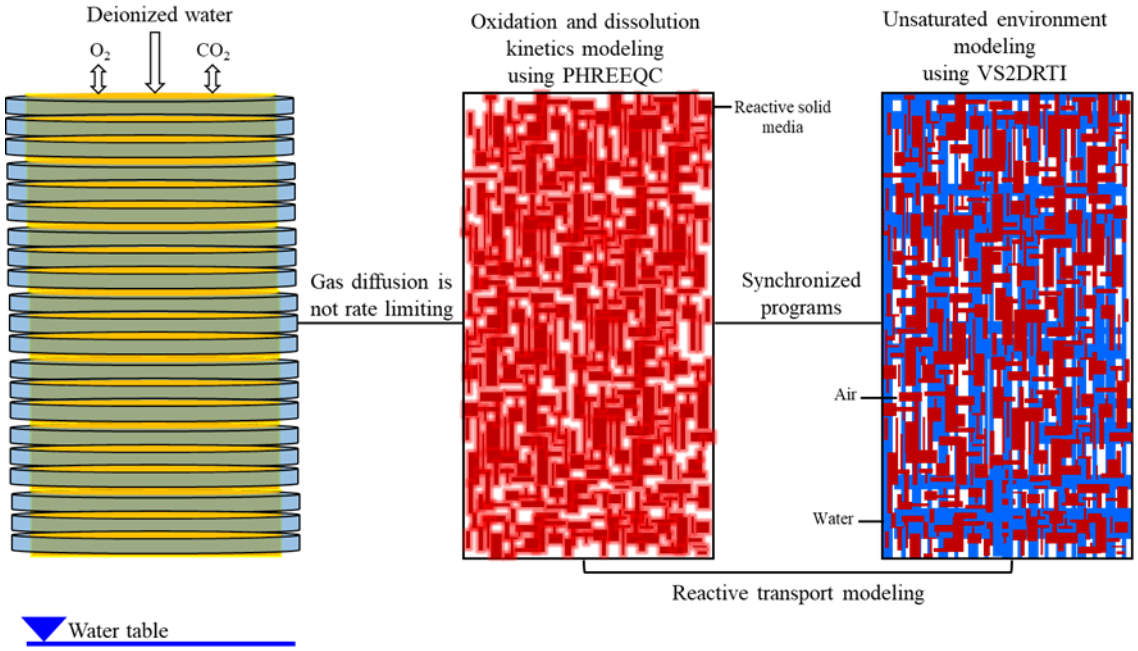


Figure S1. The conceptual model of the reactive transport simulation carried out using PHREEQC and VS2DRTI for geochemical simulation that are not O_2 diffusion-limited.

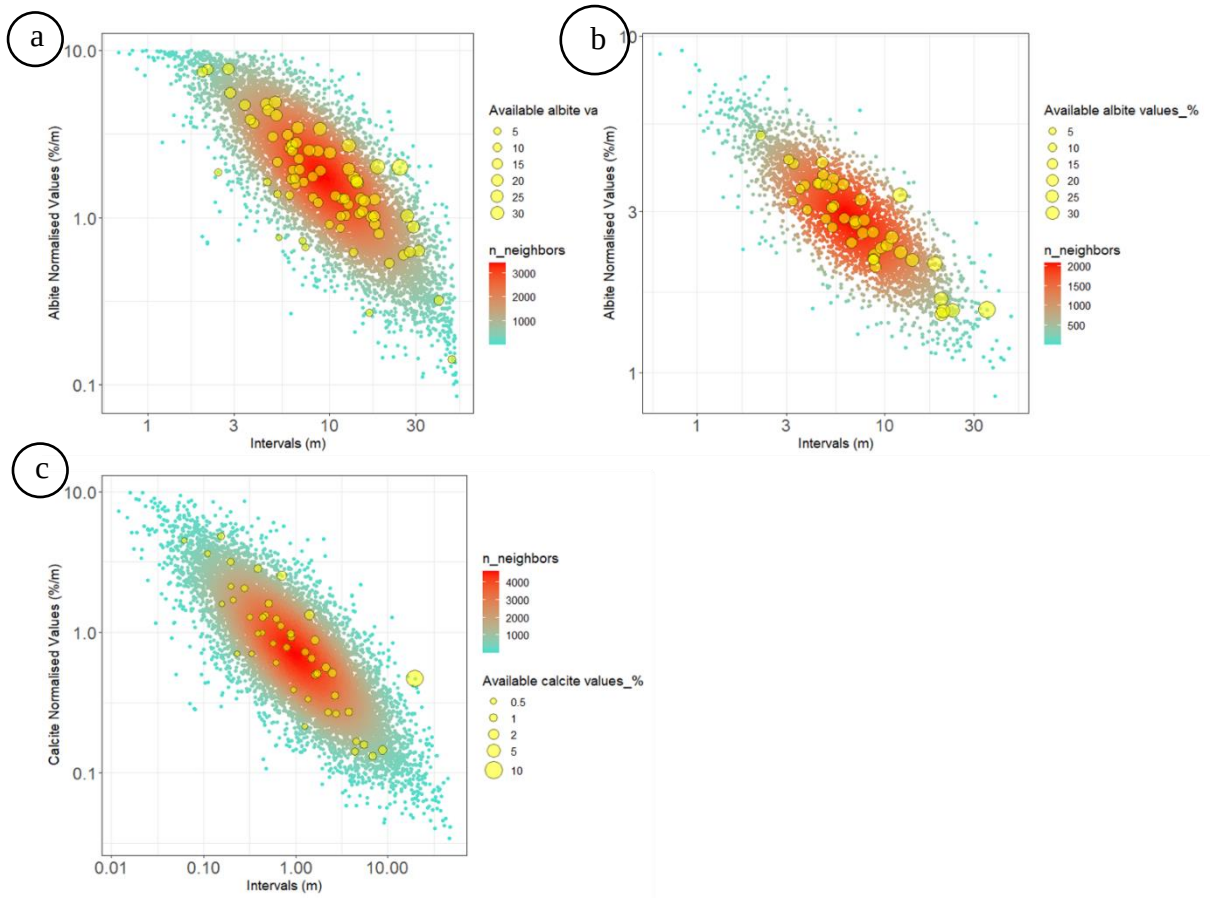


Figure S2. The Monte Carlo simulation outcome depicted for albite and calcite classes. a. The simulated and measured datasets of the class 3 of albite. b. The simulated and measured datasets of the class 4 of albite. c. The simulated and measured datasets of the class 0.1 of calcite

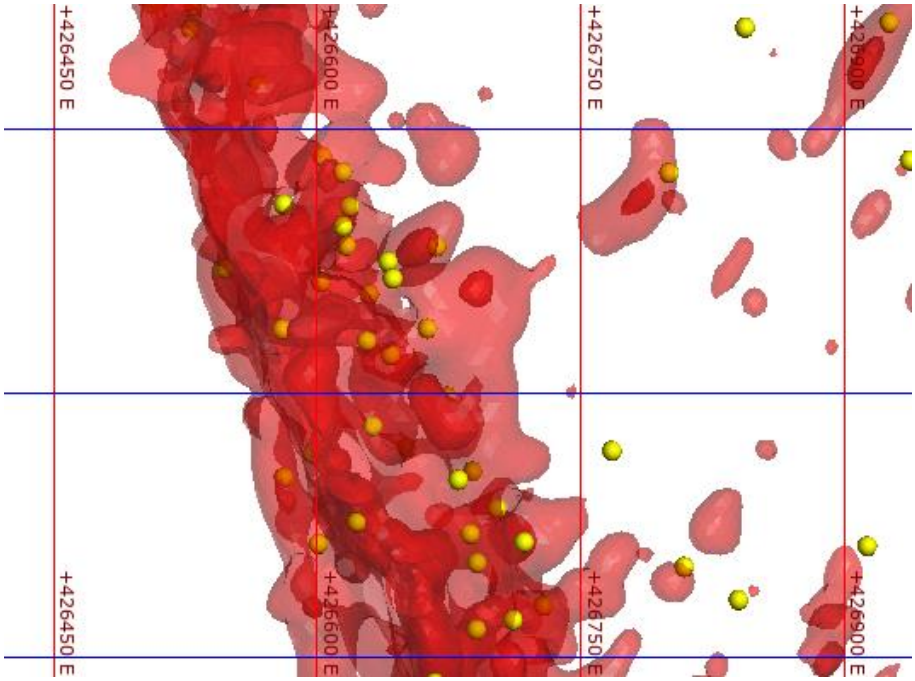


Figure S3. Measured points projected on the 3D numerical model of the pyrite. Yellow points: measured weight proportions of pyrite higher than 4.5%, red casing: the internal core of the pyrite numerical model including simulated values higher than 4.5%.

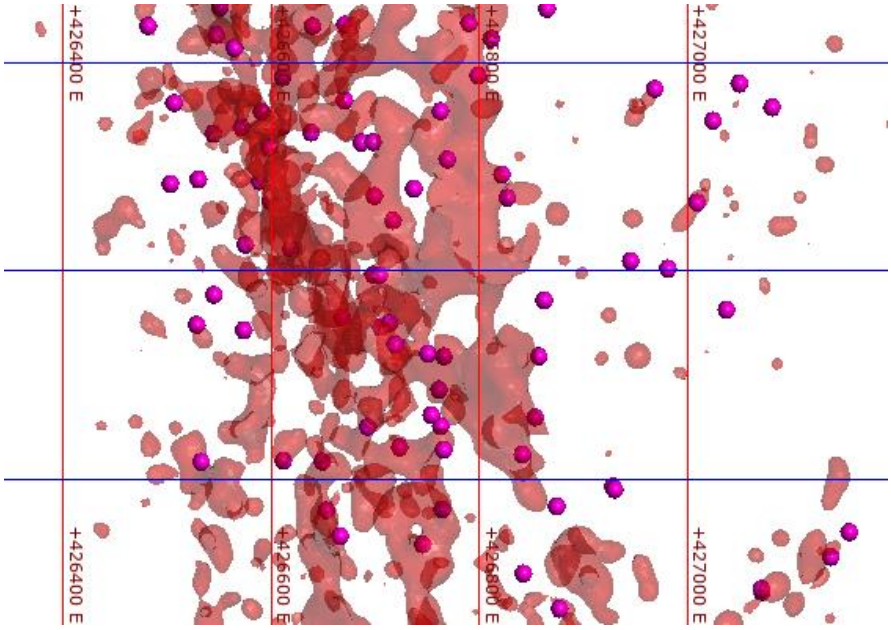


Figure S4. Measured points projected on the 3D numerical model of the albite. Purple points: measured weight proportions of albite higher than 10%, red casing: the internal core of the albite numerical model including simulated values higher than 10%.

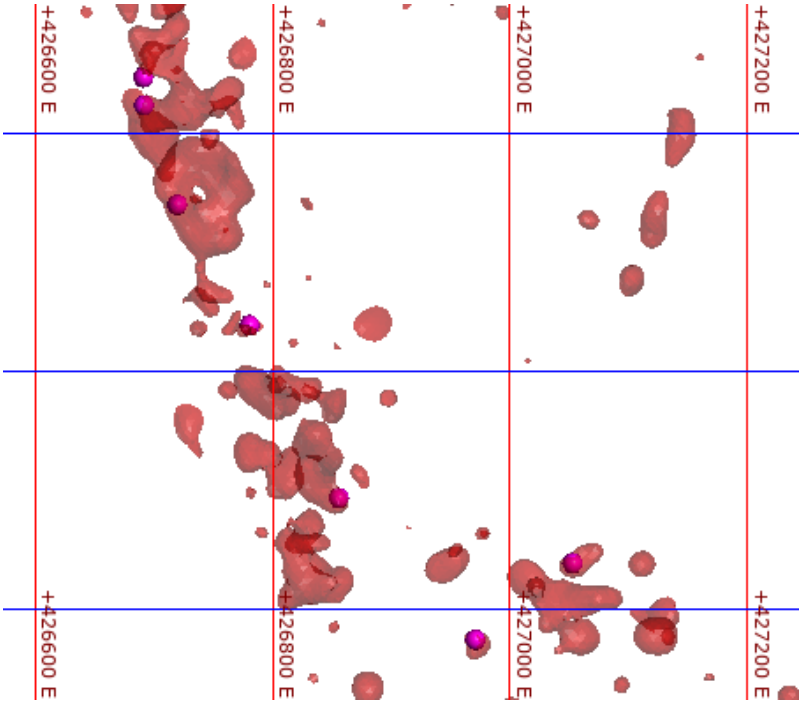


Figure S5. Measured points projected on the 3D numerical model of the calcite. Purple points: measured weight proportions of calcite higher than 1.5%, red casing: the internal core of the albite numerical model including simulated values higher than 1%.

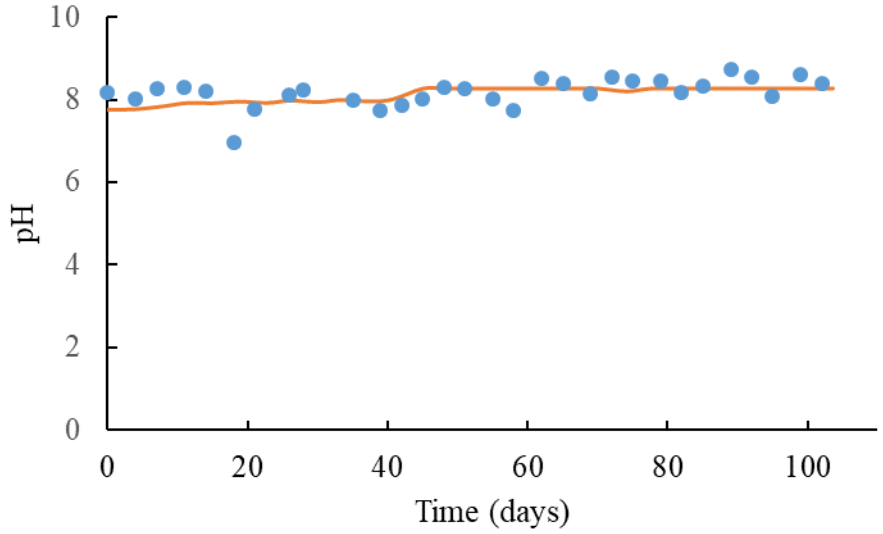


Figure S6. Measured and simulated pH values of a kinetic test containing 8.1 wt.%, 1.9 wt.% and 31.9 wt.% of pyrite, calcite and albite respectively

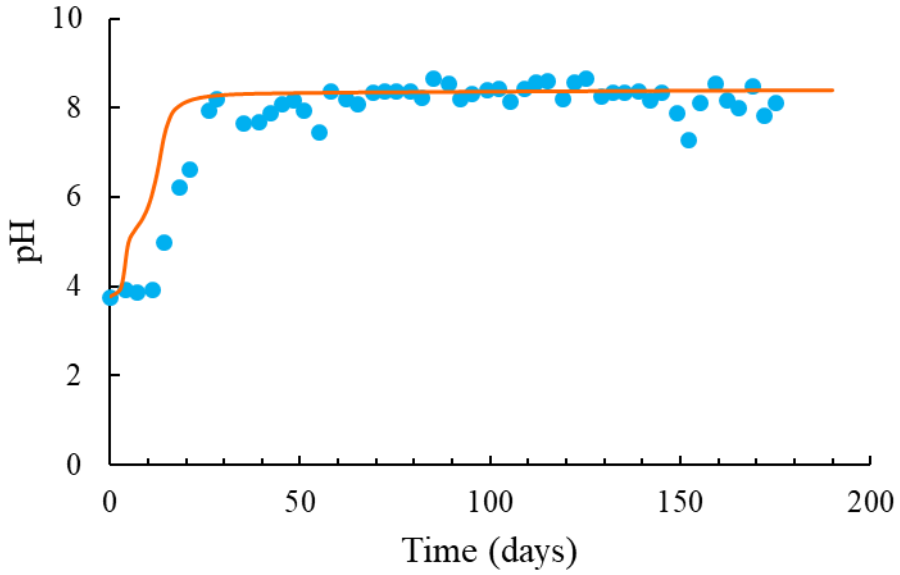


Figure S7. Measured and simulated pH values of a kinetic test containing 4.5 wt.% pyrite, 0.4 wt.% calcite and 18 wt.% albite.

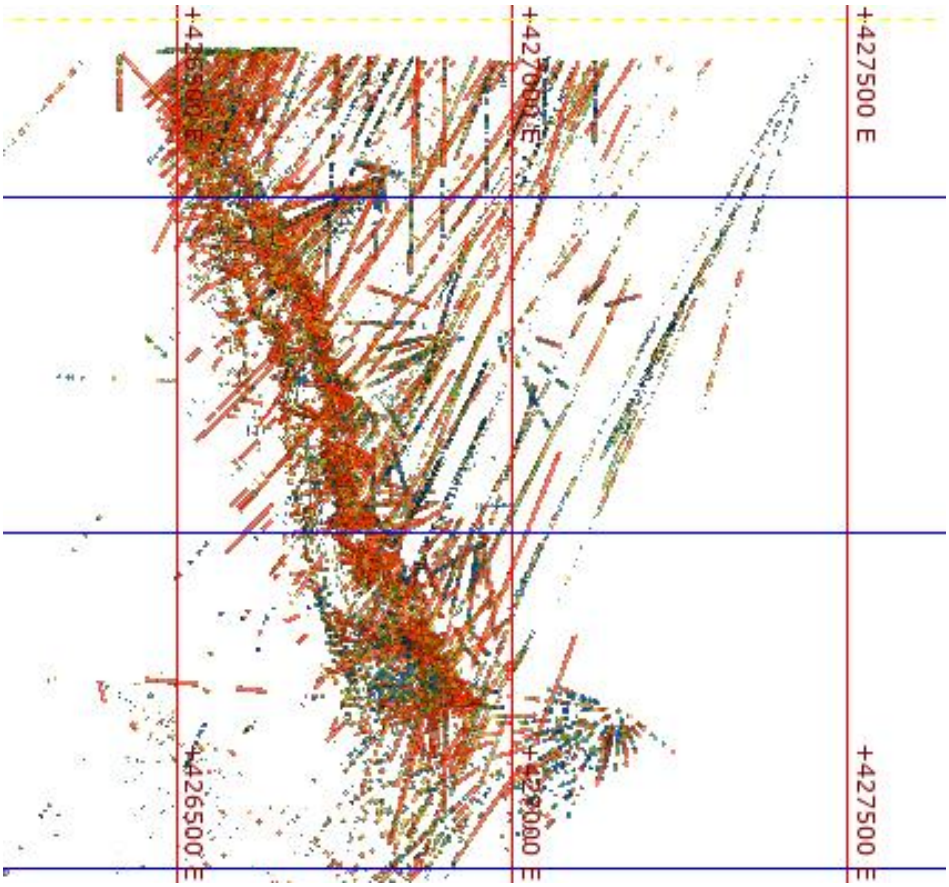


Figure S8. Drill cores described throughout the geological logging.

Description of the steps of the integrated modeling approach:

Step 1 Define the reactive minerals (the scope):

This step defines the target minerals that could be considered to perform the dynamic classification of the host rock. For instance, the present study considers pyrite, albite and calcite because they are the main minerals that will control the extent of the oxidation-neutralization process.

Step 2 Data compilation:

During this step, the user should compile the available quantitative and qualitative datasets for each mineral. For illustration purposes, the subsequent steps refer to a reactive mineral named X. The user should collect all available measurements of the X mineral weight proportions that were measured using an analytical method. Subsequently, the qualitative dataset of the mineral X should be collected from the geological logging. The geological logging should report the interval of occurrences (length of occurrences) of the mineral X in all drill cores as well as a qualitative description of each interval of occurrence. An example of the qualitative description of the intervals of occurrence could be as follows:

- 0.1 indicates thin crystals of the mineral X (less than 1 mm) and the number of the crystals is less than 10;
- 0.5 indicates thin crystals of the mineral X (less than 1 mm) and the number of the crystals is less than 30;
- 1 indicates medium crystals of the mineral X (between 1 and 2 mm) and the number of the crystals is less than 10;
- 2 indicates crystals larger than 2 mm and the number of the crystals is more than 10;

Note: All the geologists involved in geological logging should use the same qualitative description numbers (which is frequently the case in the most mining companies).

Step 3 Data classification:

The user should classify the quantitative data (measured mineral weight proportions of the mineral X) according to their corresponding class. In other words, this step consists of identifying the analyzed sample size for each qualitative class. For instance, in the present study 4187 intervals of occurrence of pyrite were attributed to the 0.1 class. From these intervals, 62 intervals were

analyzed for their pyrite content (table 1 in the main file). Therefore, for each class the analyzed sample size should be identified.

Is the available quantitative dataset sufficient to preform 3D numerical modeling?

Frequently, the measured mineral weight proportions of the mineral X are insufficient to undertake the 3D numerical modeling. Please notice from the example in the previous step that only 62 intervals were analyzed for their pyrite content while the intervals population consists of 4187 interval assigned to the 0.1 class. Therefore, with the available quantitative dataset the spatial continuity analysis needed for 3D numerical modeling could not be performed.

Step 4 Monte Carlo simulation:

This step consists of generating sufficient dataset to enable the spatial continuity analysis. The generated data of X mineral weight proportions should have the same variability as the measured data of X mineral weight proportions (i.e. ensure homoscedasticity). According to the data compilation step the user should have the following variables before carrying out Monte Carlo simulation:

- **Intervals (denoted here as variable B):** a continuous variable with complete sample size because all the intervals were measured (as pointed out earlier, an interval is the length of an occurrence of the mineral X within a given location of a drill core). Choose meter as unit of the intervals variable;
- **X mineral weight proportions (denoted here as variable A):** is a continuous variable with incomplete sample size; not all the intervals were selected to undergo analytical quantification of the X mineral weight proportions.
- **The classes of the mineral X:** is a discrete variable with complete sample size; all intervals were qualitatively classified based upon the classification agreement set by the geologists involved in the geological logging;

The objective of the Monte Carlo simulation is to estimate the probability density function (PDF) of the variable A based upon the well-defined PDF of the variable B. First, the values of the variable A should be normalized by their respective values of the variable B. For instance, if the measured mineral weight proportion of the mineral X is 20 % wt occurring in an interval of 0.1 m, the

corresponding normalized value is 20% wt divided by 0.1 m which equals to 200 (%wt/m). This normalization should be performed for each value of the variable A.

Second, the user should plot on the logarithmic scale the values of the normalized variable A/B (named the auxiliary variable) against the interval values used in normalization. A/B in the y-axis and the B variable in the x-axis. Once performed, the user will notice that a power law ($y=a.x^b$) linking the auxiliary variable and the B variable is set. A power law in the logarithmic scale exhibits a significant correlation coefficient (please make sure that both axis are in the logarithmic scale otherwise the correlation could not be exhibited).

At this stage, the user should perform an iterative Monte Carlo simulation that generates a large scatter (high number of data points), which has the same trend as the initial scatter. Therefore, the parameters of the generated power law ($y=c.x^d$) should be as close as possible to the parameters of the initial power law ($y=a.x^b$) (i.e. $a \approx c$ and $b \approx d$). To perform this Monte Carlo simulation, GoldSim software could be used as it provides the possibility to run a correlation-based Monte Carlo simulation. Three stochastic elements are set in GoldSim as indicated in the figure below (Figure S9):

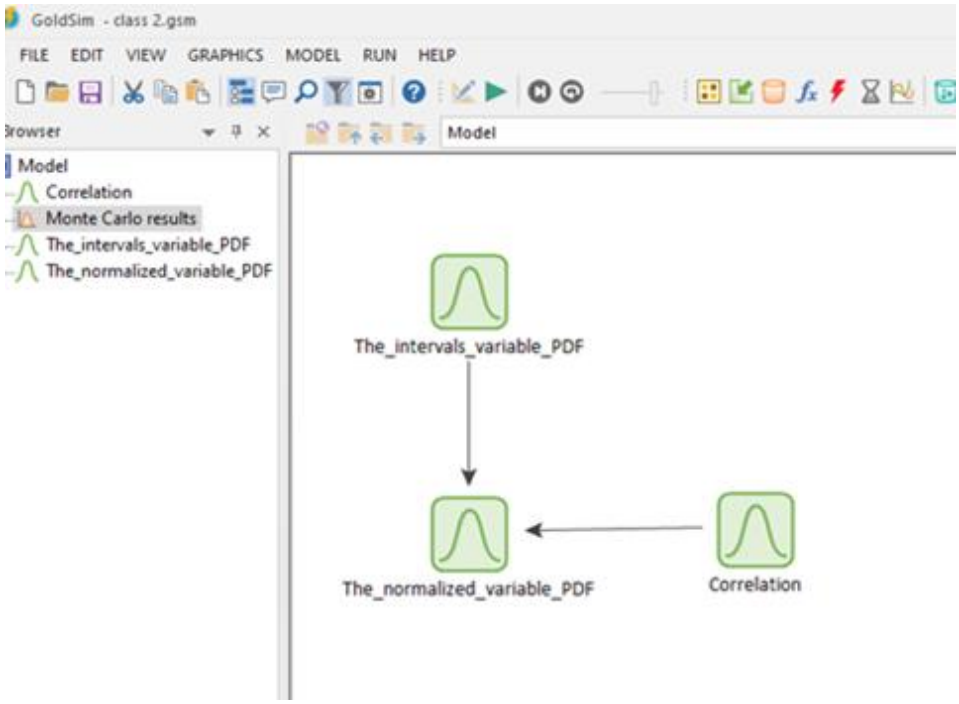


Figure S9. The stochastic elements used in GoldSim to perform a correlation-based Monte Carlo simulation.

The PDF of the intervals variable is well-defined because all the intervals were measured. In the present study, the intervals PDF is log-normal, the mean and the standard deviation used as inputs in the stochastic element of the intervals PDF. The correlation was set as a normal PDF with the mean equals to the correlation coefficient computed from the initial power law ($y=a.x^b$) and the standard deviation was at 0.5. In a previous study (Toubri et al 2021), several values of the correlation standard deviation were assessed, the results indicated that 0.5 yielded the best outcome regarding the extent of the ergodic fluctuations (ergodic fluctuations are simply the differences among different realizations generated using the same Monte Carlo simulation). The mean and the standard deviation of the PDF of the normalized variable (the auxiliary variable) could be set at any values because they will be iteratively updated until obtaining a generated power law ($y=c.x^d$) as close as possible to the initial power law ($y=a.x^b$) (i.e. $a \approx c$ and $b \approx d$). For instance, the user launches the first iteration, he compares the generated scatter power law to the initial scatter power law, if the two power laws are different, the user should modify the parameters of the normalized variable PDF and launch the Monte Carlo simulation again. The same operation should be undertaken until obtaining a generated power law as close as possible to the initial power law.

Once the iterative Monte Carlo is achieved, the generated scatter could be used to obtain a large dataset of the variable A through canceling the normalization by a simple multiplication of normalized values by their respective interval.

Step 5 Hypothesis testing:

In Toubri et al (2021), it was demonstrated using the hypothesis testing that the generated values by Monte Carlo simulation and the available measurements have the same variability features. The user could perform hypothesis testing to ensure that he generated homoscedastic populations.

Step 6 Spatial continuity analysis:

The iterative Monte Carlo simulation enabled the generation of a large dataset of the X weight mineral proportions. The dataset generated by simulation should undergo the spatial continuity analysis to assess the spatial anisotropy and to demonstrate that the spatial anisotropy of the generated dataset complies with the geological information regarding the plane with the highest spatial continuity that frequently corresponds to the major structural trend of the deposit.

SGeMS was used to compute the variogram parameters for the simulated X mineral weight proportions. As indicated in the figure below (Figure S10), SGeMS enables the calculation of omnidirectional and many other directional variograms.

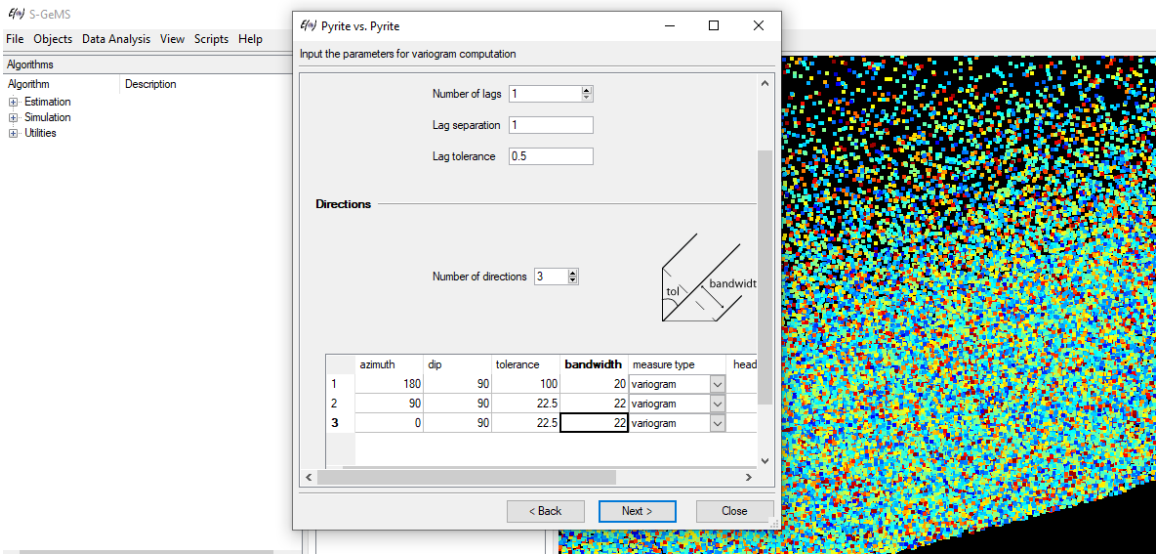


Figure S10. SGeMS and variogram calculations along various directions.

The user should compute the variograms of many directions including the direction considered by the geologists as the major structural trend. The variogram of the highest range value should correspond to the direction of the major structural trend. This agreement should be demonstrated before 3D numerical modeling because it reflects that the generated dataset complies with the geological features. In this study and in Toubri et al (2021) this requirement was fulfilled since the first generated dataset and no other attempts were needed to abide by the aforementioned requirement. This highlighted the effectiveness of the iterative Monte Carlo simulation.

Step 7 Three dimension numerical modeling:

The variogram parameters obtained for the direction with the highest spatial continuity should be used as inputs in Radial Basis Functions (RBF) interpolant of Leapfrog Geo as indicated in the figure below (Figure S11):

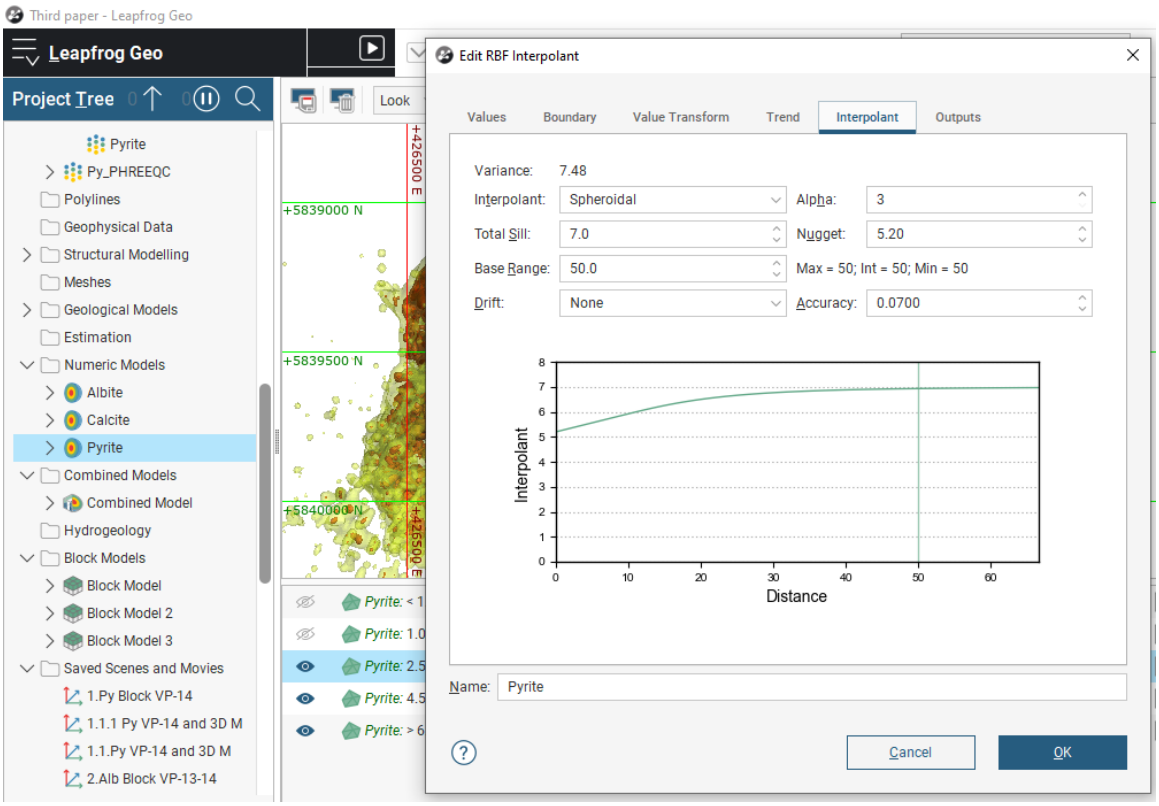


Figure S11. Variogram parameters computed using SGeMS used as inputs in the RBF interpolant of Leapfrog Geo.

Besides, the structural trends provided by the geologists during geological logging should be used as inputs in the RBF interpolant of Leapfrog Geo in the trend section as indicated in the figure below (Figure S12). Therefore, a 3D numerical model of the mineral X weight proportions could be generated.

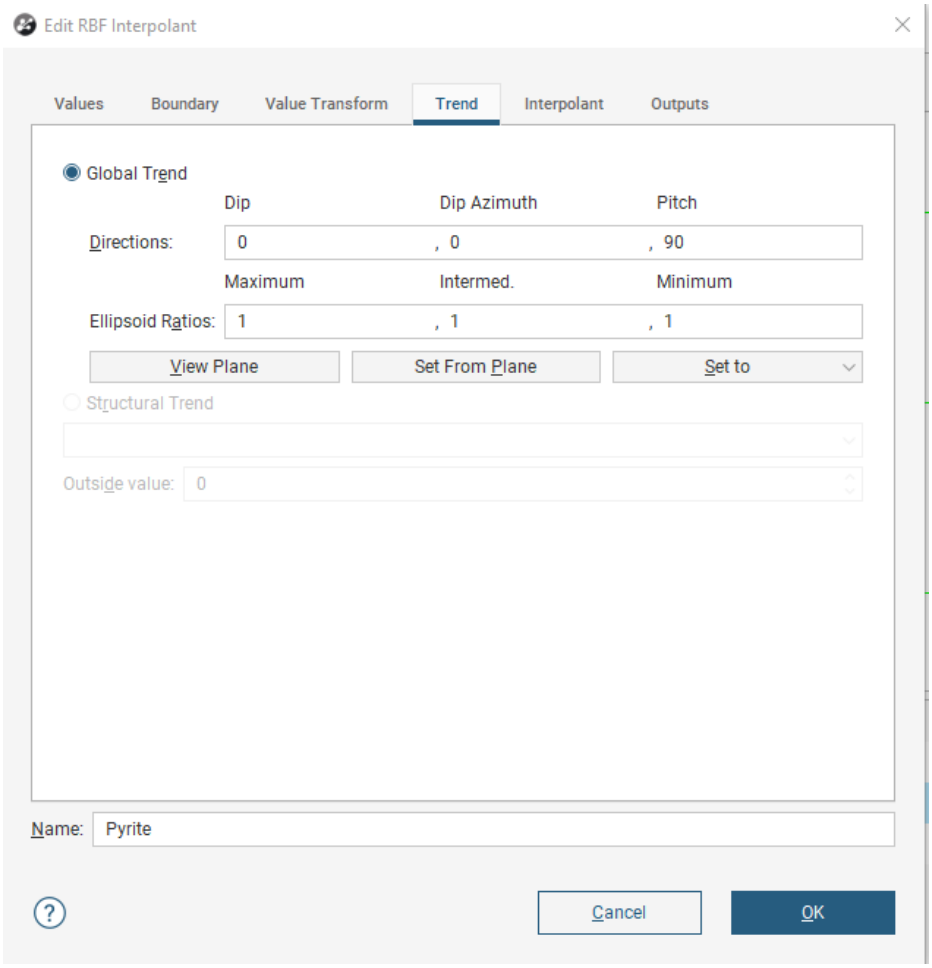


Figure S12. Structural trend used as inputs in the RBF interpolant of Leapfrog Geo.

Step 8 Benchmarking of the numerical modeling:

This step consists of importing the measured mineral weight proportions of the mineral X in Leapfrog and highlighting the agreement between the measurements of the mineral weight proportion and the 3D numerical model as indicated in Figures S2-S4 and in Toubri et al (2021).

Step 9 Block models:

From the 3D numerical model, a block model could be created using Leapfrog through choosing the dimension of the voxel of the block model. Various dimensions could be selected until obtaining the relevant dimension of voxel that needs less computation time and displays sufficient spatial detail (Figure S13).

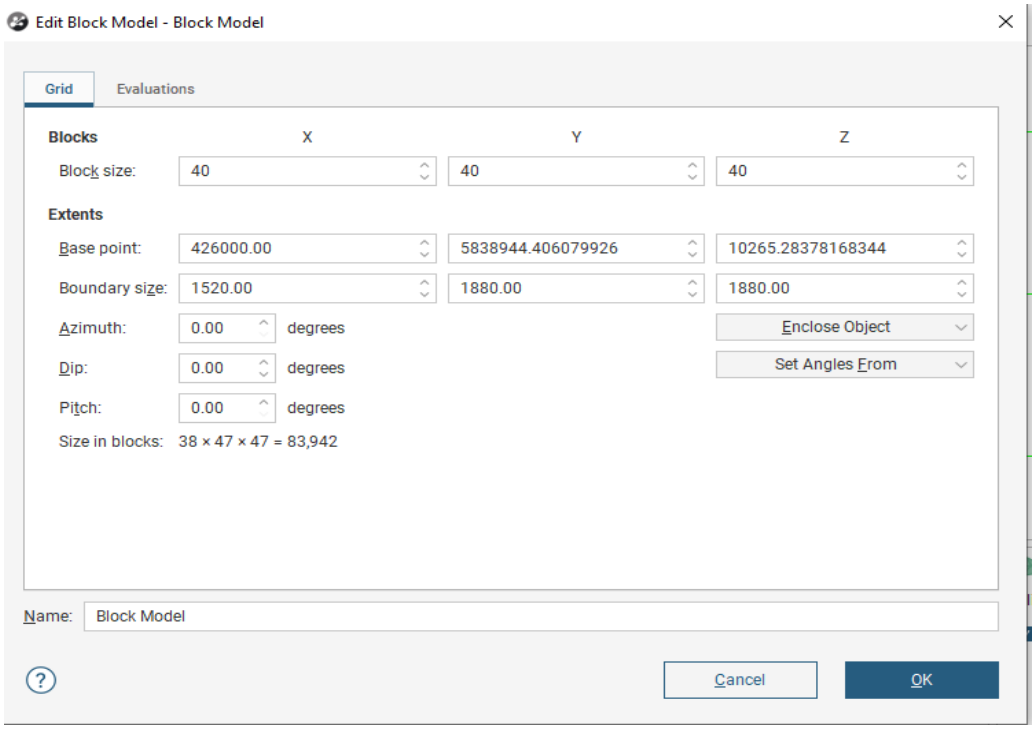


Figure S13. Specifying the dimensions of the voxel of the block model in Leapfrog Geo.

Step 10 Repeat the process:

The aforementioned steps should be performed for each reactive mineral that will be considered in the reactive transport modeling.

Step 11 The plane of the overlapping:

The user should choose a plane along which he would preform a dynamic classification based upon the pH. Once chosen, the user should overlap the 3D numerical models of the considered minerals along the aforementioned plane.

Step 12 Reactive transport modeling:

A reactive transport simulation previously calibrated and benchmarked could be used to simulate the pH that could be generated in the presence of given mineral proportions of the reactive minerals. For each voxel, a reactive transport simulation is performed assuming the same setting, only the mineral proportions that change based upon the 3D numerical model of each reactive mineral. Therefore, the established 3D numerical models are used as inputs for the reactive transport simulation.